Annalen der Meteorologie

30

23. Internationale Tagung für Alpine Meteorologie

vom 5. bis 9. September 1994 in Lindau

Offenbach am Main 1994
Selbstverlag des Deutschen Wetterdienstes
ISSN 0072-4122

Die für die Veröffentlichung als Vorabdruck zur 23. Internationalen Tagung für Alpine Meteorologie eingesandten Manuskripte sind erweiterte Zusammenfassungen der Vorträge und Poster-Darstellungen. Für ihren Inhalt sind die Verfasser verantwortlich. Die Wiedergabe der Zusammenfassungen nimmt eine spätere ausführliche Darstellung der Vorträge sowie ihre Veröffentlichung durch die Autoren an anderer Stelle nicht vorweg.

ISSN 0072-4122
ISBN 3-88148-299-7

Herausgeber und Verlag:

Deutscher Wetterdienst, Zentralamt
Frankfurter Straße 135
63067 Offenbach am Main

Redaktionsschluß: 11. Juli 1994

INHALT

Vorwort/ Foreword . . . . . XI/XII

Alpine Synoptik

KURZ, M.:
Zum Stand der operationellen numerischen Vorhersage orographischer Effekte im Alpenbereich . . 1

KERKMANN, J.; CAGNATI, A.:
Zur Problematik der Wettervorhersage für Flugwettbewerbe auf der Südseite der Alpen 6

MAYR, G.J.; McKEE, Th.B.:
Observations of the Evolution of Orogenic Blocking 10

SCHMID, W.; HUNTRIESER; H.:
The Wind Environment of Supercell Storms in Switzerland 13

WILLEMSE, S.; SCHIESSER, H.H.:
45 Years of Hailstorms North of the Alps 17

HEIMANN, D.; SEPT, V.; FUENTES, U.:
The Frequency of Convective Storms North of the Alps as a Function of the Large-scale Climate . 21

PERISTERI, M.:
First Results from the SETEX-94 Experiment 25

HAASE-STRAUB, S.; HAGEN, M.; HEIMANN, D.:
The Severe Squall Line of 21 Juli 1992 in the Region North of the Alps 28

JUDE, O.; BALUT, G.; DIMA, V.:
The Comparative Analysis of Snowstorms in November 1993 in the Carpathian-Balkan Sink 32

WERNER, R.:
Die Föhnfälle im Dezember 1989 in Vorarlberg 35

Beobachtungsmethoden und Instrumente

PÖTTSCHACHER, W.; STEINACKER, R.:
On the Relevance of Wind Measusements on Mountain Stations 39

BLUMER, F.; MAURER, Chr.; STEINEGGER, U.:
Use of a Double Fence Intercomparison Reference in High Mountain Areas to Correct Precipitation Measurements 43

NESPOR, V.:
The Wind Effect on Rain Measurement: Theoretical Approach 47

SEVRUK, B.; ZAHLAVOVA, L.:
The Effect of Systematic Error of Precipitation Measurement on Vertical Gradients of Precipitation in Switzerland 48

HELD, E.; JOSS, J.:
The Influence of the Orography on Precipitation Seen by the Swiss Radars 52

LI, L.; SCHMID, W.:
An Investigation on the Growth and Decay Patterns of Radar Echoes in Alpine Regions 56

MURSCH-RADELGRUBER, E.:
New Portable Mini-sodar and its Potential and Applicability for Complex Terrain Studies 60

YANG, D.; SEVRUK, B.; ELOMAA, E. et al.:
Wind-Induced Error on Snow-Measurement: WMO Intercomparison Results 61

VOGT, H.:
Ein Meßnetz zur Erfassung des Niederschlags im alpinen Raum 65

KRAMES, K.:
Blitzortungen mit LPATS 67

Diagnose und Simulation

Numerische Simulationen

EGGER, J.:
Lee Cyclogenesis: Cold Air Blocking and Upper-Level Potential Vorticity Anomalies 71

TAFFERNER, A.:
Life Cycle of a Mountain Generated Adriatic Cyclone 73

PICHLER, H.:
ALPEX - Simulation 78

PAUL, G.:
The ALPEX Level IIIb Analysis Produced at DWD 80

STEPPELER, J.; DAMRATH, U.; MAJEWSKI, D.:
Mountain Induced Flow in the Operational Deutschland-Modell 85

BINDER, P.; HERZOG, H.-J.:
The Effect of a Radiative Upper Boundary Condition in a 3-dimensional Meso-ß-scale NWP Model 89

HAIDEN, T.:
Modelling Orographic Upslope Rain 93

SAITO, K.; MATSUO, T.; MURAKAMI, M. et al.:
Numerical Experiments of Orographic Snowfall over the Mountainous Region of Northern Japan . 96

TAKANO, I.:
Numerical Simulation of an Orographically-induced Mesoscale Cyclone off the South Coast of Japan 100

TANNHAUSER, D. S.; MOISEYEV, N.:
The Solution of Lee Wave Problems by the Complex Coordinate Method 104

PRISTOV, N.; RAKOVEC; J.:
The Initial Interpolation for the Wind Field Analysis 105

PALMIERI, S.; D'APRANO, L.; SIANI, A.M.:
Diagnostic Modeling of Orographic and Convective Rainfall 109

VUCETIC, V.; BAJIC, A.:
Generalized Hydraulic Model Sensitivity for the Input Data 113

MAP

VOLKERT, H.:
Mesoscale Alpine Programme: Objectives, Status, and Prospects. 117

KUETTNER, J.:
American Interests in the Mesoscale Alpine Project (MAP) 121

STEINACKER, R.:
Sind Handanalysen für eine Verifikation von Mesoskalenmodellen geeignet? 122

AEBISCHER, U.; SCHÄR, Chr.:
High Resolution Simulation of Low-level Flow Features in the Alpine Region 125

BINDER, P.:
Mesoscale Initial Conditions in the Alpine Region 129

Tibet

CHEN, BOMIN; QIAN, ZHENGAN:
Numerical Predicting Tests of the Rainfall and Vortices over the Tibetan Plateau in Summer . . . 130

HUANG, FUJUN:
A Preliminary Study of Strong Storm in the East Side Edge of Tibet Plateau 134

SUN, GUOWU; ZHOU, YAJUN; LI, CHUNHU:
Some Observational Facts of Atmospheric Low-frequency Oscillations over Tibet Plateau 139

CHEN, BOMIN; QIAN, ZHENGAN; ZHANG, LISHENG:
Numerical simulation of the vortices over the Tibetan Plateau in Summer 143

SUN, GUOWU; LIU, XIAODONG; ZHOU, YAJUN:
The Numerical Experiment of Influence of Surface Heat Source over Tibetan Plateau on Runoff in Summer 147

PYREX

BOUGEAULT, P.:
Results from the PYREX Experiment 151

KOFFI, E.; BENECH, B.; DRUILHET, A.; STEIN, J.:
Application of the Linear Theory to Local Winds Around the Pyrenees Chain During PYREX Experiment 152

GEORGELIN, M.; RICHARD, E.:
A Numerical Study of the Flow Diversion around the Pyrenees 156

GENOVES, A.; CAMPINS, J.; JANSA, A. et al.:
Pyrenean Pressure Drag: Some Factors and Consequences, after PYREX 159

CACCIA, J.-L.; BENECH, B.; KLAUS, V.; TANNHAUSER, D.:
Mountain Wave Stationarity Condition Changes Observed by ST VHF Radar during the IOP3 of the PYREX Experiment 163

KLAUS, V.; SELOYAN, I.:
Turbulence Field Determination During PYREX 90 Using INSU/METEO ST Radar and PERIDOT Model Re-analysis Data 167

STEIN, J.; HEREIL, Ph.:
Nonstationary and Nonhydrostatic Simulations of the IOP 3 of the PYREX Experiment 171

v.d. EMDE, K.:
Simulation einer Gebirgsströmung mit dem Ausschnittsmodell Aladin 172

DRUILHET, A.; ATTIE, J.L.; ABREU, Sa. L. et al.:
Analysis of inhomogeneous turbulence in an atmospheric flow around a mountain range 176

ELKHALFI, A.; GEORGELIN, M.; RICHARD, E.:
Mesoscale Simulations of Hydrostatic Mountain Waves Observed during the PYREX Experiment 180

PBL, lokale Winde

KLOSE, B.:
Orographically-influenced Vertical Wind Profiles 184

EMEIS, S.:
The Effective Roughness Length for Orographically Inhomogeneous Terrain 188

RAKOVEC, J.; PRISTOV, N.:
The Reliability of the Wind Field Analysis 192

CHMELIK, M.; NEJEDLIK, P.; STASTNY, P.:
Modification of Wind Stream in Poprad Basin due to High Tatra's Massif 196

IVANCAN-PICEK, B.; TUTIS, V.:
Vorticity Diagnostics of Severe Bora Cases 200

LAZIC, L.; SAULACIC, I.:
Impact of Height and Shape of the Orography to Local Bora Wind 204

SALERNO, R.:
A Simple Prognostic Wind Field Model for Complex Areas: Applications to Local Circulation Prediction for an Alpine Region 209

VRHOVEC, T.:
Some Numerical Simulations of Dry Temperature Inversions and Associated Winds in Alpine Valleys 210

TUTIS, V.; IVANCAN-PICEK, B.:
Influence of Orography and Surface Thermal Budgets on Storm Development 215

Alpine Klimatologie

SNEYERS, R.; SIANI, A. M.; PALMIERI, S.:
Climate Change Detection in Alpine Valleys: The Example of Brera Observatory (Milan) Rainfall Series (1790-1990) 217

STEFANICKI, G.; TALKNER, P.; WEBER, R.O.:
Temperature Trends in the Alpine Region during the last Century 221

LAPIN, M.:
Possible Change of the Climate Conditions in Slovakia due to the Expected Global Warming by 1 - 2°C 225

GANDINO, C.:
Decrease of the Annual Amount of Hours With Foehn at Ispra 229

BIANCOTTI, A.; PALUDI, S.:
Le Prezipitationi nelle Valli di Lanzo durante il periodo 1915-1993 233

BLUMER, F. P.; LANG, H.:
Spatial Differences of Precipitation in the Eastern Swiss Alps 237

KRISTEV, L.; KOLEVA; E.:
Extreme Seasonal Precipitation in Mountain Regions of Bulgaria 238

WHITEMAN, C.D.; BIAN, X.:
Semiudiurnal Solar Tides in the Mountain Atmosphere 239

BÜCHER, A.; DESSENS, J.; PECH, B.:
Changes in Temperature Extremes at the Pic du Midi (Pyrenees, 2862 m), period 1882 - 1984 . . 243

BUSUIOC, A.:
The Influence of the Carpathian Mountains upon the Variability of the Romanian Precipitation in Wintertime 247

CAPKA, B.; GAJIC-CAPKA, M.:
Variation of Extreme Air Temperature across the Dinaric Alps 251

CAZACIOC, L.:
Statistical Study on the Snow Storm Phenomenon in the Mountain Area of Romania 255

KAHLIG, P.:
A New Look at Tree Rings 259

BAZAC, G.; COTARIU, R.; SIMEN, C.:
The Foehn Phenomenon in the Romanian Carpathians 260

ZANINOVIC, K.; GAJIC-CAPKA, M.:
Climatological Basis for Prediction of Road Slipperiness: Minimum Air and Soil Temperatures . . 264

LONCAR, E.; SINIK, N.; ZANINOVIC, K.:
Pressure Singularity Detected by a Mountain Station 268

MARES, I.; MARES, C.; MUSAT, I. et al:
The Influence of the Major Relief on the Climate Variability 272

MIHAILESCU, I.; RABAEA, A.; BUCSA, I.:
Longterm Air Temperature Fluctuations in the Romanian Carpathians 277

PASQUALE, V.; RUSSO, G.; SACCHINI, A.; VERDOYA; M.:
Precipitation Rate as a Possible Signal of Recent Climatic Variations 278

TODARO, C.; D'ABRAMO, F.; MIGLIARDI, E.:
Sulle Variazioni Climatiche del Numero di Giorni con nevicate in alcune Localita delle Alpi Italiane 282

KOLEVA, E.:
Air Temperature Changes in the Bulgarian Mountains 286

NIEDZWIEDZ, T.; USTRNUL, Z.:
Long-term Variability of the Potential Foehns Due to Circulation Conditions in the Western Carpathians 287

Alpine Hydrometeorologie, Schnee und Lawinenforschung

MAIR, R.:
Automatisches Meßnetz des Lawinenwarndienstes Tirol 291

MOTTA, L.; MOTTA, M.:
A Model for the Sadden Extinction of Cirque and Valley Glaciers based on a Case in the Western Alps 295

STURMAN, A.P.; OWENS, I.F.; KELLIHER, F.M. et al.:
Estimation of the Head Budget over a Glacier Snow Field, Franz Josef, New Zealand 299

GARCIA SELLES, C.; SALVADOR FRANCH, F.:
Snowfall Analysis in the Eastern Pyrenees 303

ESCHER-VETTER, H.; REINWARTH, O.:
Untersuchungen zum Niederschlag- und Abflußverhalten eines stark vergletscherten Einzugsgebietes in den Ötztaler Alpen 307

Alpine Biometeorologie

SEIBERT, P.; KROMP-KOLB, H.; KASPER, A. et al.:
Meteorological Influences on Air and Snow Pollution in the High Alps: Results of the Project ALPTRAC 311

SILBERNAGL, R.; SALZGEBER, M.; HUBER, M. u.a.:
Increase of Erythemal Effective Irradiance with Altitude between Innsbruck (577 m a.s.l.) and Hafelekar (2269 m a.s.l.) 316

VECCHI, R.; VALLI G.:
O_3 and ^7Be Measurements in Atmosphere for the Study of Vertical Exchanges and Transport . . . 320

LÜDECKE, C.:
Ergebnisse der biometeorologischen Untersuchungen im Basislager des Broad Peak, Juni 1991 . . 321

v. PRABHA, Th.; MURSCH-RADELGRUBER, E.:
The Study of Industrial Pollution of Linz Using a Diffusion Model by Incorporating the Mass Consistency Concept 325

PLANINSEK, T.; CUHALEV, I.:
Air Pollution on the Hills Around the Termal Power Plant Sostanj 329

SINIK, N.; LONCAR, E.; MARKI, A.:
Background Air Pollution on Mountain Medvednica 333

CEGNAR, T.; LESNJAK, M.:
Meteorological Conditions During Elevated Ozone Concentrations in Slovenia 336

WOOLDRIDGE, G.; ZELLER, K.; MUSSELMAN, R. C.:
Ozone Concentration Characteristics in and over High-altitude Forest 340

MATZARAKIS, A.; MAYER, H.; BALAFOUTIS, C.:
Human-biometeorologische Bewertung des thermischen Milieus in den höheren Gebirgsregionen von Griechenland 344

PELLEGRINI, U.; APADULA, F.; MARZORATI, A.:
Meteorological and Chemical Characterization of an Alpine Monitoring Station 348

PLESKO, N.;, KRSTIC-BURIC, M.; PLESKO, S.:
Dependence of Children's Sino-Bronchial Syndrome on Weather in Continental Part of Croatia . . 352

VUCETIC, M.; VUCETIC, V.:
Degree Days in the Mountain Area of Croatia 356

GOESCH, M.:
Das Literaturinformationssystem METEOROLOGIE des DWD 360

Autorenregister 365

Verzeichnis der Internationalen Tagungen 369

Vorwort

Die Internationale Tagung für Alpine Meteorologie (ITAM) findet nach zwölf Jahren wieder in Deutschland statt. Die Stadt Lindau am Bodensee wurde als Konferenzort für die 23. ITAM gewählt.

Der Deutsche Wetterdienst hat die Aufgabe übernommen, die Konferenz vom 5. bis 9. September 1994 in der Inselhalle zu organisieren und durchzuführen.

Über 100 wissenschaftliche Beiträge sind für die Konferenz angenommen worden und werden mündlich vorgetragen oder als Poster präsentiert. Dies bezeugt das große Interesse an den fachlichen Problemen der Gebirgsmeteorologie, die eine besondere Fragestellung innerhalb unserer Wissenschaft darstellt und Themen sowohl aus der Synoptik, der numerischen Simulation, der Klimatologie, der Hydrologie und Biometeorologie als auch spezielle Beobachtungsmethoden und Instrumente einschließt.

Der vorliegende Tagungsband enthält alle bis Anfang Juli 1994 eingegangenen Zusammenfassungen der Tagungsbeiträge in den Originalsprachen.

Mein Dank gilt Herrn M. Kurz und dem Organisationskomitee für die wissenschaftliche Vorbereitung der Tagung sowie den Mitarbeitern des Deutschen Wetterdienstes für die technische Vorbereitung und Durchführung der Tagung sowie die Veröffentlichung des vorliegenden Tagungsbandes.

Mein Dank gilt auch der Stadt Lindau für die gastfreundschaftliche Atmosphäre, die so viel zum Erfolg einer ITAM beiträgt, damit neben dem wissenschaftlichen Gedankenaustausch auch der persönliche Kontakt zwischen den Meteorologen der Alpenregion und darüber hinaus der Gebirgsregionen überhaupt gepflegt werden kann.

Dr. Tillmann Mohr
Präsident des Deutschen Wetterdienstes

Foreword

After twelve years the International Conference on Alpine Meteorology will once again be held in Germany. Lindau/Lake Constance has been chosen to host the 23rd International Conference on Alpine Meteorology.

The Conference will be organized by the Deutscher Wetterdienst and take place at the Inselhalle from 5 to 9 September 1994.

More than 100 scientific contributions have been accepted for the Conference, and will be presented either orally or in form of posters. This shows how great the interest is in the problems of Alpine meteorology which in itself is a specially problematic topic within our science, englobing not only subjects of synoptics, numerical simulation, climatology, hydrology and biometeorology but also special methods of observation and instruments.

The present conference report contains all summaries of the contributions in their original languages as received by the beginning of July 1994.

I wish to express my thanks to Mr. Kurz and the Organizing Committee for the preparation of the scientific part of the Conference as well as to the members of the Deutscher Wetterdienst for the preparation of the technical part and the organization of the Conference as well as the publication of the conference report.

I also wish to thank the Stadt Lindau for the hospitable atmosphere which so much contributes to the success of an International Conference on Alpine Meteorology so as not only to foster the exchange of scientific ideas but also the personal contacts between meteorologists of the Alpine region, of mountain areas in general.

Dr. Tillmann Mohr
President of the Deutscher Wetterdienst

Zum Stand der operationellen numerischen Vorhersage orographischer Effekte im Alpenbereich

M. Kurz

Deutscher Wetterdienst
Zentralamt

ABSTRACT

The performance of the NWP-models used in the DWD with regard to the simulation of the orographic effects of the Alps is demonstrated by typical examples. Macro-scale developments like lee cyclogenesis are satisfactorily forecasted by all models. The high-resolution model (DM) is even able to simulate limited meso-scale effects like the onset of foehn ahead an approaching front for some hours and the resulting changes of the frontal structure.

ZUSAMMENFASSUNG

Anhand typischer Beispiele wird der aktuelle Stand der Güte der im DWD benutzten Wettervorhersagemodelle hinsichtlich der Orographie-Effekte der Alpen dargestellt. Makroskalige Entwicklungen wie die Lee-Zyklogenese werden i.a. von allen Modellen befriedigend genau vorhergesagt. Das hochauflösende "Deutschland-Modell" ist darüber hinaus in der Lage, räumlich und zeitlich begrenzte mesoskalige Effekte wie den Einsatz von Föhn vorderseitig einer herannahenden Front und die daraus resultierende Veränderung der Frontstruktur zu simulieren.

1. Einleitung

Wie alle größeren Hochgebirge beeinflussen die Alpen Wetter und Wetterentwicklung in allen Scales. Sie stellen ein Hindernis für die Strömung dar, das entweder um- oder überströmt werden muß. Sie bilden außerdem eine hochreichende Quelle bzw. Senke für Wärme- und Feuchteflüsse. Im folgenden wird dargestellt, wie durch die im DWD operationell verfügbaren numerischen Vorhersagemodelle die orographischen Effekte simuliert werden, welche Defizite noch bestehen und worauf der in Alpennähe arbeitende Synoptiker bei der Nutzung der numerischen Prognosen zu achten hat.

2. Die verfügbaren Modelle

Im Wettervorhersagedienst des DWD ist seit Sommer 1993 eine dreiteilige Modellkette operationell verfügbar. Sie besteht aus

- einem Globalmodell (GM) mit der spektralen Auflösung T 106
- dem Europa-Modell (EM) mit einer horizontalen Auflösung von 50 - 55 km, das Europa und den Nordatlantik überdeckt, sowie
- dem Deutschland-Modell (DM) mit einer horizontalen Auflösung von 14 km,das auch den gesamten Alpenraum einschließt.

Im GM wird die Atmosphäre in 19 Schichten, im EM und DM in 20 Schichten aufgelöst. Bei EM und DM befinden sich dabei 8 Schichten in den untersten 2 km, um die Grenzschichtstruktur besser simulieren zu können. Für mittelfristige Vorhersagen wird außerdem der Output des EZMW-Modells (T 213, 31 Schichten) benutzt.

Entscheidend für die Simulation der Orographie Effekte ist natürlich die Repräsentation des Terrains in den Modellen. Sie ist entsprechend der horizontalen Auflösung sehr unterschiedlich. Während die maximale Alpenhöhe im GM nur ca. 1500 m erreicht, beträgt sie im EM 2300 m und im DM 3130 m. Die GM-Orographie enthält lediglich eine ungegliederte Senke zwischen Alpen und dem Hochland der Iberischen Halbinsel, während das EM den Alpenbogen, den Einschnitt des Rhonetals, das Zentralmassiv und die Pyrenäen auflöst. Das DM spiegelt darüber hinaus in seiner Orographie größere Gebirgszüge und Taleinschnitte in den Alpen sowie die Position der Mittelgebirge wider.

Das EZMW-Modell benutzt eine sogenannte "Envelope"-Orographie, bei der die mittlere Gebirgshöhe um die Streuung vergrößert wird, um die Hinderniswirkung besser simulieren zu können.

3. Gegenwärtiger Stand der numerischen Vorhersagen

3.1 Orographie-Effekte bei Überströmung der Alpen

Bei der Überströmung der Alpen von NW oder S resultieren typische Deformationen von Druck-, Wind- und Temperaturfeld mit einem kalten Keil an der Luvflanke, einem warmen Trog über der Leeseite sowie Föhn den Leehang hinab. Bodennah werden die im Luv anströmenden Luftmassen seitlich abgelenkt, fließen am Gebirge entlang und umströmen das Hindenis.

Bei richtig prognostizierter Grundströmung werden diese Effekte von allen Modellen mit allerdings unterschiedlicher Genauigkeit erfaßt. Erstaunlicherweise liefert das EM trotz seiner relativ großen horizontalen Auflösung häufig Vorhersagen von Bodendruck und Geopotential 850 hPa, in denen die Unterschiede zwischen Luv und Lee stark geglättet wiedergegeben werden. Das gilt auch für die Analysen dieses Modells. Im Gegensatz dazu liefert das DM meist gute Prognosen und perfekte Analysen dieser Felder. Bei Temperatur- und Windfeld sind die Unterschiede zwischen den Modellen weniger markant.

3.2 Lee-Zyklogenese über Oberitalien

Zur Lee-Zyklogenese südlich der Alpen kommt es, wenn sich ein oberes Divergenzgebiet, z. B. vorderseitig eines Höhentroges und angezeigt durch positive Vorticityadvektion, einem Leetrog überlagert. Der zyklogenetische Effekt der Höhendivergenz kann sich dort bis zum Boden durchsetzen, da die Alpen die untere Kaltluftzufuhr, die kompensierend wirken könnte, weitgehend blockieren. Wichtig ist außerdem, daß die Kaltluftzufuhr westlich der Alpen konzentriert ist, da dann der Höhentrog in eine günstige Position zum entstehenden Bodentief kommt.

Die Vorhersage dieses Prozesses hängt somit wesentlich von der richtigen Simulation des unteren Blockierungseffekts sowie der korrekten Prognose der Vorticityverteilung in der Höhe ab. Die Ergebnisse zeigen, daß prinzipiell alle verfügbaren Modelle in der Lage sind, die Lee-Zyklogenese zu simulieren. Es gibt allerdings eine weite Streuung zwischen Fällen, in denen über Tage hinweg eine konstant gute Prognose geliefert wird, und Fällen, bei denen der Blockierungseffekt der Alpen zu schwach simuliert wird und deshalb nur ausgedehnte Tröge, aber keine Leezyklonen vorhergesagt werden. Das gilt vor allem für

GM und EM, zwischen deren Prognosen trotz der unterschiedlichen Modell-Orographie meist keine signifikanten Unterschiede bestehen. Das EZMW-Modell modelliert dagegen mit seiner "Envelope"-Orographie die Zyklogenese i.a. sehr prägnant. Im DM kann dieser Prozeß wegen des begrenzten Ausschnitts nur teilweise simuliert werden.

3.3 Beeinflussung von Fronten nördlich der Alpen

Fronten, die Mitteleuropa von West nach Ost überqueren, werden nördlich der Alpen einer starken Modifikation unterworfen. Durch die Südströmung vor der Front kommt es zu einem Föhneffekt, der zum einen die Bewölkungs- und Niederschlagsverteilung verändert, zum anderen aber auch durch zusätzlichen Druckfall und die Produktion warmer Luft die Dynamik der herannahenden Front beeinflußt. Kaltfronten erfahren häufig eine starke Frontogenese, die zu einer Beschleunigung der Front führt. Nicht selten bildet sich auch eine vorlaufende neue Frontlinie an der Grenze zwischen der warmen Föhnluft und der regengekühlten Luft vor der ursprünglichen Front.

Es wurde bereits im Anschluß an das Frontenexperiment der DFG nachgewiesen, daß das EM nicht in der Lage ist, derartige mesoskaligen Effekte genügend genau zu erfassen (vgl. VOLKERT et al. 1992). Im Gegensatz dazu werden sie im DM häufig gut simuliert, was prognostisch außerordentlich wertvoll ist. Abb. 1 zeigt die geglückte Vorhersage eines kleinen Leetiefs über Südbayern, das vorderseitig einer herannahenden Okklusionsfront entstand und mit föhnbedingter Erwärmung und Austrocknung in der unteren Troposphäre verbunden war. Durch diesen Effekt kommt es dann in dem betreffenden Gebiet zunächst einmal zu recht schönem Wetter, während weiter im Westen und Norden bereits Eintrübung und Niederschlag zu verzeichnen sind. Gleichzeitig bildet sich bei einer solchen Lage ein Leetief hinter dem Westalpenbogen, während östlich davon die Strömung gegen das Gebirge gerichtet ist und Stauerscheinungen produziert.

Daß bei der Simulation solcher Erscheinungen natürlich auch zeitliche Fehler auftreten können, ist naheliegend. Das ist besonders dann der Fall, wenn die Entwicklung stark von den Bedingungen außerhalb des Modellgebiets beeinflußt wird.

3.4 Konvektion und konvektive Wettersysteme

Wie alle Gebirge erleichtern die Alpen die Auslösung der sommerlichen Konvektion. Aber auch die Formierung mesoskaliger konvektiver Systeme wird durch die Alpen beeinflußt. So ist z. B. charakteristisch, daß bei Südlagen feucht-heiße und potentiell-instabile Tropikluft durch die Lücke zwischen Alpen und Pyrenäen nach Frankreich und der Schweiz geführt wird und sich dann an den Alpen entlang nach Osten ausbreitet. Wird diese Luftmasse einer Hebung unterworfen, kann es sehr rasch zur Auslösung der Instabilität und zur Bildung von Gewitter- und Böenlinien kommen. Nicht selten geht dabei auch der auslösende Hebungsmechanismus auf Orographie-Effekte zurück.

Da die Konvektion in den Modellen nicht explizit, sondern nur in grob parametrisierter From behandelt werden kann, ist ihre Erfassung einer der größten Schwachpunkte der numerischen Prognose. Dementsprechend schwankt die Genauigkeit der Vorhersage konvektiven Niederschlags in weiten Grenzen - sowohl was den Ort des Auftretens als auch die Mengen angeht.

Mesoskalige konvektive Systeme sind mit typischen Signaturen im Wind-, Druck- und Temperaturfeld verknüpft. Mit der nachträglichen Berechnung eines Falls aus dem CLEOPATRA-Feldexperiment im Juli 1992 konnte DOMS (1994) nachweisen, daß das DM

prinzipiell in der Lage ist, solche Signaturen wie das Nebeneinander von Gewittertief und -hoch, das zugehörige große Temperaturgefälle, die Böenlinie sowie die Konvergenz- und Divergenzverteilung im Windfeld zu erzeugen und zu verlagern. Dieser Befund ist verständlich, da ja das DM den Auslöseprozeß für die Entwicklung derartiger System am besten simulieren sollte. Die Erfahrungen aus der Praxis zeigen allerdings, daß das Modell durchaus nicht bei jeder konvektiven Wetterlage solche Signaturen erzeugt und wenn ja, dann häufig nicht an den Stellen, wo die Entwicklung tatsächlich erfolgt.

4. Konsequenzen für den Wettervorhersagedienst

Aus der Darstellung folgt, daß - von der Konvektion abgesehen - die DWD-Modellkette sowie das EZMW-Modell im allgemeinen zuverlässige Signale hinsichtlich der Vorhersage der verschiedenartigen Orographie-Effekte der Alpen liefern. Wichtig ist natürlich, daß der im Vorhersagedienst eingesetzte Meteorologe oder Wetterberater diese Signale erkennt und in richtige Wettervorhersagen für seinen Bereich umzusetzen versteht.

Bezüglich der wichtigen Frage, ob sich aus einem Leetrog eine Leezyklone entwickelt, sollte unabhängig von den numerischen Prognosen die aktuelle Verlagerung des Vorticitymaximums in der Höhe verfolgt und kurzfristig extrapoliert werden. Bei einer Verlagerung über das Gebirge hinweg ist unter der Vorderseite ein stärkerer zyklogenetischer Effekt zu erwarten. Aus einem numerisch prognostizierten Trog kann sich dann durchaus ein abgeschlossenes Tief entwickeln.

Hinsichtlich der mesoskaligen Effekte im Bereich von Fronten sollte unbedingt den DM-Vorhersagen der Vorzug gegeben werden. Sie enthalten oft eine Fülle von Details, die für die Lokalvorhersage von Bedeutung sind. Fehler resultieren hier hauptsächlich mit Bezug auf die zeitliche Entwicklung. Das Verhalten aller signifikanten Strukturen muß deshalb sorgfältig mit Hilfe der Beobachtungsdaten überwacht werden. Wie in KURZ (1994) demonstriert wurde, liefert dabei vor allem das Drucktendenzfeld wertvolle Hinweise.

Die größten Probleme bereitet nach wie vor das rechtzeitige Erfassen stärkerer konvektiver Umlagerungen, die gerade in den Alpen und im Alpenvorland häufig zu Unwettern mit Sturmböen, Starkniederschlägen und Hagelfall führen. Wie oben ausgeführt, können aus dem DM-Output im Einzelfall direkte Hinweise auf die Formierung konvektiver Systeme entnommen werden. Ansonsten gilt aber, daß auf diesem Gebiet die eigene synoptische Diagnose besonders wichtig ist und nicht selten einfache Betrachtungen, die die Rolle der Vertikalbewegungen bei der Auslösung der Labilität berücksichtigen, erfolgreicher sind als die direkte Modellprognose. Nach vollzogener Auslösung bilden dann die Radardaten das ädaquate Hilfsmittel für das "Nowcasting" der konvektiven Systeme.

5. Literatur

Doms, G., 1994: Numerical Simulations with the meso-β scale models of the DWD (noch unteröffentlicht)

Kurz, M., 1994: Die Kaltfront vom 10.02.1991 - Betrachtungen zur Erscheinungsform und zur Vorhersage orographisch beeinflußter Fronten, Meteorol. Z. (in Druck)

Volkert, H., Kurz, M., Majewski, D., Prenosil, T. and Tafferner, A. (1992): The Front of 8 October 1987 - Prediction of Three Mesoscale Models

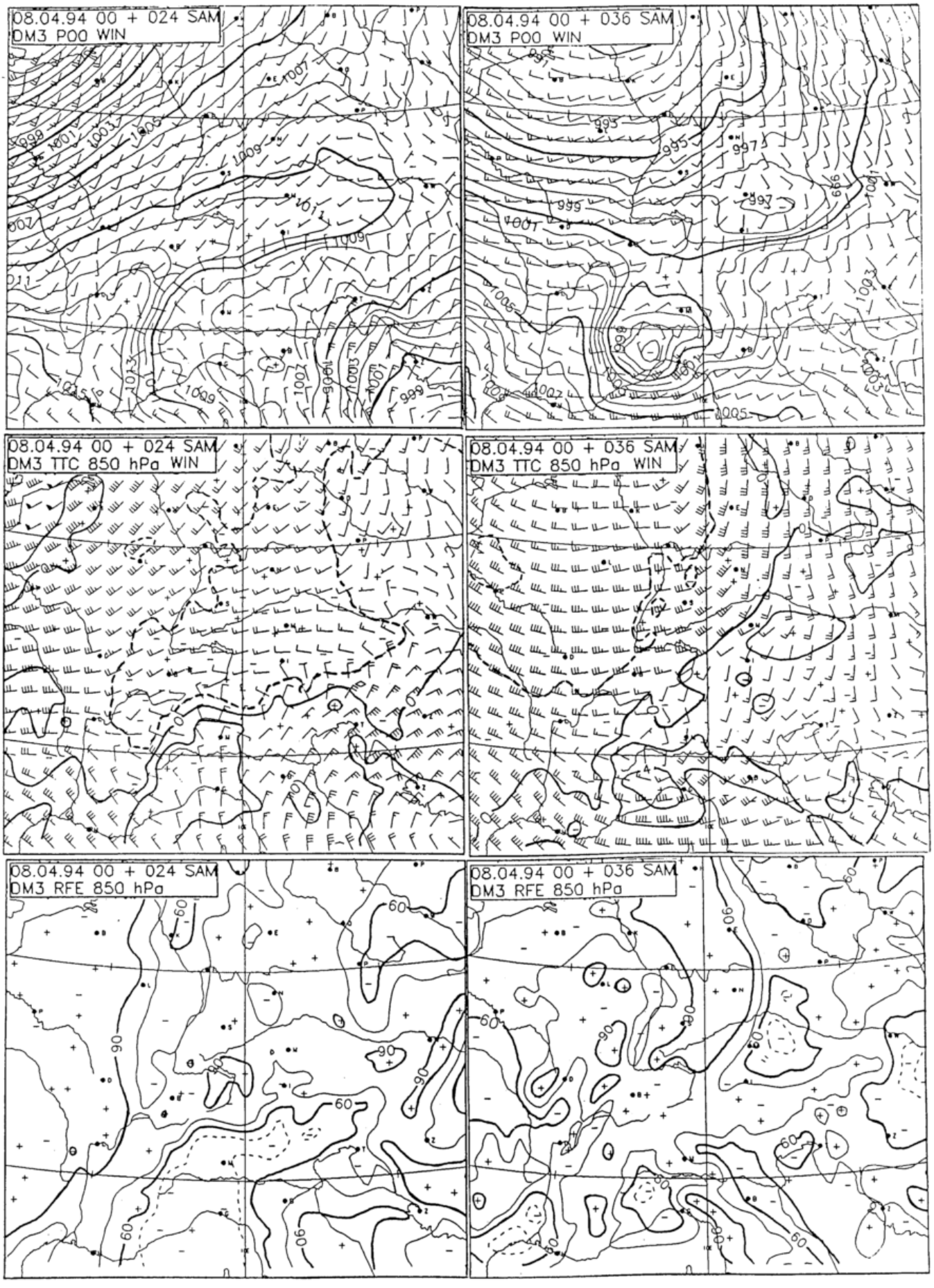

Abb. 1: Auslösung von Föhn und Entstehung von Leetiefs nördlich und südlich der Alpen in den Vorhersagen des Deutschland-Modells

Zur Problematik der Wettervorhersage für Flugwettbewerbe auf der Südseite der Alpen

J. Kerkmann und A. Cagnati

Centro Sperimentale Valanghe
e Difesa Idrogeologica
I-32020 Arabba (BL)

ABSTRACT

In the southern parts of the Alps, in the summer season, local weather prediction can be difficult due to humidity advection from the Po valley to the mountains. The massive inflow of moist air may cause the formation of extended strocumulus clouds below the inversion. The transport of the moist air is driven by the plain-mountain circulation and by the strong valley winds. In absence of other synoptic processes, the moisture and related effects may penetrate deep into the inner parts of the southern Alps.

In 1993, this phenomenon was observed several times in the Veneto Prealps. Satellite pictures show that the southern alpine regions of Lombardy and Piedmont are frequently affected by the same phenomenon. Experiences from forecasting soaring flight conditions indicate that an exact knowledge of the moisture conditions in the boundary layer is essential for a good short-range forecast. Rawinsonde informations from Milano and Udine are not sufficient, but data from automatic observing stations are needed for a correct interpretation of the situation.

ZUSAMMENFASSUNG

Der Feuchtezufluss aus der Poebene stellt im Sommerhalbjahr ein grosses Problem für die lokale Wettervorhersage in den südlichen Alpenregionen dar. Durch den massiven Zufluss feuchter Luft in den untersten Luftschichten, d.h. in Höhen bis zu 2 km, kann es unterhalb der Inversion zur Ansammlung von Feuchtigkeit und zur Bildung von ausgedehnten Stratocumulus-Feldern kommen, welche schwierig vorherzusagen sind. Die Zufuhr der feuchten Luft erfolgt dabei sowohl über die grossräumige Ebene-Gebirgswind Zirkulation, als auch über die meist kräftig ausgeprägten Tal-Bergwind Zirkulationen. Von Tag zu Tag, in Abwesenheit von anderen synoptischen Prozessen, kann diese Erscheinung tiefer in die inneren Bereiche der südlichen Alpen vordringen.

Im Jahr 1993 konnte dieses Phänomen mehrfach in den Voralpen der Region Veneto beobachtet werden. Von Satellitenbildern ist bekannt, dass auch die an die Poebene angrenzenden Gebirgsregionen der Lombardei und des Piemont häufig davon betroffen sind. Die bei der meteorologischen Betreuung von Flugwettbewerben gemachten Erfahrungen machen deutlich, dass eine richtige Einschätzung der Feuchteverhältnisse in der Grenzschicht entscheidend für eine richtige Kurzfristvorhersage ist. Die Radiosondenstationen reichen dafür nicht aus. Die Daten automatischer Wetterstationen stellen hingegen ein wichtiges Hilfsmittel bei der Beurteilung der Wetterlage dar.

EINLEITUNG

In den Jahren 1993-94 übernahm das Centro Sperimentale Valanghe die meteorologische Betreuung des internationalen Fliegerwettbewerbs Guarnieri-Trophy, das alljährlich im Piavetal zwischen Feltre und Belluno, in den südlichen Dolomiten, stattfindet. In Anbetracht der ausgezeichneten Bedingungen, ist dieser Wettbewerb in den vergangenen

Jahren mehrfach Schauplatz nationaler und internationaler Rekorde gewesen. Mit etwa 200 Teilnehmern gehört die Trophy zu einem der grössten Wettbewerbe für Drachen- und Gleitschirmflieger im gesamten Alpenraum.

In der Regel findet die Guarnieri-Trophy im April statt, doch 1993 war als Termin der 18-20. Juni ausgesucht worden, eine Entscheidung die, wie sich später herausstellte, nicht glücklich gewählt worden war. An zwei der drei Flugtage bildeten sich am Nachmittag, trotz antizyklonaler Bedingungen, ausgedehnte Stratocumulus-Felder unterhalb der Inversion, die die thermische Aktivität erheblich beeinschränkten. Ausserdem kam es nicht zur gewohnten tageszeitlichen Anhebung der Wolkenbasis. Stattdessen blieb die Basis den ganzen Tag über bei 1600 m, zu tief um Streckenflüge in der Region zu ermöglichen.

WETTERLAGE

Die rasche Passage einer nicht besonders aktiven Kaltfront am Vortag des Wettbewerbs hatte den Dolomiten Schauerniederschläge und eine leichte Abkühlung gebracht. Bereits am Abend hatte sich das Wetter wieder beruhigt und in der Nacht war es heiter. Die Bodenkarte vom 18. Juni zeigt die Kaltfront über der Balkanhalbinsel, während sich ein ausgeprägter Hochkeil vom Atlantik bis zu den Ostalpen erstreckt. In der Höhe dominiert im gesamten Ostalpenraum eine mässige Nordwestströmung mit 20-30 kn in 700 hPa, 40-50 kn in 500 hPa.

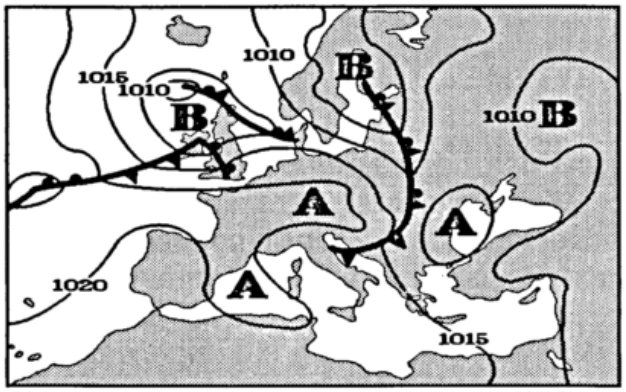

Abb.1: Bodenanalyse vom 18.06.93, 00 UTC

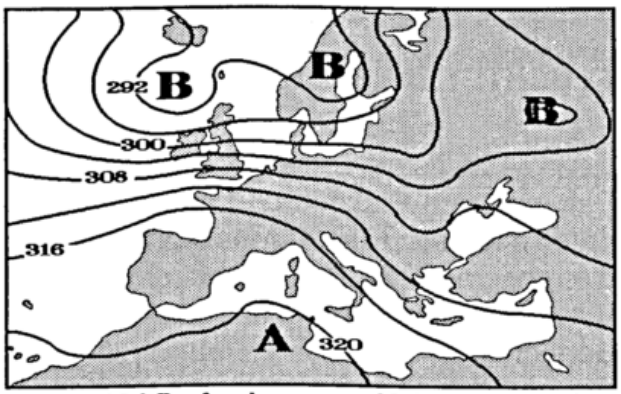

Abb.2: 700 hPa Analyse vom 18.06.93, 12 UTC

Die Radiosondenaufstiege von Mailand und Udine zeigen eine relativ hoch liegende Inversion in etwa 3500 m Höhe und eine nordwestliche Höhenströmung, die in Udine kräftiger ausgeprägt ist als in Mailand. Mit 5 bis 6°C Taupunktdifferenz ist die Luft unterhalb der Inversion recht feucht. Im Laufe des Tages verstärkte sich die Inversion und sank auf 2500 m ab.

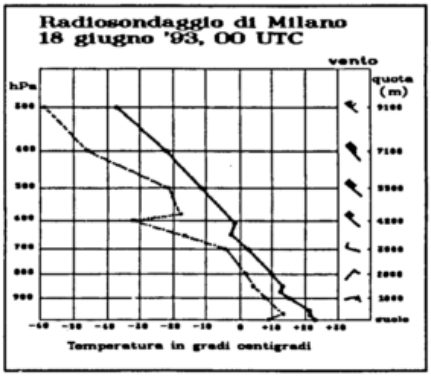

Abb.3: Temp von Mailand vom 18.06.93, 00 UTC

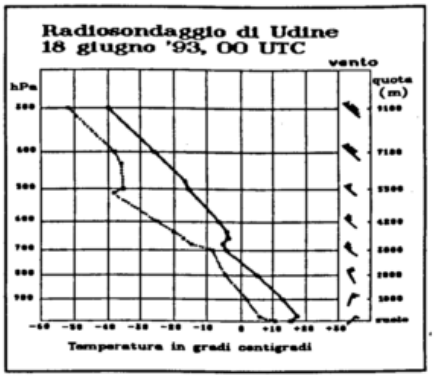

Abb.4: Temp von Udine vom 18.06.93, 00 UTC

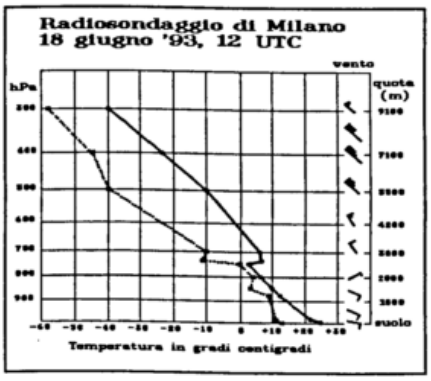

Abb.5: Temp von Mailand vom 18.06.93, 12 UTC

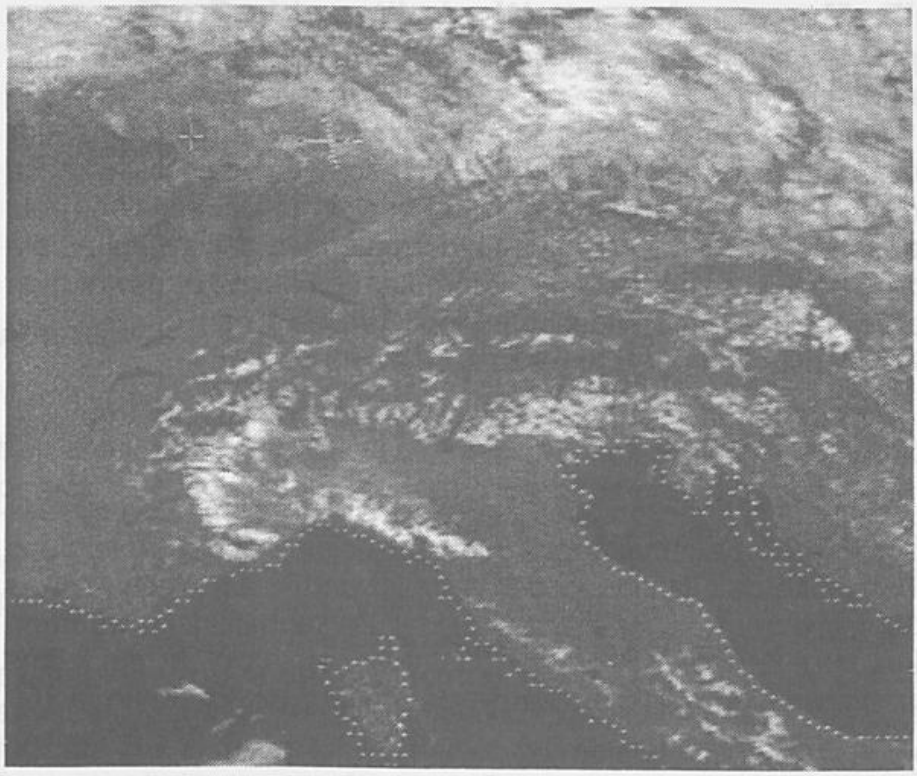

Abb.6: METEOSAT5 vom 18.06.93, 11.30 UTC

Auf dem Satellitenbild von 11.30 UTC lässt sich gut die starke konvektive Bewölkung erkennen, welche sich über weite Bereiche der Voralpen erstreckt. Der innere Bereich der Alpen ist hingegen weitgehend wolkenlos.

FEUCHTETRANSPORT ÜBER REGIONALE WINDSYTEME

Abb.7 zeigt einen Ausschnitt der Dolomiten mit den beiden Haupttälern der Provinz Belluno, dem Piavetal und dem Cordevoletal, wobei die Isohypse 1500 m die Grenzen der Täler markiert. Für 20 Messstationen sind die Windvektoren um 12 Uhr eingetragen. Über die grossräumige Ebene-Gebirgswind Zirkulation strömt feuchte Luft aus der Poebene in das Piavetal bei Belluno. Von dort gelangt die feuchte Luft über die Talwinde in die inneren Bereiche der Dolomiten. Deutlich ist zu erkennen, dass auf den Bergen eine nordwestliche Strömung vorherrscht, während der Talwind exakt der Talrichtung folgt. Im oberen Cordevoletal dominiert jedoch noch der synoptische Nordwestwind.

mittl. Feuchte	17.	18.	19.	20.	**Niederschlag**	17.	18.	19.	20.
Foen	89	78	77	73		3.6	0.0	0.0	2.4
Agordo	88	75	77	87		1.6	0.0	0.0	21.4
Caprile	80	69	74	80		2.2	0.0	0.0	10.4
Arabba	83	62	72	81		4.0	0.0	0.0	13.6
Mitteltemp.	17.	18.	19.	20.	**Max. Temp.**	17.	18.	19.	20.
Foen	18.5	17.0	18.8	19.9		23.2	24.1	26.9	27.9
Agordo	16.4	15.2	17.5	18.4		22.4	22.7	25.1	26.7
Caprile	13.5	13.5	16.1	16.2		19.3	23.8	25.7	24.8
Arabba	9.7	11.1	13.9	12.6		14.3	19.1	20.3	18.7

Tab.1: Tagesmittelwerte der relativen Feuchte und der Lufttemperatur, Niederschlag und maximal Temperatur der Stationen Foen (391 m), Agordo (578 m), Caprile (1030 m) und Arabba (1630 m) für die Tage vom 17. bis zum 20. Juni 1993

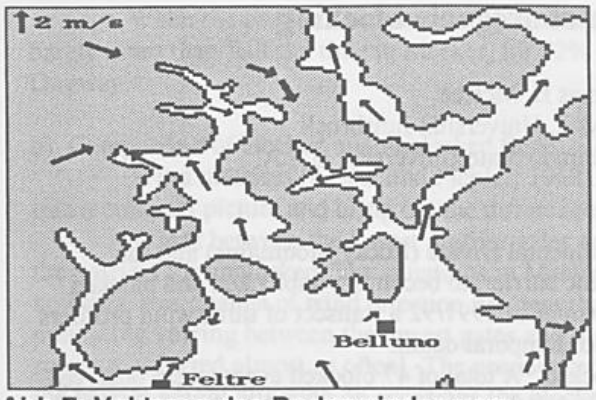

Abb.7: Vektoren des Bodenwindes vom 18.06.93, 12 Uhr (10 min. Mittelwerte)

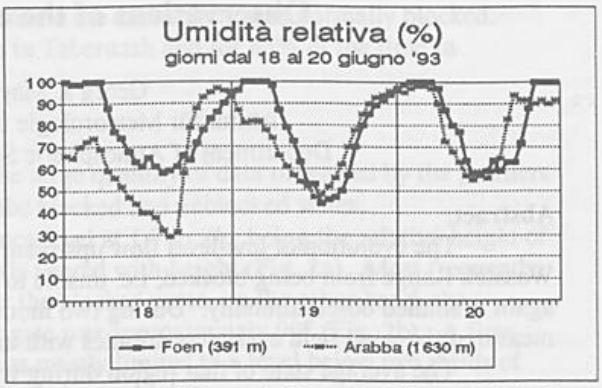

Abb.8: Verlauf der relativen Luftfeuchtigkeit vom 18-20.06.93 in Foen (Feltre) und Arabba

Die Feuchteverhältnisse in den Tälern (siehe Tab.1) weisen am 18. Juni einen deutlichen Nord-Süd Kontrast auf: trocken-warme Luft im oberen Teil der Täler (Arabba), gute Fernsicht und hohe Wolkenbasis (ca. 3000 m), Effekte der nordwestlichen Föhnströmung; hingegen feucht-kühle Luft, geringe Sicht und niedrige Wolkenbasis (ca.1600 m) im Piavetal bei Foen (Feltre). Die Berg-Talwind Zirkulation ist aufgrund der grossen Temperaturunterschiede gut ausgeprägt. Durch den advektiven Feuchtetransport über die lokalen Winde gleichen sich die Feuchteunterschiede in den folgenden Tagen aus, und die Stratocumulus-Bewölkung dringt bis weit in die Täler vor.

SCHLUSSBEMERKUNGEN

Im Sommerhalbjahr kommt es durch den Feuchtezufluss aus der Poebene in den südlichen Alpenregionen häufig zur Bildung von ausgedehnten Stratocumulus Feldern. Dieses Phänomen tritt besonders häufig in den Tagen nach Kaltfrontpassage bei nordwestlicher Höhenströmung auf, wenn die Inversion noch relativ hoch liegt und die Berg-Talwind Zirkulation aufgrund des thermischen Kontrastes (föhnig warm in den inneren Dolomiten, feucht kühl im Piavetal) besonders kräftig ausgeprägt ist. So kann es trotz scheinbar guter synoptischer Verhältnisse (nach Kaltfrontpassage, antizyklonale Strömung) zu schlechten Flugbedingungen kommen. Die Wolkendecke ist oft recht persistent; sie löst sich meist erst dann auf, wenn die Inversion absinkt oder wenn eine kräftige Strömung advektiv trockenere Luft heranbringt.

Observations of the evolution of orogenic blocking

Georg J. Mayr and Thomas B. McKee
Institut für Meteorologie und Geophysik, Universität Innsbruck
Department of Atmospheric Science, Colorado State University, U.S.A.

Abstract:

The evolution of low-level flow upstream of the Continental Divide (Rocky Mountains) and the Wasatch Range from being blocked, i.e. unable to surmount the barrier, to becoming unblocked and blocked again is studied observationally. During two months in the winter of 1991/92 a transect of three wind profilers measured the wind field every few minutes with unprecedented temporal detail.

The average state of that region during winter is blocked. A total of 47 blocked events were observed. A blocked flow event lasted on the average one and a half days but the duration varied widely from a few hours to eight days. The transition between the two states happened rapidly on the order of an hour with a minimum of 20 minutes and a maximum of four hours. The depth of the blocked layer even during one blocking episode fluctuated considerably but reached on the average half to two thirds of the barrier depth (depending on the location).

Two mechanisms seemed to force the atmosphere out of a blocked state: an approaching short wave counteracting the mesoscale high formed on the upwind side by blocking, and the growth of a well-mixed and deep boundary layer reconnecting the blocked layer with the higher cross-barrier winds above the mountain.

1. Introduction

Will air that encounters an obstacle in its path go around, become stagnant or flow over it? This question has been studied theoretically, numerically and observationally in many locations of the world for several decades. Generally, however, these investigations have only dealt with the causes for blocking (i.e. the inability of low-level air to flow over the obstacle) and not attempted to explore the evolution of blocking. How long does it take the atmosphere to switch between a blocked and unblocked state? How long and frequent are blocked periods and what mechanisms underlie blocking and unblocking in the atmosphere? To answer these questions three wind profilers were deployed in a transect along the western slope of the Rocky Mountains (Fig. 1) for two months during the winter of 1991/92 (Mayr and McKee, 1994). They measured the wind field above the lowest few hundred meters every 2-11 minutes.

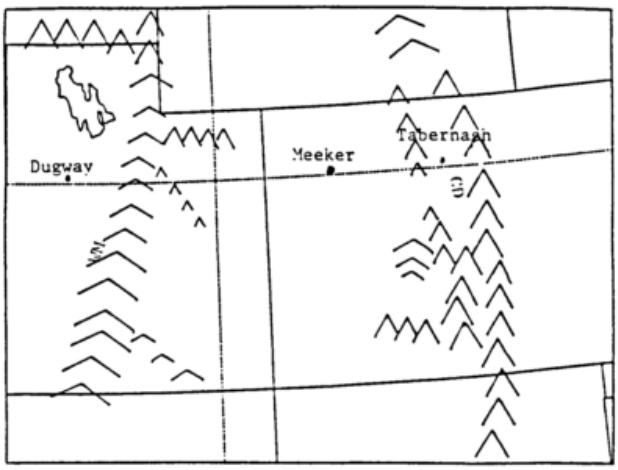

Fig. 1: Location of the 3 wind profiler sites in Colorado and Utah. State boundaries are solid lines. Wedges indicate the main mountain ranges. The Wasatch Mountains are marked WM, the Continental Divide CO.

2. Observational results

a) Statistics

From the profiler measurements 23 blocking periods were identified in Tabernash, 14 in Meeker and 12 in Dugway. The average blocking period lasted one and a half days but varied from 3 to 187 hours (nearly eight days) so that the standard deviation is large.

The depth of the blocked layer fluctuated greatly during the observational period. A steady state was never achieved; even during one blocking event the depth of the blocked layer did not remain constant. Most frequently, however, the blocked layer reached at all three sites to at least half the barrier height but rarely up to mountain top.

When the profilers were on the upwind side of the obstacle the atmosphere was normally blocked: barely more than half the time in Meeker, for 72% of the time in Tabernash and for 85% of the time in Dugway.

b) Comparison of blocked and unblocked flows

Wind matrices (Cehak and Pichler, 1968) combine the large quantity of data measured by the profilers into a compact picture and bring out the differences between the blocked and unblocked states.

Winds between the lowest profiler gates and a reference level at 1.7 h_b (h_b being the relative height of the barrier) for unblocked flow situations in Meeker dominantly veered with height (Fig. 2a). Most frequently, however, this change of wind direction was less than 40°. For the blocked cases, on the other hand, the prevailing veering between the lowest gates and the reference gate was approximately 90° (Fig. 2b). A flow reversal occurred almost as often! The pronounced turning was mostly limited to a level below two thirds of the barrier height although on occasions the blocked layer extended even higher.

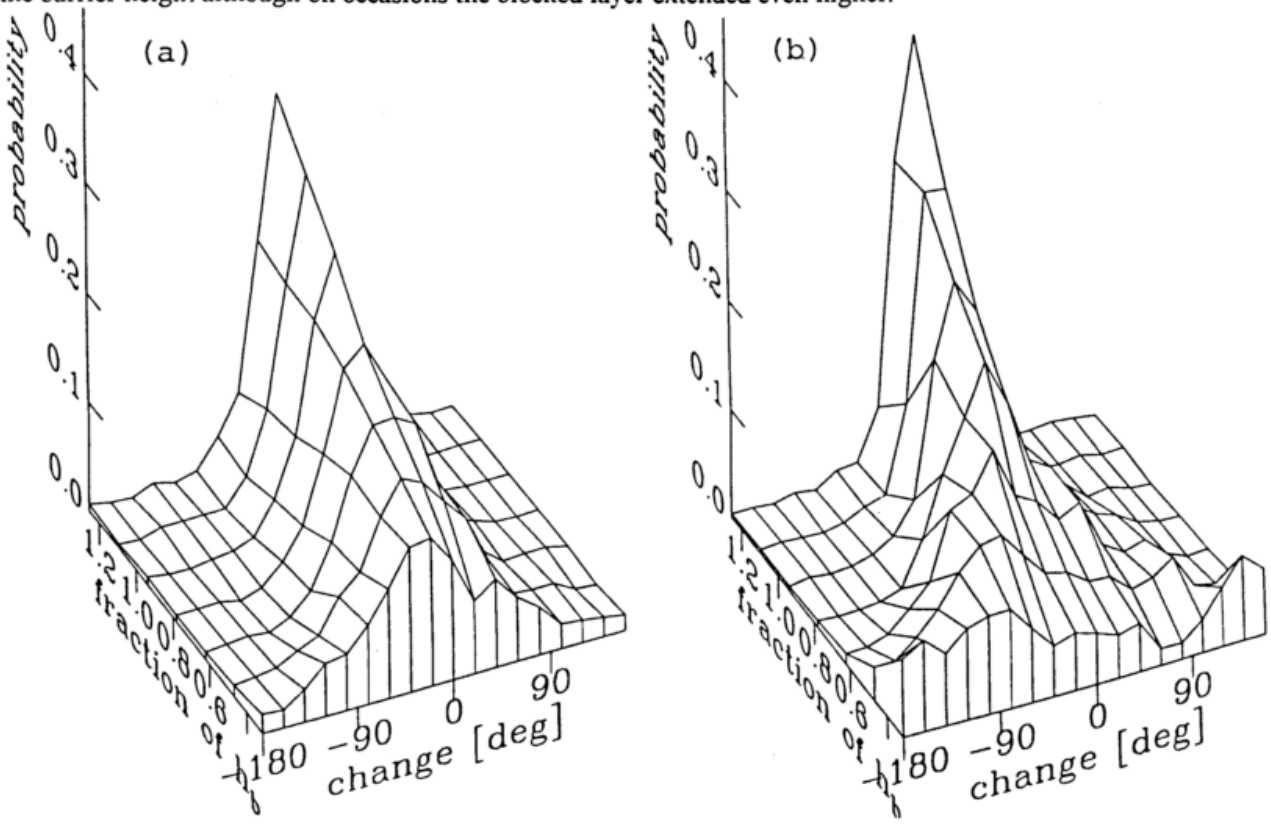

Fig. 2: Joint probability mass function of turning of wind (in degrees) between 1.7 h_b (4739 m MSL) and below for Meeker (1989 m MSL): (a) unblocked, (b) blocked. A negative change means that the wind veers with height.

3. Conceptual model of the blocking evolution

During the measuring period the cross-barrier component of the wind above the Rocky Mountains in Colorado and Utah was on average small enough and the stability strong enough to put the atmosphere into the blocked part of the parameter space (Froude number approximately 0.2). Denser air that piled up just upstream of the crest caused a mesoscale high on the upwind side, which deflected the low-level air northwards around the mountain. Two different ways were observed how the atmosphere got out of the blocked state.

In 12 out of the 18 unblocking events at the Continental Divide a short wave that approached the barrier from the west or northwest overwhelmed the orographically induced pressure maximum. The higher pressure farther upstream in the following ridge then flushed the blocked air over the barrier. The winds picked up in the lower levels to a cross-barrier speed comparable to the one above the mountains. Vertical mixing decreased the stability of the previously blocked air. All five unblocking events that the profiler in Dugway observed upstream of the Uinta Mountains followed the same pattern.

The remaining one third of the unblocking cases upstream of the Continental Divide were caused by the growth of a mixed boundary layer to almost barrier height. Most of the cases could only be observed in Tabernash where the relative barrier height is relatively low (1 km compared with 1.6 km for Meeker) and the area forested so that despite snow on the ground enough sensible heat flux was available. Towards the end of February only patches of snow remained and together with the increased solar insolation one such unblocking event occurred even in Meeker. After sunset, however, the atmosphere flipped back into its blocked state.

4. Example

The wind field measured by the profiler in Tabernash during the period January 24 - 25, 1992 may serve as an example of unblocking by a short wave, which moved in from the northwest. At 1205 LST the lowest 500 m were blocked but coinciding with the trough passage the flow unblocked within half an hour. The strong northwesterly winds mixed down to the surface and only with the passage of a short ridge could a blocked layer form again at 02 LST, January 25, which grew rapidly and reached to almost barrier height. Again, the transition took only half an hour!

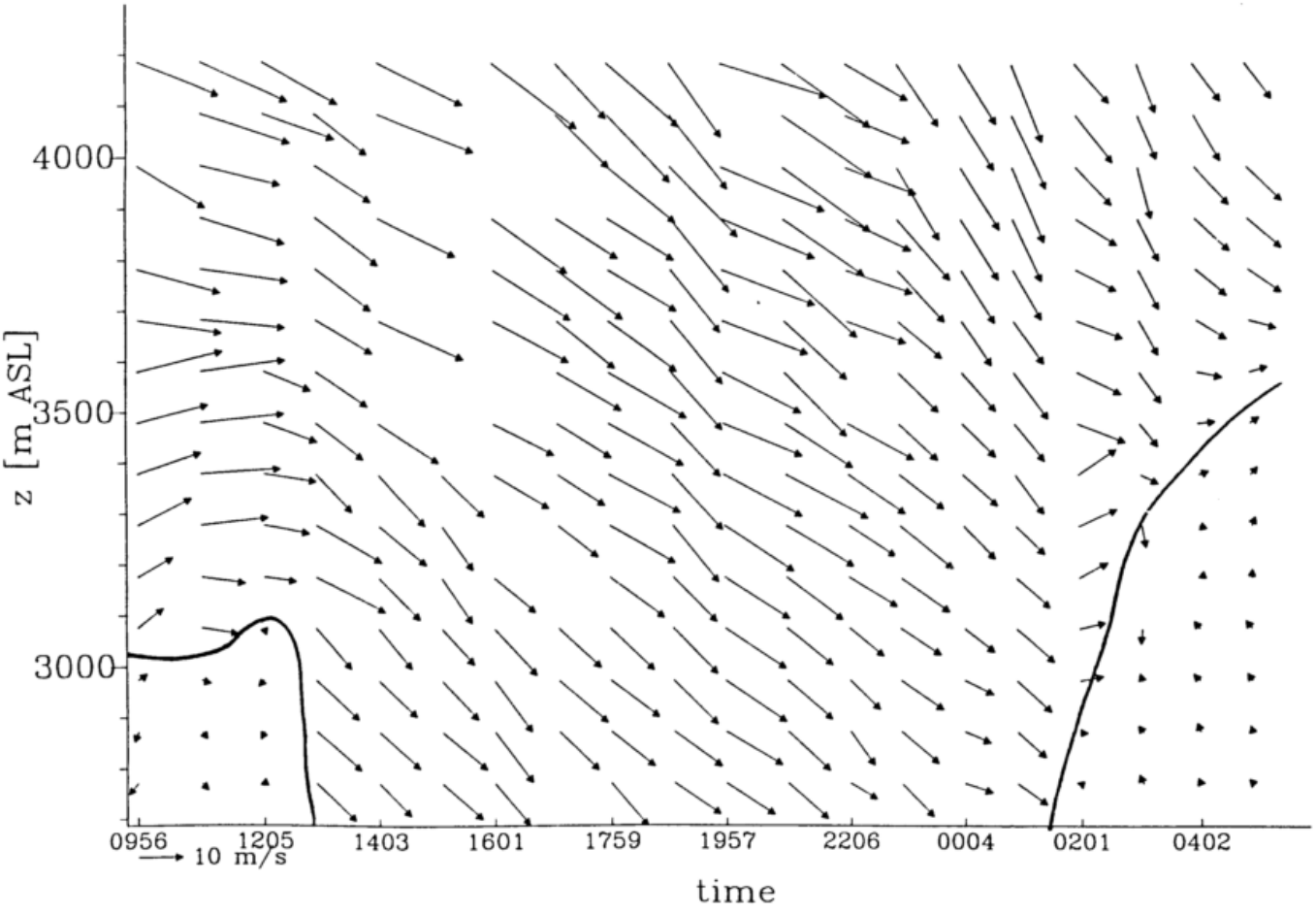

Fig. 3: Time-height cross-section of horizontal wind vectors averaged over approximately 20 minutes from the profiler in Tabernash, 0956 LST 24 January through 0420 LST 25 January 1992. A bold line marks the top of the blocked layer and a reference wind vector showing westerly wind of 10 m s^{-1} is plotted in the lower left corner.

References:

Cehak, K., and H. Pichler, 1968: Beschreibung des Stromfeldes im Alpenbereich mittels Windmatrizen. *Arch. Met. Geoph. Biokl.*, **17A**, 61-77.

Mayr, G., and T.B. McKee, 1994: Observations of the evolution of orogenic blocking. *Mon. Wea. Rev.* (accepted for publication)

The wind environment of supercell storms in Switzerland

W. Schmid and H. Huntrieser
Atmospheric Science, ETH, CH-8093 Zürich
Switzerland

ABSTRACT

The wind environment of six severe hailstorms is investigated that have significant vortex signatures. The wind profiles from the operational Payerne sounding are compared with wind profiles obtained in the vicinity of the storms with a Doppler weather radar and with ground measurements of wind. The low-level wind shear and helicity increase near the storms, compared to the values predicted by the operational sounding. Helicity is on the order of 200 m^2s^{-2} which means that the "streamwise vorticity" hypothesis is a reasonable explanation for the observed vortex signatures. We conclude that a better knowledge of the local variations of the low-level wind field is fundamental for a better understanding and prediction of supercell storms in an orographically complex region.

1. Introduction

Rotating updrafts are the primary characteristics of supercell storms. Such storms are responsible for severe damages due to hail and wind, but they also affect the evolution of mesoscale convective systems in a manner that is not necessarily predictable with numerical models. The most severe hailstorms that occur in Switzerland have significant features of supercell storms (e.g. Schmid et al. 1993). Here, we intend to present an analysis of the wind field in the environment of the storms. The main purpose of this analysis is to get insight into the most probable mechanisms that lead to the development of rotation in the observed storms.

Several conceptual models exist that try to explain the development of rotating updrafts. The most widely accepted hypothesis assumes that updraft rotation is generated by stretching and tilting of horizontally oriented vorticity associated with the environmental shear (e.g. Rotunno and Klemp 1985). An alternative explanation is given by Fujita and Grandoso (1968) and more recently by Brown (1992): a growing updraft acquires rotation by entraining and stretching ambient vertical vorticity that is formed on the downwind flank of an already existing non-rotating updraft through "obstacle-flow" processes. A third mechanism, also proposed by Rotunno and Klemp (1985), is the baroclinic generation of horizontally oriented vorticity along the low-level cold-air boundary. This latter mechanism is thought to be the source of low-level rotation whereas the former two mechanisms are thought to be the source of mid-level rotation.

Based on these mechanisms, one can define three potentially important predictors of updraft rotation: the environmental wind shear (preferably at low altitudes, typically 0-3 km AGL), the storm-relative environmental flow (typically at midlevels, 3-8 km MSL), and the existence of gust-front boundaries in the environment of the developing updrafts. These are highly variable parameters, especially in a complex orography. The presently available measuring networks (mainly radiosoundings and ground networks) are not able to capture these parameters with sufficient spatial resolution. This means that the experimental verification of the mentioned mechanisms is difficult. An experiment (called VORTEX) dealing with the question on the origin of rotating updrafts is presently carried out in Oklahoma.

Here, we intend to investigate the low-level wind shear in the vicinity of the observed storms by considering Doppler radar measurements of wind. The main question to be answered is the following: is the observed wind shear able to explain the development of updraft rotation through the first mentioned mechanism? For this, we will apply concepts that have been developed on the basis of observed U.S. supercell storms and of three-dimensional numerical model simulations. Thus: the main purpose of this study is not to give a statement on the relative importance of the three mechanisms, but to investigate if one of the three mechanisms (the most probable one) is a reasonable candidate for explaining the observed vortex signatures.

2. Methodology

a. Measurement of wind shear

The radiosounding in Payerne, operated by the Swiss Meteorological Institute (SMI hereafter), measures the profile of horizontal wind twice per day (00 and 12 UTC). The representativity of this sounding for Switzerland north of

the Alps is often questionable. We therefore take into account wind measurements of the Doppler weather radar located at ETH in Zurich (Schmid et al. 1990), and wind data from the ANETZ, a mesonetwork of 67 automated ground stations, also operated by the SMI. The Doppler radar measures the radial component of wind when radar echoes from precipitation or from insects appear. The VVP-technique (Siggia 1991) can be used to deduce the wind profile at the location of the radar. Such profiles are available in 10 min time resolution for four storms that passed the radar site when they were fully developed. For two additional storms, we consider the wind measurements of three ANETZ stations (two flatland stations and one mountain station) in the close vicinity of the storms for a correction of the wind profile at low altitudes.

b. Helicity

An important predictor of updraft rotation (and of tornadoes) is helicity (Lilly 1986), a parameter that is proportional to streamwise vorticity and the storm-relative winds:

$$H(c) = \int_0^h (v - c) \cdot \omega \, dz \qquad (1)$$

Here, v is the environmental wind vector, c is the storm's translation velocity and ω is the horizontal vorticity. Davies-Jones et al. (1990) showed that helicity is given by the area swept by the storm-relative wind vector between two boundaries in altitude, multiplied with minus two. Davies-Jones et al. (1990) suggested to calculate helicity in between 0 and 3 km AGL, since this is the layer of the storm-relative inflow of warm moist air.

c. Procedure

In the following, we will describe the low-level wind characteristics in the environment of six severe hailstorms that showed significant rotation in the Doppler radar measurements. The wind hodographs of the Payerne sounding (unmodified and modified) will be presented. The modified wind hodograph is based on wind measurements (Doppler radar and ground stations) in the vicinity of the developing storms. Helicity will be computed, and the resulting values will be compared to U.S. supercell environments. All this allows us to judge the importance of the "horizontal vorticity" hypothesis in the development of the observed updraft rotation.

3. Results

Fig. 1 shows the origin and the paths of the storms considered in this study. All six storms developed in the vicinity of rough orography, either in the south of the "Jura" mountains (storms 2 and 6) or along the northern boundary of the Alps (storms 1,3-5). Solid lines represent periods during which significant vortex signatures suggest substantial rotation within the storms. Storms 1-4 passed close to the radar when fully developed which means that the wind profiles measured with the radar ahead of the storms should represent fairly well the wind environment of the storms. Storms 5 and 6 passed in a larger distance from the radar. We decided to take into account the wind measurements from ANETZ stations Wynau and Napf (storm 5) and Luzern and Napf (storm 6) for correction of the wind profile at low altitudes.

Table 1 shows the helicity computed from the wind hodographs and the observed storm motion. One can see that helicity is above 100 m^2s^{-2} in the majority of the cases. On average, the obtained values are well within the range that is typical for U.S. tornadic supercell storms (helicity = 100 - 700 m^2s^{-2}, see e.g. Fig. 8 of Johns et al. 1993). Considerable changes of helicity are found when the modified wind profile is taken into account. In the following, we summarize the observed wind profiles and how they changed for each individual case:

21 July 1992: The marked increase of helicity (compared to the Payerne sounding) is due to an overall increase of wind shear and a turning of the wind shear vector from NE to NW at low levels, see Fig. 2a.
5 July 1993: Helicity decreased a bit (compared to the Payerne sounding), mainly due to a slight change of wind direction at 3 km MSL.
May 17 1994: The increase of helicity can be explained with more easterly winds at low altitudes compared to the Payerne sounding.
June 2 1994: The observed increase of helicity is due to a very similar change of the low-level wind profile as already observed on 21 July 1992.
The increase of the absolute values of helicity in the remaining two cases is due to an increase of wind shear at low levels (see Fig. 2b). Note that the modified values of helicity are uncertain for these cases since it is unknown on how the wind changed at 3 km altitude compared to the Payerne sounding.

Table 1: Storm motion, CAPE (convective available potential energy, computed from the unmodified Payerne sounding) and helicity, computed from the wind hodograph of the unmodified and modified Payerne sounding.

Storm number	Date	storm motion (Deg/ms^{-1})	CAPE m^{2}s^{-2}	Helicity (m^{2}s^{-2}) unmodified	modified	Data source
1	21 July 1992	217/14.4	1162	24	261	ETH-radar
2	5 July 1993	268/16.8	1626	231	140	ETH-radar
3	17 May 1994	230/28.4	405	186	343	ETH-radar
4	2 June 1994	239/25.8	1140	203	250	ETH-radar
5	20 Aug 1992	207/9.1	1528	-40	-62	ANETZ
6	21 Aug 1992	262/13.6	212	122	206	ANETZ
	Average (of abs. values)			134	210	

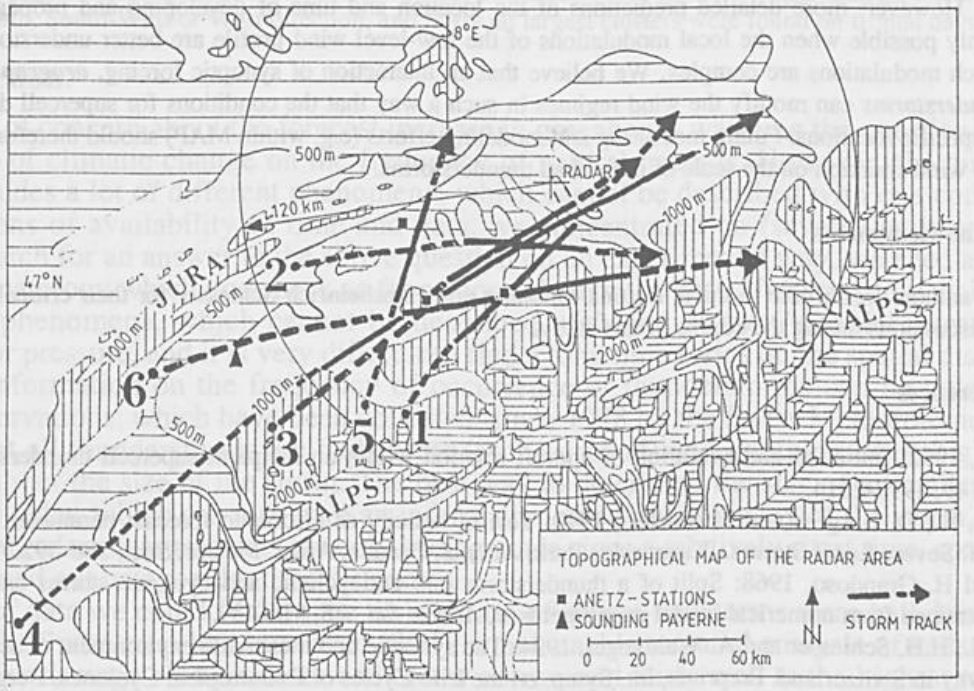

Fig. 1: The orography of Switzerland and the path of the hailstorms considered here. The solid lines indicate vortex features observed with the ETH-Doppler radar. The dots indicate the ANETZ stations Wynau, Napf and Luzern (from left to right)

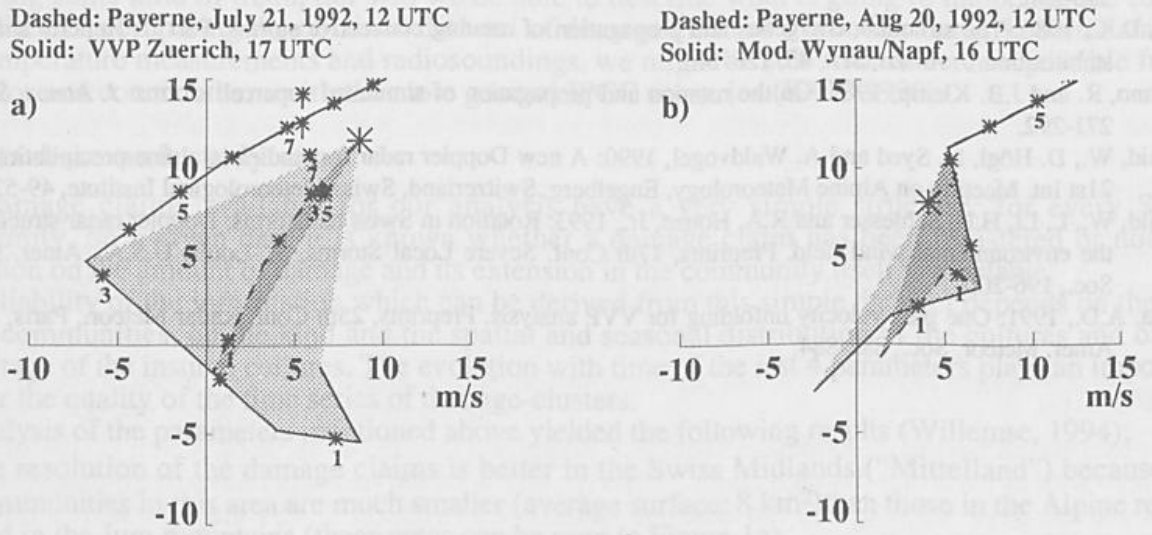

Fig. 2: The unmodified and modified wind hodographs from 21 July 1992 (a) and 20 Aug 1992 (b). The shaded areas are proportional to helicity (for details see text). The stars and the associated numbers indicate the height in km MSL. The big stars indicate storm motion.

4. Conclusions

In general, one finds substantial wind shear and helicity in the vicinity of Swiss supercell storms. This finding supports the hypothesis that the tilting and stretching of streamwise vorticity is the main source of updraft rotation. One exception is the left-moving storm from 20 Aug 1992 for which the wind shear and helicity was relatively small. The large CAPE (convective available potential energy, see Table 1) may partly compensate the low helicity in the development of updraft rotation. It's, however, also possible that the wind changed at 3 km MSL and led to a higher helicity than predicted from the ANETZ measurements alone. We intend to check this possibility with the help of the available Doppler radar data.

The Payerne sounding alone can predict to some degree the low-level wind shear that is apparently necessary for the development of supercell storms. In this sense, one can use the wind shear computed from the Payerne sounding as an additional predictor of severe storms. Recent investigations by Huntrieser et al. 1994 confirm that the overall predictive skill of the Payerne sounding for severe thunderstorms is improved when the measured wind shear is taken into account. However: more detailed predictions of the location and time of developing and propagating supercell storms are only possible when the local modulations of the low-level wind profile are better understood. The factors leading to such modulations are complex. We believe that an interaction of synoptic forcing, ***orography and already existing thunderstorms*** can modify the wind regimes in such a way that the conditions for supercell development are favorable at specific locations. Future measuring and modeling efforts (e.g. within MAP) should therefore try to capture the pre-storm wind situation on the scale of individual thunderstorms.

Acknowledgments

The authors would like to thank Bettina Messmer and Hansheinrich Schiesser for their critical comments and stimulating discussions during the course of this study.

References

Brown, R.A., 1992: Initiation and evolution of updraft rotation within an incipient supercell thunderstorm. *J. Atmos. Sci.*, **49**, 1997-2014.

Davies-Jones, R., D. Burgess and M. Foster., 1990: Test of helicity as a tornado forecast parameter. Preprints, 16th Conf. Severe Local Storms., Kananaskis Park, Atlanta, Canada, Amer. Meteor. Soc., 588-592.

Fujita, T. and H. Grandoso, 1968: Split of a thunderstorm into anticyclonic and cyclonic storms and their motions determined from numerical model experiments. *J. Atmos. Sci.*, **25**, 416-439.

Huntrieser, H., H.H. Schiesser and A. Waldvogel, 1994: The synoptic and mesoscale environment of severe convective activity in Switzerland. Preprints, Int. Symp. on the Life Cycles of Extratropical Cyclones, Bergen, Norway.

Johns, R.H., J.M. Davies and P.W. Leftwich, 1993: Some wind and instability parameters associated with strong and violent tornadoes, 2, Variations in the combinations of wind and instability parameters. The Tornado: Its Structure, Dynamics, Prediction, and Hazards. *Geophysical Monograph*, **79**, American Geophysical Union, 583-590.

Lilly, D.K., 1986: The structure, energetics and propagation of rotating convective storms. Part II: Helicity and storm stabilisation. *J. Atmos. Sci.*, **43**, 126-140.

Rotunno, R. and J.B. Klemp, 1985: On the rotation and propagation of simulated supercell storms. *J. Atmos. Sci.*, **42**, 271-292.

Schmid, W., D. Högl, N. Syed and A. Waldvogel, 1990: A new Doppler radar for studies in alpine precipitation. Proc. 21st Int. Meeting on Alpine Meteorology, Engelberg, Switzerland, Swiss Meteorological Institute, 49-52.

Schmid, W., L. Li, H.H. Schiesser and R.A. Houze, Jr., 1993: Rotation in Swiss hailstorms: Doppler radar structure and the environmental wind field. Preprints, 17th Conf. Severe Local Storms, St. Louis, U.S.A., Amer. Meteor. Soc., 196-200.

Siggia, A.D., 1991: One pass velocity unfolding for VVP analysis. Preprints, 25th Conf. Radar Meteor., Paris, France, Amer. Meteor. Soc., 882-884.

45 years of hailstorms north of the Alps.

S. Willemse and H.H. Schiesser
Atmospheric Physics, ETH, 8093 Zürich, Switzerland

Abstract

The aim of the project to be presented here is to put together a data base of hailstorm events which goes back as far as possible into the past and which will be extended into the future by a yearly monitoring of these events. For this purpose the Swiss crop-hail insurance has supplied a useful dataset of hail claims which have been collected since 1949 for the whole of Switzerland. For the years between 1983 and today hail-damage distributions have been compared with radar data of the Swiss Meteorological Institute (SMI), which are available almost without interruption since that year. The method of comparison consists mainly of a cartographic representation of the damage claims, which can be directly compared with the thunderstorm cells measured by the radar. For the period between 1949 and 1993, data on 651 hail clusters with a length of at least 25 km were collected with this method. All clusters longer than 50 km are found to be oriented in a South, South-West or West direction, and fairly all largest clusters were found on frontal days.

1. Introduction.

In these days of concern about the forecast increase in greenhouse warming the question arises as to the influence of climatic change on the frequency of natural hazards. However, the term "natural hazards" includes a lot of different phenomena, which cannot be described with one common data-set. For reasons of availability of time and data, we concentrated on (severe) hailstorms. As we decided to search for an answer to the above question on an experimental way, we need a reasonable hailstorm climatology which goes back as far as possible into the past. Unfortunately, hailstorms are complicated phenomena, which cannot be described with one or two "simple" parameters like temperature or pressure, and it is very difficult to find a long time series on the spatial distribution of hailstorms. Information on the frequency of occurrence of thunderstorms can be taken from the lightning observations, which have been collected since 1978 by the Swiss Meteorological Institute (SMI), but not all thunderstorms are hailstorms (at the ground) and lightning doesn't give a direct information about the size of the storm. The best way to determine the size of a thunderstorm is to measure it by radar, which can also give an information about the intensity of the storm. Unluckily, meteorological radar-measurements are only beeing made since a relatively short time, specially those which are carried out on a regular time distance.
The best set of data we could find on the distribution of severe hailstorms were hail damage claims collected by the Swiss crop-hail insurance (SHI), which enable a spatial analysis of hailstorm events since 1949. The damage clusters described below correspond fairly well to the highest reflectivities of the SMI-radar measurements (Schiesser and Willemse, 1992)
Climatologically, a time series of 45 years of hailstorms is quite short, independently of its quality. For this reason we won't be able to find out if the frequency and the size of thunderstorms have been following some kind of trend, nor will we be able to describe what is going to happen in the future. Nevertheless, comparing the obtained data-set of damage clusters with other better known data-sets like temperature measurements and radiosoundings, we might be able to define a few possible future scenarios and connect them with the more general IPCC scenarios (IPCC 1990).

2. Data base and study area.

The damage claims available for our analysis have a very simple structure: for every Swiss community, on a given day, it is known whether a damage claim has been registered or not. No indication on the amount of damage and its extension in the community itself is available.
The reliability of the information which can be derived from this simple data-set depends on the size of the communities, on the kind and the spatial and seasonal distribution of the cultures and on the percentage of the insured cultures. The evolution with time of the last 4 parameters plays an important role for the quality of the time series of damage-clusters.
An analysis of the parameters mentioned above yielded the following results (Willemse, 1994):

- the resolution of the damage claims is better in the Swiss Midlands ("Mittelland") because the communities in this area are much smaller (average surface: 8 km^2)than those in the Alpine region and in the Jura mountains (these areas can be seen in Figure 1a)
- most of the cultures are hail sensitive between the end of May and the beginning of September
- the largest variety of hail-sensitive cultures grows in the Midlands

- in the Midlands at least 75 % of the crops is insured
- a check of the time evolution of the cultures and of the insured areas (with agricultural statistics of the years 1955, '65, '75 and '85 and insurance statistics of 1951 and 1976) showed that, although some variations are found all over the study area, they shouldn't have influenced too much the amount and frequency of the damage claims.

These facts led to the conclusion that our study area has to be limited to the Midlands (covering an area of roughly 17'000 km$^{2)}$ and that for our hail-cluster time series only hail damages claimed between the 20th of May and 10th of September should be considered. With these constraints the whole period 1949-93 was judged to be comparable.

3. Method.

A cartographic representation of the damage-reporting communities shows how severe hailstorms leave a well recognizable hail swath. To quantify these swaths a simple method was designed: all communities, described by the horizontal coordinates x and y of their barycenter, are given a third dimension z (z=1 if the community claimed hail, z=0 otherwise), obtaining a 3-dimensional landscape of "damage hills". We define the 0.2-contours of these hills as damage clusters and choose all those having a length of more than 25 km for our hailstorm climatology. Every day between 1949 and 1993 on which at least 30 communities announced hail damage has been analyzed with this method. As an example, Figure 1a shows the distribution of the communities claiming hail on the 23rd of June 1991 and Figure 1b illustrates the resulting damage clusters. Since usually the communities are hit only partially by the hailfall, the obtained clusters have to be taken as a potential hail area.

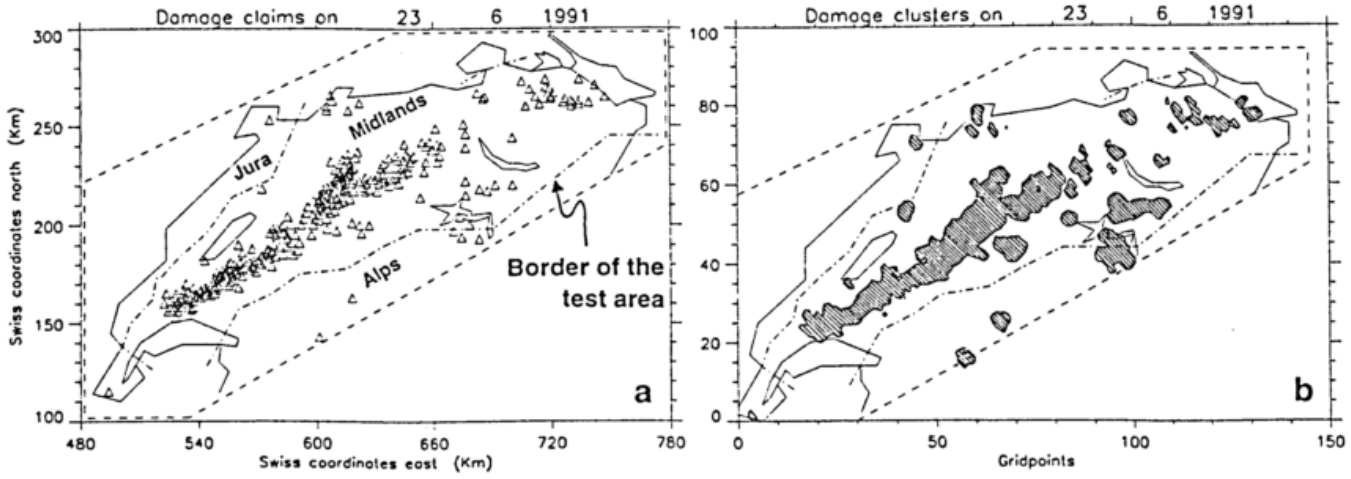

Figure 1. **(a)**Distribution of the communities claiming hail on the 23rd of June 1991 and **(b)** the corresponding damage clusters.

For each damage cluster the following parameters were recorded: date, synoptic situation (cold-frontal, prefrontal, airmass day), timing of the front (before or after 12 h local time), indication of the prevailing airmass over Switzerland at noon (maritime- and continental-polar, maritime- and continental-tropical). Furthermore, every cluster is characterized by its length, area, orientation, position relatively to the study area (completely within it or entering/exiting it), coordinates of its beginning and end points and, where possible, approximate time of the storm's occurrence recontructed with the help of daily thunderstorm-observation maps (thunder and lightning) of the SMI.

4. Results.

The observation period described in section 2 includes 5'040 days, 58 % of which (2'924 days) are haildays with at least one damage claim. 596 days (20 % of the haildays) have more than 29 claims: these are the days we used for the analysis described in section 2. 651 clusters with a minimum length of 25 km were collected on 364 of the above 596 days.
For a first analysis the irregularly spaced daily data were transformed in yearly values. Figure 2 shows the time series of the annual sum of damage claims, which oscillates between 500 and 3'000

with a local maximum in the 70[ies] and a slightly increasing trend and decreasing amplitude in the last decade. The dotted line represents the mean value of the whole series. Figure 3 displays a plot of the number of clusters per year (varying between 1 and 34), and shows an evolution which is very similar to the one of the damage claims (Figure 2). A plot of the yearly sum of the areas of these clusters, with values between 176 and 13'528 km^2, yields also a very similar curve (not shown here).

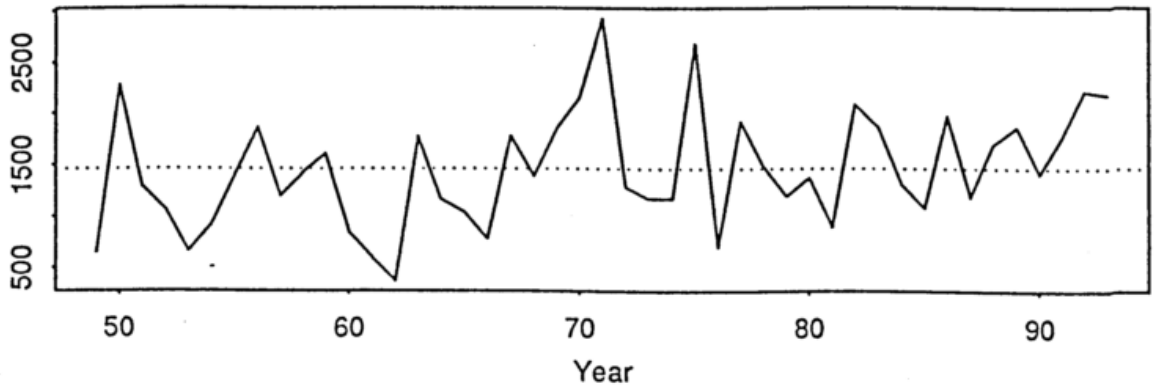

Figure 2. Annual sum of damage claims

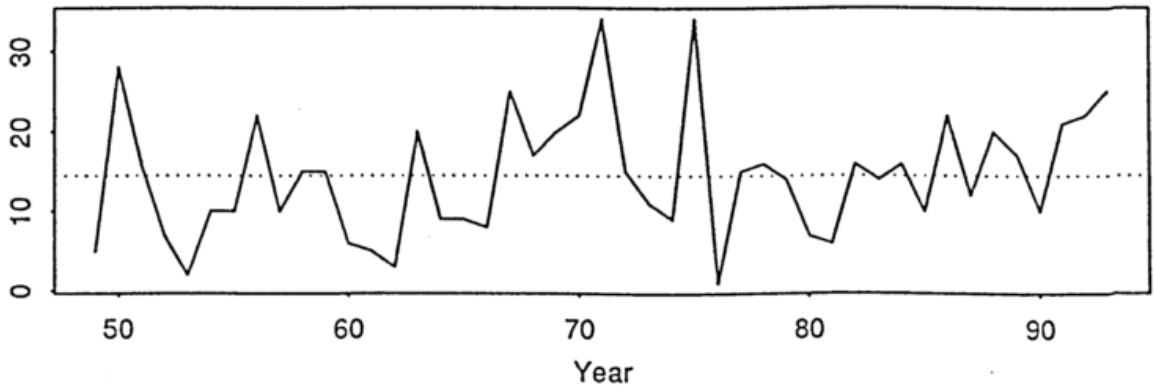

Figure 3. Number of damage clusters per year with a length > 25 km.

For 75 % of the clusters it was possible to determine, with the help of thunderstorm-observation maps of the SMI, the approximate appearance time of the storms, as mentioned in section 3. According to these clusters most of the damaging hail fell in the afternoon between 15:00 and 20:00 (CET). The area of the single clusters varies between 88 and 2'156 km^2 and their length between 25 (minimum condition to be admitted to the data base) and 179 km. 51 % of the storms built up in connection with a frontal disturbance, 22 % developed in a prefrontal region and 27 % were observed on days without approaching disturbances, mostly in situations of flat pressure distribution.
A first glance at some meteorological parameters of the days with hail clusters show that the largest clusters:

- are connected mostly with frontal disturbances (cold fronts) and with daily maximum temperatures (average of 6 mesonet stations in the study area) between 19 and 31 °C, as shown in Figure 4 (see also Huntrieser *et al.*, 1994 for typical synoptic situations),
- are always oriented in a south-west direction (see Figure 5),
- appear mostly in weather situations with south or south-westerly flow at 500 hPa,
- are found on days were, according to the radiosoundings, the 0 °C-level is rather high, namely around 4'000 m (data from 1978 to 1989)

5. Conclusions.

Although one might be tempted to extrapolate the time series of figures 2 and 3 to try to predict the future of thunderstorm activity, the data on which these series are based don't allow such kind of predictions because they hide too many uncertainties; furthermore, as we already said before, the

considered time period is still too short for climatological interpretations. However, the cluster time series seems to provide useful informations about time and location of severe hailstorms for the years without radar measurements and, all the same, they might lead to the formulation of a few possible future scenarios. For this purpose, a regression analysis with different meteorological parameters which are related to severe hailstorm activity is planned. In addition, an analysis of the radar pictures of the years 1983 to '93 is scheduled in order to make a comparison with the last decade of the damage clusters, which show a slightly increasing trend in this time span (see Figures 2 and 3).

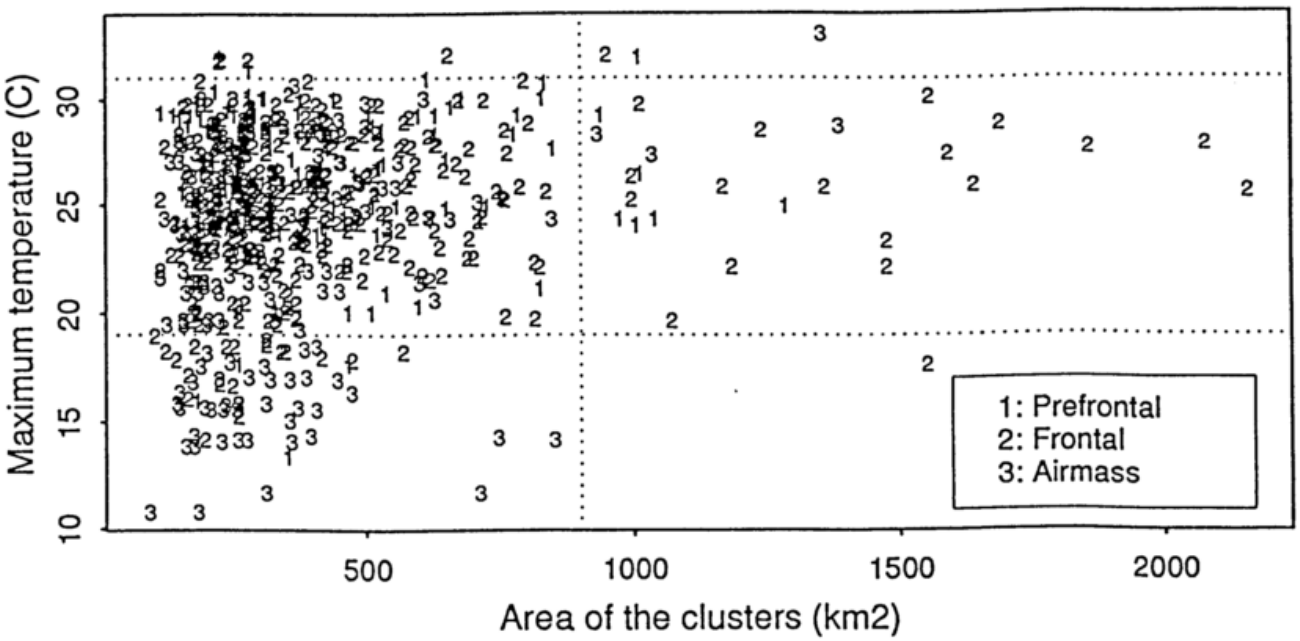

Figure 4. Area of the damage-clusters depending on the maximum temperature and on the synoptic situation.

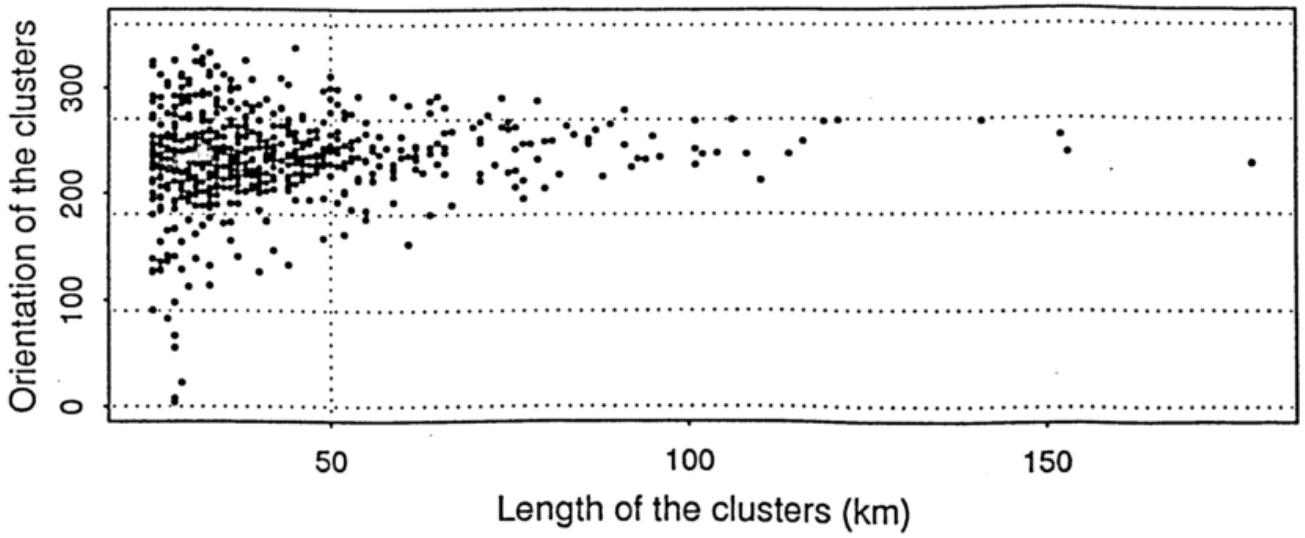

Figure 5. Length of the damage-clusters depending on their orientation.

6. References.

Huntrieser, H., H.H. Schiesser and A. Waldvogel, 1994: The synoptic and mesoscale environment of severe convective activity in Switzerland. The life cycle of extratropical cyclones, Bergen, Norway, 6 pp.

Intergovernmental Panel on Climate Change, 1990: CLIMATE CHANGE The IPCC Scientific Assessment, edited by J. T. Houghton *et al.*, Cambridge University Press, 364 pp.

Schiesser, H.H. and s. Willemse, 1992: About the origin, extent and frequency of severe hailstorms in Switzerland north of the alpine ridge. 22nd Conf. on Alpine Meteorology - CIMA 92, Toulouse, France, p. 403-407

Willemse, S., 1994: Klimatologie der Hagelstürme. In: Gruppe für Radarmeteorologie, Monitoring von starken Hagelstürmen in der Schweiz 1993. LAPETH-31, p. 11-24 (available from Atmospheric Science, ETH-Hönggerberg, 8093 Zürich)

The frequency of convective storms north of the Alps as a function of the large-scale climate

D.Heimann, V.Sept, U.Fuentes

DLR Oberpfaffenhofen
Institut für Physik der Atmosphäre

ABSTRACT

This is a precursory study of a planned application of statistical-dynamical downscaling that aims at possible changes of the regional convective storm (thunderstorm) frequency and its inner-regional spatial distribution due to global climate changes. Based on ten-years data sets (1981-1990) of regional thunderstorm observations and daily large-scale analyses over Europe we deduce statistical relations which help to classify large-scale weather situations for which thunderstorms in southern Bavaria are expected to occur. The large-scale weather situations are defined such that unequivocal input parameters for a regional model simulation can by derived for each class.

1. Introduction

In average any location in southern Bavaria, i.e. between the Alps and the Danube river, is hit by thunderstorms on 25 days per year. These storms often cause tremendous damage and even fatalities. It is speculated that the regional frequency of storms may alter when the large-scale climate conditions change, e.g. as a result of increasing greenhouse gas concentrations. It it also possible that the inner regional spatial distribution of the storm frequency changes under such circumstances. In the present climate we find distinct areas with an average number of more than 30 thunderstorm days per year (mainly near the Alpine base line and along the Danube), while the number of thunderstorms is less than 22 days per year (minumum 16) in other areas of southern Bavaria (Pelz, 1984).

Within a research project of the Bavarian climate research programme (BayFORKLIM) it is our final goal to apply a statistical-dynamical downscaling procedure on large-scale simulations of the present climate and climate scenario simulations in order to estimate the effect of large-scale climate changes on the regional frequency of convective storms (thunderstorms). This paper presents results of a very early stage of this project.

2. Statistical-dynamical downscaling

The statistical-dynamical downscaling procedure uses a sequence of daily coarse-grid meteorological fields (either analyzed or simulated) which extends over a sufficient number of years to represent a large-scale climate C. A *dynamical* limited area model is operated to generate highly resolved regional-scale meteorological fields. The link between both scales, large scale and regional scale, is based on *statistical* relations. The method is described in detail by Frey-Buness (1993) and Frey-Buness et al. (1994).

The procedure consists in four steps:
(1) The coarse-grid fields are classified into defined large-scale weather situations Φ_i where each class is represented by an individual set of meteorological parameters which later determines the initial state of a fine-mesh regional model simulation.
(2) The conditional probability $P(\Phi_i|C)$ that a large-scale weather situation Φ_i occurs in an analyzed or simulated climate C is derived by counting the number of weather situations that fall into the respective class.

(3) For all defined classes of large-scale weather situations a regional model simulation is initialized that considers the effects of regional-scale topographical features in the area of interest. By counting the number of certain regional-scale events (e.g. exceeding of a threshold value, occurrence of convective storms) in the regional model results one obtains the conditional probability $P(\varphi_j|\Phi_i)$ that the regional event φ_j occurs in a given large-scale weather situation Φ_i.
(4) Finally, the conditional probability that a regional event φ_j occurs in the climate C is given by

$$P(\varphi_j|C) = P(\Phi_i|C) \times P(\varphi_j|\Phi_i)$$

It is a general assumption of the statistical-dynamical downscaling method that the conditional probability $P(\varphi_j|\Phi_i)$ is independent of the climate.
and regional thunderstorms

3. Statistics of large-scale weather situations

Since we need to define an appropriate classification scheme we first evaluate observational reports of thunderstorms (origin DWD) and large-scale analyses in T42 resolution (origin ECMWF/DKRZ) of the present climate, i.e. the period 1981-1990. The thunderstorm days are counted from reports of eight weather stations in southern Bavaria. Since thunderstorms are rare in winter we restrict the evaluation to the summer half year (15 April to 15 October).

It turned out that thunderstorms where reported on 40 percent of all days in the summer half year. However, on 24 percent of the thunderstorm days only one of the eight stations reported a thunderstorm within only one three-hour interval of a day. On the other hand, on 20 percent of all thunderstorm days more than half of the stations reported thunderstorms. The diagramme in Figure 1 shows the number of thunderstorm days as a function of the number of reporting stations and the number of three-hour intervals per day for which thunderstorms were reported.

Next we determine the conditional probability $P(\Phi_\ell|\varphi_j)$ where Φ_ℓ stands for large-scale weather classes following an intuitive definition and φ_j distinguishes days with and without thunderstorms in southern Bavaria. The large-scale analysis data are averaged over 4×3 meshes, i.e. in an area of roughly 800×800 km^2 with the Alps in its centre. This area is almost identical with the domain of the regional model. Figure 2 exemplarily displays the frequency of the mean 850-hPa geostrophic wind direction inside the specified area for days with and without thunderstorms in southern Bavaria. It is evident that thunderstorms are very frequent in weather situations with southwesterly to westerly large-scale flow. Analogously, we test the vertical wind shear and the vertical stability as classification criteria. A final classification scheme Φ_i is defined on the experiences we obtained from the probability distribution $P(\Phi_\ell|\varphi_j)$.

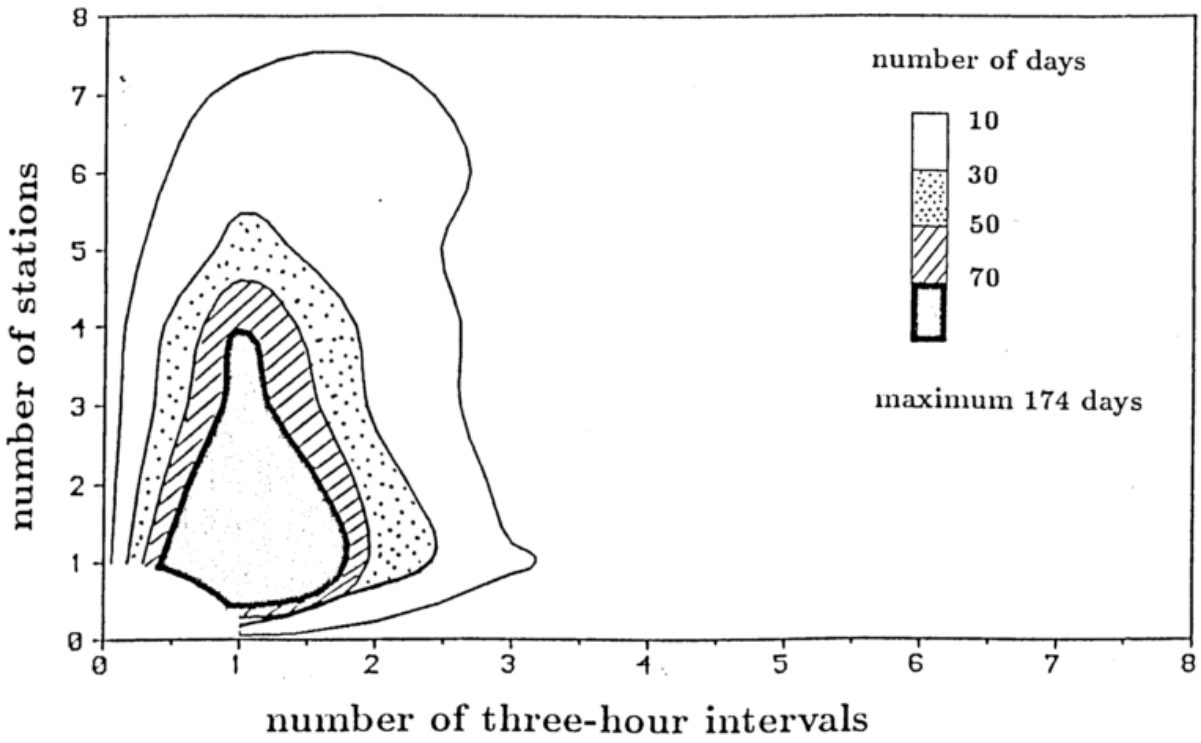

Figure 1. Reported thunderstorm days in southern Bavaria (1981-1990, only summer half year) as a function of the number of reported three-hour intervals per day and the number of reporting stations. The total number of reported thunderstorm days is 737 (= 40 percent of all days).

4. Outlook

After the final large-scale weather classes Φ_i are defined conditional probabilities $P(\varphi_j|\Phi_i)$ are determined at first from the thunderstorm reports with $\varphi_j (j = 1,2)$ distinguishing thunderstrom and non-thunderstorm days in southern Bavaria. However, the inner-regional distribution of the thunderstorm probability is hardly detectable from only eight observing stations. Hence, regional model simulations will be performed for all large-scale weather situations Φ_i. Their output is checked for appropriate threshold values of thunderstorm indicators (e.g. stability indicees) which ensure that observations and regional simulations result in the same distribution of $P(\varphi_j|\Phi_i)$ with $j = 1,2$. Apart from the general discrimination into thunderstorm days and non-thunderstorm days, the regional model offers the possibility to utilize the spatial distribution of thunderstrom indicators.

Once the probabilities $P(\varphi_j|\Phi_i)$ are found the downscaling method is ready to be applied to large-scale climate simulations for different scenarios.

References

Frey-Buness A., 1993: Ein statistisch-dynamisches Verfahren zur Regionalisierung globaler Klimasimulationen. DLR-Forschungsbericht DLR-FB 93-47, 149 S.

Frey-Buness A., Heimann D., Sausen R., 1994: A statistical-dynamical downscaling procedure for global climate simulations. Eingereicht bei Appl.Theor.Climat.

Pelz J., 1984: Die geographische Verteilung der Tage mit Gewitter in Mitteleuropa. Beilage zur Berliner Wetterkarte, SO 12/84.

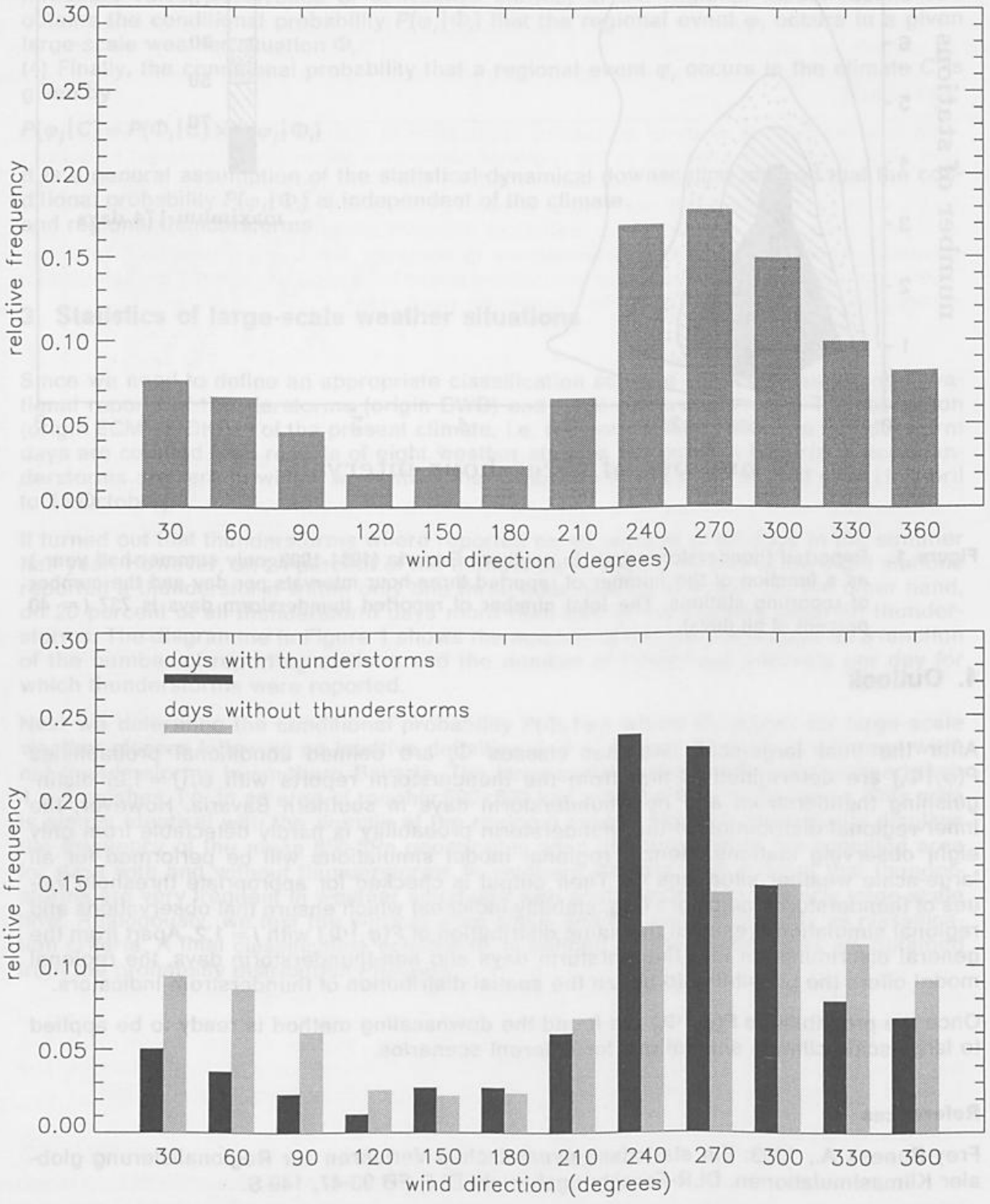

Figure 2. Top: relative frequency of the 850 hPa geostrophic wind direction (30° sectors) in the greater Alpine area (summer half years 1981-1990) as deduced from ECMWF analyses in T42 resolution.
Bottom: same as top but separated into days with and without reported thunderstorms in southern Bavaria.

First results from the SETEX-94 Experiment

M. K. Peristeri
Meteorological Institute, University of Munich

Abstract

The severe thunderstorms experiment (SETEX) was carried out during June and July 1994 to study organized severe thunderstorms in the warm moist south-westerly airstream ahead of approaching cold fronts in southern Germany and eastern Switzerland. This is the period of maximum thunderstorm frequency in the region. Some first results of the experiment will be presented.

1. Scientific aims

The SETEX field experiment is conceived as part of a longer term collaborative project (Smith *et al.* 1993). The aims of the experiment itself are

* to document the structure and life-cycle of severe thunderstorms in southern Germany and eastern Switzerland,
* to determine the preferred synoptic conditions for their formation,
* to investigate the influence of the Alps on severe thunderstorms in the region,
* to investigate the possibility of improved prediction of these storms using mesoscale numerical models such as the "Deutschland-Model" of the Deutscher Wetterdienst (DWD) and
* to provide mesoscale data sets for the initialization and/or the verification of mesoscale numerical models.

2. The experimental set up

In 1992 field observations on organized thunderstorms were carried out during the CLEOPATRA experiment which was organized by the German Aerospace Research Organization (DLR). The SETEX experiment is seen as an extension of these activities and builds upon the experience gained from them. The enhanced surface station network for SETEX, which covered a large part of southern Bavaria and Baden-Württemberg, it consisted of 11 automatic surface

stations measuring pressure, dry and wet-bulb-temperature, wind speed at a height of 2 m and wind direction at a height of 3 m. This network was embedded in the existing SYNOP-station networks of the DWD and the military meteorological service (GeoPhys) in Germany and the two meso-network, ANETZ and ENET, operated by the Swiss Meteorological Organization (SMA). Radar data were available from the DWD stations in Hohenpeißenberg and in München-Fürholzen, from the SMA in Albis, as well as extra-operational radar observations from the Doppler radars at the DLR in Oberpfaffenhofen and the Eidgenössische Technische Hochschule (ETH) in Zürich. On selected days the University of Munich (LMU) carried out serial radiosonde soundings using a Väisälä Marwinsonde system at the DLR and the ETH Zürich carried out soundings from a mobile station in eastern Switzerland in Rutschwil near Seuzach.

Decisions on making special observations were made at daily briefings and following the advice from the DWD in Munich and on the basis of telephone discussions and e-mail contact between the LMU, DLR and the ETH Zürich.

3. Results

By early June, two special observation periods had been declared and from these, two thunderstorm systems were documented in detail. Analysis of these systems will be described and an overview of other events documented will be presented.

Reference

Smith R.K., Haase-Straub S., Ulrich W., Meischner P., Hagen M., Heimann D., Schmid W., Schiesser H.H., 1993. Proposal for the Severe Thunderstorms Experiment (SETEX-94). (Available from the Meteorological Institute, University of Munich.)

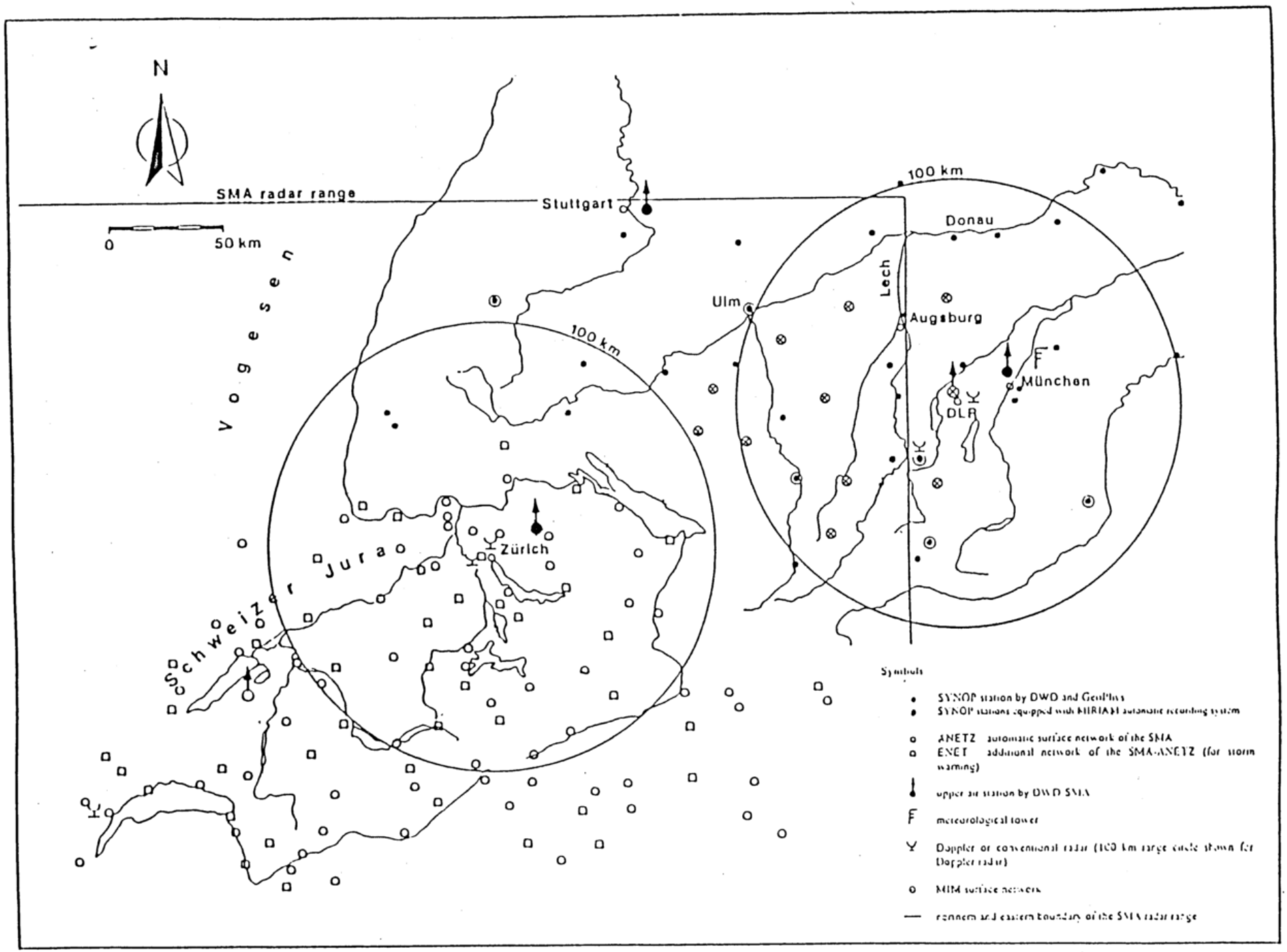

Fig. 1 Experimental area showing location of observational network (from Smith *et al.*, 1993).

The severe squall line of 21 July 1992 in the region north of the Alps

S. HAASE-STRAUB, Meteorologisches Institut der Universität München
M. HAGEN, D. HEIMANN, Institut für Physik der Atmosphäre der DLR, Oberpfaffenhofen

Summary

On 21 July 1992, during the CLEOPATRA field experiment, the evolution of a squall line was observed and analysed in detail (see Haase-Straub et *al.*, 1994). Besides routine data (synoptic surface observations and radiosonde soundings) there were radar and satellite observations at a high temporal and spatial resolution, additional radiosonde and aircraft ascents and a special mesoscale network comprising 14 surface stations covering the southwest of Bavaria (see Meischner et *al.*, 1993).

The analyses show that the squall line formed ahead of a cold front that approached the region north of the Alps from the west. Ahead of the front wind and pressure fields showed line structures, along which isolated storms and later on lines of thunderstorms formed. The latter were accompanied by strong wind gusts and heavy precipitation and moved eastward at high speed along the northern side of the Alps. As the severe-weather system crossed central Europe, fatalities and damage were reported from France, Switzerland and Germany.

1. Synoptic situation

Prior to the 21 July 1992 for about a week a cyclonic west-wind situation was prevalent over central Europe with subtropical maritime air masses influencing southern Germany and the Alpine region. By midday of the 21 July these pressure features had intensified with a strong southwesterly to southsouthwesterly upper-air flow that reached 40 m/s above Paris at a level of 300 hPa.

The surface low was located between Iceland and Norway. Its cold-frontal system extended in a wide arc over Finland and the Baltic states to the North Sea where a secondary low, which had developed at this front, was situated at midday. The front separated a cool maritime polar air mass intruding from the Atlantic ocean from warm maritime subtropic air in the east. East of the Rhine river, maritime subtropical air had already attained the character of hot continental air. The cold front, accompanied by the air-mass change, did not reach the MESONET area before midday of the following day. The acronym MESONET refers to the special CLEOPATRA mesoscale station network consisting of 14 surface stations.

2. Mesoscale development

2.1 Mesoscale analyses and radar observations

Hourly analyses have been constructed based on composites of hourly synoptic observations, radar scans from the DLR in Oberpfaffenhofen, the DWD in Hohenpeißenberg and in Frankfurt and from the SMA in Albis and LaDôle, on METEOSAT-IR images, and on data from the MESONET.

Several lines in the wind- and surface-pressure fields have been identified. By 19:00 UTC the main line had formed ahead of the cold front and was accompanied by thunderstorms in Switzerland and in the German state Baden-Württemberg (see Fig. 1a). Note the acceleration

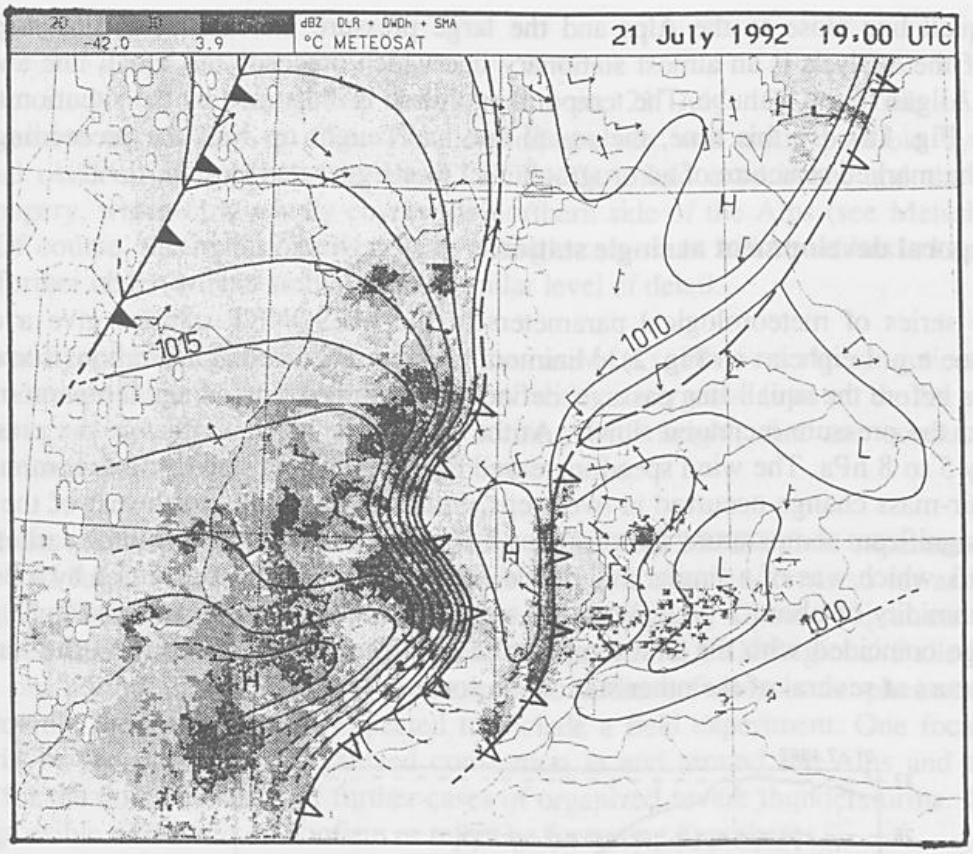

a)

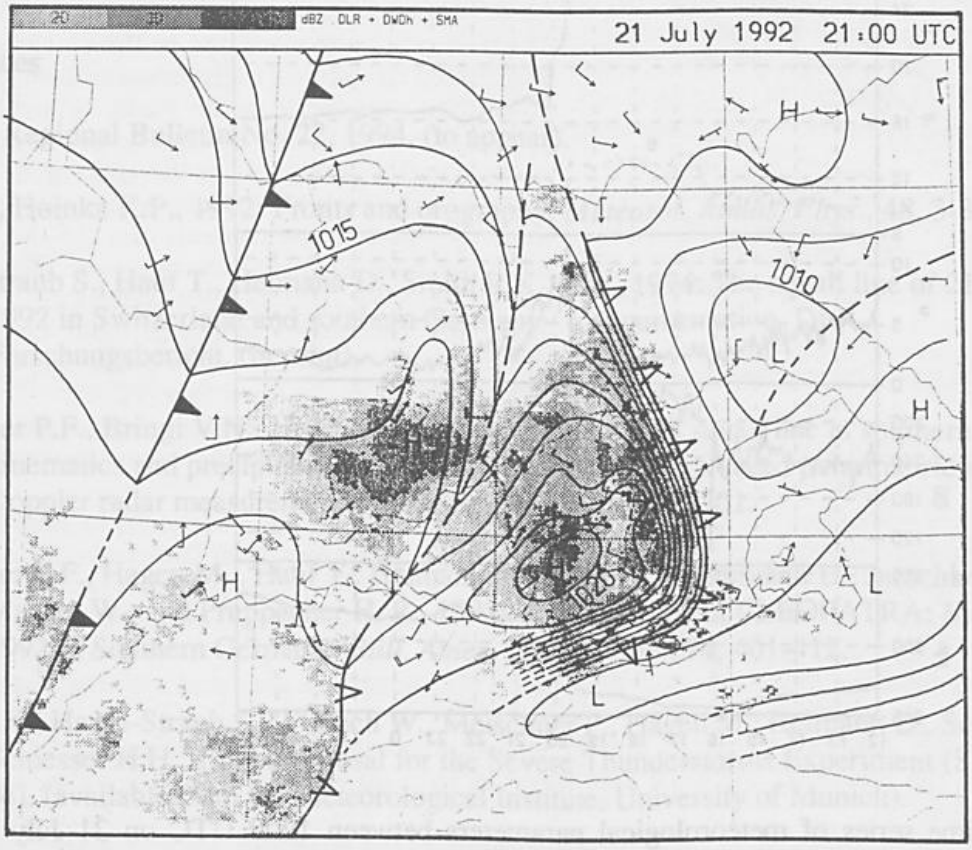

b)

Fig. 1 Analysed isobars of surface pressure reduced to mean sea level and frontal lines which are evident from one or more fields of pressure, temperature and precipitation are shown for the times **a)** 1900 UTC and **b)** 2100 UTC. Note that the analyses are based on more information than shown. In addition, composite PPI radar scans and infrared satellite images are superimposed, as indicated in the upper left corner of the figures.

of the squall line close to the Alps and the large pressure increase behind it. A prominent feature of the analysis is an almost stationary line which preceeds the squall line and extends from the Allgäu to the Danube. The temporal evolution is illustrated by the situation two hours later (see Fig. 1b). By this time, the squall line had caught up with the preceeding line and showed the marked structure of an orographic jet (see Egger und Hoinka, 1992).

2.2 Temporal development at single stations

The time series of meteorological parameters at the MESONET stations give a consistent picture (see e.g. Leipheim on Fig. 2). Minimum pressure occurred at all stations some three to four hours before the squall-line passage, defined by the time of maximum temperature change. Thereafter the pressure increased slowly. At the time of the air-mass change the pressure rose rapidly by 5 to 8 hPa. The wind speed increased rapidly, too, but only for a few minutes. Note that the air-mass change occurred in two steps. In Leipheim, in the northwest of the mesonet, the first significant temperature fall of about 5 K occurred about 20 minutes earlier than the second fall, which was of a similar magnitude. The first fall was accompanied by a decrease in specific humidity of about 3 g/kg. With the second fall the humidity increased by 1 g/kg. The wind surge coincided with the first temperature fall. The double structure in the temperature record occurs at several of the other stations to some degree.

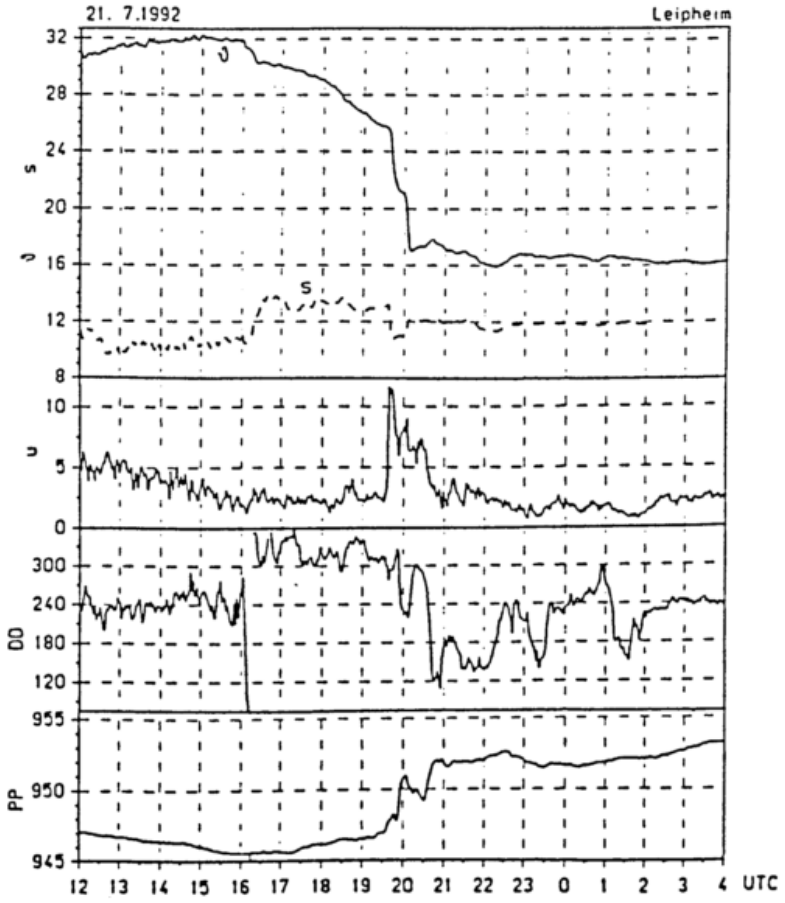

Fig. 2 Time series of meteorological parameters between 1200 UTC on 21 July and 0400 UTC on 22 July 1992 for the station Leipheim. The upper panel shows the temperature in °C and the specific humidity in g/kg. The second panel down shows the surface pressure in hPa reduced to the height of the DLR station. The third and fourth panels show the wind speed and direction, respectively. The data are based on two-minute mean values and times are UTC. (Courtesy of H. Schroers).

Discussion and outlook

The case study of the squall-line development on 21 July 1992 is one of the most comprehensive of its kind to date. The detailed analysis was made possible by the many additional observations provided by the CLEOPATRA field experiment and the composite radar imagery, which now wholly covers the northern side of the Alps (see Meischner et *al.*, 1991). Of course, the representativeness of a single case must still be addressed and this will call for further observational studies with a similar level of detail.

One of the hypotheses of the study is that in the case of a south-westerly synoptic airflow, the Alpine mountain range leads to a horizontal flow with convergence lines on the lee side as well as to patterns of vertical wind shear and turning with height, that are conducive to the generation and maintenance of severe convective systems.

Research on severe thunderstorms is continuing apace. The SETEX field experiment, planned for June and July 1994, has captured two cases of severe thunderstorms so far at the time of writing (see Smith et *al.*, 1993). An international **M**esoscale **A**lpine **P**rogramme (MAP) is being established by the countries in the Alpine region (see ALPEX Regional Bulletin No. 22). Besides promoting theoretical and climatological studies of mesoscale phenomena in the Alpine region, the programme is expected to include a field experiment. One focal point for MAP will be the problem of organized convection in and around the Alps and this should provide for the documentation of further cases of organized severe thunderstorms. This should make it possible, *inter alia*, to confirm or reject he foregoing hypotheses.

References

ALPEX Regional Bulletin No. 22, 1994, (to appear).

Egger J., Hoinka K.P., 1992: Fronts and orography. *Meteorol. Atmos. Phys.*, **48**, 3-36.

Haase-Straub S., Hauf T., Heimann D., Smith R.K., Eds., 1994: The squall line of 21 July 1992 in Switzerland and southern Germany - a documentation. DLR-Forschungsbericht, (in print).

Meischner P.F., Bringi V.N., Heimann D., Höller H., 1991: A squall line in southern Germany: kinematics and precipitation formation as deduced by advanced polarimetric and Doppler radar measurements. *Mon.Wea.Rev.*, **119**, 678-701.

Meischner P.F., Hagen M. , Hauf T., Heimann D., Höller H., Schumann U., Jaeschke W., Mauser W., and Pruppacher H. R., 1993: The field project CLEOPATRA: May-July 1992 in Southern Germany. *Bull. Amer. Meteor. Soc.*, **74**, 401-412.

Smith R.K., Haase-Straub S.P., Ulrich W., Meischner P., Hagen M., Heimann D., Schmid W., Schiesser H.H., 1993. Proposal for the Severe Thunderstorms Experiment (SETEX-94). (available from the Meteorological Institute, University of Munich).

THE COMPARATIVE ANALYSIS OF THE SNOWSTORMS OF NOVEMBER 1993 IN THE CARPATHIAN BALKAN SINK (ROMANIAN PLAIN RESPECTIVELY)

Ortansa JUDE, G. BĂLUŢ and Viorica DIMA
National Institute of Meteorology and Hydrology
Bucharest, ROMANIA

Due to Romania's geographic location on the continent and its varied relief, the most frequently encountered synoptical configuration over its territory is that of a contact area between extratropical cyclone and anticyclone.

During the cold half of the year, but especially in the winter time, there is a high frequency of situations in which an East European high pressure centre and a Mediterranean low are confronted over the 45°N parallel area, determining severe snow storms for the East and South-East of Romania. The first thorough study of this phenomenon offers a complex definition for it (strong wind intensifications drifting the snow, associated or not with snowfalls), but also points out the fact that 70% of the Romanian snow storms occur during the winter time, and for the rest of them the supremacy belongs to the month of March /1/.

The peculiarity of the 1993/1994 winter consisted in the fact that there were no snowstorms during the typical months, but the month of November focussed five snowstorms over only a 23-day period.

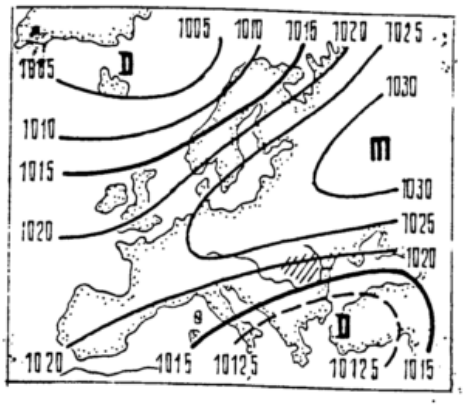

Figure 1. Baric type 1 generating snowstorms in Romania

The purpose of the present paper is to briefly present the occurrence, evolution and force of each case, but also a comparison between them, starting from the seven favouring baric types taken from the bibliography /1/.

Thus, the first snowstorm, occurred during 10 -11. XI, belong to the baric type I, subgroup Ia,/1/,(Fig.1) The concrete baric situation in the starting day was dominated by a strong high pressure field (exceeding 1045 hPa) over the Russian Plain, linked by a high pressure belt with the Asores Anticyclone, modest enough in this period (above the 1025 hPa). Thus, the activity of the Iceland Cyclone was clearly separated from the East-Mediterranean one. In the following days the East-European anticyclone became a dynamic factor for the analysed snowstorm, because it gradually developed a strong cold ridge in the Carpathian-Balkan sink, over the Western put of the Black Sea up to the Egea Sea (12.XI).

It is also to be noticed concerning the general situation it most be noticed that the effects due to the mesosynoptic process known as "Carpathian Type orographical occusion" are added.

On the 10-th of November in the morning, in about 6 hours the rain turned into sleet first, then snow, so that since noon until evening the snowstorm acted locally in Dobrudja, Muntenia and the East of Oltenia.

During the night of 10-th to 11-th of November its force became maximum, and spatially, it included the South-Eastern half of Romania.

During those days the first snow layer occurred the mountain area and also the regions of the Eastern half of the country.

This snowstorm ranged within the strong snowstorm category /1/, because on the 11-th of November in the morning, the wind was blowing with an average speed of 15 m/s in several southern places.

The second snowstorm (13-th - 14-th November) joined the subgroup I b_1 /1/ and occured at the coupling area between the former continental East-European anticyclone and the new Mediterranean cyclone that was born on the 13-th of November over the Genua Bay and moved away very fast on a Southern, trans-Balkan trajectory towards the Crete Island (15-th of November).

This can also be classified as a strong snowstorm /1/ but for a much smaller geographical area than the first one.

In the beginning, the wind speed exceeded 15 m/s in the South of Banat (region in the South-West of Romania), gradually getting stronger until it reached 25 m/s at Oravita (13-th of November at 14 o'clock).

Regarding the considerable moisture contents from the previous mentioned cyclone, the new snow cover fallen covered almost the entire country (except for the far South-East).

The synoptic situation that generated the third snowstorm of the 16-th - 18-th of November also joined type I, subgroup I a. The anticyclonic belt created was well supplied by the Asores high, and also by the East-European one, but its axis was placed much more to the North than in the previous cases.

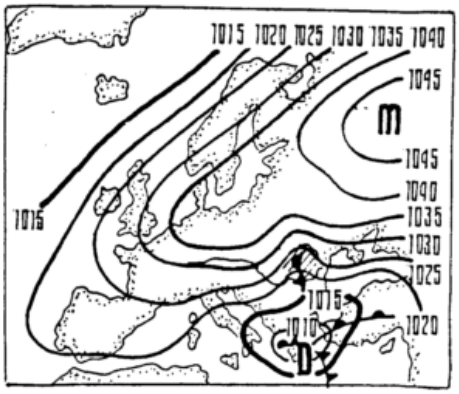

Figure 2. 16. XI h 18 UTC Carpathian orographic occlusion at the level of Romania

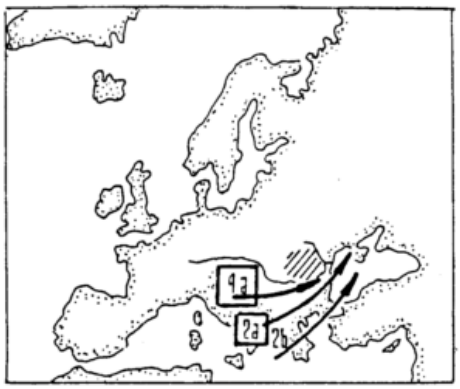

Figure 3. Processed TransBalkan cyclonic trajectories

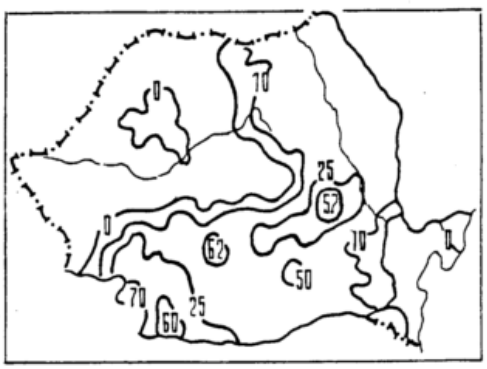

Figure 4. Distribution of the snow cover on 1. XII. h 06 UTC

This time too, the Carpathian type orographic occlusion added to the major synoptic process, amplifying the meteorological effects at Romania's scale (Fig. 2).

From the phenomenologial standpoint, on the 16-th of November, the wind was gradually intensified over the South-East of Romania, being characterized by a persistency of more than 15 hours with speeds exceeding 10 m/s, and in some places as Buzau, with over 20 m/s during more than 9 hours, ensuring a particular severeness to this third snowstorm (violent snowstorm) /1/.

The warm air advection through over the entire troposphere encouraged significant amounts of snowfall (over 15 l/m²), particularly for the Southern region added to the previous snow cover depth which, at the end of this period, covered the center, South and East of the country.

The transbalkan evolution of type 2 b /3/ (Fig.3) of the involved Mediterranean cyclone encouraged the snowstorm location in the South of Moldavia, East of Baragan and Dobrudja, on the 17-th of November and then the 18-th of November; in these regions the wind persisted over 48 hours, with speeds of about 10 m/s.

The subsequent increase of the atmospheric pressure due to the polar cold air masses spreading up to over the Black Sea basin, led to the gradual extinction of the snowstorm in these regions too (19-th of November).

After only 10 days from the first snowstorm, the fourth has occured (20-th - 22-th of November), in a baric context of type I, subgroup Ib_1 /1/.

The strong East-European baric high pressure field coupled with a new Mediterranean cyclone (on the 20-th of November) moving over the Balkanic Peninsula towards Asia Minor. Thus, a wind intensification took place up to over 10 m/s in almost the entire South of the country (strong snowstorm), but locally, in Muntenia, the snowstorm was violent (speed exceeding 17 m/s, up to 27 m/s, lasting more than 10 hours in Buzău).

The snowfalls were abundant in the extra-Carpathian regions (except for Dobrudja, where the rainfalls were prevaling), and the snow depth exceeded 15-20 cm on large areas, and in Oltenia it reached 50 cm.

On the 29-th of November the continental baric situation was dominated by the same extended high field centered over the Russian Plain. Over the Mediterranean basin another cyclone arised and developed, which, in these final days of November, situted over the Adriatic Sea and than Egea Sea. In this context

(type I, subgroup Ib_1) the fifth snowstorm occured (29-th XI - 2-th XII).
This one was similar enough with the previous one, the maximum action area of the wind at speeds of over 15 m/s was Muntenia and Dobrudja, the snowfall amounts were considerable in the South of the country too, so that the calendar winter began with an already existing snow cover almost compact over the South and East of the country (more than 25 cm up to 55 cm in Oltenia, and also the mountain area (up to 62 cm), (Fig. 4). For this case, the local Carpathian orographic cyclogenesis has not missed either. Neither in this fifth case missed the local Carpathian orographic occlusion process.
The aerological structure of all those situations did not make the subject of the present paper.

CONCLUSION

* All the five snowstorms ranged among the strong snowstorm category, and locally and temporarily had violent effects.
* All of them occurred in baric type I, subgroups Ib_1 or I a, in which persistency of the strong East-European barometric high field (1040-1055 hPa) was dominant. This one "met" a succession of young Mediterranean cyclones involved into a fast evolution at the midlatitude zone of Europe, determining for Romania the analyzed snowstorms.
* The Carpathian orographic occlusion was recurring as a mesoscale process with typical results in Romania.
* During the 23 successive days, the snow depth increased continuously for the extra-Carpathian area and the mountain area too, reaching the remarkable depth of over 5o cm in Oltenia, outstanding value even in the winter typical months.
* All these snowstorms were well forecasted by the meteorologists in Bucharest but few were the users who believed the forecastings (five successive snowstorms in November ?!).
Therefore, the inner and international transport was seriously effected, great problems occurred with food supply for the animal units or with energy supply for various industrial objectives, certain human settlements were "isolated" for days, there were human comalties.
For Romania, from the climatological, synoptic standpoint but also from the point of view of the social implications in the national economy, the month of November 1993 will remain an exception.

REFERENCES

1. Balescu, O. and Besleaga, N., (1962)
   Snowstorms in Romania, Meteorological Institute, Bucharest
2. Topor, N. and Stoica, C., (1965)
   Circulation types and atmospheric action centers above Europe., Meteorological Institute, Bucharest
3. Ecaterina Ion-Bordei, (1983)
   Rôle of the Alps-Carpathian chain in the evolution of the Mediterranean cyclones., Ed. Academiei, Bucharest.
4. Ecaterina Ion-Bordei, (1972)
   Les Carpates Roumaines - Zone de cyclogènèse orographique, a V-a Conf. de Meteorologie a Carpatilor, Bucarest.

Die Föhnfälle im Dezember 1989 in Vorarlberg

Richard Werner

Umweltinstitut des Landes Vorarlberg

ABSTRACT

Four periodes with stormy foehn from southern directions over the Alpes were analysed with pressure difference from Bozen to Bregenz, temperaturegradient, wind of 7 groundstations and meteorological observations from 13 weatherstations at different sites (valley, slope, mountain).

ZUSAMMENFASSUNG

Die vier extremen Föhnperioden im Dezember 1989 brachten bei alpenquerenden Winden mit Druckunterschieden zwischen Bozen und Bregenz von maximal 19 hPa stürmische Bodenwinde an sieben Bodenstationen. Die Summe aller Stunden mit Föhnwinden reichen landesweit von 16 bis 42 Stunden. Die Stationen Rohrspitz und Feldkirch weisen die extremsten Verhältnisse (höchste Stundenmittel: 19,2 und 18,0 m/s) auf. Die Föhnereignisse teilten sich an den dreizehn Klimastationen zu den 07-, 14-, und 19-Uhr Terminen im Verhältnis 72 : 89 : 84 auf. Durch die Stürme wurden Gebäude beschädigt, eine große Zahl von Bäumen abgedreht oder entwurzelt und Verkehrsverbindungen lahmgelegt.

1. EINLEITUNG

Die Periode vom 12. bis zum 22. Dezember wurde für die Kenngrößen Luftdruck, thermische Schichtung, der gemessene Bodenwind und Wetterbeobachtungen von Klimastationen im Land Vorarlberg untersucht. Aus den verschiedenen Unterlagen kristallisierten sich vier Föhnperioden heraus, welche zwischen 10 und 21 Stunden dauerten. Die Perioden können der Abbildung 1 mit den Druckverläufen von Bozen und Bregenz entnommen werden, wo sie mit F1 bis F4 bezeichnet und eingetragen wurden. Die Höhenströmung über dem Alpenraum herrschte in allen Fällen aus West bis Süd vor.

2. ANALYSE

Die erste Periode beginnt am 14. Dezember schon am Nachmittag, da aus den Daten der Klimastationen ersichtlich wird, daß der Föhnindex (bestimmt aus Windrichtung, Windstärke über 2 Beaufort und relativer Feuchte unter 40 Prozent) einen Wert bis 30% über alle Stationen erreicht. Stärkerer Föhn beginnt, als um 18 Uhr MEZ am Rohrspitz eine Windgeschwindigkeit von 6,9 m/s aus 200 Grad erreicht wird. Der Druckunterschied zwischen Bozen und Bregenz beträgt 16 hPa. Die Temperaturen im südlichen Teil des Alpenrheintales (Feldkirch) liegen um 19 Uhr bei 2,6 Grad Celsius, während an der Hangstation Fraxern 10,6 Grad verzeichnet werden. Der topographische Temperaturgradient von Vaduz zum Säntis beträgt -6,0 Grad je 1000 m. Der Föhn dauert in Vorarlberg ein bis acht Stunden mit einem höchsten Stundenmittelwert von 17,5 m/s. Die Föhnperiode endet gegen 5 Uhr am 15. als in Dornbirn der Wind mit 6,2 m/s aus 130 Grad gemessen wird.

Die zweite Föhnperiode beginnt am 16. gegen 11 Uhr. Nahezu zeitgleich setzt sich der Föhn am Rohrspitz (Stundenmittelwerte 11,8 m/s) in Szene, als die Feuchte in Lustenau nur mehr 45 Prozent beträgt. Sie sinkt bis 17 Uhr weiter auf 25 Prozent. Diese lange Föhnperiode wird 21 Stunden dauern und kann landesweit verfolgt werden, bis sie gegen

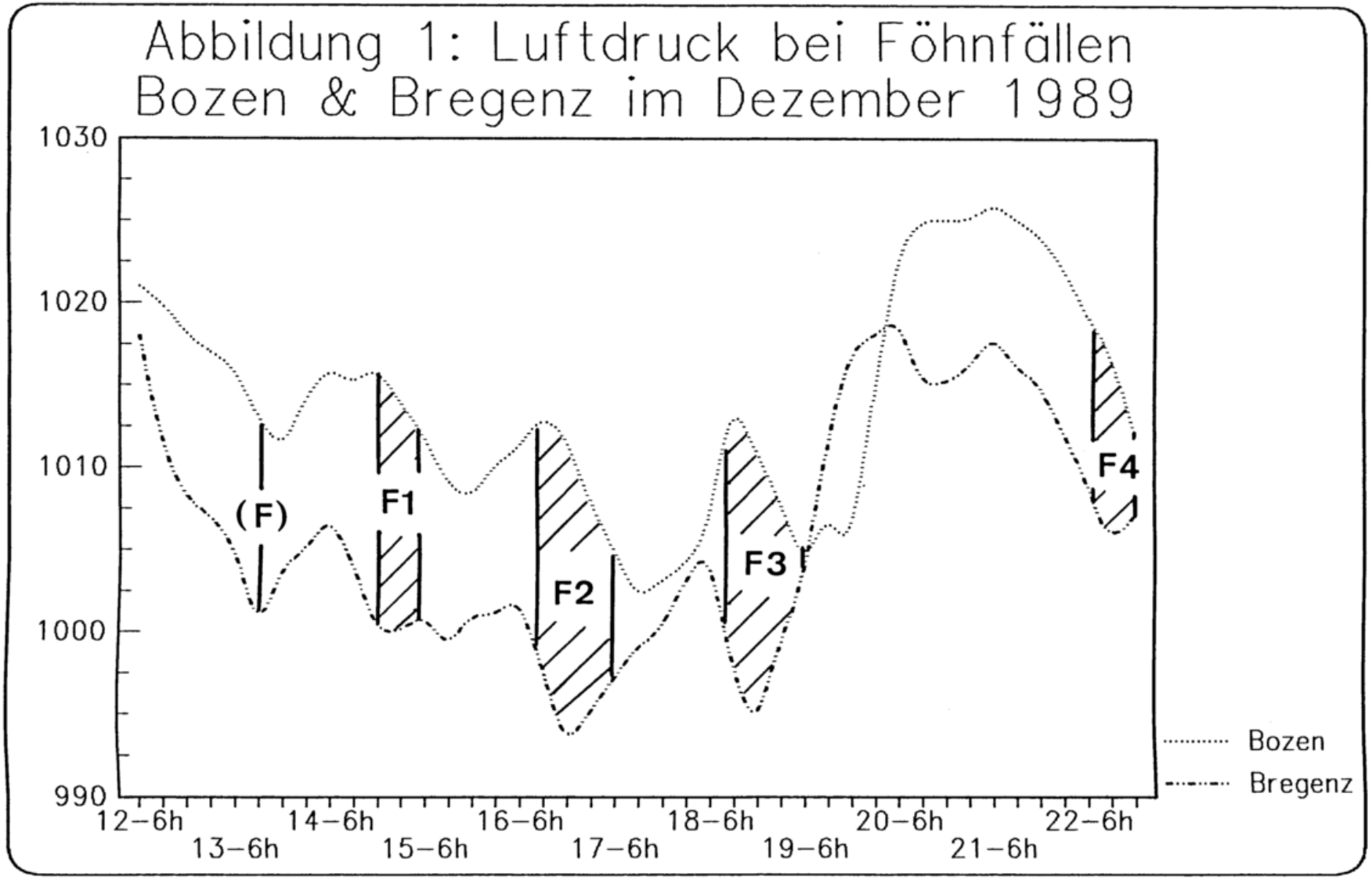
Abbildung 1: Luftdruck bei Föhnfällen
Bozen & Bregenz im Dezember 1989
1030
1020
1010
1000
990
(F)
F1
F2
F3
F4
12-6h
13-6h
14-6h
15-6h
16-6h
17-6h
18-6h
19-6h
20-6h
21-6h
22-6h
Bozen
Bregenz

7 Uhr am Folgetag zu Ende geht. Am Rohrspitz dauert sie 17 Stunden mit Geschwindigkeiten bis 19,2 m/s. In Frastanz im Walgau werden Stundemittelwerte bis 11,2 m/s registriert. Das ungewöhnliche Ereignis führt zu einem Schaden am Waldbestand, an Gebäuden und kurzfristigen Verkehrssperren. Alle Talstationen zeigen um 14 und 19 Uhr Föhnbedingungen mit einem Grad von 60% an. Der Druckunterschied zwischen Bozen und Bregenz beträgt um 12 Uhr 15 hPa und um 18 Uhr 19 hPa, sodaß dieser Sturm noch dauern kann. Die Temperaturgradienten zwischen Säntis und Vaduz betragen -7,6 bis -9,0 Grad je 1000 Metern. Im talnahen Bereich zeigen die Temperaturgradienten schon fast isotherme Verhältnisse. Zum Morgentermin (7 Uhr) finden wir einen Wert von -7,4 Grad/1000m.

Die dritte Föhnperiode dauert vom 18. Dezember 10 Uhr MEZ bis zum Folgetag um 5 Uhr MEZ; somit 20 Stunden. Der kräftige Föhn im Rheintal und Walgau entsteht bei einem massivem Luftdruckunterschied, welcher 16 hPa zwischen Bozen und Bregenz um 12 Uhr beträgt. Die Windmessungen zeigen höhere Geschwindigkeiten zwischen 4,9 und 18 m/s als Stundenmittelwert an. Die beobachteten Zeiträume betragen 12 Stunden an den Stationen Rohrspitz, Lustenau und Frastanz. Versetzte und kürzere Perioden von 6 bis 8 Stunden werden in Dornbirn, Feldkirch, Thüringen und am Sulzberg festgestellt. Die topographischen Temperaturgradienten betragen für die drei Beobachtungstermine am größeren Profil Säntis & Vaduz cirka -7,8 Grad pro 1000m und am kleineren Profil Fraxern & Feldkirch -3,2 Grad/1000m (14 Uhr) und -6,8 Grad/1000m (19 Uhr). Die sieben Talstationen (siehe Abbildung 2) zeigen um 14 und 19 Uhr Föhn an. Im Illtal (Walgau und Montafon) kann der Föhn von Partenen über Vandans nach Bürs und weiter bis Feldkirch anhand von relativer Feuchte, Windrichtungen und Windstärken bestimmt werden. Die Indizes stehen bei 60% Föhn. Die beiden Hangstationen Fraxern und Laz melden den durchgebrochenen Föhn. Für die vier Bergstationen Langen am Arlberg, Obervermunt, Schröcken und Warth gilt ebenfalls ein höchster Föhnindex aus den drei Kenngrößen. Der Föhn endet im nördlichen Teil des Rheintales gegen 22 Uhr - auch am Sulzberg erlischt er zu diesem Zeitpunkt. In Thüringen endet die stürmische Periode um 5 Uhr mit Windgeschwindigkeiten von 8 m/s aus 240 Grad.

Die vierte Föhnperiode betrifft den Walgau, sowie den Raum Feldkirch mit Windgeschwindigkeiten bis 9,8 m/s. Sie dauert am 22. Dezember zehn Stunden und endet um 18 Uhr mit zwei Windstößen in Thüringen Die Druckdifferenz über die Alpen ist mit 12 hPa (12 UTC) etwas geringer. Die Gradienten der Temperatur betragen -8,6 Grad/1000m am größeren Profil. Zwischen Feldkirch und Fraxern ist zum Morgentermin eine massive Inversion (14 Grad/1000m) festzustellen, welche bis zu Mittag aufgelöst wird. Dann wird eine Temperaturgradient von -11,1 Grad/1000m gemessen. In den Morgenstunden zeigen nur die Klimastationen entlang der Ill den Föhn an. Zur Mittagszeit weisen bis auf Bregenz alle Talstationen ein bis drei Kenngrößen für Föhn auf.

3. LITERATUR

Hann J. (1857): Föhnwinde, Handbuch der Klimatologie, 1. Band, 332 - 351, Stuttgart.
Waibel K. (1984): Statistik des Föhns im Bodenseeraum im Vergleich mit dem Reusstal, Arbeitsbericht der Schweizerischen Meteorologischen Zentralanstalt, No. 118, Zürich.

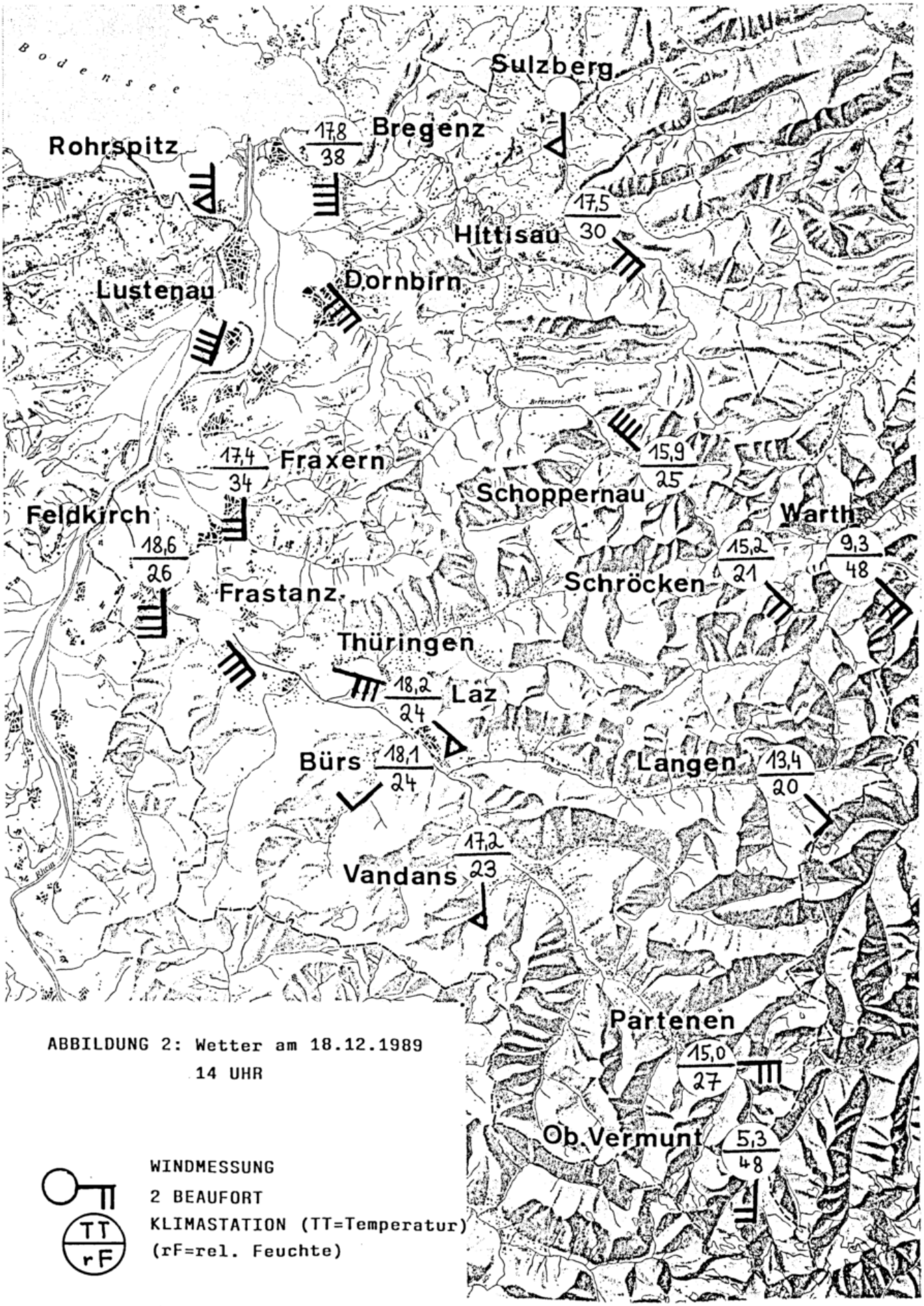

ABBILDUNG 2: Wetter am 18.12.1989
14 UHR

WINDMESSUNG
2 BEAUFORT
KLIMASTATION (TT=Temperatur)
(rF=rel. Feuchte)

On the relevance of wind measurements on mountain stations

Pöttschacher W. und R. Steinacker
Institut für Meteorologie und Geophysik, University of Vienna, Austria

The wind measurements on high Alpine mountain stations are compared with the windfield of ECMWF uninitializied analyses. It is investigated, if the measurements on some stations can be used to improve the wind field analyses e.g. at 700hPa.
In the present study, which will be soon published as a Diploma Thesis, the 7 stations: Säntis (06680), Jungfraujoch (06730), Corvatsch (06791), Zugspitze (10961), Sonnblick (11146), Kredarica (13008) and Plateau Rosa (16052) are investigated in detail.
Flow regime periods of 1992 are considered, which are lasting at least for two days. The data of the ECMWF analyses on pressure-levels are interpolated to isentropic levels using the method of Nickus and Vergeiner (1984). The observed wind is used as initial value for 6-hourly backward trajectories on that isentropic level which touches the corresponding mountain station. Trajectories are also computed with the kinematic (Pettersen, 1956) as well as with the dynamic method (Steinacker, 1984). Kinematic trajectories "lose" their memory about the initial value instantly, whereas dynamic trajectories keep it over the whole range of integration.

The difference between the two trajectories may be caused by several reasons:
1) Synoptic scale influence: Depending on the direction and the speed of the basic flow the trajectories show the influence of the Alps as a whole (flow over the obstacle on the meso alpha scale). This effect is already included in the analysed wind field of the ECMWF.
2) Flow blocking: The ECMWF orography is smoother than actual (Fig. 1), so that mountain top stations generally lie above the model (analysis) topography.

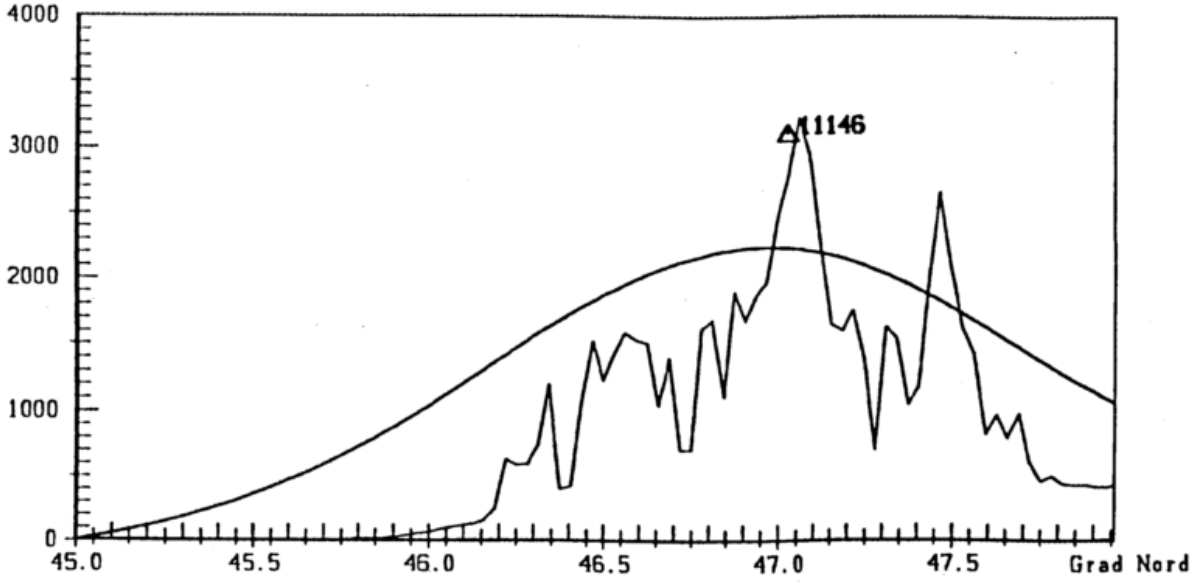

Fig. 1: N-S section at 12°57'E (longidude of Sonnblick). Bold is the orography of ECMWF (analysis) model, thin a high resolution orography by H. Volkert (1989).

Therefore it must be assumed that the blocking effect of single mountain ranges are underestimated in the analyzed wind field.
3) Surface friction: This effect tends to decelerate and deviate the flow, depending on the location of a mountain station with respect to the general flow direction (windward or leeward). Energy considerations (Bernoulli equation) help to identify this effect.

4) Local effects: The wind measurement on a mountain observatory is also influenced by the characteristics of the site (single steep mountain peak, e.g. Zugspitze, col, e.g. Jungfraujoch, or slope, e.g. Kredarica). This effect may be studied by a comparison of different directions of the basic flow and the corresponding channeling at the station.

First let us consider the mean of the observed wind, the analyzed wind (ECMWF analyses) and the geostrophic wind. The geostrophic wind is computed from the gradient of the Montgomery potential in the ECMWF analyses at the location of the corresponding station on the isentropic level which touches the station (used grid distance approx. 45km).

		OBSERVED WIND			ANALYZED WIND			GEOSTROPHIC WIND		
Stat. Nr.	ng	dd	ff	stead.	dd	ff	stead.	dd	ff	stead.
06680	32	279	3,7	0,69	334	8,1	0,88	331	15,1	0,97
06730	28	304	6,9	0,94	351	8,8	0,86	49	25,7	0,97
06791	46	17	4,5	0,89	344	10,4	0,94	41	15,1	0,96
10961	37	351	6,4	0,94	326	8,7	0,95	345	12	0,81
11146	41	340	6,3	0,84	319	13,4	0,96	48	14,5	0,92
13008	32	318	6,1	0,99	333	10	0,88	312	7,9	0,76
16052	43	1	11,5	0,85	350	10	0,89	22	23,7	0,95

Tab. 1: Mean of the observed wind, the analyzed wind and the geostrophic wind during northwesterly flow regimes. Stat. Nr. is the WMO-code of the station, ng the number of observations used. dd is the direction, ff the speed (m/s) and stead. the steadiness of the corresponding wind.

During northwesterly flow regimes most of the winds have a high steadynes due to the high velocity of the basic flow during these regimes. At Zugspitze there is no big difference between the windvectors. That seems to be reasonable, because Zugspitze is an isolated steep peak located north of the Alpine main ridge. On Corvatsch the situation is different during northwesterly flow regimes, because Corvatsch is a mountain peak with the much higher Berninamassiv in its vicinity. This can also be seen in Fig. 2 and 3.

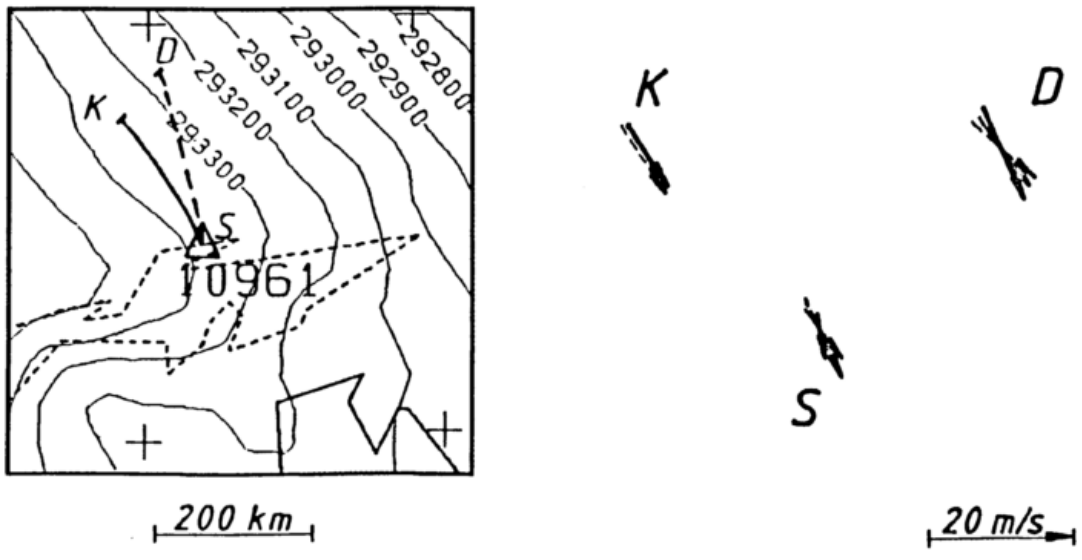

Fig. 2: Left: Mean Montgomery stream function M in m^2s^{-2} on the isentropic level which touches the station Zugspitze during northwesterly flow regimes (mean of 37 cases). The continuous line represents the kinematic, the dashed line the dynamic backward trajectory for 6 hours. Right: Mean wind vectors at the station (S), at the final (upstream) point of the kinematic (K) and the dynamic backward trajectory (D). The bold vector represents the observed wind at S, or the kinematically computed wind vector at K and the dynamically computed wind vector at D. The thin vector is the analyzed wind (ECMWF) and dashed the geostrophic wind.

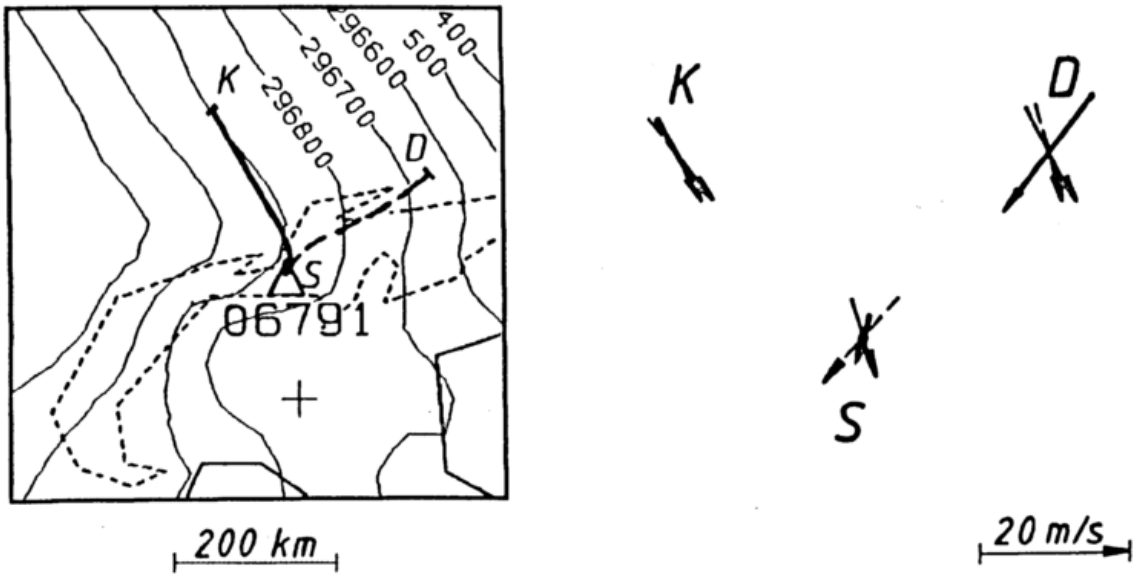

Fig. 3: Same as Fig. 2, but for Corvatsch (mean of 46 cases).

The synoptic scale influence on Zugspitze is dominant. This becomes evident by the small spatial difference between K and D and the small difference between the wind vectors at D. For northwesterly flow regimes the observed wind on Zugspitze is highly representative for the wind in the "free atmosphere", whereas the wind observed on Corvatsch is mainly determined by local influences. And therefore it shouldn't be used directly to refine wind field analyses.

On all stations the difference between the observed wind and the analyzed wind (ECMWF) depends on the direction of the general flow. This fact is documented in Fig. 4 and 5 where the situation on Sonnblick for northeasterly and southwesterly flow regimes is shown.

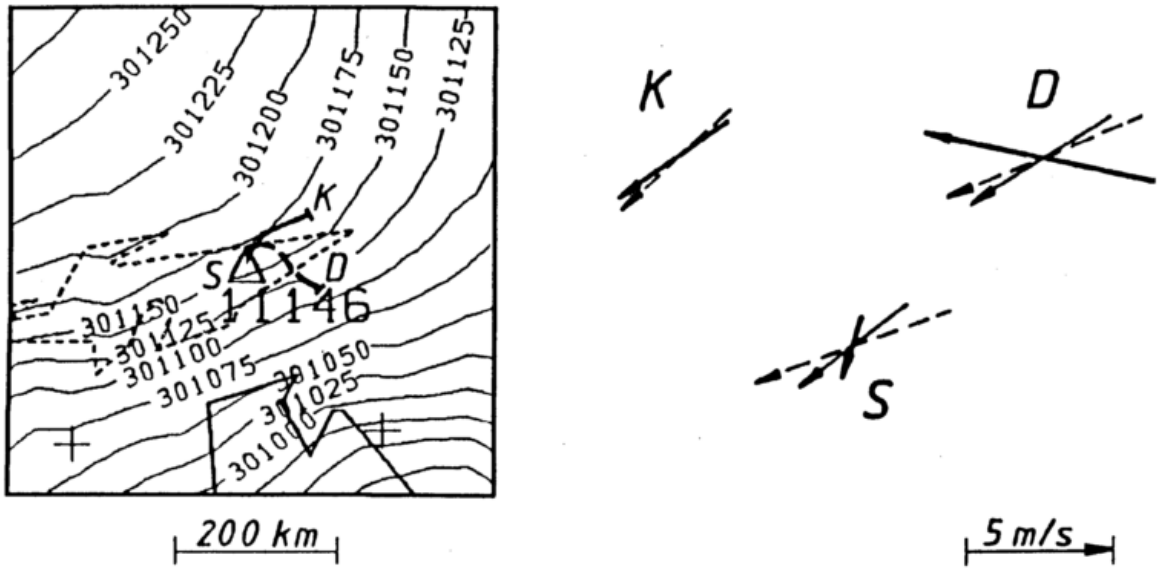

Fig. 4: Same as Fig. 2, but for Sonnblick and during northeasterly flow regimes (mean of 34 cases).

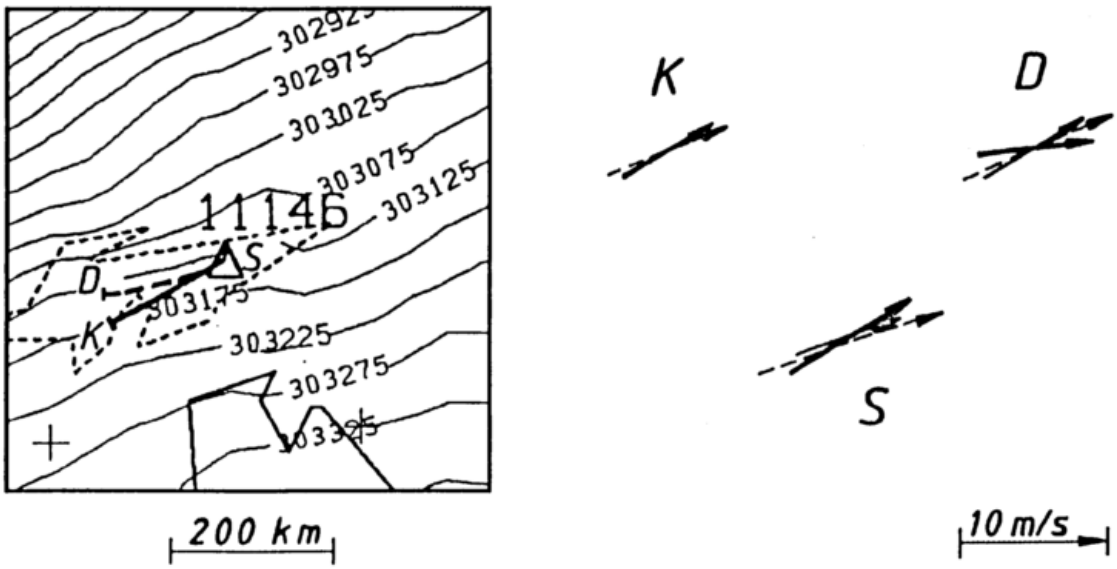

Fig.5: Same as Fig. 2, but for Sonnblick and during southwesterly flow regimes (mean of 32 cases).

In cases with northerly flow, the observed wind differs much stronger from the analyzed wind, as compared to a southerly flow regime. The northern slope of Sonnblick is very steep. This seems to influence the local flow characteristics much more than the smoother southern slope. That means, that the observed wind on Sonnblick can well be used to refine the wind field analyses during a southwest flow regime, whereas a direct use during a northerly flow regime is problematic.

REFERENCES:

Nickus U., I. Vergeiner, 1984: The thermal structure of the Inn valley atmosphere. Arch. Met. Geophys. Biocl. 33A, pp 199 - 215

Pettersen S., 1956: Weather analyses and Forecasting. Mc Graw Hill Book Company, pp 27 - 30

Steinacker R: ,1984: Airmass and frontal movement around the Alps. Riv. Met. Aer. 43, pp 85 - 93

Volkert H., 1989: An Alpine Orography Resolving Major Valleys and Massifs. Int. Conf.on Mount. Met. and Alpex, Garmisch Partenk., pp 148 - 150

Use of a Double Fence Intercomparison Reference in High Mountain Areas to correct Precipitation Measurements

Felix P. Blumer, Christian Maurer and Urs Steinegger
Swiss Federal Institute of Technology, Department of Geography, Hydrology Section,
Winterthurerstr. 190, 8057 Zurich

ABSTRACT

Precipitation measurements based on the gauging technique are influenced by wind-induced measurement losses. A variety of windshields and wind fences are used to reduce such effects. The Double Fence Intercomparison Reference (DFIR) is suggested by the WMO as a means to correct solid precipitation measurements. The DFIR consists of two octagonal fences with diameters of 4 m for the internal fence and 12 m for the external fence, respectively. In autumn 1991 the Department of Geography of the Swiss Federal Institute of Technology installed the first DFIR in the European Alps at the top of Gamserrugg (47°12'N/9°21'E; 2074 m a.s.l.). Intercomparison measurements between a Belfort gauge protected by the DFIR and an unprotected Belfort gauge showed a measurement increase of about 48% on average. Measurement differences between the two gauges increase with decreasing temperatures and increasing wind velocities. For velocities higher than 8 m/s, measurement differences decrease because in such cases the DFIR itself acts as an obstacle.

1. INTRODUCTION

Precipitation measurements based on the gauging technique are influenced by wind-induced measurement losses. For rainfall events, Sevruk (1986) gives values of 2 - 10% depending on the gauge exposure. In high mountain areas where the ratio of snow on the annual precipitation amount is very high, measurement losses are much higher. At well-protected observation sites, measurements of the water equivalent of the new snow are much better than the gauging technique (Martinec, 1986; Sevruk, 1983).

Measurements of the water equivalent are also not reliable at very exposed observation sites because the snow accumulation is disturbed by the wind influence.

For this reason precipitation gauges at exposed measurement sites in alpine regions are protected by windshields. Well known are the Nipher-, the Alter- and the Tretjakov- windshield. Another way to reduce the wind-induced measurement losses is by setting up special wind fences.

2. THE HISTORY OF THE DFIR

The first attempts to reduce the wind speed above precipitation gauges with the aid of wind fences were done by Shipchinsky (1921), reported by Golubev (1986). Previous attempts had been carried out by Orlov (1938) and Golubev, who developed and tested four different types of wind fences at the Valdai Branch of the USSR Hydrological Institute.

The first type was an octagonal vertical double fence (DFIR), inscribed into circles 4 m and 12 m in diameter. The inner fence was 2.0 m high and the outer one 2.5 m. The fences were made of wooden picket boards 1.5 m high and 0.05 m wide, with a gap between the vertical bars of 0.05 m. The distance between the ground and the bottom of the picket boards was 0.5 m for the inner fence and 1.0 m for the outer fence. A Tretjakov gauge was installed in the center of the fence with the orifice 2.0 m above ground.

The second type differed from the first one in terms of fence installation: the two fences were not vertical, but inclined at an angle of 15° away from the precipitation gauge.

Compared to the DFIR a third fence differed by the elevation of the fence. It was 1.0 m higher, i.e., the outer fence was 3.5 m high while the inner fence was 3.0 m high. The receiving surface was 3.0 m above ground.

The fourth variant differed from the first one by the dimensions of the circles into which the fences were inscribed: the outer fence was inscribed into a circle of 4 m in diameter, while the inner fence into a circle of 2 m in diameter.

The results from these four protected precipitation gauges were compared with the results from a gauge surrounded by bushes (Table 1).

Table 1: *Ratios of total precipitation measured by 4 Tretjakov gauges protected by different wind fences compared to a Tretjakov gauge surrounded by bushes (100%) (Golubev, 1986).*

Kind of protection	Elevation of the gauge	Jan.	Feb.	Mar.	Apr.	May	June	July	Aug.	Sep.	Oct.	Nov.	Dec.	Year
Vertical 1st type	2.0 m	0.92	0.96	0.94	0.96	0.94	0.96	0.99	0.96	0.94	0.97	0.94	0.96	0.95
Inclined 2nd type	2.0m	0.89	0.92	0.96	0.98	0.96	1.02	0.99	0.99	0.97	0.99	0.93	0.92	0.96
Vertical 3rd type	3.0 m	0.87	0.92	0.91	0.95	0.94	0.96	0.90	1.00	0.97	0.92	0.94	0.91	0.93
Vertical 4th type	2.0 m	0.85	0.91	0.88	0.89	0.98	0.95	0.95	0.93	0.93	0.92	0.85	0.88	0.91
Tretjakov unprot.	2.0 m	0.67	0.65	0.65	0.87	0.95	0.97	0.98	0.98	0.95	0.94	0.81	0.66	0.84
Tretjakov unprot.	3.0 m	0.48	0.46	0.56	0.72	0.92	0.98	0.93	0.92	0.94	0.89	0.70	0.53	0.75

For the whole year the best results (0.96) were produced by the inclined fence. During the winter season with a high ratio of solid precipitation, the measurement values of the 1st type (DFIR) are better. For this reason the WMO recommends this type for the Solid Precipitation Measurement Intercomparison program (WMO, 1985). In fact, there exist 19 DFIRs worldwide for this intercomparison program, but the station on Gamserrugg is the only one in the Alps.

3. THE OBSERVATION SITE

In autumn 1991 the Hydrology Section of the Swiss Federal Institute of Technology installed a DFIR (Fig. 2) on the top of Gamserrugg (47°12'N/9°21'E; 2074 m a.s.l.) (Fig. 1). A Belfort gauge was installed in the center of the DFIR so that these results could be compared with those from an unprotected Belfort gauge at a distance of only about 50 m, used in the project Precipitation Conditions in the Alps (Blumer & Lang, 1993, 1994).

Fig. 1: *Gamserrugg (47°12'N/ 9°21'E; 2074 m ü. M.) in the eastern part of the Swiss Alps viewed from Chäserrugg (J. Rinderknecht, 1. 1. 1992).*

Fig. 2: *The DFIR at the top of Gamserrugg. The inner fence is 4 m in diameter and 2.0 m high, the outer one is 12 m in diameter and 2.5 m high. The protected Belfort gauge on the Gamserrugg catches on average 48% more solid precipitation than an unshielded Belfort gauge.*

4. RESULTS

During the winter seasons 1991/92 and 1992/93, 56 precipitation events were compared with a total precipitation amount of 523 mm for the unshielded gauge and 776 mm (48.4%) for the DFIR protected Belfort gauge. Maurer (1993) shows that measurement differences between the two gauges increase with decreasing temperature. For precipitation events with wind velocities of less than 8 m/s there can also be found a general increase of measurement differences with increasing wind velocity. For events with higher wind velocities the DFIR acts as an obstacle and measurement differences between the two gauges get lower (Table 2). In Table 3 increasing differences can be found for decreasing precipitation intensities.

Table 2: *Measurement values of a DFIR protected Belfort gauge compared to an unprotected Belfort gauge (100%) dependent on temperature and wind velocity at the top of Gamserrugg.*

	wind velocity	$0 < u \leq 3.5$ (m/s)	$3.5 < u \leq 8.0$ (m/s)	$8.0 < u$ (m/s)	Total (m/s)
snow	Temp. < -1°C	153.4%	167.2%	156.3%	159.5%
snow/rain mixed	Temp. ≥ -1°C	123.3%	155.8%	129.7%	135.3%
		138.5%	162.6%	143.9%	148.4%

Table 3: *Measurement values of a DFIR protected Belfort gauge compared to an unprotected Belfort gauge (100%) dependent on temperature and precipitation intensity at the top of Gamserrugg.*

	precipitation intensity	$0 < I \leq 0.4$ (mm/h)	$0.4 < I \leq 0.9$ (mm/h)	$0.9 < I$ (mm/h)	Total (mm/h)
snow	Temp. < -1°C	165.6%	190.8%	140.4%	159.5%
snow/rain mixed	Temp. ≥ -1°C	160.0%	139.7%	125.6%	135.3%
		164.5%	157.7%	133.7%	148.4%

Only 6 of these 56 events show a higher value for the unshielded gauge. However, these are generally small events, where other measurement errors of the two gauges are greater than the influence of the DFIR. Compared to other intercomparison measurements (i.e., Goodison, 1978; Elomaa, 1988), the differences between the two gauges are low because of the relatively high temperatures and the generally intense precipitation events.

During the summer season measurement differences between the two gauges are normally less than 5%. Using the average of the DFIR of 48% for the winter season and a value of 10%, according to Sevruk (1986), for the summer season, the annual precipitation amount at the top of Gamserrugg increases from 1332 mm to 1627 mm in 1990 and from 1270 mm to 1548 mm in 1991.

5. ACKNOWLEDGEMENTS

The authors wish to thank the Wildhaus-Oberdorf-Gamsalp AG for support in field work, to the Bundesamt für Militärflugplätze (BAMF) and to the Kommando der Flieger- und Fliegerabwehrtruppen (KFLF) for transportation help by helicopter.

6. REFERENCES

Blumer, F. P. and H. Lang, 1993: Altitudinal dependence of precipitation in the eastern Swiss Alps. Precipitation Variability & Climate Change. B. Sevruk and M. Lapin (eds.). Proceedings of the International Symposium on Precipitation and Evaporation, Bratislava, 20. - 24. Sept. 1993, Vol. 2, 141 - 146.

Blumer, F. P. and H. Lang, 1994: Spatial differences of precipitation in the Eastern Swiss Alps. 23. Internat. Tagung für Alpine Meteorologie, in this volume.

Elomaa, E., 1988: Solid precipitation measurement intercomparison. Final Report of the Third Session, WMO, Geneva, 12 p and appendicies.

Golubev, V. S., 1986: On the problem of standard conditions for precipitation gauge installation. ETH/IAHS/WMO Workshop on the Correction of Precipitation Measurements. Zurich, 1. - 3. April 1985, B. Sevruk (ed.), Zürcher Geographische Schriften, 23, 57 - 59.

Goodison, B. E., 1978: Canadian snow gauge measurement, accuracy implications, alternatives, needs. Water Stud. Inst., Saskatoon, Saskatchewan. 7 - 15.

Martinec, J., 1986: Correction of winter precipitation data, by computed snow accumulation. Correction of Precipitation Measurements. ETH/IAHS/WMO Workshop on the Correction of Precipitation Measurements. Zurich, 1. - 3. April 1985, B. Sevruk (ed.), Zürcher Geographische Schriften, 23, 67- 72.

Maurer, Ch., 1993: Der Winterniederschlag auf dem Gamserrugg. Diplomarbeit am Geographischen Institut der ETH Zürich, 77 p. (unpublished).

Orlov, G. I., 1938: Rezultaty ispytaniy dozhdemerov raznogo ustroistva v raznykh usloviakh (Test result of different rain gauges under various conditions). Trans Voyekov Main Geophys. Observ., GGO, 21, 39 - 50.

Sevruk, B., 1983: Correction of measured precipitation in the alps using the water equivalent of new snow. Nordic Hydrology, 14(2), 49 - 58.

Sevruk, B., 1986: Correction of precipitation measurements: Summary report. ETH/IAHS/WMO Workshop on the Correction of Precipitation Measurements. Zurich, 1. - 3. April 1985, B. Sevruk (ed.), Zürcher Geographische Schriften, 23, 13 - 23.

Shipchinsky, A., 1921: Vlianie zabornoi zashchity na pokazania dozhdemera (Fence protection effects on rain gauge readings). Meteorologicheskiy vestnik, N 1 - 2, 21 - 32.

WMO, 1985: International Organization Committee for WMO Solid Precipitation Measurement Intercomparison, Norrkoping, 8p and some appendicies.

THE WIND EFFECT ON RAIN MEASUREMENT: THEORETICAL APPROACH

Vladislav NESPOR

Swiss Federal Institute of Technology

The wind-induced error of precipitation measurement is estimated using a procedure which is based on (i) three-dimensional numerical simulation of the flow, and (ii) computation of particle trajectories and determination of the error from relative areal densities of drops. The results are verified in wind tunnel.

The flow around a gauge is simulated numerically using PHOENICS, a general software for computational fluid dynamics. The three-dimensional flow is considered to be symmetrical with the vertical plane of symmetry parallel to the flow and going through the centre of the gauge. Computations were done in cylindrical coordinates.

The wind field is computed for different wind velocities and then used for determination of trajectories of water drops of various size. The change of the drop position in the wind field is computed from the balance of forces acting on it. Drag coefficient is evaluated from the terminal velocity of a water drop of the particular diameter falling in the stagnant air. Relative areal densities of rain drops in the horizontal plane level with the gauge orifice are determined by computation of drop trajectories starting from nodes of a horizontal rectangular grid above the gauge. This relative areal densities depend strongly on the drop diameter and they tend to be lower in the windward and higher in the lee of the gauge. With decreasing size, drops follow the air stream more closely which results in formation of an area with zero relative density on the windward edge of the gauge orifice. With further decreasing diameter this area extends over the whole orifice causing zero efficiency of the gauge. The estimated wind-induced error of the gauge is plotted as a function of wind velocity and drop size. If the type of drop size distribution, the rain intensity and the wind speed are known, the wind-induced error of the gauge can be directly estimated. The procedure is applied to various types of rain drop spectra and different types of precipitation gauges.

The results from flow simulation are compared with similar measurements in a wind tunnel. In both cases contour lines of normalized magnitude of velocity plotted in the vertical plane of symmetry show similar pattern. Also normalized vertical velocity profiles above the centre of the gauge based on measurements and flow simulation, respectively, agree well. Finally, the resulting estimates of wind-induced error are compared with previous studies.

The Effect of Systematic Error of Precipitation Measurement on Vertical Gradients of Precipitation in Switzerland

Boris Sevruk, and Luba Zahlavova

Department of Geography, Swiss Federal Institute of Technology, ETH Zurich
Slovak Technical University, Bratislava

The spatial distribution of vertical gradients in the mean annual and seasonal precipitation, 1951-1980, in Switzerland indicates a regional pattern. Moreover, there was an influence of altitude indicating smallest gradients in the lower reaches and increasing gradients in the middle reaches, up to 1500-2000 m a.s.l., and large gradients in the high alpine regions, mainly in the South. The difference can be very large as shown, for example, in the Grisons (Graubünden): The gradient below 1500 m a.s.l. is 14 mm per 100 m and above 1500 m a.s.l. the gradient is 110 mm per 100 m. In the Valais (Wallis), the respective gradients are 11 and 161 mm per 100 m. However, over the range of all altitude zones, the gradients for these two regions were 44 and 93 mm per 100 m, respectively. Below 700-800 m a.s.l., the spatial variability of precipitation in some regions does not seem to depend on altitude at all, and the gradients are very small or even negative. In addition, there is also a difference between the seasonal values of gradients. Over a large part of the Swiss territory the winter gradients generally exceed the summer ones by approximately 30%.

The analysis was based on data from 340 Swiss stations uniformly covering the entire territory of Switzerland including the Alps, up to 4000 m a.s.l. The data were first corrected for the systematic error of precipitation measurements due to wind and wetting using the special algorithms developed for this aim at the ETH. The main variables are monthly wind speed, temperature, the fraction of snow in the total precipitation, the number of days with precipitation and the degree of gauge site exposure. Some of the variables increase with altitude. This is reflected also by the increase of corrections with altitude. Then the data were subdivided into eleven groups according to the climate regions and large river basins, and fitted by means of linear regression analysis. In the case of gradients appearing to be non-linear, the data in a particular group were additionally subdivided according to altitude zones, and fitted separately for each zone by linear regression. An example of the summer season from April to September and the winter season from October to March from the region of Valais (Wallis) in the south-western part of Switzerland is shown in Table 1. Here, the altitude dependent differences are very large not only between the gradients but also between the correlation coefficients (R^2). Both variables increase considerably in the upper reaches of Valais as is shown in the plot of winter precipitation totals against altitude in Figure 1, on the top.

The corrected gradients were roughly 30 % greater than those based on non-corrected precipitation data. The difference varied according to region, season and altitude, and was largest in the winter season in the regions with the smallest gradients. Plots of corrected and non-corrected precipitation data against altitude with the respective gradients are compared in Figure 1.

Table 1 The seasonal vertical gradients, intercepts and R^2 values as subdivided according to altitude zones in the region of Valais, 1951-1980.

Range of altitude (m a. s. l.)	Summer season Gradient (mm)*	Intercept (mm)	R^2	Winter season** Gradient (mm)*	Intercept (mm)	R^2	Number of stations
350-2000	4.3	462	0.00	4.7	447	0.00	21
1500-3400	72.5	-761	0.97	88.4	-1012	0.89	11
350-3400	41.8	62	0.73	50.8	8	0.73	28

* mm per 100 m ** see also upper diagram in Figure 1

For the purpose of comparing of regional gradients, an average, linear gradient over the whole range of altitude zones of a particular region was used. Such gradients are compared in Table 2. They are ordered from the largest to the smallest values. The range of the average regional and river basin gradients in annual precipitation was from 15 to 160 mm/100 m, but over two-thirds of the Swiss territory including a great part of the Alps, they varied between 80 and 90 mm/100 m as seen from Table 2 (cfr. Midland, Central and West Switzerland, Valais, Zurich and Prealps).

Table 2 Regional gradients and differences between the gradients as computed from corrected and non-corrected precipitation data subdivided according to season, 1951-1980.

Region	Range of altitude (m a. s. l.)	Year Gradient (mm)*	Difference (mm)	(%)	Summer Gradient (mm)*	Difference (mm)	(%)	Winter Gradient (mm)*	Difference (mm)	(%)
East Switzerland	400-1100	158	9	6	98	3	3	60	6	11
Valais	300-3800	93	24	35	42	6	16	51	18	56
Zurich	400-1200	90	22	32	39	5	15	51	17	49
Midland	300-1500	87	12	16	37	3	7	50	9	22
Central Switzerl.	400-1800	88	14	19	40	5	13	48	9	24
West Switzerland	400-1700	82	15	22	44	4	10	38	11	37
Prealps	400-3300	80	17	27	32	7	25	48	13	38
North Switzerl.	250- 900	65	9	16	34	2	6	31	7	29
Grisons	400-2500	44	10	32	23	3	16	21	7	52
Ticino	200-2100	23	15	190	2	5		21	10	93
Engadin	990-2400	15	5	45	8	2	20	7	3	94

* gradient based on corrected precipitation data, in mm per 100 m

The greatest variability of gradients was obtained in the eastern half of Switzerland, in the regions near the Austrian borders. The maximum occured in the East Switzerland, in an area below Lake Constance, dominated by a relatively small and isolated massif, the Säntis, open on all sides, and the minimum occured in Ticino (Tessin) with very high precipitation, and in the southern part of Grisons (Engadine). Smaller values were also found in the external North, in a region along the German border and Lake Constance. In contrast, in the western half of Switzerland and along the

line Geneva - Zurich and Sion - Zurich, across the Alps, the variability of regional gradients was generally very small, from 80 mm per 100 m above the Lake Geneva and the southern part of the Jura, to 90 mm per 100 m in the Valais and Central Switzerland up to the region of Lake Zurich.

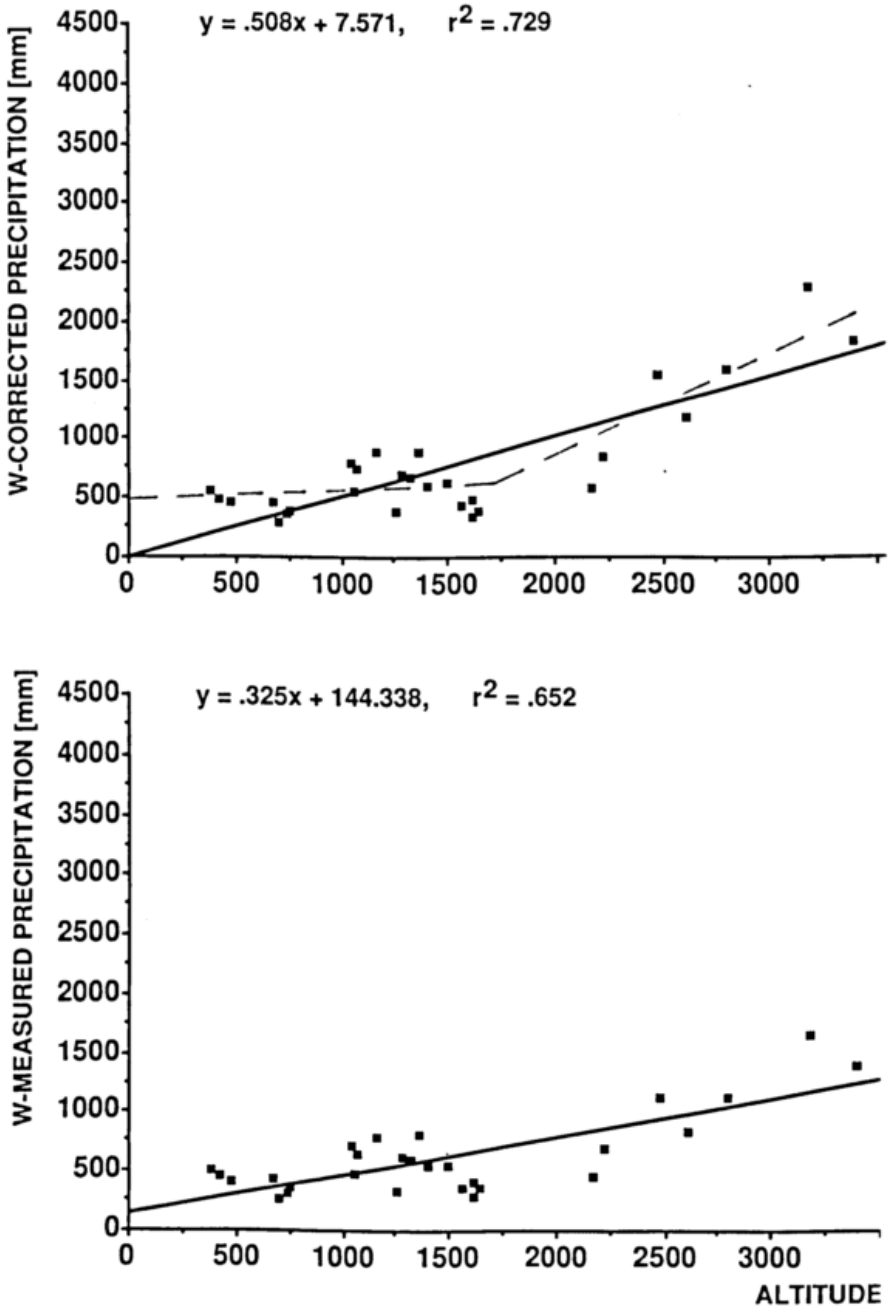

Fig. 1 Plot of corrected (top) and non-corrected (bottom) winter season precipitation totals against altitude. Region of Valais.
Dashed line indicates gradients for different altitude zones. (Cfr. Tab. 1).

The scatter in Figure 1 indicates that the variability of gradients within a region can be large. For instance, in the humid region of Ticino, which is a rather special one with a small regional, annual gradient of 23 mm/100 m, the gradient varies between -12 mm/100 m in the north-eastern part (5 gauges), 24 mm/100 m in the north-western part (6 gauges) and 44 mm/100 m in the southern part (9 gauges). Curiously enough, merging the two northern regions with a total of 11 gauges, results in

a gradient of 36 mm/100 m. However, when the north-western or north-eastern region is merged with the southern region, the gradients amount to 14 or -14 mm/100 m, respectively.

To understand this phenomenon, it is important to know, that in addition to the scaling problem, the gradients in smaller basins or a group of basins depend not only on the region and altitude, but primarily on the inclination and aspect of a particular basin to moisture-bearing air masses. In addition, there are also precipitation network specific variables such as the siting, number and representativeness of gauge sites which have not sufficiently been accounted for in the present study. Since the precipitation data used have been corrected for the systematic error of precipitation measurement, and by extention, the effect of gauge site exposure can be assumed to have been eliminated, at least to some extent, the physiographical characteristics of gauge site locations can be considered the crucial factor for the accuracy of gradient estimate. The gradient can be different for a sample of gauges, all situated in the valley or on the windward or leeward slopes.

In a case where there is a sample consisting of a few gauges in the lower reaches of a basin and only one gauge in the upper reaches, the gradient estimate depends essentially on the location of the upper gauge (slopes, valley) and can deviate considerably from "the true gradient". Similarly, in a sample of several gauges, the gradient estimate depends to a great extent on the deviation of only one gauge from the regression line or on the elimination - for whatever reason - from the sample of another gauge. In both of the above-mentioned cases, the regional gradient based on a large number of gauges proves more representative and samewhat helpful for evaluating the local gradient.

The square of correlation coefficient, R^2 , seems to depend on the gradient magnitude and varies from 0.7 to 0.9 for the larger gradients as obtained in the West, Midland and East, representing approximately 70 % of the Swiss territory, and from 0 to 0.5 for smaller ones in the Ticino, Grisons and the North. Generally, higher R^2 values have been obtained for corrected precipitation data than for non-corrected ones. Deviations from the regional regression line of point precipitation values at the same altitude amounted to +/-25 %. This is why, in some smaller sub-regions or basins with an altitude difference of a few hundred meters, the gradient can appear either to be very large, or even negative (Fig. 1). It is interesting to note the extremely large variability of regional values of intercept ranging from 70 mm in the relatively dry region of Valais, to 1711 mm in the very humid region of Ticino.

The study shows that (i) the altitude appears to explain a considerable portion of spatial variability of precipitation over a large part of the Swiss territory, (ii) that the vertical gradient in seasonal and annual precipitation totals shows regional pattern, (iii) that the gradient is in general not linear and varies according to altitude and season and (iv) that the application of corrections of systematic error of precipitation measurement for the studies of vertical gradients in precipitation totals in mountainous areas is needed.

Acknowledgement: This study was sponsored by the Swiss National Hydrological Service in Bern. The authors would like to express their thanks to Dr. W. Kirchhofer from the Swiss Meteorological Institute in Zurich who provided the data set used in the study.

The Influence of the orography on precipitation seen by the Swiss radars

E. Held and J. Joss

Swiss Meteorological Institute, Osservatorio Ticinese, CH-6600 Locarno-Monti

Abstract

To what extent can the influence of the orography on precipitation be detected in radar data? The low spatial resolution of the rain gauges often makes it difficult to study the impact of the orography. Here the radar with its spatial resolution of 2km holds promise. The relative contributions of the orography (the Alps) and variables describing the weather situation (e.g. the wind) to the spatial variation of the rain amount estimated by the radar are calculated. Before correlating, a correction of the rain amount for the vertical profile of reflectivity combined with reduced visibility is made (caused by geometrical shielding by mountains and the earth curvature). This adjustment is optimized using an independent data set of over 400 rain gauges at ground level.

1. The aim

In the project NOWRAD (NOWcasting of precipitation by RAdar) in the Swiss program NFP-31 (Joss 1992) the use of radar to understand and forecast heavy rain is addressed. Here we will make a step towards answering the first two of following questions rose in this project:

1.1. What corrections should be applied to radar data before studying the orographic influence on precipitation?

1.2. Can we confirm (quantify?) the relations between orography and precipitation with radar data, such as a height dependence of the rain amount (Blumer and Spiess, 1990) and Luv/Lee-effects? Can radar data lead to a similar precipitation distribution as shown on precipitation maps e.g. on the "Niederschlagskarte der Schweiz" (Kirchhofer and Sevruk, 1992)? Can we use the radar data to explain e.g. distributions of heavy precipitation in Southern Switzerland (as presented by Spinedi,1992)?

1.3. Where are the possibilities and limitations of the radar as an instrument for nowcasting in an orographically complex area?

2. Corrections applied to the radar data

To illustrate the corrections applied to the radar data, we look at a period of 48 hours during 7/8 July 1990 (Fig. 1). This period was characterized by a strong cyclonic northwest flow and caused precipitation up to 80mm in the NE of Switzerland. Western Switzerland received little, the South almost no rain. If we try to use the original uncorrected data we obtain very modest results. The linear correlation coefficient $c_{R,G}$ between the original radar-estimated rain and the data of the rain gauges is 0.47.

There are several reasons for this low correlation coefficient: the influence of the bright band, clutter echoes and shielding effects reducing the visibility of precipitation significantly (Joss and Pittini, 1991). To reduce the influence of the bright band, a correction has been applied, eliminating concentric structures around the radar at Albis. With these changes $c_{R,G}$ rose to 0.54.

Clutter echoes of ground targets also cause a loss of information: at the location where they occur blank holes are left (no data, reduced visibility). To correct for reduced visibility, the vertical profile of the reflectivity $r(h)$ is estimated: knowing the lower limit of the height h of the measurement of the radar echo (height of visibility), we can extrapolate the estimated rain rate to the ground. Correlation of the radar data with more than 400 gauges in Switzerland (daily amounts) as an independent dataset is used for optimizing this profile (Fig.2). The highest correlation coefficient between radar and gauges defines the "best" profile $r(h)$ marked with the asterisk in Fig. 2. As a result we chose a mean gradient of -40%/km and the correlation rose to $c_{R,G} = 0.61$.

As a third treatment, the radar data was smoothed (i.e. every pixel was substituted by the medium value of the surrounding pixels). Smoothing not only reduces the clutter problem, but also eliminates small scale structures (often artifacts). Again the highest correlation coefficient between radar and gauges is used as a criterion to find the optimal smoothing area (Fig.3). This size of smoothing may be an indication for the area of influence of the orography on precipitation. After correcting for the influence of the bright band, for visibility and after smoothing over $(40km)^2$, our correlation coefficient $c_{R,G}$ for the comparison of radar and rain gauge data rose

from initially 0.47 up to 0.74.

Fig. 2

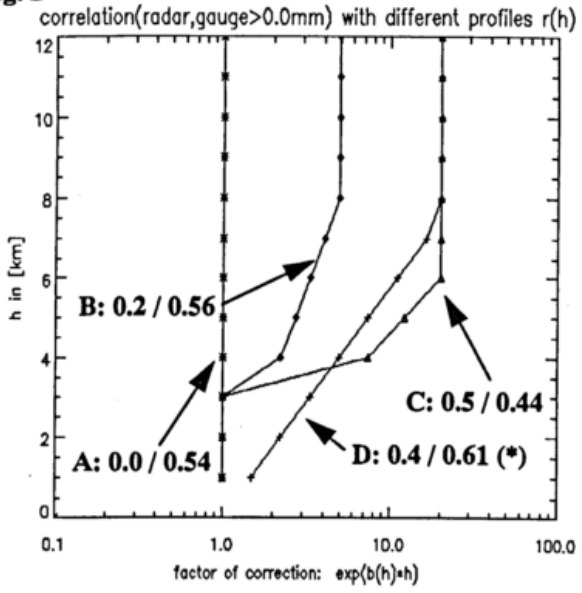

Fig. 3

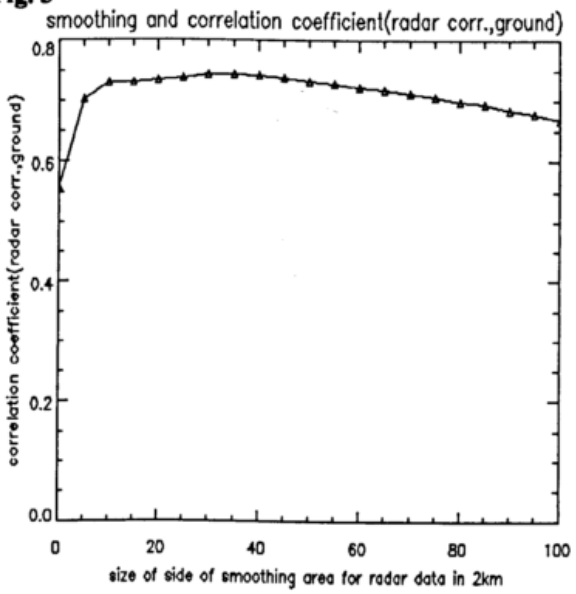

*Fig. 2: The dependency of the correlation coefficient from different profiles. The first number stands for b in the segment, where exp(b*h) is not constant, the second for the linear correlation coefficient, obtained with radar data (corrected with the corresponding profile) and over 400 rain gauges. Factors were limited to 20, visibilities to 8km. Because the maximum projection of the archived Swiss radar data was used, the profiles A, B and C are without a correction below the bright band (here 3km). D is the "best" profile with a decrease of the reflectivity of 40%/km. The corrected radar data (using profile D) yields a linear correlation coefficient with the rain gauge data of $c_{R,G}$=0.61.*

*Fig. 3: The influence of smoothing on the correlation between radar and gauge. The best correlation between the radar data (corrected with profile *) and rain gauge data is found with a smoothing area of (35[2km])^2. To avoid unnecessary loss of information by smoothing, only (20[2km])^2 were chosen leading to a $c_{R,G}$=0.74, see Figures 4 to 6.*

3. An approach to quantify relations between precipitation and orography

To answer the second question a multiple regression was applied, allowing to quantify the variance of the rain distribution correlated to the orography:

$$P_R = k_0 + k_1 \cdot height + k_2 \cdot V_{vertical} \qquad (1)$$

For eq. (1) we need 3 parameters: the corrected precipitation seen by radar (P_R in [mm]) as dependent variable, the absolute height (*height* in meters above sea level) and the vertical windspeed ($V_{vertical}$ in m/s) as independent variables. The latter is found by a vector multiplication of the ground gradient with the horizontal wind. This results in a vertical wind speed, a scalar quantity. It is a fictitious component of the wind at the surface along the slope of the hill. The wind for the vector multiplication is gained from radio soundings and is hoped to represent the wind of the entire area of investigation. This procedure is a rough first step. In future we will try to add further variables, e.g. windspeed and direction and humidity of the Swiss High Resolution Model (gridsize 15km).

In addition to k_0, k_1 and k_2, eq. (1) gives two results: the multiple correlation coefficient m_{cc}^2 and the relative error s_r. The latter is defined in eq. (2):

$$s_r = \frac{\sqrt{(1 - m_{cc}^2) \cdot var(P_R)}}{avg(P_R)} \qquad (2)$$

m_{cc}^2 indicates how much of the variance of the radar reflectivity is explained by the variation of *height* and $V_{vertical}$. The residual root mean square s_r describes the width within which the rain can vary without being explained by either of the two independent variables (containing 68% of the points of a normal distribution). The area of investigation is the marked square (in Fig. 1 - 4) and all the following statements are related to these (200x160)km^2.

Fig. 1 7./8. July 1990, original rain in [mm]

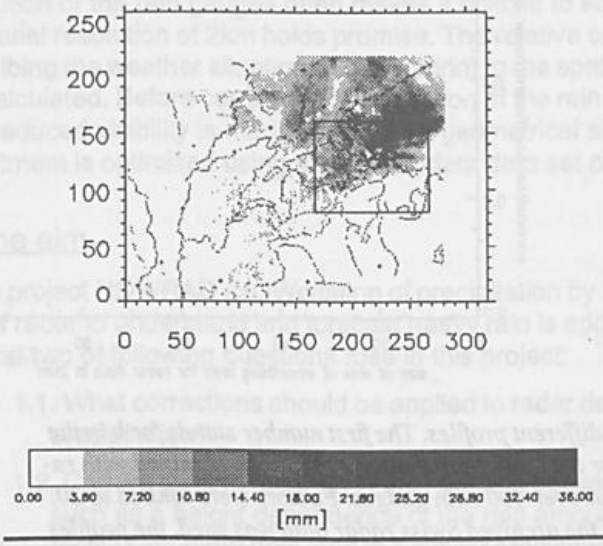

Fig. 4 7./8. July 1990, corrected and smoothed rain

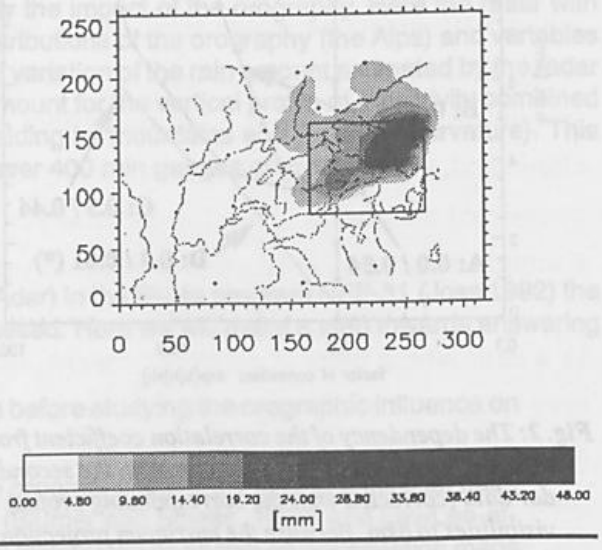

Fig. 5 Smoothed topography in [m AMSL]

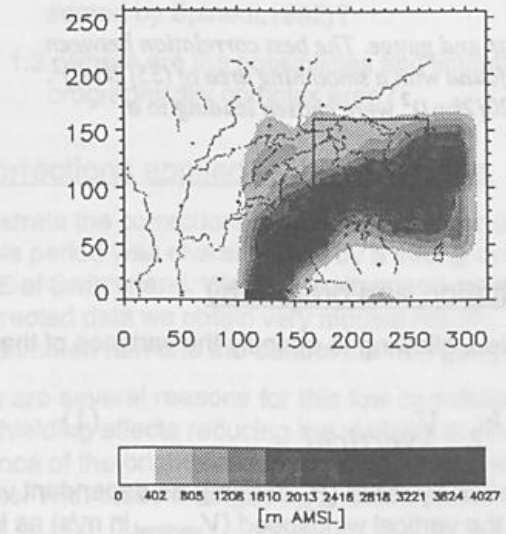

Fig. 6 Smoothed vertical velocity in [0.01m/s]

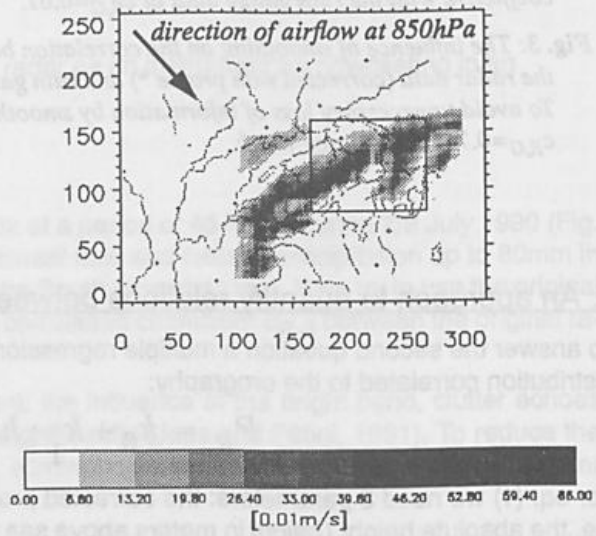

Fig. 1: *The original radar rain accumulated over 48h of 7/8 July 1990. The square indicates the area of data analyses, "holes" in the data are caused by the elimination process of clutter echoes, radial sectors by reduced visibility and the influence of the bright band is reflected in concentric bands of enhanced reflectivity.*

Fig. 4: *Same as Fig.1, but corrected for bright band, vertical profile * in Fig.3 and smoothed over an area of (20[2km])^2, resulting in the elimination of some of the small scale structure of Fig. 1. This corrected radar rain yields the highest correlation with the gauges ($c^2_{R,G}=0.74^2=0.55$).*

Fig. 5 + 6: *Smoothed orography and smoothed vertical windspeed at a wind direction of 315° (NW). With these two independent sets of data we can explain 47% of the variance in Fig. 4.*

The gradient of the orography explains 30%, the absolute height 17% of the variance of the rain. The remaining unexplained relative variation e_r is 54%: i.e. rain amounts vary 54% without being explained by eq. (1). The values for the coefficients in eq. (1) tell us that an increasing of the height of the terrain by 1km results in 3mm less rain (k_1=-3.2mm/km). If the air is lifted by $V_{vertical}$ equal 0.1m/s we expect 2mm more rain (k_2=22.4mm/m/s). The negative correlation between P_R and *height* is probably caused by the choice of the area of investigation and reflects the fact that the maximum precipitation did not coincide with the highest part of the Alps (Fig. 4)

variable	average	standard deviation
P_R	8.4mm	6.3mm
height	1705m	805m
V_v	0.15m/s	0.15m/s

Tab.1: Average values and standard deviations of the variables used for the multiple regression. Applying eq. (1) to the modified radar data (P_R in Fig. 4), we can explain 47% (= m_{cc}^2) of the variance in the radar image with the two independent variables (the smoothed height in Fig. 5 and the smoothed $V_{vertical}$ in Fig. 6).

4. Conclusions

In our example we can explain almost half of the variance (spatial distribution) of the rain with the orography. The unexplained part is caused by other effects like variation of air masses and non meteorological influences, such as reduced visibility, clutter etc. which have not been eliminated.

The study also shows the importance of the correction with the vertical profile *r(h)* and the influence of smoothing. The orography bears twofold influence: on real precipitation and on the amount measured by radar, an artifact. This latter one is a consequence of clutter (more echoes) and shielding (reduced visibility, less echoes). This twofold influence causes of a lot of complications and sometimes confusion, which may explain why little operational use of radar was made so far for precipitation measurement and flood forecasting. Therefore we should not extend the range of analyses beyond good visibility (e.g. the precipitation should be seen at least down to 4km and the distance from the radar station should not exceed 150km).

References

Blumer F. and R. Spiess, 1990: Investigation on Altitudinal Dependence of Precipitation in the Swiss Alps, in: Tagungsbericht zur 21. Internationalen Tagung für Alpine Meteorologie, Engelberg, September 1990, pp 415-418

Joss J. and A. Pittini, 1991: Real-Time Estimation of the Vertical Profile of Radar Reflectivity to Improve the Measurement of Precipitation in an Alpine Region, J. of Meteorology and Atmospheric Physics 47, pp 61-72

Joss J., 1992: Projekt NOWRAD (NOWCASTING von Niederschlägen mittels RADar für Kurzfrist- und Abfluß-prognosen des NFP 31, Klimaänderungen und Naturkatastrophen)

Kirchhofer W. and B. Sevruk, 1992: Mittlere jährliche korrigierte Niederschlagshöhen 1951 - 1980. Hydrologischer Atlas der Schweiz, Tafel 2.2.

Spinedi F.,1992: Synoptical Analysis of the Events of Heavy Precipitation on the Southern Slope of the Swiss Alps, 1961-1990, ICS/ICTP/WMO International Workshop on Mediterranean Cyclones Studies, Trieste, Italy, May 1992

An investigation on the growth and decay of radar echoes in alpine regions

L. Li and W. Schmid
Atmospheric Physics, ETH
CH-8093, Zuerich
Switzerland

1. Introduction

It is well known that the distribution of precipitation patterns in alpine regions is strongly associated with the local topography. This phenomenon has been investigated by many researchers with the help of ground measurements of precipitation and numerical model simulations. Bernath (1992), for instance, used the data from a network of 28 raingauges to study the distribution of precipitation and its dependence on altitude in an alpine basin near Gletsch. The results showed that the variability of the distribution of precipitation in summer is significant, whereas in winter the distribution of snow showed a strong precipitation-altitude relationship. Giorgi et al. (1990) used a Limited-Area Model nested in a General Circulation Model for regional climate simulations over Europe. They examined the frequencies of precipitation events over 10 simulated Januaries. The model results revealed frequency maxima over the alpine regions, and the frequencies decreased over the Mediterranean basin and southeastern Europe. More recently, Widmann and Schaer (1994) analysed the distribution of precipitation by means of principal component analysis. This study is based on the daily precipitation measurements from 300 Swiss ground stations over thirty years. One important result is the strong relation between the dominant empirical orthogonal functions, i.e. the dominant spatial precipitation patterns, and topography.

Kuo and Orville (1973) studied the climatology of convective clouds in the Black Hills regions (Rapid City, United States) using weather radar. They investigated the annual echo frequencies in relation to the local orography. The strong orographic control of the maximum cloud development was found to appear downwind of the mountain peaks. However, similar work using radar data in alpine regions has been rarely done up to now. The existence of a correlation between enhanced radar echoes and topography is helpful to understand the distribution of growing and decaying radar patterns and, hence, to enhance the prediction of the future coverage of radar echoes. Such a study may also provide an additional dataset for the verification of regional numerical prediction models. An important premise of such an expectation, however, is an analysis method that permits the identification of the growth and decay of small scale radar patterns. The internal motion vectors of radar patterns provide the basis for the quantitative identification of small scale development and dissipation of radar echo patterns over the period of echo tracking.

In this contribution, an objective analysis method to obtain the growth and decay patterns within radar echoes is presented. The proposed method is an extension of TREC (TREC = Tracking Radar Echoes by Correlation, Rinehart 1978). Radar data for this analysis are available from projects "Winterregen" and from special rain measurements during July 1993. A statistical analysis of the growth and decay patterns of radar echoes is presented that can be related to orography.

2. Methods

a) COTREC method

The internal motion of small scale radar patterns can be obtained with the TREC method first described by Rinehart and Garvey (1978). The TREC technique computes translation vectors of small partitions of radar echo patterns that were observed twice within a short time interval. However, the TREC-vectors often show an inconsistent and noisy behavior that is mainly due 1) to ground clutter and shielding effects and 2) to failures in tracking radar echo patterns (Rinehart 1981). An objective method, referred to as COTREC (CONtinuity of TREC-vectors), is proposed

with the motivation to correct the erroneous TREC-vectors and to isolate the divergent-free component of the TREC-vector fields. This is needed for identification of the growth and decay patterns within radar echoes. A variational method that considers continuity for the retrieved motion field as a constraint is used for this purpose. For more details about this method we refer to Li et al. (1994).

The method to obtain the patterns of echo growth and decay is straightforward: one calculates the difference in mean radar reflectivity between a box of the second scan and the corresponding box of the first scan. The location of the box of the second scan is determined by the given field of the COTREC motion vectors. This procedure is repeated for each box of the first scan. Areas of positive values for the calculated difference represent regions of echo growth, while areas of negative values indicate regions of echo decay. In contrast to the approach used in Kou et al., the COTREC method gives the growth and decay patterns of radar echoes instead of the frequencies of occurrences of radar patterns. It is believed that the distribution of the growth and decay patterns within radar echoes are directly connected to local orography.

b) Example for the determination of echo growth and decay

Here, we will present an example to show the growth and decay of radar echoes. A precipitation event that occurred in the early morning of 11 March 1992 was selected for this analysis. The precipitation was caused by a cold front that passed over Switzerland within a westerly wind field (20 m s^{-1} approx.) in the free atmosphere. The temperature at the Rigi mountain (1620 m MSL) dropped from 3° to 0° between 0130 and 0230 UTC. Widespread precipitation with embedded convection was mainly observed in the hours after the frontal passage at the ground. Doppler radar data were collected at 10 min intervals. PPI-scans were taken at an elevation angle of 1.5°. The time interval between two consecutive PPI scans was lowered to 2 min at specific periods for application of COTREC. The COTREC method was applied to the PPI-scans taken at 0330 and 0332 UTC, 0340 and 0342UTC, ..., 0430 and 0432UTC. A box size of 16 km was defined and a grid spacing of 10 km was selected.

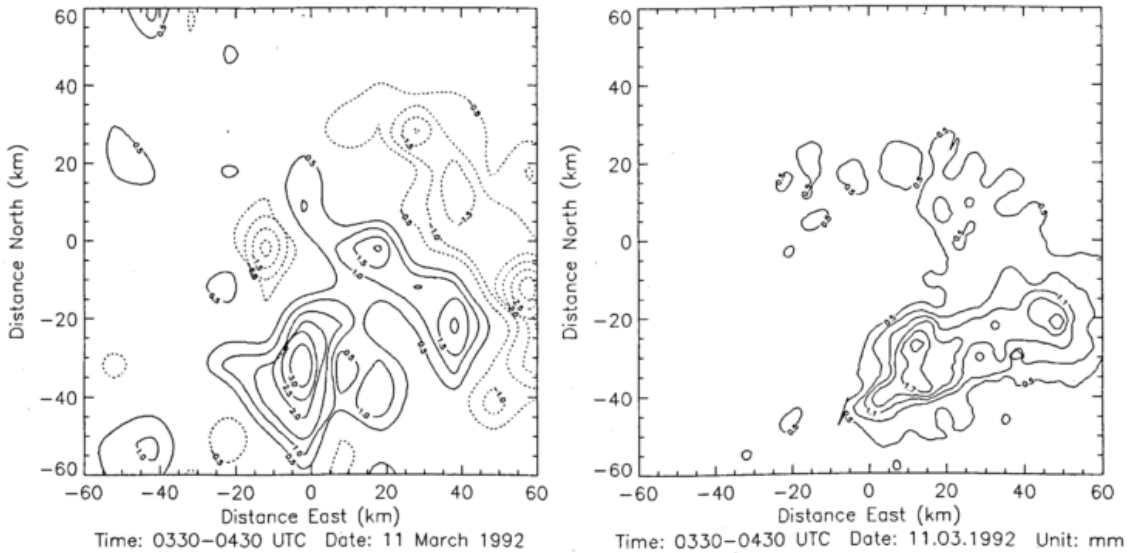

Fig.1: (a) Areal distribution of the echo growth and decay within a range of 60 km around the ETH radar. The result is an average of the growth and decay patterns (calculated from COTREC) over the period of 0330UTC to 0430UTC. Contour values start at 0.5 dB/min and continue in increments of 0.5 dB/min. The solid lines indicate regions of the growth of radar echoes and the dashed lines represent the decay. (b) The accumulated rainfall obtained from radar measurements over the same period. The unit is in mm, starting at 0.5 mm with intervals of 0.3 mm.

Fig. 1a shows the patterns of averaged echo growth (solid contours) and decay (dashed contours) in units of dB min^{-1}. These patterns were fairly stationary during the period. Three significant centers of echo growth can be recognized which are located on the upwind flank of two mountain ridges (compare Fig. 1a and Fig.2b). For comparison, the accumulated precipitation rainfall

obtained from radar measurements over the same period is given. The regions of enhanced rainfall is located downwind of the regions ofradar growth (compare Figs. 1a and 1b). All these observational facts and analysis results give strong support that the growth and decay patterns of radar echoes are well related to an orographic impact on the associated precipitation patterns.

3. Growth and decay patterns of radar echoes in July 1993

In this section, we will present a statistical analysis of the echo growth and decay patterns over the period of rainfall events in July 1993. The data were obtained with the ETH Doppler radar (for details see "Group for Radar Meteorology" 1994). One primary purpose of these measurements is to obtain statistics on the spatial and temporal distribution of precipitation for a one month period. The collected large amount of radar data yields a good opportunity to evaluate the growth and decay patterns of radar echoes. Averaging the patterns over the considered rainfall period are expected to lead to a geographic distribution of precipitation enhancement due to topography. The dataset used for this analysis is restricted 1) to trackable echo patterns; 2) to intermediate types of convective and widespread precipitation. The former requirement is fundamental for COTREC, and the latter minimizes the effect of the random development and decay of radar echoes due to strong convective activity. In total, the radar data of 15 days were selected. For each precipitation event, a sequence of radar data in five minute intervals were analyzed using COTREC for calculation of the growth and decay patterns. Finally, the growth and decay patterns were averaged over the whole selected precipitation periods (see Fig.2a). The geographic distribution of the growth and decay patterns and the corresponding map of topography is given in Fig.2a and 2b. The most significant features seen in Fig.2a are two major patterns of echo growth. One is located in the south of the radar site within the range between 0 km and 35 km. In this growth region, three subcenters are further identified (marked with "x" in Fig.2a). Two of them were located upwind of a mountain ridge marked as a dashed line in Fig.2b, whereas the third subcenter close to the radar site is mainly assciated with an elongated topographical terrain (see the middle of Fig.2b). Another growth center is found at 25 km E-ESE of the ETH radar, i.e. in the region of the " Zuercher Oberland". All these growth patterns of radar echoes occurred on the upwind flank of hills and are strongly related to local topography. Decay regions appear mainly in the northeast or northwest of the radar site. The large area of decay in the northwest is probably caused by a foehn effect when the precipitation systems move from the Jura towards the Swiss plateau.

4. Discussion and future work

The discussion on the distribution of the growth and decay patterns of radar echoes in complex orography can not be concluded without consideration of the shielding effect. In mountain areas, the radar coverage is seriously affected by shielding of ground targets which leads to "blind areas" where precipitation will not or only partly be seen. A stationary growth/decay couplet along the two boundary flanks of the shielded area has to be expected when precipitation systems cross the shielded regions. These "false" growth and decay patterns can lead to mis-interpretations when related to orographic effects. Therefore, the patterns of echo growth and decay should be interpreted with caution. The shielding effect caused by the "Uetliberg" mountain is signifcant mainly in the south of the radar range. The sector of the shielded area is marked by two straight dashed lines in Fig.2a. As seen in the figure, the growth and decay regions caused by the shielding effect are close to two flanks of the shielded area. However, the extent and intensity of the growth region are larger compared to the decay region. On average, the growth of radar echoes (net effect) in the "shielded" area is still dominant and supports an orographic effect on the radar echoes.

In summary, distinct patterns of the growth and decay of radar echoes have emerged from applying COTREC to the radar data of precipitation events of 15 days. These patterns strongly support the fact that topography influences the formation and dissipation of radar echoes. Further analysis is needed by collecting more complete radar datasets and by separating these data with respect to the direction of movement of the radar echoes, the type of precipition, and different

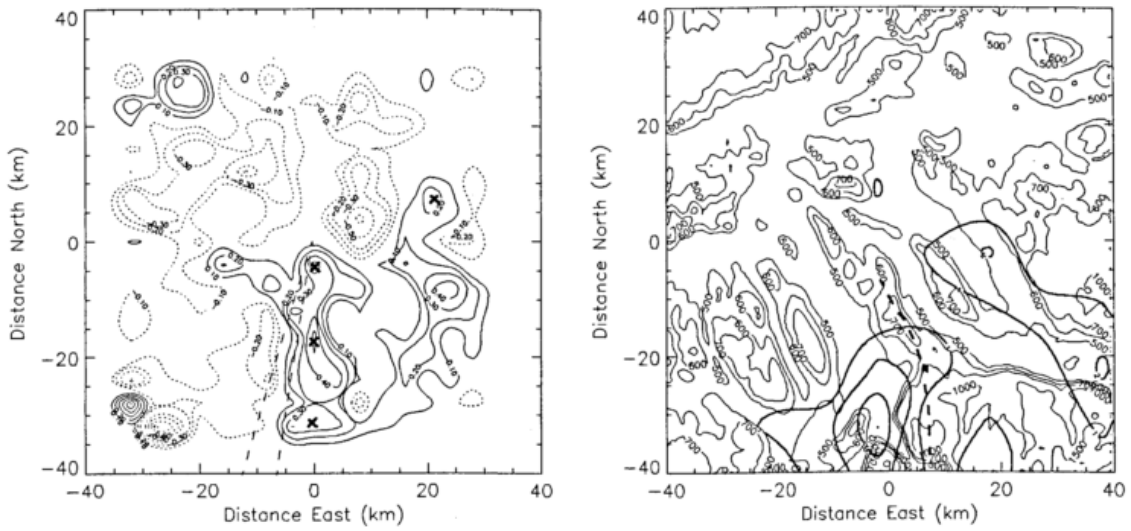

Fig.2: (a) Geographic distribution of the patterns of the growth and decay of radar echoes within a range of 40 km around the ETH radar. The result is an average of the growth and decay patterns (calculated from COTREC) over 15 days of precipition events. Contour values start at 0.1 dBl/min in increments of 0.1 dBl/min. The solid lines indicate regions of the growth of radar echoes and the dashed lines represent the decay. The sector of "shielded" data is indicated by two straight dashed lines in the figure.(b) Topographical map in the experimental area surrounding the ETH-radar. Contours of the terrain are in meters MSL The growth centers shown in Fig.1a are also superimposed over the topographic map with thick lines. The values of the lines start at 1.0 dBl/min in increments of 1.0 dBl/min.

seasons. Such detailed analysis can lead to a better understanding of a radar climatology of the growth and decay patterns in alpine regions and can help to reveal the coupling between the enhancement (dissipation) of precipitation and orography, thus to improve the nowcasting of precipitation.

Acknowledgement:

We would like to thank Dr. Juerg Joss for his interest in this work and for many critical discussion.

References:

Bernath A., 1992: Precipitation measurements in the alpine basin Gletsch during the ALPEX/ RHONEX project: Distribution and elevation dependency. *Preprints, 22th International Conference on Alpine Meteorology*, Toulouse, France, 156-160.

Giorgi, F., M. R. Marinocci, and G. Visconti, 1990: Use of a limited area model nested in a general circulation model for regional climate simulation over Europe. *J. Geophys. Res.* **95**, 18413-18431.

Group for radar meteorology, 1994: Monitoring of severe hailstorms in Switzerland 1993. LAPETH. Available from Institute of Atmospheric Sciences, ETH, CH-8093, Zuerich, Switzerland.

Kou, J. , and H. D. Orville, 1973: A radar climatology of summertime convective clouds in the Black Hills. *J. Appl. Meteor.*, **12**, 359-369.

Li, L., W. Schmid, and J. Joss, 1994: A method to deduce the motion, growth and decay of radar patterns in complex orography. submitted to *J. Appl. Meteor.*

Rinehart, R. E., and E.T. Garvey, 1978: Three-dimensional storm motion detection by conventional weather radar. *Nature*, **273**, 287-289.

Widmann M. and C. Schaer, 1994: Principal component and trend analysis of precipitation in the Alpine Region. Poster presentation. *European conference on the global energy and water cycle*, 18-22, July, London.

NEW PORTABLE MINI-SODAR AND ITS POTENTIAL AND APPLICABILITY FOR COMPLEX TERRAIN STUDIES

ABSTRACT

A new portable, high frequency Mini-SODAR for investigating the structure and dynamics of the lower planatary boundary layer is discussed. The design concept is centered around multiple beam and multible frequency mode, which allows simultaneous measurement of different velocity components. Also the plus repetition rate can be smaller than 1 sec. This offers good estimates of turbulence characteristics including flux estimates. For potabillity and vertical resolution a special micro antenna system using arrays of small piezoelectric tweeters was developed. Combined with a special electronic design the Mini-SODAR fits in a suitcase box and can be handled by one person. The vertical resolution is about 5m.

Results from measurements in a small valley system show the potential and the applicability of this very portable instrument. The high resolution of continuos profiles offer insight into flow interaction and dynamic forcing mechanism of flow structures in complex terrain.

Wind-Induced Error on Snow Measurement: WMO Intercomparison Results

Yang, D.[1], B. Sevruk [2], E. Elomaa[3], V. Golubev[4] , B.Goodison[1] and Th. Gunther[5]

[1] Atmospheric Environment Service, Downsview, Canada
[2] Swiss Federal Institute of Technology, ETH Zurich, Switzerland
[3] Finnish Meteorological Service, Helsinki, Finland
[4] State Hydrological Institute, GGI, St. Petersburg, Russia
[5] Deutscher Wetterdienst, ZHEA, Potsdam, Germany

The aim of the WMO Solid Precipitation Measurement Intercomparison, initiated in 1986 and completed in 1993 was to: determine the wind-related errors in national methods of solid precipitation measurement, including considerations of wetting and evaporation losses; derive standard methods for correcting solid precipitation measurements, and introduce a reference method for general use to calibrate any type of precipitation gauge. The Double-Fence Intercomparison Reference, DFIR, was used as the reference at all the intercomparison stations, while the national standard precipitation gauges were operated according to national methods. The DFIR is shown in Figure 1. It consists of a shielded Tretyakov gauge encircled by two, 1.5 m high octagonal lath fences of 4 m and 12 m diameter, respectively and mounted 3.5 m and 3 m above ground.

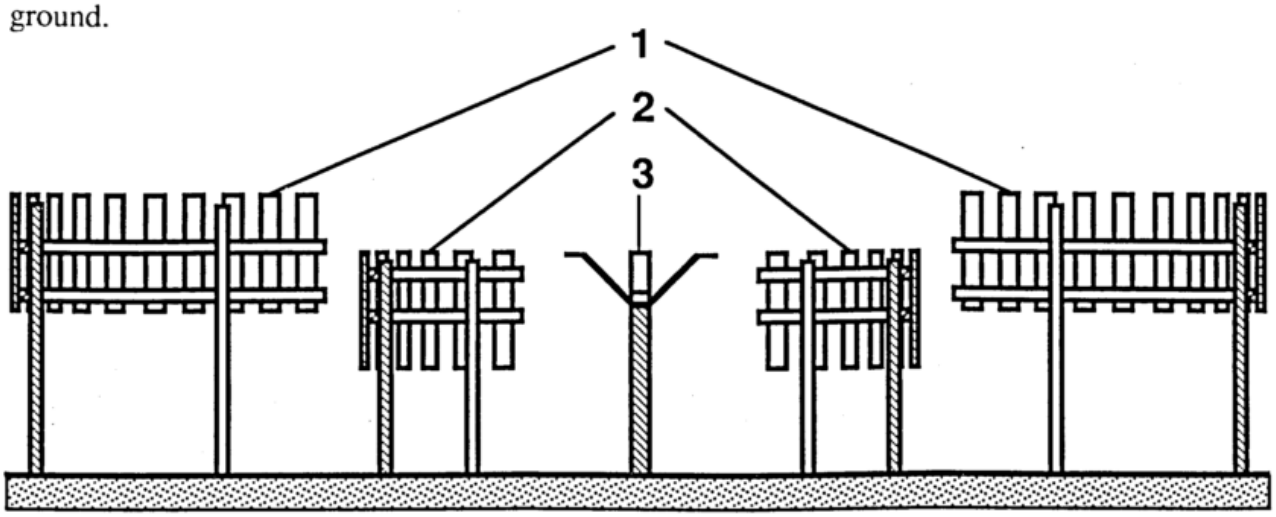

Figure 1 The Double Fence Intercomparison Reference, DFIR: 1 indicates the outer fence; 2 the inner fence and 3 is the Tretyakov gauge.

The wind-induced error of the DFIR was checked against the completely protected "bush gauge" (shielded gauges sited in bushes kept at gauge heights) which was deemed to provide the best estimate of "ground true", and was found to be less than 10% as shown in Table 1.

The measurements clearly show the need to correct the DFIR to be equivalent to the "ground true" value of the gauge in the bushes. Methods to correct the DFIR for the effect of wind and other

environmental factors were developed and applied when assessing the catch of national gauges compared to the DFIR.

Table 1 Average differences in measured precipitation between the DFIR, the bush gauge and some of the other gauges operated at the Valdai Experimental Station in the Russian Federation.

Gauge type	Total rain + snow (mm)	Per cent of the "bush reference"
Tretyakov in bushes	367	100
DFIR (Tretyakov)	339	92
DFIR (Canadian Nipher)	342	93
Canadian Nipher shielded	314	86
Tretyakov	258	70
8" USA Alter shielded	273	75
8" USA unshielded	208	57

Over 16 countries participated in the comparison at sites selected in their own country, sampling during at least five winter seasons a range of climatic and snowfall conditions. Members which submitted complete data summaries for analysis were: Canada, China, Croatia (formerly Yugoslavia), Denmark, Finland, Germany (formerly German Democratic Republic), Norway, Russia (formerly USSR), Sweden and the United States. Other countries collecting comparative measurements for at least one winter included Bulgaria, India, Japan, Romania, Slovakia (formerly Czechoslovakia) and the United Kingdom. The systematic errors in the measurement of solid precipitation were determined quantitatively in the intercomparison for over 20 different precipitation gauge and shield combinations.

The intercomparison data consisting of daily or twice-daily measurements as collected at 16 different sites, representing a great variety of climate, are completely comparable relative to the DFIR in terms of the wind-induced losses for the same type of gauge. The wind speed at the height of the gauge orifice and three classes of precipitation (snow, rain and mixed) were used in the analysis. Only events with a measured precipitation amount of at least 3 mm (DFIR) were used.

This paper summarizes results from analysis of the field data for several types of gauges tested in different countries and discusses potential problems in correcting solid precipitation measurements. Data from all experiment sites confirm that solid precipitation measurements must be corrected for wetting loss (for volumetric measurements), evaporation loss and undercatch due to wind speed. Systematic losses vary according to type of gauge and precipitation (snow, mixed snow and rain,

and rain) and season. Table 2 shows the possible range of losses of national standard gauges and recording gauges due to different gauge types, wind shields and construction parameters.

Table 2 Deviations of snow catch of different gauges from the DFIR measurements. Jokioinen, Finland, 1987 - 1993.

Gauge (shielded)	Per cent catch	Gauge (unshielded)	Percent catch
DFIR	100		
Canadian Nipher	82	Danish Hellmann	48
Tretyakov	74	Tretyakov	46
Wild	57	Wild	40
Swedish	69		
Norwegian	66		
Geonor (weighing)	62		
Tipping Bucket (heated)	62		

Evaporation and wetting loss varied according to gauge type and time of year. Evaporation loss was a problem with gauges which had no preventative funnel in the bucket, especially in late spring as for instance the Tretyakov gauge and the Swedish gauge. Losses in April of over 0.8 mm/day were measured in the Finnish Station Jokioinen. Losses during winter were much less than during comparable summer comparisons. The magnitude of wetting loss is also a function of the number of times the gauge is emptied. Average wetting loss can be up to 0.2 mm per observation. At synoptic stations where precipitation is measured every 6 hours, this can become a very significant loss. At some Canadian stations, wetting loss was calculated to be 15-20% of measured winter precipitation.

Wind speed has been found, once again, as the most important variable affecting the gauge catch of snow. The wind-induced losses increase considerably with wind speed for all types of gauges, varying by gauge type, wind shield used, type of precipitation and, in some instances, air temperature, as shown in the example from Herzgerode in Germany in Table 3.

The above-mentioned results have been confirmed by intercomparison data from four stations with the German Hellmann gauge and from 11 stations with the Russian Tretyakov gauge. The unshielded Hellmann gauge catches only one half of fallen snow, if wind speed approaches 3 m/s, as shown in Figure 2, but the Tretyakov gauge catches on average ten per cent or more than the Hellmann gauge under the same conditions (Table 3). Similarly, a better performance of all shielded gauges, particularly the Canadian Nipher gauge was obvious.

The tables and figures below are intended to provide only a comparative summary of the results of the intercomparison. Complete results and equations which can be used to correct measured data

for wind-induced error will be included in the final report of the experiment. The regression functions of wind-induced losses versus wind speed have been derived for snow and mixed precipitation and can be used to correct precipitation data from different types of gauges.

Table 3 Wind effect on the per cent catch of shielded and unshielded gauges as compared to the DFIR catch.

Wind speed	TRET/DFIR (shielded)			HELL/DFIR (unshielded)		
m/s	%			%		
	snow	mixed	rain	snow	mixed	rain
1.1- 2.0	86	85	92	68	80	94
2.1- 3.0	71	76	91	56	69	91
3.1- 4.0	49	62	90	42	57	89
4.1- 5.0	49	52	88	26	46	86
5.1-20.0	33	56	83	22	50	87

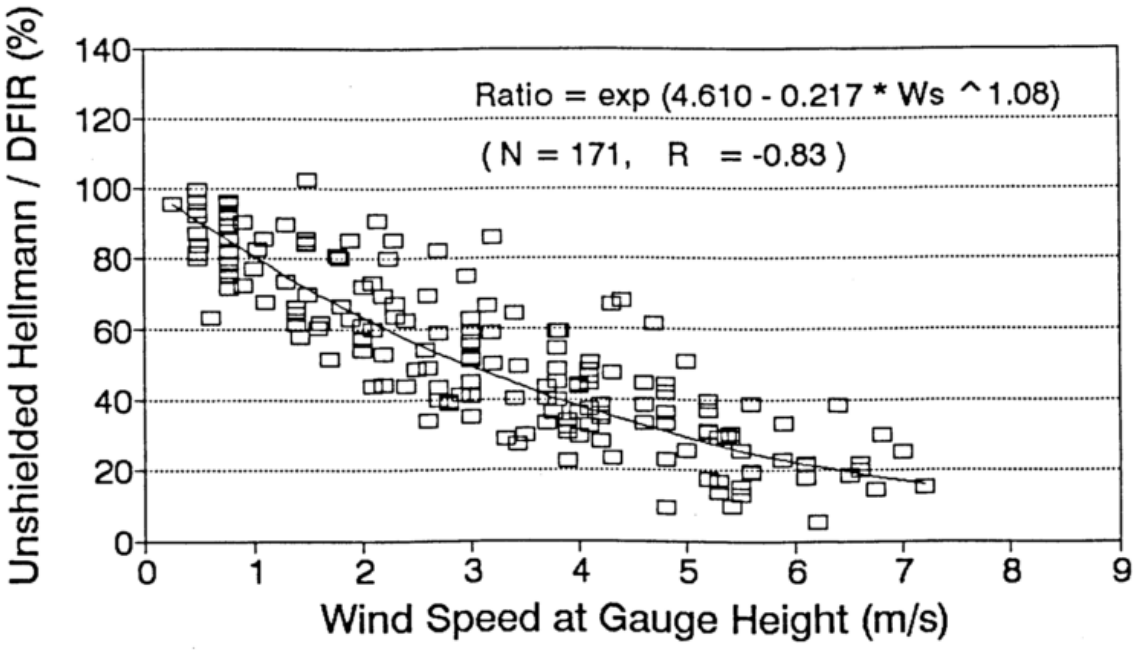

Figure 2 Plot of snow catch ratio, Hellmann/DFIR, against wind speed. Three sites: Valdai, Jokioinen and Herzgerode.

It is clear that to achieve data compatibility when using different gauge types and shielding during all weather conditions, significant corrections to the actual measurements are necessary. Shielded gauges catch more than their unshielded counterparts. Therefore, gauges should be shielded either naturally (e.g., forest clearing) or artificially (e.g., Alter, Canadian Nipher type, Tretyakov wind shield) to minimize the adverse effect of wind speed.

Ein Meßnetz zur Erfassung des Niederschlags im alpinen Raum

ORR H.Vogt, Nationalparkverwaltung Berchtesgaden

Dem Nationalpark Berchtesgaden stellt sich als Haupt - aufgabe wissenschaftlicher Untersuchungen die Ökosystem-forschung. Dabei darf davon ausgegangen werden, daß deutliche Veränderungen von Ökosystemen auch auf der Variabilität des Wasserhaushalts beruhen.Dies kann sowohl durch natürliche Schwankungen als auch durch Kulturmaßnahmen hervorgerufen werden. Zur Erfassung und Erklärung der Reaktionen der Natur kann auch die Klimatologie, sowohl durch die Erhebung von Meßdaten, wie durch eine synthetische Klimatologie (G. Enders) ihren Beitrag leisten. Im Gegensatz zu einer Reihe meteorologischer Parameter gelingt es beim Niederschlag jedoch nicht, eine zeitlich wie räumlich allgemeingültige Abbildungsgleichung zu erstellen, die die zeitlich - räumliche Variabilität des Niederschlags be - stimmbar macht. Vielmehr unterliegen die das Niederschlagsverhalten beeinflussenden Parameter einer großen Vielfalt, die bei der Konzeptionierung und Installation eines Meß - netzes berücksichtigt werden müssen:

1. Meteorologische Einflußgrößen

   a. Großwetterlage
   b. lokale Wetterentwicklung
   c. Niederschlagstypus
   d. Luv - und Lee-Effekte
   e. Höhe des Kondensationsniveaus

2. Invariable Lageparameter

   a. vorgelagerte Gebirgsbarrieren
   b. Exposition
   c. Meereshöhe
   d. geographische Orientierung
   e. lokale Reliefsituation

Das Niederschlagsmeßnetz im Wimbachtal bei Berchtesgaden mußte also diesen Steuerungsvariablen Rechnung tragen und setzt deshalb eine repräsentative vertikale und horizontale Verteilung der Niederschlagsmeßstationen voraus. Dies konnte nur durch eine längere experimentelle Phase der Standortauswahl und eine multivariate Überprüfung der Meßergebnisse erreicht werden.
Die Instrumentierung des 34 qkm großen Wimbachtals mit einem Höhenintervall von rund 2100m erfolgte überwiegend mit

Niederschlagswaagen. Dies erweist sich deshalb als besonders praktikabel, da Gebiete mit hohen niveometrischen Koeffizienten häufig eine Heizung der Geräte voraussetzt, was sich sowohl aus fehlertechnischen Gründen (Verdunstung) als auch auf Grund energietechnischer Gründe als nicht durchführbar erweist.
Die Betreuung der mit Wochenumlaufzeit ausgestatteten Geräte erfolgt durch Mitarbeiter der Nationalparkverwaltung.
In der Regel sind Meßlücken selten, sie entstehen nur beim Eintritt widriger Bedingungen, wie sie im Gebirge etwa bei Lawinengefahr auftreten können.
Eine Verdichtung des Meßnetzes erfolgte durch Hochgebirgs - totalisatoren, so daß sich eine mittlere Stationsdichte von einer Station pro 3,1 qkm ergibt.
Für topoklimatologische Untersuchungen oder Berechnungen des Gebietsniederschlags ist zusätzlich eine Ausweitung des Meßnetzes auf die Umrahmungen des Wimbachtales durchgeführt worden.
Um die Parameterisierung des Luv-und Lee-Effekts zu erzielen, erfolgte an einem repräsentativen Profil die Installation von Windmessern in Kombination mit Niederschlagsmeßgeräten. Gesicherte Ergebnisse liegen aber hierfür noch nicht vor.
Erste Anwendungen bestätigen die Repräsentativität des Niederschlagsmeßnetzes. So erwies sich die auf der Basis der Meßstellenverteilung mit Hilfe einer multiplen Regression durchgeführte Gebietsniederschlagsberechnung für ein Einzelereignis als signifikanter Input für das Hochwassermodell TR20.

Blitzortungen mit LPATS

Karl Krames
Marientaler Au 45, 56856 Zell

ABSTRACT

For the civil and military aviation - especially in the low level - the exact information over the zones with a minimum hazard of crash caused by lightning flash is very important. The statistics proves, that for the modern aircraft - carbon fibre compcsites, electronic installations - the sufficient protection against lightning discharges is missing. It is essential therefore to put the meteorological informations into practice in cooperation with LPATS datas. In any case the synoptical and climatological documents alone are not sufficient for the forecaster. For the recommended flight route the pilot must be exactly informed over the isolines of flash/km^2/time. The LPATS informations are a conditio sine qua non for the flight safety during the passage of thundery fronts, especially in the Alps.

ZUSAMMENFASSUNG

In der zivilen und militärischen Luftfahrt - besonders im Tiefflug - ist die genaue Information über die Bereiche mit minimaler Unfallgefahr durch Blitzschlag sehr wichtig. Statistiken beweisen, daß bei modernen Luftfahrzeugen - kohlefaserverstärkte Kunststoffe, Elektronik - ein ausreichender Schutz gegen elektrische Entladungen nicht gewährleistet ist. Deshalb erscheint es notwendig, in der Praxis die meteorologischen Informationen mit LPATS Daten zu verknüpfen. Jedenfalls sind die synoptischen und klimatologischen Unterlagen allein für eine sichere Beratung nicht ausreichend. Der Pilot muß bei der Festlegung der empfohlenen Flugstrecke genau über die Isolinien der Blitzzahl/km^2/Zeit unterrichtet werden. Die LPATS Daten stellen hierbei eine conditio sine qua non für die Flugsicherheit während des Durchgangs von Gewitterfronten - besonders in den Alpen - dar.

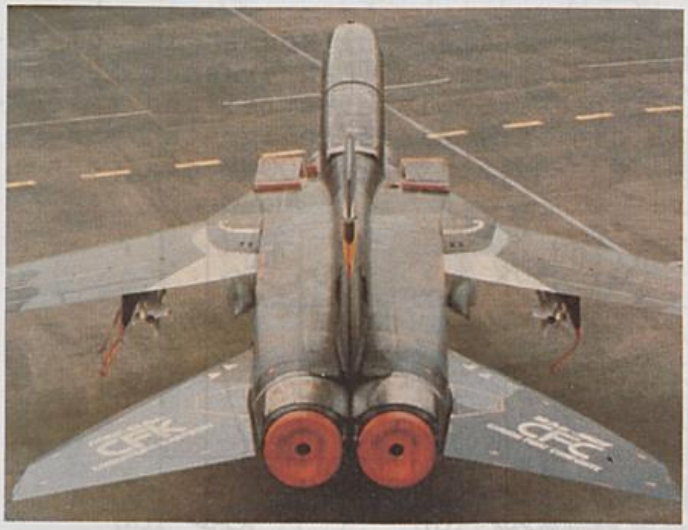

Bild 1

Bei der Wetterberatung ist die genaue Lokation von Gewittern eine unerläßliche Voraussetzung für die Verbesserung der Flugsicherheit. Dies gilt vor allem für moderne Luftfahrzeuge mit Bauteilen aus Kunstfaserstoffen und empfindlicher Elektronik, z.B. Tornado CFK Taileron, Bild 1. Der Verlust eines derartigen Flugzeugs mit CFK Unterflügeln und Außentanks durch Blitzschlag, z.B. am 6.2.1984 bei Friedeburg in Ostfriesland, zeigt die Bedeutung einer rechtzeitigen und geographisch detaillierten Gewitterwarnung.

Bei Kosten - Nutzen - Rechnungen für die Installation geeigneter Blitzortungsgeräte müssen selbstverständlich auch die häufigen Schäden berücksichtigt werden, die zwar nur zu Zwischenfällen führen, deren Behebung aber insgesamt enorm hohe Kosten verursacht.

Nach den langjährigen Erfahrungen des Verfassers ist vor allem bei Hubschraubern eine Minimierung des Flugsicherheitsrisikos bei Gewitter durch genaue Angaben der optimalen Flugstrecke möglich. Auch diese Luftfahrzeuge werden nämlich zunehmend, wie z.B. die neue EC 135, unter Verwendung von Kevlar - Carbonfaser - Sandwich - Komponenten gebaut.

Bislang können für die Flugvorbereitung nur die synoptischen Unterlagen und die klimatologischen Karten der Gewittertage/Jahr herangezogen werden. Der Verfasser wies bereits früher für Bayern, Baden - Würtemberg und Schleswig Holstein nach, daß die Klimawerte nach der von ihm durchgeführten Überarbeitung bessere Informationen liefern als häufig angenommen wird. Sie weisen nämlich mit den Auswertungen der automatischen CIGRE Blitzmessungen zufriedenstellende Übereinstimmungen auf /1-3/.
Von russischer Seite ist allerdings eine weniger enge Korrelation gefunden worden /4/. In diesen Fällen ist davon auszugehen, daß die CIGRE Meßdaten im Ob-Bereich bei Tomsk die Blitzgefährdung exakter angeben. Die höheren Blitzzahlen in Flußnähe sind nämlich das Resultat der orographischen Konvergenz, die zur Labilitätssteigerung führt.
Für die Beratungspraxis genügen natürlich die statistischen Jahreswerte nicht. Hilfreicher wären Häufigkeitsangaben von Gewittern und Blitzzahlen für exakt definierte Wetterlagen bei bestimmten Tages- und Jahreszeiten.
Wegen der bekannten Fehlermöglichkeiten bei audiovisuellen Gewitterbeobachtungen und der mangelnden Verfügbarkeit von CIGRE Daten zur Echtzeit ist von militärischer Seite bereits früher ein in der Praxis brauchbares Blitzortungsgerät auf dem Fliegerhorst Lechfeld getestet worden. Hierbei wurden mit dem Gerät von W. Schmidt Elektronik-Meteorologie in Lindau recht brauchbare Ergebnisse erzielt /5/.
In den letzten Jahren sind von der Industrie wesentlich leistungsfähigere Instrumente zur exakten Blitzortung gebaut und von verschiedenen Stromversorgungsunternehmen erprobt worden. Der Verfasser hat gelegentlich der letzten Tagung in Toulouse das LPATS (Lightning Positioning an d Tracking System) der Fa Atm. Research in Florida vorgestellt, das in Deutschland von Siemens in der BLIDS (Blitzinformationsdienstleistung von Siemens) Version installiert worden ist und seit 1991 zufriedenstellend arbeitet /6/.
Auf eine Wiederholung der technischen Daten wird an dieser Stelle verzichtet. Stattdessen soll eine vorläufige geophysikalische Interpretation der Meßdaten des genannten Systems erfolgen, das auch in anderen Ländern erfolgreich getestet wurde.
Wegen der geringen zur Verfügung stehenden Seitenzahl können im folgenden die synoptischen Karten nicht vorgelegt werden. Man erkennt jedoch sofort, daß die LPATS Daten hinsichtlich der Gewitterverteilung wesentlich mehr Informationen bieten. Durch die Wahl eines geeigneten Maßstabs läßt sich jeder Blitz mit einer Genauigkeit bis 200 m eingrenzen.

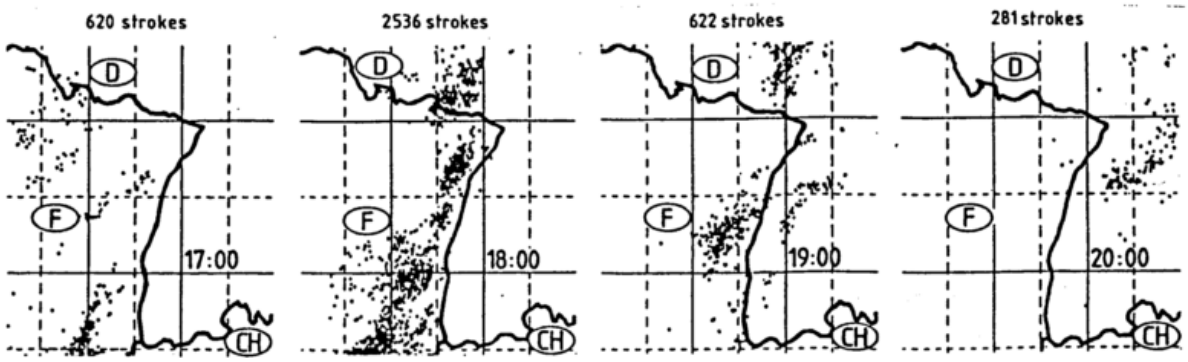

Bild 2 Durchzug einer Gewitterfront am 27.4.1992, 17 - 20 Uhr, nach /7/

Die in Bild 2 dargestellte Blitzverteilung bestätigt die in früheren Untersuchungen vom Verfasser vertretene Auffassung, nach der normalerweise bei Westströmung im Lee der Vogesen eine Zone abflauender Gewitteraktivität zu erwarten ist /8,9/. Mit Hilfe umfangreicher klimatologischer Unterlagen ist diese Meinung später auch von J. Pelz bestätigt worden /10/.
In Übereinstimmung hiermit stehen die statistischen LPATS Auswertungen

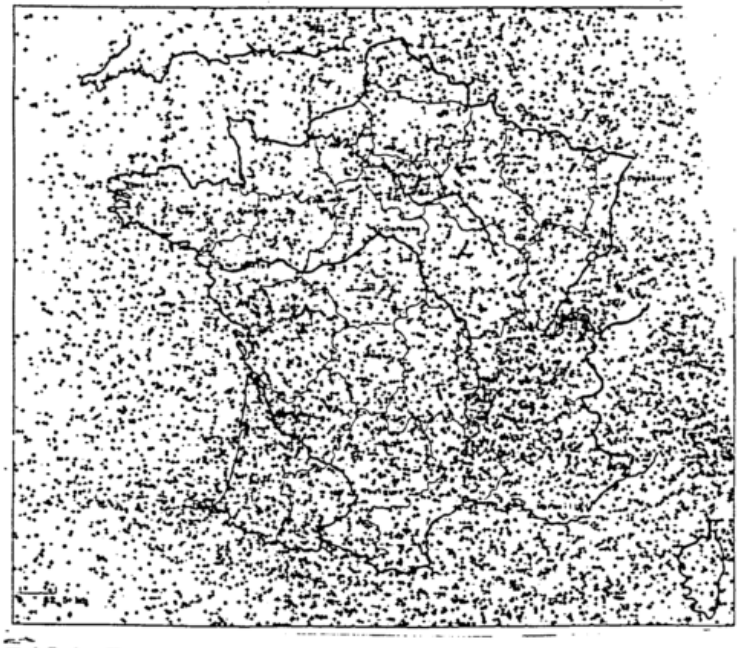

Bild 3 Blitzdichte in Frankreich 1.7.1987-30.6.1989 nach /11/

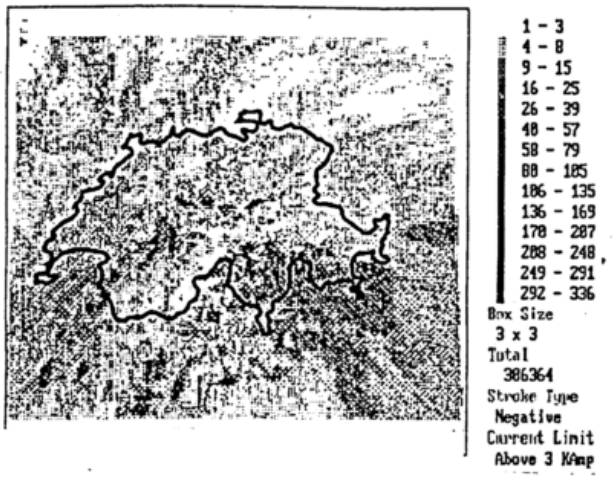

Bild 4 Blitzdichte in der Schweiz, Sept. 1991-Sept. 1992 nach/12/

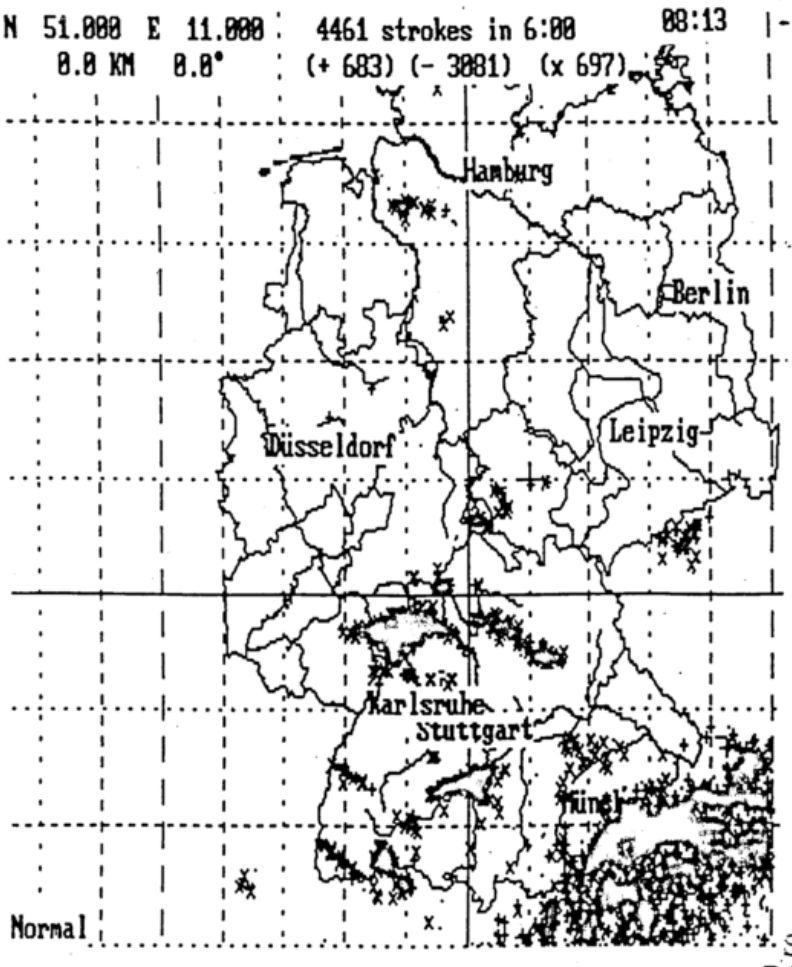

Bild 5 Blitzdichte innerhalb von 6 Stunden am 17.7.1991

in Frankreich und in der Schweiz, Bild 3 u. 4. Leider konnte die von Siemens zwischen Sept. 1991 und Sept. 1992 durchgeführte Meßkampagne und die auf dieser Basis gewonnene "First lightning frequency map" von Deutschland zum Vergleich nicht herangezogen werden, weil ihr Kauf mit enorm hohen Kosten verbunden ist. Die zur Verfügung stehenden LPATS Daten von Frankreich und der Schweiz zeigen trotz der relativ geringen Meßdauer bemerkenswerte Details, die im Rahmen dieses Beitrags nur in groben Zügen skizziert werden können. Höhere Werte treten in den Savoyer, Berner und Glarner Alpen auf. Maxima werden im Tessin, in den Rätischen Alpen, im Ortlergebiet und in den Bergamasker Alpen verzeichnet. Auffallend ist die Leewirkung des Zentralmassivs, die sich bis in die französischen Alpen nachweisen läßt. Höhere Dichtewerte treten auch im Schweizer Jura auf.

Die Zuordnung der Daten zu bestimmten Wetterlagen und die Verwendung geeigneter Maßstäbe ließe Einzelheiten erkennen, die für die Flugwetterberatung von Bedeutung sind.

Zur Beurteilung des Blitzrisikos in den verschiedenen Flughöhen

sind die LPATS Hinweise auf die verschiedenen Blitzarten - Wolke-Wolke, Wolke-Erde, Erde-Wolke - von besonderer Bedeutung.
Entscheidend wird jedoch die Flugsicherheit durch die Verfügbarkeit der Unterlagen zur Echtzeit verbessert.
Die in Bild 5 dargestellte Situation gibt für einen 6 Stundenzeitraum sehr genau die Gefährdungsbereiche in Deutschland wieder. Maximalwerte der Blitzdichte treten im Alpengebiet auf. Höhere Zahlen werden auch im Odenwald, im Bauland, in der Schwäbischen Alb, im Erzgebirge und im Thüringer Wald registriert.
Von besonderem Interesse ist die Tatsache, daß sogar Moränenzüge mit geringer Erhebung - zwischen Hamburg und Bremen - stärker blitzgefährdet sind. Dieses Ergebnis wird im übrigen durch Messungen in Holland und in Schweden bestätigt /13,14/.
Insgesamt dürften die ersten Erläuterungen der LPATS Unterlagen deutlich zeigen, daß ihre Nutzung die Flugsicherheit bei Gewitterlagen erheblich verbessern würde. Dies gilt vor allem für den alpinen Raum.
Nachdem nunmehr auch in Österreich das "Austrian Lightning Detection & Information System ALDIS" installiert worden ist, kann davon ausgegangen werden, daß in Zukunft der größte Teil der Alpen flächendeckend im Hinblick auf die Gewitteraktivität überwacht werden kann /15/.

SCHRIFTTUM

/1/ Krames K. Die Blitzbedrohung in Süddeutschland ITAM 82
/2/ Krames K. Kritischer Vergleich zwischen Gewitterbeobachtungen und Blitzzählungen... ICLP 88
/3/ Krames K. Influences of Geophysical Factors on the Pilot-Aircraft-System. HSSLF, AGARD Conf. Proc. No 267, Lisbon, 1979
/4/ Rakov et al. Annual ground flash density from lightning flash counter records, 20 th ICLP, Interlaken 1990
/5/ Fischer K.E. Gewitterortung, Promet 4, 1981, 11-13
/6/ Krames K. Auswirkung von Gewitterfronten auf das unterschiedliche Flugsicherheitsrisiko in den Bayerischen Alpen, CIMA 92
/7/ Fister V. et al. Lightning Positioning in Electric Power Supply Systems, 21st ICLP, Berlin '92, 6.14
/8/ Krames K. Optimale Flugroute im Oberrheintalgraben bei Gewitter, Int. Symp. on Urban and Local Climatology, Freib. Geogr. H. 26, 1986
/9/ Krames K. Die Problematik des REEP Verfahrens zur Gewittervorhersage in den Naturräumen des Oberrheintalgrabens, Freib. Geogr. H. 26, 1986
/10/Pelz J. Gewitterkarte, Beil. zur Berliner Wetterkarte 49, 1986
/11/Le Boulch The Meteorage Thunderstorm Monitoring System, 20 th ICLP, 6.13, Interlaken 1990
/12/Montandon E. Analysis of Lightning Strike Density and Recorded Waveforms by the Swiss Lightning Position and Tracking System, 21 st ICLP, 6.04, Berlin 1992
/13/Janssen M.J.G. The New Lightning Detection System in the Netherlands, 19 th ICLP, 1.9, Graz 1989
/14/Lundquist S. Study of a Local Intensive Thunderstorm in South Sweden, 21 st ICLP, 6.12, Berlin 1992
/15/Diendorfer G. The Austrian lightning detection and information system ALDIS, 21st ICLP, 6.05, Berlin 1992

Lee cyclogenesis: cold air blocking and upper-level potential vorticity anomalies

J. Egger

Meteorologisches Institut
Universität München

ABSTRACT

An idealized model of the role of cold-air blocking by a mountain and the passage of positive anomalies of potential vorticity at the upper levels over this mountain during lee cyclogenesis is presented. This concept is tested for a case of cyclogenesis in the lee of the Atlas mountains.

ZUSAMMENFASSUNG

Ein stark idealisiertes Modell des Zusammenspiels von kalter Luft an einem Gebirge und der Bewegung eines Zentrums potentieller Vorticity über die Berge während der Entstehung einer Leezyklone wird vorgestellt. Dieses Bild wird anhand einer numerischen Simulation einer Sharav-Zyklone im Lee des Atlas einem Test ausgesetzt.

1. Conceptual model

The model atmosphere consists of three homogeneous layers of uniform potential vorticity P_i except for an anomaly embedded in the upper layer. A surface front is located where the interface of the lowest (coldest) layer with the intermediate layer intersects the ground. A zonal mean wind U transports the cold front and the anomaly towards the mountain. No depression is seen in the surface pressure field if the anomaly P_3^* is above the coldest air (Fig. 2a). If, however, the cold air is blocked by the mountain, the anomaly overtakes the surface front and induces a depression in the lee. Thus, a lee cyclone is generated (Fig. 2b).

2. Test

The conceptual model is exposed to a relatively mild test. We interpret an idealized case of cyclogenesis in the lee of the Atlas mountains in the light of this concept. This lee cyclone forms while a cold-air outbreak from the north-east is blocked by the barrier and an upper-level trough is moving over the mountain. No surface cyclone is seen underneath the vorticity maximum linked to the trough as long the trough is to the north of the mountain. However, a lee cyclone forms almost exactly underneath the trough as soon as the trough crossed the barrier. This evolution of the flow is in qualitative agreement with the conceptual model. However, deficiencies show up as soon more quantitative aspects are exposed to the test.

3. Conclusion

The test suggests that the conceptual model as displayed above describes part of the lee cyclogenesis mechanisms during lee cyclogenesis at west-east oriented barriers. However, the concept is two-dimensional and excludes baroclinic conversion and is, therefore, incapable of capturing all the essential features of lee cyclogenesis.

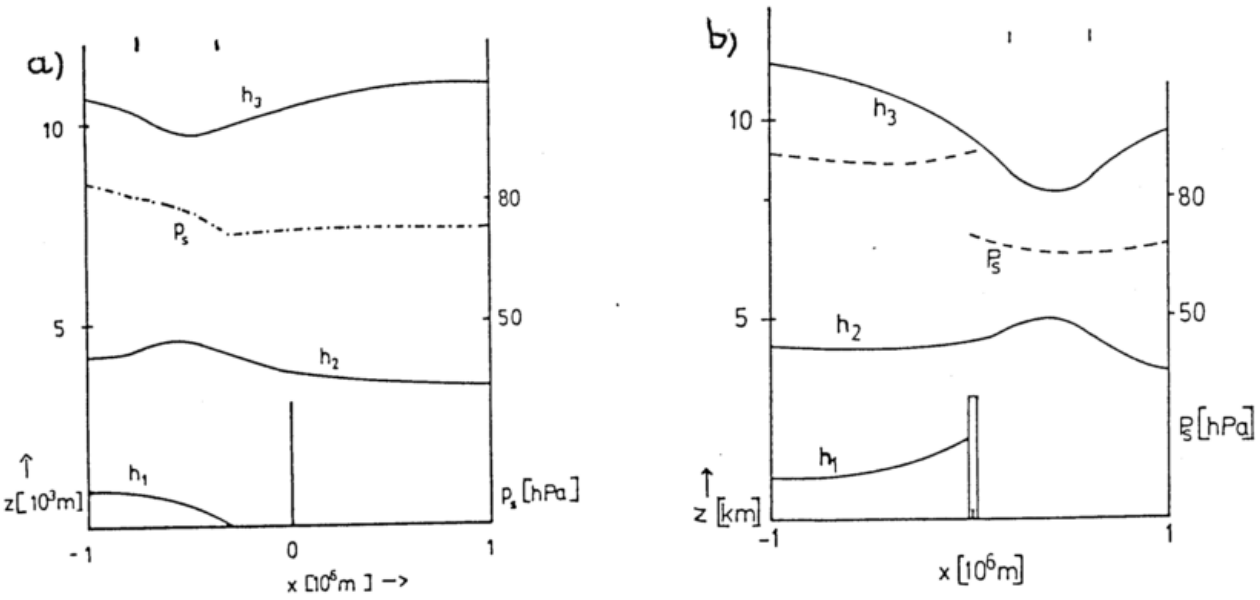

Fig. 1. Interface heights h_i (m) and surface pressure p_s (dashed, deviation from reference value) for a situation (a) where the PV-anomaly is above the cold air and where the cold front is upstream of the mountain and (b) 25hrs later, when the cold air is blocked by the mountain while the PV-anomaly is in the lee. The tick marks give the position of the PV-anomaly.

Life Cycle of a Mountain Generated Adriatic Cyclone

Arnold Tafferner

Meteorologisches Institut der Universität München
München, Germany

Abstract

An Adriatic cyclone is investigated by numerical simulation. During the first 24 hours of forecast a shallow low-level lee side vortex is found within flow perturbations envoked by the Alps. During the second day this vortex triggers cyclogenesis over the Adriatic when an upper-level trough moves over the Alps. Probably due to the lack of moisture in the model physics the forecast lateron fails to reproduce the observed strength of the cyclone while it moves toward the eastern Mediterranean. No cyclone develops without model Alps.

1. Introduction

Cyclones in the lee of mountain ranges have received widespread attention during the past ten years. In particular Alpine lee cyclones have been treated in numerous investigations in the wake of the field experiment ALPEX (review by Mesinger and Pierrehumbert, 1986). Due to the orography of the Mediterranean area and the shape of the major mountain ranges the gulf of Genoa is a preferred place for cyclogenesis. To a minor fraction cyclones are also generated in the western Mediterranean near the Balearic Islands and in the Adriatic Sea. Here we discuss the life cycle of a cyclone which generated in the Adriatic Sea on 19 January 1983 and moved into the eastern Mediterranean during the following days.

In many of the investigations the role of the mountains was questioned as to whether lee cyclogenesis is invoked by the mountains or only modified. Considering the outcome from the great number of numerical simulations it is suggesting that the mountains have a determining influence where and when cyclogenesis is ensued from a particular synoptic situation, but „real" lee cyclones are rare in the sense that a corresponding no-mountain simulation does not produce a cyclone. Besides theoretical aspects (summarized in Mesinger and Pierrehumbert 1986, discussed in Egger, 1988 and Tafferner and Egger, 1990), the life cycle of a typical Alpine lee cyclone has been constructed. As noted already by Buzzi and Tibaldi (1978) a lee cyclone undergoes a two-stage development: rapid pressure fall within about six hours on the lee side of the mountains followed by a maturing phase of about 24 hours. Rapid pressure fall sets on when cold air at ground levels is blocked by the mountains while the upper-level trough continues to proceed over the mountain. Tafferner (1990) has discussed this situation in a conceptual model based on conservation of potential vorticity. He argued that on the lee side upper-level massflux divergence ahead of a moving potential vorticity maximum is not balanced by lower-level massflux convergence because cold air advection is retarded by the mountains. As a consequence low level convergence is forced on the lee side to balance the mass loss aloft. This in turn produces cyclonic vorticity at low levels. Depending on the overall synoptic situation this crude picture is modified. E.g. part of the vorticity at low levels could also be provided by particels entering the cyclogenetic area near Corsica through the Rhone gap. Thereby a conversion from shear into curvature vorticity can be found (Pichler and Steinacker, 1987). Tafferner (1990) and Lanzinger (1992) noted that the maturing phase consists of phase locking between potential vorticity maxima at upper and lower levels in the troposphere as described by Hoskins et al. (1985) for the general case of extratropical cyclogenesis.

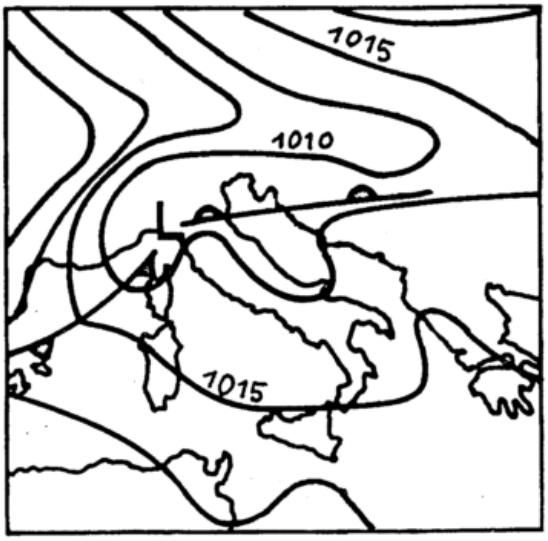

Figure 1. Sealevel Pressure on 19 January 1983 06 UTC. Depicted from the surface chart of Deutscher Wetterdienst.

Moist processes do not seem to play an important role during the first development phase as dry models are able to capture that part of the genesis. During the mature phase however, the cyclone's strength is likely to be influenced by moisture fluxes from the sea and release of latent heat depending on air/sea parameters and the time span available for diabatic processes to act. Often Alpine lee cyclones grow into a cut off cyclone, stay in place and decay after about two days.

Here report is given of the life cycle of an Alpine lee cyclone which does not follow the typical life cycle described above. As will be seen from the numerical simulation discussed in chapter 3, there are important differences in the first development phase. It also turns out that this cyclone is a „real" lee cyclone in the sense outlined above.

2. Synoptic Situation

A synoptic-scale trough situated at 18 January 1983 OO UTC over England approached the Alps from northwest and it's front side reached the lee of the Alps 24 hours later (upper-level charts at 500 mbar, Berliner Wetterkarte, FU Berlin; not shown). Underneath the trough cold air advected toward the mountains experienced blocking as is evident from the anticyclonic bending of the isobars upstream of the Alps in the sealevel pressure chart on 19 January 1983 06 UTC (Fig. 1). There is a low near Genoa at this time but no closed isobar is found. During the following day the upper level trough deepened considerably and continued to progress over the Alps (500 mbar chart from 20 January 1983 00 UTC; not shown). Given such a situation one would expect rapid growth of the lee cyclone near Genoa. The synoptic charts one day later reveal that this is not the case. On the contrary a cyclone developed not before 24 hours later and not in the gulf of Genoa but the southern Adriatic Sea (Fig. 2). On 21 January 00 UTC a closed contour in the 500 mb height field shows up indicating the vertical growth of the Adriatic cyclone (not shown). Lateron the cyclone progressed over Greece and reached the eastern Mediterranean on 22 January 1983. There it decayed when the upper-level cut off low got vertically aligned with the low level cyclone.

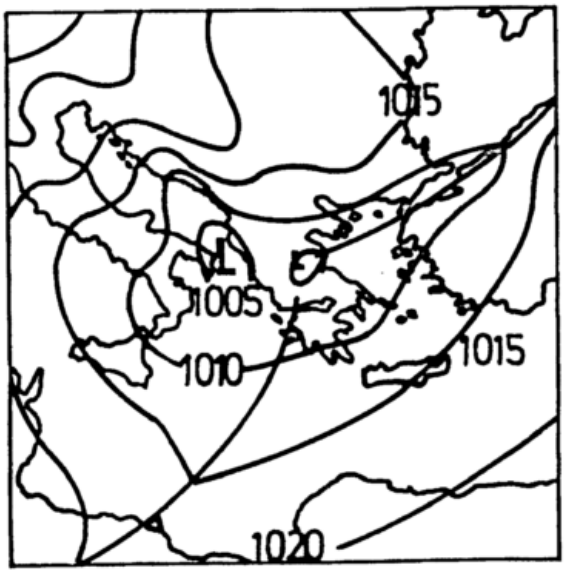

Figure 2. Sealevel pressure on 20 January 1983 12 UTC. Depicted from the surface chart of Deutscher Wetterdienst.

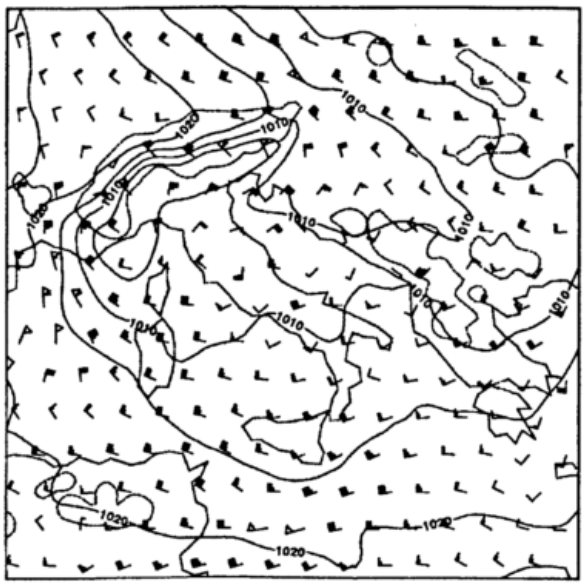

Figure 3. Seavel pressure (hPa) and surface wind (knots). 18 hour model forecast for 19 January 1983 06 UTC. Only part of the model domain is shown.

3. Results of Simulations

We use Bleck's (1984) isentropic model designed to simulate mesoscale features (details of the model setup can be found in Tafferner and Egger, 1992). Grid size is about 50 km and the computing domain encompasses the area as seen in Fig. 6. Twenty isentropic levels are used in the vertical. Objective analysis of Montgomery potential and wind is performed using Bleck's (1975) analysis scheme. Initialization and updating of the boundaries is performed using 12 hourly analyses. We start the model run on 18 January 1983 12 UTC and extend the simulation over 60 hours. In parallel to a control run with full orography a „no-mountain" forecast is carried out where the height of the Alps is set to a constant value of 550m. The life cycle of this cyclone is investigated by diagnosing dynamical quantities on the 900 hPa pressure surface for the near ground development and on isentropic surfaces 300K to 320K for upper-tropospheric levels together with cross sections along the Adriatic Sea. Furthermore, trajectories on isentropic surfaces are calculated from half hourly model output.

At starting time a surface cold front running from west to east over northern France and Germany has not yet touched the Alps (surface chart of Deutscher Wetterdienst from 18 January 1983 12 UTC; not shown). The 18 hours forecast for 19 January 06 UTC is in overall agreement with the observation, but a closed contour of 1005 hPa is already seen in the direct lee of the mountains (Fig. 3; to be compared to Fig. 1). The model overpredicts the onset of north-foehn which leads to a warming in the Po valley. We note that there is a low also in the observation at this time (Fig. 1). In contrast to the location of the pressure minimum in the immediate lee of the Alps vorticity production is strongest in the northern Adriatic as seen on the 900 hPa surface (Fig. 4a). There, a cyclonic cell is found in the order of 1.5 times the magnitude of the Coriolis parameter. In the immediate lee of the Alps on the other hand there is a row of vorticity cells of changing sign. Such a vortex structure has recently been identified to be typical for flow over the Alps (U. Aebischer, ETH Zürich, prilim. res. of PhD thesis). There is also a pronounced cyclonic maximum north of Corsica, typically found in lee cyclonesis (Pichler et al., 1990; Tafferner, 1990). It will be seen that the larger cell in the northern Adriatic Sea continues to exist

Figure 4a. Relative vorticity (10 E-5/s; negative values dashed) on level 900 hPa after 18 hours of forecast for 19 January 1983 06 UTC. The area of the Alps and the Dinaric mountains is stippled. Continental outlines are drawn too.

Figure 4b. As in 4a, but from the no-mountain simulation.

and lateron acts as a trigger for deep cyclogenesis. The corresponding no-mountain forecast after 18 hours does not produce the vortex cells mentioned above (Fig. 4b). Although there is a cyclonic cell in the northern Adriatic it's magnitude is only one third of that from the full mountain run. Also during the following hours it does not grow in amplitude. Before we go on to the mature phase

Figure 5. Particle trajectory on 287.5 isentropic surface calculated kinematically from half-hourly model output backward and forward from forecasting time 18 hours. Little squares mark two-hourly positions. Numbers denote forecasting hours. The 1200m contour marks the Alps and the Dinaric mounatins.

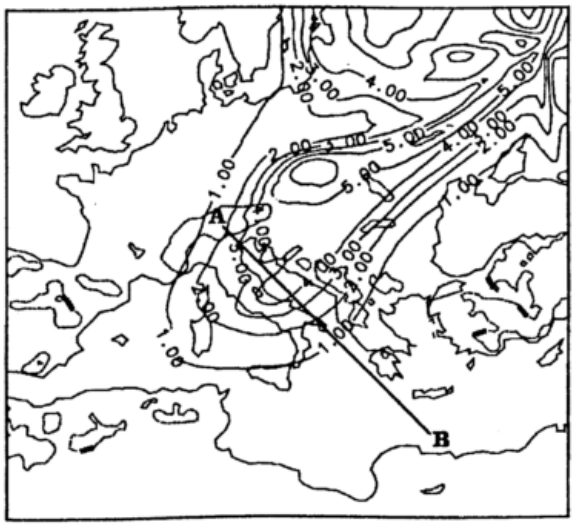

Figure 6 (left). Potential vorticity (PVU) on 300 K isentropic surface after 48 hours of forecast for 20 January 1983 12 UTC. Whole model domain is shown. The line A-B marks the location of the sections in Fig. 7.

of cyclone development we ask what caused the generation of the cyclonic vorticity maximum in the full orography run. Trajectories calculated kinematically backward and foreward from half hourly model output reveal that particles within the vorticity maximum in the northern Adriatic Sea originated in the western Mediterranean. Fig. 5 shows the path of one such particle on the near ground

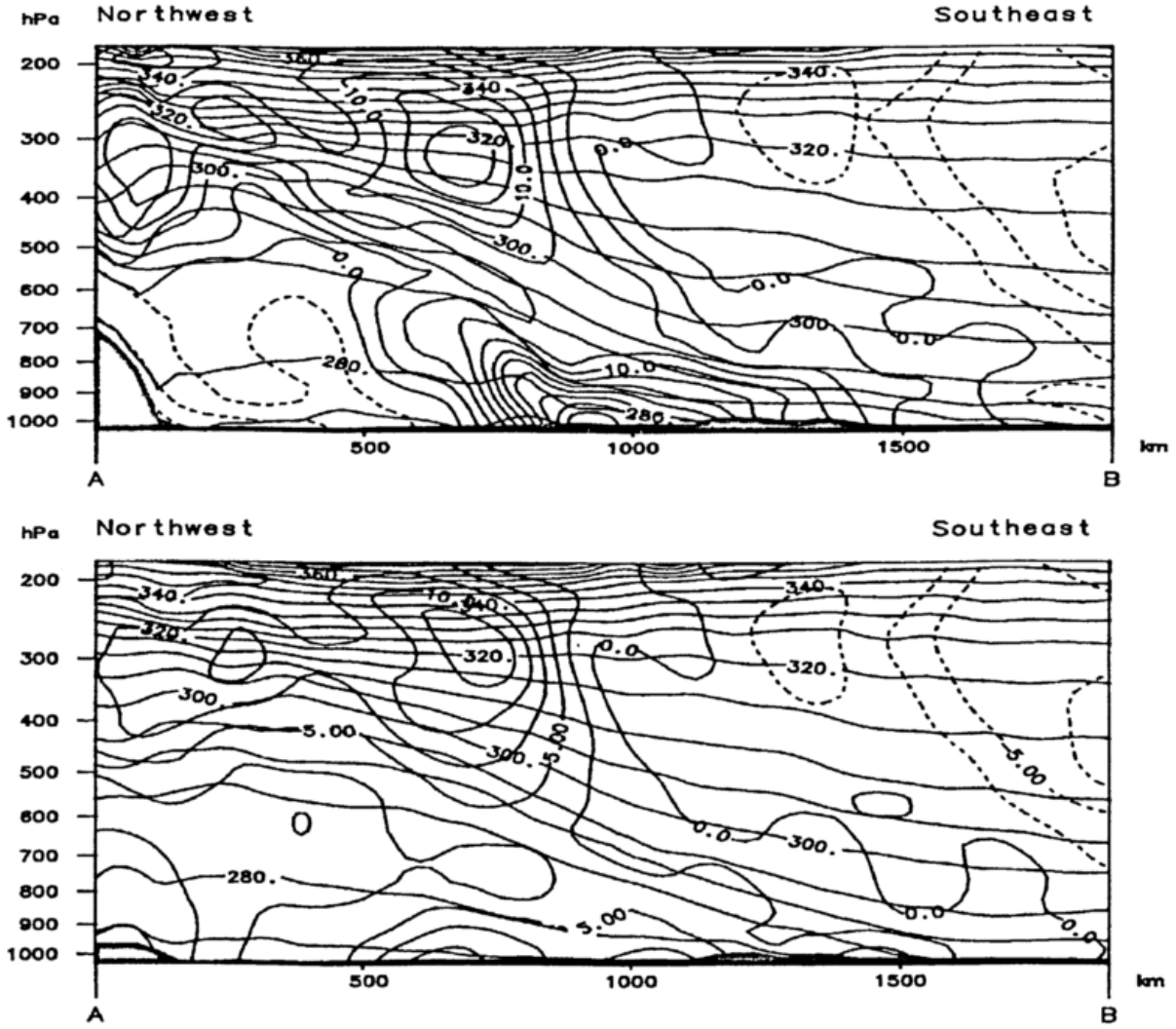

Figure 7. Cross section along the line A-B marked in Fig. 6. Shown is relative vorticity (10 E-5/s; negative values dashed) and isentropes (K; quasi-horizontal lines) after 48 hours of forecast for 20 January 1983 12 UTC. a) full mountain forecast (top); b) no-mountain forecast (bottom).

isentropic surface 287.5 K. Starting from the southern tip of the Alps it turned cyclonicaly around the pressure fall area in the lee of the Alps (compare Fig. 3) until it entered the northern Adriatic Sea. There it was deflected anticyclonically after 12 hours while it migrated through the region of anticyclonic vorticity in the gulf of Triest (Fig. 4a). It did not acquire cyclonic vorticity before it entered the region where the vorticity maximum is found after 18 hours. Therefore, it does not seem that vorticity advection at low levels has contributed to vorticity generation. It is more plausible that the cyclonic vortex is a stationary feature in the low level flow. The anticyclonic deflection of cold air around the eastern edge of the Alps leads to a strong cyclonic jump in wind direction in the northern Adriatic Sea. The surface wind barbs show this clearly (Fig. 3; note that only every third wind barbs is drawn). The cyclonic turning in that area is weak in the no-mountain run. There the flow in the Po valley and the gulf of Triest is straight from the north (not shown) in contrast to the northeasterly flow in Fig. 3. Therefore, it can be concluded that the cyclonic cell in the northern Adriatic is a direct consequence of the anticyclonic deflection of the near ground flow around the eastern edge of the Alps. Inspecting consecuting charts of wind and vorticity on 900 hPa we find that this flow configuration at low levels does not change considerably during the next 18 hours. Note the very slow movement of the particle bewteen 18 and 36 hours (Fi.g 5). Lateron the vorticity maximum gets superpositioned by the upper-level potential vorticity maximum which has progressed in the mean time over the Alps (Fig. 6). After 48 hours a connection between the vorticity maxima at upper and lower levels is established as is found typically in the maturing phase of a extratropical cyclone (Fig. 7a). This process cannot take place in the no-mountain run where no low-level vorticity maximum has been generated during the previous hours (Fig. 7b). We therefore find a new cyclone only in the full orography run (Fig. 8a), but not in the no-mountain run (Fig. 8b). It's depth is a little weaker than observed (compare Fig. 2), but the location is right.

The model forecast has been continued another 12 hours but lateron fails to reproduce the observed strength of the cyclone. This can be attributed to the lack of moisture in the model physics. It seems plausible that moisture fluxes from the sea helped to strengthen the cyclone while it moved toward the eastern Mediterranean.

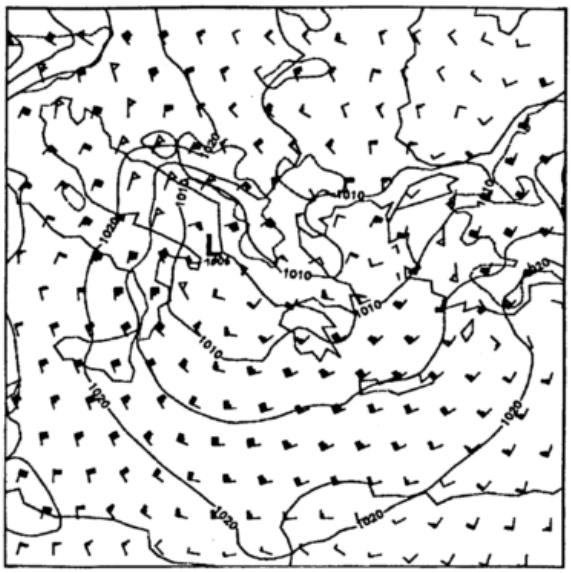

Figure 8a. Sealevel pressure (hPa) and surfeace wind after 48 hours of forecast for 20 January 1983 12 UTC.

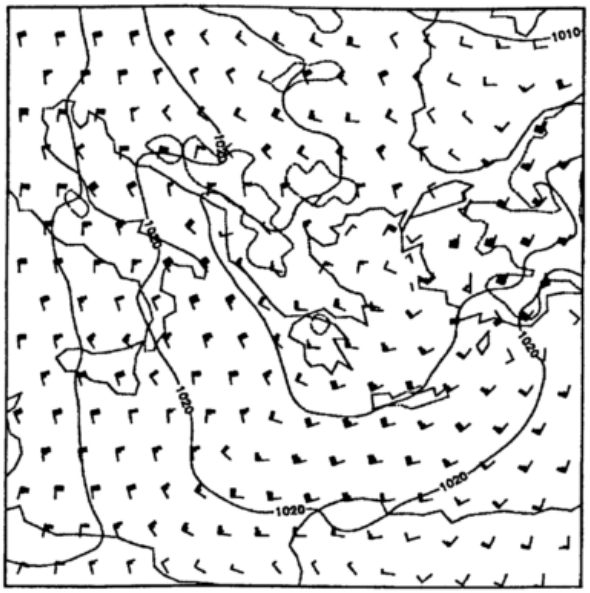

Figure 8b. As in Fig. 8a, but no-mountain forecast.

4. Conclusions

By now it cannot be said if the processes found in this study are typical during the life cycle of an Adriatic cyclone. More cases need to be taken under investigation. It is quite plausible that the cyclonic vortex at low levels in the northern Adriatic Sea is a frequent feature when there is a flow deflection around the eastern Alps into the gulf of Triest. Once generated the low level vortex seems to play the same role in triggering cyclogenesis as does the low level vortex found often in the gulf of Genoa during lee cyclogenesis. Despite the generation of the cyclone in the Adriatic Sea instead of the lee of the Alps, it should be termed a „lee cyclone" as it would not have existed without the Alps. The maturing phase of baroclinic growth was found to consist of the typical vorticity coupling between an upper and a lower level cyclonic disturbance as has been identified in other studies of Alpine lee cyclones. With the dry adiabatic model used here we were not able to catch the late phase of the cyclone following the baroclinic growth.

Acknoledgement
I am grateful to the Deutscher Wetterdienst for providing radiosonde data for this case.
Remark
This paper has been presented during the Symposium on "The Life Cyle of Extratropical Cyclones" in Bergen, Norway, 27 June - 1 July 1994

References:

Bleck, R., 1975: An economical approach to the use of wind data in the optimum interpolation of geo- and Montgomery potential fields. Mon. Wea. Rev., **103**, 807-816

Bleck, R., 1984: An isentropic coordinate model suitable for lee cyclogenesis simulation. Riv. Meteor.Aeronaut. **44**, 189-194

Buzzi, A. and S. Tibaldi, 1978: Cyclogenesis in the lee of the Alps: A case study. Quart. J. Roy. Met. Soc.,**104**, 271-287

Egger, J., 1988: Alpine lee cyclogenesis: verification of theories. J. Atmos. Sci., **45**, 2187-2203

Hoskins, B. J., M. E. McIntyre and A. W. Robertson, 1985: On the use and significance of isentropic potential vorticity maps. Quart. J. Roy. Meteor. Soc. **111**, 877-946

Lanzinger, A., 1992: Upper and lower level PV-coupling associated with Alpine lee cyclogenesis. Meteor. Zeitschrift., N.F. **1**, 173-181

Mesinger F., and R. T. Pierrehumbert, 1986: Alpine lee cyclogenesis: Numerical simulation and theory. Scientific Results of ALPEX, GARP Publ. Series No. **27**, Vol. I, WMO

Pichler, H., and R. Steinacker, 1987: On the synoptics and dynamics of orographically induced cyclones in the Mediterranean. Meteor. Atmos. Phys., **36**, 108-117

Pichler, H., R. Steinacker and A. Lanzinger, 1990: Cyclogenesis induced by the Alps. Meteor. Atmos. Phys., **43**, 21-29

Tafferner, A., 1990: Lee cyclogenesis resulting from the combined outbreak of cold air and potential vorticity against the Alps. Meteor. Atmos. Phys. **43**, 31-47

Tafferner, A., and J. Egger, 1990: Test of theories of lee cyclogenesis: ALPEX cases. J. Atmos. Sci., **47**, 2417-2428

Tafferner, A., and J. Egger, 1992: Modification of fronts by the Alps: simulation and numerical experimentation. Meteorol. Atmos. Phys., **48**, 193-203

ALPEX-Simulation

H. Pichler

Institut für Meteorologie und Geophysik, University Innsbruck

Abstract

In a project "ALPEX-Simulation", sponsored by the "Österreichischer Fond zur Förderung der wissenschaftlichen Forschung (FWF), all eight cases of ALPEX-SOP cyclones were numerically simulated with a fine mesh isentropic model of the atmosphere. These numerical simulations in six-hourly intervals allow a deeper insight into the synoptics and dynamics of the cyclogeneses in the Western Mediterranean, especially into the genesis of the two basic types of cyclones: the so-called "Überströmungs"-type and "Vorderseiten"-type. In the first phase of cyclogenesis of the "Überströmungs"-type, the blocking and flow splitting of the cold air due to the Alps and the canalization between the Alps and the Massif Central are important. Cold air flows cyclonically around the western part of the Alps, creating a vorticity maximum at the south western edge of the Alpine bow and leads also to an enhanced PV. In connection with warm air in the Mediterranean, a strong baroclinic zone is generated. The interaction between the arriving PV maximum in the upper troposphere and the enhanced PV at the bottom leads to cyclogenesis in the Western Mediterranean. In the case of the "Vorderseiten"-type warm air advection dominates with the expection of a shallow layer of cold air in the inner Po-Valley, which is shielded by the Alpine ridge. A well pronounced PV maximum builds up and couples with the PV maximum arriving at upper levels, even before the cold air, coming from the north-west, has surrounded the Alps. The cold air only intensifies the development by raising the baroclinity. Therefore, the "Vorderseiten"-cyclogenesis is an *orographically modified cyclogenesis*, in the course of which the cyclonic development is triggered by the Alps, whereas the "Überströmungs"-cyclogenesis is an *orographically induced cyclogenesis* i.e. a "true" lee cyclogenesis.

For more details the reader will find extented versions of "ALPEX-Simulation" in:

a) H. Pichler, R. Steinacker, E. Hagenauer and A. Jäger (1994 or 1995): ALPEX-Simulation. Meteorol. Atmos. Phys. (in print), Springer Wien-New York.

b) H. Pichler, R. Steinacker, E. Hagenauer and A. Jäger (1993): ALPEX-Simulation, Atlas of short range forecasts in comparison to analysis of ALPEX-SOP cyclones in the Western Mediterranean. Department of Meteorology and Geophysics, University Innsbruck; 423 pp.
This publication can be ordered from Department of Meteorology and Geophysics, University Innsbruck, Innrain 52, A-6020 Innsbruck, Austria.

The ALPEX level IIIb Analyses produced at the DWD

Gerhard Paul
Deutscher Wetterdienst - Zentralamt, 63067 Offenbach, F.R.G.

1 INTRODUCTION

The Research Department of DWD has been producing ALPEX IIIb analyses for the SOP-Period with its forecasting system. It consists of the global Model(GM) and the Europa-Model(EM) embedded into the GM. The GM(T106) is based upon the ECWMF model. The EM has a horizontal resoluton of 0.5^{o} on a rotated spherical grid and 20 vertical levels in a hybrid terrain following coordinate system. Eight layers are used in the lowest 2 km of the atmosphere to reproduce the structure of the boundary layer sufficiently well. The initial data for both models are prepared by two separate, 6-hourly intermittent data assimilation cycles, consisting of a multivariate three-dimensional optimum interpolation, a nonlinear normal mode initialization, and a 6-hour forecast. The status of the project is : The set of reference analyses(using only GTS Data) is being completed, the analyses including the additional checked and corrected SOP data will be produced in 1994.

2 FEATURES OF THE DATA ASSIMILATION SYSTEM

The main differences between GM and the current ECMWF model are the horizontal and vertical resolution (T106 vs. T213, L19 vs. L31), the orography (mean vs. envelope-type) and the radiation scheme. GM is used for large-scale predictions, the regional EM for the synoptic and meso-αscale. Fig.1 shows the data assimilation streams for the GM and EM. Both streams run in parallel and the EM is only coupled via the boundary data written by the GM every 3 hours. Analysed variables are horizontal wind, geopotential, relative humidity(optimum interpolation) on model levels, snow depth, sea surface temperature (correction method). For the 11 standard pressures levels(1000,950,850,700,500,400,300,250,200,100,50 hPa) analyses are provided too. The structure functions of the 6-hour forecast error for the GM/EM used in the OI scheme are presented in Fig.3. The correlation component length scale of the EM(240 km) is shorter than for the GM(400 km). In the analysis for the EM smaller scales can be corrected and the balance between mass and wind is appropriate.
The correlation function as used at ECWMF in 1982 is broader as the present one. Thus, the old analyses are smoother and show less detail.
The description of the orography is more realistic in the EM (Fig.2a) as in the GM(Fig.2b). The maximum height for the Alps is only around 1500 m for the GM, whereas the barrier extends to a height of up to 2300 m in EM. Main features such as the shape of the Alps and the river Po-valley are existent in the EM allowing a realistic flow over and around the Alps.

3 MONITORING OF THE DATA ASSIMILATION SYSTEM

The complete 2 data assimilation systems were started for the 13th of February 1982 from climatological fields(so called cold start) and run for 14 days to get a realistic state of the atmosphere. The runs were controlled by the experiment system: start, executing, archiving and the graphical output is operating in a continuous manner. The requirements for the storing device are 0.6 GBytes and for computing time 20000 CPU-sec for 1 day of EM/GM data assimilation(CRAY YMP4). Under real application condition 1 day of data assimilation is done in one calendar day.
For monitoring the quality of the assimilation verification statistics from radiosonde data the three quantities: Observation minus 6-hour Prediction(O-P), Observation minus Analysis(O-A), Observation minus Initialized analysis(O-I) for the variables geopotential, wind and relative humidity are calculated.
For a horizontal uncorrelated observing system as radiosonde the mean difference shows systematic error in the assimilation, the standard deviation of the differenc(O-A) is a measure of either the local accuracy of the analysis to observations and/or the random error of the radiosonde. The reduction of the quantity (O-P) to (O-A) gives some limit of the response of the analysis to the observations. The quantity (O-I) shows, how well the analysed fields are in balance with the numerical models solutions.
The quality of the alpex assimilation is similar to the actual one in 1994. For alpex assimilation a deficit is still in the upper tropospheric humidity analysis (in the operational analysis code already removed) and the stratospheric geopotential analysis shows greater differences to observations. This may be caused by the minor observation quality of radiosondes in the early eihties.

4 THE CHARACTERISTICS OF THE EM ANALYSES

Comparing the EM Analyses to numerical analyses produced in 1982 (e.g. ECMWF) the main structures in the mass field are very similar. Only phenomena of the meso-α scale are more concise, minima of lows, short troughs, blocking in the luv of the Alps, temperature gradients. The EM analyses profits mostly in the wind field. In Fig.4 the windfield in 10 m above ground is given for 4th of march 1982; the shaded area depicts the model orography above 600m. This is the early stage of the most significant leecyclogenesis occuring during the SOP. A pronounced cold front approaches the Alps and an initial wave is forming in the lee (Fig.5). In the EM Analysis many details of the observed phenomena can be detected: N to NW winds including mistral in Rhone valley behind the cold front, the flow around the Alps.
In general the EM analyses are able to produce the relevant orographically stimulated phenomena of the meso-α scale and the main advantage is the well balanced 4-dimensional set of atmospherical fields for the SOP.

5 AVAILABILITY OF THE ALPEX ANALYSES

The data format for the analyses, initialized analyses and 6-hour forecasts for the EM and the GM is the GRIB-Format. The set of reference analyses(using the GTS data only) is completed until September 1994, the set of analyses(using the additional data) will be produced towards the end of 1994. Delivery of data is foreseen on magnetic tapes and orders may be addressed to:
Deutscher Wetterdienst, Department of Climatology, Postfach 100465
63004 Offenbach, Germany.

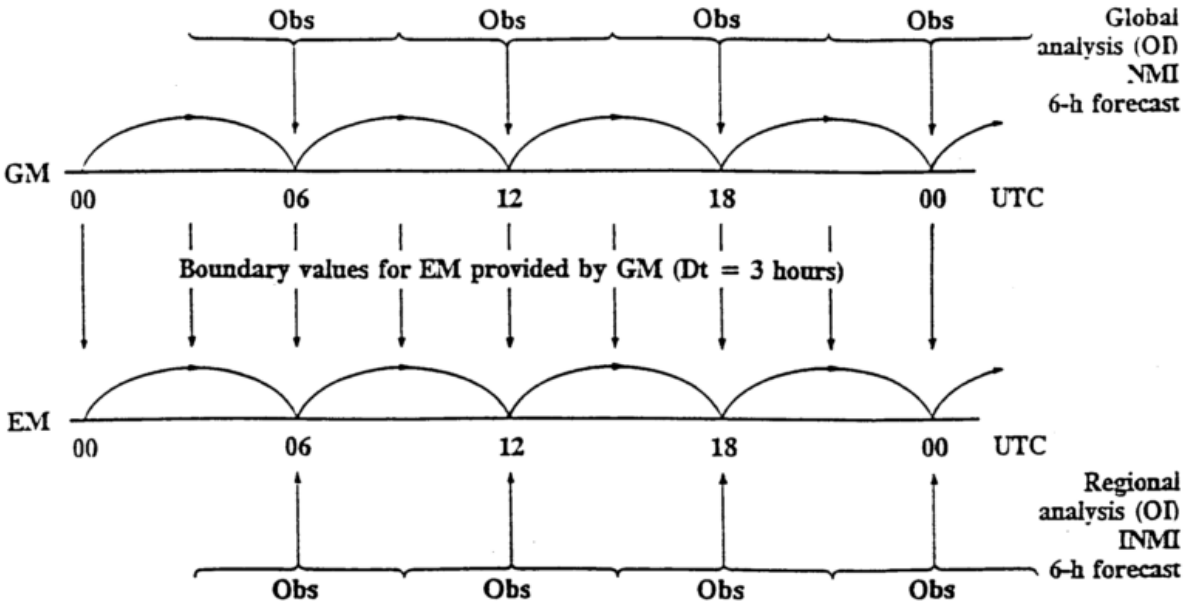

Fig. 1 4dim. data assimilation for GM and EM

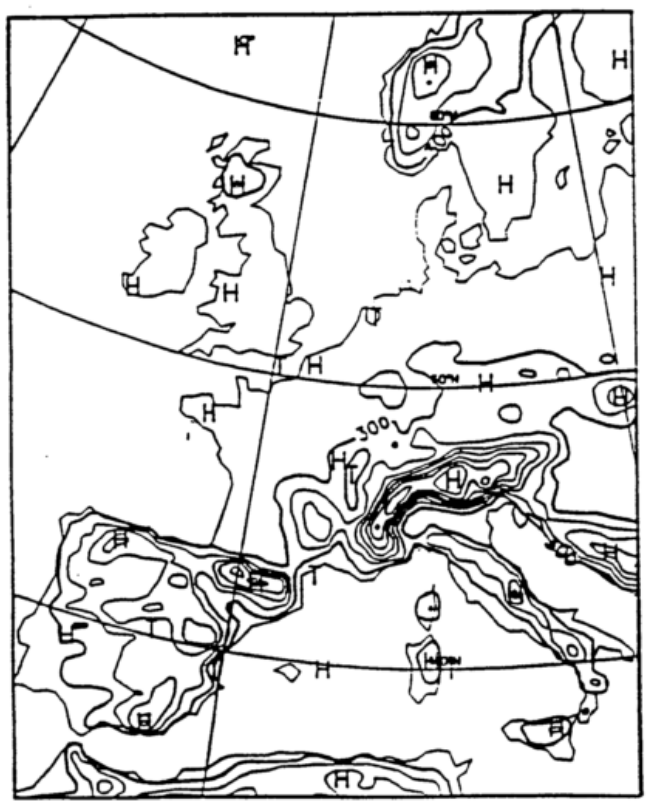

Fig. 2a Orography of Europa-Modell (EM) for Central Europe.

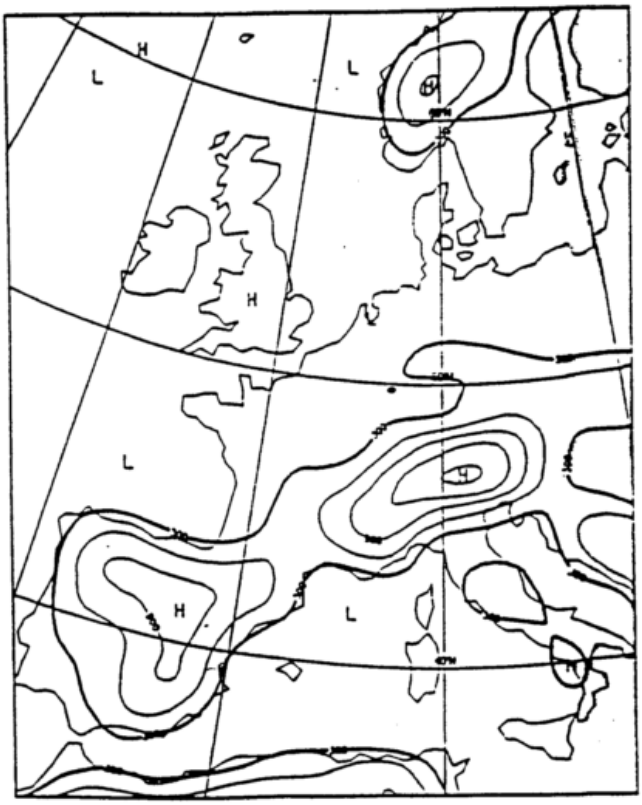

Fig. 2b Orography of Global-Modell (GM) for Central Europe

Reference line: 300 m; increment 300 m.

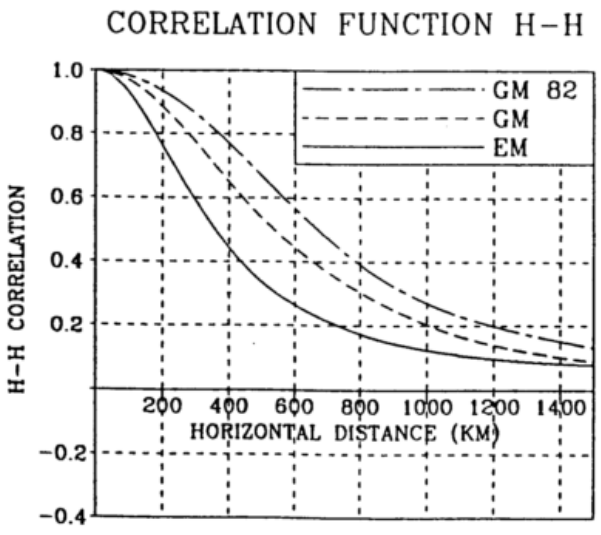

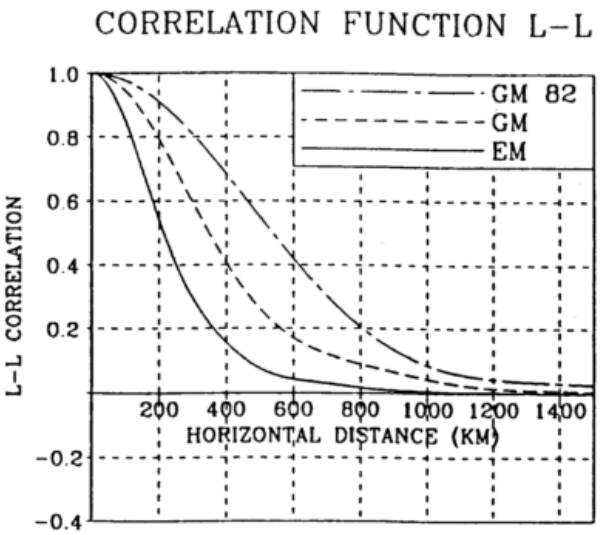

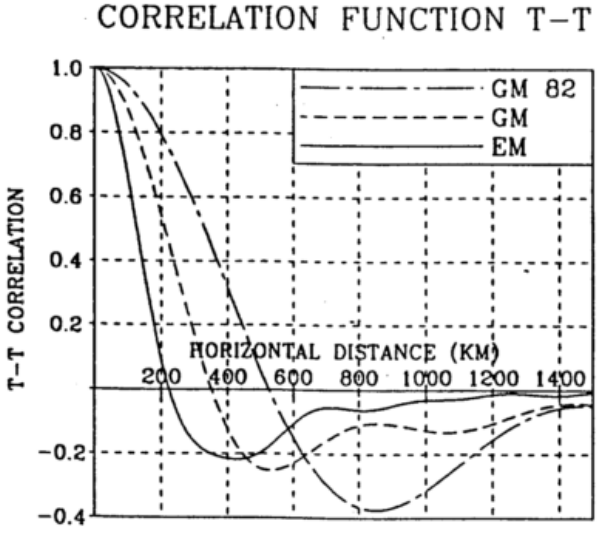

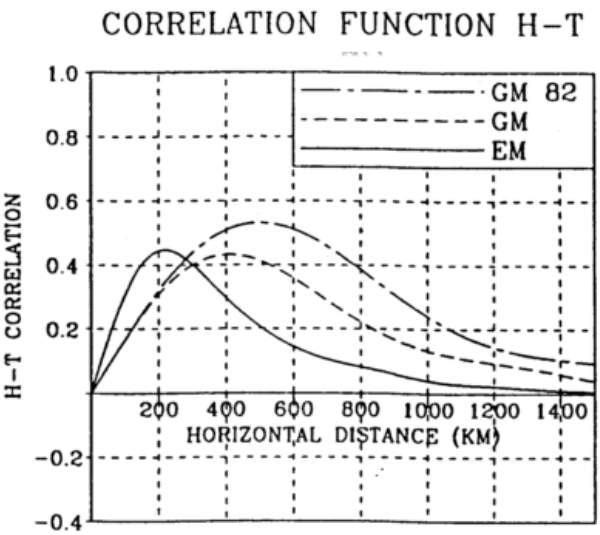

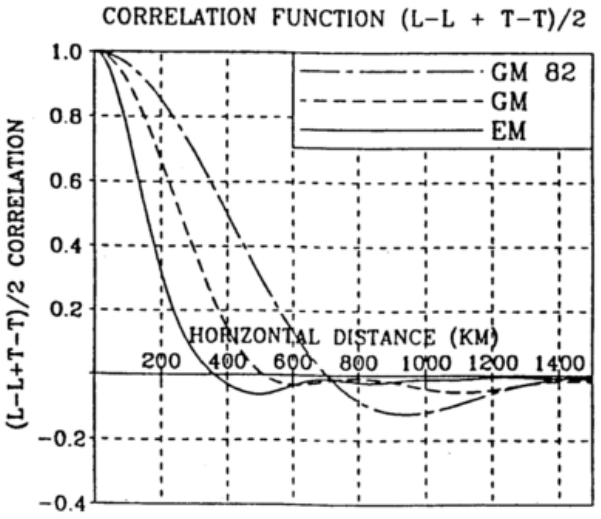

6-HOUR FORECAST ERROR CORRELATIONFUNCTION OF THE EUROPA MODEL / GLOBAL MODEL

H-H HEIGHT CORRELATION
L-L LONGITUDINAL VELOCITY CORRELATION
T-T TRANSVERSE VELOCITY CORRELATION
H-T HEIGHT/TRANSV.VELOCITY CORREL.
(L-L + T-T)/2 VELOCITY CORRELATION

Fig. 3 Correlationfunction

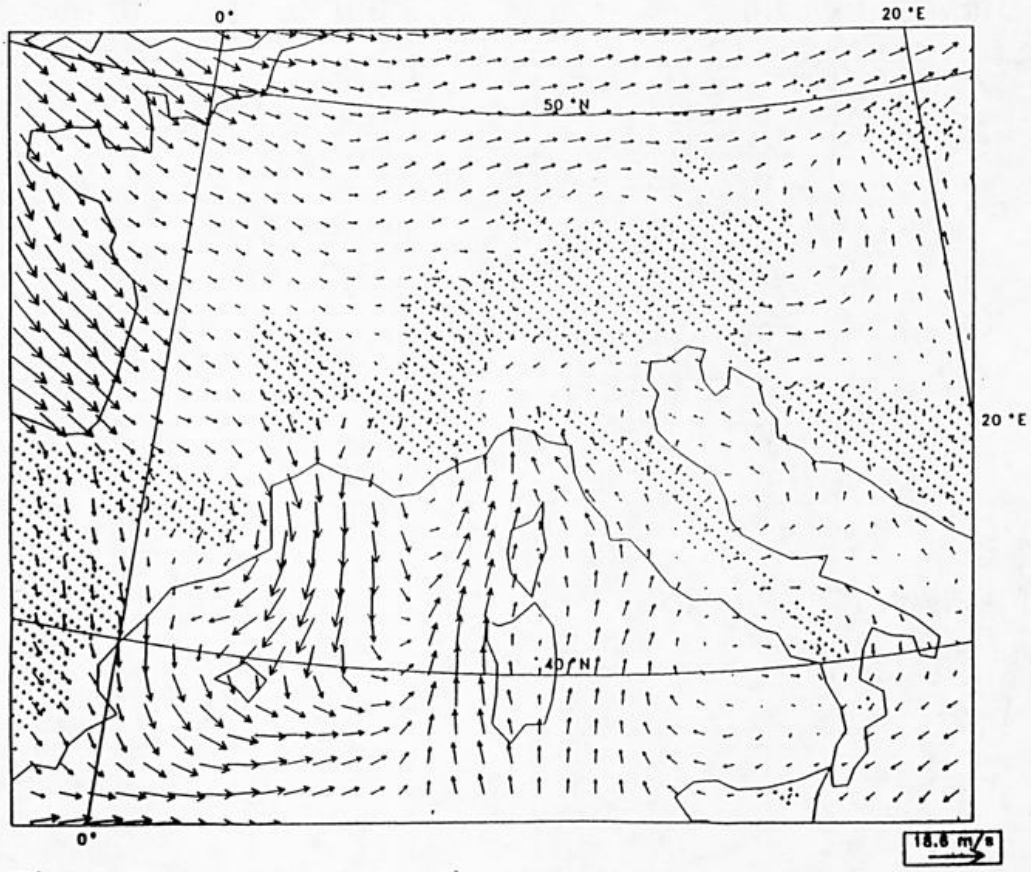

Fig.4 Europa-Analysis Windvector 10m 4.3.1982 12 UTC

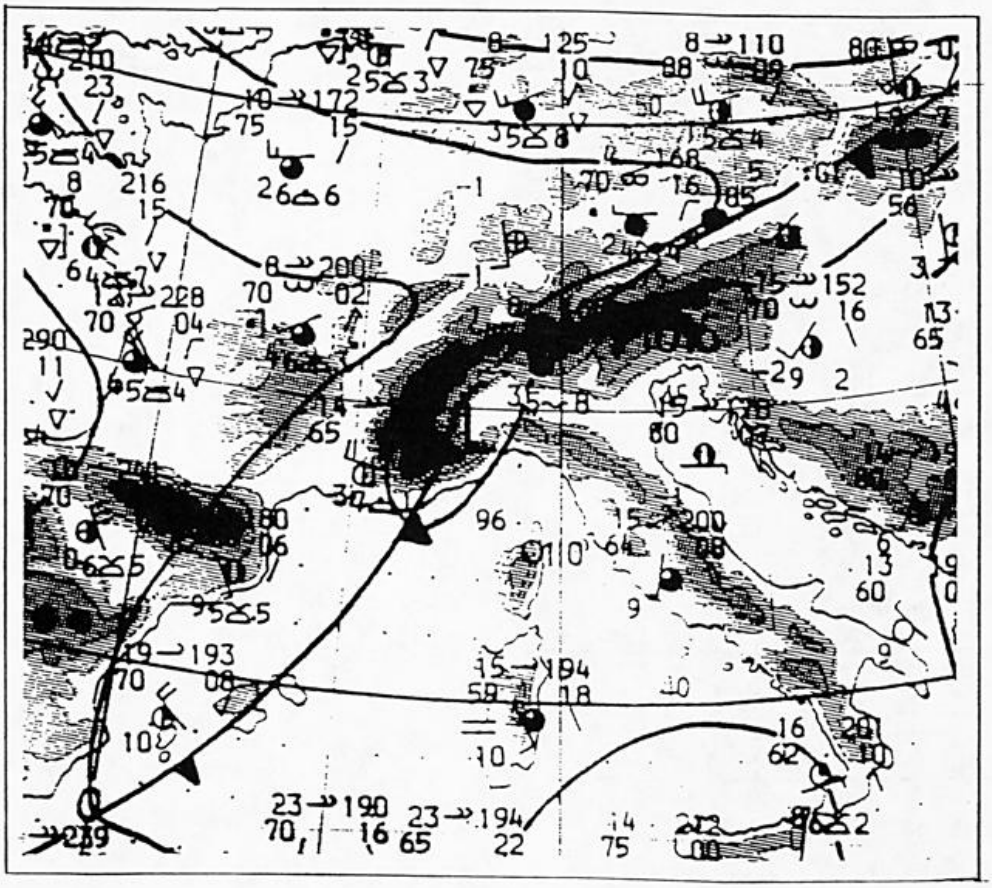

Fig. 5 Surface-Analysis(DWD) 4.3.1982 12 UTC

Mountain Induced Flow in the Operational Deutschland-Modell

J.Steppeler, U.Damrath, D.Majewski
DWD,Offenbach

Since the first of July 1993 the Deutschland-Modell (DM) of DWD with horizontal meshlength 14 km is in operational use. Some characteristic features of this model, and of the Europa-Modell (EM) with a horizontal meshlength of 56 km are given by Majewski and Schrodin (1994).

The purpose of the DM is to provide small scale details, which are not captured by the coarser mesh of the EM. Figs. 1,2 give the example of the 2m wind forecast with EM and DM from 1 June 1994. At the coasts of Germany and the Netherlands small scale deformations of the wind field are observed, including a substantial change in wind direction, as compared to the result of the Europa-Modell. Such differences are important for weather forecasting in coastal areas. The weakening and turning of the wind to northerly directions can be verified by synop observations at 15UTC. An inspection of the model results reveals that small scale orographic features are causing such differences. In this case it is the minor orography associated with the land-sea contrast, mainly by the resulting temperature difference.

One of the most important forecast information of the DM is small scale precipitation. Fig.3 shows the precipitation forecasts for DM and EM accumulated for the period of 17 to 23 of December 1993. This is associated with the so called Christmas flood. The observations are from the climatological raingauge system, involving about 5000 observation sites in Germany and Switzerland. The EM captures some of the coarse structures of the rainfall areas. It misses the small scales and the strong peaks up to 280 mm in the observed field. The DM forecast provides valuable realistic details to this picture. In particular the areas of very strong precipitation are captured well by DM. Also the areas with low precipitation in the Rhine valley are well indicated in the DM forecast. The rainfall in the Alpine region also shows a marked mesoscale structure, which the DM forecast captures with some realism, while the EM obviously has a too large scale to capture these details. Precipitation verification for a period of three months is done using 220 selected stations in Germany and Switzerland. Table 1 shows a contingency table verifying the rainfall forecast (18-30h). The number of cases is given, where a class of precipitation (0-0.1,0.1-2,2-10,$>$10mm) is forecasted. This is shown against the class which actually occurs. The diagonal elements of the table, containing the number of classes which have been forecasted correctly, are much larger than the side-diagonals, containig the forecasts with an error. A a small problem concerns the class with precipitation $>$10mm. Here the side diagonals contain more cases than the off diagonals, and it even occurs that more than 10mm of rain is forecasted, when in reality there is less than 0.1mm. The table contains greater numbers below the diagonal than above. This points to a tendency of DM to overpredict precipitation.

The quality of several DM forecast elements as compared to EM is shown in Fig. 4. It gives

monthly averages dependent on forecast time for each month of the year. The verification quality for the different elements can depend strongly on the lead time of the forecast and on the season of the year.

REFERENCE

Majewski, D. and R. Schrodin, 1994: Short description of the Europa-Modell (EM) and the Deutschland-Modell (DM) of Deutscher Wetterdienst (DWD), April 1994,28pp, DWD

Prog/Observation	0-0.1mm	0.1-2mm	2-10mm	>10mm
0-0.1mm	3062	286	93	9
0.1-2mm	4210	2158	1168	94
2-10mm	574	929	1648	261
> 10mm	78	71	291	192

Table 1:
Contingency table of total precipitation for DM forecasts, starting 00 UTC, December 93 January and February 94 for 220 stations in Germany and Switzerland

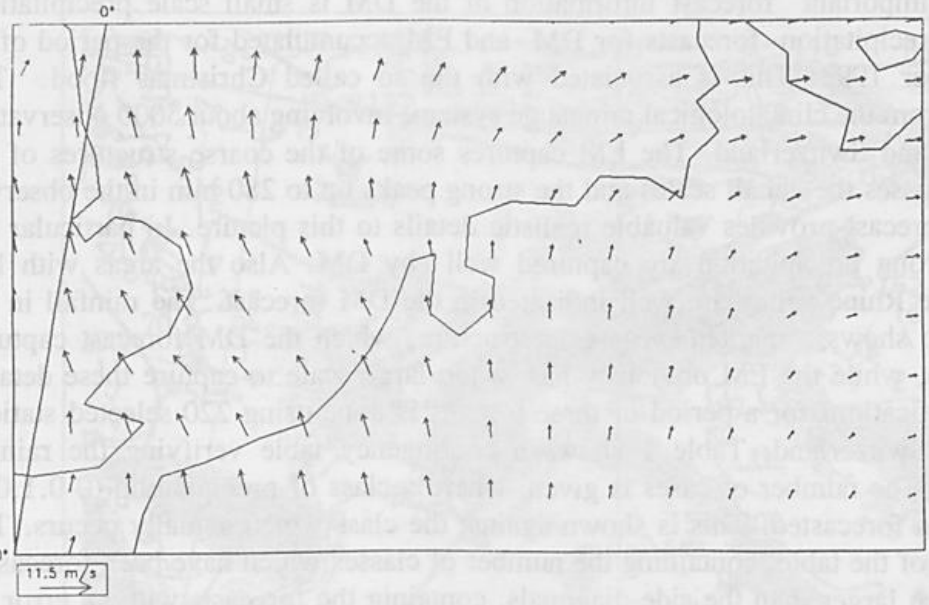

Fig. 1 :
15-h forecasts of EM of winds at 10 m, valid at 15 UTC on 1 June 1994.

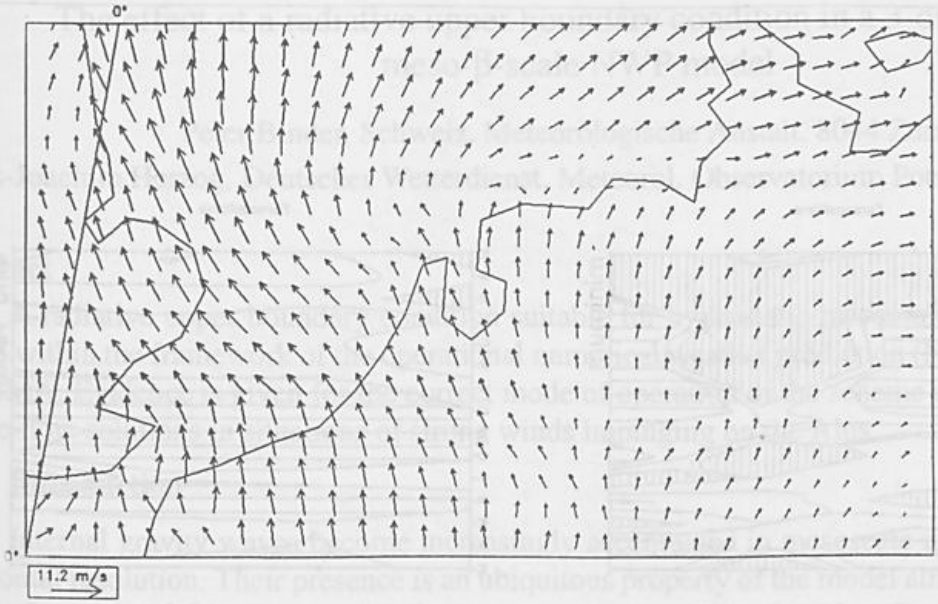

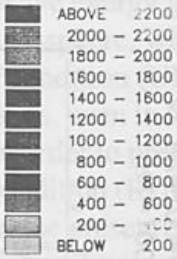

Fig. 2 :
As fig. 1 for DM.

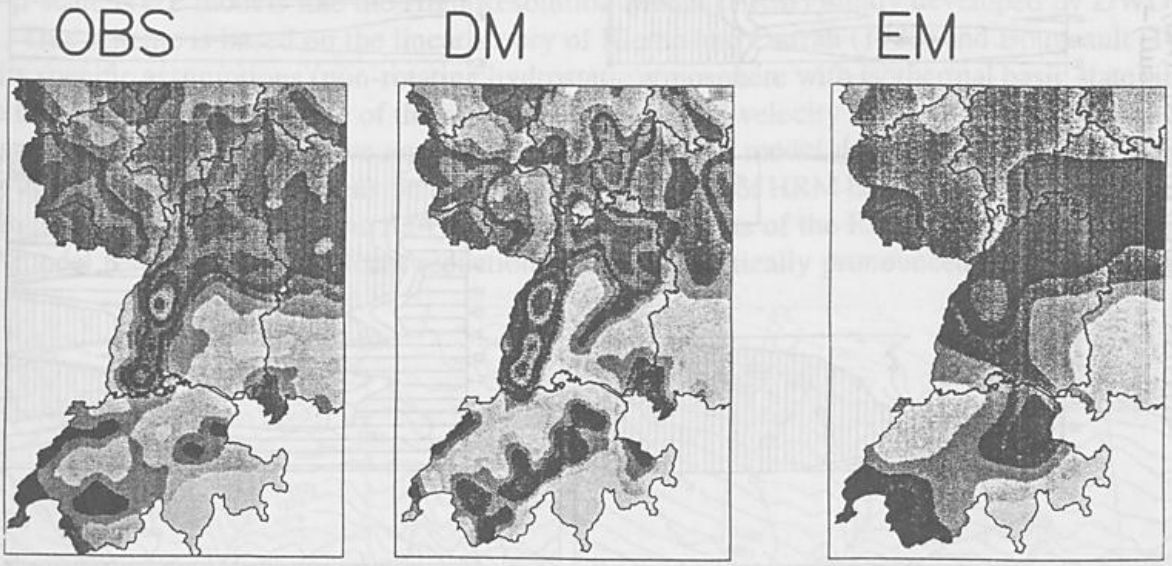

Fig. 3 :
Sum of precipitation during the "Christmas flood" in the south-western Part of Germany (17. 12. 1993 06 UTC until 23. 12. 1993 06 UTC.

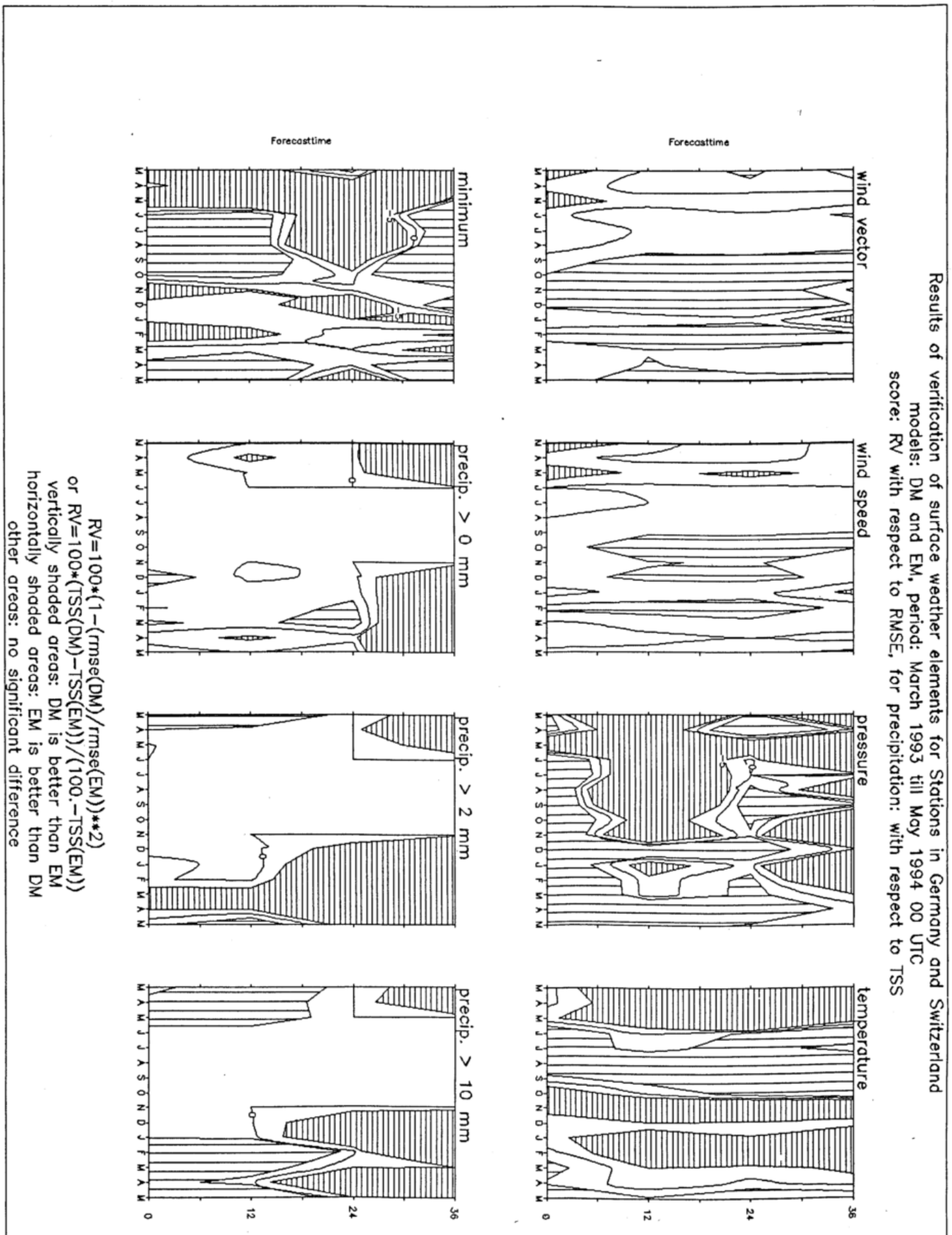
Results of verification of surface weather elements for Stations in Germany and Switzerland
models: DM and EM, period: March 1993 till May 1994 00 UTC
score: RV with respect to RMSE, for precipitation: with respect to TSS
Forecasttime
wind vector
wind speed
pressure
temperature
minimum
precip. > 0 mm
precip. > 2 mm
precip. > 10 mm
M A M J J A S O N D J F M A M
0
12
24
36
RV=100*(1-(rmse(DM)/rmse(EM))**2)
or RV=100*(TSS(DM)-TSS(EM))/(100.-TSS(EM))
vertically shaded areas: DM is better than EM
horizontally shaded areas: EM is better than DM
other areas: no significant difference

Fig. 4 :

The effect of a radiative upper boundary condition in a 3-dimensional meso-β-scale NWP model

Peter Binder, Schweiz. Meteorologische Anstalt, 8044 Zürich
Hans-Joachim Herzog, Deutscher Wetterdienst, Meteorol. Observatorium Potsdam, 14473 Potsdam

Abstract

A radiative upper boundary condition suitable for hydrostatic mesoscale numerical models is tested within the framework of the operational numerical weather prediction (NWP) models of DWD and SMA. Evidence is given for the correct mode of operation of the scheme and its positive impact on the flow solutions in situations of strong winds impinging on the Alps.

1. Introduction

Internal gravity waves become increasingly accentuated in mesoscale models with increasing horizontal resolution. Their presence is an ubiquitous property of the model atmosphere, in particular due to flow over highly structured and steep mountain areas like the Alps. Gravity wave energy generated by orography is propagated upwards and reflected at the top of the model atmosphere, where most commonly a lid-type boundary condition is used. This type of upper boundary condition (UBC) can be responsible for the contamination of the model's flow solution by reflected waves, even in lower-levels of the model atmosphere which are of immediate meteorological interest. In order to prevent from this undesirable reflection, the implementation of a radiative upper boundary condition (RUBC) into a complex mesoscale numerical weather prediction (NWP) model is described in the present contribution. A radiative scheme has been developed by Herzog (1994), which applies to hydrostatic meso-β-scale NWP models like the High Resolution Model (HRM) jointly developed by DWD and SMA. This scheme is based on the linear theory of Klemp and Durran (1983) and Bougeault (1983) with its specific assumptions (non-rotating hydrostatic atmosphere with isothermal basic state) in order to find a reasonable estimate of the non-vanishing vertical velocity at the upper model boundary, corresponding to mesoscale wave energy radiation out of the model domain. Gravity wave experiments with a nonlinear two-dimensional vertical-plane version of HRM have clearly demonstrated the advantages of the RUBC over the lid-type condition. First tests of the RUBC in a full meso-β-scale NWP model resulted in a significant reduction of the unrealistically pronounced ridge-trough struc-

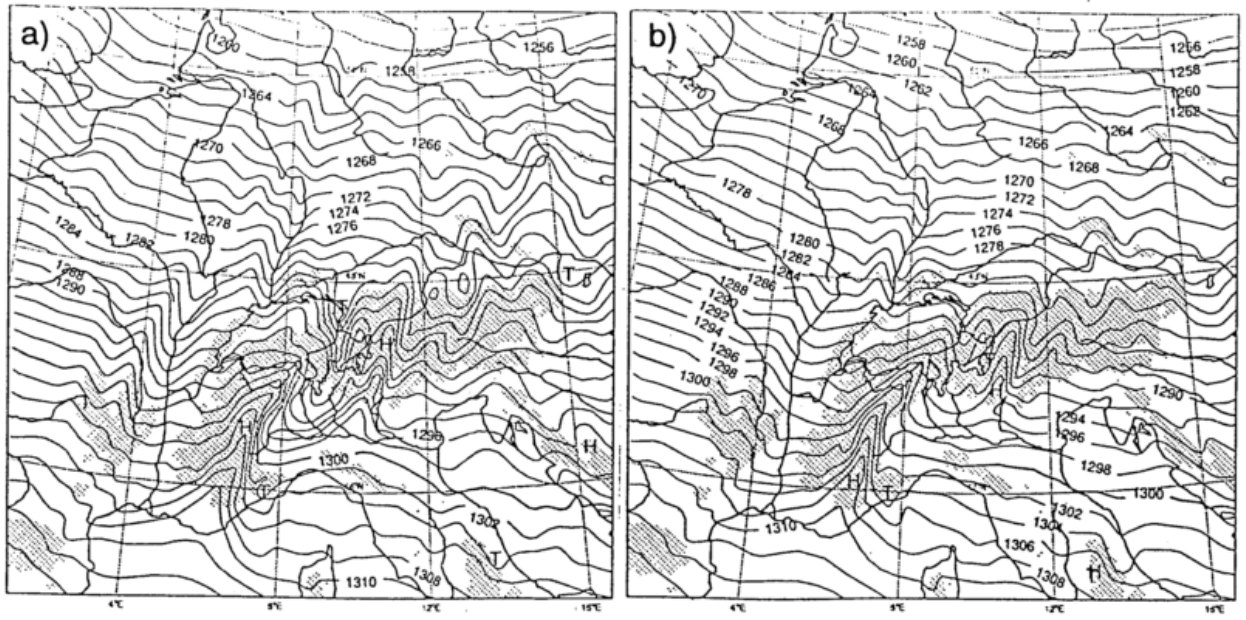

Fig. 1: Geopotential height field (dam) at 165 hPa, 8.12.93 12 UTC +24 h. Terrain heights above 750 m a.s.l. are shaded. Full model domain of 97 x 91 grid points.
a): Lid-type upper boundary condition; b) radiative upper boundary condition (RUBC).

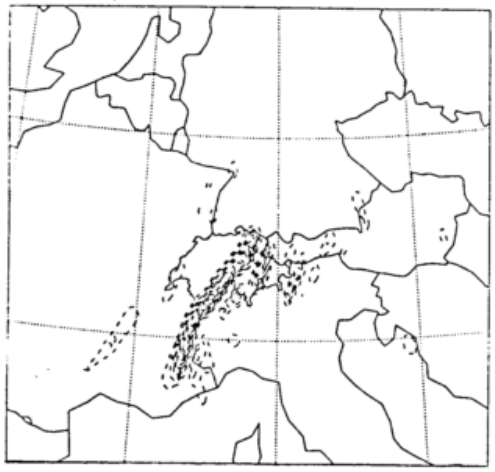

Fig. 2: Instantaneous wave energy flux through the top of the model atmosphere (arbitrary units): 8.12.93 12UTC +24h.

tures, which were present in the vicinity of the Alps in the simulations using the lid-type UBC. From that starting point more systematic investigations were initiated to give evidence of the effect of the RUBC and to reveal its possible meteorological impact.

2. Evidence of the effect of the RUBC as revealed by the simulation of 8.12.93 12UTC +24h

As a representative example for synoptic situations with strong flow towards the Alps, the case of 8/9 December 1993 with prevailing WNW-flow over Europe is chosen for illustration. Similar results are found for synoptic situations with other wind directions like strong N- or S-flow. Simulations are carried out with the following configuration of HRM, which is a hydrostatic primitive equation model with hybrid vertical coordinate (Majewski, 1991): horizontal grid distance 1/8° lat/lon (~14km), 97x91 grid points, 30 vertical levels, semi-implicit time stepping with Eulerian advection, time step 90s. Fig. 1a shows the strong orographically excited perturbations of the basic WNW flow in the upper model atmosphere, if the commonly used lid-type upper boundary condition is used. Application of the RUBC (Fig. 1b) leads to a much smoother geopotential height field: the wave pattern on the region of the Massif Central and the river Saône has almost disappeared, the ridge-trough structure over the western Alps is distinctly damped as well as the trough over the eastern part of Switzerland, finally perturbations over the eastern part of the Alps are significantly reduced. It is also remarkable that by use of the RUBC the flow field at some distance from the Alps has generally a smoother appearance.

In Fig. 2 the regions of most intense energy flux through the upper model boundary are shown. Obviously the RUBC scheme works correct in the sense, that most hydrostatic mountain wave energy

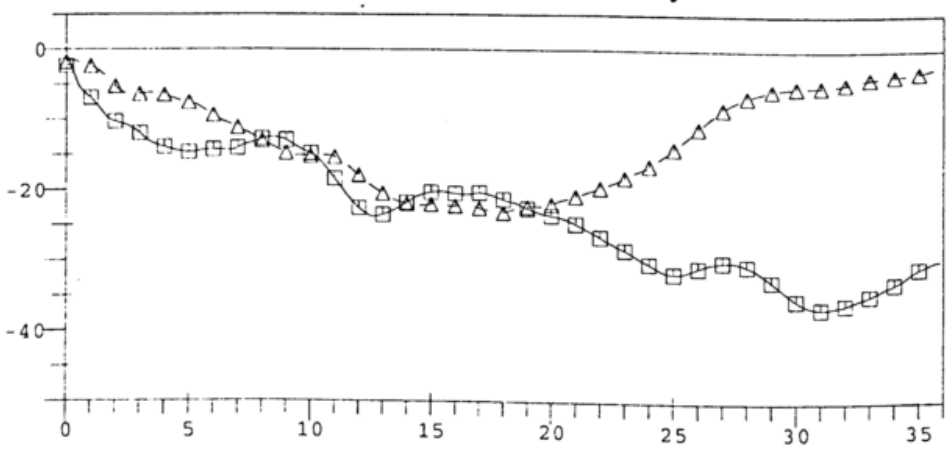

Fig. 3: Time series of an estimate of the area averaged (full domain without lateral boundary zone) energy flux through the model upper boundary for two weather situations: 8.12.93 12UTC (squares) and 27.1.93 00UTC (triangles). The forecast range [h] is indicated on the horizontal axis.

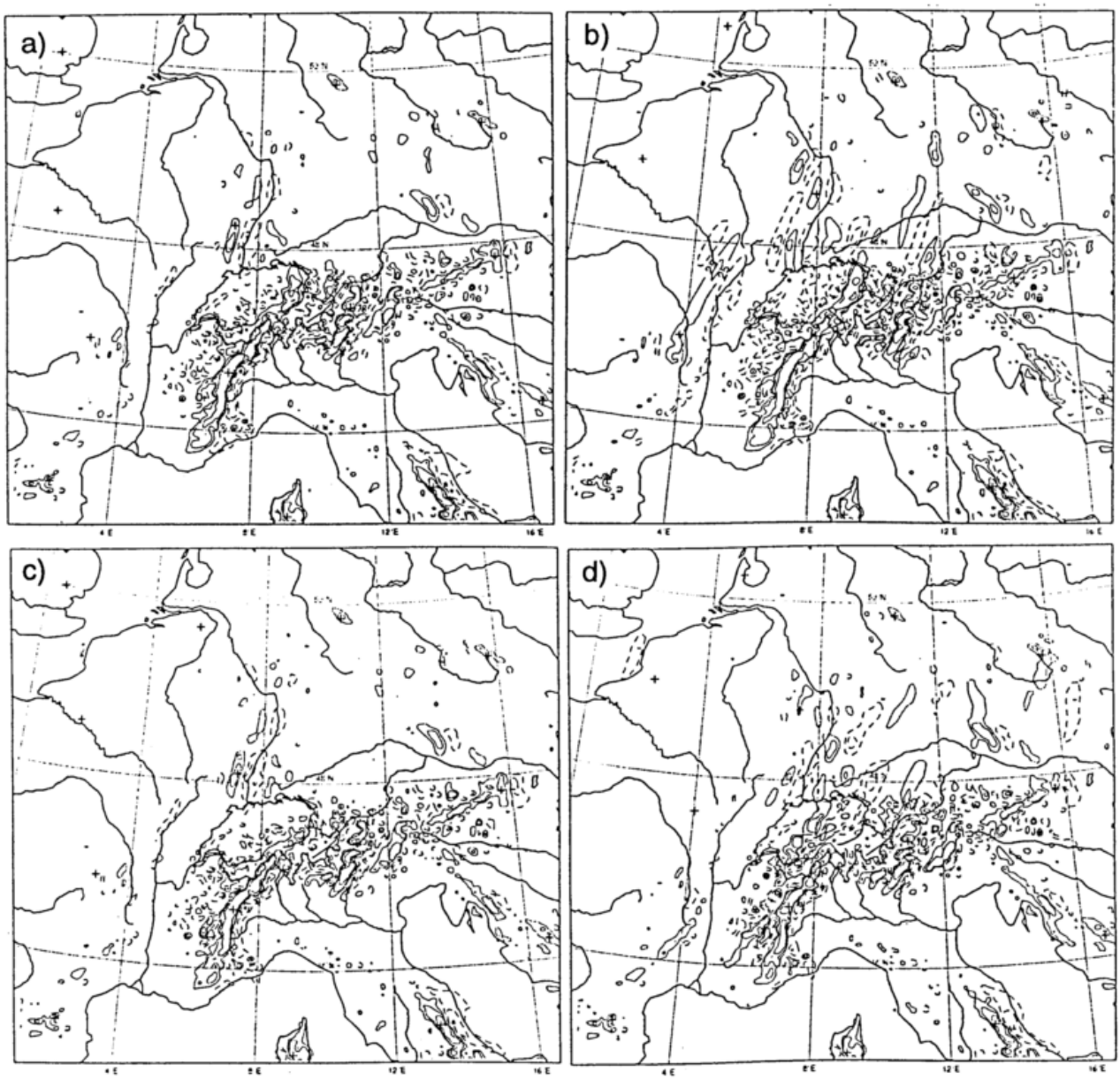

Fig. 4: Vertical p-velocity (ω) at 700hPa for 8.12.93 12UTC +24h.
a) RUBC 30 levels b) LID 30 levels
c) RUBC 20 levels d) LID 20 levels isolines: ±2.5,5,10 Pa/s.

is radiated to space above the region of its origin. In the present flow situation these are the mountains of the Massif Central and most pronounced the western part of the Alps.

The evolution of the area averaged energy flux through the upper model boundary is given in Fig. 3. First, all values are negative which means that wave energy leaves the model domain, thus the energy flux has the correct direction. Second, the time of most intense wave generation and radiation can be identified from these curve. For the situation of 8/9 October 1993 most energy is radiated to space at +31 h. For comparison the time series of a second weather situation (NWN-flow towards the Alps) is also shown in Fig. 3.

3. On the meteorological impact of the RUBC

So far, we discussed the effect of the RUBC in the upper model atmosphere. The relevant question in the context of NWP is, whether there will also be some recognizable impact or potential improvement in model layers immediately relevant for weather prediction. Consideration of the vertical motion field (ω) at 700hPa yields some interesting insights (Fig. 4). The ω-pattern of the experiment using the RUBC (Fig. 4a) appears generally smoother than that using the lid-type UBC (LID) (Fig. 4b). The LID-case shows some maxima which are absent in the RUBC simulation (eastern France, river Danube). The principal maxima at the eastern flank of the western Alps and in the region

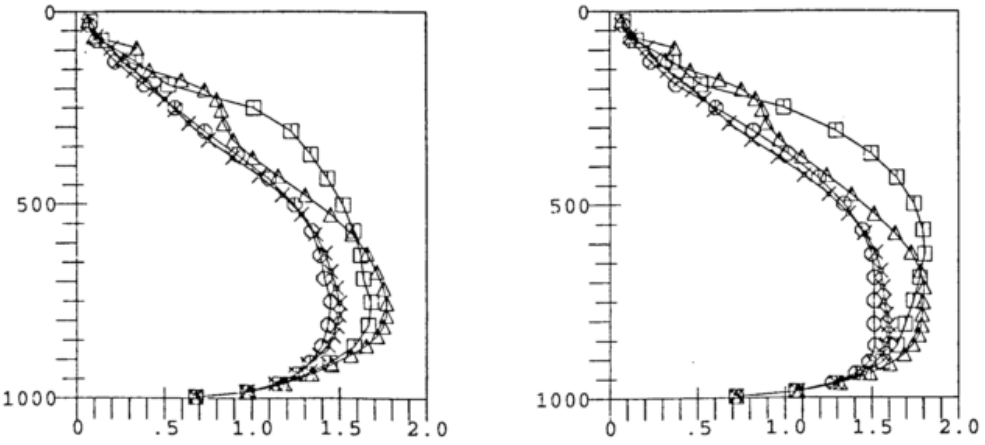

Fig. 5: Vertical profile of the area average (full model domain without lateral boundary zone) of the absolute values of ω [Pa/s]. Pressure is indicated on the vertical axis. 8.12.93 12UTC +24h (left panel) and +30h (right). cross: RUBC 30 levels; triangle: LID 30 levels; circle: RUBC 20 levels; square: LID 20 levels.

of the Brenner Pass are found in both experiments. For comparison the RUBC and LID simulations were repeated with only 20 model levels (Fig. 4c and d respectively). This modification alters the vertical resolution of the model and therefore has an impact on the representation of the vertically propagating waves. Most interestingly, the ω-patterns in the lower model atmosphere differ quite considerably in the LID-simulations, whilst they are very similar in the RUBC-runs. Thus, the reduction of the number of model levels affects the flow solution significantly in the LID-case, but not in the RUBC-case (the same is true if only the distribution of model levels is changed). Evidence for this finding is given in Fig. 5: Here vertical profiles of the area averages of the absolute values of ω are compared for the four experiments. Again, the profiles of the RUBC-simulations are much more similar than those of the LID-experiments. This is an indication that the RUBC removes an undesirable and uncontrollable degree of freedom from the model. Furthermore, from comparison of LID- and RUBC-profiles in Fig. 5 it follows that the model atmosphere is less noisy in the RUBC-cases. Since the vertical motion field is linked to cloudiness and precipitation an impact of the RUBC on these weather parameters must be expected. We also expect differences in the horizontal wind field.

4. Concluding remarks

- A radiative upper boundary condition has been formulated for vertical hybrid coordinates and implemented in a full meso-β-scale NWP model.
- It has been demonstrated that the RUBC works correctly.
- The magnitude of the effect of the RUBC depends on the flow situation.
- An impact of the RUBC on predicted weather elements is probable, but further investigations are needed.
- The RUBC eliminates a degree of freedom, which is related to the choice of the vertical discretization of the model atmosphere, i.e. the number and distribution of model levels.

References

Bougeault, Ph., 1983: A non-reflective upper boundary condition for limited-height hydrostatic models. Mon. Wea. Rev., **111**, 420-429.

Herzog, H.-J., 1994: Testing a radiative upper boundary condition in a nonlinear model with hybrid vertical coordinate. submitted to Meteorol. Atmosph. Phys.

Klemp, J.B., and D.R. Durran, 1983: An upper boundary condition permitting internal gravity wave radiation in numerical mesoscale models. Mon. Wea. Rev., **111**, 430-444.

Majewski, D., 1991: The Europa Modell of the Deutscher Wetterdienst. Proc. ECMWF Seminar on numerical methods in atmospheric models, Vol. II, Sept. 1991, 147-191.

Modelling orographic upslope rain

T. Haiden

Institut für Meteorologie und Geophysik
Universität Wien

ABSTRACT

A two–dimensional, linear model of flow over mountains is used to assess orographic precipitation enhancement in the Alpine region. Nonlinear effects of stratification are parameterized by using the 'dividing streamline' concept. Orographically induced vertical motion is calculated as the sum of an upslope and a blocking component. The upslope component results from directly forced lifting above the orography, and the blocking component from the mass budget of air at lower levels which stagnates because of the stratification. Comparison with observed distributions of precipitation shows to which extent the upslope/blocking mechanism can be captured without explicitly resolving the details of the flow.

1. Introduction

Orography of Alpine dimensions strongly influences the mesoscale distribution of precipitation. The most prominent physical mechanisms are forced lifting of air on the windward side of an orographic barrier, and triggering of deep convection by thermally induced circulations (Smith, 1979; Banta, 1990). In the latter case the daytime heating of the boundary layer and the nonlinear dynamics of dry and moist convective circulations inevitably introduce time–dependence to the problem. The formation of upslope rain, on the other hand, may be regarded as a quasi–steady phenomenon, undergoing changes only in response to changing conditions in the oncoming airflow. Thus these two main types of orographic precipitation enhancement require quite different modelling strategies, and only non–convective effects will be treated here.

2. Estimating orographically forced lifting

A characteristic feature of airflow past high mountains is the occurence of nonlinear stratification effects. While air which originates from above a certain level below mountain top crosses the barrier in a manner similar to what potential flow theory predicts, air below that level is mainly deflected horizontally or gets completely blocked (Blumen, 1990).

Central to the 'dividing streamline' concept is the assumption that the depth of the flow actually crossing the mountain is determined by the ratio between inertia and buoyancy in the flow, given by cU/N (U... magnitude of wind speed, N...buoyancy frequency). According to laboratory experiments, the nondimensional coefficient c has a value between 0.5 and 2 and depends on mountain shape (Baines and Hoinka, 1985). Although in the real atmosphere the formation of waves and the presence of friction modifies the flow, we adopt the dividing streamline approach as a first order approximation to realistic lifting rates in a model as simple as possible.

nized into parallel strips oriented along the direction of the mean flow. On each strip, for each mountain top, the dividing streamline level is determined and an idealized flow field, consisting of several layers within which linear flow is assumed, is calculated from bottom up. The linear flow within a layer is obtained by Fourier series technique. The resulting field of vertical motion represents directly forced uplift.

Vertical motion caused by the retardation of low-level air is calculated from mass conservation. For this calculation the maximum lateral dispacement of air parcels, and the maximum increase of wind speed due to channelling within valleys are prescribed.

3. Parameterization of cloud physics

The sum of upslope and blocking components of vertical motion enters the condensation term in the cloud microphysical equations. The spatial distributions of cloud and rain water are calculated. Autoconversion of cloud to rain water, accretion of cloud water by rain, and evaporation of rain are treated according to the bulk parameterization of Kessler (1969). The equations are solved by a semi-analytical method which also accounts for wind-drift effects (Kerschbaum, 1992).

Significant orographic precipitation in continental regions requires the presence of seeding precipitation formed at higher levels by synoptic-scale vertical motion (Cotton and Anthes, 1989). Seeding precipitation leads to efficient washout of orographic clouds. To model the 'seeder-feeder' mechanism explicitly, the synoptic-scale precipitation rate is prescribed at the top of the domain ($\approx$4 km).

4. Application and results

The model was applied to a recent case (21.-24. Oct. 1993) of intense precipitation in the southern Alpine region (Eastern Tyrol, Carinthia), where at some places 12 h-precipitation amounts in excess of 50 mm and 4-day totals up to 150 mm were encountered. Routine radiosonde data was used to calculate the distribution of humidity at the inflow boundary. As a substitute for the seeding precipitation rate at 4 km the distribution of precipitation rate predicted by the ECMWF, reduced by a constant factor, was used. Mean wind speed and direction, atmospheric stability, and wet bulb potential temperature were also estimated from radiosonde data. Within each 12 h-period all boundary conditions were held at constant values.

It was found that the model correctly reproduces several of the precipitation maxima on the southern Alpine slopes, in particular an area near Kötschach-Mauthen and one in the vicinity of the Loibl pass. Both areas are well known to be recurrently affected by heavy rain if cyclonic activity south of the Alps occurs (Nobilis et al., 1991). Generally weak precipitation enhancement at the Brenner pass, and strong precipitation at Obergurgl with southeasterly, but not with southwesterly flow, are qualitatively reproduced. The overall quantitative reliability of the model, however, strongly depends on the quality of the synoptic-scale precipitation forecast. The model results are also quite sensitive to the choice of mean wind direction, which is difficult to define if baroclinicity is high.

References

Baines, P.G. and K.P. Hoinka (1985): Stratified flow over two-dimensional topography in fluid of infinite depth: a laboratory simulation. *J. Atmos. Scvi.*, **42**, 1614-1630.

Banta, R.M. (1990): The role of mountain flows in making clouds. In: Blumen, W. (Hrsg.), *Atmospheric Processes over Complex Terrain,* Am. Met. Soc., Boston, 229-283.

Blumen, W. (1990): *Atmospheric Processes over Complex Terrain.* Meteor. Monogr., **23**, No. 45.

Cotton, W.R. and R.A. Anthes (1989): *Storm and Cloud Dynamics.* Int. Geophys. Series, Vol. 44, Academic Press, San Diego.

Kerschbaum, M. (1992): Modellierung von Wolken- und Niederschlagsbildung bei zweidimensionaler Bergüberströmung. Dissertation, Wien.

Kessler, E. (1969): On the distribution and continuity of water substance in atmospheric circulations. Meteor. Monogr., **10**, No. 32.

Nobilis, F., T. Haiden and M. Kerschbaum (1991): Statistical considerations concerning probable maximum precipitation (PMP) in the Alpine country of Austria. *Theor. Appl. Climatol.*, **44**, 89-94.

Smith, R.B. (1979): The influence of mountains on the atmosphere. Adv. Geophys., 21, 87-230.

Numerical Experiments of the Orographic Snowfall over the Mountainous Region of Northern Japan

K. Saito, T. Matsuo, M. Murakami, H. Mizuno and M. Ikawa

Meteorological Research Institute, Nagamine 1-1, Tsukuba, Ibaraki, 305 Japan

Abstract

Two-dimensional numerical experiments using a nonhydrostatic model of MRI (Ikawa and Saito, 1991) are conducted to investigate the cloud microphysical aspects of the orographic snowfall over the mountainous region of Northern Japan. The model incorporates cloud microphysics which predict the mixing ratios of six water species (water vapor, cloud water, rain, cloud ice, snow and graupel) and the number concentrations of three ice species (cloud ice, snow and graupel). Sensitivity experiments are conducted to study the orographic change of the snow clouds and the following results are shown. 1) The basic structures of the snow clouds and concentration of the snowfall over the windward slope of the mountainous region are reproduced by the simulation. 2) In warm rain process, the precipitation amount decreases significantly since the condensed cloud water does not converts to rain effectively without ice phase. 3) The ice nucleation by the decrease of the cloud temperature due to orographic ascent plays important role to the orographic enhancement of the snowfall.

1. Introduction

The mountainous and coastal regions of northern Japan, facing the Sea of Japan, are famous for heavy snowfall in winter. The convective snow clouds initially develop over the Sea of Japan by the abundant heat and moisture supply from the relatively warm sea surface (10°C). The snow clouds gradually increase their cloud top height when they approach the coastal region of northern Japan and concentrate snowfall over the windward side of the mountainous region of northern Japan. Although a general explanation for the development of the convective snow clouds in terms of mountain-forced updraft has been made from dynamical point of view, the cloud microphysical aspects of the terrain-induced heavy snowfall have not been fully investigated so far.

Ikawa *et al.* (1991) performed a simulation of the convective snow cloud using a 3-dimensional model with a bulk parameterization scheme of cloud microphysics and succeeded in reproducing the basic characteristics of an isolated convective snow cloud which developed over the Sea of Japan. They also made sensitivity experiments to the ice crystal nucleation rates and showed that the increase of the number concentration of ice crystals results in the increase of snow in mass and number. Similar results have been reported by an 1-dimensional Euler-Lagrangian model by Matsuo *et al.* (1994) where detailed microphysics are incorporated. Although Ikawa *et al.* (1991) gave some numerical experimental support to the possibility of controlling the snow cloud by artificial seeding, their simulation was performed without orography and the roll of the orography to the snowfall over northern Japan were not studied.

Murakami *et al.* (1994) performed a numerical simulation of the convective snow clouds over the Sea of Japan using a 2-dimensional cloud model with orography. They used an observed profile in Siberia for the inflow boundary condition and succeeded in reproducing the observed mixed layer development over the sea surface. Their simulation showed good agreement with observational results in terms of cloud fetch distance, cloud top and base height and air temperature increase in the mixed layer, while investigation of the mechanisms of orographic enhancement of the snowfall using sensitivity tests was not performed.

In this study, we perform sensitivity tests to the mountain height and ice crystal nucleation rates using a 2-dimensional model to investigate the mechanisms of the orographic enhancement of the snowfall. Additionally, artificial seeding experiments are made to study the seeding effect to the snow clouds in the situation with orography.

2. Winter Snowfall over Norther Japan

Figure 1 shows a visible GMS satellite image of 12 JST 2 February 1989, which is a typical one with the winter monsoon outbreak over the Sea of Japan. Convective snow clouds which develop over the sea of Japan bring snowfall over the coastal region facing the Sea of Japan and the mountainous region of northern Japan. Figure 2 shows the schematic structure of the winter monsoon snow cloud derived from the ground and aerological observation made from 2 to 3 February 1989. The cloud develops over the mountainous slope and the cloud top height increases from about 2.4 km over the sea off the coast to about 3 km over the coastal plain. Intermittent snowfalls of 1 - 2 mm/h were observed at the coastal region from 06 JST 2 to 06 JST 3 February.

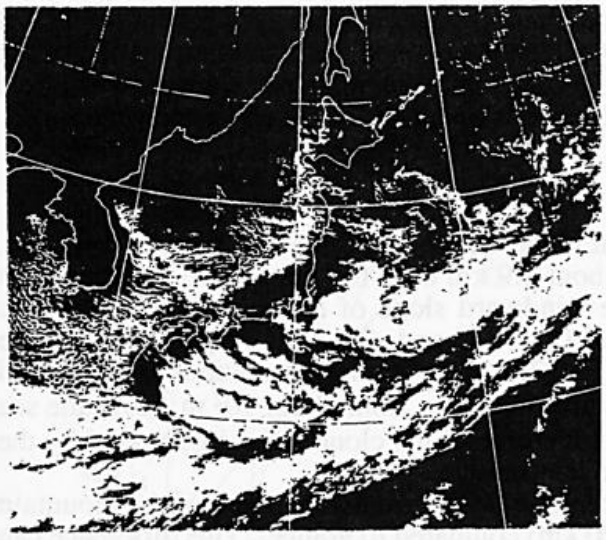

Fig. 1. Visible GMS satellite image of 12 JST 2 February 1989.

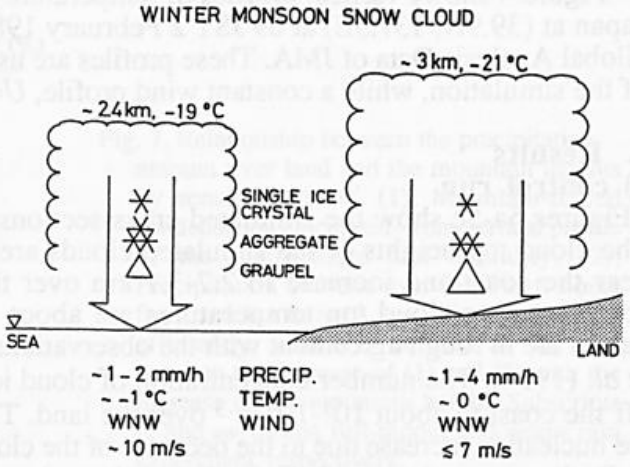

Fig. 2 Schematic structure of the winter monsoon snow cloud derived from the ground and aerological observation made from 2 to 3 February 1989.

3. Numerical model and design of experiments

The dynamical framework of the model is the anelastic version of the nonhydrostatic model developed at the Forecast Research Department of the MRI (Ikawa and Saito, 1991). A bulk parameterization scheme of cloud microphysics same as in Ikawa *et al.* (1991) is incorporated, which predicts the mixing ratios of six water species (water vapor, cloud water, rain, cloud ice, snow, and graupel) and the number concentrations of three ice species (cloud ice, snow, and graupel). For the parameterizations of the ice crystal nucleation, 1) Fletcher's deposition/ sorption nucleation, 2) Bigg's freezing of cloud droplets, and 3) Hallet and Mossop's secondary ice multiplication process are implemented.

For the subgrid-scale turbulence, a turbulent closure model determines the diffusion coefficients. For the boundary layer physical processes, a resistance law calculates surface momentum and heat fluxes according to the distribution of sea and land. The sea surface temperature is assumed to be 10°C while the ground temperature is fixed to the same value of the reference temperature in the simulation. Lateral boundary condition is open, which incorporates Orlanski's radiation condition.

Model domain of the simulation is taken along a orography perpendicular to the direction of northern Japan (a solid line in Fig. 3). The orography is simplified as a symmetric mountain with 1000 m height and 160 km width. The dimensions of the model domain are (Lx, H)=(600 km, 13.8 km), with the grid number of (Nx, Nz)=(302, 30). A variable grid mesh is used in the z-coordinate, whose grid distance varies from 40 m to 900 m.

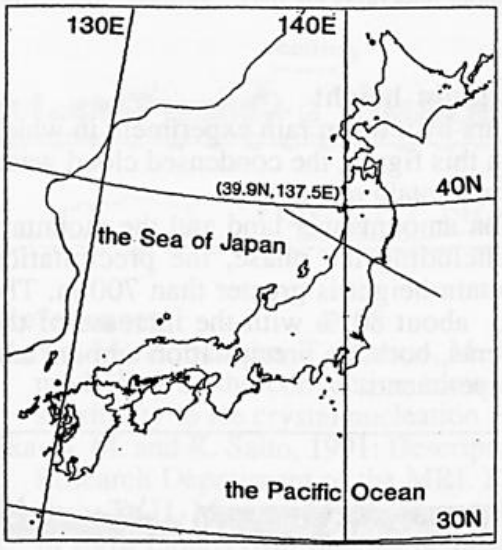

Fig. 3. Map around Japan. Model domain of the 2-dimensional simulation is taken along a solid line crossing northern Japan.

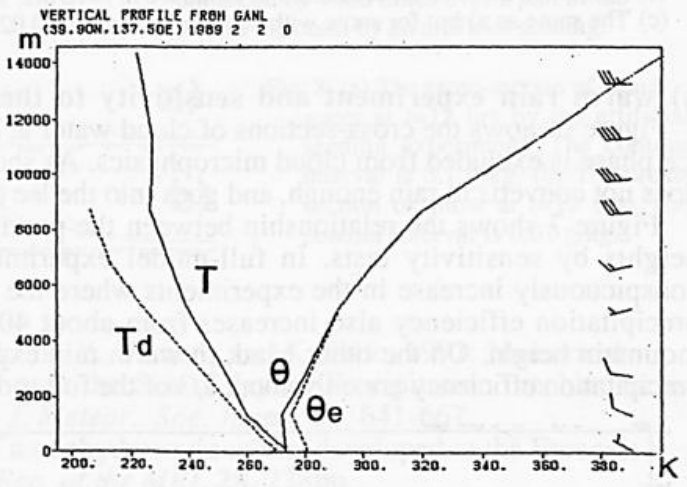

Fig. 4. Vertical profiles of temperature (T), dew point temperature (Td), potential temperature (θ) and equivalent potential temperature (θe) at 09 JST, Feb. 2, 1989 at (39.9N, 137.5E) obtained from the Global Analysis Data of JMA.

Figure 4 shows vertical profiles of temperature and humidity over northeastern part of the Sea of Japan at (39.9N, 137.5E) at 09 JST 2 February 1989, which is obtained from an interpolation of the Global Analysis Data of JMA. These profiles are used for the initial and reference environmental field of the simulation, while a constant wind profile, U=10 m/s, is assumed for the reference wind.

4. Results

a) control run

Figures 5a-5c show the simulated cross-sections of cloud water, cloud ice and snow at t=12 hrs. The cloud top heights of the simulated clouds are about 1.9 km over the sea off the coast, 2.3 km near the coast and increase to 2.7-3.1 km over the windward slope of the mountain range. The corresponding cloud top temperatures are about -16 C, -19 C and -21-23 C respectively. These values are in rough agreement with the observations (Fig. 2) and the former simulations as Murakami *et al.* (1994). The number concentration of cloud ice also increases from about 10^2 m^{-3} over the sea off the coast to about 10^3-10^4 m^{-3} over the land. This increase of the cloud ice is interpreted by the ice nucleation increase due to the decrease of the cloud temperature.

Both snow and graupel (figure is not shown) concentrate on the windward slope of the mountain range, while snow concentrate more leeward (about 20 km) compared to graupel. This difference can be explained by the smaller fall velocity of snow (about 1 m/s) than that of graupel (2-3 m/s).

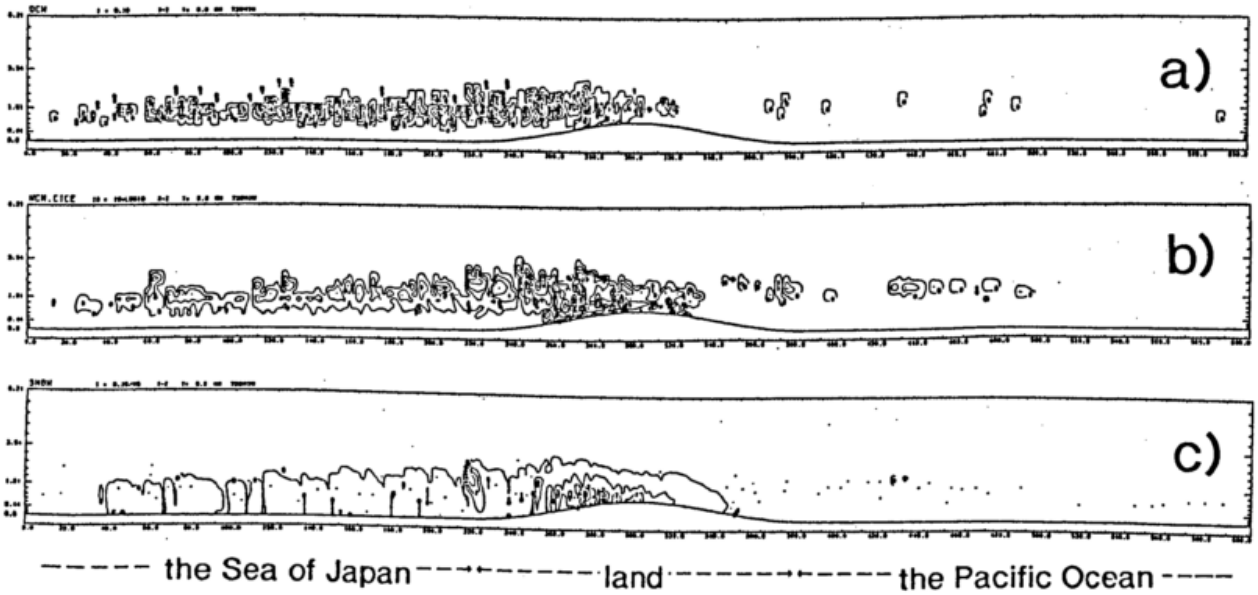

Fig. 5. (a) Simulated liquid cloud water content at t=12 hrs with contour intervals of 0.1 g/kg.
(b) Simulated number concentration of cloud ice at t=12 hrs. The contour interval is log (Ni).
(c) The same as a) but for snow with contour intervals of 0.02 g/kg.

b) warm rain experiment and sensitivity to the mountain height

Figure 6 shows the cross-sections of cloud water at t=12 hrs by a warm rain experiment in which ice phase is excluded from cloud microphysics. As shown in this figure, the condensed cloud water does not converts to rain enough, and goes into the lee of the mountain range.

Figure 7 shows the relationship between the precipitation amount over land and the mountain heights by sensitivity tests. In full-model experiments including ice phase, the precipitation conspicuously increase in the experiments where the mountain height is greater than 700 m. The precipitation efficiency also increases from about 40 % to about 80 % with the increase of the mountain height. On the other hand, in warm rain experiments, both the precipitation amount and precipitation efficiency are only about 1/3 of the full-model experiments.

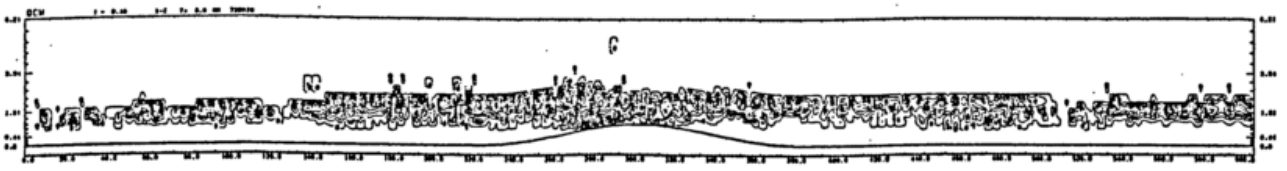

Fig. 6. Simulated liquid cloud water content at t=12 hrs with contour intervals of 0.1 g/kg.

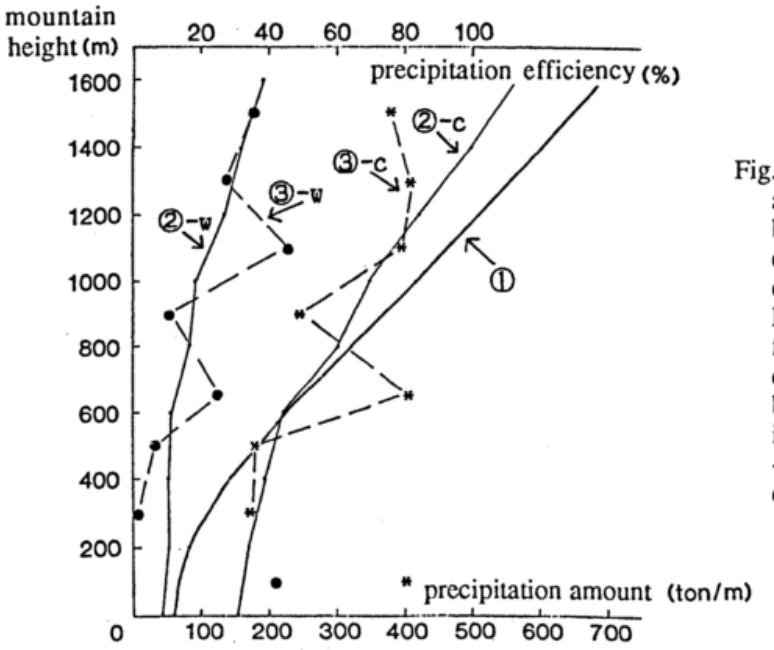

Fig. 7. Relationship between the precipitation amount over land and the mountain heights by sensitivity tests. (1); Mountain-forced condensation calculated from vertical profile of the temperature and humidity. (2); Precipitation amount over land in 6 hours from t=6 hrs to t=12 hrs. (3); Precipitation efficiency, which is defined as the rate between the increase of (1) and (2) with the increase of the mountain height. Subscripts -c and -w means full-model and warm rain experiment, respectively.

c) sensitiviy to the ice crystal nucleation rates

Table 1 summarizes the results of the various sensitivity experiments. When both the freezing of cloud droplets and the deposition/sorption nucleation are switched off, the precipitation over the land decreases by 50% compared to the control run. In case that both ice nucleation rates are suppressed over the land, the precipitation over the land decreases by 30%. On the other hand, even in the case without mountain, the surface precipitation (snowfall) increased with the enhancement of the ice nucleation rates over the land (table not shown here).

Figures 8a and 8b show the cross-section of cloud water and snow at t=12 hrs by an artificial seeding experiment. In the seeding area (x=150-180 km in Fig. 9) almost all cloud water changes into snow by the artificial nucleation. The surface snowfall over the sea in the lee of the seeding area is intensified, while total precipitation over the land decreases by 10% compared to the control run.

experiments with mountain	average precipitation	precipitation over the land (maximum)
control run	0. 8	2. 2 (5. 8)
no Fletcher's nucleation	0. 8	2. 1 (5. 6)
no Bigg's cloud freezing	0. 7	1. 9 (5. 0)
no Fletcher no Bigg	0. 4	1. 2 (3. 2)
warm rain	0. 3	0. 6 (1. 6)
suppression ice over land	0. 6	1. 5 (3. 9)
artificial seeding	0. 8	2. 0 (4. 7)

Table 1. The precipitation amount in 6 hours from t=6 to t=12 hrs obtained by the various sensitivity experiments (mm). *'suppression ice over land'* means the experiment in which ice nucleation terms are suppressed by 1/100 over land. *'artificial seeding'* means the experiment in which ice nucleation terms are enhanced by 1000 times over a part of the sea off the coast by an artificial seeding.

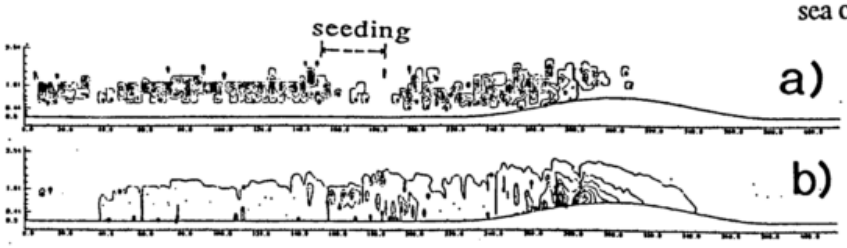

Fig. 8. (a) The cross-section of cloud water at t=12 hrs by the artificial seeding experiment. The contour interval is 0.1 g/kg. (b) The cross-section of snow at t=12 hrs. The contour interval is 0.01 g/kg.

References

Ikawa, M., H. Mizuno, T. Matsuo, M. Murakami, Y. Yamada and K. Saito, 1991: Numerical modelling of the convective snow cloud over the Sea of Japan -Precipitation mechanism and sensitivity to ice crystal nucleation rates-. *J. Meteor.. Soc. Japan,* **69**, 641-667.

Ikawa, M. and K. Saito, 1991: Description of a nonhydrostatic model developed at the Forecast Research Department of the MRI. *Tech. Rep. of the MRI,* **28**, 238pp.

Matsuo, T., H. Mizuno, M. Murakami and Y. Yamada, 1994: Requisites of graupel formation in snow clouds over the Sea of Japan. *Atmos. Res.,* **30** (in press).

Murakami, M., T.L. Clark and W.D. Hall, 1994: Numerical simulation of convective snow clouds over the Sea of Japan; Two-dimensional simulation of mixed layer development and convective snow cloud formation. *J. Meteor. Soc. Japan,* **72**, 43-62.

Numerical Simulation of an Orographically-Induced Mesoscale Cyclone off the South Coast of Japan

Isao Takano

Meteorological Research Institute, Tsukuba, Ibaraki, Japan.

Abstracts

Numerical simulation by use of a high-resolution limited-area model is performed for a mesoscale cloud system induced by the orographic influence of the high mountains over Japan. It was found that the leeward shear line preceded the cyclogenesis and that the later development of the disturbance was largely controlled by the diabatic heating effects of precipitation and the vertical coupling with a middle-level trough.

The central part of Japan is occupied by several mountain ranges which in aggregate constitute the Chubu Mts. The Chubu Mts. have an overall horizontal dimension of 200 km and include several mountains exceeding 2500m in altitude. These Chubu Mts. give substantial influence on the atmospheric conditions around Japan. In cold seasons a low-level mesoscale cloud system associated with an orographically-induced shear line (horizontal scale 100 km) often develops in the lee side, i.e., off the south coast of central Japan when the environmental low-level wind is northerly. Occasionally, a mesoscale cyclone evolves out of the cloud system.

We have performed numerical experiments using a high resolution limited-area model (20 km-grid version of a JMA operational prediction model JSM (Japan Spectral Model, Segami et al., 1989)) for the 14 Oct. 1991 case in which active cyclogenesis occurred (Fig. 1). The model (Fig. 2) represents the small-scale features of the Chubu Mts. well. The experiment using a mesoscale analysis that was obtained from the forecast-analysis cycle of JSM captured some key features of the observed disturbance.

The growing process of the disturbance outlined by the model (initial time; 12UTC, 13 Oct. 1991) may be divided into the following stages.

a. Shear-line formation stage (6h< Forecast Time <12h)

After the passage of a typhoon near the south coast of Japan, strong northerly wind dominated over Japan. As the northerly wind in the windward side gradually weakened, splitting of low-level inflow occurred around the Chubu Mts. The existence of a stable layer in the windward side seems to be a favorable condition for the low-level flow splitting. In this stage, low-level wind is weak in the lee of the mountains, and high θe air is accumulated in this area.

After FT=6h, easterly wind gradually intensified south of the mountains, which led to the NW-SE oriented shear line between the easterly wind and the northerly wind downstream of the west of the Chubu Mts. (Fig. 3-b). The shear line has strong positive vorticity. The shear line is also characterized by strong moisture contrast across it, with humid air in the NE side and fairly dry air in the SW side. A band-shaped precipitation area was simulated north side of the shear line. The disturbance first appeared as a low-level cloud system due to the capping stable layer near 600 hPa.

b. Cyclone formation stage (12h< FT <18h)

The low-level geopotential height also shows local depression around the shear line. Abrupt downward motion accompanying mountain wave is simulated for the northerly wind over the lee side of the Chubu Mts. Thus, the adiabatic heating due to the downward motion over the Chubu Mts., together with the stagnant relatively warm air in the lee side, accounts for the negative low-level pressure anomaly.

c. Cyclone developing stage (18h< FT)

As another cyclone accompanying a middle-level trough approached north Japan, the northerly wind ceased in the windward side. The mesoscale disturbance then began to move eastward along the shear line away from the coast. Relatively strong precipitation and intensified cyclonic circulation with wind speed of 30 kt are simulated at this stage. The middle-level stable layer found in the earlier stage is no longer seen over the cloud system. The low-level cyclone combined with the middle-level trough and developed further as a synoptic-scale cyclone (Fig. 4).

In order to make the developing mechanism more clear, we made additional experiments in which the precipitation processes of the model are turned off (Fig. 5). Although a cyclone is simulated off the south coast of Japan, the central pressure is shallower and the wind speed is weaker than those of the control case. It clearly indicates that latent heat release played an important role for the further development of the cyclone over the sea. The simulated results show that the initial growth of the cyclone is triggered by the orographic effects, and that the later development is strongly influenced by the approach of the middle-level trough, as well as the diabatic processes.

References

Segami, A., K. Kurihara, H. Nakamura, M. Ueno, I. Takano and Y. Tatsumi, 1989: Operational mesoscale weather prediction with Japan Spectral Model. J. Meteor. Soc. Japan, 67, 907-924.

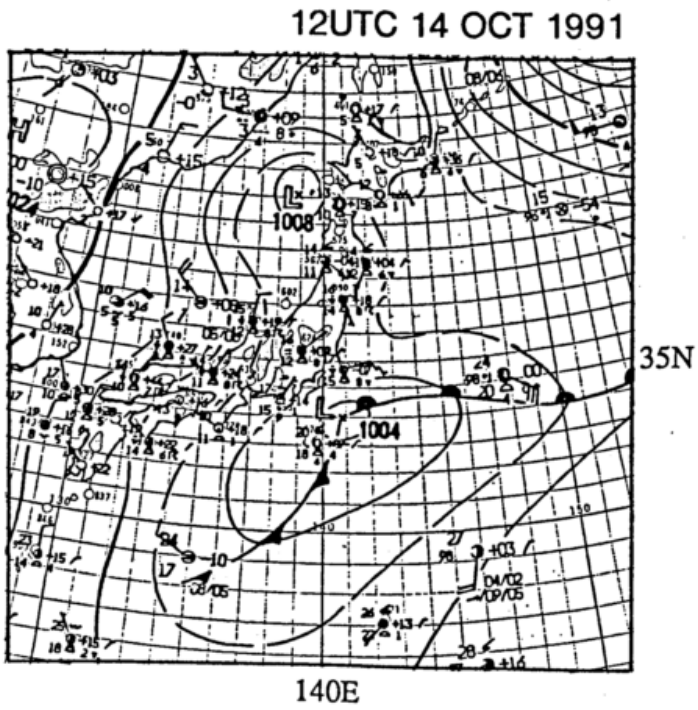

Figure 1. Surface weather map 12UTC 14 Oct., 1991

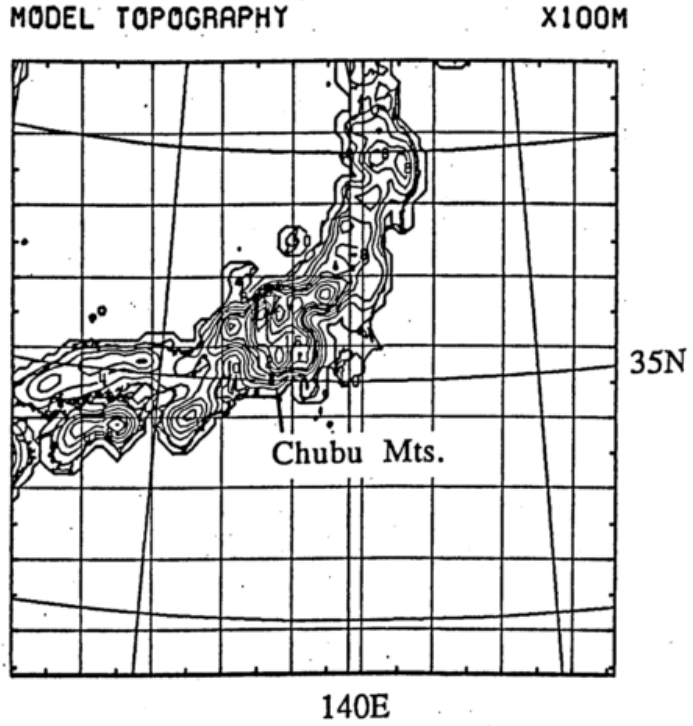

Figure 2. Model domain and topography

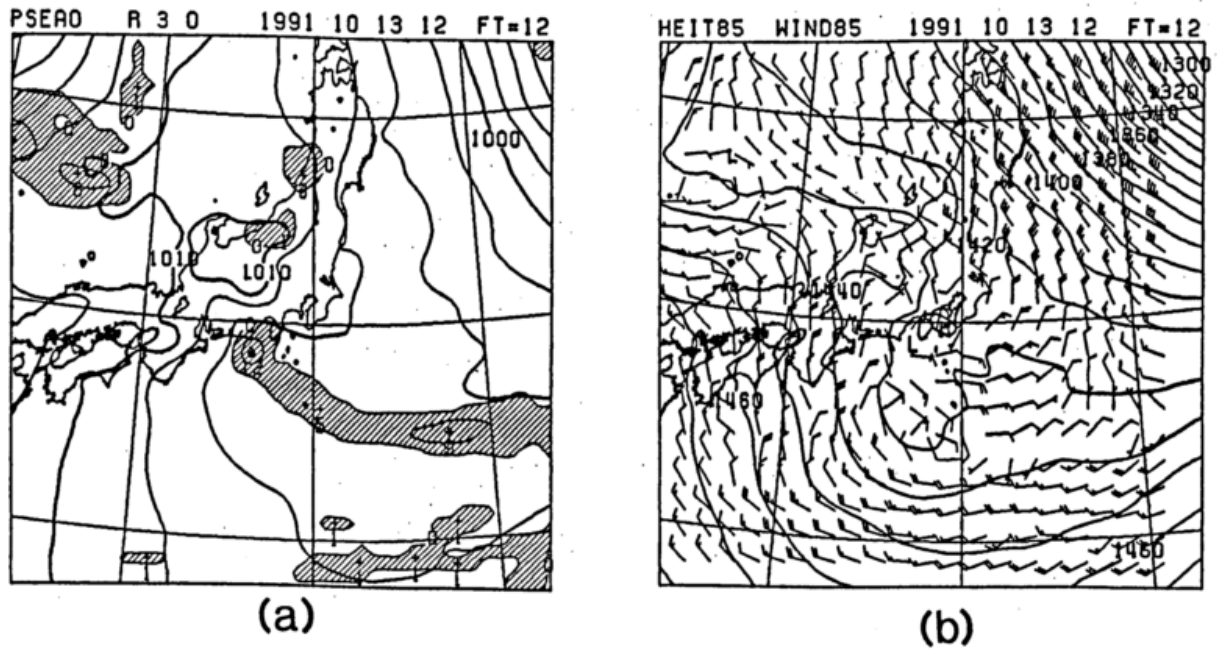

Figure 3. 12 hour forecast results starting at 12 UTC 13 Oct.
(a). Surface pressure (contour interval; 2 hPa) and 3 hourly accumulated precipitation (shaded areas, contour interval; 5 mm).
(b). Geopotential height at 850 hPa (contour interval; 10 m) and wind at 850 hPa.

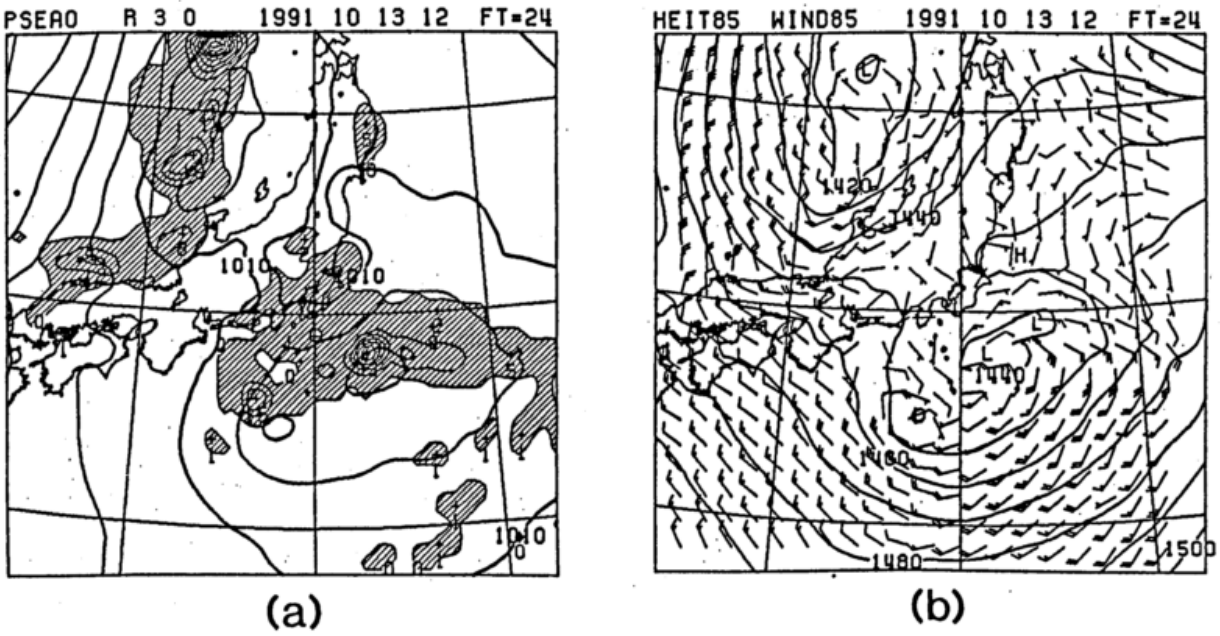

Figure 4. As in Fig. 3 except for 24 hour forecast.

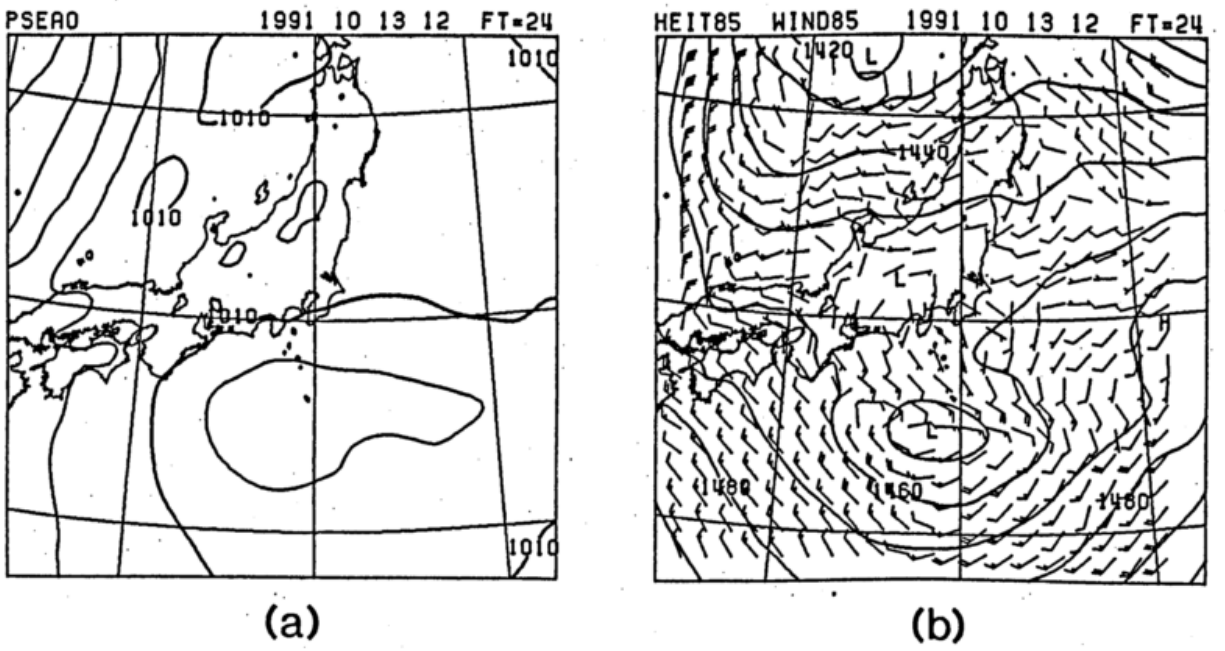

Figure 5. 24 hour forecast results starting at 12 UTC 13 Oct. No precipitation case.

THE SOLUTION OF LEE WAVE PROBLEMS BY THE COMPLEX COORDINATE METHOD

D.S. Tannhauser, Department of Physics
and
N. Moiseyev, Department of Chemistry
Israel Institute of Technology, Haifa, Israel

April 1, 1994

Stationary mountain waves play a significant role in the transfer of momentum from the atmosphere to the ground. Their properties have been reviewed by Smith[1] and others and their structure has been calculated by many authors. An important part of a mountain wave field are the completely or incompletely trapped lee waves.

The wave field can be calculated by a numerical solution of the basic hydro- and thermodynamic equations. For a two dimensional model of the lee waves the field can also be calculated analytically, and the two methods of solution can then be compared. The altitude dependence of the amplitude in the analytic method is given by a solution of the Helmhotz equation

$$\frac{d^2\tilde{w}_0}{dz^2} + [l_S^2(z) - k^2]\tilde{w}_0 = 0 \qquad (1)$$

which has been solved by many authors by various methods. The principle of the solution of this equation by a new method known as the *Complex Coordinate Method* is described. This method is based on a FORTRAN program and is easy to apply and to verify. Its results for various published Scorer profiles which have been solved by other methods are discussed.

This research was supported by the Fund for the Promotion of Research at the Technion.

1) R.B. Smith, The influence of mountains on the Atmosphere, *Advances in Geophys.* 21, 87-230 (1979)

The initial interpolation for the wind field analysis

Neva Pristov and Jože Rakovec
University of Ljubljana, Department of Physics
and
Hydrometeorological Institute of Slovenia

ABSTRACT

Different methods of horizontal and vertical interpolation are tested for obtaining initial wind field in all model point of variational wind analysis. At upper levels bilinear interpolation of geopotential is applied, at the ground three "closest" stations are used with $1/r$ as a weight (r being modified "distance"), while for vertical interpolation the atmosphere is divided into three sub-layers.

1. Introduction

For the variational analysis of the wind field it is crucial to make a satisfactory initial interpolation. It is only initial field which relates the individual case with the appropriate measured values and so separates individual cases each from the others. In a smooth terrain the proper choice of the interpolation is, at least in principle, obvious (horizontal interpolation at the ground and a the top of the model, the use of the Ekman law and the log- linear law). In mountainous, complicated terrain the choice is even in principle not trivial: the height of the level of geostrophic wind is affected by mountains and there is no clear semi-analytical solution for vertical interpolation. Different interpolations have been applied in a set of numerical experiments. In this paper it is shown which results are obtained with the combination of (quasi-horizontal) interpolation at the ground, the interpolation of geostrophic wind in a free atmosphere, and introduction of different layers for the needs of vertical interpolation.

As we deal with meso-β scale (horizontal domain of the model of the order of 100 km, resolution of the order 10 km), we can neglect the curvature of the Earth and so we use a local Cartesian co-ordinate system (x, y, z), with high vertical resolution at the ground and stretched towards the upper levels. Into the model we introduce the so called "stepped" or "block" mountains, so that the plateaux coincide with model levels. The Arakawa C-grid is used. Small concave shapes, consisting of only one grid block are corrected to become flat areas. If it happens that the point with measurement is in block relief close to the "wall" (one component is set to zero to obey the boundary conditions) it is not corrected. If such measuring point falls into a "corner" (both components should be zero) the data of such station are moved to the nearest, less obstacled grid point.

2. The methods of interpolation

We dived the initial interpolation procedure in three parts:

a) separate (quasi-horizontal, terrain following) interpolation of the ground level wind over whole lower boundary of the analysis model, based on measurements on ground stations,

b) separate (again quasi-horizontal) interpolation of the upper level winds on standard pressure levels of 500, 700, and $850hPa$ levels, based on radio soundings and with linear interpolation to obtain the wind at a height of the upper boundary of the model, and

c) filling the whole interior of the model with the use of vertical interpolation between these two boundaries.

For interpolation of surface layer wind we have in our area typically one measurement per $100-150km^2$. Available data from measurements are for operational use denser for Slovenia, where we can include a lot of stations e.g. also automatic stations, and coarser in the neighbouring countries, from which operationally only the data from GTS are available. We extend the idea of Vrhovec (1988) to introduce into the "distance" which we use as a weight not only the measure σ for eventual mountain ridge between the two points, but we use also additional weight k_h for vertical distance:

$$r^2 = (x - x_m)^2 + (y - y_m)^2 + k_h^2(h - h_m)^2 + (k_\sigma \sigma)^2$$

Tests have shown that the use of $1/r$ gives better results than e.g. the use of $1/r^2$, that the values of k_h and k_σ should be quite large (we use for both weights the value of 150), and that the inclusion of three closest stations gives in average better result than the inclusion of only one or two stations, and almost the same average error as the inclusion of four closest stations (according to the modified distance).

As regards the interpolation of upper levels winds on standard pressure levels are for operational purposes on disposal typically some 5 soundings for the area. Some earlier tests (Vrhovec and Rakovec, 1991) have shown that it is better to use initially bilinear than some other interpolation (e.g. least-square polynomial). With variational coupling of the wind and geopotential field the same tests have shown that it is better to geostrophically convert the wind into gradient of geopotential than opposite. After solving the equation (with relaxation) we compute the wind field using the geostrophic equation.

In hilly terrain there is no obvious choice of the type of vertical interpolation between the ground field and the top wind field. Many of authors have simply used potential law. As we try to resolve also the wind in valleys, basins etc., we use the following approach to divide the atmosphere into three layers:

- from h_s to $h_s + \Delta h$ polynomial (quadratic) coupling between the surface wind and the Ekman profile,

- from $h_s + \Delta h$ to $h_s + h_{PBL}$ Ekman profile,

- and above $h_s + h_{PBL}$ linear interpolation between standard pressure levels.

Here is h_s the averaged height of relief (averaging over 49 neighbouring grid points), while h_{PBL} we determine subjectively, by inspection of soundings from Udine and Zagreb. (We have developed also objective algorithm for this procedure, based on PBL resistance laws but automation does not behave well in some cases of more complicated vertical structure of the atmosphere.) Δh is determined as the greatest of differences (calculated over 25 neighbouring points) between the average and grid point heights.

3. Results

We tested the described method of initial interpolation on a very mountainous part of the area (part of the mountains on the border between Slovenia and Austria - Karavanke mountains and Kamnik/Savinja Alps, see Rakovec and Pristov 1994, this proceedings).

Table 1 shows the average errors on 25 stations at the ground, after the initial quasi-horizontal interpolation at the ground, caused by two reasons:

- the data do not exist and must be interpolated; here this is artificially simulated by omitting the data from each of 25 stations, and then comparing interpolated values with the measured ones,

- the separate components of the wind data must be in our case of using the Arakawa stagerred C-grid averaged into their respective locations; here we test three ways of doing it: a) interpolation exactly into a central (station) point (true value, no error), b) interpolation of u and v components into their appropriate positions in the staggered grid and than averaging into a central point, and c) interpolation into a central point, averaging of u and v values to their positions in staggered grid and then averaging back into a central point.

a		b		c	
incl.	omitted	incl.	omitted	incl.	omitted
m/s deg	m/s deg	m/s deg	m/s deg	m/s deg	m/s deg
- -	2.8 43	1.4 28	3.1 42	2.2 27	2.6 55

Table 1: Average of absolute errors after simulating the wind on 25 stations with three types of representing data in staggered grid (see text), and for cases when data for a station were or included or omitted. Average wind speed is $4.7 m/s$ in this case

The results for initial vertical interpolation according to the described model with three layers are compared to the two other methods of interpolation: with one which uses potential law, and one with the use of Ekman profile through whole atmosphere below h_{PBL} down to the ground. In all case the height of PBL is set to $h_{PBL} = 800m$ (Figure 1).

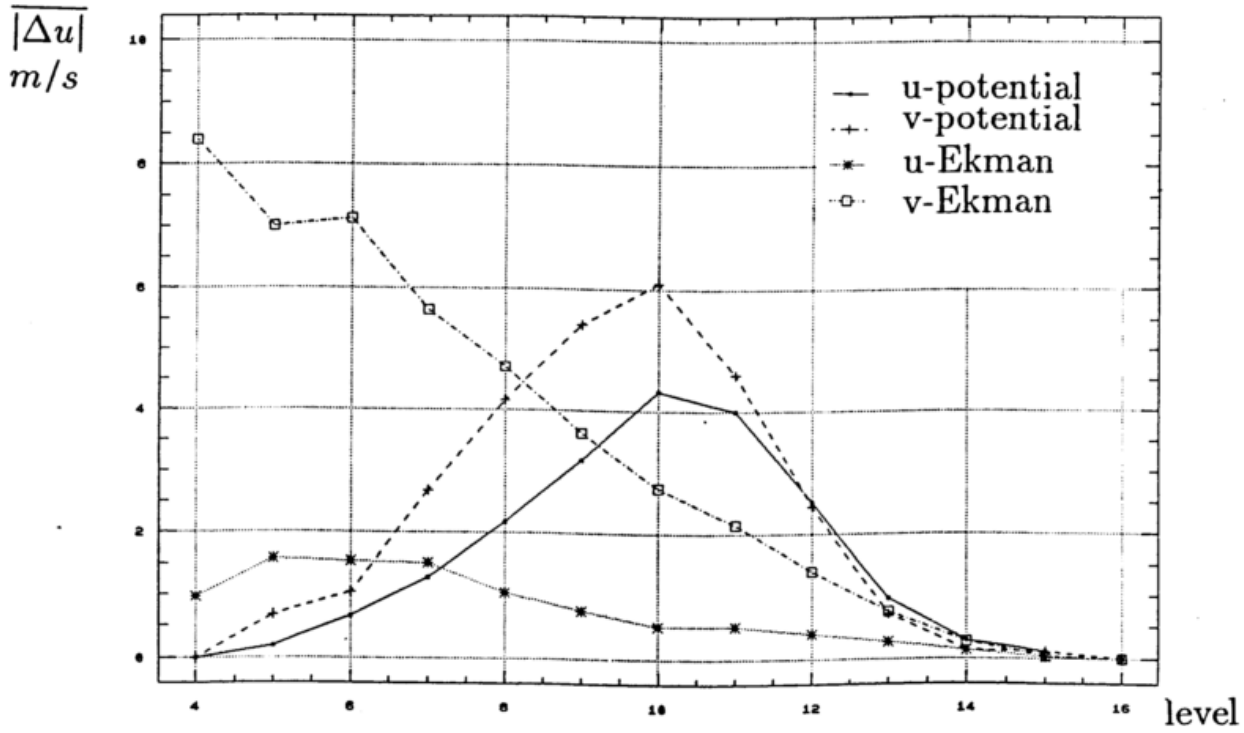

Figure 1: Average absolute differences betweenthe 3-layer vertical interpolation, the Ekman-to-the-ground, and potential vertical interpolation for all layers in the model

The figures show that differences between methods are great if Ekman law is applied down to the ground: in this case the interpolation does not take into account the measured winds at the ground. The use of potential law on the other hand does not take into account the change of wind direction with height, and so here the differences are great at some elevated level (in our case of $h_{PBL} = 800m$ this is at approx. $1200m$.

Nevertheless, it is difficult to judge objectively for how much the initial interpolations differ from the real wind field (for such a comparison the data of e.g. wind profiler should be used. But according to the test for different idealised and real cases we can judge that the three-layers model is better than the other two.

References

Vrhovec. T., and J. Rakovec, (1991): Variacijska geostrofska analiza vetra (Variational geostrophic wind analysis). Univ. Ljubljana, report URP:C1-0507, 76-79.

Vrhovec, T., 1988: Analysis of three-dimensional mesometeorological wind fields. CIMA 88, Sestola 18-25 Sept. 1988.

DIAGNOSTIC MODELING OF OROGRAPHIC AND CONVECTIVE RAINFALL

Sabino Palmieri, Leonardo D'Aprano, Anna Maria Siani
(University of Rome "La Sapienza", Dept of Physics, P.le A. Moro n.2, I-00158 Rome, Italy)

ABSTRACT
A model for diagnostic high resolution estimate of rainfall fields (including topography and convection) is described. Sensitivity tests of the model are presented togrther with some applications to extreme events occurred in Italy. The possibility of using the model as a tool for analysing the local impact of long term climate fluctuations (predicted by general circulation models) is also discussed.

1. INTRODUCTION

The diagnosis of rainfall in mountain areas is generally difficult : concurring causes are a) the poor number of conventional stations, b) the limited reliability of radar precipitation estimates on account of the orographic effects , c) the high space variability of rainfall determined by topographical features. On the other hand there is a keen interest in the estimation of the water balance , in the determination of the flooding risk, in coping with flood events and , last but not least, in estimating climate change effects that may occur on the scale of a watershed , all elements requiring a detailed knowledge of rainfall .
In reference to climate simulation, current available general circulation models (CGM) , presently used for this purpose, make use of grid scales on the order of 300-500 km, while nested regional models involve scales on the order of 50 to 100 Km. There remains therefore the need to study precipitation at watershed scale in order to study climate change scenarios for the purpose of reservoir management or other local problems.
The introduction of simple orographic models for the detailed diagnosis of precipitation was pioneered by Rhea (1970). Collier (1975) formulated a model of orographic rainfall with an elaborate method of estimating vertical velocity in the vicinity of orographic features. Bell (1979) introduced a scheme for treating cloud physics processes together with orographic forcing, Haiden et al. (1989, 1992) formulated an analytical model of stable upslope rain and suggested the inclusion of both orographic and convective component of rainfall in diagnostic models, Medina (1991) proposed the use of rainfall diagnostic models as a tool for climate impact studies at the watershed level. More recently Barros and Lettenmaier (1992) introduced the concept of transport of moist static energy and total water through a finite element grid, where precipitation is the only scavenging agent of both variables. A preliminary application of orographic rainfall modeling in which the blocking effect of the relief was considered.was described by Palmieri et al. (1992).

2. MODEL DESCRIPTION

The threedimensional atmosphere over the watershed is devided in a number of cells . For each cell the basic precipitation formula derived from water continuity equation is applied in the form:

$$(1) \qquad P = -\alpha\beta\gamma\delta\,\omega\,(dq/dz)\,\rho\,dz$$

where α is set equal to unity when vertical motion and humidity do allow precipitation to form, β is related to the time the growing droplets spend in the orographic cloud, γ is an element which parameterizes the intensity of convection as a function of the thermal stratification of the atmosphere, the vertical wind shear, the potential buoyancy energy, the vertical extent of the buoyancy energy; δ is a coefficient which expresses the overall efficiency of the microphysical condensation and rain formation processes; ω is the

vertical velocity in pressure coordinates related to the wind component across mountains and to the slope, dr/dp is the derivative of saturated humidity mixing ratio for a saturated adiabatic ascent; ρ is the air density; dz is the thickness of the layer. In the vertical integration three main processes are taken into account : seeder-feeder accretion of rain (washout), evaporation of droplets, drift of rainfall due to the horizontal drift. The model produces precipitation estimates integrated over desired time periods at each grid point of a selected array.

3. RESULTS AND DISCUSSION

The model was applied to two cases: The Valtellina flood event occurred on 18-19 July 1987 in the southern slopes of Central Alps and the Isola del Gran Sasso torrential rain event (Central Italy, eastern slopes of the Appennines) of 9-10 April 1992. Results are presented in Fig. 1 and 3 , while maps of the two basins are shown in Figg. 2 and 4. The sensitivity study shows that the contribution of convection is vital for the correct modeling of the Alpine rainfall event. The other elements like washout and drift play a minor role.
In the case of Gran Sasso event the study shows that the drift is more important than convection and washout in determining the detailed distribution of precipitation.
From the meteorological point of view the two cases are quite different: in the Alpine event the blocking effect of the mountain retarded the cooling of the atmosphere in the lower layers, while cold air could freely flow across the range at higher levels giving rise to extreme instability; in the Appennine case warm moist air from southwest was running over a very cold layer of air flowing from east (stable stratification of the atmosphere); this frontal situation persisted for many hours giving rise to an appreciable contribution to rainfall. This is why in the latter case the model (which does not include frontal rainfall phenomena but solely topographic and convective effects) tends to understimate somewhat the actual precipitation.
In conclusion the application of the model provide results which are consistent with the observed fields and coherent with the synoptic differences of the two considered events.
As far as climate simulation is concerned, keeping in mind that current available general circulation models (CGM) , presently used for this purpose, make use of grid scales on the order of 300-500 km, while nested regional models involve scales on the order of 50 to 100 Km, we are planning to study precipitation at watershed scale in order to derive climate change scenarios for the purpose of reservoir management or other local problems. We intend to make use of the input provided by climate simulation experiments which do not take into account the detailed forcing of local topographic effects.

REFERENCES

Barros A.P., Lettenmaier D. P.(1993) -Dynamic modeling of the spatial distribution of precipitation in remote mountainous areas- Monthly Weather Review, 1993, April, pp.1195-1214.
Bell R.S. (1978)- The forecasting of orographically enhanced rainfall accumulation using 10-level model data- Meteorological Magazine, n.107, pp 113-124.
Collier, C.G. (1975) - A representation of the effect of topography on surface rainfall within moving baroclinic disturbances- Quarterly Journal R. Met. Soc. 101, pp 407-422.
Haiden T. Kerschbaum M. (1989)- An analytical model of stable upslope rain- Beitr. Phys. Atmosph., 1989, pp 327-331.
Haiden T., Kerschbaum M., Kahlig P. , Nobilis F. (1992)- A refined model of the influence of orography on the mesoscale distribution of extreme precipitation- Hydrological Sciences Journal, 37, 5, 10/1992.
Medina J.G. (1991)- Application of a simple local scale numerical model in the study of altered climate impacts on watershed precipitation- AMS, II Symposium on global change studies, Jan 14-18, 1991, New Orleans, La.
Palmieri S., Scrocca A., Siani A.M. (1992)- Application of an orographic rainfall model to a storm case in southern Alps- XXII International Conference on Alpine Meteorology, Toulouse, 7-11 Sept., 1992.

Rhea J.O. (1977)- Orographic precipitation model fro hydrometeorological use- PhD dissertation. Dept Atmospheric Sciences, Colorado State University, Fort Collins, Colorado.

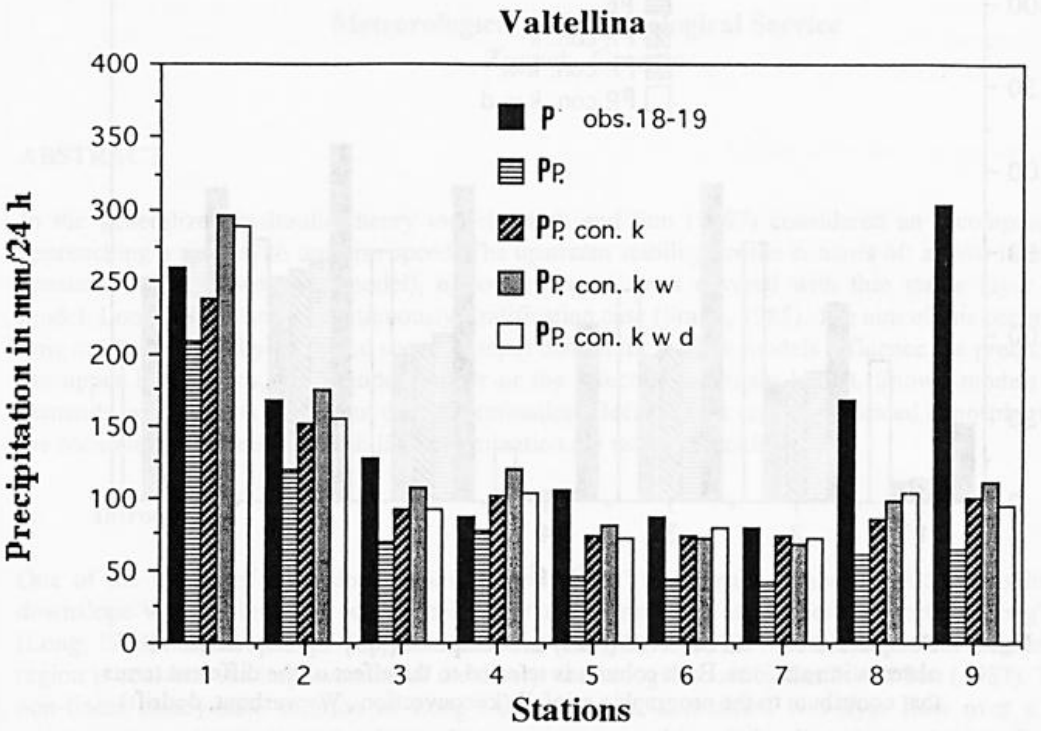

Fig: 1 – Comparison between observed (Pobs) and computed (Pp.) precipitation in 9 observation stations. Each column is referred to the effect of the different terms that contribute to the orographic rainfall (k=convection , W=washout, d=drift)

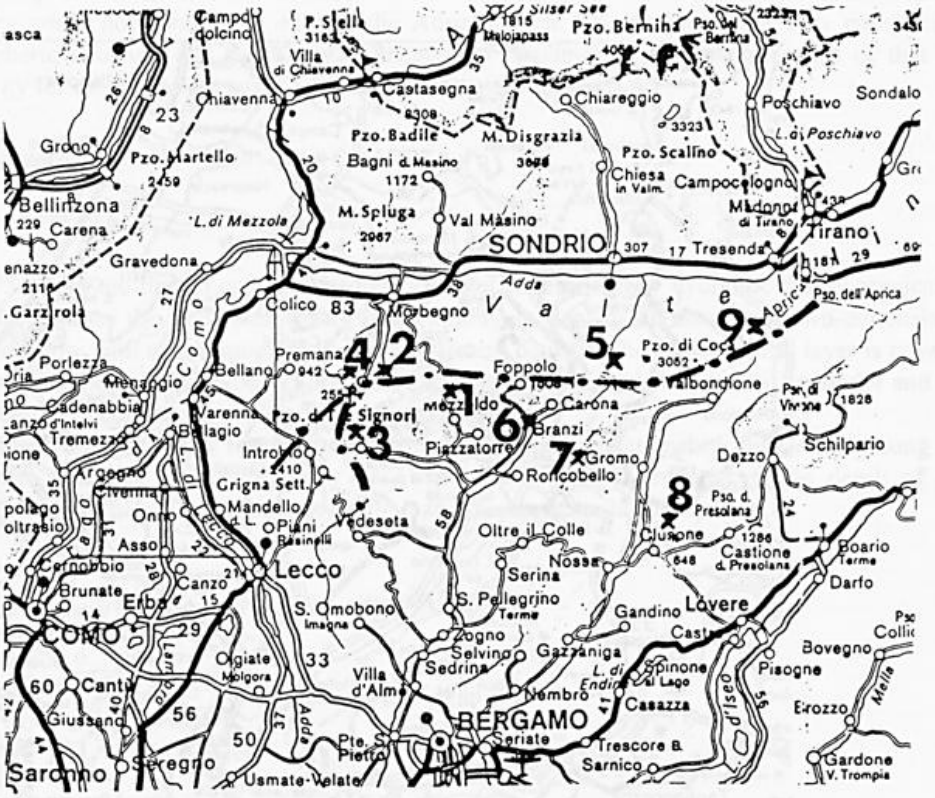

Fig: 2 – Basin map, watershed line and rainfall stations

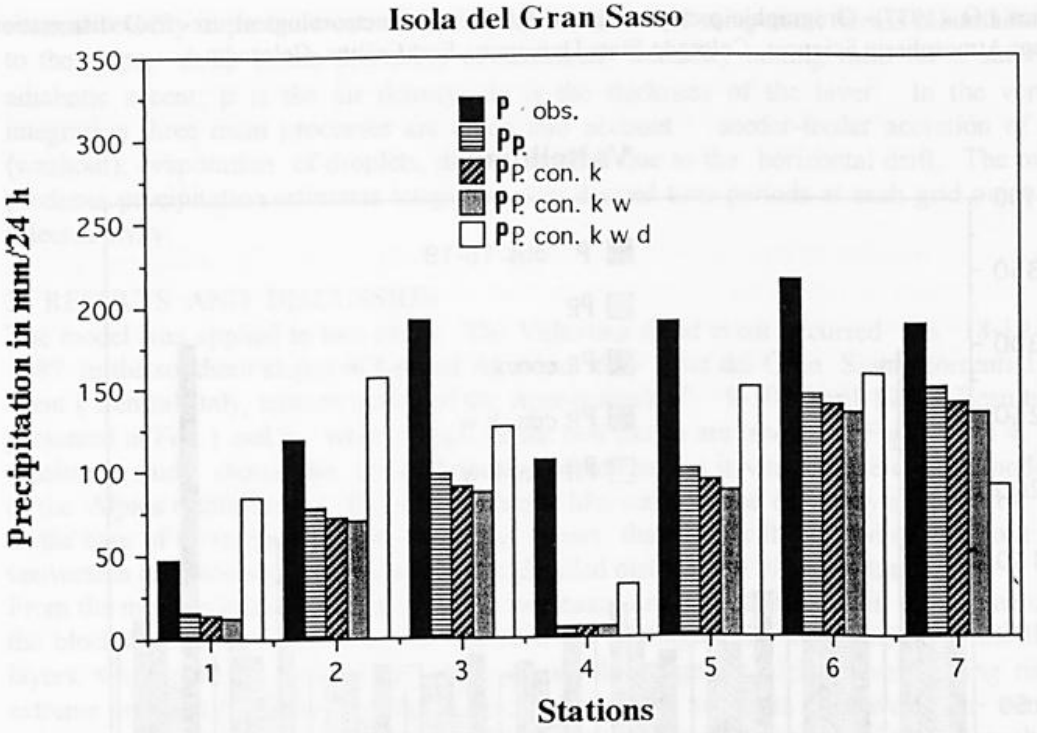

Fig: 3 – Comparison between observed (P_{obs}) and computed ($P_{p.}$) precipitation in 7 observation stations. Each column is referred to the effect of the different terms that contribute to the orographic rainfall (k=convection , W=washout, d=drift)

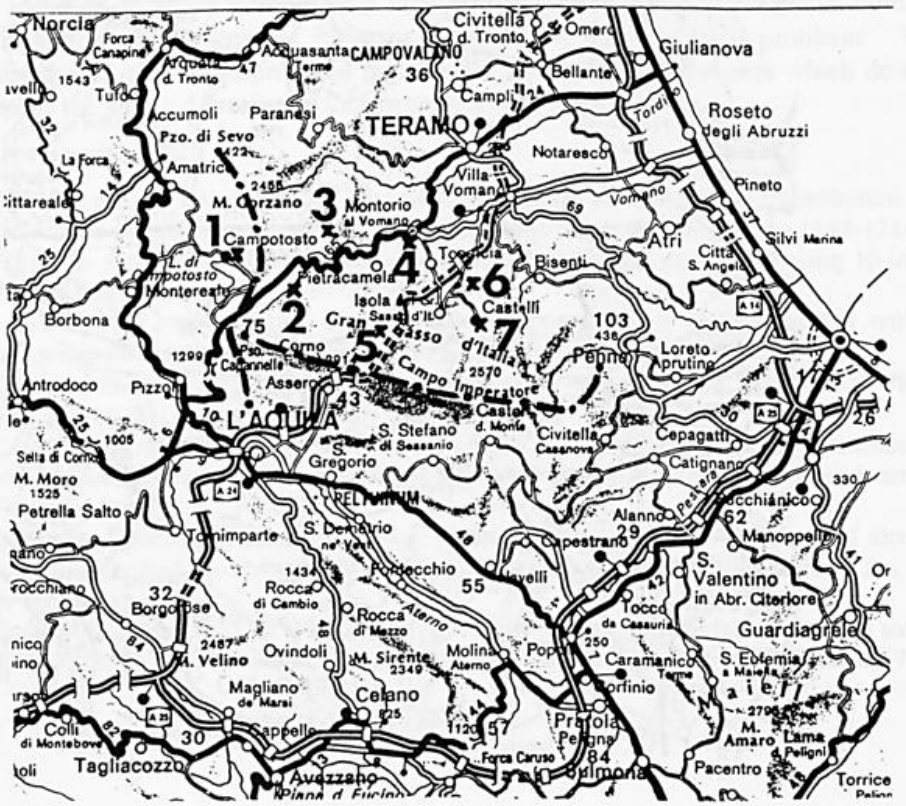

Fig: 4 – Basin map, watershed line and rainfall stations

Generalized Hydraulic Model Sensitivity for the Input Data

V. Vučetić, A. Bajić

Meteorological and Hydrological Service
Zagreb, Croatia

ABSTRACT

In the generalized hydraulic theory model Smith and Sun (1987) considered an incompressible flow approaching a ridge with uniform speed. The upstream stability profile consists of: a) two layers, each of constant stability (two-layer model), b) lower neutral layer covered with thin stable layer (one-layer model, Long, 1953), and c) continuously stratification case (Smith, 1985). The aim of this paper is to show how much the stability and wind speed as input data in these three models influence the predicted values: the upper layer depth, the Froude number or the effective mountain height. Shown models sensitivity demands great caution with input data determination. Because of a very complicated atmospheric structure the accurate wind speed and stability determination are rather difficult.

1. Introduction

One of the theory of downslope windstorms is Smith' mathematical model (1985). This links severe downslope wind to breaking waves in a continuously stratified atmosphere by solving Long's equation (Long, 1953) subject to the assumption that the overturning region is well mixed, so that the density in that region is constant. An improvement of the theory was brought about by Smith and Sun (1987). They found non-linear steady-state solution of Long's equations for a stratified two-layer flow over a ridge that encompass any distribution of stability. In parameter space this solution lie between the interfacial case of Long (1953) and the constant stratification case of Smith (1985).
Strong downslope NE wind in Croatia is the bora wind that blows across a mountain barrier parallel to the eastern Adriatic coast. The theory is applied to five ALPEX bora cases (Smith 1987) and many bora cases on northern and mid-Adriatic (Bajić, 1991; Jurčec, 1990: Vučetić, 1993). Although the application of this theory successfully estimated the maximum bora velocity, analyses show that the two-dimensional hydraulic theory could not completely explain the Adriatic bora. The problem is a very complicated vertical atmospheric structure and sensitivity of theoretical results on input data. Because of that the models sensitivity for the input data will be discussed in the next section.

2. Models sensitivity for the input data

2.1. One-layer model

Long (1953, 1954) was the first to consider theoretically and experimentally hydraulic theory application to a uniform flow across the mountain with a discontinuity in density. It assumes a two-dimensional hydrostatic steady flow with two homogenic fluids of different density. The lower neutral layer is covered with a very thin temperature inversion. In that case the model is reduced to a one-layer model and the motions and continuity equations for shallow water are valid.
According to the hydraulic theory for single layer model, a certain relationship must exist among the uniform upstream wind U_0, the stability N_2^2 (N_2 - the Brunt-Väisälä frequency), the depth of the temperature inversion d, the critical mountain height h and the upstream layer depth H_0:

$$\frac{h}{H_0} = 1 + \frac{1}{2} F_0^2 - \frac{3}{2} F_0^{2/3} \qquad (1)$$

$$F_0 = \frac{U_0}{\sqrt{g' H_0}}, \quad g' = N_2^2 d, \quad N_2 = \frac{g}{\rho} \frac{\partial \rho}{\partial z} \qquad (2)$$

For which initial conditions the fluid undergoes a transition from subcritical flow to supercritical flow can be seen in Fig, 1a. The subcritical flow is associated with a weak wind and a strong stability of the inversion layer. The Froude number is also less than 1 for the strong wind ($U_0 \geq 10$ ms^{-1}) and the upstream layer H_0 higher than 3 km. The flow is always supercritical for the severe wind despite the upstream stability. The supercritical flow can be occurred with a weak wind but the stability is less than 0.5×10^{-2} s^{-1}. The mean upstream flow in the real atmosphere during the severe bora on the northern Adriatic was subcritical with the mean Froude number equals 0.74 (Jurčec, 1990).

2.2. Continuous stratification model

The analyses of aircraft measurement during bora occasion on the northern Adriatic in the ALPEX period (March-April 1982) helped Smith to construct a new hydraulic model using Long's equation for the continuous stratification N_0 and uniform upstream flow U_0 (Smith, 1985). It is presumed that the critical streamline at the level H_0 splits over the mountain with the lower branch descending rapidly, by δ_c, towards the lee side. Above H_0 a weak flow is present, at least in comparison with the strong perturbance below. Between the split streamlines the air is well mixed so that the density in that region is constant. The vertical profile of velocity perturbations $u_p(x_1, z)$ is obtained from the relation:

$$u_p(x_1, z) = U_0\,(1-\delta_{c_1}\cos lz) \qquad (3)$$

$$\delta_{c1} = \frac{\pi}{2} - \mathbf{H}_0, \quad \mathbf{H}_0 = H_0\, l, \quad \mathbf{h} = h\, l \qquad (4)$$

h is the effective mountain height and $l = N_0/U_0$ is the Scorer parameter. Smith (1985) supposed that transitional flows over the effective mountain height higher than 1 are not possible because of the complete blocking on the windward side.
It is interesting to see for which values of U_0 and N_0 as input data for the different mountain heights, the criteria $\mathbf{h} \leq 1$ is valid. The transient flow across the obstacle is possible for the every uniform flow $U_0 \geq 10$ ms^{-1} despite on the stability, but the mountain height should not be exceed 500 m. The model of continuous stratification for the criteria $\mathbf{h} \leq 1$ requires stronger wind and higher stability inside the upstream layer H_0 for the mountain higher than 1000 m.
The theory application in the situations with $\mathbf{h} \leq 1$ shows that the mean upstream wind speed is 8-20 ms^{-1} with the upstream stability 0.7-1.8×10^{-2} s^{-1} and h = 800 m (Jurčec, 1990: Vučetić, 1993).
The predicted critical streamline height H_{op}, can exceed the tropopause in the cases with strong wind speed ($U_0 \geq 15$ ms^{-1}) and small atmospheric stability ($N_0 \geq 0.5\times10^{-2}$ s^{-1}).
However, such ratio $U_0/N_0 > 3000$ m is not noticed in the real atmosphere during the severe Adriatic bora. This means that there is not a vertical propagation of gravity waves throughout the troposphere. Instead of that in the lower atmosphere the hydraulic flow exists (Smith and Sun, 1987). If the NE flow is throughout the entire troposphere, U_0/N_0 ratio is approximately 1000 m with the wind speed about 10 ms^{-1} and a moderate stability (Ivančan-Picek and Vučetić, 1990).
The estimated surface lee wind speed agrees with the empirical bora speed for the low mountain height (Tab 1.). For the small and moderate stability and the higher mountain barrier the theoretical values of u_p are close to the observed bora gusts.

Table 1 Hydraulic parameters for the model of continuos stratification for different input data: upstream wind speed U_0, upstream stability N_0 and critical mountain height h. The index 1 means $N_0 = 0.5\times10^{-2}$ s^{-1} and the index 2 means $N_0 = 2.0\times10^{-2}$ s^{-1}.

	h = 500 m				h = 1000 m			
U_0 [ms^{-1}]	u_{p1} [ms^{-1}]	u_{p2} [ms^{-1}]	$H_{0\,p1}$ [m]	$H_{0\,p2}$ [m]	u_{p1} [ms^{-1}]	u_{p2} [ms^{-1}]	$H_{0\,p1}$ [m]	$H_{0\,p2}$ [m]
5	14.9	31.7	3350	1750	20.9	52.2	4750	2760
10	22.7	41.8	5700	2350	29.8	63.4	7100	3450
15	29.9	50.9	7700	2950	37.8	73.8	9300	4100
20	36.8	59.5	9650	3550	52.8	83.5	11350	4750

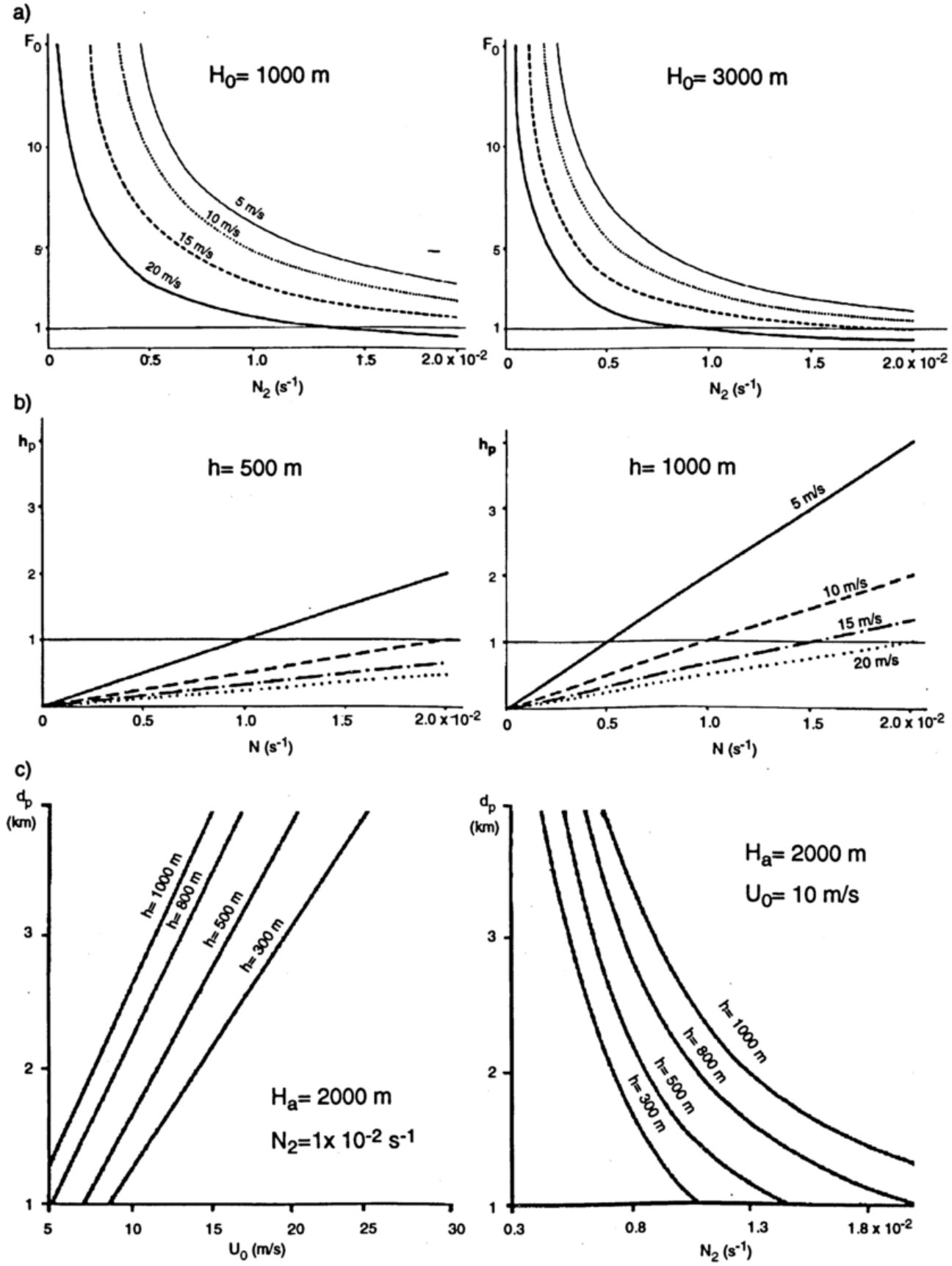

Fig. 1 a) The predicted Froude number F_{0p} for the one-layer model in dependence on upstream wind speed U_0 , stability of the thin inversion layer N_2 and upstream layer depth H_0.

b) Predicted effective mountain height $\mathbf{h_p}$ for the model of continuous stratification in dependence on upstream wind speed U_0 and stability N_0 inside the upstream layer H_0 and critical mountain height h.

c) Predicted upper layer depth d_p for the two-layer model in dependence on: upstream wind speed U_0 and critical mountain height h (left) and upper layer stability N_2 and critical mountain height h (rihgt).

2.3. Two-layer model

For the two-layer model (Smith and Sun, 1987) the vertical profile of stability consists of two layers with stability N_1 and N_2. In order to simplify that, it is presumed that the lower layer is neutral ($N_1 = 0$). Knowing the empirical values of the critical mountain height h, the lower neutral layer depth H_a, the upper layer stability N_2 and the uniform upstream wind speed U_0 we may apply the theory in order to obtain the predicted depth of the upper layer d_p For an analogous definition of the Froude number F_0 as in the one-layer model, Smith and Sun presumed that a thick stable layer might be approximated by a thin density interface of equal strength located at its mean position. This is why they introduced the effective altitude $H_{ef} = H_a + 0.5$ d and the Froude number equals

$$F_0 = \frac{U_0}{\sqrt{g' H_{ef}}} \qquad (5)$$

How much the stability N_2 and wind speed U_0 as input data influence the predicted upper layer depth d_p is shown by Bajić (1991) and can be seen in Fig. 1c. The flow approaching the mountain with the same critical height with only 5 ms^{-1} difference in speed causes a difference of more than 1000 m in the predicted upper layer depth. The situation is similar when stability is used as input parameter. Relatively small changes in the stability value ($0.8\text{-}1.0\times10^{-2}$ s^{-1}) result in the differences of a few hundred meters in the upper layer depth.

Two-layer vertical structure of atmosphere is observed in five cases during the ALPEX boras according to the Zagreb soundings (Bajić, 1988 and Vučetić, 1988) and in only eight cases during the severe bora at Senj on the northern Adriatic in the period 1957-1986 (Bajić, 1991). In these situations the mean upstream flow was 5-16 ms^{-1} with the stability of $1.2\text{-}2.1\times10^{-2}$ s^{-1} and h= 800 m. Thus, the initial wind speed and stability are in the interval where the predicted value of d_p could vary near to 1000 m.

All presented results show reasonably good agrrement with the theory, considering complicated vertical structure in the real atmosphere and the theory's sensitivity to input data.

References:

Bajić A., 1988: The strongest bora event during ALPEX-SOP, Rasprave-Papers 24, 1-9.

Bajić A., 1991: Application of a "generalized hydraulic theory" to the severe northern Adriatic bora, Meteorologische Rundschau 44, 129-133.

Ivančan-Picek B. and V. Vučetić, 1990: Bora on the northern Adriatic coast during the ALPEX-SOP 20-25 March 1982, Rasprave-Papers 25, 1-12.

Jurčec V., 1989: Mountain drag and surface pressure variations during severe Adriatic bora storms, Rasprave-Papers 25, 25-36.

Long R. R., 1953: Some aspects of the flow of stratified fluid, I A theoretical investigation, Tellus 5, 42-58.

Long R. R., 1954: Some aspects of the flow of stratified fluids, II Experiments with a two-fluid system, Tellus 6, 97-115.

Smith R. B., 1985: On severe downslope winds, J. Atmos. Sci. 42, 2598-2603.

Smith R. B., 1987: Aerial obseravtions of the Yugoslavian bora J. Atmos. Sci. 44, 269-297.

Smith R. B and J. Sun, 1987: Generalized hydraulic solutions relevant to severedownslope winds, J. Atmos. Sci. 44, 2934-2939.

Vučetić V., 1988: Bora on the northen Adriatic 12-18 April 1982, Rasprave-Papers 24, 27-44.

Vučetić V., 1993: Severe bora on the mid-Adriatic, Rasprave-Papers 28, 19-36.

Mesoscale **A**lpine **P**rogramme

objectives, status, and prospects

Hans Volkert

Institut für Physik der Atmosphäre, DLR-Oberpfaffenhofen,
D-82230 Weßling, Germany

1. Introduction

Over the past 15 years, i.e. since the planning of ALPEX, operational numerical weather predicition (NWP) has made tremendous progress. Horizontal resolution, to mention one parameter, increased by more than a factor of ten. For instance, since summer 1993 a high-resolution model with less than 15 km meshsize is run twice a day at DWD and SMA to produce 36 h forecasts.

Discussions involving the meteorological services, university institutes and research laboratories revealed that a fresh, concerted research effort dealing with applied and basic aspects of mountain meteorology is highly desirable. This should take **mesoscale** aspects and issues related with the new operational models as its foci; the **Alpine** region is to serve as area of immediate interest and as exemplary mountain range when the impact to larger-scale circulations is considered; finally, the research activities should be organized as an integrated **programe** including modelling and theoretical studies and, if possible, also leading to a major field campaign. These three issues are reflected in the general title: **M**esoscale **A**lpine **P**rogramme or **MAP** for short.

2. Objectives

Two primary scientific objectives have been defined:

a) improve the understanding of dynamical and physical processes over complex topography, and
b) to improve the predictive capability of mesoscale NWP models in mountainous terrain.

These objectives have some overlap as an improved parameterization of mountain drag, say, necessitates a better understanding of the dominant processes.

Furthermore, two supporting objectives should be taken into account:

c) to establish a climatology of mesoscale systems in the Alpine region
d) to organize the collection and exchange of non-GTS data

Objective (a) will be subdivided in four to five topics, e.g.:

a1) Convective and severe storms;
a2) Downslope wind, orographic blocking, flow splitting, gravity waves;
a3) Orographic modification of fronts; possibly also mesoscale cyclogenesis;
a4) Upper-level effects including trans-tropopause exchange and also gravity waves;
a5) Boundary layers in mountainous terrain, transport problems.

Research groups from the meteorological services, university departements and research laboratories are at present asked to identify their interests within these topics.

An analogous subdivision was made by the NWP community for objective (b). Besides technical issues as mesoscale analysis schemes the following four focus areas have been identified:

b1) Orographic precipitation and deep convection (to include upslope precipitation and orographically-influenced convection)

b2) Low-level wind systems (to include shear and convergence lines, mesoscale vortices, Bora, Mistral, Shirocco, and shallow Foehn)
b3) Orographically-modified fronts
b4) Gravity waves (to encompass all aspects of mountain-induced gravity wave effects that do not fit into the other areas)

3. Status

At present, MAP undergoes its definition phase. An international workshop will take place at ETH in Zürich during the week following ITAM'94. More than 60 scientists from European countries, the United States, and New Zealand will gather to finally specify the scientic objectives for MAP.

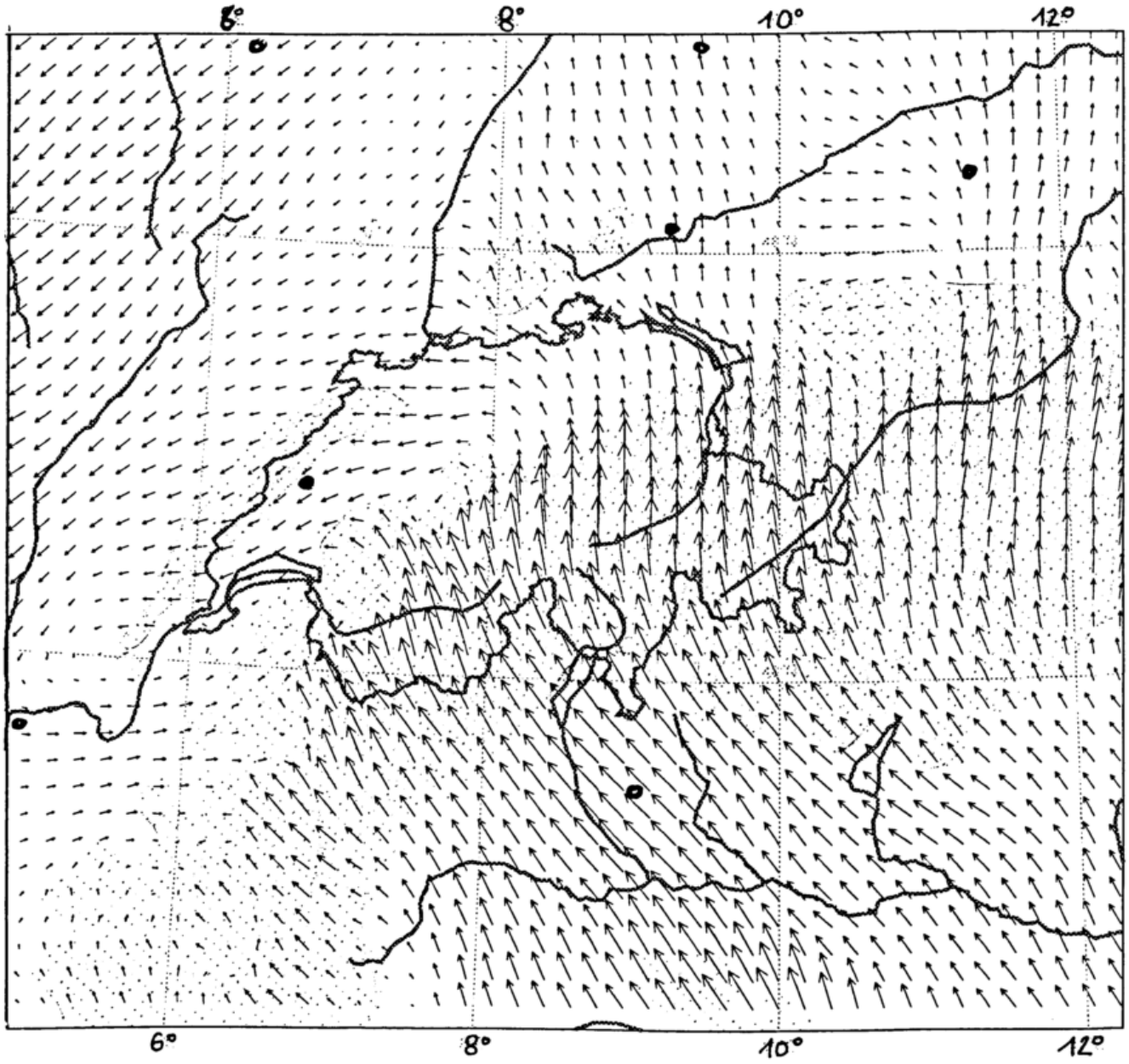

Figure 1. Regional wind field about 1000 m above ground. 24 h forecast valid for 24 Sept. 1993 obtained with the operational SM-model. Major rivers and Swiss borderlne are included; model orography above 750 m is shaded. The approximate positions of the regular radiosounde stations are given (•). Courtesy of P. Binder (SMA).

The research departements of a number of European National Meteorological Services have expressed interest in MAP. It is anticipated that they also will detail their research interest in the context of MAP during the Zürich workshop.

About two dozen U.S. scientists made proposals for research projects that they intend to integrate into MAP. The observation and simulation of orographically generated gravity waves is of particular interest.

More details can be found in issue 23 of the ALPEX-regional Bulletin, which can be obtained from SMA in Zürich.

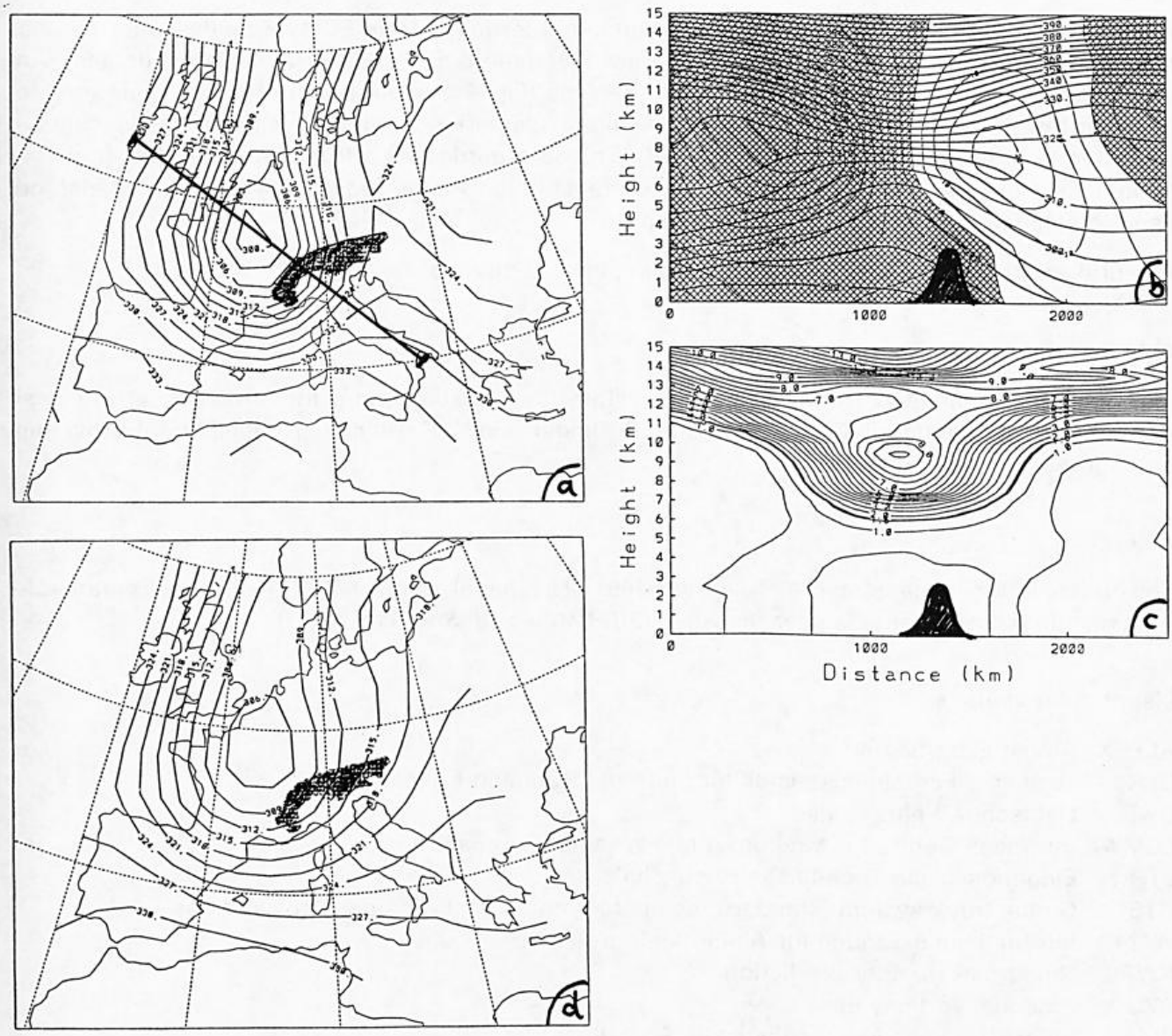

Figure 2. Potential temperature ($\Delta\theta = 3$ K) on the tropopause defined by the 1.6 PVU potential vorticity surface (a), cross-sections from Ireland to southern Italy of normal wind and potential temperature (b) and potential vorticity (c) for 4 May 1987, 00 UTC. Potential temperature as in (a) but averaged over the 8 most similar cases from the 1985-92 dataset. Data from ECMWF. Figure courtesy of K.-P. Hoinka (DLR).

4. Prospects

It is, of course, difficult to specify the prospects of new research programme in its early phase. But the proven international co-operation during and after ALPEX and the established contacts between the interested institutions should be very beneficial. The problem of adequate funding has to be tackled now.

Two, admittedly arbitrary example may illustrate where progress during MAP can be expected. Figure 1 shows the operational wind field forecast at about 1000 m above ground for Switzerland and its surroundings together with the coarse network of regular radiosonde stations in the area. The flow field exhibits a pronounced Foehn structure over the main Alpine ridge and a modification into a northeasterly Bise over the Swiss Mittelland. Although these features appear plausible, there are at present no means to validate them at levels above the surface. Denser upper air wind observations are badly needed.

Figure 2 (a to c) reflects the synoptic scale forcing determined from ECMWF analyses for the situation of the so-called papal front early in May 1987 (see e.g. Volkert et al. 1991 for details). An anomalously low tropopause extended over the Alps (Fig. 2c) and a dome of cold air laid next to their northwestern flank (Fig. 2b). By applying a clustering technique similar cases can be extracted from the ECMWF archives (Fig. 2d). This is regarded as a first step to establish climatologies of a number of relevant mesoscale systems in the Alpine region. These data can also be used to estimate the trans-tropopause transport.

The presentation at the conference may well contain further examples.

Acknowledgements:

This overview benefitted from discussions within the working group for MAP and at the past ALPEX-regional meeting in Zürich last June. P. Binder and K.-P. Hoinka are thanked for providing the Figures.

Reference:

Volkert, H., L. Weickmann, and A. Tafferner, 1991: The papal front of 3 May 1987: a remarkable exmaple of frontogenesis near the Alps. *Q.J.R.Meteorol. Soc.* **117**, 125-150.

List of abbreviations:

ALPEX	Alpine Experiment
DLR	Deutsche Forschungsanstalt für Luft- und Raumfahrt e.V.
DWD	Deutscher Wetterdienst
ECMWF	European Centre for Medium-range Weather Forecasts
ETH	Eidgenössische Technische Hochschule
GTS	Global trunk system (standard means to communicate meteorological data)
ITAM	Internationale Tagung für Alpine Meteorologie
NWP	Numerical weather prediction
PVU	Potential vorticity unit
SMA	Schweizerische Meteorologische Anstalt

Abstract

American Interests in the Mesoscale Alpine Project (MAP)
by
Joachim Kuettner, NCAR
Boulder, USA

American scientists and institutions have indicated considerable interest in certain aspects of MAP, among them:

- Testing and observational verification of (near-) operational meso-ß prediction models over orography and related parameterization schemes.
- Gravity wave effects, including wave breaking and momentum transport into the Middle Atmosphere.
- Front/mountain interaction.
- Foehn and downslope wind dynamics.
- Chemical transports (horizontal and vertical) over orography.

Also discussed are observational requirements, measurement techniques, potentially available platforms and some planning and data management aspects. Close contact is being maintained with the European Working Group for MAP.

Sind Handanalysen für eine Verifikation von Mesoskalenmodellen geeignet ?

R. Steinacker

Institut für Meteorologie und Geophysik
Universität Wien, Österreich

ABSTRACT

Some advantages of fine scale hand analysis of meteorological fields are outlined, which allow a verification of even todays high resolution forecast models in the low troposphere over central Europe. At upper levels, however, the sparse radiosonde network prohibits a verification of small scale structures. A collection of a spatial and temporal dense data set for at least selected areas and a development of an objective high resolution data analysis/assimilation scheme is an urgent need for the scientific community.

ZUSAMMENFASSUNG

Vorteile von hochaufgelösten Handanalysen meteorologischer Felder werden diskutiert, die eine Verifikation selbst der heute operationellen mesoskaligen Modellen in der unteren Troposphäre Mitteleuropas erlauben. In höheren Niveaus ist dagegen eine solche Verifikation von feinskaligen Strukturen, bedingt durch den großen räumlich-zeitlichen Abstand der Radiosondenmessungen nicht möglich. Eine Gewinnung eines durchgehend dichten Datensatzes zumindest für ausgewählte Gebiete und die Entwicklung eines objektiven feinmaschigen Analyse/Assimilations-schemas stellt ein dringendes Anliegen dar.

1. Einleitung

Seit kurzer Zeit werden hochaufgelöste Prognosemodelle für Mitteleuropa operationell eingesetzt. Eines davon, das Deutschlandmodell des Deutschen Wetterdienstes weist eine horizontale Auflösung (Gitterdistanz) von ca. 14 km auf. Das konventionelle Bodenbeobachtungsnetz (SYNOP) kommt selbst im Gebiet mit der höchsten Datendichte nur auf rund 35 km, das Radiosondennetz (RAWIN) nur auf rund 250 km mittleren Stationsabstand. Damit lassen sich bodennah und insbesondere in der freien Atmosphäre die vom Modell gelieferten Strukturen in den kleinen Skalen feldmäßig nicht direkt verifizieren.

Man kann einzelne Beobachtungen mit aus Gitterpunktswerten interpolierten Modellergebnissen überprüfen, nimmt dabei jedoch in Kauf, daß lokale Eigenheiten von Beobachtungsstationen den Vergleich verzerren, was insbesondere für Gebirgsstationen zutrifft, an welchen der Unterschied zwischen Stationshöhe und Modelltopographie erheblich sein kann.

Der Vergleich zwischen objektiv analysierten Feldern und den Modellfeldern ist dadurch verzerrt, daß sinnvolle Analyseschemata (z.B. Optimum Interpolation) ein (kurzfrist-)prognostiziertes Feld als first guess benötigen. Der im Verhältnis zur Gitterdistanz große Stationsabstand bewirkt i. a., daß die Beobachtungsinkremente (Beobachtung minus first guess) eine nur geringe räumliche Korrelation aufweisen und daher der Lärm in den Daten (nichtrepräsentativer Anteil des Meßwertes plus Beobachtungsfehler) das Signal (Analyseinkrement = Analyse minus first guess) übertrifft. Einfacher ausgedrückt, heißt dies, daß die Analyse in hohem Maße vom first guess-Feld abhängt und ein Vergleich der beiden sehr ähnlichen Felder keine unabhängige Verifikation des Modells zuläßt.

2. Verifikation mit Handanalysen

Wie kann eine Handanalyse sinnvollere (für Verifikationszwecke geeignetere) Ergebnisse liefern als eine objektive Analyse ?

- *Eine gute Handanalyse berücksichtigt den meteorologischen Lärm:* ein versierter Synoptiker sollte durch Erfahrung aus zahlreichen Vergleichsfällen die Eigenheiten einzelner spezifischer Stationsbeobachtungen kennen, intuitiv Einzelfehler aufspüren können und systematische Beobachtungsfehler besonders sorgfältig verfolgen (vgl. Abb. 1).
- *Eine gute Handanalyse ist multivariat:* Die analysierte Feldverteilung einer Variablen sollte immer aus einer Synthese aller beobachteten Größen entstehen. Für eine Analyse eines Druckfeldes sollte z.B. immer zumindest die Wind- und Temperaturinformation gleichzeitig betrachtet werden.
- *Eine gute Handanalyse berücksichtigt anisotrope Strukturen:* Gerade kleinskalige atmosphärische Strukturen weisen eine erhebliche räumliche Anisotropie auf. Wird etwa eine Frontstruktur von nur wenigen eng benachbarten Stationspaaren aufgelöst, so läßt sich guten Gewissens diese Struktur auch auf datenarme Gebiete transferieren. Dasselbe gilt für orographisch induzierte Strukturen, bei denen durch die genaue Kenntnis der Topographie ein detaillierter Informationstransfer bewerkstelligt werden kann.
- *Eine gute Handanalyse ist "4-dimensional":* Durch die gleichzeitige Betrachtung von Stationen in verschiedener Höhe und der zeitlichen Konsistenz (Analyse des Vor- und Nachtermins) gelingt eine quasi 4-dimensionale Verknüpfung der Daten. Dies erlaubt insbesondere bei transienten Strukturen eine signifikante Erhöhung der Auflösung.

3. Schluß

Durch eine sorgfältige Handanalyse kann in der untersten Troposphäre besonders über dem Alpenraum eine Auflösung erzielt werden, welche durchaus vergleichbar ist mit den heute operationellen hochauflösenden Modellen. Damit kann auch eine unabhängige feldmäßige Verifikation der Prognosen durchgeführt werden. In der freien Atmosphäre ist hingegen durch den zu großen Stationsabstand (Radiosonden) selbst bei sorgfältigster Analyse keine Verifikation der feinen Skalen möglich. Hier ist dringender Handlungsbedarf gegeben: zumindest für einen beschränkten räumlichen und zeitlichen Bereich muß durch eine entscheidende Erhöhung der Datendichte und -frequenz die Basis für eine Verifikation von Mesoskalenmodellen geschaffen werden. Zu diesem Zweck scheint eine international konzertierte Aktion wie MAP (Mesoscale Alpine Programme) unumgänglich. Eine Verbesserung der Modelle kann schließlich nur durch die Erfassung von Modelldefiziten durch Verifikationsstudien erzielt werden.

Eine Handanalyse hat neben ihren Vorzügen natürlich den gravierenden Nachteil, daß sie zeitaufwendig ist. Die oben geschilderten Vorzüge einer guten Handanalyse sind aber nicht auf die "Hand" beschränkt. Ein automatisches (objektives) Analyseverfahren, das hochauflösend, multivariat und vierdimensional (assimilierend) ist, Beobachtungsfehler und den meteorologischen Lärm, sowie die Anisotropie mesoskaliger Strukturen berücksichtigt, leistet dasselbe, sogar in wesentlich kürzerer Zeit; nur ist ein solches Verfahren bis heute nicht verfügbar. Auch hier ist daher ein großer Handlungsbedarf gegeben, eine weitere wichtige Aufgabe für MAP.

Danksagung: Für die Zurverfügungstellung der geplotteten Ostalpenkarten als Basis für die Feinanalysen sei der Wetterabteilung der Zentralanstalt für Meteorologie und Geodynamik in Wien gedankt.

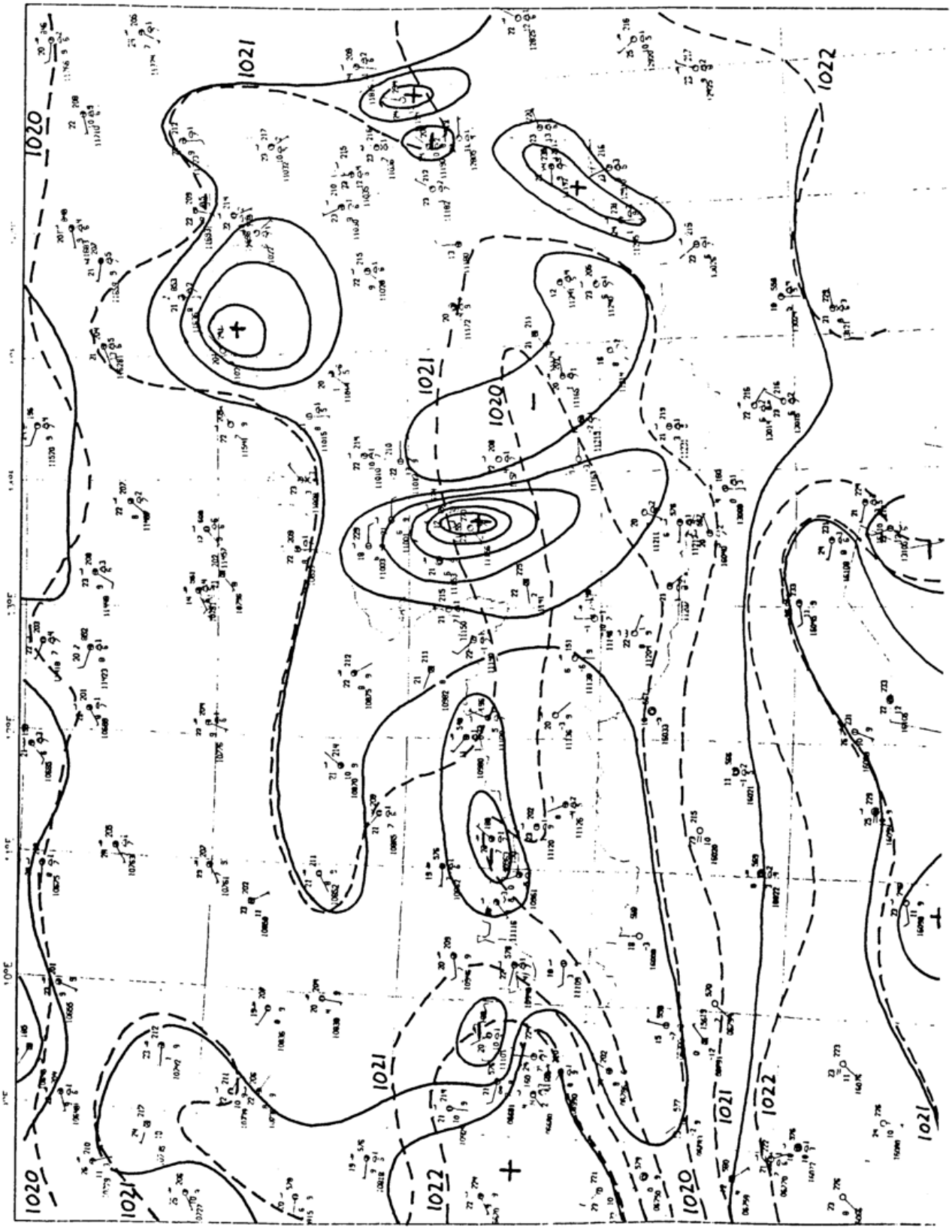

Abb. 1. Vergleich einer Bodendruckanalyse über dem Ostalpenraum unter strikter Verwendung der gemeldeten Druckwerte (durchgezogen) und unter Berücksichtigung der Meßfehler, der topographischen Gegebenheiten sowie der Temperatur- und Windinformation (stichliert) für den 30.4.1994, 12 Uhr UTC. Der Isobarenabstand beträgt jeweils 1 hPa. Die Korrektur erfolgte aufgrund von Zeitreihenuntersuchungen, wobei an rund 10% aller Stationen signifikante systematische Fehler des Luftdrucks entdeckt werden können.

High resolution simulation of low-level flow features in the Alpine region

Urs Aebischer and Christoph Schär
Atmospheric Physics ETH, 8093 Zürich, Switzerland

Introduction

Atmospheric flow past high topographic obstacles is often associated with the splitting of the incident stream of air at low levels. It can lead to the generation of vortices and shearlines downstream (Etling 1989, Smith and Grubisic 1994, Thorpe et al. 1993). These flow features are of significance for mesoscale weather and forecasting, since they permanently alter the downstream conditions and can interact with other synoptic and mesoscale flow structures. In dynamical terms, the lee-vortices and shearlines are distinct through their value of potential vorticity (PV). The latter arises from a violation of PV-conservation, which can, in principle, arise from diabatic processes, dissipation, or surface friction.

The aforementioned processes have been investigated in several numerical studies using idealized terrain. Smolarkiewicz and Rotunno (1989) showed that lee vortices can form even in the absence of surface friction, and they argue that the vertical vorticity develops owing to the tilting of horizontally oriented vorticity. In contrast, Schär and Smith (1993a,b) suggest that the violation of PV-conservation is significant and results from dissipation in the interior of the flow which is induced by flow-splitting. In addition, consideration was also given to the effects of complex terrain (Smith and Smith 1994), and to surface friction (Thorpe et al. 1993, Grubisic et al. 1994).

In this study, low level effects of flow past the Alps are investigated with high-resolution hydrostatic numerical simulations. Two case studies will be presented. The discussion will focus on the PV distribution at low levels and to the lee of the topography.

The model

The model utilised in this study is the EM/HRM Europa-Modell developed by the German Weather Service (Majewski 1991, 1994) which is also operationally used by the Swiss Meteorological Institute. The simulations have horizontal resolutions of 0.5° (~ 56 km) and 0.125° (~ 14 km), respectively, and a vertical resolution of 30 layers in hybrid coordinates. The HRM model is one-way nested into the EM-simulations, whereas initial and lateral boundary data for the EM simulations derive from ECMWF-analysis fields.

Case Studies

The first case to be considered is associated with an Alpine lee cyclogenesis event, which subsequently leads to a period of northerly flow past the Alpine massif. Fig.1 shows the ECMWF analysis (on December 6, 1992, 06 GMT), and the corresponding fields for the EM simulation after 42 h of integration. A comparison of the two panels in Fig.1 indicates that the formation of the lee cyclone, its progression over Italy, and the subsequent phase of North-Föhn is very well captured by the model.

Here we concentrate on the results pertaining to the period of northerly flow past the Alps. Fig.2 shows the resulting fields of potential vorticity at 850 hPa for both the EM and HRM runs. These simulations have 56 km

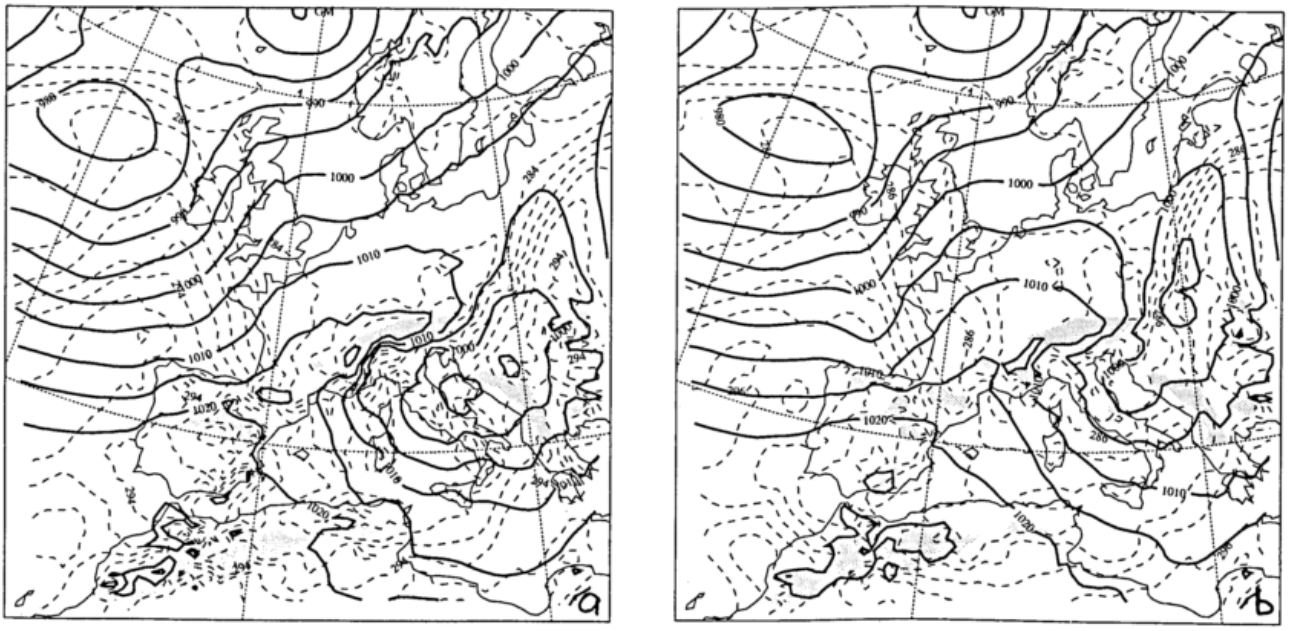

Figure 1: The synoptic situation of case 1 on 92-12-06 6 UTC as run with ECMWF-analysis (a) and EM (b) showing a lee cyclone in the Adriatic sea. The reduced surface pressure in hPa is solid, the potential temperature on 850 hPa is dashed (every 2K), the area with an altitude greater than 1000 m is shaded.

and 14 km horizontal resolution, respectively. The dark shaded areas in the panels indicate regions with PV>0.8 pvu, which is well above typical lower tropospheric values. The white areas (except for locations where the 850 hPa surface intersects the topography) show regions with negative PV values. In the low-resolution experiment in Fig.2a, the center of the lee cyclone is visible as a positive PV anomaly, while there are few features directly associated with the topography. On the other hand, the high-resolution simulation in Fig.2b resolves numerous bands of potential vorticity. At the time shown, the bands are still growing while being advected off the topography by Föhn winds from the north. Individual positive and negative pairs of bands can be attributed to peaks in the model topography. Note for instance the bands leading away from the Mount Rosa Massif in the Wallis (south-western Switzerland). Looking downstream, a negative (positive) band of PV forms to the left (right) of the massif. This is a clear indication of the importance of flow splitting for the formation of these bands.

The vertical structure of the bands is depicted in Figs.3 and 4. Figure 3 shows a S-N cross-section as indicated by a solid line in Fig.2b along a positive PV band south of the Alps. It can be observed that the PV band origi-

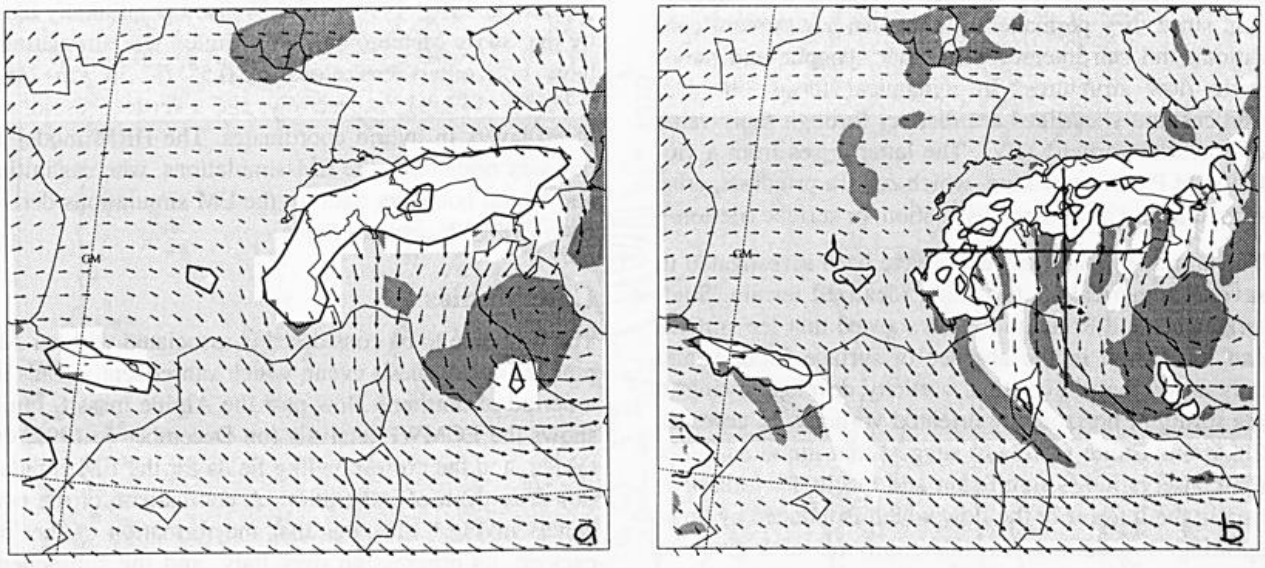

Figure 2: Potential vorticity shown on 850 hPa on 92-12-06 6 UTC 42 h after starting the EM-simulation (a), HRM-simulation (b), respectively. White areas indicate negative PV values (except within the h=1000 m isoline), PV values between 0 and 0.8 pvu are shaded, PV values > 0.8 pvu are shaded dark. The heavy lines denote altitudes of 1000 m and 2240 m, respectively, of the topography. The solid lines in b indicate the S-N (W-E) cross-section of Fig.3 (Fig.4).

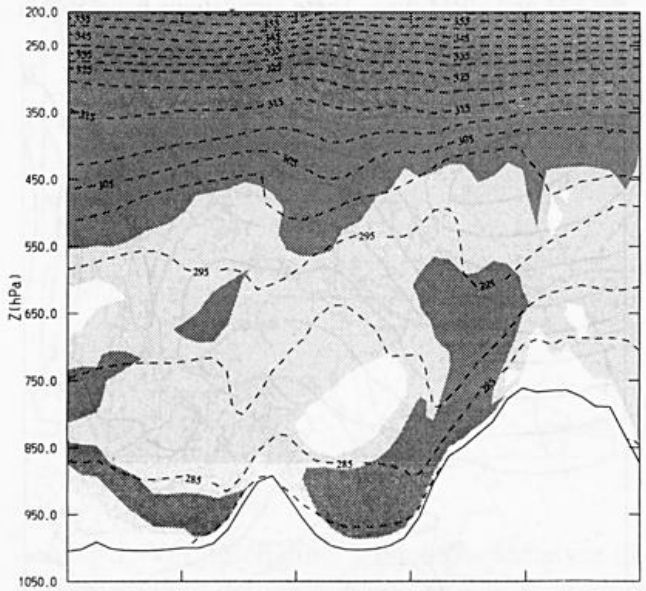

Figure 3: A vertical S-N cross-section through a positive PV band of Fig.2b (as indicated by a solid line). White areas indicate negative PV values, PV values between 0 and 0.8 pvu are shaded, PV values > 0.8 pvu are shaded dark. Potential temperature is dashed (every 5K).

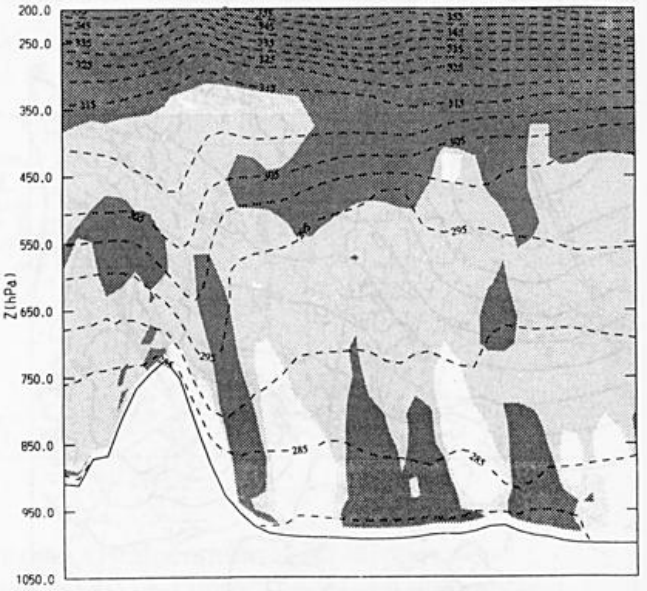

Figure 4: A vertical W-E cross-section through the situation of Fig.2b (as indicated by a solid line) along the Alps and perpendicular to Fig.3 showing a section across several PV bands. Same settings as in Fig.3.

nates at mountain peak height, but appears in addition to be fed from higher above through gravity wave breaking (or the model's representation of this process). This is suggested by the form of the isentropes, which show a hydraulic-jump-like structure, and the high levels (near 600 hPa) where the PV band originates from. Figure 4 shows a W-E section across the western part of the Alps and the Po-valley. For most of it, the section is oriented perpendicular to the PV bands. It can be observed how the bands extend surprisingly deep into the free troposphere. The vertical tilt of the bands is a result of differential advection with height.

Orographic bands of potential vorticity appear to be fairly common in the Alpine region, as well as near other topographic obstacles. For illustration, Fig.5 shows the results of an additional 42 hours high-resolution integration on September 14, 1993, 06 GMT (case 2). An elongated cold-front is oriented N-S along the Rhone valley throughout the computational domain. It is connected to a cyclone in the Mediterranean Sea, which steers cold air from N to S across the Pyrenees, and warm air from S to N across the Alps. To the lee of both the Alps and the Pyrenees, impressive bands of potential vorticity can be observed.

Conclusions

Results from two high-resolution numerical simulations have been analysed with respect to the distribution of potential vorticity at lower levels. In both cases, positive and negative PV bands evolve after some simulation time when the winds turn into a direction crossing the Alps or Pyrenees. After formation, the bands are ad-

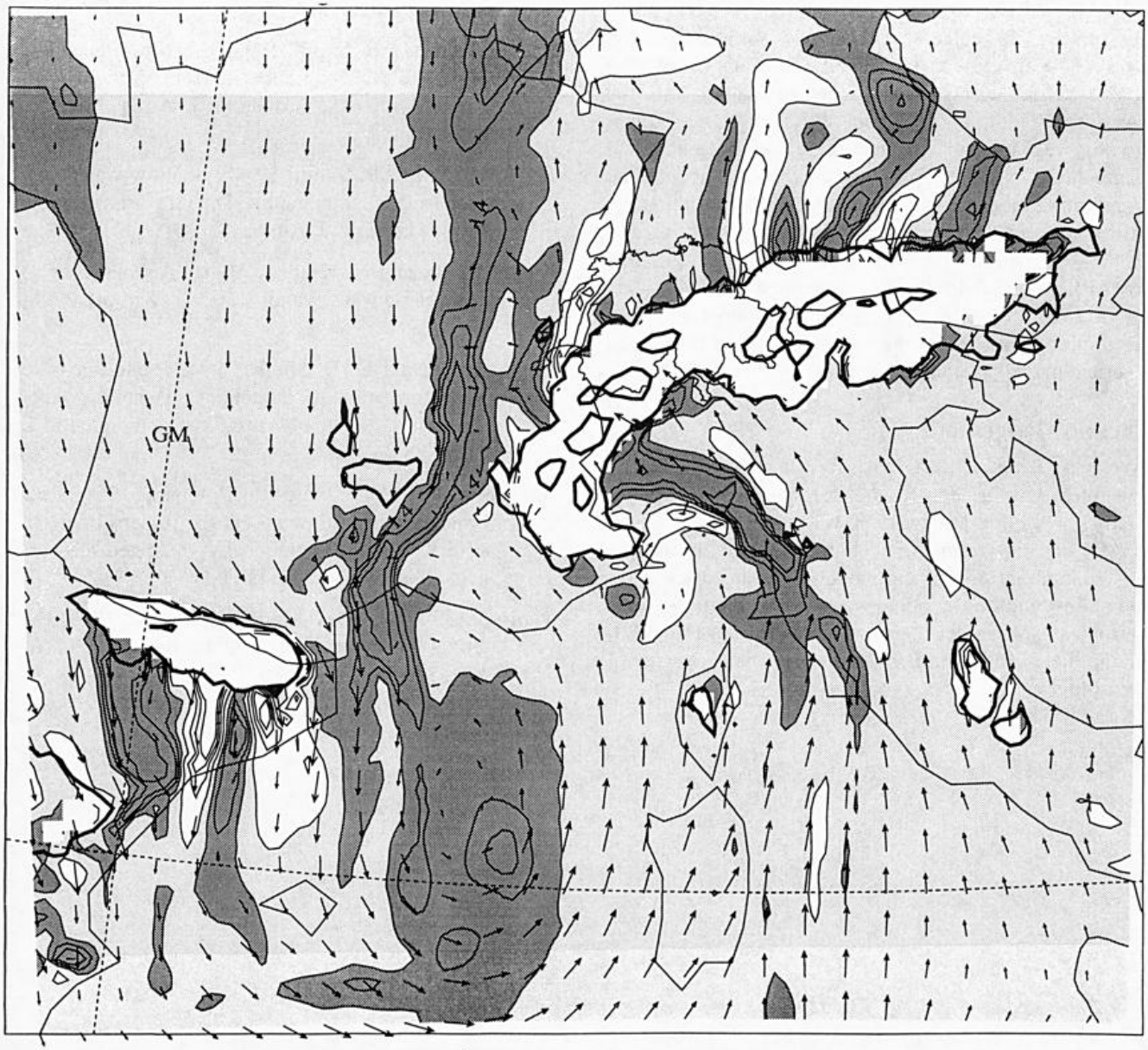

Figure 5: Bands of potential vorticity shown on 850 hPa on 93-09-23 6 UTC (case 2) 42 h after starting the HRM simulation. White areas indicate negative PV values (except within the h=1000 m isoline), PV values between 0 and 0.8 pvu are shaded, PV values > 0.8 pvu are shaded dark. The solid lines show the isolines of PV=-2,-1.4, -0.8, 0 (within the white area) and 0.8, 1.4,2,3 (within the dark area). The heavy lines denote altitudes of 1000 m and 2240 m, respectively, of the topography.

vected downstream by the ambient flow. In this way, some of the bands attained a length of more than 400 km. The orographic bands usually occur as pairs of positive / negative PV anomalies which can be attributed to mountain peaks in the model topography.

Orographic bands of potential vorticity must be distinguished from frontal bands, which usually result from diabatic processes in the frontal zone. Frontal bands of potential vorticity have recently received a great deal of attention, and they have been identified as one of the key-elements in small-scale cyclogenesis. This pinpoints towards the possibly important role played by orographic bands of potential vorticity, for instance in relation to Alpine lee cyclogenesis. Further attention in future research will also be devoted to the effects of surface friction, and to the sensitivity with respect to terrain-resolution.

It appears difficult to validate the simulated flow-features with current-day operational data. While the PV-bands are elongated and extend far away from the Alps, their width is only about 50 km and thus difficult to observe. This apparent inability to validate numerical simulations is quite typical for current-day operational forecasting models, which have reached a resolution beyond that of the observational networks. This issue is addressed within the Mesoscale Alpine Programme (MAP), whose field-phase is scheduled for 1998. One central aim of this programme is to provide high-resolution data-sets for the validation of mesoscale numerical models in complex terrain.

Acknowledgement

We are indebted to the German Weather Service (DWD) for providing access to the Europa-Modell. Special thanks to Detlev Majewski (DWD) and to Jean Quiby (SMI) and his group for technical support during the installation and use of the model. The diagnostic computations and the graphics was done with the IVE graphics package developed by Dale Durran, Harry Edmond, Pete Miller and Dave Warren at the University of Washington, Seattle.

References

Etling, D., 1989: On atmospheric vortex streets in the wake of large islands. Meteorol. Atmos. Phys. 41, 157-164

Grubisic, V., R. B. Smith, and C. Schär, 1994: The effect of bottom friction on shallow-water flow past an isolated obstacle. Submitted to J. Atmos. Sci.

Majewski, D., 1991: The Europa-Modell of the Deutscher Wetterdienst. ECMWF Seminar on numerical methods in atmospheric models, Vol.2, 147-191.

Majewski, D., 1994: Short description of the Europa-Modell (EM) and Deutschland-Modell (DM) of the Deutscher Wetterdienst (DWD) as at January 1994. 70pp [Available from: Deutscher Wetterdienst, Zentralamt, 63004 Offenbach am Main].

Schär, C., and R. B. Smith, 1993a: Shallow-water flow past isolated topography. Part I: Vorticity production and wake formation. J. Atmos. Sci. 50, 1373-1400.

Schär, C., and R. B. Smith, 1993b: Shallow-water flow past isolated topography. Part II: Transition to vortex shedding. J. Atmos. Sci., 50, 1401-1412.

Smith, R. B., and V. Grubisic, 1993: Aerial Observations of Hawaii's Wake. J. Atmos. Sci. 50, 3728-3750.

Smith, R. B. and D. F. Smith, 1994: Pseudo-inviscid wake formation by mountains in shallow-water flow with a drifting vortex. To be submitted to J. Atmos. Sci.

Smolarkiewicz, P. K., and R. Rotunno, 1989: Low Froude number flow past three dimensional obstacles. Part I: Baroclinically generated lee vortices. J Atmos. Sci. 46, 1154-1164.

Thorpe, A. J., H. Volkert, and D. Heimann, 1993: Potential Vorticity of Flow along the Alps, J. Atmos. Sci. 50, 1573-1590.

Mesoscale initial conditions in the Alpine region

Peter Binder, Schweizerische Meteorologische Anstalt, 8044 Zürich

At present no method exists to establish proper initial conditions for meso-β-scale numerical weather prediction (NWP) models. In practice the initial fields are interpolated from larger-scale representations and the fine-structure is expected to evolve during the integration (an exception is the optimum interpolation (OI) analysis for the Deutschland Modell of DWD). Especially in highly complex and steep orography as present in the Alpine region these approaches might not constitute the best possible solution of the analysis problem.

The following key issues are related to meso-β-scale initial conditions:

- formulation of balance conditions on the meso-scale in the presence of steep orography
- incorporation of active diabatic processes into the initial state
- adequate spatial and temporal resolution of observations, in particular including the vertical dimension
- initial conditions are closely linked to the spin-up behaviour of a NWP model

Requirements for the preparation of initial conditions increase with increasing model resolution and with the increasing sophistication of NWP models. For instance, at present time, three-dimensional humidity fields are poorly initialized by the conventional methods and data sources available. This can lead to serious spin-up effects and badly affect forecasts. This is in contrast to the primary ambition of high-resolution NWP models to better predict weather parameters like cloudiness and precipitation.

These general thoughts are illustrated by examples taken from daily operations of the meso-β-scale Schweizer Modell (SM). Then, possible and desirable contributions of the future project MAP to improve meso-scale initial conditions will be outlined, including the three main research fields involved in the preparation of meso-scale initial conditions, namely theories and methods of analysis and data assimilation, observational devices and methodologies, NWP models and experimentation.

Numerical Predicting Tests of the Rainfall and Vortices over the Tibetan Plateau in Summer

Chen Bomin Qian Zhengan

(Lanzhou Institute of Plateau Atmospheric Physics, Chinese Academy of Sciences, Lanzhou, China)

Abstract

In this paper, firstly, the errors of the wind and relative humidity (RH) fields of FGGE level-Ⅲb data set over the Tibetan Plateau from June to July 1979 were analysed. Then, by utilizing a limited model, comprehensively correcting initial wind and RH fields of the model, modifying parts of its physical processes, and increasing its horizontal resolution, six predicting experiments were designed and a set of 24-h forecasts of two plateau vortex / shear line precipitation process cases were performed.

1. Introduction

The Tibetan Plateau vortex here refers to the 500 hPa low pressure over the Tibetan Plateau (TP) in Summer. It occurs within the boundary layer over the TP and is main rain-producing system over the TP in Summer as well. Thus the improvement of the numerical prodiction for the TP vortex is need.

2. Model, data and cases

The model used is the primitive equation model with the C-type staggered grid, the horizontal resolution of 1.875° × 1.875° Lat. / Lon. and six vertical layers, covering full model physics and rather real topograph of the the TP terrain (the maximan height of 5200 m) (Yan, 1987).

A part of the FGGE level Ⅲb (hereafter FGGE) data, real temperature, humidity and wind data over the plateau and its neighbourhood, and Tiros-N satellite's cloud image for June to July 1979 were used.

Two cases of the TP vortex events during 30-31 July (case 1) and 23-24 June 1979 (case 2) were chosen.

3. Modified schemes and a design for forecasting experiments

Our efforts will be directed to altering the model intial fields, physical processes and horizontal resolution.

3.1 An analysis and correction of the initial field

Through analysing, we found that the FGGE wind and RH have obvious errors over the westen TP because the data of the temporary stations were not collected. For example, at 1200 GMT 30 July, the FGGE wind and RH fields over the eastern TP were rather consistent with the truth, but its wind direction tended to be opposite with the real one and its RH values were considerably overestimated over the westen TP (Fig. 1a-b; 2a-b).

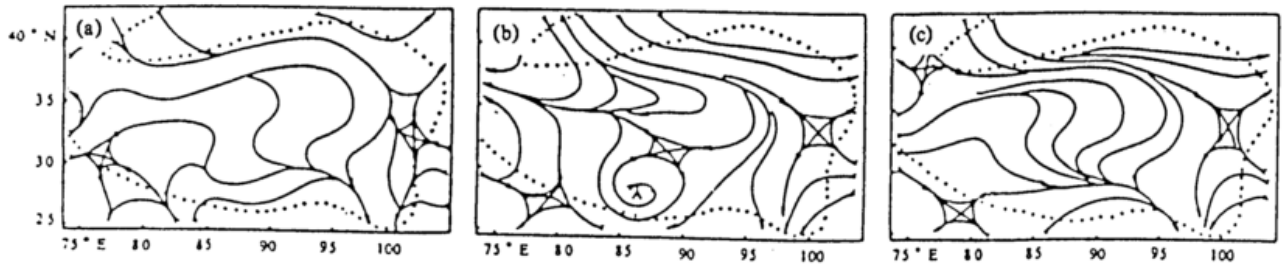

Fig. 1 The real flow field (a), original FGGE flow field (b), and that altered by comprehensive correction (c) over the TP 1200 GMT 30 July 1979. Dot line stands for outline of the TP tarrain.

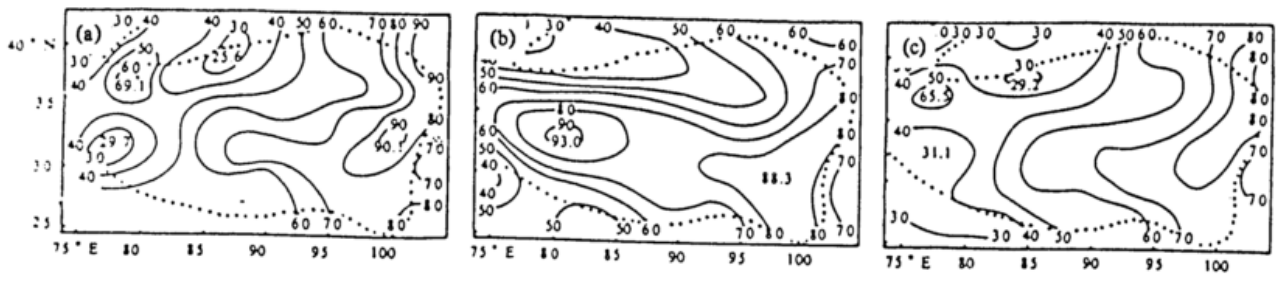

Fig. 2 As in Fig. 1, but for RH field (× 10^2).

We utilize the data of TIPMEX and Cressman's successive correction approach (Cressman, 1959) to modify the FGGE wind and RH fields . Iteration is carried out five times with the "scaning" radius of 2000, 1500,

1000, 500 and 250 km respectively. Then comprehensive correction is made by using the real wind field and satellite cloud image.

After correction, both the wind and RH fields are much close to the observed (Fig. 1c, 2c).

3.2. Modification of partial model physics

3.2.1 Drag coefficient C_D

The earth–air momentum, sensible and latent heating exchange in the model were dealed with by bulk aerodynamic method (Yan, 1987), in which all the C_D values over the TP are 0.005.

Now the monthly averaged C_D value of July derived from observed data during TIPMEX of 1979 (Zhang et al., 1988) are used.

3.2.2 Cloudness parameterization

An altered Slingo's cloudness parameterization scheme (Yan, 1987) was employed in the model.

In the paper, an altered ECMWF cloudness parameterization scheme (Qian et al., 1992) will be used to improve the radiative calculation.

$$N=\left[max\left(\frac{RH-RH_c}{\Delta RH},0\right)\right]^2 \qquad \Delta RH=\begin{cases}0.15 & high\ cloud\\ 0.35 & middle\ or\ low\ cloud\end{cases}$$

where N is cloudness; RH and RH_c respectively represent relative humidity and its critical values, and the latter are set as 0.35, 0.35, 0.50, 0.50, 0.70 and 0.80 from the highest model layer to lowest one sucessively.

3.2.3 Cumulus parameterization

Cumulus convection was originally parameterized by means of a modified Kuo–type scheme (Yan, 1987).

A modified Krishnamurti's multiple regression scheme by considering the the characteristics of the TP cumulus activities is used over the TP (Chen and Qian, 1992).

$$\frac{\partial T}{\partial t}=g(1-b)\frac{L}{c_p}W_L(1+\eta)\frac{(\theta_{se})_c-\theta_{se}}{\int_{p_T}^{p_B}[(\theta_{se})_c-\theta_{se}]dp} \qquad b=\frac{0.640\times10^5D_4-0.650\Delta\theta_{se}+2.69}{-0.410\times10^4D_4-1.404\Delta\theta_{se}+4.00}$$

$$\frac{\partial q}{\partial t}=gbW_L(1+\eta)\frac{q_s-q}{\int_{p_T}^{p_B}(q_s-q)dp}+\omega\frac{\partial q}{\partial p} \qquad \eta=-0.410\times10^4D_4-1.40\Delta\theta_{se}+3.00$$

where the tendencies of $T$and q stand for convective heating and moistening rate respectively, W_L, the large–scale efficient moisture convergence; b, the moistening coefficient; η, the mesoscale moisture convergence parameter; $(\theta_{se})_c$ and θ_{se}, the pseudo–equivalent potential temperature inside and outside cloud; q and q_s ,the specific humidity and saturation specific humidity; D_4 and $\Delta\theta_{se}$, the convergence at layer 4 and pseudo–equivalent potential temperture diference between layers 5 and 3; p_T and p_B, the pressure at cloud top and base.

3.3.3 Nested forecast of the model

Horizontal resolution of the model is increased from 1.875 ° × 1.875 ° Lat. / Lon. (coarse–mesh) up to 0.9375 ° × 0.9375 ° Lat. / Lon. (fine–mesh) with the vertical layers unchanged and, correspondingly, the time integration step length decreased from 4–min to 2–min. Observed lateral boundary condition is used for the coarse–mesh part of the model, and one–way interaction one for its fine–mesh part.

Based on the above modification schemes, six forecasting experiments are designed in Table 1.

5. Analyses of the forecast experiments

5.1 Forecasts of the original model schemes

For case 1, in observed flow field there is a shear line near to 30 ° N over the TP, a vortex at the west end of the shear–line (Fig. 3a) and the real rain regions were located to the south of the shear–line (Fig. 4a). Exp. 1 fails to forecast the vortex, and forecasts the shear–line to somewhat north and west of the verifying position (Fig. 3b). Overpredicted rain regain larger than 10 mm, with the maximum of 25mm, covers almost all the area to the south of 35 ° N over the TP (Fig. 4b). For case 2 there are similar forecast errors (Figs. 5b, 6b).

5.2 Effects of correcting initial RH and wind fields

Exp. II reduces the rain region over the west of the TP with only correcting the initial RH field (not shown) in case 1, but does not substantially improve the rainfall forecast with only correcting 500 hPa initial

Table 1 A summary of the six experiments and their performances

Exp.	Initial fields		Model physics			Horizontal resolution	Performance	
	RH	wind	C_D	cumulus parameterization	cloudness parameterization		precipitation	500 hPa flow field
I	original	original	original	original	original	coarse	overpredicted	shear-line predicted vortex not given
II	corrected only case 1	corrected only case 2	original	original	original	coarse	improved only in case 1	improved little
III	corrected	corrected	original	original	original	coarse	improved only in case 2	improved little
IV	corrected	corrected	modified	original	original	coarse	improved little	improved little
V	corrected	corrected	modified	modified	modified	coarse	improved	improved
VI	corrected	corrected	modified	modified	modified	fine	overpredicted	improved

wind field in case 2 (Figs. 6c). Once correcting both the initial RH and wind fields for the two cases, Exp. III more clearly improves the rainfall forecast over the middle and western TP in case 2 than that in case 1 (Figs. 6c–d, 4c–d). Nevertheless, predicted flow fields are not importantly improved by modifying the initial fields (not shown).

5.3 Effects of modifying C_D value, cloudness and cumulus parameterization

Exp. IV modifying the C_D value over the TP shows that, both forecasted precipitation and flow fields are altered little (Fig. 4c), maybe relate to short intergration time.

Exp. V, further modifying the cloud amout and cumulus parameterization schemes, gives better flow and precipitation. In case 1, the originally E–W oriented narrow rainbelt larger than 10 mm extended in the south part of the TP in Exp. II, III and IV is now broken up into four pieces with its raincore and position

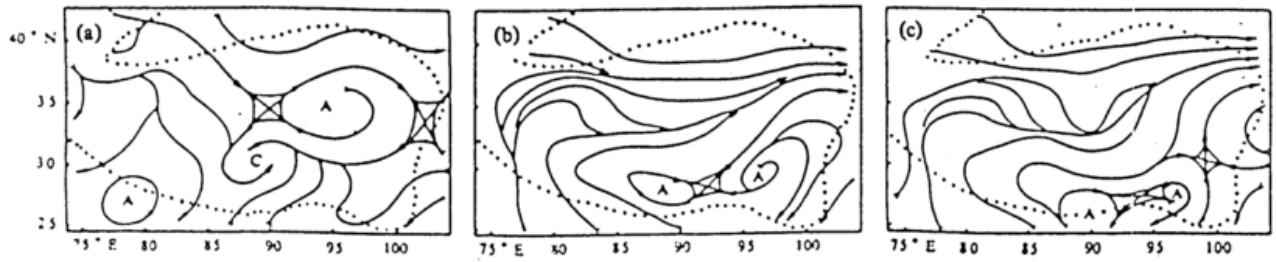

Fig. 3 500 hPa flow field observed (a) and predicted by Exps. I (b) and V (c) over the TP valid 1200 GMT 31 July 1979.

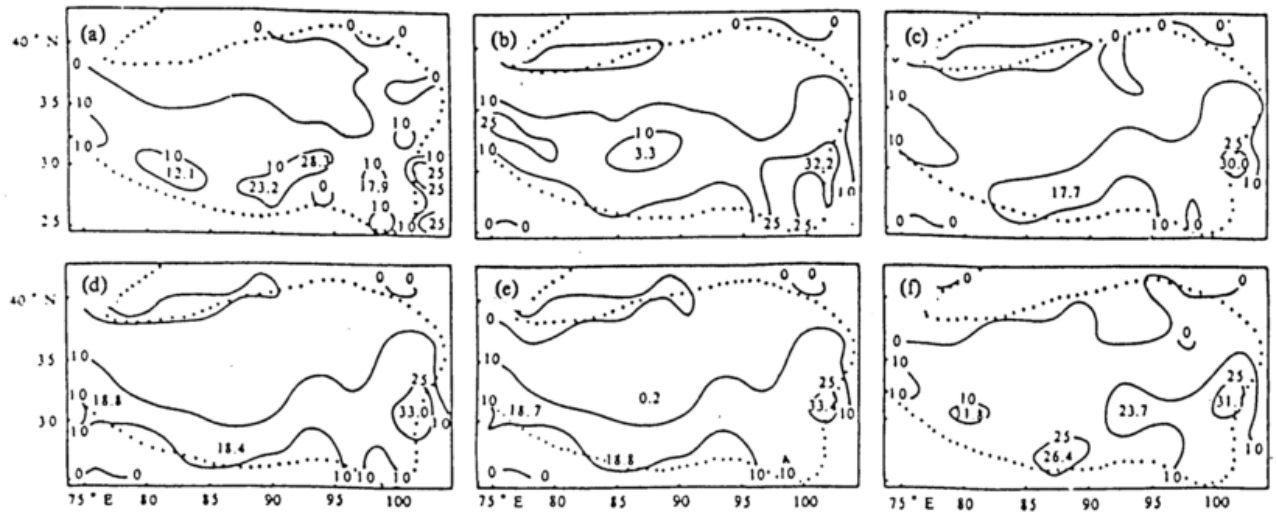

Fig. 4 Precipitation observed (a) and predicted by Exps. I (b), II (c), III (d) IV (e) and V (f) over the TP from 1200 GMT 30 July to 1200 GMT 31 July 1979.

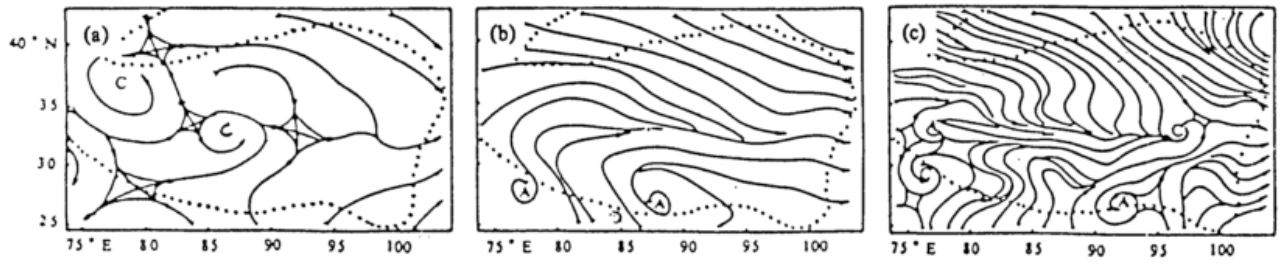

Fig. 5 500 hPa flow field observed (a) and predicted by Exps. I (b)and VI (c) over the TP valid 1200 GMT 23 June 1979.

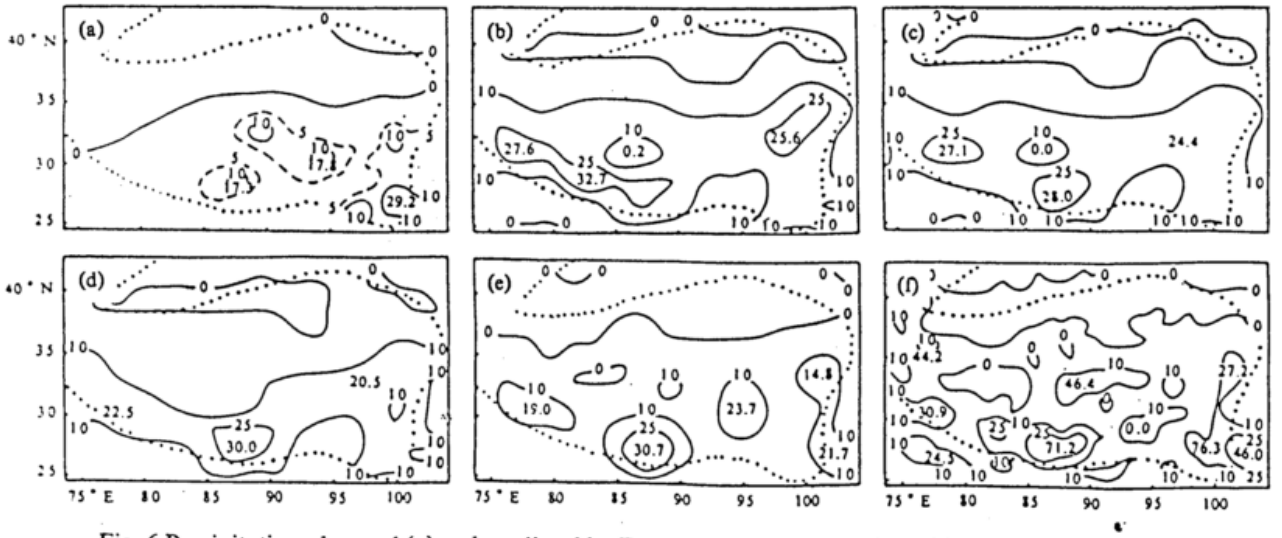

Fig. 6 Precipitation observed (a) and predicted by Exps. I (b), II (c), III (d), V (e) and VI (f) over the TP from 1200 GMT 23 June to 1200 GMT 24 June 1979.

very much close to the observed (Figs. 4a, f). The forecasted shear–line position over the middle TP given by Exp. V is quite near the real one (Fig. 3c), and the cyclonic curvature over the real vortex is increased, only well–closed vortex is not presented yet. In case 2, there are similiar improvements and deficiences of (Figs. 6a–c, 5a–b).

5.4 Effects of increasing horizontal resolution

Nest–forecasted field at 500 hPa in case 2 by Exp. VI presents a clearer shear line over the middle TP and further enhances the cyclonic curvature over the real vortex region. Namely the flow field forecast is altered more or less. However precipitation is considerably overestimated (Fig. 6f). For this reason, some parameters for controling precipitation are turned and tested, but little alteration is produced.

5. Conclusions

Primary conclusions to be drawn from the above analyses and discussion are the following:

1) The wind and RH fields of FGGE data of 1979 had clear deviations from the truth over the west of the TP and shoud be corrected.

2) The model can produce quite good precipitation over the TP and has also certainly forecast ability for the shear–line over the middle TP when comprehensive corrections of its initial RH and wind fields and modification of its cloud amount and cumulus parameterization are made, but the closed vortex is not presented yet. The next efforts should be directed to make better performance of the TP vortex flow field.

References

Chen, B. M and Z. A. Qian, 1992, An altered Kuo–type cumulus parameterization scheme suitable for the Qinghai–Xizang Plateau area, *Plateau Meteorology* (in Chinese), **11**, 1–12.

Cressman, G. P., 1959, An operational objective analysis system, *Mon. Wea. Rev.*, **87**, 367–374.

Qian, Z. A. et al., 1992, Comparison tests of parameterization schemes for cloud cover over Aisa and the effect of cloud cover, *Acta Meteorologica Sinica* (in Chinese), **50**, 50–59.

Yan, H., 1987, The design of a nested fine–mesh model over the complex topography, Part one and two, *Plateau Meteorology* (in Chinese), **6**, No.2 (suppl.), 1–139.

Zhang, J. J. et al., 1988, Progress of the Tibetan Plateau Meteorology (in Chinese), Science Press, Beijing, China, 70–77.

A Preliminary Study of Strong Storm in the East Side Edge of Tibet Plateau

Huang Fujun
Chengdu Meteorology Center

Tibet Plateau have a great influence upon the synoptic- climate of China and east Asia even, upon The Northern Hemisphere The SW-Vortex in the east side edge of Tibet Plateau induced by terrain often trigger the strong convevtion, gail and heavy hail in its developing process and cause heavy disaster. The average economic loss of one year is 1.5 billion RMB and southands of pepeole are dead and hurtful. Acorrding to the statistics from 1981 to 1994 of April and May (Table 1)

	time	class	area	affecting systems
1	20/9/5/81		West and south of SiChuan	baroclinic disturbances pleateau distrubance cold front
2	24/4/83		Whole sichuan	baroclinic disturbance
3	13/5/83		Whole sichuan	baroclinic pteteau disturbance
4	21/5/83		Northwest of Sichuan basin	cold front pteteau trough
5	12/5/86		Southwest of Sichuan basin	pteteau shear trough
6	29/5/86		East of Sichuan basin	Pleteau waves
7	19/5/87		North of Sichuan	Hetao transversal trough
8	19/4/87		southwest of sichuan	pleteau trough
9	24/4/87		whole sichuan basin	pleteau trough
10	24/5/87		East of Sichuan	pleteau trough
11	31/5/88		Whole sichuan	pleteau ridge
12	3/5/88		Whole sichuan basin	pleteau warm ridge
13	19/4/89		LuZhou	pleteau waves
14	20/4/89		Whole Sichcan	baroclinic cold front
15	17/4/92		North and central of sichuan	cold advection before ridge
16	30/4/92		Whole Sichuan	baroclinic pleteau disturbance
17	24/4/93		West of Sichuan	baroclinic disturbance cold front
18	30/4/93		West of Sichuan	baroclinic disturbance cold front
19	2/5/94		East of Sichuan	baraclinic disturbance cold front

table 1 Strorg advection Weather Processes happened in Sichuan—East side of Q-Z pleateau .

the cross of spring and summer , there are nighteen gail and heavy hail process in this region . Among them , four belong ones in type, which the influential area are not very large but there are high destruction power fifteen, relate to the large-scale baroclinic disturbances. An extremely heavy hail occured in the south of Sichuan province in April 20, 1989 and hardly seen for fifty years.

It is very interest that the spout phenomenon accompany with strong convection is not common, and this apparently distinguish with the spout phenomenon of the storm in East side edge of Rocky mountains in US .

In this paper , we study the form, the development and its mechnism of the heavy storm in April. 20 1989 ("4. 20" storm)

1、The evolution character of single station element

Accoring to Fig 1. the 10 min . temperature lapse rates are -3.5℃-5.4℃, -9.7℃, -8.3℃and -5.7℃ respectively when the storm passed by Jinggan Zhigong Luzhou and Naxi; and the temperature decreased with mavement. It is need to note that the temperature lapse rate has the characteristic of precursor before the stoum's getting its strength. From the pressure change in 20 minutes when passed the stations , the pressare rising rate is correspondent with the temperature lapse rate from and it shows the cool airmass and middle-high pressure formed at the same time and was caused by the downburst in the back of the storm. (Fig 1)

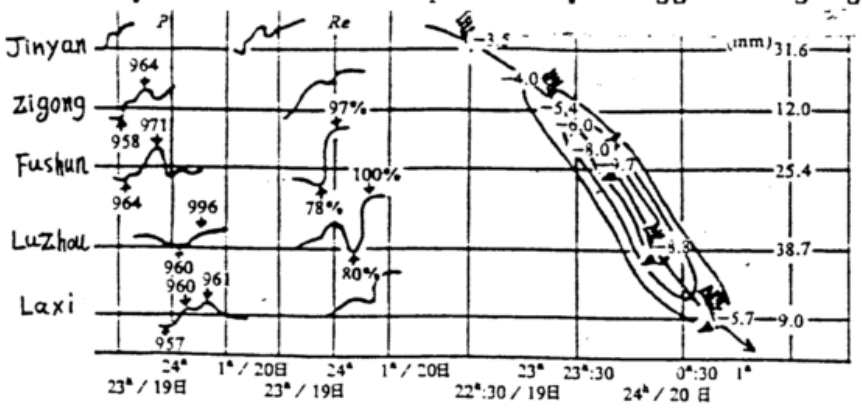

figl. The syntnetic Auto-dipicted chart of surface pressue , temperature and humidty

When the "4.20" storm passed through a station the curve of pressure didnt exhibit a "V "change which the tornado generally has and the wind direction are all north. Thus exclude the possibility of tornado and of squall line from the radar echo and satellite cloud chart .

It was very similar to the "downburst " Fujita [1] proposed. And the strong wind of zhigong. Fushun Naxi reached the standard of F1 which Fujita stipulated in 1973.

2. The characteristic of the general circulation when "4. 20" storm happened and developed

In 500hpa map on 20: ooBT, April 19, 1989 (fig. omitted. BT: Beijing Time). The meridional circulation predominated in Europin and Asia continent. There was a moving long-wave trough between the polar vortex centre (87.5° E , 62.5° V) and Alamutu and the corresponding front line located in the northwest of China (40° N). The circulation was flat in south of 40° N. The Q- Z Plateau and Sichuan basin were controlled by southwest stream and a mesoscale disturbence existed at the west of sichuan (102° E). In 200hpa , subtropical westerly jet move slowly morthward. The axis of jet located at 29° N steadly on 20: ooBT, April 19, where the stream were divergence. "4.20" storm just happened in the area of mesoscale α-wave acting and extrance of high- level jet. The cold front was far away and showed no relation with the storm which is very different from the thunderstonm previously described.

3. The external conditions when the "4.20" storm happened and developed.

a. Energy

From the stratification curve of three stations——Chengdu, Yibin, Chorgging we find Yibin (in south of Sichuan) had a inversion layer between 725 and 710 and 710hpa which stored the unstable energy and supprass the happenig of weak convection. Negative unstable encrgy was much more than the positive one at Chongging station. Campareed the stratification curve of Chengdu and Yibin ; three character are concluded as follows: (1) The free convection level were at 770hpa and 550hap respectively at Chengdu and Yibing (2) The limit level of convective was on 240hpa and above 200hpa respectively in Chengdu and Yibin , which is seldom seen in summer. (3) The unstable energy of Chengdu concentrated in the lower and middle level of troposphere and in the middle and high level in Yibing , which was the important reason for the development of the storm .

the θ se vertical distribution map of Chengdu and Yibing on which much higher energy air existed in Yibing, where θ se was more than 65℃ at 600hpa and reached 78℃ at 700hpa We can find strong potential instability in Yibing because the cases that: $\frac{\partial \theta se}{\partial p}>0$ in 950-800hpa; $\frac{\partial \theta se}{\partial p}<0$ in 800-700hpa; $\frac{\partial \theta se}{\partial p}>0$ in 700 -400hpa; $\Delta \theta$ se (700-600) =13℃/100hpa. Thus the "warm cover" lecated in 800-700hpa which suppress the development of disturbance and the accumulation of energy between 700-400hpa level, the showed convection changed into deep convection (Fig omiffed). Fig 2 showed a sinle mesoscale air mass with high energy in intersection area of Yunan, Sichuan and Guizhou province. It centre was in Yibing where θ se was as high as 78℃ and formed a strongest energy front. Meanwhile, southern stream transport the high energy air to the area of storm. At 08: 00BT, April 20, the high energy air mass and energy front disappeared when heavy storm passed away and thus conclude that they were the dominant external forces for the strong development of the storm which is different from what was thought that thelong-living storm happened in the area and its nearby of large-scale energy front.

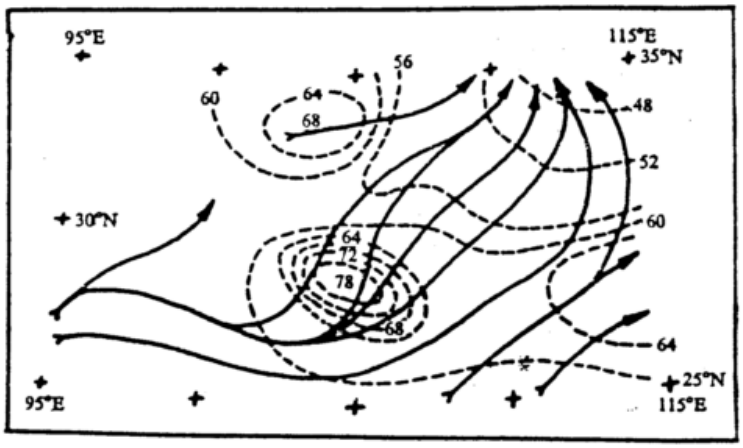

Fig 2. The θ se fields and flow chart in 700hpa on 20: 00BT Apri 19, 1989. solid arrous represent the flow and dashed lines the θ se. (BT: Beijing Time)

b. Trigger Condition

The combination of the vertical movement drived by warm and differential advection of lower-middle level, and the rising movement triggered by the fast movement of cold dome in thunderstorm, was the trigger mechanism for the release of unstable energy.

c. Ri value and the development of disturbence

According to theory, the Ri value canbe used to judge the development of the mesoscale disturbence. In moist air , $Ri=\frac{1}{\rho}\frac{\partial \ln \theta_{se}}{\partial p}/\left(\frac{\partial V}{\partial p}\right)^2$, the bigger the vertical shear $\left(\frac{\partial V}{\partial p}\right)$ of wind , the smaller the Ri value. $\frac{\partial V}{\partial P}$ represents the strength of baroclinic instability. Fing 3 shows the distribution of Ri value of 700Hpa over the Basin and its nearby. The storm in luzhou appeared near the minimum axis of Ri value which was extremly favourable to the developmint of mesoscale storm when convergence flow of 700hpa and the disturbence of 500hpa impended.

The disturbence transfered along the minimum Ri value axis and strengthed storm in its eastward moving.

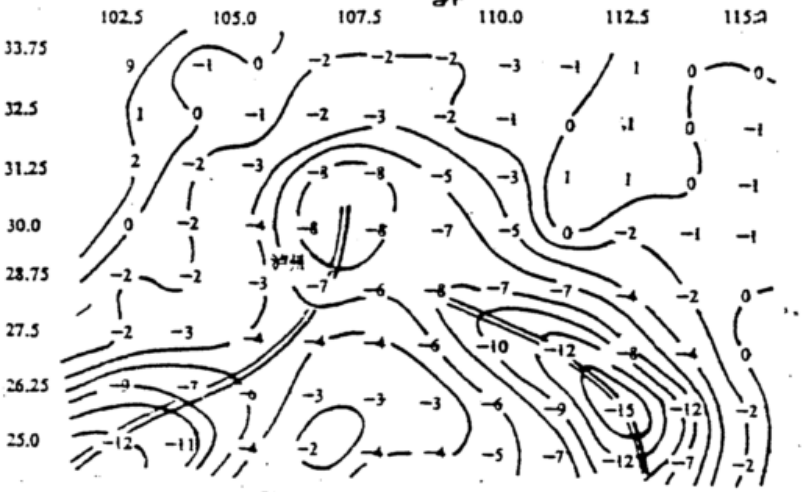

Fig 3 Ri value distribution in 700hpa on 20: ooBT Apri 19, 1989.

a. The initial stage of storm

According to fig 4

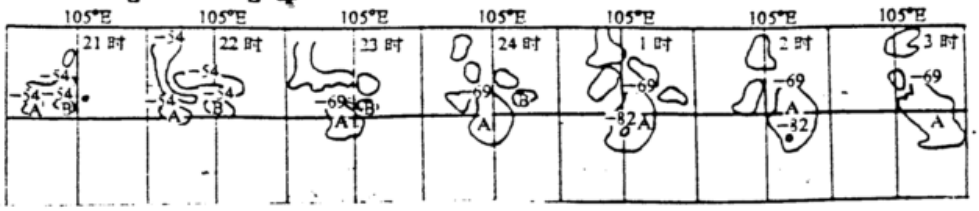

Fig4 The pseudo-color cloud pictures by GMS-3 from 21: ooBT, Apr1 19 to 03: ooBT, April 19, 1989. (once an hour) The values in the picture are temperatures of top clouds.

the cloud system of large scale trough was above 90° E while the west Sichuan basin was fine with unstablity on 20: ooBT April. 19on GMS-3 satellite cloud picture. But on 22: 00BT, a convective cloud cluster started to develop with the center on 103. 5° E, on 23: 00BT, the cloud cluster developed and extended to southeast with the area of 2000km², the descent of cloud top from -54℃ to -69° . This convective cloud cluster was combined by two β-cloud according to the colour of the cloud cluster and its strongest center was in southeast of the cloud.

b. The developing stage

On24: ooBT, the main body of cloud cluster arrived on 105° E, 29° N, with the 4000km² area. Its cirrus plume raised to southeast and the storm occured just in the back of raising cloud clouster corresponding to Fushun , Luzhou on

ground . on 01:00BT, Apri 19, the storm developed to its strongest , while the area of cloud clouster reached 50000km² and the temperature of cloud top descented to -80℃ with white bright dot in the cloud center at 106° E. 28.5° N, while on the ground of luzhou and Naxi occured 12 grade gale and hale respectively on 00:15BT and 00:25BT, Apri, 20. On 02:00BT, April 20, the storm body entered Guizhou province. On 03:00BT, the bright dot disappeared. Fig. 6 is the radar echo of Leijang station from 00:38BT to 00: 53BT April 20, in which the strip of echo delineated the convective rainfall clouds (length of 140km and width of 12km) and looked like a bow. It demenstrated that the wind velosity above the convective clouds was disconnected and the echo formed a fork on its lower reaches, which curred as cyclone path and showed the specific character of downburst in strong devastating storms. (Fig 5)

6. Conclusion

①From 1981 to (May) 1994, Nighteen gail and hevy hail processes happened in sichuan province and almost focused in Apri or May. Most of them belong the sort of baroclinic disturbances or pletean disturbances.

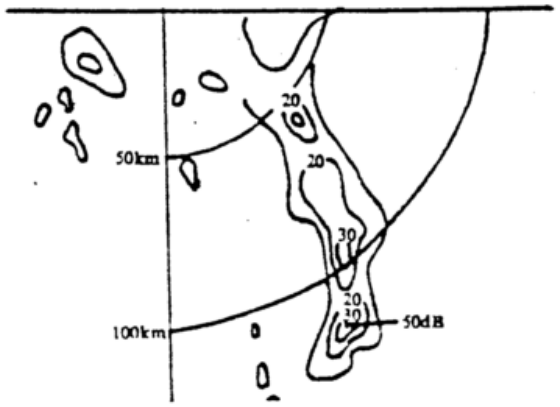

Fig5 The radar echo of Leijang station from 00:38BT to 00:53BT, April 20, 1989.

②The storm at Zhigong and luxhor in Apri 20, 1989 was caused by the downburst in the rear part of storysuper-storm. Its intensity reached F1 and its verosity was morethan 30m/s.

(a) "4.20" storm has much difference from previous strong storm in mang ways. Its duration is short and its scale was rather small and its intensity was very strong. Its happened in the non-stable warm south area of sichuan where then the cold front was 1000km far away.

(b) The high energy air mass and energy front were the major fores for the happening and development of the "4.20" storm.

(c) The condition for triggering the storm and its downburst is the cold dome in the strong storm, which forcerbly lift the warm and humid air in the front of strong convection cell farther more, its warm advection in middle lower level and its differential vortex advection result in vertical motion. The other triggering conditons may be the disturbence in East of Q-Z pleateau in 500hpa and the non-stability of small Ri values.

(D) The pseudo-color satellite cloud pictures (once an hour) showed that the storm developed by two middle p-scale convective clouds which quickly combined and enforced.

SOME OBSERVATIONAL FACTS OF ATMOSPHERIC LOW-FREQUENCY OSCILLATIONS OVER TIBET PLATEAU

Sun Guowu Zhou Yajun Li Chunhu
(Lanzhou Arid Meteorological institute, Lanzhou 730020, P.R.China)

1. INSTRODUCTION

The tibet Plateau's (TIP's) atmospheric physical feature resembles to that in equatorial and tropical areas in many aspects. Equatorial and tropical area is the source place of atmospharic low-frequency oscillation (LFO) with period of 30-50 days, how about Tibet Plateau (TIP)? Authors have studied the oscillations and propagation of TIP's atmospheric low-frequency wave. In this paper the facts of TIP's atmospheric LFO will be discussed further.

2. POWER SPECTRUM OF THE ZONAL WIND OVER TIP

The different frequency oscillation in time domain exists in atmospheric activity, all kinds of circulation systems and meteorological factors have different frequency oscillation features. The objective of this paper is to discuss the LFO over TIP, hence we use the TIP's zonal wind data of 500hPa to analyse whether it includes the low-frequency oscillation with period of 30-50 days.

The distribution of selected stations and 500hPa zonal wind power spectrum over TIP and its surroundings have been given in Fig.1. and Fig.2. (omitted) respectively, The results was not performed smooth and were computed independently, and Shiqianhe, Gaize, Zhongba and Shuanghu among the stations were newly butit during Tibetan Plateau Meteorological Experiment in 1979.

From these results, the U's power spectrum of single station performs 2-4 days, 6-8 days, 10-15 days, and 30-50 days period, in which the oscillation with 30-50 day period is the most obvious. The wave spectrum peak of 30-50 days period passed through the red-noise test. Therefore, Fig.2. (omitted) indicates the zonal wind of 500 hPa over TIP possesses evident low-frequency oscillation features.

Considering LFO with evident annual variation, the analyse of 1979 mentioned above is perhaps limited , and for convenience of data and catcutation, the 500 hPa height field of 1980-1991 will be analyzed as following.

3. THE RATIO OF HEIGHT VAREATION OVER TIP

In order to investigate the proportion of 500 hPa height's LFO variation (LOV) in total variation (TV) over TIP, and to compare with other area, we have calculated the ratio of LOV over TV of May-Sept. from 1980 to 1991 (LOV/TV), together with the computing range of 20° N-80° N, 60° E -140° E with grid 5° ×5° .

From each year's LOV/TV distribution, it may be divided into three patterns, the large values area is located at, (1) North-west of TIP and its surroundings, such as 1980, 1981, 1983, 1988 and 1990. (2)South-west of TIP and its surroundings, such as 1984, 1987, and 1991. (3) North-east or East of TIP and its surroundings, such as 1985, 1986 and 1989.

On the whole, 500 hPa sruface over TIP exists large values area of LOV /TV all along in summer, only in different position in each year. Without regard to large annual variation of LOV/TV, it may be indicated that TIP is one of LFO active area based on the analyes of section 1 and 2.

4. THE LOW—FREQUENCY SYSTEMS (LFS) OVER TIP

Refering to Batterworth band-pass filter and using the grid data of ECMWF in the summer (May-sept.) of 1980—1993. The low-frequency wind field charts in each day has been gotten (500hPa) and LFS may be taken as the definition of synlptics (low-frequency cyclone and anticyclone).

It is found that LFS usually produced in TIP by each day's low-frequency wind field chart. It seems TIP is the source place where LFS form. As an example, we will discuss Fig.3. which is one processes of LFS production and evalution over TIP in the summer of 1983. For the purpose of saving space, only shows the low-frequency flow field chart of 1, 2, 41 day. From Fig.3. when time series index is 1, a low-frequency cyclone produced in Norther-west of TIP, centerde at around 36° N, 81° E. After its mantaining up to 21 day, a low-frequency anticyclone appeared lying on the same position to 41 day, it was alternated by another cyclone.

The production of LFS over TIP is not limited at one or two examples, so we will analyse the composite structure of TIP's LFS. The reference center of composition was located at the middle part of TIP(32.5° N, 87.5° E) Fig4 is a compositing chart based on 31 times of LFS producing in the main part of TIP, it could be seen further that TIP is an important source place of LFS.

Aad all this, the period of low-frequency cyclone (low-frequency anticyclone) is reponded to rainy spell (dry spell) in TIP as well as rich water

time (poor water time) in upper reaches of Yellow Rirer.

5. SUMMARY

The primary results on this paper could be summaried as following,

(1)Based on analyse of power spectrum and variation, it was found that 500hPa zonal wind and geopotential height of summer half year over TIP possess low-frequency (30-50 day period) oscillation features, TIp is an active area of LFO with period of 30-50 day.

(2)The low-frequency systems on low-frequency wind field chart usually produce and oscillate on TIP, together with the period of 30-50 day. TIP is one of the highest frequency area where LFS produce. Therefore, TIP is not only one of active areas of LFO but also the source place of LFS.

(3)The low-frequency systems are related to TIP's recipitation and Yellow River flow.

REFERENCES,

Sun Guowu , Chen Baode , The oscillation and meridional propagation of atmospheric low-frequency wave over TIP, Chinese J. Atmos. Sci., 12, 250—256, 1988.

Murakami, T. and t. Nakazawa, Tropical 45 day oscillations during the 1979 northern hemisphere summer, J. Atoms. Sci., 42, 1107—1122, 1985.

Lau, K.M. and D.H. Chan, Aspects of the 40—50 day oscillation during the northern summer as inferred from outgoing longwave radiation, Mon. Wea. Rev., 114, 1354—1367, 1986.

Lau, K.M. and L. Peng, Origin of low-frequency (intraseasonal) oscillations in the tropical atmosphere, Part 1, basic theory, J. Atmos. Sci., 44, 950—972, 1987.

Krishnamurti, T. N. and S. Gadgil , On the structure of the 30 to 50 day mode over the globe during FGGE, Tellus, 37A, 336—360, 1985.

Krishnamurti, T. N. and D. Subrahmanyam , The 30—50 day mode at 850 mb during MONEX, J. Atmos. Sci., 39, 2088—2095, 1982.

Pedgley, K.E. and Krishnamurti, T.N., Structure and behaviour of a monsoon cyclone over west Africa, Mon. Wea. Rev., 104, 149—167, 1976.

Hoskins, B.J. and R. pearce, Large scale dynamical processes in the atmosphere, Academic Press, 1983.

He Jinhai et al., The circulation and vapour transport variations of 40-50 day period oscillation over Asian mooson region in 1979 summer, Journal of N.M.I. No. 2, 163—175, 1984.

Li Chongyin, The intraseasonal oscillation in atmosphere, Chinese J. Atmos. Sci., 14, 32—44, 1990.

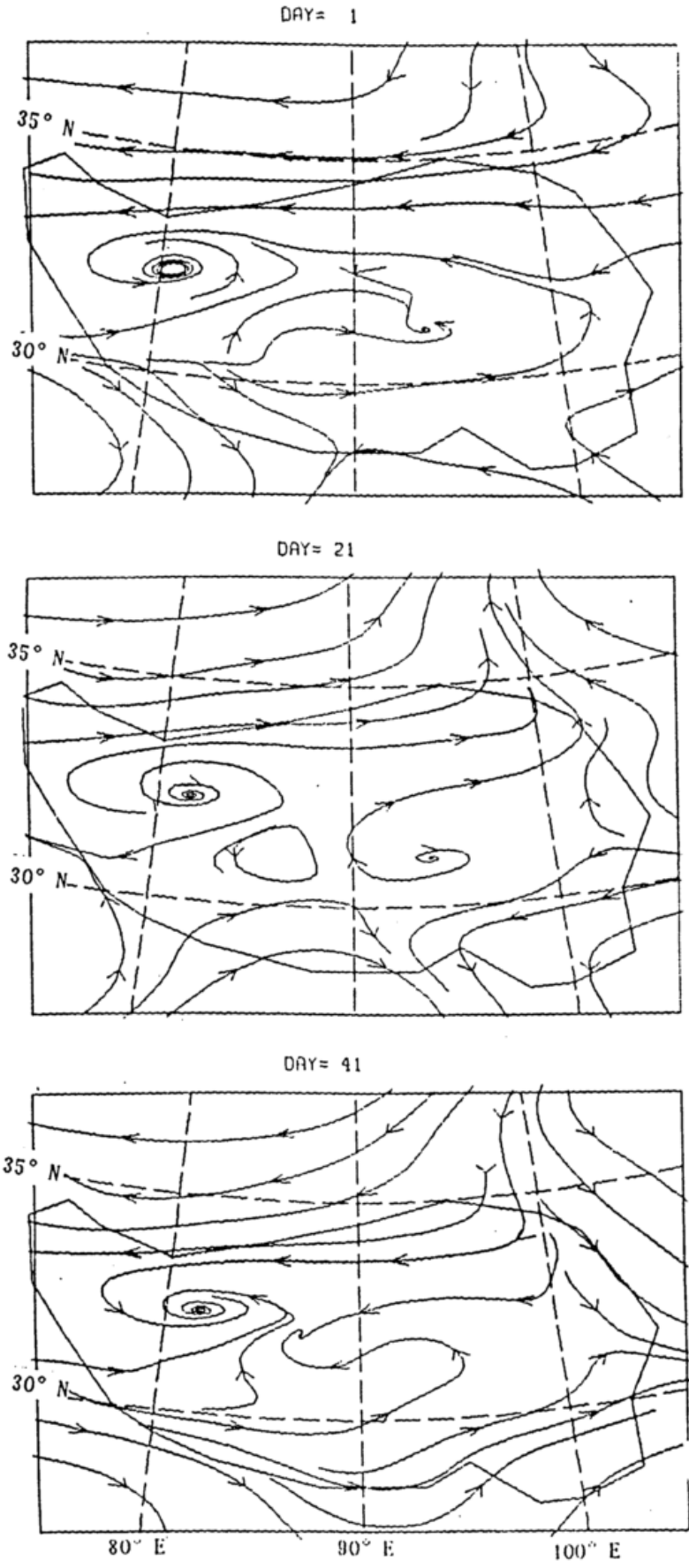

fif.3 500hPa low-frequency flow chart in 1983 summer. The solid line is TIP orography

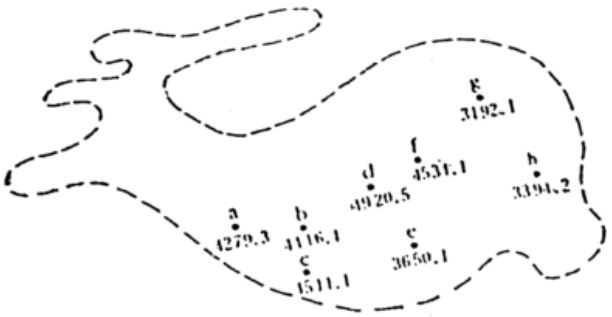

fig.1 The stations distribution of TIP's zonal wind power spectrum. a: Shiqianhe; b: Gaize; C: Zhongba; d: Shuanghu; e: Lasha; f: Tuotuohe; g: Dulan; h: Ganzhi. the number is the height above sea level and the dashed line shows the TIP orography

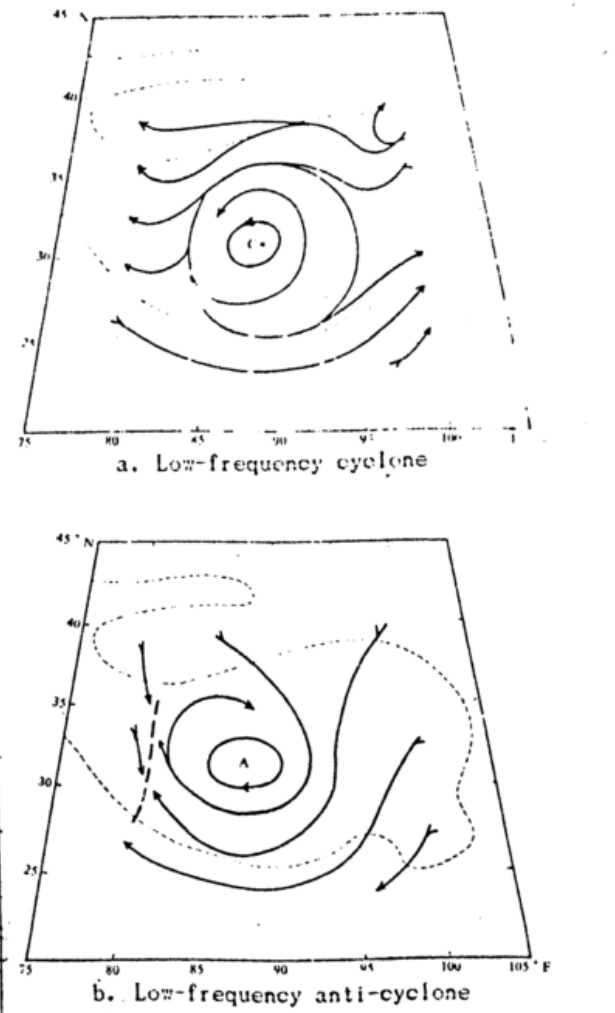

fig.4 Compositing chart of LFS over TIP (500hPa)

Numerical Simulation of the Vortices over the Tibetan Plateau in Summer

Chen Bomin Qian Zhengan Zhang Lisheng

(Lanzhou Institute of Plateau Atmospheric Physics, Chinese Academy of Sciences, Lanzhou, China)

Abstract

In this paper, three typical vortex cases including the genesis and / or development stages in summer 1979 were chosen. A set of ten experiment schemes with a consideration of influences of the TP terrain elevation, surface fluxes, friction, latent heating, the temperature lapse rate and baroclinicity of air column was designed and their 24–h or 48–h simulation were performed by using a limited numerical model suitable for complex terrain which parts of physical process parameterization were improved and utilizing the comprehensively–corrected FGGE level Ⅲb data.

1. Introduction

The Tibetan Plateau vortex here refers to the 500 hPa low pressure which occurs withen the boundary layer over the Tibetan Plateau (TP) in summer. It is the product of the TP complex terrian dynamic and thermodynamic influences, and is main rain–producing system over the TP. Occasionally, some TP vortices can move eastwards out of the TP on condition of preferable largerscale patterns. Therefore simulation of the TP vortex is important for both the theory of the TP Meteorology and improvements of forecast skill over the TP and to its east side.

However, existing simulations of the TP vortex are nearly one–case studies and the data used were not corrected. Qian et al (1984) summaried six factors favourable to the vortex–genesis and proposed the physical picture about its formation and development, which have not been examined and modified. Hance, multiple case simulations paying attension to different stages of the vortex is needed to give an insight into the TP vortex genesis and development.

2. Model, data and cases.

The model used is the primitive equation model with the C–type staggered grid, the horizontal resolution of 1.875 ° × 1.875 ° Lat. / Lon. and six vertical layers, covering full model physics and rather real topograph of the TP terrain (the maximan height of 5200 m) (Yan, 1987).

The comprehensively–corrected FGGE level Ⅲb data from June to August 1979 (Chen and Qian) were employed.

Three cases of the TP vortex events during 23–25 June (case 1), 22–23 July (case 2) and 11–12 August 1979 (case 3) were chosen. In case 1, the typical patterns favourable to the TP vortex genesis exited over the TP at 1200 GMT 23 June, the vortex would form over the midst in 24h (Fig. 1a), and then developed and moved over the eastern TP at 1200 GMT 25 June (Fig. 2a). In case 2 and case 3, only genesis and development stages of the vortices were considered respectively.

3. Schemes for simulations and analyses of results

Based on Qian et al (1984), Ten experiments for simulation are designed and listed in Table 1.

Table 1. A list of simulating schemes

Exp.	Initial $\partial \lvert V \rvert / \partial p$	Boundary Layer Lateral Fricition	The Surface Friction	Initial $\partial T / \partial \ln p$	The Surface Sensible Heating	The Surface Evaporation	Largescale Latent Heating	Convective Heating	The TP Elevation
1	Unaltered	Yes	Yes	Unaltered	Yes	Yes	Yes	Yes	Unaltered
2	Increased	Yes	Yes	Unaltered	Yes	Yes	Yes	Yes	Unaltered
3	Unaltered	No	Yes	Unaltered	Yes	Yes	Yes	Yes	Unaltered
4	Unaltered	No	No	Unaltered	Yes	Yes	Yes	Yes	Unaltered
5	Unaltered	Yes	Yes	Decreased	Yes	Yes	Yes	Yes	Unaltered
6	Unaltered	Yes	Yes	Unaltered	No	Yes	Yes	Yes	Unaltered
7	Unaltered	Yes	Yes	Unaltered	Yes	No	Yes	Yes	Unaltered
8	Unaltered	Yes	Yes	Unaltered	Yes	Yes	No	Yes	Unaltered
9	Unaltered	Yes	Yes	Unaltered	Yes	Yes	No	No	Unaltered
10	Unaltered	Yes	Yes	Unaltered	Yes	Yes	Yes	Yes	Decreased

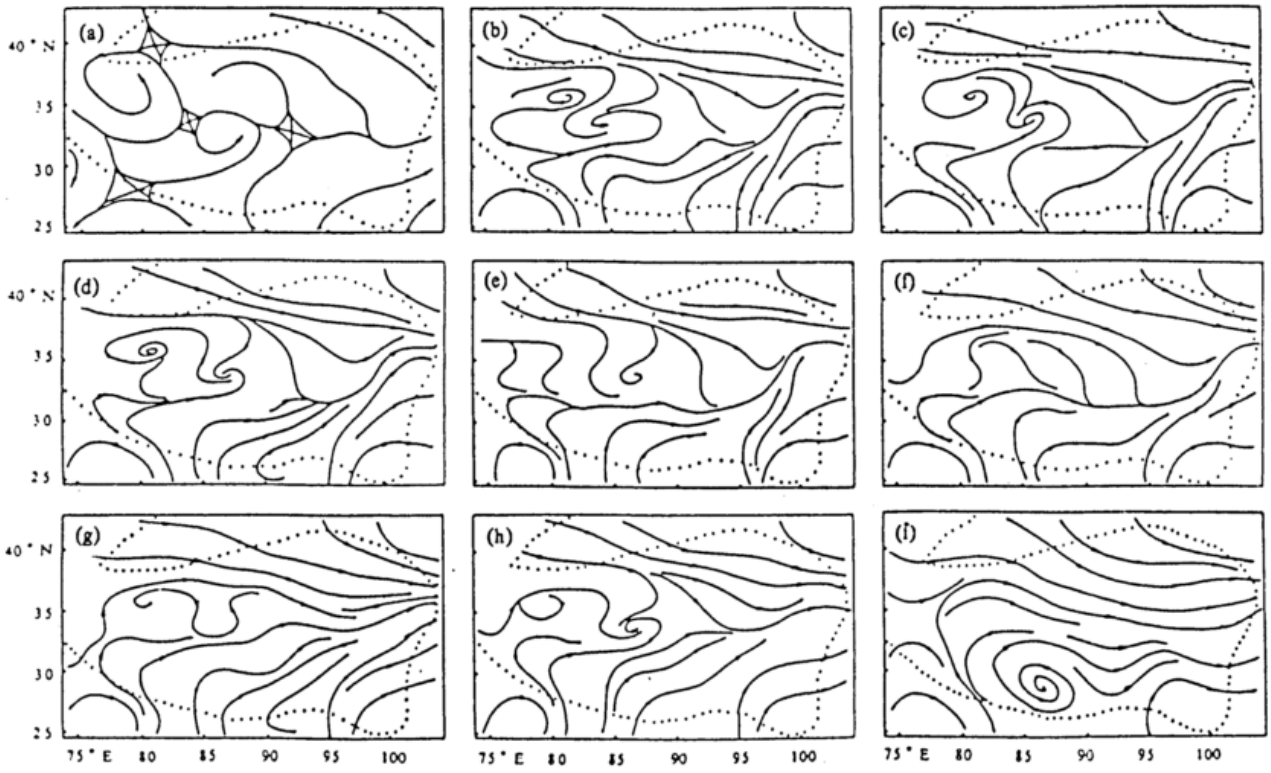

Fig. 1 500hPa flow fields of case 1 in reality (a), and that simulated by Exp. 1 (b), 2 (c), 3 (d), 5 (e), 6 (f), 7 (g), 9 (h) and 10 (i) at 24h.

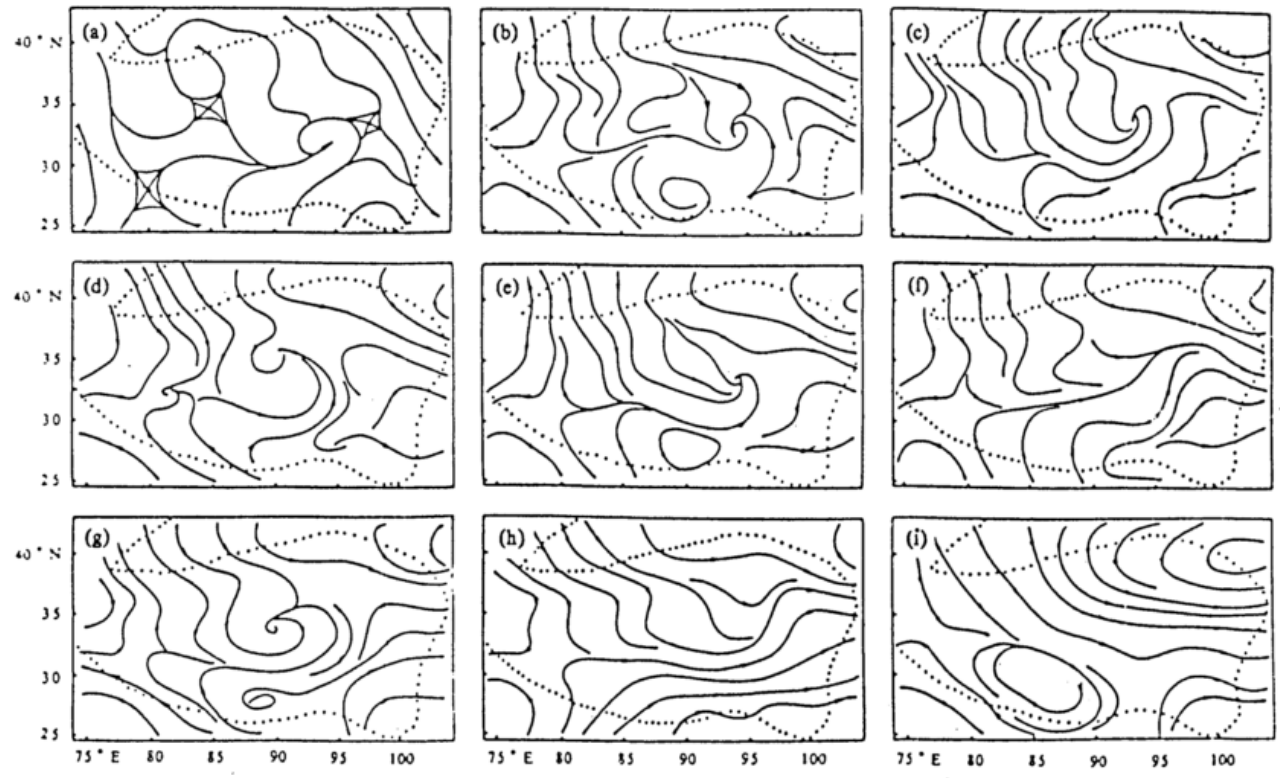

Fig. 2 500hPa flow fields of case 1 in reality (a), and that simulated by Exp. 1 (b), 2 (c), 4 (d), 6* (e), 7* (f), 8 (g), 9 (h) and 10 (i).

3.1 Controlling experiment

Exp. 1 successfully presents the vortex genesis and development of the three cases (Fig. 1a, b; Fig. 2a, b; Fig. 3a, b; Fig. 4a, b). It gives rether real vorticity and 0–24h precipitation score over the vortex of case 1 (Ta-

ble 1). Although the daily rainfall in case 2 and that for 24–48h in case 1 are overforecasted, the model make a good forecast of the vortices on the whole. Therefore it can be used for simulating of the TP vortex.

3.2 Effect of baroclinicity (vertical shear of wind) in intial field

Enhancing the initial baroclinicity, Exp. 2 weakens the vortex in case 1 (Fig.1c, 2c), but causes intensification of the vortices in case 2 and 3. Two opposite effects of vertical shear of wind on the TP vortex were proposed by Qian et al.(1984) and Sun et al. (1988) respectively. The experiment seemly suggests that the importance of the two effects is variable.

3.3 Effect of Friction

In Exp. 3, without the boundary layer lateral friction, the feature and intensity of the vortices change little (Fig. 1d). However, further removing the surface frition in Exp. 3, Exp. 4 increases the vorticity over the vortex of case 1 (Fig. 2d), which means the surface friction have a few contributions on the vortex.

3.4 Effect of temperature lapse rate

After the temperature lapse rate of the initial field is decreased (Exp. 5) , only a very weak vortex is produced in case 1 (Fig. 1e), while no vortex is presented in case 2 and 3 (Fig. 3c). This shows the summertime TP vortex has, indeed, a close relation to stratification stability over the TP.

3.5 Effect of sensible heating and evaporation on the surface

When the surface sensible heating is concealed (Exp.6), no vortices is formed in case 1 and 2 (Fig. 1f, 3d), and the weak vortex exited in initial field of case 3 disappears at the begining of integration (Fig. 4c).

When the surface evaporation is removed (Exp.7), the vortices in case 1 and 2 are formed, but obviously are damped (Fig. 1g, 3e). The vortex in case 3 is notmaintained also (Fig. 4d). To more correctely understand

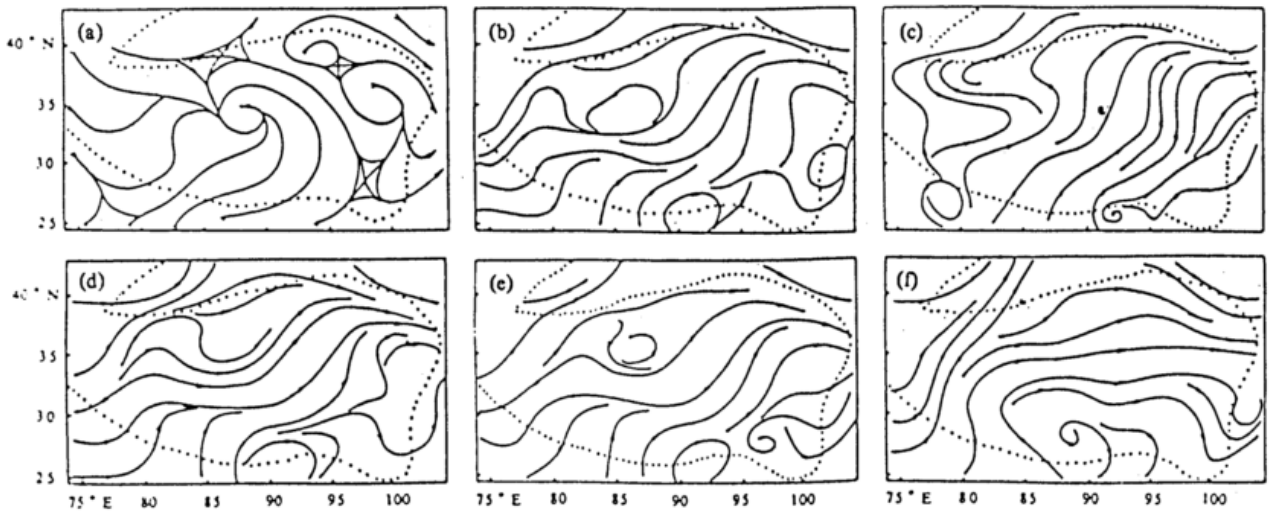

Fig. 3 24h 500hPa flow fields of case 2 in reality (a), and that simulated by Exp. 1 (b), 5 (c), 6 (d), 7 (e), 10 (f).

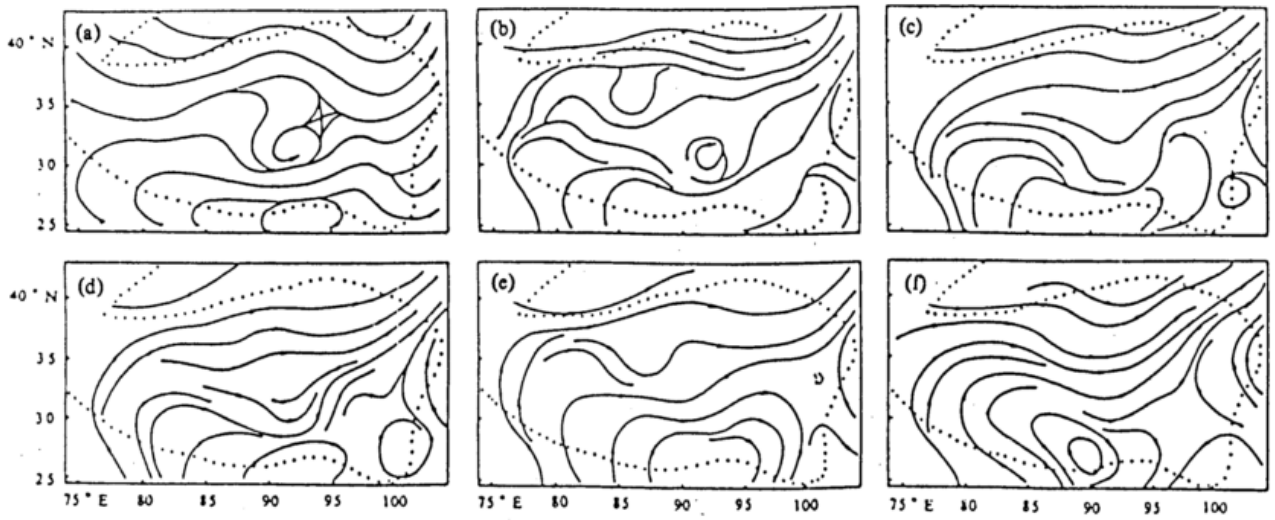

Fig. 4 24h 500hPa flow fields of case 3 in reality (a), and that simulated by Exp. 1 (b), 6 (c), 7 (d), 9 (e), 10 (f).

Table 1. Simulation schemes and maximum of 500hPa relative vorticity ($\times 10^{-5}$ s^{-1},), 300–500hPa averaged vertical velocity ($\times 10^{-3}$ hPa • s^{-1})and daily precipitation(mm)over the TP vortices simulated by the schemes.

Exp.	500hPa Relative Vorticity				300–500hPa Averaged Vertical Velocity				Daily Precipitation			
	Case 1		Case 2	Case 3	Case 1		Case 2	Case 3	Case 1		Case 2	Case 3
	24h	48h	24h	24h	24h	48h	24h	24h	0–24h	24–48h	0–24h	0–24h
1	1.7	5.9	3.8	8.8	−4.6	−9.4	−6.1	−3.0	17.8	41.5	2.4	40.4
2	0.8	5.6	4.4	9.5	−4.7	−7.9	−6.0	−3.7	12.9	47.3	2.0	30.2
3	2.6	5.0	2.9	9.0	−7.3	−8.6	−6.3	−3.8	12.8	41.7	2.2	35.7
4	2.7	7.2	3.5	8.7	−8.2	−11.6	−7.5	−4.2	12.9	26.0	1.7	39.8
5	0.8	4.8	0.7	7.5	−3.9	−4.3	−5.1	−2.0	2.4	37.4	1.6	52.5
6	0.1	2.6	5.6	8.4	−2.1	−6.3	−2.6	−3.9	16.0	52.2	2.3	23.6
6*		5.6				−7.7				41.4		
7	0.9	1.9	2.1	5.7	−2.2	−1.9	−4.7	−2.5	6.4	12.6	2.0	21.8
7*		3.8				−3.6				33.7		
8	1.2	4.4	2.7	1.2	−4.1	−4.4	−4.7	0.9	16.4	24.8	2.1	18.3
9	0.8	2.8	1.6	2.2	−2.8	−3.5	−4.3	0.7	6.7	14.7	1.1	10.3
10	−1.1	−0.8	2.9	2.2	0.4	−0.2	−3.7	−0.5	2.0	0.0	0.0	0.0
Truth	1.7	2.9	2.8	3.1					10.6	15.4	16.2	34.4

the importance of the surface sensible heating and evaporation at the stage of the vortex maintenance or development, complementary experiment Exp. 6 and 7 (i.e. Exp. 6* and 7*) are made for case 1, by using their 24h results of Exp.1 as initial field and repeating Exp.6 and 7 with 24h integration. Fig. 2e, f indicate that the vortex is relutantly maintained in Exp. 6*, but not in Exp. 7*.

3.6 Effect of latent heating

In Exp. 8, the vortex of case 3 is not presented (Fig. 4e) and that of case 2 and 3 weakens as the largescale and / or the convective latant heating is not considered. The vortex in case 1 is filled during 24–48h of integration after convective heating is further removed in Exp. 9 (Fig. 2g, h).

3.7 Effect of the TP elevation

In Exp. 10, the TP elevation is decreased with the maximum only equal to the half of the original one. The vortices in all the three cases are not produced either at 500 hPa or 700 hPa. Besides, the feature of the flow patterns over the TP also differs from those in Exp. 1 (Fig1i, 2i; Fig. 3f; Fig. 4f).

4. Conclusion

From the above analyses, main conclusions could be obtained as follow,

the TP terrain elevation plays an essential role in both the genesis and development stages of the vortices, and the effects of the surface sensible heating on its genesis and the surface latent heating on its development are also very much important; the next will be the influences of the latent heating in the air column and temperature lapse rate. It is seemly that the baroclinicity in the air column and the friction has only a few contributions.

References

Chen, B. M. and Z. A., Qian, Numerical predicting tests o the rainfall and vortices over the Qinghai–Xizang (Tibetan) Plateau in summer,to be published in *Chinese J. Atmos. Sci.*.

Qian, Z. A. et al., 1984, A statistics of the vortices over the Qinghai–Xizang Plateau and investigation of climatic factors of the vortices genesis, *Paper collection of the Tibetan Plateau Meteorological Science Experiment* (II) (in Chinese), Scientific Press, Beijing, China, 182–194.

Sun, G. W. and B. D., Chen, 1988, Dynamic processes of the moving and developing lows on the Qinghai–Xizang Plateau during the early Summer, *Jounral of academy of Meteorological Science* (in Chinese), **3**, 56–63.

Yan, H., 1987, The design of a nested fine–mesh model over the complex topography, Part one and two, *Plateau Meteorology* (in Chinese), **6**, No.2 (suppl.), 1–139.

The numerical experiment of influence of surface heat source over Tibetan Plateau on runoff in summer

Sun Guowu Liu Xiaodong Zhou Yajun

(LanZhou Arid Meteorological Institute, Lanzhou 730020, P. R. China)

Abstract

Based on statistical facts, the heat source variation of the Tibetan Plateau is related with the the flow of upper reaches of Yellow River. A numrical experiment of influence of the heat source variation over the Tibetan Plateau on the flow of upper reaches of Yellow River in the summer is perfomed with a model of GCM. The results show that while the heat source of the Plateau is weaken, the runoff is decreased and flow is decreased. As a result, the heat source variation of the Tibetan Plateau is one of important causes which led to flow variation of the upper reaches of Yellow River.

Keyword: Heat source of the Plateau; runoff; Flow; Numerical experiment.

1. Introduction

Land surface hydrology processes are very important in climate system. The numerical experiments with GCM indicated that atmosphere is sensitive to many elements in land surface processes. At the condition of the fixed solar radiation, the climate in the future maily depends on slow varying state of land surface. Other papers indicated terrain and surface heat condition of Tibetan Plateau had obvious effect on atmospheric circulation and dry and rainy days of Tibetan Plateau and Eastern Asia. This paper first analysed the statistical facts between Tibetan Plateau heat source and the flow of Yellow River upper reaches, and then do a numerical experiment of influence of the heat source variation over Tibetan Plateau on runoff using GCM. At last, this paper indicated that the method may be a good one for forecasting flow of Yellow River upper reach.

2. The statistical analysis of surface heat source over Tibetan Plateau and flow varying of Yellow River upper reaches

June to July in 1986, China and America did a Tibetan Plateau Planetary Experiment (be referred as TIPMEX-86). fig. 1 is the surface net radiation in Lasha (29° 40′ N, 90° 08′ E) during experiment and the flow of Yellow River upper reaches. Varying tendency of the net radiation and flow are consistent in fig. 1. Although TIPMEX-86 only had these data, it provided us the clue between Tibetan Plateau net radiation and flow.

In fact, the consistency between heat source intensity of Tibetan Plateau and varying tendency of flow of Yellow River upper reaches have verified to pass 30 years test, and its correlation coefficient is 0.73 (22/30). This is consistent with TIPMEX-86 daily data.

TABLE 1. The heat source anomaly of Tibetan Plateu and the flow anomaly of Yellow river upper reachin summer from 1958-1987

Year	1958	1959	1960	1961	1962	1963	1964	1965	1966	1967
flow	+	-	-	+	-	+	+	-	+	+
heat	+	-	-	+	-	-	+	+	+	-
Year	1968	1969	1970	1971	1972	1973	1974	1975	1976	1977
flow	+	-	-	-	-	-	-	+	+	-
heat	-	-	-	-	-	-	-	-	+	+
Year	1978	1979	1980	1981	1982	1983	1984	1985	1986	1987
flow	-	+	-	+	+	+	+	+	+	-
heat	-	+	-	-	+	+	+	+	+	+

The details above specify the consistency between surface heat source of Tibetan Plateau and flow of Yellow River upper reaches. Its physical cause may be when Plateau surface heat source intensifies, Plateau vortices and convective actions intensify, the precipitation around Yellow River source will increase through surface runoff. It is a statistical fact that there exists positive correlation between precipitation over Plateau and flow of Yellow river upper reach.

3. Numerical experiment of influence of the heat source over Tibetan Plateau on runoff

We designed two experiments with OSU GCM: ①. Control experiment (be referred as CNT), There are 9 kinds surface type which have different albedo. The albedo with snow will increase. If α_{sb} is albedo without snow, α_{sc} is the maximum albedo with snow, then albedo α that snow covers is s is determined by following equation:

$$\alpha_s = \begin{cases} \alpha_{sb} + \sqrt{s}\,(\alpha_{sc} - \alpha_{sb}) & s < s_c = 1 g cm^{-2} \\ \alpha_{sc} & s \geqslant s_c \end{cases}$$

The albedo over Tibetan Plateau in summer is general 0.2-0.25, it's similar with average albedo of 6 stations during Tibetan Plateau Meteorological Experiment in 1979. ②. Albedo increase experiment (be referred as ABD). The only difference between ABD and CNT is increasing surface albedo α_s which heights are beyond 3 km over Tibetan Plateay.

α_s is defined as:

$$\alpha_s = \begin{cases} 0.15 + 0.1Z & Z_s > 3km \\ \text{be same as CNT} & Z_s \leqslant 3km \end{cases}$$

TABLE 2 Albedo of different surface type

surface type	surface future	α	α
1	grass field, shrub, plant	0.12	0.50
2	forest	0.10	0.41
3	drygrassland	0.13	0.58
4	wilderness	0.20	0.53
5	desert	0.25	0.55
6	tundra	0.19	0.70
7	water	0.07	0.07
8	land ice	0.45	0.80
9	sea ice	0.45	0.80

The albedo over Tibeteau Plateau beyond 3 km was increase averagely 0.22. The inital field was 20 June. The whole integration time was 40 days.

In CNT, sea level pressure in July was simulated (fig. 3a) . The continental low and Oceanic high in northern hemisphere and other systems were better simulated. The surface temperature (fig. 3b), besides the temperature is lower in permanent ice area, the simulated value in most areas were better.

If albedo over Tibetan Plateau were increasing, large rain areas over Plateau disappearred, shown as Table 3, then runoff over Plateau will decreasing.

TABLE 3 The differences between ABD and CNT precipitation(unit:mm/d)

Tibetan Plateau	Loess Plateau	Yungui Plateau	Mongolia Plateau
-2.48	-1.47	0.46	1.87
Huabei Plain	Huai River Valleys	Changjiang River Valleys	
-0.35	-0.15	-0.32	
Southeast Inshore	Heilongjiang River Valleys	Liaohe River Valleys	
0.42	-1.98	2.82	

The runoff differences between ABD and CNT are shown as fig. 4. The maximum negative center was over Tibetan Plateau. When runoff into Yellow River upper reach was decreasing, the flow of Yellow River reach was correcponding decreasing. Heat source variation over Tibetan Plateau was indeed one important reason of causing variation of runoff of Plateau areas and flow of Yellow River upper reach.

4. Discussion and conclusion

The statistical analysis and numerical experiment indicated that surface heat source variation over Plateau affected precipitation and runoff in this area through atmosphere, then affected flow of Yellow River upper reach. Precipitation also affected heat field. Its correlation are shown as follow:

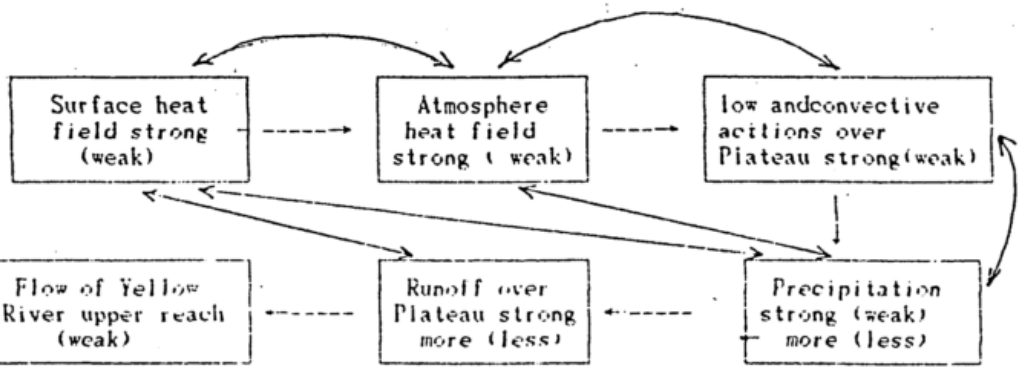

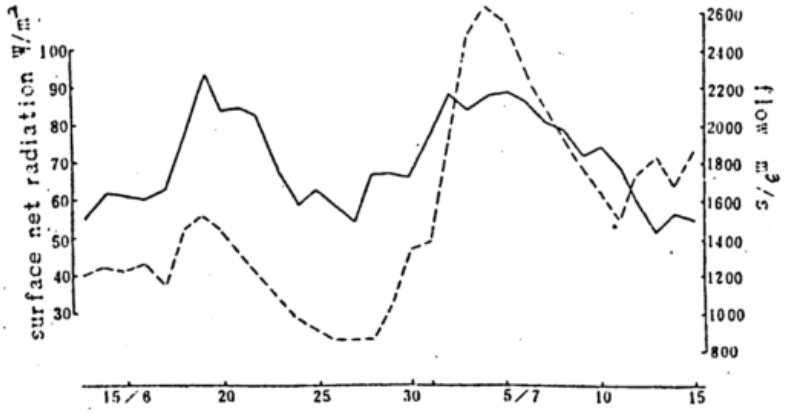

fig.1 5-day runing average of Lasha net radiation (real) and the flow of upper reaches of Yellow River (dash) from 13, June to 15, July in 1986

It would be specified that numrecal experiment indicated that precipitation and runoff over Tibetan Plateau were affected by surface heat source, but due to the limitation of GCM, there were climate drifts in pressure, temperature and the precipitation field. In land surface, especially in sophisticated terrain, simulated results may be worse. We use better GCM to simulate in the future.

Reference (omitted)

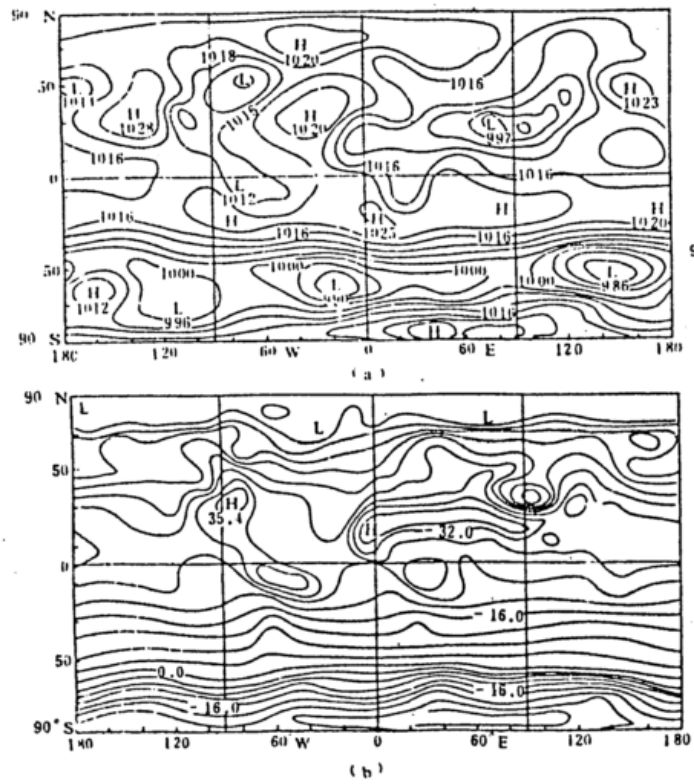

fig.3 Sea level pressur (a) and surface temperature (b) in July by simulated with CNT

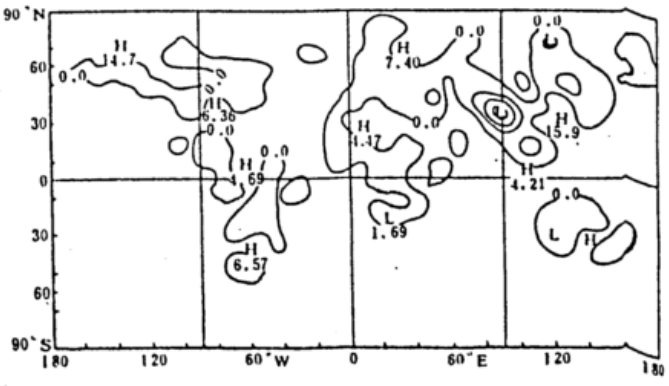

fig.4 The defference of runoff betwwn ABD and CNT

Results from the PYREX experiment

by P. Bougeault, METEO-FRANCE, CNRM

The talk will discuss the main experimental and modelling results obtained at the time of the conference. The emphasis will be put, as can be foreseen one year in advance, on :

i) the comparison of numerical modelling results with observations from the PYREX data base

ii) the morphology of the flow around the Pyrénées, including a discussion of the flow regime in terms of non dimensional parameters

iii) the momemtum budget

iv) the potential vorticity budget of these flows.

The teachings of PYREX in terms of reasonable objectives for the forthcoming MAP project could be discussed either during this talk or in another occasion, depending of the suggestions of the organizing committee.

APPLICATION OF THE LINEAR THEORY TO LOCAL WINDS AROUND THE PYRENEES CHAIN DURING THE PYREX EXPERIMENT.

E. Koffi, B.Benech, A.Druilhet (Laboratoire d'Aérologie,LA CNRS, Université Paul Sabatier , Toulouse, France) **and J. Stein** (Météo France, CNRM, Toulouse, France)

Abstract:

The interaction between the synoptic flow and the Pyrenees chain induces a pressure perturbation and generates at low level local winds around the chain. Following Smith (1982) and Phillips (1984), linear solutions of pressure and wind perturbations induced by an elliptical mountain of variable extension have been numerically determined and applied to the case of synoptic flows perpendicular to the Pyrenees mean axis. The Coriolis effect is introduced into the linear equations system and acts on the intensity of the pressure dipole and on wind deviations at the low levels. In general, the comparison between experimental data obtained during the PYREX experiment and the linear model simulations are in good agreement concerning the local winds intensity aa well as the dissymmetry of the flow on lateral edges of the mountain chain.

1 - Introduction :

The aim of this study is to explain the basic mechanism of local winds generated around the Pyrenees chain by applying the linear theory to normal synoptic flows. This theory already applied by Smith (1982) to the local winds around a mountain is extended to the Coriolis effects. We present at first , the model description , next the confrontation of the model simulations to the experimental data obtained during PYREX experiment which was realized from October to November 1990 around the Pyrenees chain. The domain and experimental means of PYREX experiment are described in Bougeault et al. (1993).

2 - The model description.

We consider a hydrostatic , incompressible fluid, Boussinesq model, stably stratified with uniform wind profile over a simple bell shape mountain with a elliptical horizontal cross sections (figure 1). Perturbations of pressure fields, wind and density are described by the following linear equations:

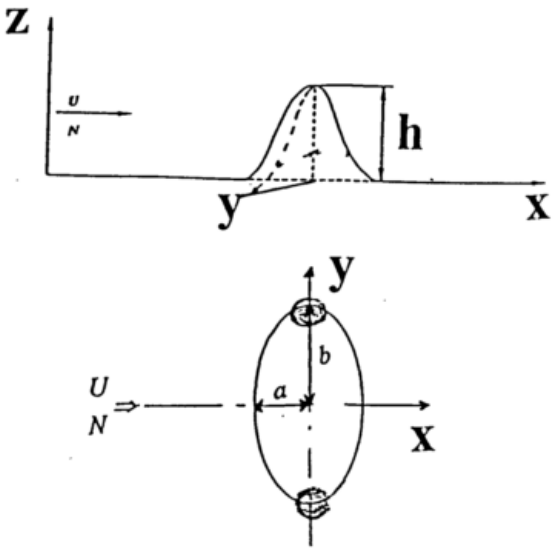

Figure 1: Conceptual diagram of the model with a homogeneous flow over a bell elliptic mountain . U and N are respectively the wind normal component and the Brunt Vaisala frequency The geometric scales are given by a,b and h.

$$\rho_0 U \frac{\partial u'}{\partial x} = -\frac{\partial p'}{\partial x} + \rho_0 f v' \qquad (1)$$

$$\rho_0 U \frac{\partial v'}{\partial x} = -\frac{\partial p'}{\partial y} - \rho_0 f u' \qquad (2)$$

$$\rho_0 U \delta \frac{\partial w'}{\partial x} = -\frac{\partial p'}{\partial z} - \rho' g \qquad (3)$$

$$U \frac{\partial \rho'}{\partial x} + w' \frac{\partial \rho_0}{\partial z} = 0 \qquad (4)$$

$$\frac{\partial u'}{\partial x} + \frac{\partial v'}{\partial y} + \frac{\partial w'}{\partial z} = 0 \qquad (5)$$

$\delta = 1$ non hydrostatic case

$\delta = 0$ hydrostatic case

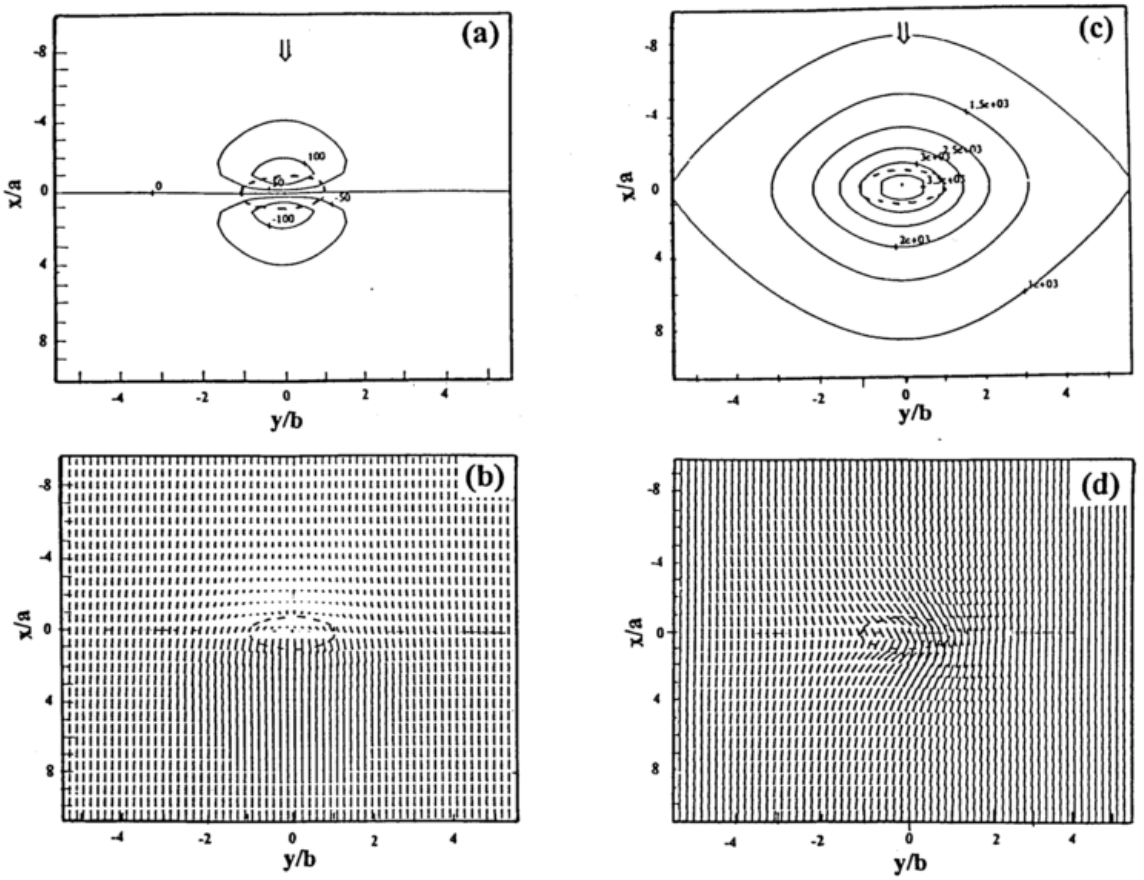

Figure 2: Perturbation of the surface pressure (a, c) and surface wind fields (b, d) in the vicinity of a mountain similar to Pyrenees shape parameterized by $\gamma = 1/5$ et $\mu = 1$; *(a) and (b): simulation for* $R_0 = \infty$ and $F_r = 0.66$; *(c)and (d): simulation for* $R_0 = 0.2$ and $F_r = 0.66$. *Isobars in Pa. The relief is marked by a dashed ellipse.*

With x, y, z longitudinal , transverse and vertical axes; u', v' , w', ρ', p' are respectively the longitudinal, transverse and vertical wind fluctuations, the density and pressure fluctuations. ρ_0 , U, N are respectively the density, the normal component of the incident flow, the Brunt Vaisala frequency defined in the upstream; g is the acceleration of the gravity and f the Coriolis parameter.

The surface pressure and wind perturbations , p' , u' and v' describe the local winds generated on the lateral sides of the obstacle. The non dimensional analysis shows that:

$p'/\rho_0 U^2 = f_1(F_r, R_0, \gamma, \mu)$, $u'/U = f_2(F_r, R_0, \gamma, \mu)$ and $v'/U = f_3(F_r, R_0, \gamma, \mu)$

with $F_r = U / Nh$, Froude number quantifying the non linear effects.

$R_0 = U / fa$, Rossby number which quantifying the earth rotation influence on the flow .

$\gamma = a / b$, the aspect ratio of the mountain.

μ, a parameter caracterizing the mountain shape.

We note h, the maximum height of the mountain , a its half length and b its half width (figure 1) The solutions of the linear equations are computed by FFT algorithm of spectral solutions (Koffi, 1994). We present in figure 2 simulations of surface pressure and wind perturbations with weak($F_r = 0.66$, $R_0 = \infty$), and strong ($F_r = 0.66$, $R_0 = 0.2$) Coriolis effects in the vicinity of a mountain similar to the Pyrenees given by $\gamma = 1/5$, $\mu = 1$. For the case $R_0 = \infty$, the surface pressure p' shows a pressure dipole between upstream and downstream sides of the mountain with an amplitude egal to 2hPa (figure 2a). The wind field (figure 2b) shows a blocking upstream of mountain and symmetrical deviation at the lateral edges . For $R_0 < 1$ (figure 2c), the Coriolis effects become large, the pressure dipole disappears and a positive perturbation of 35hPa is centered on the relief. The wind field becomes dissymetric with an increase of the flow on the left side of the obstacle and a decrease on the right side (figure 2d).

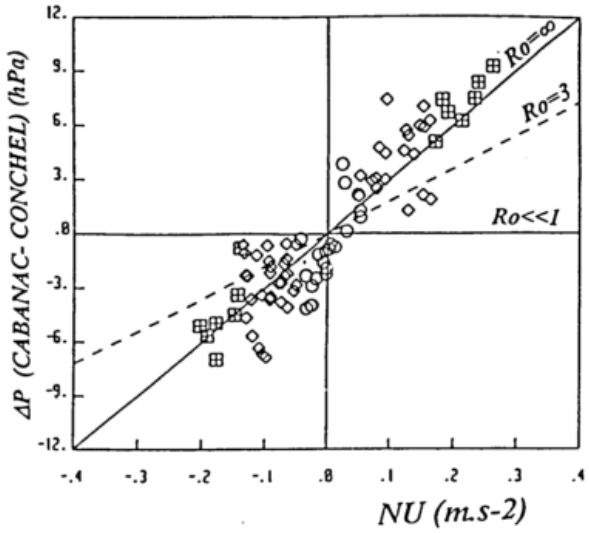

Figure 3: Pressure difference between French(Cabanac) and Spanish(Conchel) stations as a function of NU for the all the PYREX experiments. F0r Southerly flow (NU < 0), values of NU are obtained at 3000 m from the radiosondings at Saragossa, andfor northerly flow (NU > 0), they are obtained from the radiosoundings at Toulouse.

3- Application to the PYREX experiment.

The Pyrenees chain is a barrier to atmospheric flow of 3000 m maximum heigth (h), oriented nearly east - west with 400km of length ($2b$) and 60 to 100km of width ($2a$). The results concern the northern and southern synoptic flows normal to the mountain for the pressure dipole; for winds, we present only results on north synoptic flows.

Froude and Rossby numbers, and upwind air mass acceleration NU, are deduced in the case of north wind from the radiosondings made at the station of Toulouse located 120km upstream of the Pyrenees, and in the case from south wind from those made at the station of Saragossa located 150km upstream. We find for all the cases of PYREX, $F_r < 0.5$, $R_0 < 5$ (with a maximum occurence for $R_0 = 3$) and $NU < 0.4$. The pressure dipole is measured along an axis centered and normal to the Pyrenees mean axis (Bessemoulin et al.,1993). According to the linear theory, the intensity of the pressure dipole is a linear function of NU . On the figure 3, the intensity of the dipole pressure deduced from experimental data corroborates this theorical result. Nevertheless, the intensity of the dipole pressure for the case $R_0 = 3$ underestimates the reality; However, the upwind overpressure increases significantly.

On figure 4, the wind intensity (FF) deduced from the experimental data normalized by the incident flow (U) is related to the Froude number. The wind data include radiosoundings (Port la Nouvelle :east side, Pamplona; west side), constant volume balloons and aircraft measurements made on the Pyrenees edges. Asymptotic curves obtained for $R_0 = \infty$ and $R_0 \to 0$ for two types of mountains parameterized by $\gamma = 1/5$ et $\mu = 1$ and $\gamma = 1/4$ et $\mu = 2$ are also presented. On the east side of the Pyrenees (figure 4a), the ratio FF / U increases when the Froude number decreases, which is in agreement with the linear theory. On the west edge (figure 4b), the ratio FF/U shows that the slowing of the flow is well anticipated by the linear theory. The mountain defined by $\gamma = 1/4$ and $\mu = 2$ gives results relatively well fitting to experimental data. Figure 5 presents the difference of wind between east and west sides (ΔFF) normalized by the incident flow (U) as a function of the Rossby number. This difference increases when the Rossby number decreases. The flow becomes dissymmetric on the lateral sides of the relief. The difference decreases when the Rossby number increases, the flow tends to become symmetrical in accordance with the linear theory.

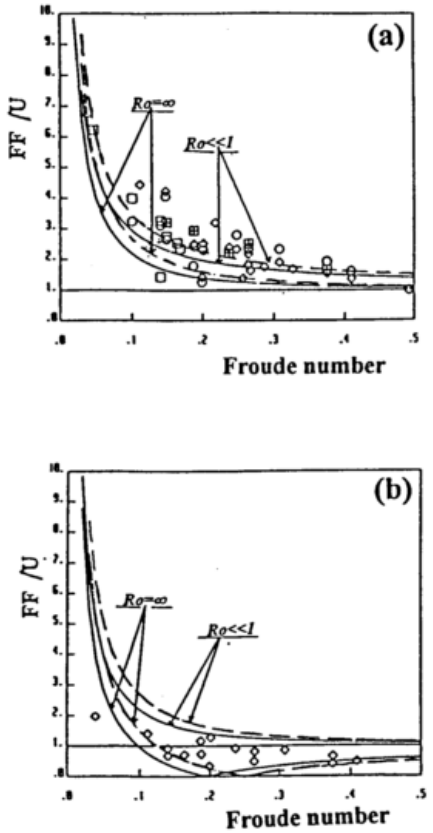

Figure 4: Intensity of the wind at 500 m height on the lateral Pyrenees edge by flow from the north normalized by the normal wind to Pyrenees at the level 3000 m as a function of the Froude number evaluated at Toulouse. Asymptotic solutions of the linear model are also given ($R_0 = \infty$, $R_0 << 1$) for the mountains : ($\gamma = 1/5$ et $\mu = 1$:—) and ($\gamma = 1/4$ et $\mu = 2$:- - -). a) on the left edge (east side of Pyrenees) b) on the right edge (west side of Pyrenees).

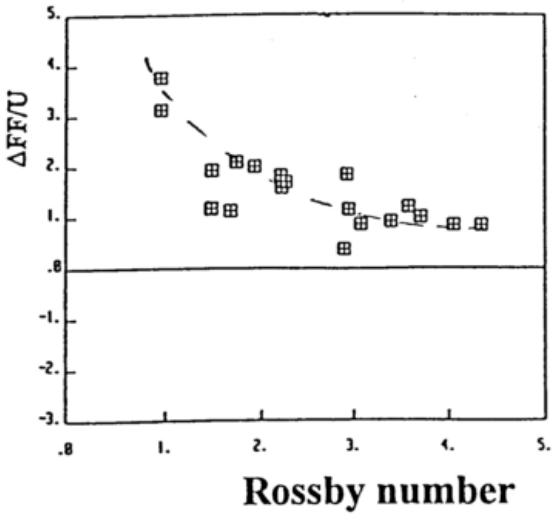

Figure 5: Flow dissymmetry as a function of the Rossby number, between the east edge (Port la Nouvelle) and the west edge(Pamplona) deduced of the difference of wind at the level 500 m normalized by the incident flow at 3000 m at Toulouse

Conclusion:

By comparing theorical results for simplified atmospheres flowing over schematic mountain with real data from PYREX experiment , we show that the linear theory including Coriolis effects can explain a large part of the local winds generated around the Pyrenees for northerly synoptic flows. The local winds are linked to the upstream surface pressure perturbation induced by the mountain. The dissymmetry of the flow on the lateral sides of the relief varies as an inverse function of the Rossby number. The intensity of local winds increases when the Froude number decreases.

References:

Bessemoulin, P., P.Bougeault, A.Genoves,A.Jansa Clar and Puech, 1993: Mountain pressure drag during PYREX. Beitr.Phys. Atmos.,305-325.

Bougeault et al.,1993: The atmospheric momentum budget over a major atmospheric mountain range: first results of PYREX program. Annales Geophys., 11:395-418

Koffi, E., 1994: Caractéristation expérimentale de l'écoulement atmosphérique autour d'un massif montagneux (expérience PYREX), thèse de l'Université Paul Sabatier , Toulouse.

Phillips, D.S., 1984: Analytical surface pressure and drag for linear, hydrostatic flow over tree-dimensional elliptical mountains. J.Atmos.Sci., 41,1073-1084

Smith,R.B., 1982: Synoptic observations and theory of orographically disturbed wind and pressure. J. Atmos.Sci., 45, 3889-3896

A NUMERICAL STUDY OF FLOW DIVERSION AROUND THE PYRENEES

M. Georgelin, and E. Richard

Laboratoire d'Aérologie, Université Paul Sabatier
Toulouse, France

1. INTRODUCTION

Frequently for real flows, the lower part of the atmosphere cannot rise enough to cross a mountain, it has to go around the mountain, generating local characteristic winds. The transition between crossing and non crossing flow is characterized by the existence of a stagnation point where the wind speed is zero. Below this stagnation point, the oncoming flow is divided in two different parts each going around one side of the obstacle . If the mountain is elongated in the direction perpendicular to the flow, these diverted winds become low-level jets parallel to the ridge-line. Hunt and Snyder (1980) have performed laboratory studies of this mechanism, Smolarkiewicz and Rotunno (1990) have carried out numerical experiments analyzing the upwind characteristics of a low Froude number flow past an elongated obstacle.

2. THE TRAMONTANA

The Tramontana is a low level jet occurring when a northerly synoptic flow impinges on the Pyrenees mountain range, 400km long and 70 km wide, lying between France and Spain. This wind blows first parallel to the ridge, then strengths within the conscricted valley between the southern edge of the Massif Central and the Pyrenees and finally turns towards the south when it reaches the Mediterranean Sea. It achieves its maximum wind speeds off shore at the exit of the gulf of Lions. A sheltered zone is created behind the mountain, separated from the Tramontana by a strong shear line.

The PYREX experiment (Bougeault et al., 1990; 1993), which took place over the Pyrenees during October-November 1990, provides a good data set to study Tramontana events. The case of the Intensive Observing Period 6 (November 4, 1990) has been chosen for our study.

3. NUMERICAL RESULTS

Corresponding author address: Laboratoire d'Aérologie, Université Paul Sabatier, 118 route de Narbonne, 31062 Toulouse, France.

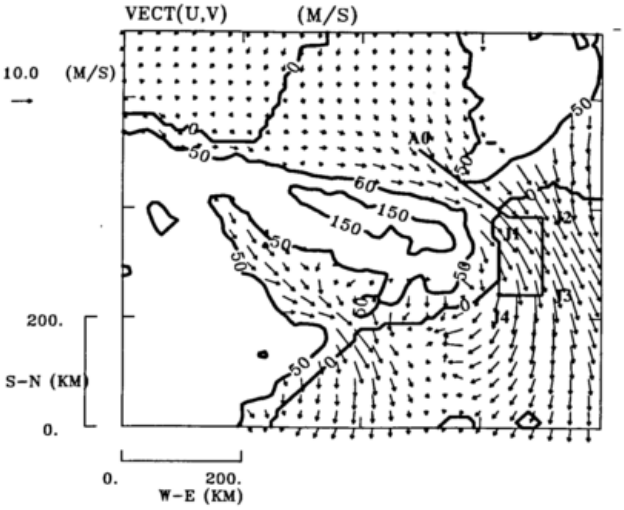

Figure 1. Horizontal wind field for November 4, 11 UTC.

The IOP 6 situation was simulated with an hydrostatic mesoscale model (Nickerson et al., 1986). The simulation has been carried out from 9 UTC to 14 UTC. Short term forecasts of the French operational model have been used to initialize the mesoscale model and to update its lateral boundary conditions. Figure 1 presents the 950 hPa wind field computed for 11 UTC over the PYREX area. This wind field reproduces all the above-mentioned climatological features of the Tramontana. The thick black line (A0-J1-J2-J3-J4) in fig.1 shows the flight legs followed at different altitudes by 2 instrumented aircrafts.

Figure 2 focuses on surface streamlines upwind of the mountain. One notices the presence of a singular point (saddle point), at the bottom of a downslope reversal current, where the flow splits in two different directions. This feature is consistent with the experimental and numerical work of Hunt and Snyder (1980) and Smolarkiewicz and Rotunno (1990).

A sodar located in Lannemezan (noted L in fig.1) measured the horizontal wind between ground and 360 m. Figure 3 shows the time evolution of the horizontal wind profile measured by this instrument between 10 UTC and 13 UTC. The weak intensity of the wind ($\leq$ 2.8 m/s) indicates

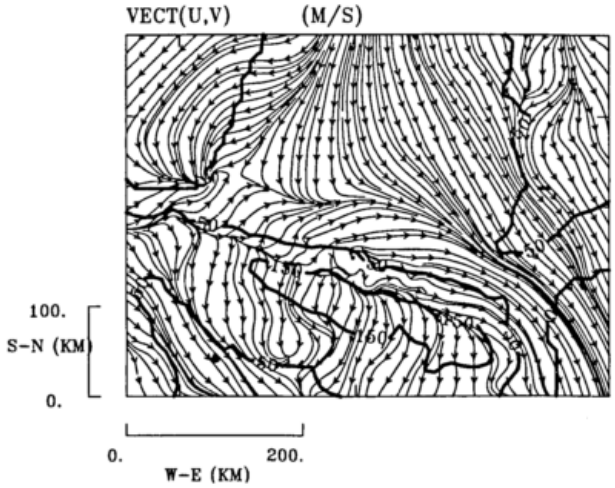

Figure 2. Surface streamlines for November 4, 11 UTC.

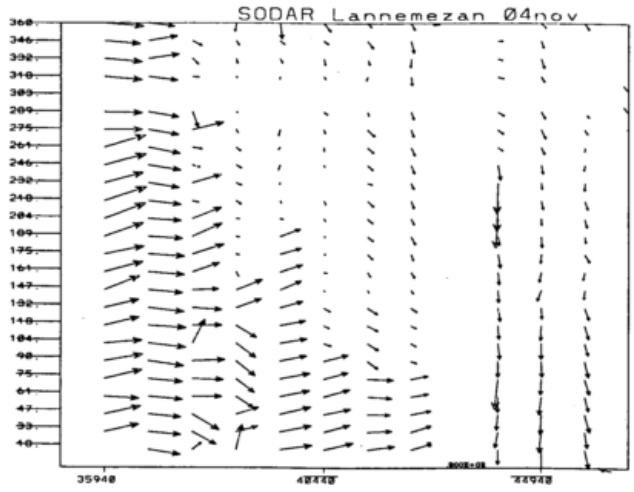

Figure 3. Time evolution of the horizontal wind vertical profile measured by a sodar located in Lannemezan

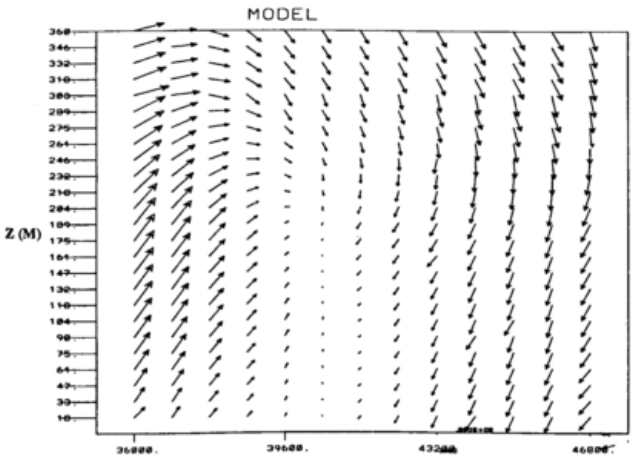

Figure 4. Time evolution of the horizontal wind vertical profile computed by the model above Lannemezan

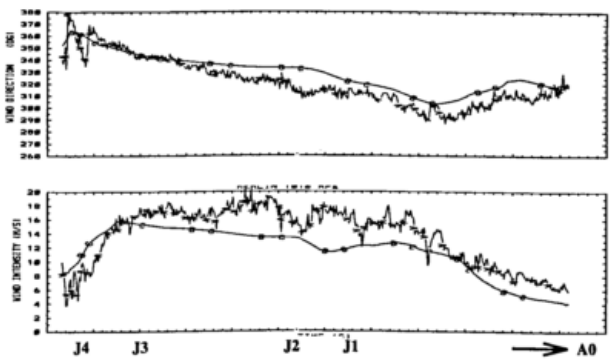

Figure 5. Comparison between observed and computed wind intensity and direction along the 950 hPa flight leg (J4-J3-J2-J1-A0) followed by the Fokker aircraft.

that this sodar was in the blocking (stagnation) zone. The left side of the figure (10-11 UTC) shows winds going away from the mountain (which run parallel to a line oriented 100° east of north): this is an illustration of the reversal flow seen by the sodar. The right side of this figure shows that the wind is no longer diverted but crosses over the altitude of the sodar. A rapid transition between the two types of flow occurs around 12 UTC. Figure 4 is deduced from the model computation and represents the same horizontal wind evolution above the sodar location. As shown in Fig.4 the model qualitatively reproduces the observed evolution of the low-level winds and is able to capture the sudden change in direction around 12 UTC.

An automatic network of 14 microbarographs set on a central transect of the range recorded the time evolution of the surface pressure drag during the entire experiment (Bessemoulin et al., 1994). Koffi and al. (1993) have found that for all the experimental cases, the intensity of the Tramontana is well correlated with the drag. For the IOP6, the drag between 10 UTC and 15 UTC slightly increases from 2.3 Pa to 2.7 Pa while model estimation of the drag shows an increase from 2.1 Pa to 2.7 Pa for the same period. This confirms the good representation of the blocking by the model.

Where the Tramontana is well established, close to and over the Mediterranean Sea, the model

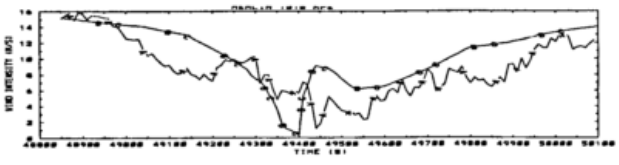

Figure 6. Comparison between observed and computed wind intensity along the flight track section crossing the shear line.

prediction can be checked against the aircraft measurements. Figure 5 presents an example of comparison between observed and computed winds along a J4 to J1 flight leg performed at 500 m above sea level. The agreement between measured and simulated winds is very good in direction, and fairly good in intensity in spite of a slight underestimation near the point J2.

Figure 6 shows a similar comparison but is focused on a zone located between J4 and the coast, where the aircraft crossed the shear line which separates the Tramontana from the sheltered area. The position of this transition, important for navigation, is accurately predicted by the model.

4. WHY THE REVERSAL FLOW DISAPPEAR WITH TIME?

During IOP 6, upwind conditions remain roughly the same over the simulation period. The evolution of the reversed flow is therefore unlikely to be due to a change in the upwind Froude number. The disappearance of the reversed flow might be caused by a thermal effect. By continuity the reversed flow, generates a vertical circulation analogous to a nocturnal downslope breeze. Above the top of the reversal current, air from higher altitude is entrained into the circulation, this air experiences an adiabatic compression resulting in the heating of the air above the slope. This heating tends to create another circulation in opposition to the previous one, and as a consequence the reversed flow disappears. Diurnal heating (and nocturnal cooling) could surely amplify this phenomenon (Reisner and Smolarkiewicz, 1994), they cannot however account for the elimination of the reversed flow since surface temperature was almost constant during the course of the simulation.

5. CONCLUSION

A 3 D numerical simulation was compared with observations of the Tramontana, obtained during IOP 6 of the PYREX experiment. The model was effective in simulating the spatial structure and time evolution of the low level flow blocked by the Pyrennes. In particular the model captured the transition from laterally diverted low-level flow to cross-mountain low-level flow observed at Lannemezan. Good agreement was also obtained between the observed and numerically simulated low-level winds along the aircraft flight tracks over the Mediterranean Sea.

6. REFERENCES

Bessemoulin, P., P. Bougeault, A. Genoves, A. Jansa Clar and D. Puech, 1993: Mountain pressure drag during PYREX. *Beitr. Phys. Atmos.*, **66**, 305-325.

Bougeault, P., A. Jansa Clar, B. Benech, B. Carissimo, J. Pelon and E. Richard, 1990: Momentum budget over the Pyrenees: the PYREX experiment. *Bull. Amer. Meteor. Soc.*, **71**, 806-818.

Bougeault, P., A. Jansa, J.L. Attié, I. Beau, B. Benech, R. Benoit, P. Bessemoulin, J.L. Caccia, J. Campins, B. Carissimo, J.L. Champeaux, M. Crochet, A. Druilhet, P. Durand, A. Elkhalfi, P. Flamant, A. Genoves, M. Georgelin, K.P. Hoinka, V. Klaus, E. Koffi, V. Kotroni, C. Mazaudier, J. Pelon, M. Petitdidier, Y. Pointin, D. Puech, E. Richard, T. Satomura, J. Stein, and D. Tannhauser, 1993 : The atmospheric momentum budget over a major atmospheric mountain range: first results of the PYREX program. *Annales Geophysicae*, **11**, 395-418 .

Hunt, J.C.R., and W.H. Snyder, 1980: Experiments on stably stratified flow over a model three-dimensional hill. *J. Fluid. Mech.*,**96**, 671-704.

Koffi, E., B. Benech, P. Durand, A. Druilhert, P. Bessemoulin, A. Jansá et C. Campins, 1993: Etude expérimentale ders vents locaus autour des Pyrénées. *Atelier de modélisation de l'atmosphère, CNRM, Toulouse*, Proc. 111-122.

Nickerson, E.C., E. Richard, R. Rosset, and D.R. Smith, 1986: The numerical simulation of clouds, rain, and airflow over the Vosges and Black Forest mountains : a meso-β model with parameterized microphysics. *Mon. Wea. Rev.*, **114**, 398-414.

Reisner, J.M., and P.K. Smolarkiewicz, 1994: Thermally forced low Froude number flow past three-dimensional obstacles. *J. Atmos. Sci.*,**51**, 117,133.

Smolarkiewicz, P. K. and R. Rotunno, 1990: Low Froude Number Flow Past Three- Dimensional Obstacles. Part II: Upwind Flow Reversal Zone. *J. Atmos. Sci.*, **47**, 1498-1511.

PYRENEAN PRESSURE DRAG: SOME FACTORS AND CONSECUENCES AFTER PYREX

A. Genovés[1], J. Campins[1], A. Jansá[1],
P. Bessemoulin[2], E. Koffi[3] and B. Benech[3]

[1] Instituto Nacional de Meteorología
Centro Meteorológico Territorial de Baleares

[2] Météo France
Centre National de Recherches Météorologiques

[3] Université Paul Sabatier
Centre de Recherches Atmosphérics

ABSTRACT

The French-Spanish Pyrenean Experiment PYREX has provided a high quality two-month serie of mountain pressure drag measurements. The existence of big pics on the drag values, up to 8 Pa, together with quite frequent values above 5 Pa, is a result worthy to be commented. This contribution will stress, a) The different behaviour of the flow-mountain interaction, in terms of drag value, for northern and southern flow, b) The importance of the hydrostatic contribution to the drag, mainly in northern situations, c) The outstanding meso-alpha scale manifestation of the orographic interaction as an intense dipolar pressure anomaly, d) The relevant significance of the dipolar pressure anomaly in the generation of local winds, mainly the Tramontane.

1. Pyrenean pressure drag. Results from observations

A high quality serie of pressure measurements, along the 150 Km main Pyrenean transect, between 200 and 2400 m of altitude, has been obtained from the 14 AWS network installed for PYREX Experiment, developped during October-November of 1990. From that high resolution network, it has been possible the estimation of mountain drag values, with a temporal resolution of 10 minutes (Bessemoulin et al., 1993). From Davies and Phillips (1985), the pressure drag component along the transect, per unit length (in $N.m^{-1}$) becomes:

$$D/l=\int_{z_b}^{z_t}\Delta p dz \qquad (1)$$

and the drag per unit area (in Pa) is:

$$D/\Delta=D/(Ll) \qquad (2)$$

where z_b is the altitude of the lowest station, z_t is the altitude of the highest station, $\Delta p(z)$ is the pressure difference across the mountain at height z and L is the width of the instrumented section. That was considered the most suitable method to estimate the drag in PYREX case, by one hand, because the 2D character of the Pyrenean range, by the other, because only observed pressure (not reduced at

sea level) and their differences are concerned, so it would be took the advantage of the good relative accuracy of the sensors (Bessemoulin et al., 1993).

By convention, grad p being positive when the pressure is higher on the northern side of the range, the pressure drag during the two-month observation period was ranging between 8 and -7 Pa. In northern flow situations, the drag was frequently ranging between 4/6 Pa, being of -2/-4 Pa in southern ones. The mean value was close to 2.2 Pa, indicating that the Pyrenees could be a major sink for momentum.

2. Factors influencing the drag. Differences between northern and southern situations

In order to determine the governing parameters of the incident flow, i. e., the Froude and Rossby numbers, F and R_0, respectively, the available upstream soundings were considered, namely, Zaragoza for southern situations and Toulouse for the northern ones. Only the cases where the upstream wind was nearly perpendicular to the range and where the mean stabilities for layers 950-850 and 850-700 hPa were aproximately the same, were selected. The computations showed, according to conditions of blocked flow from Pierrehumbert and Wyman (1985), that the IOP's were characterized most of the time by the upstream blocking and significant non geostrophic flow response (Bessemoulin et al., 1993). The linear value of drag understimate the high values of the observed one in an important percentage. It can be considered a predictor of the order of magnitude of observed drag along the principal mountain axis, as a first aproximation.

Correlations Drag/UN were calculated in the layers 850-700 hPa, again from Toulouse and Zaragoza soundings, in order to determine the parameterization of drag in terms of UN (lineality). Correlations of 71% for northern cases and a 12% for southern ones were encountered. This result shows an important difference from linear behaviour between northern and southern situations. The differences were again evident when the contributions of different layers of the mountain range to the total drag were computed. In doing that, two important observations can be done. By one hand, the drag was evenly distributed on the mountain; by the other, the relative importance of the upper section of the mountain clearly decreases in the northern cases compared to the southern ones. All of these results can be interpreted as follows: the major correlation and "linearity" of drag values in northern cases can be explained in terms of the greater homogeneity and non perturbed upstream flow (in Toulouse), in front of the probably upstream perturbed flow in southern cases (Zaragoza) due to the presence of the Iberic Mountains. However, the greater contribution of low layers of the mountain in northern cases could be interpreted as a contribution of blocked colder air (and then non linear effects) in front of southern ones.

3. Different contributions to the drag

To corroborate the last hipothesis, the different components of drag were computed.
From wave momentum fluxes computations, it was concluded that the wave drag was only a small fraction of the surface pressure drag (Bessemoulin et al, 1993).

The hydrostatic drag was computed by interpolating the temperature observations to obtain a thermal profile, and then the hydrostatic equation was integrated on both sides of the mountain from the highest level down to the lowest one. This yielded a pressure profile on both sides of the mountain explainable solely in terms of temperature. A horizontal pressure gradient was then determined and the hydrostatic drag finally computed from Eq.(1).

Total Drag Range (Pa)	Mean Hydrostatic Drag Range (Pa)	Wave Drag Range (Pa)	Hydrostatic Contribution (%)
+1/+4	+1.27/+2.60	+0/+2	70-80%
+4/+6	+4.39/+5.47	+2/+3	45-55%
>+6	+2.59/+2.52	>+3	30-40%
-1/-5	-0.52/-2.15	-0/-3	40-50%
<-5	-1.62/-1.71	<-3	25-30%

The comparison between total drag and hydrostatic drag for the whole campaign is shown in Figure 1. The hydrostatic component appears to be a significant part of the total drag. Quantitative estimations of the magnitude of the hydrostatic drag have been derived from hourly observations. The results are shown in Table I. The hydrostatic contribution ranges between 30 and 85%, being this contribution larger for northerly flows. This behaviour can be easily understood considering the blocking of cold air on the northern side of the Pyrenees during this type of event.

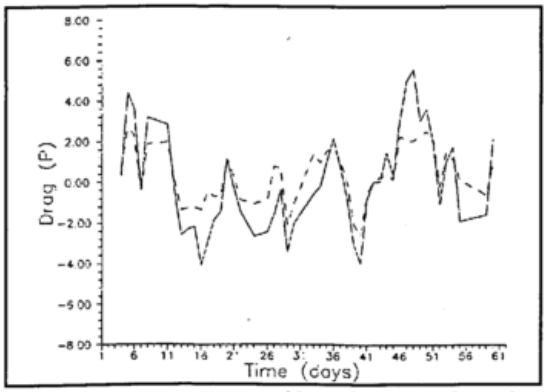

Figure 1. Contribution of the hydrostatic drag (dotted line) to the total drag (full line).

4. Relationship with Meso-Scale horizontal structures

From an observational point of view, based in the daily operative meso-analysis techniques, the orographic effects of the Pyrenees are mainly revealed by a dipolar sea-level pressure perturbation consisting of more or less well defined high and low centers of limited extension. A statistical analysis of the Mediterranean zone has shown that the frequency of occurrence of low pressure centers south of the Pyrenees is comparable to the frequency of occurrence of meso-scale low pressure centers in the Genoa Gulf area (Genovés and Jansá, 1989). The orographic dipole is considered to be a key phenomena for the organisation and intensification of local winds observed in the area, like the Tramontane, as we will see below. The negative part of the dipole forces a strong pressure gradient in the upper Ebro Valley, contributing to produce the Cierzo wind. Similarly, southerly situations generate the Autan wind in France. Moreover, it is suspected that these orographic high-low perturbations can generate or reinforce important convergence zones where convective processes can develop. Finally, the role of these low centers in generating or favouring the development of deep cyclogenetic processes in the Mediterranean is not yet wellknown.

A high correlation (r=0.91) exists between the horizontal pressure gradient (dipole intensity), measured as pressure difference Pau-Zaragoza, and the drag. The regression line being: drag = 0.01003 Δ P - 0.68, where both, drag and Δ P are expressed in Pascals.

5. The Tramontane as an orographic effect

Tramontane is a local wind that blows northwesterly over inland France, turns north over the sea and sometimes reaches Balearic Islands (Campins et al., 1994). Both Tramontane and Mistral constitute the most important wind system in Western Mediterranean basin. Data collected from constant level balloons, soundings and Piper Aztec and Merlin flights have provided a 3D analysis of the estructure of Tramontane (Campins et al, 1994). Basically, it has revealed like a low level cold jet, with maximum wind speed, in the range of 23-33 m/s, at the axis of Pyrenees, 90-100 Km from Port la Nouvelle. The presence of a shear line (with gradients of 7 m/s in 10 Km), between the zone where the Tramontane blows and the sheltered zone, with two different orientations (NW-SE and NNE-SSW) allows to distinguish two types of Tramontane, determining its penetration in Mediterranean Sea.

Significant correlations drag/wind at different levels, reveal the orographic origin of Tramontane. A correlation of 0.60 has been encountered for NNW surface wind at Perpignan.

A diagnostic study based on the comparison between numerical modelling results and observations, consisting of the evaluation of terms of the momentum equation

$$\frac{d\vec{V}}{dt} = -\nabla_h \phi - f\vec{k}x\vec{V} + \vec{R}$$

confirms that the main responsible force for the intensity and location of a strong maximum of wind speed within the Tramontane domain is the pressure force, reinforced by the pressure anomaly on the windward side of Pyrenees, due to flow/orography interaction.

BIBLIOGRAFY

Bessemoulin, P., P. Bougeault, A. Genovés, A. Jansá and D. Puech, 1993: Mountain Pressure Drag during PYREX. *Contributions to atmospheric Physics,* **66,** 305-325.

Davies, H. C., and P. D. Phillips, 1985: Mountain Drag along the Gotthard Section during ALPEX. *Journal of the Atmospheric Sciences,* **47,** 2093-2109.

Campins, J., A. Jansá, B. Benech, E. Koffi and P. Bessemoulin, 1994: PYREX Observations and Model Diagnosis of the Tramontane Wind. (Submitted to).

Genovés, A. and A. Jansá, 1989: Statistical approach to mesoscale non-alpine West Mediterranean cyclogenesis. *Report of the Third Session of the Steering Group on Mediterranean Cyclones Study Proyect,* WMO PSMP Rep. Series No. **31** (WMO/TD No. 298), 77-85.

Pierrehumbert, R.T. and B. Wyman, 1985: Upstream effects of mesoscale mountains. *J. Atmos. Sci.*, **42,** 977-1003.

Mountain wave stationarity condition changes observed by ST VHF radar during the IOP3 of the PYREX experiment

J-L.Caccia[1], B.Benech[2], V.Klaus[3] and D.Tannhauser[2]

[1] Laboratoire de Sondages Electromagnétiques de l'Environnement Terrestre, Université de Toulon, 83957 La Garde, France.
[2] Laboratoire d'Aérologie, Université Paul Sabatier, 31062 Toulouse, France.
[3] Météo-France, Centre National de Recherches Météorologiques, 31057 Toulouse, France.

ABSTRACT

The IOP3 of PYREX was a case of strong mountain/lee waves generated by a northward wind crossing the Pyrénées. Upstream radiosoundings, aircraft measurements along the chain transect, and observations by constant volume balloons launched from the crest gave wavelength and amplitude of the mountain wave at the times they worked. Two ST VHF radars, one located on the crest and another one below the wave field, observed temporal variations of the wave amplitude measured in a fixed vertical direction. The analysis of these observed variations and their vertical distribution allow the stationary nature of the wave to be studied. It has been found that the stationarity conditions were far from being constant during the wave life-time but that some periods, never longer than 1h30, existed during which such constant conditions can be assumed.

1 - INTRODUCTION

The PYREX experiment took place around the Pyrenean chain during October and November 1990. It was dedicated to the study of the dynamical influence of the Pyrénées on the atmospheric circulation. The program and the scientific purposes were decribed by Bougeault et al (1990) and the first results presented by Bougeault et al (1993). The study of mountain/lee waves was one of the main purposes.

When the wind is perpendicular to a mountain chain the air accumulation on the upwind side of the relief creates a high pressure zone which slows down the incident flow. Part of the air is deflected upwards, giving rise to mountain waves. In the frame of the 2-D linear theory (see Scorer, 1949, or more recently Atkinson, 1981) when the Scorer-parameter vertical profile, i.e. the atmospheric stability to horizontal wind ratio, is not far from being uniform this wave radiates upward and downwind. In this case the air motion amplitude very rapidly decreases from the crest in the horizontal direction leading to a short horizontal wave extension. On the other hand, if the Scorer-parameter decreases with height, the wave is reflected downward and the atmosphere acts as a duct leading to a possible horizontal extension of several tens of kilometers. Such a wave is called trapped lee, or mountain, wave. In any cases, if the upstream atmospheric conditions are stable in time these waves are stationary, which means the wave field is fixed with respect to the ground. If it is not, vertical propagation for the non-trapped case, and horizontal propagation for the trapped case are possible.

Our purpose is to give a complete description in space and time of the mountain/lee wave which occurred from 00:00 to 11:00UT Oct. 15 1990, and investigate its stationary nature. Note that all the experimental results presented below are interpreted in terms of orographically induced processes only.

2 - EXPERIMENTAL TECHNIQUE AND RESULTS

2.1. General description

The relevant instruments included in our analysis are:

- Upstream radiosoundings (RS) allowing wind and atmospheric stability profiles to be obtained.
- Aircraft measurements made along the Pyrenean chain transect allowing the horizontal structure of the wave to be established at a given time and altitude. Four flights A1, A2, A3, and A4 are taken into account.
- Two constant volume balloons, also called constant level balloons, CVB1 and CVB2, launched from the crest giving Lagrangian measurements by following the airstream perturbed by the wave.
- Two ST VHF radars observing in a fixed vertical direction the temporal evolution and the vertical distribution of the wind velocity field. The one located on the crest is called crest-radar (CR) and the one to the north of the Pyrénées, thus exactly below the mountain wave field, lee-radar (LR).

Figures 1a and 1b respectively show their geographic and orographic situations. The acronyms used in these figures are those presented here above. The straight line B1-B4 is a ground projection of the aircraft flights and the incident flow is schematically represented by the grey arrows.

For all the instruments, except RS, the relevant parameter used here is the air vertical velocity W. The reason for this choice is that this quantity reflects the mountain wave structure, and is measured by all the instruments at different times and/or locations.

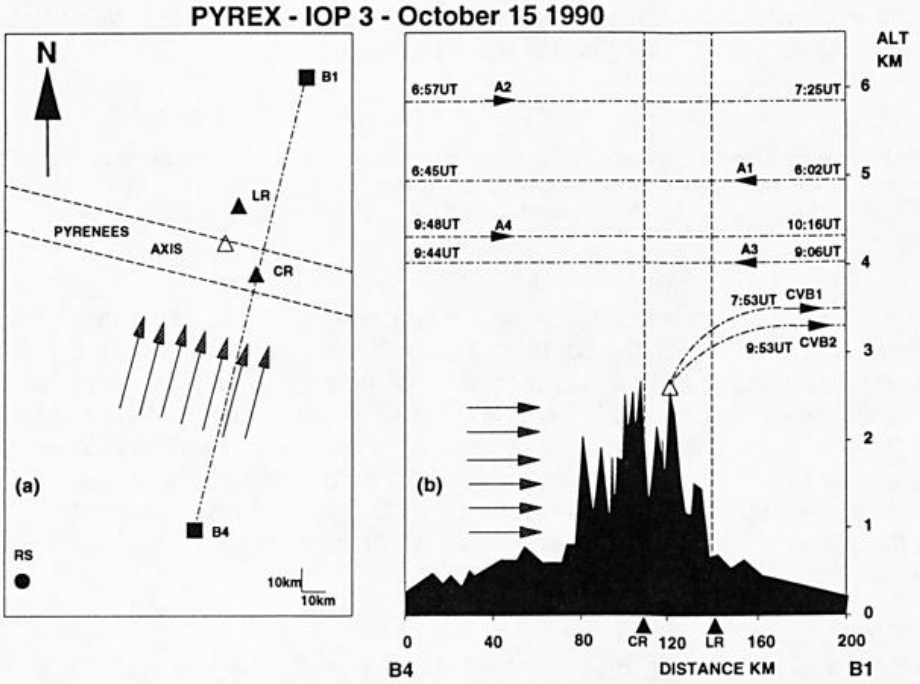

Figure 1: Geographic (a) and orographic (b) situation of the crest-radar (CR), the lee-radar (LR), and the meteorological radiosounding station (RS). The ground projection of the four aircraft flights A1, A2, A3, and A4 is the B1-B4 straight-line. The wind direction during the IOP3 is schematically represented by the grey thin arrows both in a horizontal (a) and vertical (b) plane. The white small triangle indicates the location of the Pic du Midi from where the constant volume balloons CVB1 and CVB2 were launched. Their UT launch times are noted in (b), as also the UT times of the aircraft passages above B1 and B4. The small black arrows correspond to their flight ways. In (b) the vertical dotted-lines show the radar sounding directions. All in (b) is depicted in an orthogonal projection onto the vertical plane above B1-B4 where the mean Pyrénées profile along B1B4 is shown in the lower black part.

2.2. Radiosoundings and airborne measurements

The experimental results obtained by RS, CVB's, and airplanes have been already reported and analysed by Benech et al., 1993. They have been interpreted in the frame of the 2-D linear theory. A good agreement, in time and altitude, was found between the horizontal wavelengths measured by the airborne instuments and that calculated from the Scorer-parameter profile deduced from RS. More particularly, from the 05:00-06:00UT RS, a decrease of this profile with altitude essentially due to an increase of the wind is found. Such a behaviour is compatible with a trapped lee wave situation. As a confirmation a horizontal extension from the crest of about 60km for the wave was observed almost at the same time by the A1 flight. For the later flights such a comparison is impossible since no RS's were simultaneously made. The limit of the wave was detected from the crest at 35km by A2, 40km by CVB1, 45km by A3, and 35km by A4 and CVB2. The other wave characteristics obtained by the airborne instruments in the 3-6km altitude-range were 8-12km for the horizontal wavelength, and 5m/s for the maximal *W*-amplitude.

Wave crest position variations with altitude and time (not shown here) were also observed from one flight to the next. In association with the wave horizontal extension variations a first indication of stationarity condition changes, or nonstationarity, for the lee wave can be drawn. It is noticeable that these nonstationarities can be changes in characteristics associated with a given type of wave, trapped or non-trapped, but also transitions between these two regimes. Such behaviour was already reported by Ralph et al., 1992, in the case of trapped lee wave induced by the Colorado mountains.

2.3. ST VHF Radar measurements

Preliminary remarks:

The radar *W*-profiles are obtained along fixed vertical directions above their installation sites. Therefore as long as the mountain wave stationarity conditions are unchanged these profiles are constant in time. On the other hand, the periods during which significant temporal variations are observed correspond to variations for the stationarity conditions. Theoretically, for the same periods, variations in the RS profiles should be observed. Unfortunately, in the case studied here, such profiles were only obtained every six hours which is obviously too slow to be directly related to the radar *W*-profile temporal variations. For this reason the stationarity nature of the waves is mainly investigated using radar data.

The Crest-Radar (CR):

The CNRM ST VHF radar, CR, was installed at St-Lary exactly on the Pyrénées axis (see Fig.1).

This location was nevertheless in a valley which explains its low altitude, 600m, compared with that of the main crest, 2800m. A vertical profile of *W* was obtained every 12mn using vertical complementary high and low resolution modes, respectively 375m, below 8km, and 2250m above. As already reported elsewhere the results were found to be consistent with the airborne measurements.

A classical behaviour of *W*-profiles in mountain wave event is negative *W*-values in a first height-range above the crest. The upper limit *H* of this range is of high interest since it is directely related to the upstream atmospheric conditions. From the CR data *H* as a function of time has been computed and is shown in Fig.2. The *NO WAVES* period from 18:00 to 01:00UT is so called because *W* is positive immediately above the crest which is incompatible with a mountain wave situation. After 01:00UT and until 11:00UT the data indicate that the wave system is established. In this figure C1, C2, and C3 indicate periods longer than 50mn during which *H* is constant with time according to the accuracy of 750m. This suggests that the mountain wave was stationary within these periods.

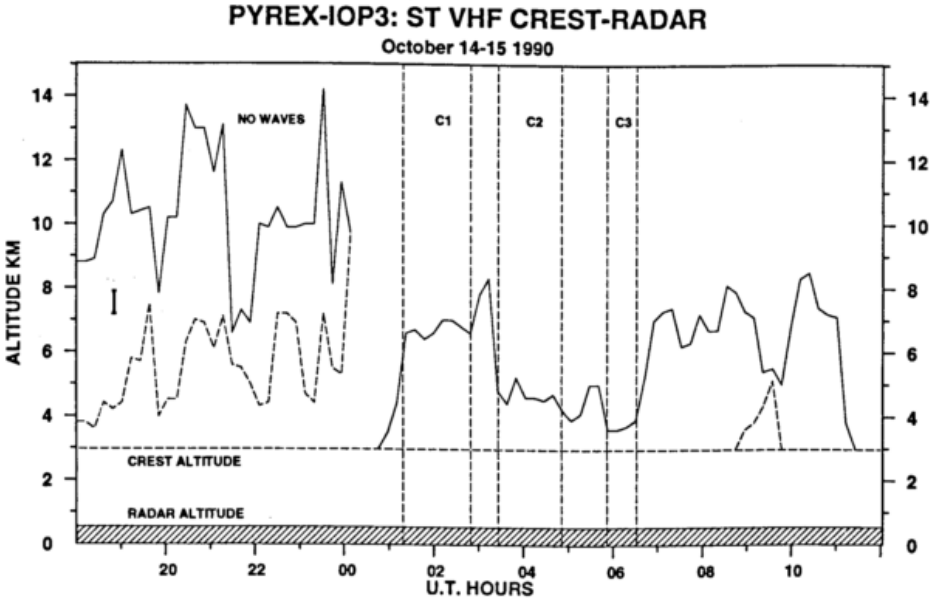

Figure 2: Time evolution of the first altitude *H* above the crest where *W* goes from negative values to 0 (solid curves). The dotted curves indicate the altitude, if it exists, where W goes from positive values to 0. The periods for which no curve exists correspond to cases where *W* is positive in all the altitude-range.The *NO WAVES*, C1, C2, and C3-periods are defined in the text. The thick vertical dash on the left shows the accuracy, here 750m, for the *H* estimation.

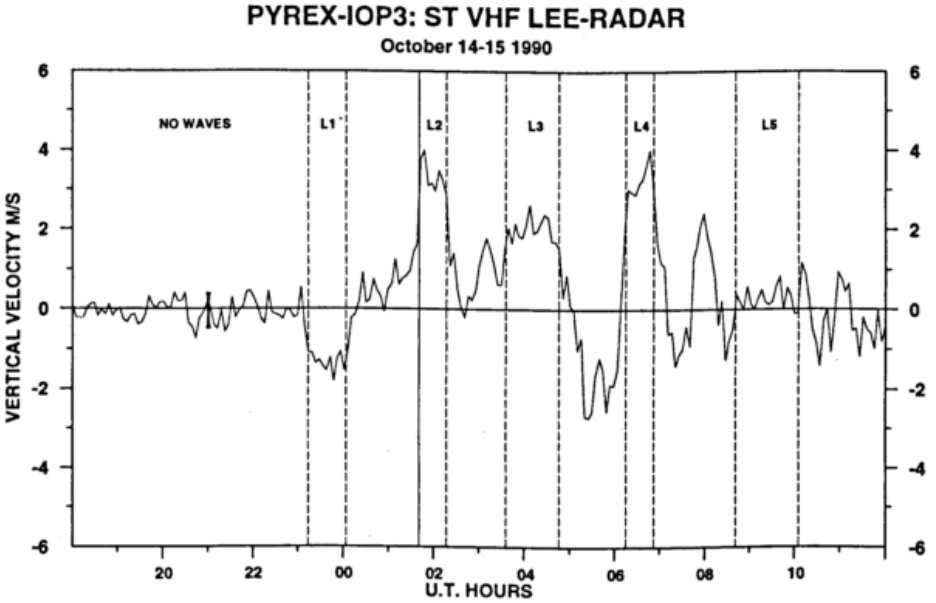

Figure 3: Time evolution of *W* in the wave field vertically averaged in the 2-6km altitude-range. The periods named *NO WAVES*, L1, L2, L3, L4, and L5 are defined in the text. The thick vertical dash superimposed to the *NO WAVES* data indicates the *W*-fluctuation range,i.e. -40 to 40cm/s. It is considered to be the noise level in *W*-values obtained in the wave field.

The Lee-Radar (LR):

The LSEET ST VHF radar, LR, was installed at Lannemezan at about 40km to the north of the crest (see Fig.1). This location is below the mountain wave field. A *W*-vertical profile is obtained every 4mn50s with a 1mn30s of time-resolution and from 2250m to 15750m of altitude with a vertical step and resolution of 750m. In our study we use data obtained from 2250m to 6000m which is a range where the wave had a maximal activity and where the airborne measurements presented here were made. In this height-range and during the whole IOP3 six time-series of *W* were recorded. As for CR, the results were found to be consistent with airborne data.

These six *W*-time series, not presented here, show that the significant time variations occurred simultaneously, coherently, and without any vertical sign shift in the whole altitude range from 23:00 to 02:30UT and from 03:30 to 08:30UT. This is a radar signature of horizontal crest wave motions and thus of a trapped lee wave. As a consequence we can average these time series without smoothing the variations at least for these time intervals. These averaged values are presented in Fig.3. Here, the *NO WAVES* period corresponds to small *W*-values ranging from -40 to 40cm/s classically observed in situations not perturbed by waves. Here, L1, L2, L3, L4, and L5 indicate periods longer than 35mn during which *W* is constant according to a -40 to 40cm/s possible fluctuation range, and thus stationarity is suggested.

3 - RADIOSOUNDINGS/AIRBORNE/CREST-RADAR/LEE-RADAR DATA COMPARISON

As already mentioned the *W*-values obtained by all the instruments are in global agreement taking into account their features, locations and acquisition instants.

The best period for a complete description of the wave is 05:00-06:30UT since RS, A1 flight, CR and LR data are available. At this time RS and A1 suggest a trapped lee wave, whereas CR and LR indicate a stationary nature, respectively, from 05:50 to 06:35UT (see C3 in Fig.2), and from 06:10 to 06:55 (see L4 in Fig.3). The stationarity duration is 45mn in each case but LR observed it 20 mn later.

Furthermore a global agreement is found between the C1, C2, and C3-periods of Fig2, and the L2, L3, and L4-periods of Fig.3. Their time locations and durations are clearly indicated in these figures.

The stationarity found by LR during the L5-period of Fig.3 is only apparent and due to the averaging made on the data. At this time there were vertical *W*-sign shifts which caused the small values in the corresponding interval.

The subsidence obtained by LR during L1 (see Fig.3) is not in agreement with the CR data and a mountain wave effect since at this time the air is found by CR to move upward from the crest which is not a wave signature. This case needs further investigations.

4 - CONCLUSIONS AND PERSPECTIVES

The mountain/lee wave event of the IOP3 of PYREX has been described in space and time using RS, airborne and radar data. Three periods of stationarity of 35-90mn, 80mn, and 45mn have been quite consistently identified using an ST VHF radar located on the crest axis and another one below the wave field. In addition during these periods and using this second radar the wave was found to be trapped, which was confirmed by a radiosounding for the 45mn-case. For time-scales longer than 45mn, and except for the three previous cases, the mountain wave was found to be unstationary.

The temporal evolution of the upstream atmospheric profile is required to complete and validate our analysis only based on wave field direct observations. These missing data do not allow us to understand the mechanism of transition from a stationary state to a nonstationary one, and vice versa.

One solution would consist in interpolating upstream radiosounding profiles obtained every six hours and verifying if at least slow variations in the wave field can be retrieved.

REFERENCES

B.W.Atkinson, *Meso-scale atmospheric circulations* Acad.Press, 1981.

B.Benech et al, *Observation of lee waves above the Pyrénées (French Spanish PYREX experiment)* Technical Soaring, **18**, 7-12, 1993.

P.Bougeault et al, *Momentum budget over the Pyrénées: The PYREX experiment* Bull.Am.Meteorol.Soc. **71**, 806-818, 1990.

P.Bougeault et al, *The atmospheric momentum budget over a major mountain range: first results of the PYREX field program* Ann.Geophysicae **11**, 395-418, 1993.

F.M.Ralph et al, *Nonstationary trapped lee waves: wind profiler, RASS, and satellite observations* **6th Conf. on Mountain Meteorology**, Portland, 29 Sept-2 Oct., 1992.

R.S.Scorer, *Theory of waves in the lee of mountains* Q.J.R.Meteor.Soc. **75**, 41-56, 1949.

Turbulence Field Determination during PYREX 90 Using INSU/METEO ST Radar and PERIDOT Model Re-analysis Data

V. Klaus, I.Seloyan

Météo-France
Centre National de Recherches Meteorologiques, 31057, Toulouse

ABSTRACT

In this paper, we investigate the possibility of getting a three-dimensional distribution of turbulence over the Pyrenees mountains during PYREX 90 Experiment. Using the particularly rich data set available during this compaign, first we compute the refractivity structure constant Cn^2 by applying the Warnock-VanZandt model to the re-analysis data provided by the meso-scale PERIDOT model. Parallely, the validity of the results is checked by a systematic comparison with the Cn^2 measurements directly given by the ST radar network operating during these periods. Then, removing the influence of humidity, we calculate the turbulent rate ε distribution which will be compared to the airborne measurements.

1 - ST RADAR MEASUREMENTS OF CN2

ST radars are able to measure the refractivity turbulence structure constant Cn^2 which is directly obtained from the wind signal power observation. Several investigations have shown that this constant can be related to the intensity of atmospheric turbulence parameterized by the eddy dissipation rate ε (for example Gage et al, 1980). By this way, ST radars give new prospects for the study of turbulence in the free atmosphere.

$$\frac{Signal}{Noise} = \frac{S}{N} = \frac{Pt.\frac{a^2.A.c.\tau}{8.\pi.r^2}.k'.Cn^2.\lambda^{-1/3}}{K.(a.Tc+Ts).\frac{\beta}{\tau}}$$

Where:

Pt = Radar Peak power	λ = signal wave length
a = loss coefficient	r = range
A = Antenna surface	K = Boltzmann constant
c = light celerity	Tc = Cosmic noise temperature
τ = pulse width	Ts = Receiver noise temperature
k' = 0.38	β = Matched filter coefficient

This equation shows that Cn^2 can be directly obtained from the power-to-noise ratio and the range r using a radar constant K':

$$Cn^2 = K'.r^2.\frac{S}{N}$$

An example of ST radar capabilities to provide high resolution measurements oc Cn^2 above the radar site is given by figure 1.

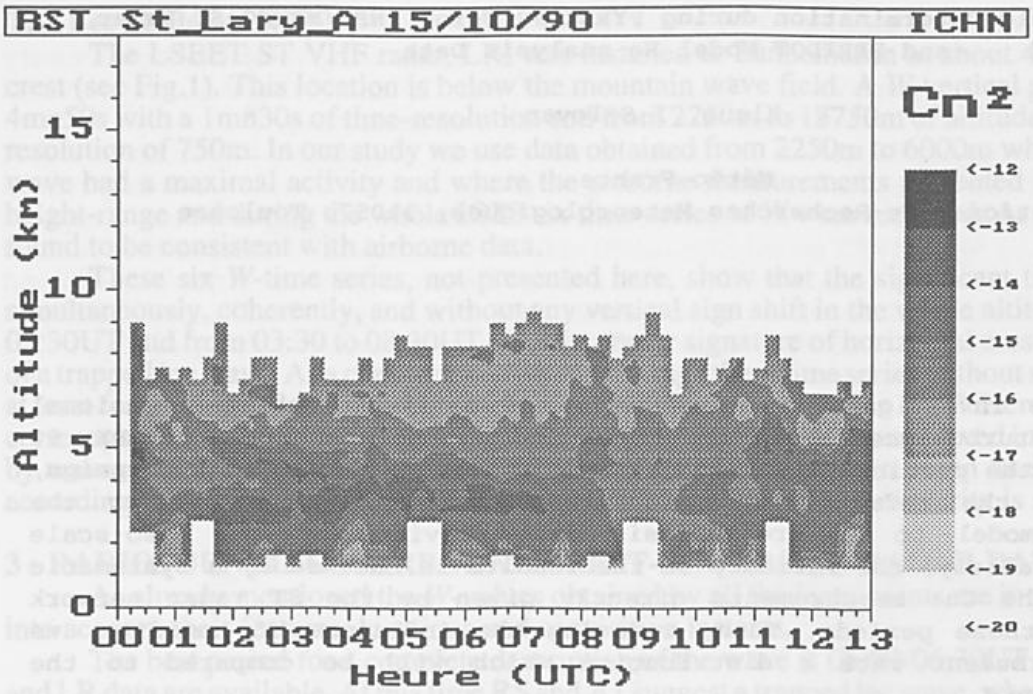

Fig. 1 - Evolution of Cn^2 profile measured by the INSU/Meteo ST radar at Saint Lary during PYREX 90 experiment on 15 october 1990 between 0 AM and 1 PM. Data were obtained with a radial resolution of 375 m, the antenna pointing to the North at 13° from zenith.

2 - MODEL COMPUTATION OF CN2 AND ε

Further studies have allowed to implement a statistical model that estimates the mean values of Cn^2 and ε in the free atmosphere from routine radio soundings or model outputs profiles including altitude, pressure (P), wind speed and direction (V) and humidity (U) (Warnock et al, 1985):

$$C_n^2 = f(P,T,H,V)$$

The main difficulty lies in the fact that the atmosphere is composed of a number of turbulent layers embedded in the large-scale laminar flow. Consequently, a probability approach has been implemented for estimating a mean Cn^2 value in a slab countaining statistical number of thin turbulent layers:

$$\overline{C_n^2} = \int_{L_{min}}^{L_{max}} dL \int_{Ri \le 0.25} \int dS.dN^2 . \int_{-\infty}^{+\infty} dq' . p . C_n^2 \qquad \overline{\varepsilon} = \int_{L_{min}}^{L_{max}} L^2 . dL \int_{Ri \le 0.25} \int S^3 . dS . dN^2 . \int_{-\infty}^{+\infty} p . dq'$$

L = outer scale
S = wind shear
Ri= Richardson number ($Ri=N^2/S^2$)
p = multipariate probability distribution function, $p=p(L,S,N^2,q')$

Several comparisons between vertical Cn^2 profiles measured by ST radar and the model have been reported (for example Green et al., 1984), and a good agreement has been found. At CNRM, the model was tested with synotic radio sounding data for a three months period. The results show quite strong variations of Cn^2 in the lower

The same comparisons have been made with the data obtained during PYREX 90 respectively by the ST radar located in St Lary and the PERIDOT model profile from the closest grid point. They show a quite good agreement.

3 - CN2 THREE DIMENSIONAL DISTRIBUTION

The previous results encouraged us to investigate further the possibilities provided by the PYREX data bank. More precisely, we decided to apply the Cn^2 model computing to all the data of the PERIDOT model in order to get a three-dimensional distribution over 52x52x15 points covering roughly a major part of Spain and the Southern half of France.

The figures show some samples of optical Cn^2 horizontal distribution computed with the Warnock-VanZandt model using the data from the fine mesh PERIDOT re-analysis model. The optical Cn^2 is obtained by expunging humidity contribution from the computation. It allows a better correlation with the turbulence influence. The data are given in logarithms.

The selected period is IOP 9 characterized by a northern wind: We notice a sensitive increase of the Cn^2 to the vicinity of the Pyrenean relief which demonstrates its influence on the atmospheric turbulence during meridian wind. At 3000 m, The Cn^2 is especially high in two regions in the middle part of Pyrenees.

CONCLUSION

The Cn^2 profile obtained with the Warnock-VanZandt model can be an interesting tool for studying the atmospheric turbulence. This model has been successfully tested through comparisons with the INSU / METEO ST radar measurements. It can be used notably when the instrumental set allows a precise fine-mesh atmospheric modelisation of the three-dimensional field of P, T, U and V. In the presentation, we shall compare the turbulence fields with those obtained from aircraft measurements during this experiment.

REFERENCE

Bougeault P., A. Jansa Clar, J.L. Attié, I. Beau, B. Benech, R. Benoît, P. Bessemoulin, J.L. Caccia, B. Carissimo, J.L. Champeau, M. Crochet, A. Druilhet, P. Durand, A. Elkhalfi, A. Genoves, M. Georgelin, K.P. Hoinka, V. Klaus, E. Koffi, V. Kotroni, C. Mazaudier, J. Pelon, M. Petitdidier, Y. Pointin, D. Puech, E. Richard, T. Satomura, J. Stein and D. Tannhauser, 1993, The atmospheric momentum budget over a major moutain range; First results of the PYREX field program, Annales Geophys., Vol.11, N°5, 395-418.

Green J.L., J. Vernin, T.E. VanZandt, W.L. Clark, and J.M. Warnock, 1984, A comparison of optical and radar measurements of Cn^2 height profiles, Preprints, 22nd Conf. on Radar Meterol., Zurich, Suisse, 10-14/09/1984, 470-475.

Hocking, W.K., 1985, Measurement of turbulent energy dissipation rates in the middle atmosphere by radar techniques: a review, Radio Science, Vol. 20, N°6, 1403-1422.

Petitdidier M., V. Klaus, F. Baudin, M. Crochet, G. Penazzi, and P. Quinty, 1986, The INSU and DMN network of ST radars, Handbook for MAP, Vol. 20, 347-348.

Tatarskii, V.I., 1961, Wave propagation in a turbulent medium, Mc Graw Hill, New York.

Warnock J.M and T.E. VanZandt, 1985, A statistical model to estimate the refractivity turbulence structure constant Cn^2 in the free atmosphere, NOAA Technical Memorandum, ERL AL-10, november 1985.

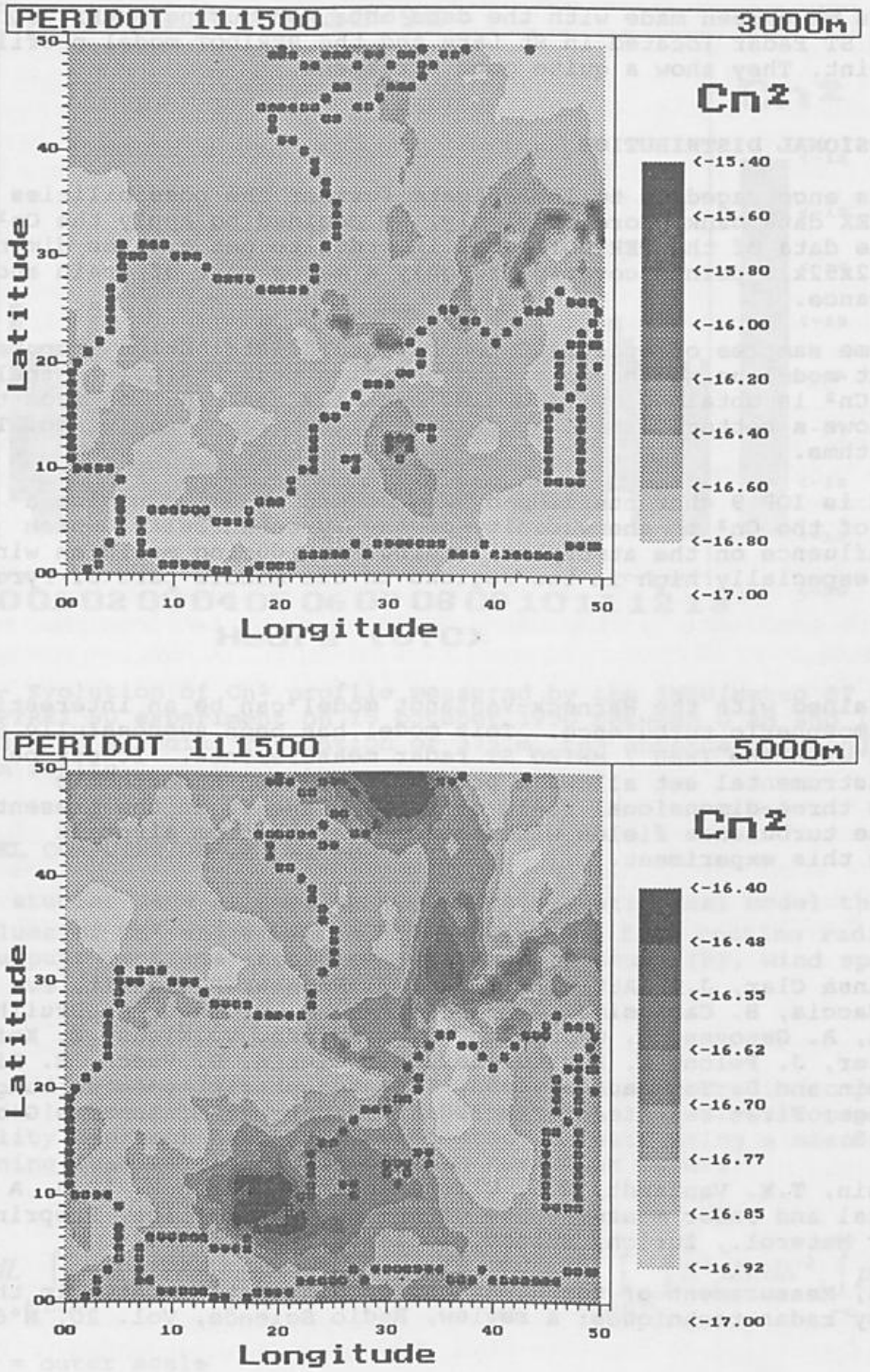

Fig. 2 - Optical Cn^2 horizontal distribution at 3000 and 5000 m respectively computed by the Warnock-VanZandt model using the data from the fine mesh PERIDOT re-analysis model. The Cn^2 data caption is in logarithm.

NONSTATIONARY AND NONHYDROSTATIC SIMULATIONS OF THE IOP 3 OF THE PYREX EXPERIMENT

J.Stein and Ph. Hereil (CNRM/GMME, 42 avenue Coriolis, 31057 Toulouse, France)

We simulate the Pyrex's IOP 3 (15/10/1990), characterized by intense trapped lee-waves, which developped downstream the Pyrénées. The model is an anelastic, twodimensional model, we compare its results with the airplane data extracted from the Pyrex database. Firstly, the stationnary responses are obtained after 5 hours when the model is initialized with the radio-soundings of Sarragoza at 0, 6 12 hTU. Then, a 12 h simulation forced by the time-dependent radio-sounding of Sarragoza, has been realized, which can be easily compared with the data. We show by sensitivity experiments that the friction plays a crucial role to obtain a quantitative agreement with the data for the drag, lee-wave amplitude and vertical momentum flux.

corresponding address:
STEIN Joel,
METEO-FRANCE / CNRM / GMME,
42, Av. Coriolis 31057 Toulouse,
FRANCE,
phone: (33) 61 07 96 58
fax : 61 07 96 26
session: 3 - Diagnosis and simulation of orographically-influenced processes
oral presentation

Simulation einer Gebirgsüberströmung mit dem Ausschnittsmodell Aladin

Klaus v. d. Emde

Zentralanstalt für Meteorologie und Geodynamik
Hohe Warte 38, A-1190 Wien, Österreich

ABSTRACT

A new Limited Area Modell (Aladin) has been developped in the framework of the collaboration between the french and central-eastern european weatherservices. This modell takes the initial and boundary fields from the global forecast model (Arpege) of the french weather service. In this presentation, the limited area modell is applied to a case study of the Pyrex90 (IOP3) field experiment. The goal was to test the model in the case of a highly resolved steep orography. The results show, that the model is able to simulate the observed hydrostatic mountain wave above the pyrenees as well as some local wind systems. Also the simulated wave drag produced by the pyrenees corresponds very well with the observations.

ZUSAMMENFASSUNG

Im Rahmen der Zusammenarbeit zwischen dem französischen und den zentral- sowie osteuropäischen Wetterdiensten wurde ein neues Limited Area Modelle (Aladin) entwickelt. Dieses Modell verwendet Anfangs- und Randbedingungen von dem globalen Vorhersagemodell des französischen Wetterdienstes (Arpege). In der vorliegenden Arbeit wird dieses Modell auf einen Fall des Pyrenäen Experimentes Pyrex90 (IOP3) angewendet. Das Ziel war, an Hand einer Überströmung eines hochaufgelösten steilen Hindernisses die Fähigkeiten des Modelles zu testen, inwieweit es beobachtete Strukturen simulieren kann. Dabei zeigte sich, daß die über den Pyrenäen beobachtete Gebirgswelle sowie einige lokale Windsysteme gut erfaßt wurden. Hervorzuheben ist, daß der simulierte Gebirgswiderstand der Pyrenäen mit den Messungen gut übereinstimmt.

1. Einleitung

Einer Einladung von Météo-France folgend hat in den letzten Jahren eine Gruppe zentral- und osteuropäischer Wissenschaftler an der Erstellung einer LAM Version (genannt Aladin) des globalen Prognosemodelles des französischen Wetterdienstes (genannt Arpege) gearbeitet. Im Rahmen dieses Projektes wurde eine Studie durchgeführt, die zum Ziel hatte, das Verhalten dieses neuen Limited Area Modelles bei der Simulation einer hochaufgelösten Gebirgsüberströmung zu untersuchen. Hierfür wurde eine Fallstudie des im Herbst 1990 von Frankreich und Spanien durchgeführten Feldexperimentes Pyrex90 verwendet.

2. Die numerischen Prognosemodelle

Das neue globale Prognosemodell des französischen Wetterdienstes wird in Kooperation mit dem Zentrum für Mittelfristvorhersage (ECMWF) in Reading entwickelt. Ein

besonderes Merkmal dieses spektralen Modelles ist die Möglichkeit mittels einer Koordinatentransformation ein Gebiet der Erdkugel stärker aufzulösen (Courtier und Geleyn, 1988).

Das Ausschnittsmodell Aladin ist so konzipiert, daß alle Berechnungen, die nicht den spektralen Raum betreffen, von den entsprechenden Modellteilen des globalen Modelles berechnet werden können. Daher ist ein Großteil des Modelles Aladin (ca. 60%) identisch mit dem des globalen Modelles. Dies betrifft z.B. die 'Physik' des Modelles, wobei allerdings unterschiedliche Werte einiger Parameter verwendet werden. In Aladin werden die abhängigen Variablen in bi-Fourier Reihen entwickelt, wobei die Anzahl der Wellen durch eine 'Elliptische Truncation' bestimmt wird. Zur Minimierung des numerischen Lärmes bei der Fourierentwicklung wird eine Erweiterungszone ohne geographischen Bezug um das innere Prognosegebiet gelegt. Die prognostischen Gleichungen für den horizontalen Wind, die Temperatur, die Feuchte und den Bodendruck können auf verschiedenen konformen (z.B. polar stereographisch) Projektionen integriert werden. Das Initialisierungsverfahren basiert auf der Digitalen Filter Technik (Lynch et al., 1992). Für die Kopplung an das globale Modell werden die entsprechenden Randbedingungen in einer Relaxationszone (Davies, 1976) am Rand des Gebietes mit geographischer Bedeutung vorgeschrieben. Dabei wird für die Feuchte eine andere Kopplungsfunktion verwendet als für die übrigen Variablen. Der Zeitschrittalgorithmus ist ähnlich dem Schema in Arpege und enthält eine semi-Lagrange Behandlung der Advektion. Die Gestaltung der semi-impliziten Korrektur der Schwerewellenausbreitung erlaubt es, daß die prognostischen Gleichungen nur im inneren Integrationsgebiet gelöst werden müssen und nicht in der Erweiterungszone.

3. Das Experiment

Zur Erstellung der Anfangs- und Randbedingungen wurde, unter Verwendung der reassimilierten Daten vom ECMWF, mit dem globalen Modell Arpege eine Prognose über 24 Stunden durchgeführt. Die Ergebnisse wurden alle 3 Stunden abgespeichert. Für Aladin wurde eine polarstereographische Projektion gewählt, wobei das innere Integrationsgebiet, mit 94*94 Gitterpunkten und einer Gitterdistanz von 10 km (exakt bei 60 Grad Nord) so gelegt wurde, daß sich die Pyrenäen genau in der Mitte des Gebietes befinden. Die Erweiterungszone für die Periodisierung wurde mit 14 Gitterpunkten in x- und y-Richtung festgelegt. Die spektrale Auflösung wurde durch einen kreisförmigen Abhackgrad auf 35 Wellen beschränkt. In der Vertikalen wurde die Atmosphäre in 31 Schichten unterteilt. Um die Reflexion von Wellen am oberen Rand des Modelles zu reduzieren, wurde in den Schichten über 15 km Höhe die Horizontaldiffusion verstärkt.

Die synoptische Situation war im Verlauf des 14.-15.10.1990 durch einen Trog über dem östlichen Atlantischen Ozean charakterisiert. Dadurch kam es über Spanien und Frankreich in höheren Schichten zu einer süd- bzw. südwestlichen Strömung und über den Pyrenäen bildete sich eine Gebirgswelle aus. Das synoptische System driftete langsam nach Osten, und der Wind wurde während der Nacht zum 15.10.1990 immer stärker. Die Luftmassen, die auf die Pyrenäen trafen, waren ziemlich feucht und bildeten auf beiden Seiten des Gebirgszuges Wolken. Trockenere Luft kam erst nach dem Durchzug einer schwachen Front am 15.10.1990 um ca. 12 GMT in dieses Gebiet.

Als Beispiel für die Ergebnisse der Simulation mit Aladin ist in Abb.1 das Windfeld in 10m Höhe über dem Boden dargestellt. Es zeigt die für diese synoptische Situation

typischen lokalen Strömungsverhältnisse: die Strömung das Ebro-Tal aufwärts im Süden der Pyrenäen, der schwache Wind im Nordwesten der Pyrenäen und der Wind Autan im Nordosten der Pyrenäen. Diese Struktur zeigt sich auch in den Beobachtungen (Abb.2), wobei der Autan-Wind den Meßungen zu folge im Modell zu schwach war (Bougeault et al., 1992). Die hydrostatische Gebirgswelle über den Pyrenäen reichte bis in die Stratosphäre. Eine Abschätzung des Gebirgswiderstandes ergab eine gute Übereinstimmung zwischen den berechneten (4.8, 5.3 Pa) und den beobachteten Werten (5.6, 5.0 Pa um 6 und 9 Uhr GMT).

4. Zusammenfassung

Diese erste Fallstudie zeigte, daß mit dem Limited Area Modell Aladin unter Verwendung von Anfangs- und Randbedingungen aus dem globalen Modell Arpege, eine Überströmung der hochaufgelösten (Gitterweite von 10 km) Pyrenäen simuliert werden kann. Hervorzuheben ist dabei, daß das Modell den Gebirgswiderstand richtig erfaßt. Unterschätzt wurde hingegen der Autan-Wind, der im Lee der Pyrenäen in den unteren Schichten der Atmosphäre parallel zum Gebirgszug weht. Die beobachteten lokalen Windsysteme wie die Strömung das Ebro-Tal aufwärts und die Region mit schwachen Winden im Nordwesten der Pyrenäen stimmen mit den Modellergebnisse überein.

Das Model Aladin wurde von J.-F. Geleyn, unter der Mitarbeit von M. Batka, R. Bubnova, E. Cordoneanu, V. Ducrocq, V. Ivanovici, I. Ihász, M. Janousek, M. Jerczynski, A. Joly, A. Horányi, S. Malardel, V. Pescaru, G. Radnoti, H. Seidl, L. Spacek und V. Spiridonov entwickelt.

Literatur:

Bougeault, Ph., I. Beau and J. Stein, 1992: Validation of Meteorologiocal Models and Parameterizations with Observations of the PYREX Field Experiment. ECMWF-Seminar: Validation of Models over Europe, 7–11 Sept., 1992, Reading.

Courtier, Ph. and J.-F. Geleyn, 1988: A global spectral model with variable resolution – application to the shallow-water equations, Q.J.R. Meteorol. Soc. **114**, 1321–1346.

Davies, H.C., 1976: A lateral boundary formulation for multi-level prediction models. Q.J.R Meteorol. Soc., **102**, 405-418.

Lynch, P. and X.Y. Huang, 1992: Initialization of the HIRLAM model using a digital filter. Mon.Wea.Rev., **120**, 1019-1034.

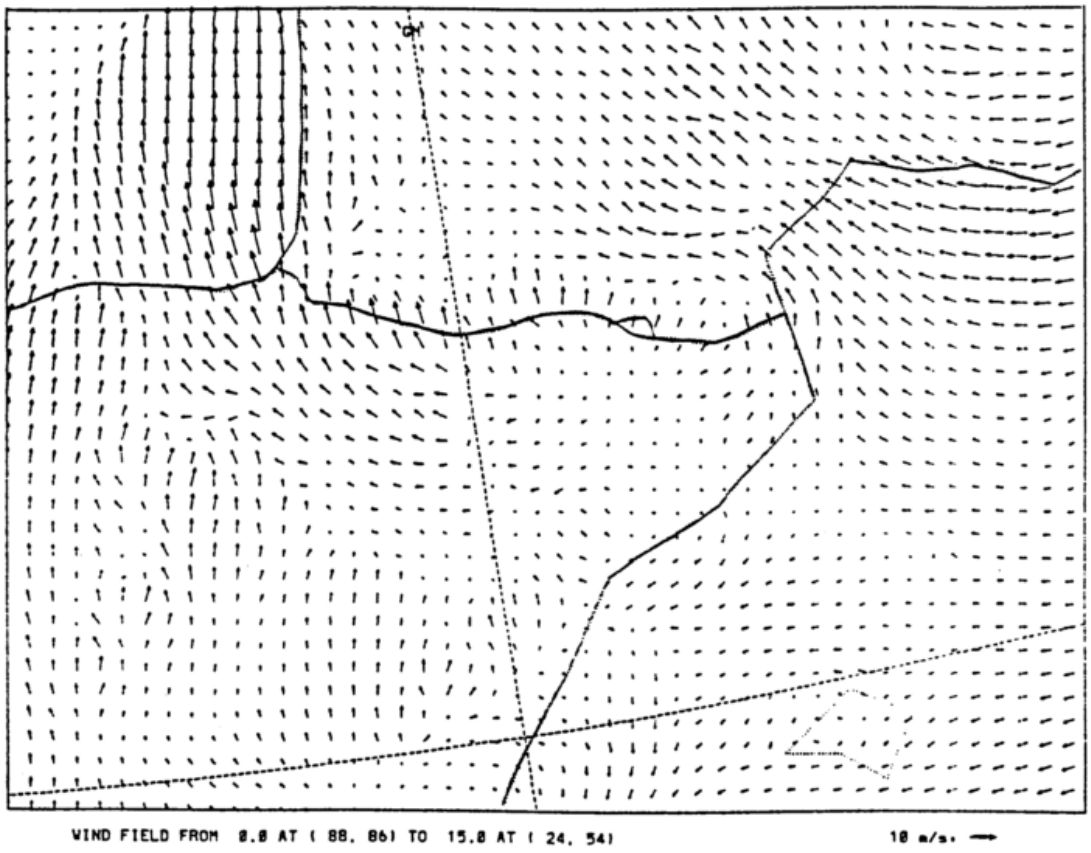

Abb.1: Wind in 10 m Höhe über dem Boden nach 9 Stunden Integration, 15.10.1990 um 9 GMT.

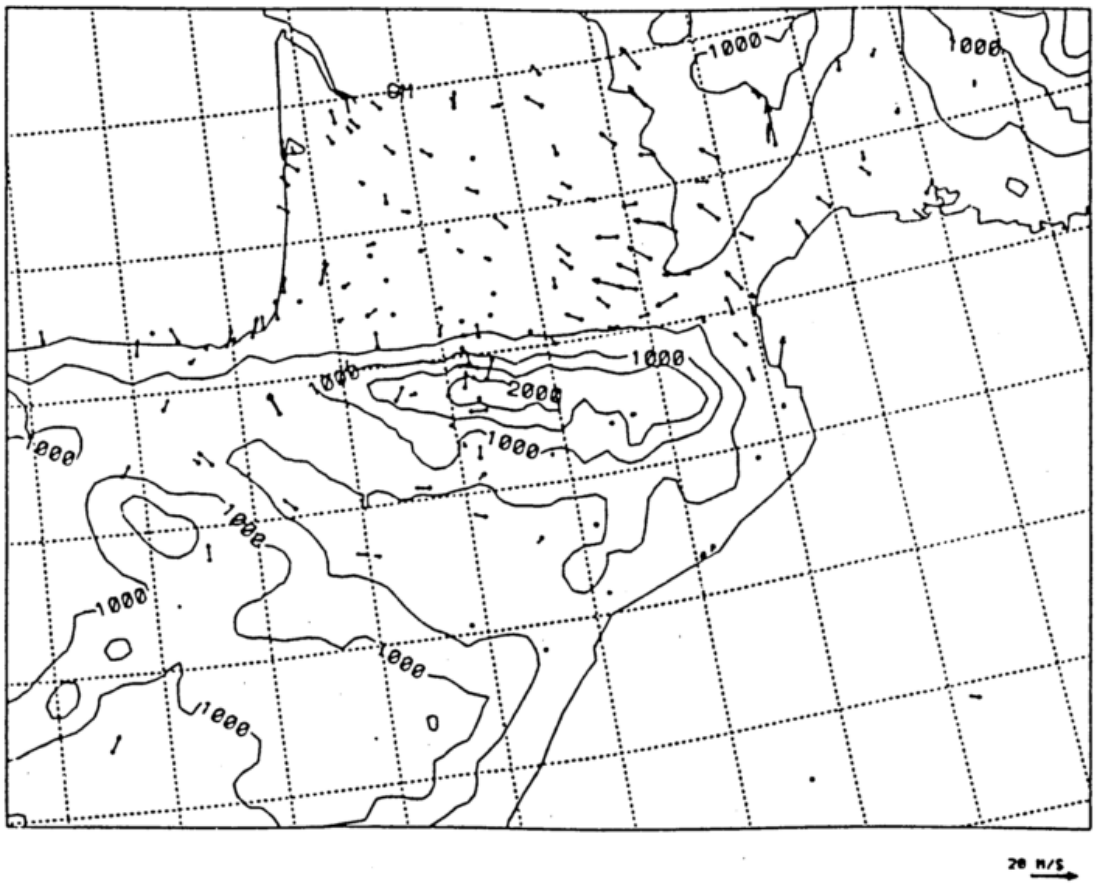

Abb.2: Wind in 10 m Höhe über dem Boden, gemessen am 15.10.1990 um 9 GMT.

Analysis of inhomogeneous turbulence in an atmospheric flow around a mountain range

Druilhet, A., Attié, J.lL., Abreu Sa L., Durand, P. and Bénech, B.

abstract

Wavelet transform was used to analyse aircraft data in the case of inhomogeneous turbulence. The data was gathered during a meteorological experiment (PYREX) to study the airflow around a mountain ridge: the Pyrénées. Four specific flows are analysed:
1) Mechanical turbulence in the lee side of the mountain;
2) Mountain lee waves and small scale turbulence;
3) Coherent structures within Tramontana wind over the
Mediterranean sea and
4) Inhomogeneous and strongly turbulent valley wind (Cierzowind).
These two latter local winds are generated by the Pyrénées mountain range.

1-Introduction}

For a long time, only homogeneous turbulence was investigated. The resulting knowledge was a parameterization of the turbulent flow characteristics. This parameterization is used in numerical models of the atmospheric flow (weather forecasting or the modeling of diffusion-transport of effluents).

Afterwards, sensors and measurement techniques for atmospheric turbulence were adapted to be embarked onboard instrumented aircraft. With such mobile-type platforms, measurements could be performed on domains lacking in experimental dataset, such as averaged properties of heterogeneous surfaces or flow distortion due to the relief. In such conditions, the thermodynamic parameters are more complex, because of the accumulation of various mechanisms which greatly disturb the steady state.

The aim of this contribution is to present some characteristics of non-stationary turbulent signals, gathered with instrumented aircraft during the PYREX experiment [2,3], whose goal Airborne measurements. Inhomogeneous signals are studied segment-by-segment with the Short-Time Fast Fourier Transform (SFFT) and particularly by wavelet transform.[The wavelet is used for determining the spectral structure of the signals (represented as a time-frequency or a space-wavenumber). So, the analysing function is a complex Morlet-type wavelet (Grossmann, A. and J. Morlet, 1984).

To illustrate this, we have chosen some examples of turbulent samples measured on board instrumented aircraft in the proximity of the Pyrénées relief during the PYREX experiment. They are: 1- inhomogeneous turbulence, close to the relief; 2- leewaves and associated turbulence above the relief;.3- mechanical structure of the "Tramontana" wind; 4- inhomogeneous turbulence and fluxes in a valley wind (the "Cierzo")

2-Turbulence close to the mountain

Flight legs very close to the mountain were made by the Merlin IV aircraft of Météo-France on November 16, 1990. The synoptic meteorological situation was characterized by a northerly wind. Strongly turbulent zones associated with the roughness are spread out on the downwind side of the mountain. Figure 1 shows the turbulent zones observed on the vertical velocity of the air close to the relief. Figure 2 presents the wavelet transform (real part and energy) performed on the flight legs 1 and 2. The wavelet transform

provides a spectral description of the turbulent zones and their characteristic scales. The energy diagram allows to put in evidence the link between the zones of turbulent energy production and the zones of dissipation. These diagrams show the existence of areas, of around ten kilometers in horizontal length, in which the turbulence is very strong, with fluctuations in vertical velocity of more than 5 m.s-1.

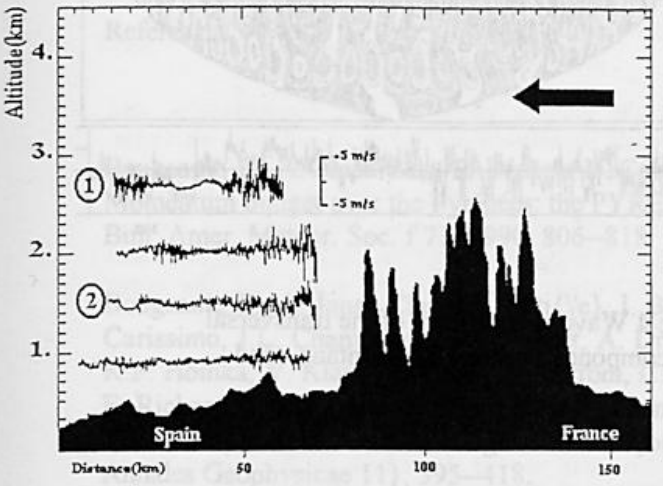

Figure 1- Vertical velocity of the air close to the Pyrénées on 16 Nov 1990

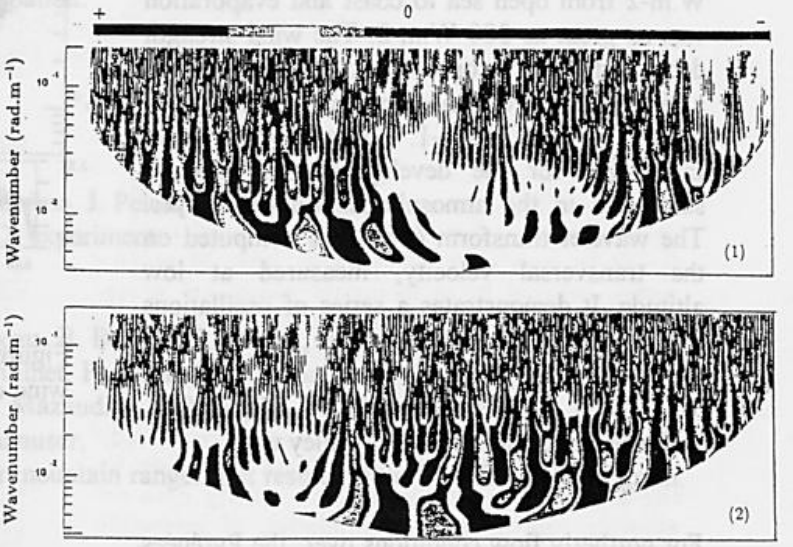

Figure 2- Wavelet Transform performed on legs (1) and (2) (real Part)

3- Lee waves and turbulence

Figure 3 presents a sample of data measured by the Fokker 27 aircraft. It corresponds to a straight and constant level run, 200 km long performed at 4000 m altitude. On the downwind side of the mountain, an area of very clear lee waves is observable in the air temperature and vertical velocity signals. The wavelet transform has been applied to the fluctuations in the vertical velocity w' and in the temperature Θ. The wavelet transform demonstrates quite clearly the continuity in scale between lee waves and high frequency turbulence where the waves degenerate and the turbulent kinetic energy dissipates.

4- Coherent structures within Tramontana wind

The data was collected by the two instrumented aircraft (MerlinIV and Fokker27) on legs located in an East-West vertical plane, from the open sea to the coast of Spain (November 4

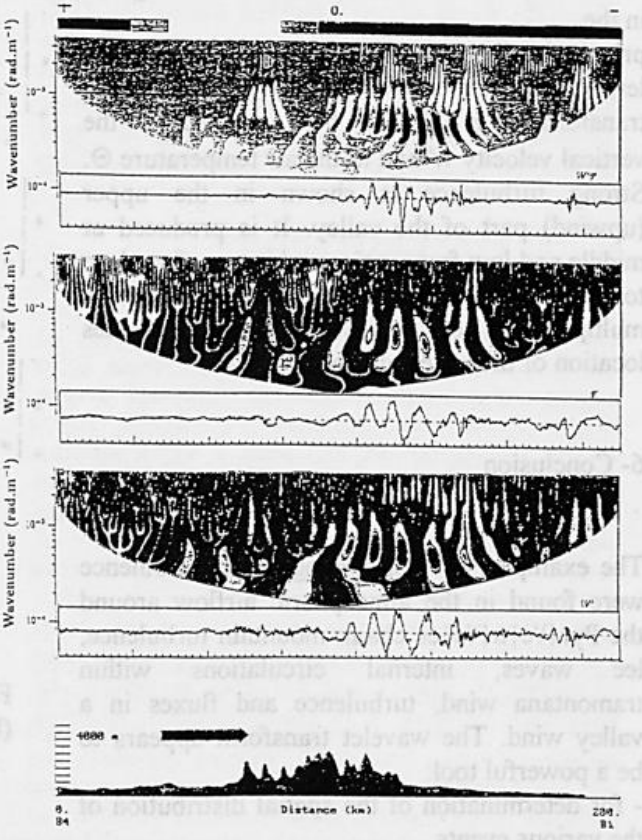

Figure 3 Wavelet transform of lee wave case.

1990). This plane is perpendicular to the Tramontana wind. During this study, boundary conditions over the sea were the following: sensible heat flux varied from 60 W.m-2 to 30 W.m-2 from open sea to coast and evaporation was as great as 280 W.m-2. The wind strength decreased from the open sea to the coast, giving a simultaneous variation in the frictionvelocity from 0.25 to 0.1 m.s-1. These conditions are favourable for the development of coherent structures in the atmospheric boundary layer. The wavelet transform (fig. 4) is computed on the transversal velocity, measured at low altitude. It demonstrates a series of oscillations of about 5 km in wavelength.

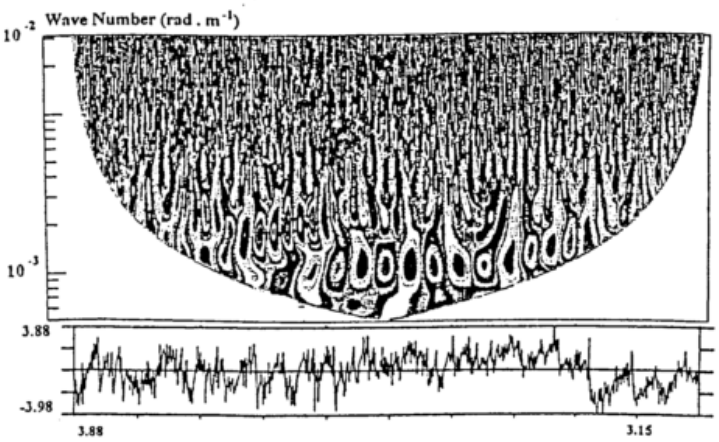

Figure 4 Wavelet transform of the transversal wind component: case of Tramontana wind.

5- Turbulence and fluxes in a valley wind

For northerly flow conditions over the Pyrénées range, a strong wind develops in the upper Ebro valley and extends up to the Mediteranean shore. This wind, called "Cierzo", has been investigated in the
principal valley axis with a straight and constant level flight run of 100 km long,.The wavelet transform (fig. 5) has been applied to the vertical velocity w' and to the air temperature Θ. Strong turbulence is shown in the upper (upwind) part of the valley. It is produced at middle and low frequencies and is transferred up to the inertial subrange (local dissipation).The multiplication of the two diagrams enables location of the zones of heat transfer.

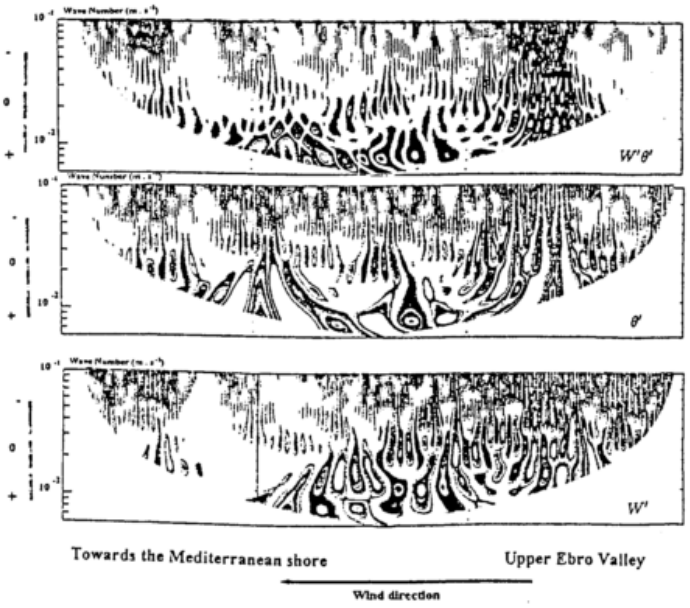

Figure 5 Wavelet transform of vertical velocity (bottom), temperature (middle) and

6- Conclusion

The examples of non homogeneous turbulence were found in the atmospheric airflow around the Pyr{\'e}n{\'e}es chain: mountain turbulence, lee waves, internal circulations within tramontana wind, turbulence and fluxes in a valley wind. The wavelet transform appears to be a powerful tool:
- for determination of the spatial distribution of the various events,
- for the characterization of frequencies contributing to the transfer,

- for isolating the physical mechanisms and
quantifying theirspecific contribution,
- for the identification of secondary structures within the turbulent flow and finally
- for the representationof the path followed by
the turbulent kinetic energy towards viscous dissipation.

References

Bougeault, P., A. Jansa Clar, B. Bénech, B. Carissimo, J. Pelon, and E. Richard,
Momentum budget over the Pyrénées: the PYREX experiment
Bull. Amer. Meteor. Soc. f 71, 1990, 806--818.

Bougeault, P., A. Jansa Clar, J.L. Atti{\'e}, I. Beau, B. Bénech, R. Benoit, P. Bessemoulin, J.L. Caccia, B. Carissimo, J.L. Champeaux, M. Crochet, A. Druilhet, P. Durand, A. Elkhalfi, A. Genoves, M. Georgelin, K.P. Hoinka, V. Klaus, E. Koffi, V. Kotroni, C. Mazaudier, J. Pelon, M. Petitdidier, Y. Pointin, D. Puech, E. Richard, T. Satomura, J. Stein and D.S. Tannhauser,
The atmospheric momentum budget over a major mountain range: first results of the PYREX field program.
Annales Geophysicae 11}, 395--418.

Grossmann, A. and J. Morlet,
Decomposition of Hardy functions into square integrable wavelets of constant shape.
SIAM J. Math. Anal.,15 (1984), 723--736.

MESOSCALE SIMULATIONS OF HYDROSTATIC MOUNTAIN WAVES OBSERVED DURING THE PYREX EXPERIMENT

A. Elkhalfi, M. Georgelin, and E. Richard

Laboratoire d'Aérologie, Université Paul Sabatier
Toulouse, France

1. INTRODUCTION

Mountain barriers exert a significant influence on atmospheric flows. When a stratified fluid is forced to pass over an obstacle, internal gravity waves, referred to as mountain waves, are generated. These waves exert a drag on the upper levels of the atmosphere that is believed to affect the global circulation and needs to be parameterized in numerical weather prediction models.

The Pyrex experiment whose aim was to study the dynamical influence of a large mountain on the atmosphere provides a good quality data set allowing for the precise validation of mesoscale models regarding their capability to reproduce mountain waves and the associated transfer of momentum. In this paper, we present numerical results obtained with 2D simulations of several mountain waves events observed during PYREX. Our purpose is to evaluate from real case studies the validity of the 2D approximation for this flow regime. This point is of some importance considering that most of the parameterizations used in numerical weather prediction models derive from the results of idealized 2D mesoscale simulations.

2. THE PYREX EXPERIMENT

The PYREX experiment (Bougeault et al., 1990; 1993) took place over the Pyrenees at the French-Spanish border. The Pyrenees form a continuous barrier extending east-west over a length of nearly 400 km from the Atlantic Ocean to the Mediterranean Sea with a width varying from 30 to 70 km and an averaged height of 2400 m along the crest line. Given the large aspect ratio of the Pyrenees, a large number of measurements were focussed along a vertical cross section perpendicular to the range in its central part. The observing framework along this cross section included upwind and downwind radiosondes (Toulouse in France and Zaragosa in Spain), an automatic network of 14 ground stations allowing for the surface pressure drag computation, and aircraft measurements taken at different altitudes. Among the 10 Intensive Observing Periods of the experiment, the cases of IOP 3 (18 hour long) and IOP 9 (60 hour long) have been retained for our study. They correspond to the best observed cases of mountain wave from the south and the north respectively.

Corresponding author address: Laboratoire d'Aérologie, Université Paul Sabatier, 118 route de Narbonne, 31062 Toulouse, France.

3. MODEL DESCRIPTION

The model used is the 2D version of the hydrostatic model described in Nickerson et al. (1986) and Richard et al. (1989). The vertical grid is composed of 60 levels with a vertical mesh increasing from 40 m near the ground to 500 m in the upper part of the domain. An absorbing layer, in which diffusion increases with height, occupies the 15 upper levels and prevents spurious refection from the model top boundary. The horizontal domain contains 84 grid points, 10 km apart and is centered over the instrumented cross section previously mentioned.

The standard parameterizations of the model were turned on except for the surface parameterization. No heat flux was allowed at the surface, but the momentum flux was locally enhanced by the use of an effective roughness length devoted to the representation of the subgrid scale orography (Georgelin et al., 1994). All simulations presented were conducted with the Coriolis parameter set equal to zero.

The model is initialized with the upwind radiosoundes data, either from Zaragosa or Toulouse depending on the synoptic flow direction. The wind intensity is computed as the projection of the total wind along the cross section considered in the model. The model is forced at the boundaries by the 6 hourly observed upwind radiosondes data using the relaxation method of Davies on the first and last four lateral grid points of the domain.

4. IOP 3 SIMULATION

The model has been run from October 15, 00 UTC to October 15, 12 UTC. Figures 1 and 2 present the wind field and the potential temperature field obtained for 06 UTC, i.e. at the time of maximum wave activity. A wave of

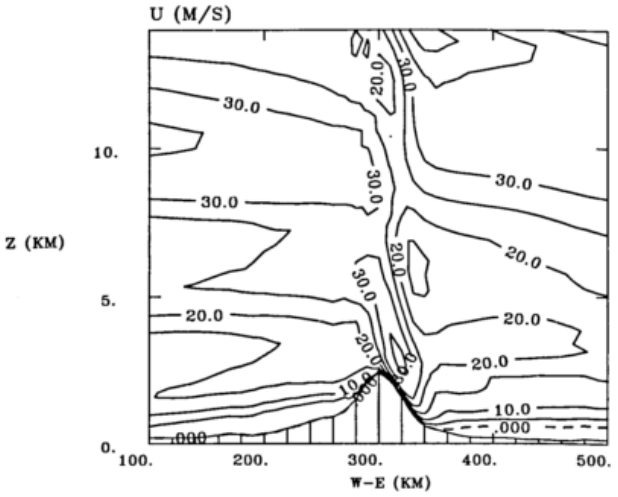

Figure 1. Horizontal wind field for October 15, 06 UTC.

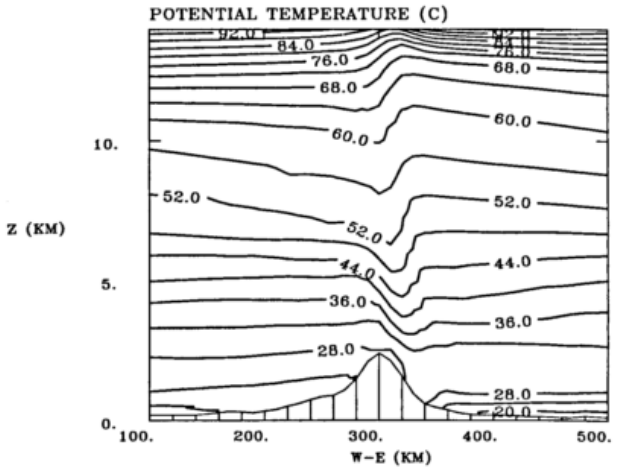

Figure 2. Potential temperature field for October 15, 06 UTC.

significant amplitude is present all over the depth of the troposphere. The wind intensity above the lee slope reaches 33 m/s. Comparisons performed with the aircraft measurements taken between 06 UTC and 10 UTC (not shown) gave a good verification of the amplitude of the modeled wave.

The ground station network installed along the transect allow the computation of the observed surface pressure drag (Bessemoulin et al., 1994). Figure 3 shows a comparison between the time evolutions of the measured and computed surface pressure drags. Two modeled curves are plotted on the figure. They correspond to different values of the roughness length. Curve B results from

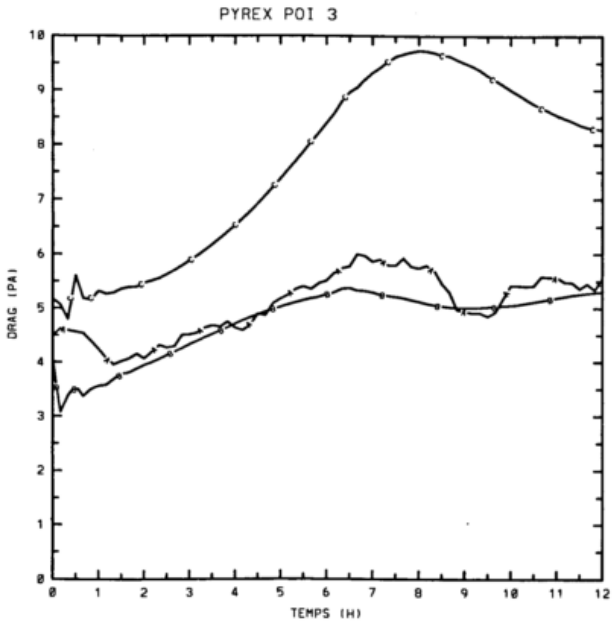

Figure 3. Time evolution of the surface pressure drag in the case of IOP 3: observed (curve A), simulated with the subgrid scale orography parameterization turned on (curve B) and off (curve C).

our reference simulation in which the subgrid scale orography is accounted for through the concept of "effective roughness length" developed by Mason (1988). In this case the effective roughness length deduced from the Pyrenees topography reaches 17 m. Curve C was obtained in the absence of the subgrid scale parameterization, the roughness length characterizes only the roughness due to the vegetation and has a uniform value of 20 cm. These results confirm Georgelin's results obtained with a 3D simulation for the same case study. In the absence of the parameterized subgrid-scale orography, the model gives a wave amplitude and a surface pressure drag much stronger than the observed ones.

5. IOP 9 SIMULATION

The model was run from November 14, 06 UTC to November 16, 18 UTC. During the course of the simulation, the wave structure undergoes a significant evolution due to the modifications of the upstream profiles. The time evolution of the surface pressure drag is plotted in figure 4. Up to 45 hours the agreement between computations and observations is fairly good. At the end of the period, the drag decreases more rapidly in the

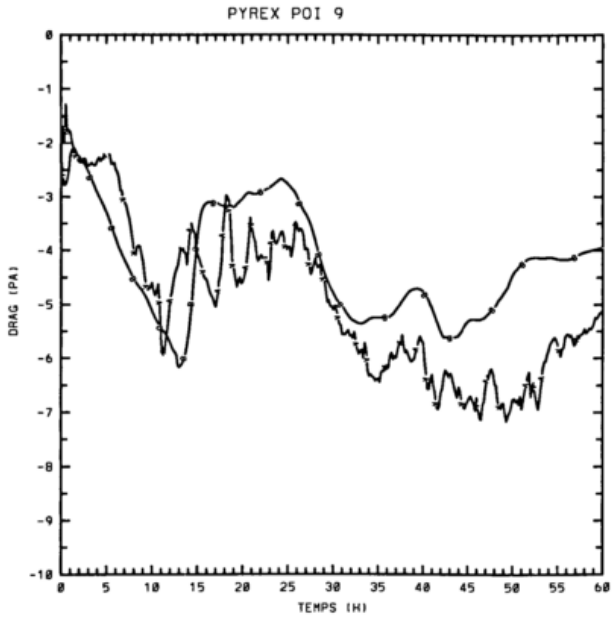

Figure 4. Time evolution of the surface pressure drag in the case of IOP 9: observed (curve A), simulated (curve B).

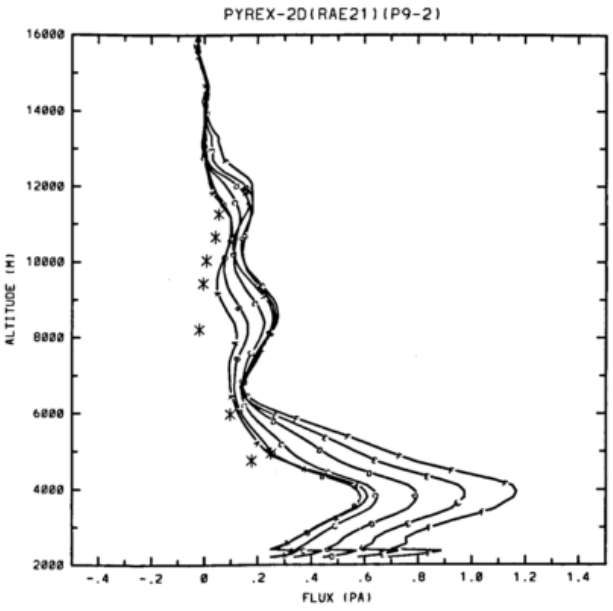

Figure 5. Time evolution of the vertical profile of horizontal momentum flux computed for November 15 from 06 UTC (curve A) to 11 UTC (curve F). The stars correspond to the observed values.

simulation than in the observation, however the error remained less than 1 Pa.

The velocities measurements performed on each day of the IOP 9 by research aircraft flying along different constant height legs allow the computation of the vertical flux of momentum. Figure 5 presents an example of a comparison between the observed flux and the flux deduced from model outputs for the second day of the IOP. The agreement between observations and computations is remarquably good. The modeled flux profile shows a weak maximum at the 12 km level that is correlated with wave breaking in the low stratosphere and is confirmed by the observations. In the low troposphere the flux becomes divergent .

6. CONCLUSION

Two-dimensional numerical simulations were performed for 2 PYREX events in which there was significant cross-mountain flow, IOP 3 which lasted less than one day and IOP 9 which lasted two and one-half days. The time evolution of the large-scale flow was incorporated in the model through time dependent boundary conditions which were updated using soundings from Toulouse or Zaragoza. The numerically simulated mountain waves agreed well with the available aircraft observations. Good agreement was also obtained between the simulated and observed vertical momentum flux profiles which are second-order quantities. In addition the model generated cross-mountain pressure drag accurately followed the time evolution of the observed drag for periods as long as two and one-half days.

7. REFERENCES

Bessemoulin, P., P. Bougeault, A. Genoves, A. Jansa Clar and D. Puech, 1993: Mountain pressure drag during PYREX. *Beitr. Phys. Atmos.*, **66**, 305-325.

Bougeault, P., A. Jansa Clar, B. Benech, B. Carissimo, J. Pelon and E. Richard, 1990: Momentum budget over the Pyrenees: the PYREX experiment. *Bull. Amer. Meteor. Soc.*, **71**, 806-818.

Bougeault, P., A. Jansa, J.L. Attié, I. Beau, B. Benech, R. Benoit, P. Bessemoulin, J.L. Caccia, J. Campins, B. Carissimo, J.L. Champeaux, M. Crochet, A. Druilhet, P. Durand, A. Elkhalfi, P. Flamant, A. Genoves, M. Georgelin, K.P. Hoinka, V. Klaus, E. Koffi, V. Kotroni, C. Mazaudier, J. Pelon, M. Petitdidier, Y. Pointin, D. Puech, E. Richard, T. Satomura, J. Stein, and D. Tannhauser, 1993 : The atmospheric momentum budget over a major atmospheric mountain range: first results of the PYREX program. *Annales Geophysicae*, **11**, 395-418.

Georgelin, M., E. Richard, M. Petitdidier and A. Druilhet, 1994: Impact of subgrid scale

orography parameterization on the simulation of orographic flows. *to appear in Mon. Wea. Rev.*.

Mason, P.J., 1988: The formation of areally-averaged roughness lengths. *Quart. J. Roy. Meteor. Soc.*, **98**, 213-221.

Nickerson, E.C., E. Richard, R. Rosset, and D.R. Smith, 1986: The numerical simulation of clouds, rain, and airflow over the Vosges and Black Forest mountains : a meso-β model with parameterized microphysics. *Mon. Wea. Rev.*, **114**, 398-414.

Richard, E., P. Mascart and E.C. Nickerson, 1990: Examples of the Role of Surface Friction in Downlope Windstorms. *Meteorol. Atmos. Phys.*, **43**, 163-172.

OROGRAPHICALLY-INFLUENCED VERTICAL WIND PROFILES

Brigitte Klose

Meteorological Institute, Humboldt University at Berlin, Germany

Abstract. The atmospheric boundary layer (ABL) of a mountainous region is characterized by acceleration effects in a significant manner so that the observed wind profiles differ markedly from the well-known Ekman profile. In order to study these effects an analytical solution of the modified equation of motion was derived taking into account the influence of vertical motion, velocity divergence and curvature vorticity. The obtained solutions allow to compute vertical wind profiles up to 1500 m height both for a barotropic and a baroclinic ABL in case of stable, unstable and neutral stratification.

1. Introduction

Vertical motions in a mountainous region are caused by synoptic scale developments (lee cyclogenesis, front events), thermally driven micro-scale circulations (mountain and valley winds, slope winds) and overflow phenomena (e.g.'Föhn'-effects). For synoptic scale motions the vertical velocities have a typical magnitude of 10^{-2} to 10^{-3} ms^{-1}, i.e. they are three to four orders of magnitude less than the horizontal wind velocity. Despite of this fact vertical velocities have a great influence on thermodynamical processes in the atmosphere. They are connected with the vertical component of the gradient in each total derivative of a physical quantity and we know that the vertical component of a gradient is more than one order of magnitude greater than its horizontal components. Furthermore, the vertical velocity field is connected with the horizontal flow divergence by the continuity equation so that the influence of vertical motions and that of horizontal accelerations on the vertical wind profile in the ABL have to be treated simultaneously.
Considering all these facts it was made an attempt to gain an analytical solution of the equation of motion including the above described characteristics of the ABL using some simplified assumptions.

2.Theoretical Aspects

In order to derive an analytical solution we write the equation of motion in a complex form

$$\frac{dV}{dt} - k\frac{d^2V}{dz^2} + ifV = ifV_g, \qquad (1)$$

where V and V_g are the complex horizontal and geostrophic wind vectors, k is the eddy viscosity coefficient and f the Coriolis parameter; the other symbols in Eq. (1) have their usual meaning. Next we split the total derivative dV/dt into its local, advective and convective parts and gain the following equation

$$\frac{\partial V}{\partial t} + V\cdot\nabla V + w\frac{\partial V}{\partial z} - k\frac{\partial^2 V}{\partial z^2} + ifV = ifV_g$$

(w means the velocity component in the z direction). In this equation we transformate the advective acceleration term in terms of velocity divergence $\partial V/\partial s$ and curvature vorticity V/r using natural coordinates and obtain

$$\frac{\partial V}{\partial t} + V\cdot\left(\bar{s}\frac{\partial V}{\partial s} + \bar{n}\frac{V}{r}\right) + w\frac{\partial V}{\partial z} - k\frac{\partial^2 V}{\partial z^2} + ifV = ifV_g \qquad (2)$$

($\bar{s}$ and $\bar{n}$ represent the horizontal unit vectors in direction and perpendicular to the horizontal streamlines, r is the streamline curvature radius). For $\partial V/\partial s = D = \text{const}$ and $V/r = D^* = \text{const}$ we get after rearranging of these terms in Cartesian coordinates the following partial differential equation (see /1/ to /5/)

$$\frac{\partial V}{\partial t} + w\frac{\partial V}{\partial z} - k\frac{\partial^2 V}{\partial z^2} + V(if + iD^* + D) = ifV_g\,. \qquad (3)$$

If we assume that D is constant with respect to height a linear profile results for w(z) up to the top of ABL by using the continuity equation for incompressible fluids. In this case the vertical velocity w at the top h of the ABL can be written as

$$w(h) = -\int_0^h (D_v + D_\Psi)dz = -D_v h$$

neglecting the direction divergence D_Ψ. That means the vertical velocity will be 1 cms^{-1} at a height of 1000 m if the velocity divergence D_v has a value of 10^{-5} s^{-1}.
Furthermore, for a baroclinic ABL the geostrophic wind vector can be expressed by $V_g = V_{go} + C_g z$, whereas V_{go} is the geostrophic wind vector near the ground and C_g the complex geostrophic shear vector. Thus, we obtain finally

$$\frac{\partial V}{\partial t} - Dz\frac{\partial V}{\partial z} - k\frac{\partial^2 V}{\partial z^2} + (if+iD^*+D)V = ifV_{go} + ifC_g z\,. \qquad (4)$$

In order to solve this second order partial differential equation we choose

$$V(z,t) = \Phi(z,t)e^{-Bt}e^{-Dz^2/2k} + (if/B)V_{go} + (if/N^*)C_g z, \qquad (5)$$

where $B = (if+iD^*+D)$ and $N^* = if + iD^*$. After some rearrangements of all terms we get now the following homogeneous differential equation

$$\frac{\partial \Phi}{\partial t} + Dz\frac{\partial \Phi}{\partial z} - k\frac{\partial^2 \Phi}{\partial z^2} + D\Phi = 0\,. \qquad (6)$$

Letting $\Phi(z,t) = e^{-Dt}\,\Omega(z)$ like it is usual in problems of mathematical physics Eq.(6) becomes

$$Dz\frac{\partial \Omega}{\partial z} - k\frac{\partial^2 \Omega}{\partial z^2} = 0. \qquad (7)$$

After integrating Eq.(7) using $\Omega'(z) = \mu(z)$, $\Omega''(z) = \mu'(z)$ we obtain $\Omega = C_1\int e^{Dz^2/2k}\,dz + C_2$. If we substitute $\Omega(z,t)$ the solution of the differential equation (1) takes the form in case of velocity divergence ($D > 0$) or velocity convergence ($D < 0$)

$$V(z,t) = e^{-(if+iD^*+2D)t}e^{-Dz^2/2k}\{C_2 + C_1\int e^{Dz^2/2k}\,dz\} + (if/B)V_{go} + (if/N^*)C_g z \qquad (8a)$$

$$V(z,t) = e^{-(if+iD^*-2D)t}e^{Dz^2/2k}\{C_2 + C_1\int e^{-Dz^2/2k}\,dz\} + (if/B)V_{go} + (if/N^*)C_g z\,. \qquad (8b)$$

In the second solution the integral term corresponds to the error integral which is tabulated or can be solved using polar coordinates. Specifying and applying the boundary conditions

$$V(z=z_o,t) = C_o e^{i\alpha} e^{-2Dt} \text{ resp. } V(z=z_o,t) = C_o e^{i\alpha} e^{+2Dt} \quad (9a)$$

$$V(z=z^*,t) = (if/B)V_{go} + (if/N^*)C_g z^*, \quad (9b)$$

(where z^* is the depth of the ABL (1500 m) and $C_o e^{i\alpha}$ the horizontal wind vector in a given height z_o) we find following solutions in case of velocity divergence or convergence

$$V(z,t) = e^{-D(z^2-z_o^2)/2k} \cdot \{C_o e^{i\alpha} e^{-2Dt} - (if/B)V_{go} - (if/N^*)C_g z_o\} \cdot \left(1 - \frac{\int e^{Dz_o^2/2k}\,dz - \int e^{Dz^2/2k}\,dz}{\int e^{Dz_o^2/2k}\,dz - \int e^{Dz^{*2}/2k}\,dz}\right) +$$
$$+ (if/B)V_{go} + (if/N^*)C_g z$$

$$V(z,t) = e^{D(z^2-z_o^2)/2k} \cdot \{C_o e^{i\alpha} e^{+2Dt} - (if/B)V_{go} - (if/N^*)C_g z_o\} \cdot \left(1 - \frac{\int e^{-Dz_o^2/2k}\,dz - \int e^{-Dz^2/2k}\,dz}{\int e^{-Dz_o^2/2k}\,dz - \int e^{-Dz^{*2}/2k}\,dz}\right) + \quad (10)$$
$$+ (if/B)V_{go} + (if/N^*)C_g z\,.$$

Applying the Euler formula and separating the real from the imaginary part we get the components of the horizontal wind vector and can now compute hodographs or vertical wind profiles. Due to gain realistic profiles we choose $C_o = u^*/\ln(z_o/z_{oo}) + 0.2$ ms^{-1} (with z_o = 1 m, z_{oo} = 10 cm) and α=22.5° and become u(1) = 2.31 ms^{-1} and v(1) = 0.96 ms^{-1} for all simulations.

3. COMPUTED VERTICAL WIND PROFILES

On the basis of the derived analytical solutions we computed vertical wind profiles using a constant eddy diffusion coefficient k=10. In case of descending (ascending) air we obtained decreasing (increasing) wind speeds with increasing quantity of vertical velocity up to about 300 m (up to 500 m) and increasing (decreasing) wind speeds with increasing quantity of vertical velocity in the upper part of ABL (compare Fig. 1 and 2).This behaviour results from the noticable diminuation of the angle of deviation in the lower part of the ABL which is connected with an ageostrophic wind component in direction of the streamline. In the upper part of the ABL the influence of the velocity divergence dominates alone. Since velocity divergences are connected with an ageostrophic wind component perpendicular to the horizontal flow the v-component of the horizontal wind vector is markedly influenced. Thus, in case of velocity divergence (descending air) we get an ageostrophic wind component to the lower pressure and in case of velocity convergence (ascending air) a component to the higher pressure.

In a baroclinic ABL with a shear vector of -0.0025 s^{-1} a low-level wind maximum developes under nearly neutral stratification (k = 1.0 m^{2}s^{-1}). The maximum speed reaches 8.25 ms^{-1} at 550 m height for a given vertical velocity of -2.5 cms^{-1}. Less vertical velocities reduce the maximum speed. Thus, we get 8.0 ms^{-1} in 700 m and 7.7 ms^{-1} in 800 m if we choose vertical velocities of -1.5 or -1.0 cms^{-1} (see Fig.3). The angle of deviation normally reduces up to the height of the low level wind maximum and increases above it, because we have here a negative shear of the horizontal wind vector and hence an ageostrophic flow to the lower pressure. In case of ascending air a wind speed maximum exists also.The velocities are 4.7, 4.6 and 4.2 ms^{-1} in 400, 450 and 500 m height for vertical velocities of 1.5, 1.0 and 0.5 cms^{-1} (see Fig. 4). As expected, the angle of deviation rotates in all levels to right with respect to the height.

4. References

/1/ KLOZE, B.: Vlijanie vertikal'nogo dviženija i baroklinnosti na razvitie nočnogo strujnogo tečenija v pogranično sloe atmosfery. AN SSSR, FAO **24**(1988), 1134-1141.

/2/ KLOSE, B.: Ausgewählte Charakteristika der stabilen nächtlichen Grenzschicht. Meteorol. Rdsch. **44**(1991)1, 55-61.

/3/ **KLOSE, B.:** Empirische und theoretische Befunde zum Windregime in der nächtlichen Grenzschicht. Wiss. Z. Humboldt-Univ. Berlin, Math.-Nat. Reihe, **41**(1992)2, 107-115.

/4/ **KLOSE, B.; SJAROV, M**: Über den Einfluß strömungsparalleler und strömungssenkrechter Beschleunigungskomponenten auf die Ausbildung eines nächtlichen Low-Level Jets. Z. Meteorol **40**(1990)3, 211-217.

/5/ **SJAROV, M**: Zum Einfluß von Geschwindigkeitsdivergenz und Krümmungsvorticity auf die Entwicklung nächtlicher Windmaxima in der Planetarischen Grenzschicht. Dipl.arbeit, Humboldt-Univ. Berlin, 1989, 85 pp.

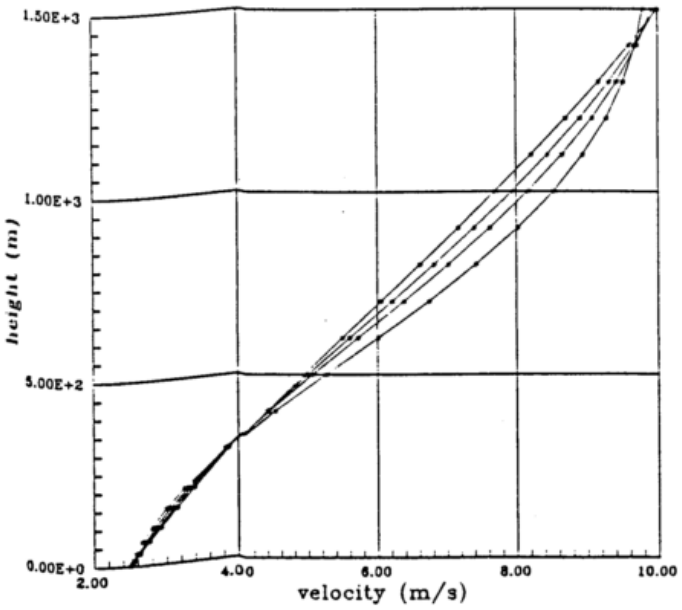

Figure 1: Vertical wind speed profile
(D>0; w = -0.5, -1.0, -1.5, -2.5 cms^{-1})

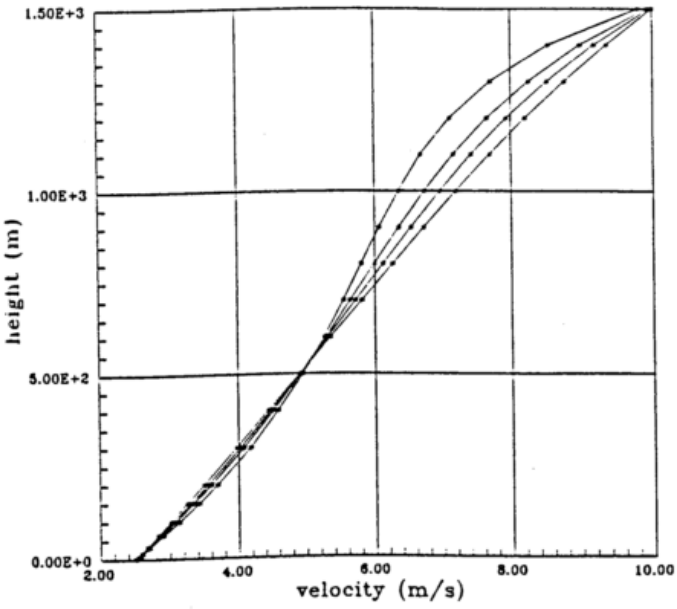

Figure 2: Vertical wind speed profile
(D<0; w = 0.5, 1.0, 1.5, 2.5 cms^{-1})

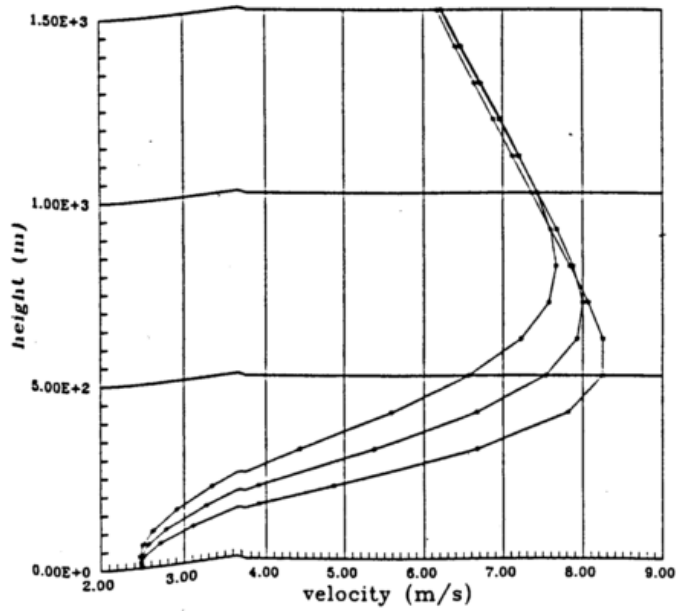

Figure 3: Low-level wind maximum
(baroclinic ABL; w = -1.0, -1.5, -2.5 cms^{-1})

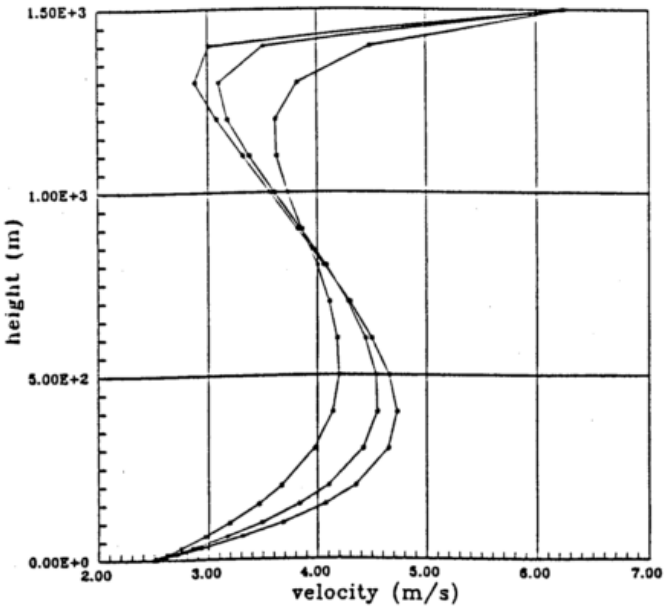

Figure 4: Low-level wind maximum
(baroclinic ABL; w = 1.0, 1.5, 2.5 cms^{-1})

The effective roughness length for orographically inhomogeneous terrain

S. Emeis

Institut für Meteorologie und Klimaforschung
Kernforschungszentrum Karlsruhe / Universität Karlsruhe
Postfach 3640, D-76021 Karlsruhe

ABSTRACT

Here form drag will be parameterized in terms of an effective roughness length. Firstly the dependence of form drag on the geometric parameters of the orography will be derived from a scaling of the equation of motion, and from numerical simulations with a mesoscale model. Then this dependence will be translated into a dependence of the effective roughness length on these parameters using the resistance law from Rossby-number similarity theory. We find that effective roughness length is mainly a function of the mean slope of the terrain, the size of the orographic structures, and the roughness of the surface. Finally the dependence of pressure drag on wind direction will be demonstrated for an area of 200 x 240 km^2.

1 Introduction

Orography influences considerably the lower boundary condition for the atmospheric (angular) momentum budget. In contrast to the heat or the moisture budget, the presence of obstacles in the flow adds an additional momentum flux to the momentum budget, the pressure drag. It can be divided in three different parts: form drag due to the viscosity of the air (here mainly turbulent viscosity), wave drag due to restoring forces (here mainly the atmospheric stratification), and hydrostatic drag due to blocking of colder air masses upstream of an obstacle.

In numerical models (climate models and prognostic models) the influence of orographic structures smaller than the grid distance must be parameterized. For wave drag and hydrostatic drag this task has been solved in the last ten years (BURRIDGE 1990).Therefore only form drag will be considered in the following.

2 Form drag as function of orographic parameters

We start with the first equation of motion (a 2D flow in the x-z-plane is considered here for simpicity). Applying the Boussinesq approximation, using the β-plane approximation, assuming stationarity, splitting the pressure p into a geostrophic basic state p_g and a ageostrophic deviation caused by an obstacle p_{ag}, and integrating over a control volume which includes the complete obstacle, we yield

$$\iint_{z\,x} \frac{\partial p_{ag}}{\partial x} dx dz = -\int_x \rho_0 u w_{oben} dx - \int_x \rho_0 (\overline{u'w'}_{oben} + u_*^2) dx + \iint_{z\,x} \rho_0 f_0 (v - v_0) dx dz + \\ + \iint_{z\,x} \rho_0 \frac{\partial f}{\partial y} v y dx dz \qquad (1)$$

u_* is the stress at the surface which is assumed to be unchanged by the pressure forces. The primes denote subgridscale fluctuations, the overbar indicates averages over one grid volume.

Scaling (1) (EMEIS 1990) and normalizing it with the kinetic energy of the undisturbed incident flow ($\frac{1}{2}U^2$), we get the pressure drag coefficient

$$C_W = \frac{H^2}{L^2}(-Fr \int u^* w^* dx^* - Re_t^{-2/3} \int \overline{u'^* w'^*} dx^* + Ro_o^{-1} \iint v^* - v_0^* dx^* dz^* +$$

$$+ Ro_p^{-1} \iint v^* y^* dx^* dz^*) \qquad (2)$$

Asterisks mark non-dimensional quantities. H/L is the mean slope of the obstacle (H is height and L is streamwise length scale of the obstacle), Fr is a Froude number (NL/U, N: Brunt-Väisälä frequency, U: velocity scale), Re_t is a turbulent Reynolds number (UL/ν_t, ν_t is the turbulent viscosity of air), Ro_o is a Rossby number (U/fL), and Ro_p is a planetary Rossby number ($U/\beta L^2$, β is the (constant) meridional gradient of the Coriolis parameter f). If the scaling was correct, the integrals over the non-dimensional velocities should be order of one.

Some more important parameters influence the pressure drag. In a 3D flow it becomes decisive whether the flow is deviated around the obstacles or across the obstacle. This is described by the parameter B/L (B: cross-wind length scale of the obstacle). The number of obstacles per unit area is important, therefore λ ($=nH/L_xL_y$, n: number of obstacles, L_x, L_y: horizontal extension of the domain with obstacles) must be taken into account. Finally the roughness of the surface influences the magnitude of pressure drag, therefore we have to consider the parameter Ro_s ($=U/fz_0$, z_0 roughness length).

Empirically from numerical simulations with KAMM2D (ADRIAN and FIEDLER 1991) we have for $0,3 \cdot L$ larger than δ and B/L larger than 10 for the pressure drag W_D

$$W_{D\,neutral} = 19,5\rho u_g^2 \left(\frac{H}{L}\right)^{2.17} Re_t^{-2/3} \left(1 + \frac{Re_t^{2/3}}{18Ro_o}\right) \left(1 + 0,15 \cdot \frac{10^5}{Ro_s}\right) f(\lambda) \qquad (3a)$$

For $0,3 \cdot L$ less than δ and B/L larger than 10 we have

$$W_{D\,neutral} = 19,5\rho u_g^2 \left(\frac{H}{L}\right)^{2.17} Re_{t\delta}^{-2/3} \left(1 + \frac{Re_{t\delta}^{2/3}}{18Ro_o}\right) \left(1 + 0,15 \cdot \frac{10^5}{Ro_s}\right)$$

$$\left(1 + \frac{C_D}{\kappa} \ln\left(\frac{0,3Lf}{\kappa u_*}\right)\right)^2 f(\lambda) \qquad (3b)$$

with $Re_{t\delta} = UL_m/\nu_t$ and $L_m = 700$ m empirically from numerical simulations.

3 Effective roughness length as function of orographic parameters

Form drag is physically equivalent to friction. Form drag comes from viscous forces which act on obstacles which are larger than the smallest resolvable scale, whereas friction acts on structures smaller than the smallest resolvable scale. Usually friction is parameterized by a roughness length or a friction velocity. Roughness length, friction velocity, and undisturbed (geostrophic) wind-speed are linked via a resistance law.

Because of this physical equivalence we will parameterize form drag by introducing an effective roughness length. The effective roughness length gives over homogeneous terrain the same downward momentum flux as it is observed over orographically inhomogeneous terrain (FIEDLER and PANOFSKY 1972).

Division of the resistance law with the effective quantities by the resistance law for the homogeneous Ekman layer gives (EMEIS 1987)

$$z_{0eff} = z_0 \cdot \frac{C_{Deff}}{C_D} \cdot e^{\sqrt{\frac{\kappa^2}{C_D^2} - B^2} - \sqrt{\frac{\kappa^2}{C_{Deff}^2} - B^2}} \qquad (4)$$

After inserting (3) into (4) we have plotted the effective roughness length as function of L/z_0 (Fig. 1) for a sine-shaped orography (here H/L and λ are linked by a fixed relation). From this figure we propose the following relations for the effective roughness length for $0.05 \leq H/L \leq 0.2$, $B/L \geq 10$, and $Ro_s \leq 10^8$ in order to parameterize form drag

- for $Ro_o \geq 100$:

$$\ln\left(\frac{z_{0eff}}{z_0}\right) = 0,57 \cdot \frac{H}{L} \cdot \ln^{1,8}\left(\frac{L}{z_0}\right) \tag{5a}$$

- for $Ro_o \leq 10$:

$$\ln\left(\frac{z_{0eff}}{z_0}\right) = 0,21 \cdot \frac{H}{L} \cdot \ln^{2,0}\left(\frac{L}{z_0}\right) \tag{5b}$$

4 Real orographies

Orography is directionally unisotropic. We have chosen an area of 200 km by 240 km including the Black Forest, the Vosges mountains, and the Swiss Jura in order to calculate the pressure drag as function of wind direction and wind speed. Wind data are from two years (1990 and 1991) of 12-hourly observations in 850 hPa from radiosonde ascents at Stuttgart. Using a cluster analysis 120 classes have been formed from this data (ADRIAN 1994, personal communication). Then 120 runs with the mesoscale model KAMM3D (ADRIAN and FIEDLER 1991) have been performed. The ICAO-standard atmosphere has been used to initialize the stratification for these model runs. Therefore the pressure drag form these simulations contains contributions from all three parts of the drag listed in the introduction.

The result is plotted in Fig. 2 which shows isolines of pressure drag (normalized with the whole simulation area) in Pa. The abszissa shows the u-component, the ordinate the v-component of the 850-hPa wind at Stuttgart for the 120 classes. We have relatively low drag values for winds from West, North-West, and East. For these directions channeling in the Rhine valley occurs. Higher drag values are found for 850-hPa winds from North and South. Here channeling is less and the surface airflow is crossing the mountains.

5 Acknowledgements

Parts of this study have been financed by the Deutsche Forschungsgemeinschaft via the Sonderforschungsbereich 210.

6 References

Adrian, G. and F. Fiedler, 1991: Simulation of Unstationary Wind and Temperature Fields over Complex Terrain and Comparison with Observations. *Beitr. Phys. Atmosph.*, **64**, *27-48.*

Burridge, D. M., 1990: New Results and Progress of the Model Development at ECMWF. *EGS XV General Assembly Copenhagen. Ann. Geophysicae,* **1990 Special issue,** *219.*

Emeis, S., 1987: Pressure Drag and Effective Roughness Length with Neutral Stratification. *Bound.-Lay. Meteorol.*, **39**, *379-401.*

Emeis, S., 1990: Pressure Drag of Obstacles in the Atmospheric Boundary Layer. *J. Appl. Meteorol.*, **29**, *461-476.*

Emeis, S., 1994: Bestimmung und Parametrisierung des Druckwiderstands an Hindernissen in der atmosphärischen Grenzschicht. *Habilitationsschrift, Fakultät für Physik, Universität Karlsruhe, 189 S.*

Fiedler, F. and H. A. Panofsky, 1972: The Geostrophic Drag Coefficient and the 'Effective' Roughness Length. *Quart. J. Roy. Meteorol. Soc.*, **98**, *213-220.*

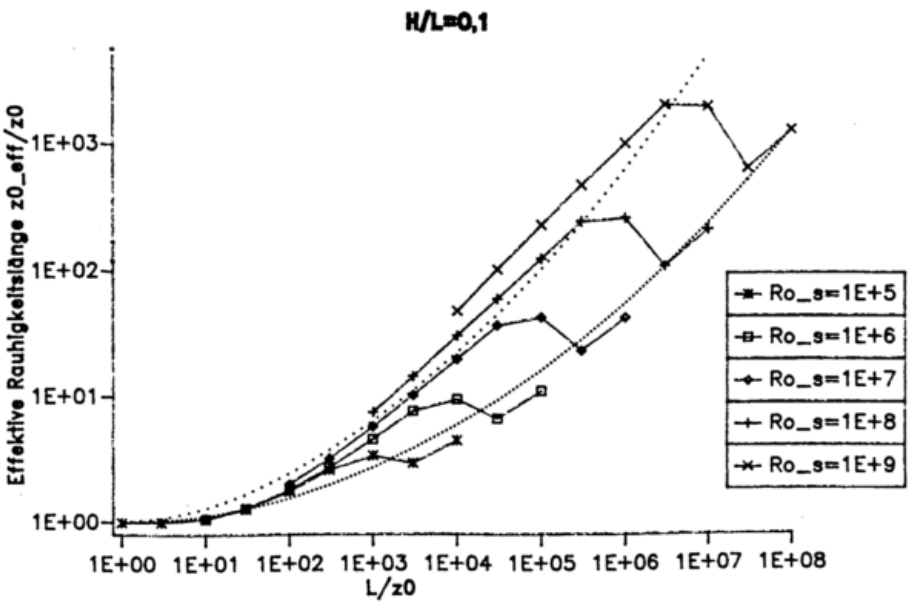
Normierte effektive Rauhigkeitslänge
H/L=0,1
Effektive Rauhigkeitslänge z0_eff/z0
1E+03
1E+02
1E+01
1E+00
1E+00 1E+01 1E+02 1E+03 1E+04 1E+05 1E+06 1E+07 1E+08
L/z0
Ro_s=1E+5
Ro_s=1E+6
Ro_s=1E+7
Ro_s=1E+8
Ro_s=1E+9

Fig. 1

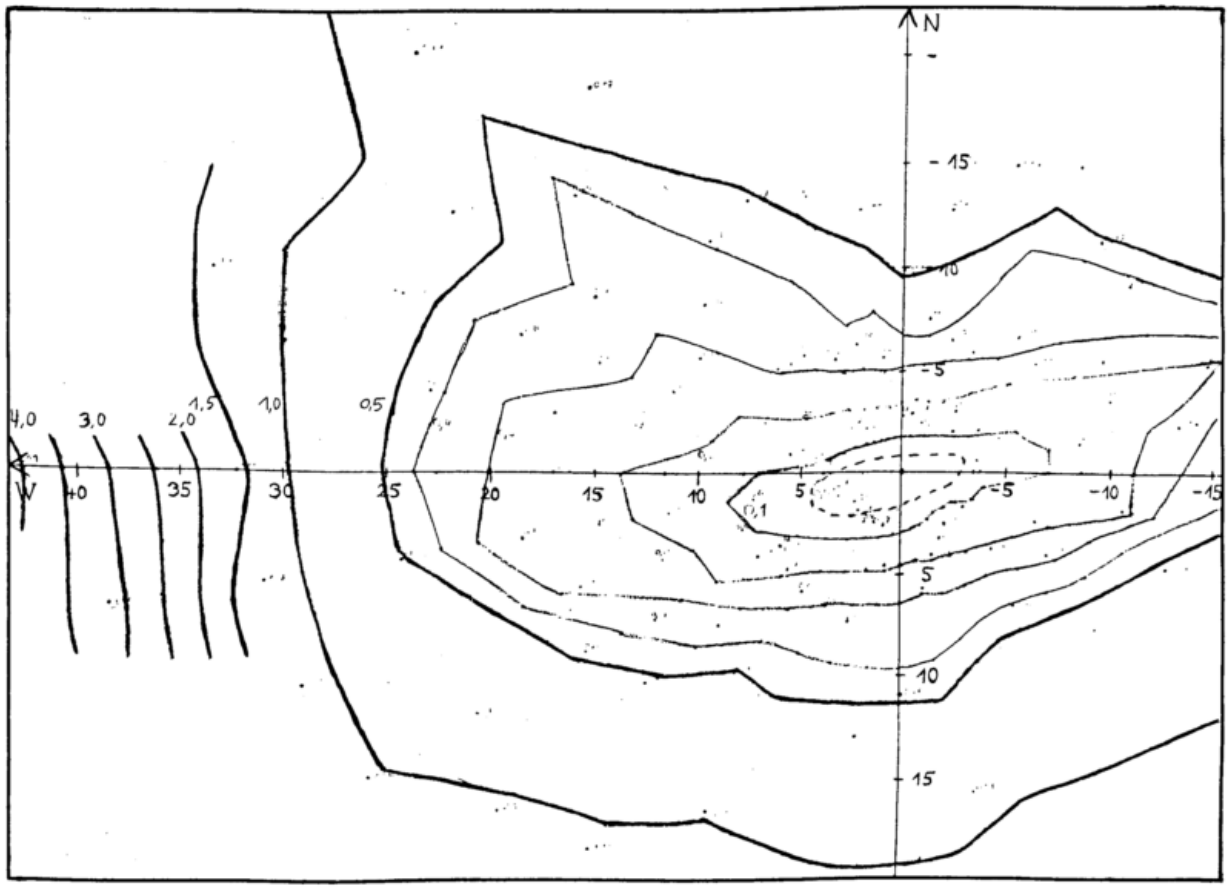
N
W
4,0
3,0
2,0
1,5
1,0
0,5
0,1
15
10
5
5
10
15
40
35
30
25
20
15
10
5
5
10
15

Fig. 2

The reliability of the wind field analysis

Jože Rakovec and Neva Pristov
University of Ljubljana, Department of Physics
and
Hydrometeorological Institute of Slovenia

ABSTRACT

Some test were done to see how variational analysis of wind can reconstruct wind field in a very hilly terrain, where due to rather scarce data unavoidable initial interpolation introduces a lot of error. This was done by omitting some ground measured data. The results were then compared with these omitted data.

1. Introduction

Variational analysis of wind is based on observed data and on some constraint; in our case the incompressibility strong constraint is applied. However, in a complicated mountainous terrain the wind is extremely unhomogenious and is in general not appropriately covered with measurements. With such scarce data the wind simulation relies mainly on the constraint and is only in some points supported by measurements. In a process of analysis are the measured data interpolated into each of the model points. This is the first (crucial!) step as regards the final result. We describe some results on this interpolation in Pristov and Rakovec (1994, this proceedings). Next steps are the process of consecutive approaching to the desired incompressibility (steps in numerical process of relaxation). But better incompressibility (smaller remaining divergence) does not necessarily mean also closer fit to the data - in principle is final result is a compromise between the observations and the incompressibility (in our case strong constraint). An ensemble of numerical experiments has been done to obtain a measure of the quality of analysis and in each of these experiments one measurement was omitted from the set of the initial data and then the simulated vector compared with the measured wind vector in that point.

2. Approach to the incompressibility

In a functional, which is formed in a process of variational analysis with strong constraint, with Lagrange multiplicator λ for incompressibility (Sasaki 1970, Daley 1991), and in a correspondent differential equation, which follows from the minimisation of that functional, horizontal and vertical components of velocity can (and should) have different weights; α for horizontal, and μ for vertical velocity.

Initial wind (u, v, w) is observed in only few points, and in all other points without measurements it is interpolated; in lack of information we are often forced to put $w = 0$ initially. The final wind velocity U, V, W is then computed from the equation

(here we write only discrete form of equation for U component, the ones for V and W are similar):

$$U_{i,j,k} = u_{i,j,k} + (1/2\alpha\Delta x)(\lambda_{i+1,j,k} - \lambda_{i,j,k})$$

When approaching to the nondivergent field we can prescribe to stop the process when e.g. the difference $\Delta\lambda$ between the values of λ in the two consecutive relaxation steps differ for less than e.g. ϵ (we can choose maximum difference, or average difference, etc.). As regards the remaining divergence in the wind field this means that not only the value of ϵ, but also the applied ratio α/μ, the magnitude of α, and the grid distance Δx influence the remaining divergence $|divU|$:

$$\Delta|divU| \approx .(1/\alpha)(\Delta|\nabla^2\lambda|) \leq \epsilon$$

3. Test on the case on Jan. 29, 1994

We tested the approach to incompressibility on the case for high mountains area on the border between Slovenia and Austria (part of Karavanke mountains and Kamnik/Savinja Alps, Fig. 1).

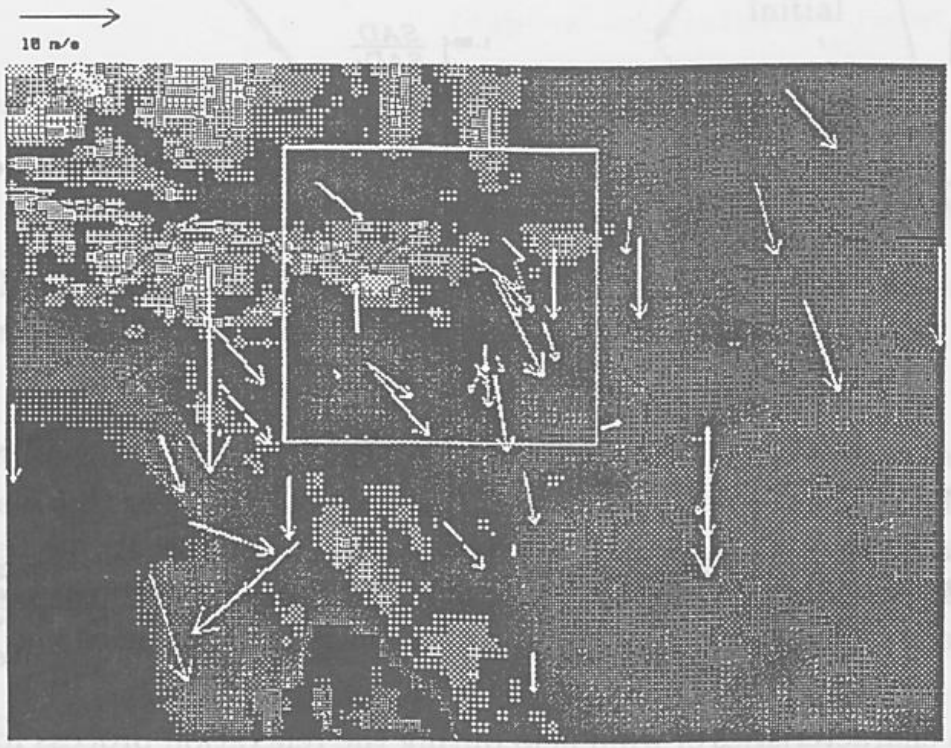

Figure 1: The broader area and the test area of the model, with observed wind vectors at the ground

The size of the area is approx. $100kmx100km$, sub-mountain areas are approx. $300m$ above m.s.l. and highest peaks have $2500m$. Our model goes up to the height

of $5000m$. There are $32x28x18$ grid points with $\Delta x = 3200m, \Delta y = 3470m$, while Δz varies from $50m$ at sea level to $720m$ in the uppermost model layer. For the results shown on Fig. 2 are applied values of $\alpha = 0.01$ and of $\mu = 1$ or 10 or 100.

The case of Jan. 29, 1994 was the case of relatively strong, mostly northern wind (one must take into account that $7m/s$ as in this day, is for the area in a lee of the Alps already strong wind - average January velocity for Ljubljana in a basin is $1.0m/s$ and for the $2515m$ high observatory Kredarica also only $7.3m/s$).

Figure 2 (left) shows that the value of α/μ (grater value of this ratio means that adjustment of vertical velocity is stronger) results also in stronger vertical winds - when w is allowed to take greater part in elimination of divergence it also becomes greater. What is here interesting, and different to the cases of idealised hill shapes, is shown on Fig. 2 (right). This figure shows the sum of absolute divergences SAD in all grid points, relative to the same sum at the beginning of the relaxation SAD_0. It is clear that in this test for the realistic relief the different values of $\alpha/\mu = 0.01, 0.001, 0.0001$ have only small influence on the convergence of relaxation. This result for real terrain is very different from the cases with idealised mountains (e.g. axis-symmetrical hill)! With idealised hills the convergence is namely in general much quicker if α/μ is greater (what means that the possibility of adjusting vertical velocity helps a lot to incompressibility in idealistic, symmetrical, and not so much in real relief).

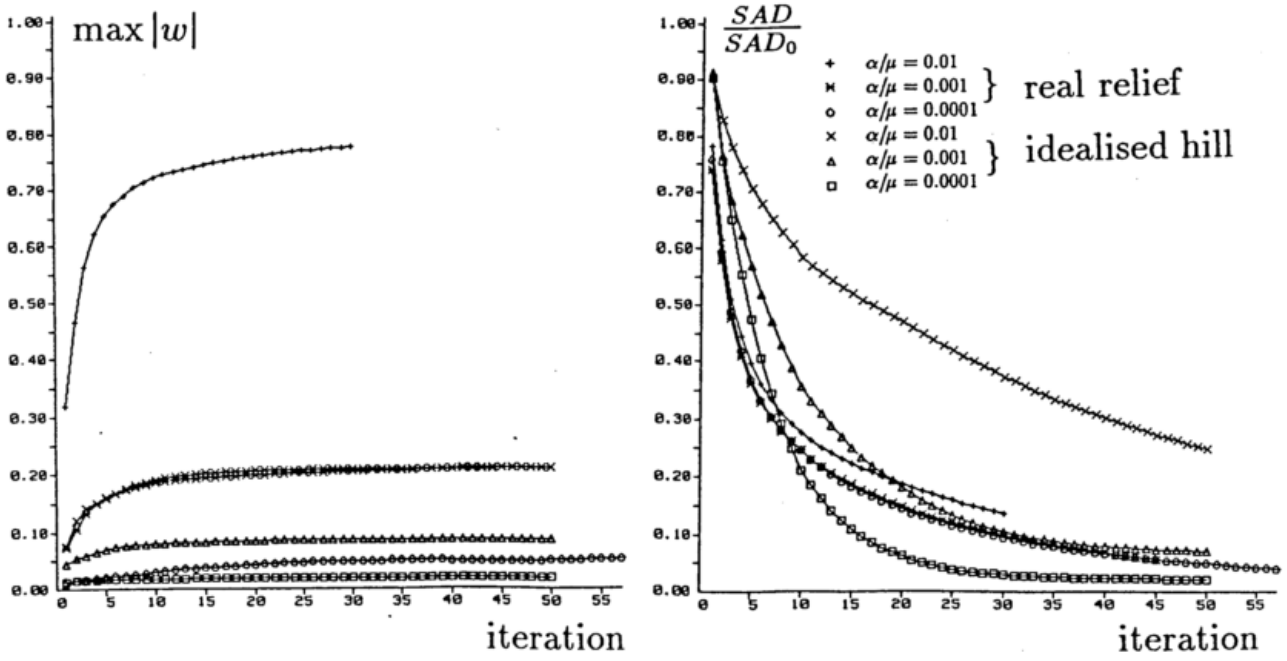

Figure 2: Two characteristics of wind field during the relaxation process for idealised and for real relief for $\alpha/\mu = 0.01, 0.001, 0.0001$: left - maximum absolute vertical velocity $max|w|$, right - summ of absolute values of divergences (relative to the initial value) $\frac{SAD}{SAD_0}$

Small remaining divergence does not necessarily mean that also the wind field is reconstructed realistically. The main weakness of the method is initial interpolation

into grid points close to the ground; the grid points at upper levels suffer less from the initial interpolation.

How the wind can be reconstructed after unavoidable interpolation by using variational analysis is presented here only for two particular stations:

- for one case of the station in a basin (measured $3m/s$ from $320deg$) and with relatively well interpolated initial data from three stations (one of them on the top of the mountain with $10.8m/s$ from 333, two in a basin: 4.3 from 316, and $5.4m/s$ from $331deg$).

- and one case of the station on the top of the mountain (measured $8m/s$ from $350deg$), and with rather bad initial interpolation (all three stations are also on hills, but only one measured strong wind:$6.6m/s$ from $356deg$, while the other two measured low wind from different directions: 3.3 from 27, and $2.0m/s$ from $110deg$).

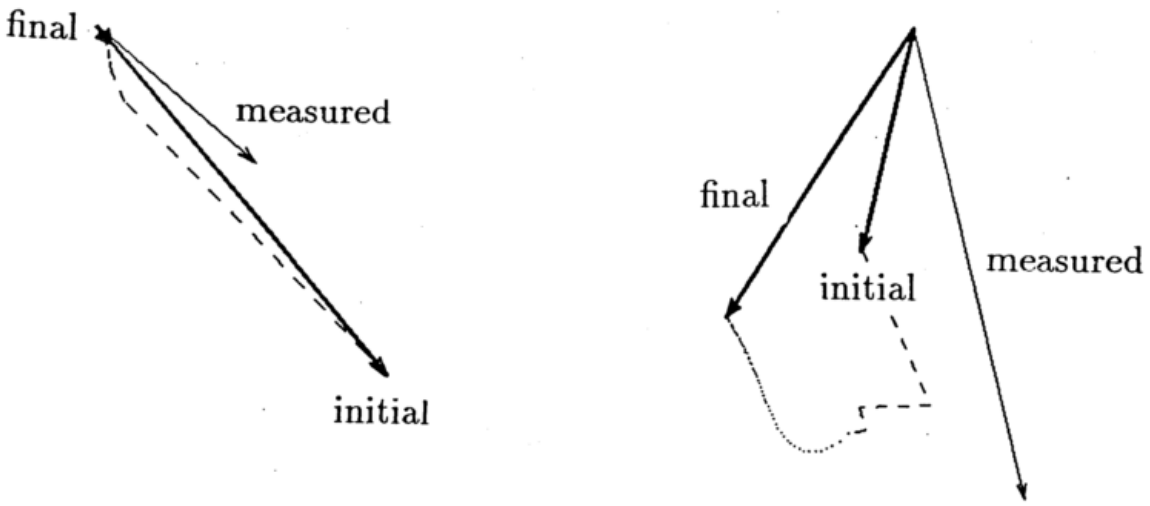

Figure 3: The development from the initial, interpolated wind vector to the final wind vector: left - for a station in a basin, right - for a station at the hill; thin line - measured

Figure 3 shows the approach from the (not very successfully) interpolated values to the final (relaxed) value. It is obvious that the measured wind is not reconstructed well: in one case already the interpolation was bad. But even in a case of relatively good interpolation the incompressibility constraint forces the wind to change from that initial one to some other wind, which responds better to the constraint.

References

Sasaki, Y, 1970: Some basic formalisms in numerical variational analysis. Mon. Weath. Rev. 98, 875-883.

Daley, R, 1991: Atmospheric data analysis. Cambridge Univ. press, Cambridge etc. xiv + 457 pp.

Modification of wind stream in Poprad basin due to High Tatra's Massif

M.Chmelík, P.Nejedlík, P.Šťastný
Slovak Hydrometeorological Institute, Bratislava

Abstract

The paper deals with relationship between the upper wind and wind conditions within the boundary layer. The data of one aerological and three ground stations situated on the bottom of Poprad basin and south slopes of High Tatras were used for describing the influence of Tatra massif on the airflow. The three pressure levels 850, 700 and 500 hPa were taken into consideration. The influence of 500 hPa presure level on surface wind isn't expressed strongly enough, so as the 700 hPa pressure level was chosen as a level at which the wind data were compared to ground stations. Statistical outputs have showed the decline, the rise of some directions, respectively according to the ground location and also good developed local circulation, as well.

Introduction

High Tatras is the highest range of mountains in Slovakia. 30 km long ridge that follows approximately W - E direction reaches about 2300 m a.s.l. It largely influences the wind conditions on the bottom of the southward Poprad basin. The prevailing west to the north-west air streaming in free atmosphere is turned to basin axis in general. The thermal and deformational factor of airflow depends strongly on the position within the basin. The local circulation is well expressed due to relatively large area of southern faced slopes and 1300 m ridge rise over the basin. See fig. 1.

Methodics

The data of the three ground stations were calculated to investigate wind deformation. Štrbské Pleso is situated on the southern slope of High Tatras. Poprad and Gánovce are placed on the basin bottom. The aerological station is under work in Gánovce.

Fig. 1. Localization of High Tatra's and Poprad basin region

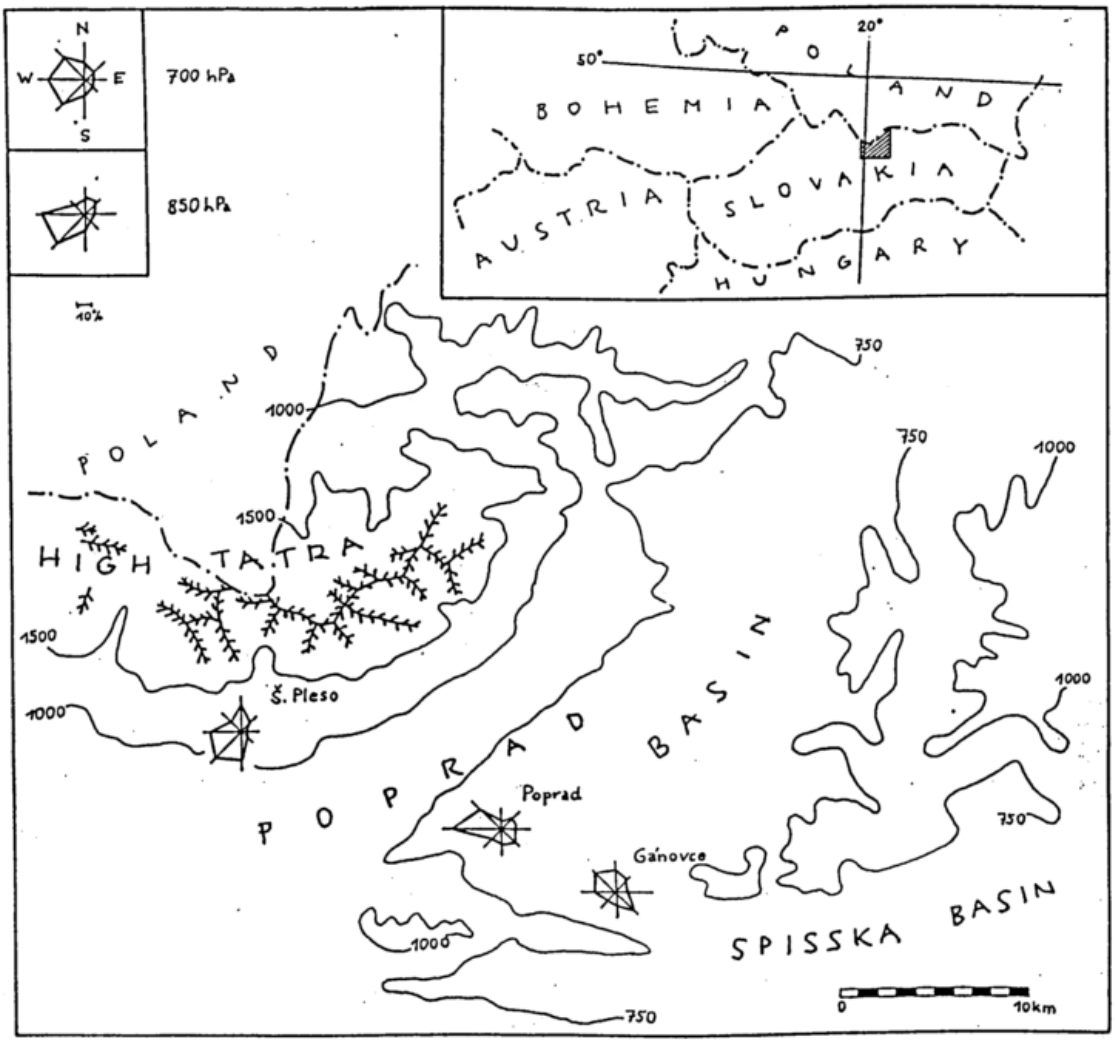

Tab. 1 Data of anemographics stations

Station	λ	φ	h[m]	Location	Ridge dist.
Štrbské Pleso	20° 04' 00"	49° 07' 18"	1330	south slope	5 km
Poprad	20° 14' 44"	49° 04' 08"	695	basin bottom	15 km
Gánovce	20° 19' 27"	49° 02' 06"	703	basin edge	20 km

The wind data sets of the ground stations involve hourly wind direction and mean wind speed. The aerological sets consist of 00°° and 12°° GMT data approximately up to 35 km level. The intersection of these sets gives the possibility to investigate midday and midnight hour of observation. The three levels, 850 hPa, 700 hPa and 500 hPa were compared to ground data in the period 1981-90.

To find out relationship between upper and ground layer wind field it was necessary to neglect the local mountain - valley breezes and slope wind within the basin. 500 hPa level wind hasn't shown any meaningful influence on the surface wind. This was much better expressed at 700 hPa level that is about 800 m above the mean ridge height. 850 hPa level is practically inside the basin and wind

stream follows more closely the basin axes. It was found out that the local circulation is strongly enough restrained at 60 km/h wind speed at 700 hPa level. According to this criterion the wind roses were drawn for all stations and 700 and 850 hPa levels at 00°° and 12°° GMT term. See fig.2.

Fig.2. Wind roses distribution within the investigated area

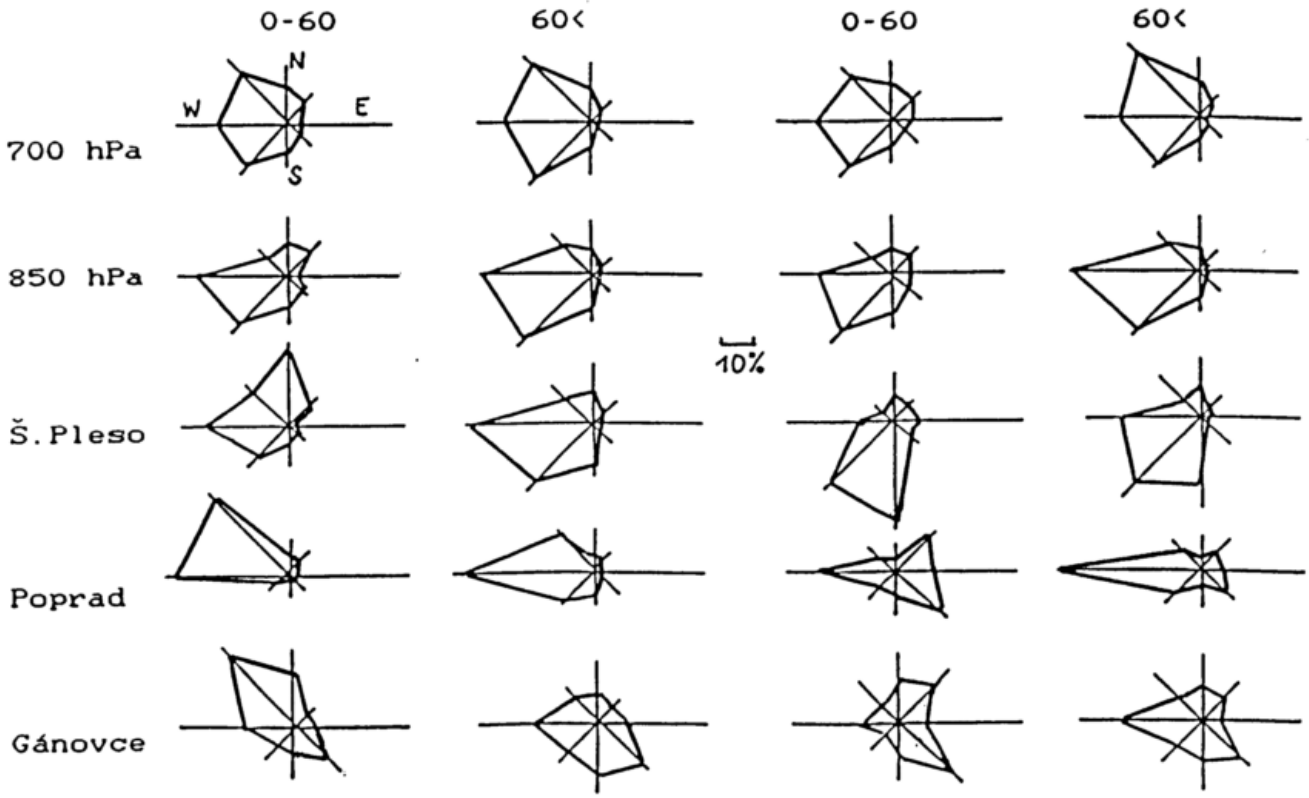

There wasn't recognized any influence of local circulation on wind direction changes at 700 hPa level that exceeds the High Tatra's ridge over 700 m. The frequency of the wind speed over 60 km/h is only about 14 %. The wind rose over this wind speed border doesn't almost differ to the wind rose without speed restriction. 850 hPa level is situated around the halfway between the basin bottom and the ridge. The frequency of prevailing west wind components that are parallel to the basin axis is in arise.

"Wind roses at Štrbské Pleso station illustrate the south slopes circulation. We can see mountain-valley breezes at low wind speed at 700 hPa pressure level at first. The north direction frequency reaches 26 % and is equal to general prevailing west direction. The most frequent midday direction is the south one, 32 %. The anabatic wind frequency even surpasses the valley wind which is supported by global streaming. Under high wind speed at upper level the wind

rose at Štrbské Pleso is characterized by big dispersion of prevailing wind directions from south to the west. The orography impact is not expressed so clearly, of course.
Central part of the basin bottom has got narrow wind rose that precisely follows west-east axis of the basin, see Poprad station. At wind speed over 60 km/h at 700hPa pressure level the frequencies of the directions perpendicular to prevailing west direction are restrained. The katabatic air stream running down the south slopes at low wind speed at the upper level during the night turns and step by step follows the basin axis, W=35%, NW=32%. At midday term the east components exceeds the west. That is also caused by anabatic wind stream towards the south slopes.
Gánovce station is located at south-east edge of the basin and is the most distanced from the Tatra's ridge. Prevailing NW and SE directions claim the air mass exchange between Poprad basin and neighbouring Spišská basin. This is expressed through the whole wind speed spectrum. This is the evidence of a nonhomogenity of the bottom wind regime.

Conclusion

The analyze of wind conditions in Poprad basin in relationship to upper level air streaming has showed an increased role of mountain- valley breezes up to the 60 km/h wind speed at 700 hPa pressure level. The thermal compounds of ground air stream at midday term are different from prevailing wind direction. This fact stresses the intensity of anabatic airflow at south slopes of High Tatra's. When the wind speed at 700 hPa pressure level is over 60 km/h there isn't any remarkable difference between midday and midnight wind stream. The impact of Tatra's massif certainly drops down according to the distance from the massif ridge. There is a relevant influence of eastward situated Spišská basin on the wind regime in south-east part of Poprad basin and points out on the air mass exchange between these basins.

Literature:

Chmelík, M.: Aeroclimatics characteristics on Poprad station SHMU, Bratislava, 1987

Nejedlík, P., Šťastný, P.: The influence of Carphatian ridge on the airflow in East-Slovak region, Proceedings from 16th International Conference on Carpathian Meteorlogy, Smolenice, Bratislava, 1993 p.46-53.

VORTICITY DIAGNOSTICS OF SEVERE BORA CASES

Branka IVANČAN-PICEK and Vlasta TUTIŠ

Meteorological and Hydrological Service, Zagreb, Croatia

ABSTRACT

Mesoscale conditions influencing the severe downslope Adriatic wind bora are investigated. The results of isentropic vorticity diagnostics of recent, unusually severe bora (26/29 March 1993) along the entire Croatian Adriatic coast, give us a proof for two different origins of the bora flow. The ageostrophic motions were dominant only along the middle and south Adriatic coast. The conversion term U<0 confirms the goestrophic origin of the severe bora along the northern Adriatic.

1. INTRODUCTION

Detailed investigation of vorticity and divergence dynamics during the severe downslope wind bora periods may improve our understanding of this mesoscale process. It has been shown that bora can occur under a wide range of conditions, but a supply of low level cold air on the windward side is necessary for its occurrence. Wind turning or reversal aloft is a common, but not an essential feature.
We present here the results of isentropic vorticity diagnostics on selected isentropic levels of the recent, unusually severe bora (26/29 March 1993) which caused a lot of damage and complete traffic disturbance along the entire Croatian Adriatic coast. Such severe bora (maximum gust observed in Split: 36.6 m/s) was primarily caused by the strong cyclone centered over the southern Adriatic (Ivančan-Picek and Tutiš, 1994). The cyclone vortex was well developed throughout the whole troposphere, but the flow reversal at a height of 3-4 km unambiguosuly defined the "bora layer" upwind of the Dinaric Alps.

2. ISENTROPIC VORTICITY DIAGNOSTICS

In this paper, conventional synoptic studies have been performed with detailed investigation of vorticity and divergence dynamics during severe bora periods. To get more to the insight of governing dynamical processes and to consider the severe bora from several points of view, it is convenient to have a look at the derived quantities on selected levels (eg. potential vorticity, conversion terms).
The vorticity diagnostics may be used for possible dynamical mechanisms which can create conditions for a hydraulic flow and severe wind.
In the isentropic coordinate system the vorticity equation for frictionless adiabatic motions becomes very simple (Lanzinger, Pichler and Steinacker, 1991):

$$\frac{\partial h}{\partial t} + \nabla_\theta \cdot \left(\eta V_h\right) = 0 \qquad (1)$$

i.e. the absolute vorticity is sourceless in such a frame.

The term U

$$U = -\left[K_t V \frac{\partial V}{\partial s} + \frac{\partial}{\partial n}\left(\frac{\partial M}{\partial s}\right)\right] \qquad (2)$$

indicates the conversion rate from shear into curvature vorticity (U > 0), where K_t= curvature of trajectory, projected horizontally, and M = Montgomery potential. It can be easily examined, that conversion represents an ageostrophic effect. In case of geostrophic equilibrium, hence, no interaction between shear and curvature can take place.

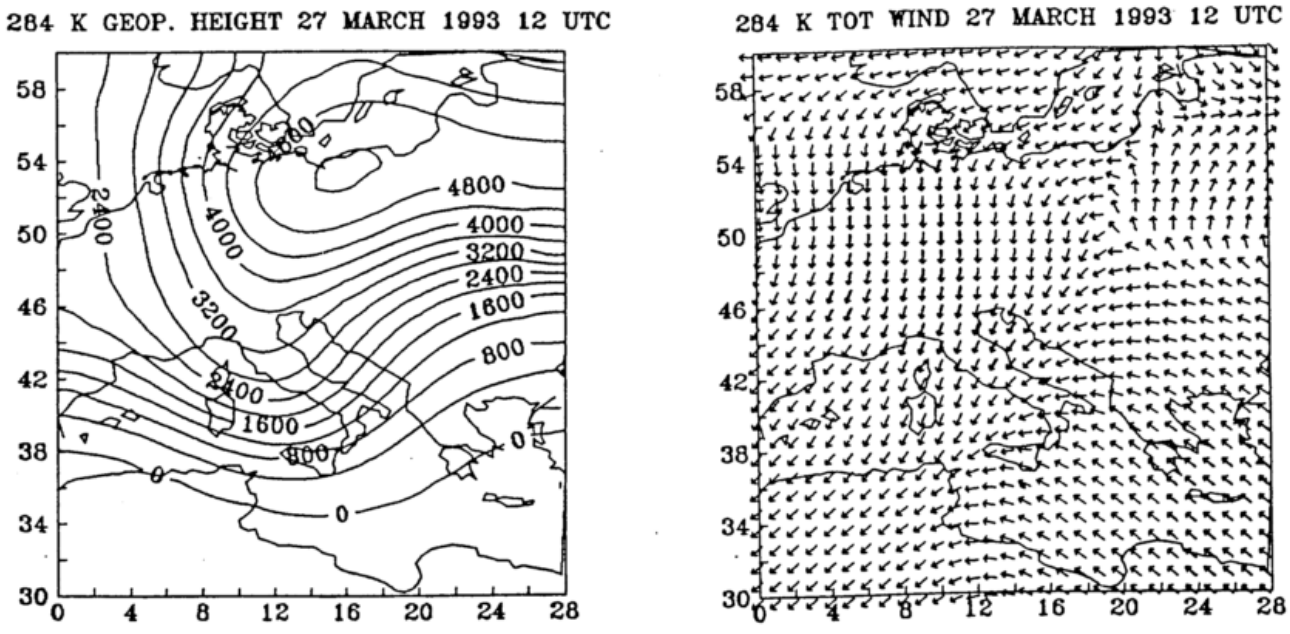

Fig. 1: Geopotential height and wind field on 284 K level, 27 March 1993, 12 UTC.

Here we present the results of isentropic vorticity diagnostics on 284 K level (Fig.1). A strong lowering of 284 K surface from the northern to southern part of Europe is evident, with strong gradients in the geopotential field over the Dinaric Alps.
The wind field at 284 K surface is plotted in Fig.1. We clearly see that the cold air supplying bora flow originates also partly in NW, so when the air goes around the Alps it gains eastern component, appearing to be NE wind at the windward side of the Dinaric Alps.
Over the southern Adriatic the cyclonic vorticity and strong convergence remain in the wind field during the existence of cyclonic activity (Fig.2).

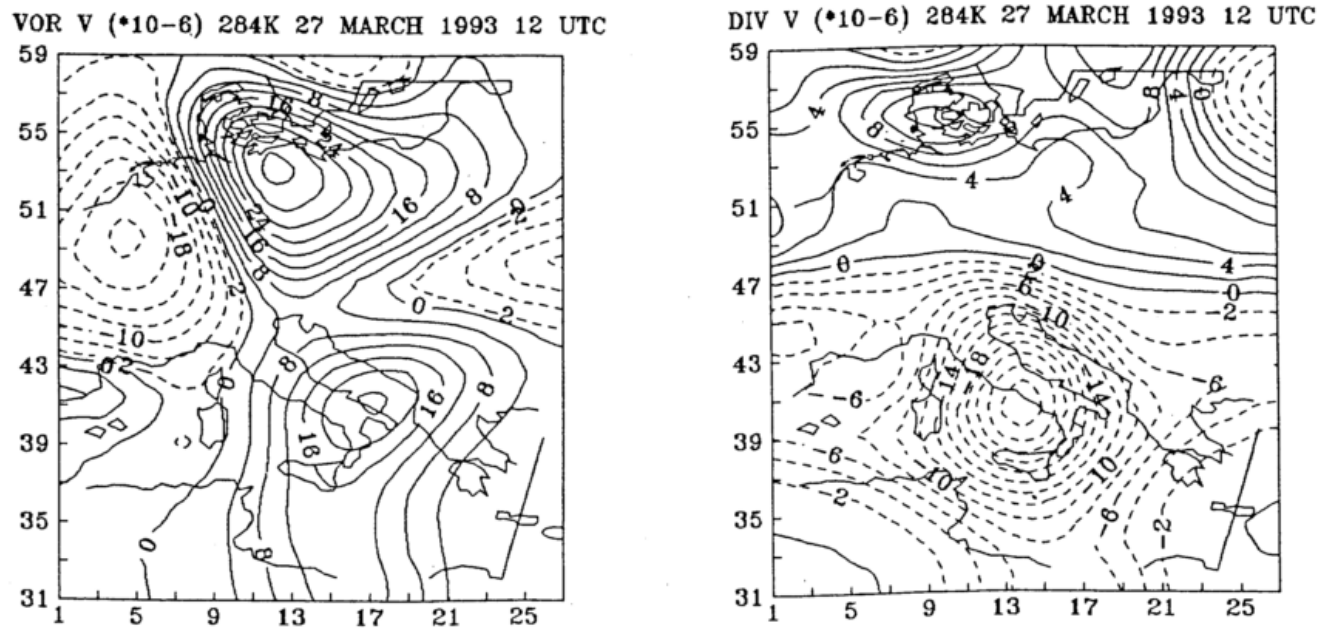

Fig. 2: Vorticity and divergence fields on 284 K level, 27 March 1993, 12 UTC.

Several diagnostic case-studies indicated that the cold air supply in the surface "bora layer" on the windward side of the Dinaric Alps is accompanied by high positive values of potential vorticity. The isentropic potential vorticity (IPV) is a product of absolute vorticity and static stability and it is also a conservative property of air particles (assuming adiabatic processes). IPV maxima at lower levels (284 - 296 K) correspond to the cold air northerly of the Alps (Fig.3).

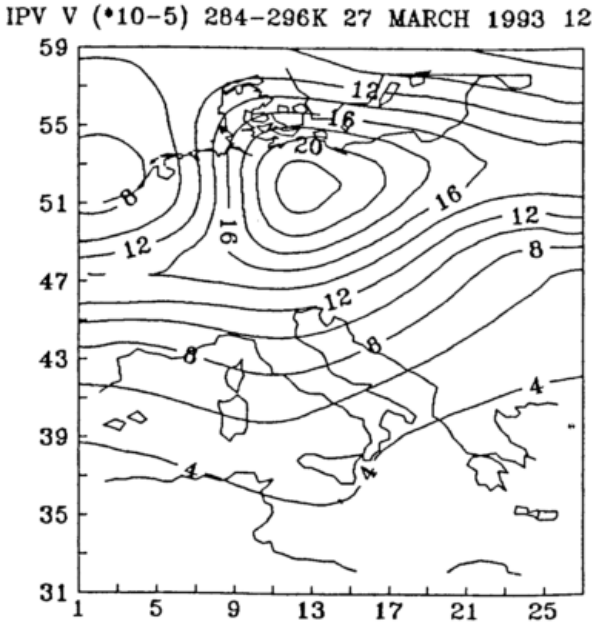

Fig. 3: Isentropic potential vorticity in the layer 284 - 296 K, 27 March 1993, 12 UTC.

Near the center of the cyclone the conversion term U (Lanzinger,Pichler and Steinacker,1991) usually acts as a damping mechanism for the growth of curvature. The magnitude of conversion term occasionally approaches the magnitude of the advection and divergence term of curvature vorticity and hence it cannot be neglected. The magnitudes of the conversion term are very similar with maximum values (U>0) near the center of the cyclone (Fig.4), so we may conclude, that for the particular severe bora case, the ageostrophic motions were significant only along the middle and the south Adriatic coast. However, over the Alps, western part of Croatia and the bora region along the northern Adriatic coast, the conversion term is in the same time U<0 (due to the conversion from curvature to shear vorticity)g and small enough to indicate the geostrophic origin of the severe bora in that case or a weak ageostrophy.

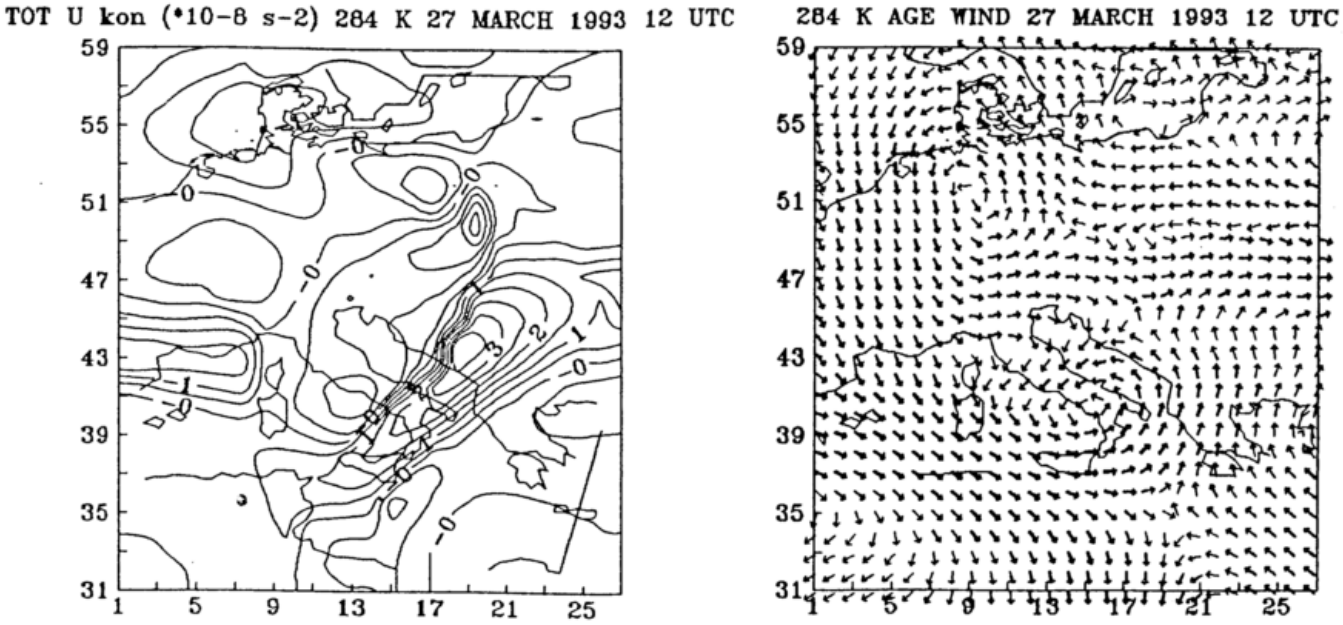

Fig. 4: Conversion term U and ageostrophic wind on 284 K level, 27 March 1993, 12 UTC.

3. CONCLUSION

The investigation of dynamic and kinematic properties of the atmosphere indicates different physical origins for the severe bora on the Northern Adriatic and the severe bora in Dalmatia, which is more evident by the observation of the frequency and duration than of the intensity of the maximum wind speed.

The maximum values of U (U>0) are observed near the center of the cyclone so we may conclude, that ageostrophic motions due to the conversion from shear to curvature vorticity are prevailing over the south Adriatic, while small negative values of the conversion term confirm the prevailing geostrophic environment of the severe bora over the northern Adriatic.

REFERENCES

IVANČAN-PICEK,B.,V.TUTIŠ 1994: Severe bora 26-29 March 1993. Extraordinary Meteorological and Hydrological Events in Croatia in 1993.

LANZINGER,A.,H.PICHLER,R.STEINACKER, 1991: ALPEX-Atlas; Case studies of ALPEX-SOP cyclones in the western Mediterranean. Osterreichische Beitrage zu Meteorologie und Geophysik, Heft 4, Zentralanstalt fur Meteorologie und Geodynamik, Wien, 234 pp.

Impact of height and shape of the orography to local bora wind

Lazar Lazić and Ivana Saulačić
Department of Meteorology, Faculty of Physics
University of Belgrade, Yugoslavia

1. Introduction

Bora is local, cold, strong, northerly or north-easterly wind over Adriatic coast. It is caused by a very cold air outbreak in a deep upper tropospheric trough which usually develops into a cut-off low in the Mediterranean. This process is often accompained by a cut-off high in the northeastern Atlantic. Such a blocking type circulation prevents the wormer air from the Atlantic to invade the European continent which is occupied by a broad cold surface anticyclone. The latter builds up a large pressure gradient toward the Mediterranean cyclone which is particularly strong at the northern Adriatic coast (Jurčec, 1989). The essential ingredients of bora are thermal stratification of the incoming cold air, vertical wind structure above the upstream bora layer and terrain configuration.

Numerical simulations of the local bora wind are still based on extremely simple atmospheric structure of 2-D models in comparison with the real atmosphere. Spatial and temporal variations of bora speed and gusts along the Adriatic coast can simulate only by 3-D models.

In this paper, numerical simulations for a case of bora wind based on observed data by the Eta Model are performed, in order to assess the state-of-the-art model performance in simulating bora with eta mountain representation. This model has shown excellent capabilities for simulation of mountain-induced phenomena. The impact of height and shape to the local bora wind are studied by calculation of forward trajectory over different height of step eta mountains in the region with impact to bora. The latter implies different shape, which comes from the eta coordinate definition.

2. Model summary

The model used for simulation of this case is a limited area primitive equation model with step-mountain coordinate, so-called Eta Model. The vertical coordinate η (Mesinger, 1984) is defined as

$$\eta = \frac{p - p_T}{p_S - p_T}\eta_S, \tag{1}$$

with

$$\eta_S = \frac{p_{rf}(z_S) - p_T}{p_{rf}(0) - p_T}. \tag{2}$$

Here p_T and p_S are the top and the surface pressure, respectively, z is geometric height and $p_{rf}(z)$ is a suitably defined reference pressure as a function of z. The ground surface heights z_S are permitted to take only a discrete set of values, chosen so that mountains are constructed from the three dimensional grid boxes in the model. The velocity components normal to the sides of mountains are set to zero.

The U.S. NAVY high resolution (10′ x 10′) orography dataset, provided by NCAR, was used to compute mountains. Heights of the mountains were obtained by averaging over group of four neighbouring model points and were subsequently rounded-off to the nearest reference interface elevation.

The model uses the semi-staggered (E) grid; the technique preventing grid separation is combined with split explicit time differencing; the horizontal advection has a built-in nonlinear energy cascade control; and the internal boundary conditions at the sides of the step-mountains preserve all major properties of horizontal advection. A more detailed description of the dynamical part of the model can be found in Mesinger et al. (1988).

The physics package of the model includes the Mellor-Yamada level 2.5 planetary boundary layer and Mellor-Yamada level 2 "surface" layer; large scale precipitation, convective parameterization based on the Betts and Miller scheme; surface flux of sensible and latent heat; and radiative processes. The

model physics package has been described in more detail by Janjić (1990, 1994).

The horizontal resolution used for the experiments was 0.25° x 0.25° (20 km x 20 km) with 16 layers in the vertical. The model horizontal domain was defined between 0° to 30° E and from 40° N to 50° N.

Time-dependent lateral boundary values are taken from ECMWF (European Centre for Medium-Range Weather Forecasts) analyses, linearly interpolated between analysed fields available at 6 h intervals. The boundary grid points of the outermost row affected by this forcing extend inwards to affect the next row. The integration domain of the model excludes these two outermost rows. The second row within the outer boundary is a blend (four-point space interpolation) of the outer row and the third row inside which is included in the integration.

3. Trajectory calculations

Trajectories are defined as the paths followed by air parcel with time. They are calculated from simulated wind fields, with both horizontal and vertical wind components, derived from the Eta Model. Trajectories can be calculated forward and backward in time. Forward trajectories are calculated by specifying initial parcel locations and time and then tracing the parcels with increasing time to determine their final positions. Backward trajectories are calculated by specifying final parcel locations and time and than tracing the parcels with decreasing time to ascertain their origins. Forward trajectories are calculated within the Eta Model itself, using wind components from every time step.

Horizontal wind components (u,v) from the Eta Model are defined on a latitude-longitude (λ, φ) grid, and vertical component of motion is $\dot{\eta} = d\eta/dt$ defined on each eta surface of the model. For a given position and time, the new location for an integration of one time step (Δt=90 s in this study) was accomplished by a two-step approach. To derive the needed wind components at a given position, bilinear horizontal and linear vertical interpolation are performed. First, bilinear interpolation is performed horizontally on the two η model levels that bracket the trajectory position in the vertical. Then, linear vertical interpolation is done on the two horizontally interpolated values to obtain the wind component at the parcel's current position. This process gives the interpolated wind components at the current trajectory position. This interpolation is done for all three wind components. Using these interpolated wind components $(u_1, v_1, \dot{\eta}_1)$, a first guess of the new position $(\lambda_1, \varphi_1, \eta_1)$ for the parcel was obtained. A new set of wind components $(u_2, v_2, \dot{\eta}_2)$ in the second-step approach was than calculated in the same manner for this new location. The final displacement was calculated using the average of the two sets of wind components:

$$\lambda^{\tau+1} = \lambda^{\tau} + \frac{(u_1 + u_2)}{2} \Delta t \frac{180/\pi}{R \cos((\varphi_1{}^{\tau+1} + \varphi^{\tau})/2)}, \tag{3}$$

$$\varphi^{\tau+1} = \varphi^{\tau} + \frac{(v_1 + v_2)}{2} \Delta t \frac{180/\pi}{R}, \tag{4}$$

$$\eta^{\tau+1} = \eta^{\tau} + \frac{(\dot{\eta}_1 + \dot{\eta}_2)}{2} \Delta t, \tag{5}$$

where τ is time level, R is mean radius of the earth, the $180/\pi$ factor is needed to convert (λ, φ) from radians to degrees. This procedure is repeated until the desired final time is reached.

4. Results

From 0000 UTC 01 December to 0000 UTC 03 December 1990, a typical bora case was occurred over Adriatic coast in synoptic case, as explained above. The numerical simulation by the Eta Model starts at 0000 UTC 01 December with ECMWF analysis as the initial condition.

To study impact of heights and shape of mountains to bora wind in these numerical experiments, mountains are varied only over region with significant orography influence to bora wind. For that reason

we introduced "bora masks", with values equal 1 inside, and 0 outside the bora region. Orography in the bora region used in the experiments in this study was: 0%, 25%, 50%, 100%, 150% and 200% of real (standard, control) models orography. By varying the heights of orography, shape of mountains are changed automatically (from definition of eta coordinate (1) and (2)).

The 48 h Eta Model based 3-D trajectories are calculated forward, from a given initial horizontal position (20°E, 47°N) and from the lowest eight model levels in the vertical. Results for 0% (zero mountains), 50%, 100% (control case) and 150% are shown on Figs. 1 and 2.

Trajectories demonstrate large changes in their behaviour when comparing calculations over different mountains in the bora region. Increasing heights of mountains, the blocking effect of the step eta mountains deforms bora wind trajectories above them. In case of zero mountains, no accumulation of air in front of mountains and flow in the bora direction is quite uniform, without acceleration along trajectories. A small impact to bora can be seen in case of 25% and 50% of control mountains. In control case there is accumulation of air with small wind speed in front of mountains, what can be seen from the small distances between one-hour positions on the trajectories. Just over and in the lee side of mountains, a stronger bora wind speed and its acceleration can be seen. In case of 200% of control mountains in the bora region (not shown on Figs.), mountains completely blocked the flow. The air accumulated in front of obstacle going around.

It is well known from the literature that the necessary condition for height of mountains in the bora region is 800 - 1200 m. Analysing trajectories from this study, it is confirmed. Only in the control case with mountains about 1000 m the local bora wind is well developed.

5. Conclusions

Numerical simulation of synoptic events for the case of severe bora storm over Adriatic coast by the Eta Model with high resolution (20 km x 20 km) shows satisfactory results. Bora is associated with a strong cold outbreak leading to a cut-off process in the Mediterranean. The maximum bora speed is predicted in the lee of the tree-dimensional mountains in step eta representation.

Increasing heights of mountains from zero elevation, the blocking effect of the step eta mountains deforms wind above them. Two times higher mountains then in the control case completely blocked the flow in the bora direction. The air in that case moves around the obstacle.

Mountains from the control experiment with height about 1000 m in the bora region satisfied necessary condition for bora wind known from the literature. That condition for height of obstacle is 800 - 1200 m.

Aknowledgments

This study was partly supported by the U.S.-Yugoslav Joint Fund for Scientific and Technological Cooperation in cooperation with the NSF under grant JF 990-71 and partly by the Association for Science of Serbia under grant 0704.

References

Janjić, Z.I., 1990: Physical package for the step-mountain, eta coordinate model. *Mon Wea Rev,* 118, 1429-1443.

Janjić, Z.I., 1994: The Step-mountain Eta Coordinate Model: Further Developments of the Convection, Viscous Sublayer and Turbulence Closure Schemes. *Monthly Weather Review,* 122, 927-945.

Jurčec, V., 1989: Severe Adriatic bora storms in relation to synoptic developments. *Paperes of Meteorological Society of Croatia*, 24, 11-20.

Mesinger, F., 1984: A blocking technique for the representation of mountains in atmospheric model. *Riv Met Aeronautica*, 44, 195-202.

Mesinger, F., Z.I. Janjić, S. Ničković, D. Gavrilov and D.G. Deaven,1988: The step-mountain coordinate: model description and performance for cases of Alpine lee cyclogenesis and for a case of an Appalachian redevelopment. *Mon Wea Rev*, 116, 1493-1518.

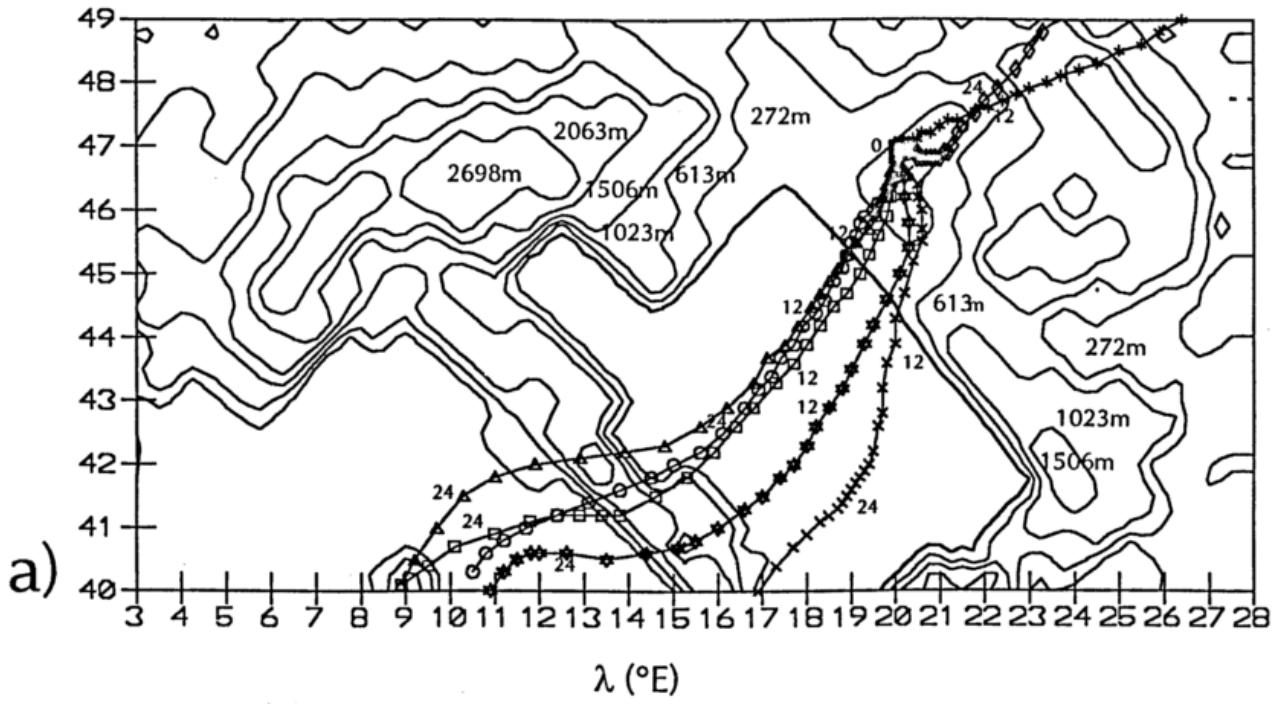

* LT=1 (z=3820m) ◊ LT=2 (z=3057m) O LT=3 (z=2380m) Δ LT=4 (z=1784m) □ LT=5 (z=1264m) ✡ LT=6 (z=818m) X LT=7 (z=442m)

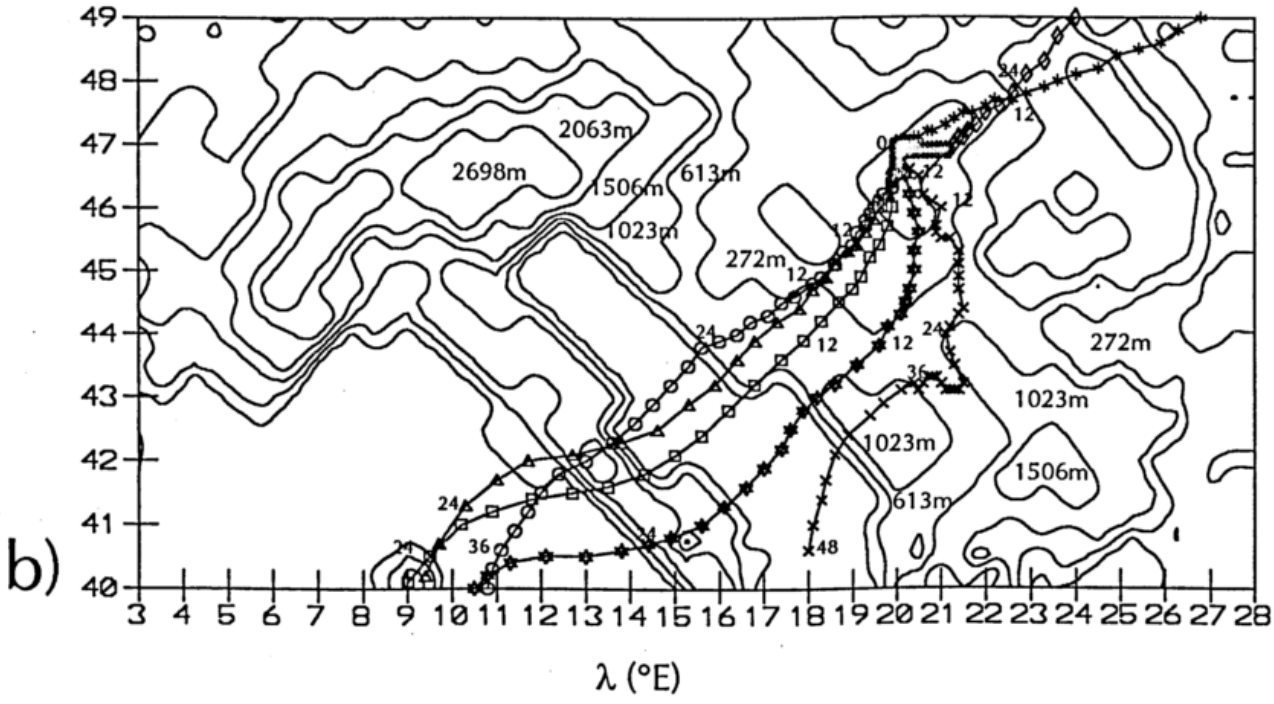

Fig.1 Horizontal trajectory projections for initial levels as in legend: a) with zero mountains, b) with 50% of control mountains over Adriatic coast. Numbers along trajectories indicate integration time.

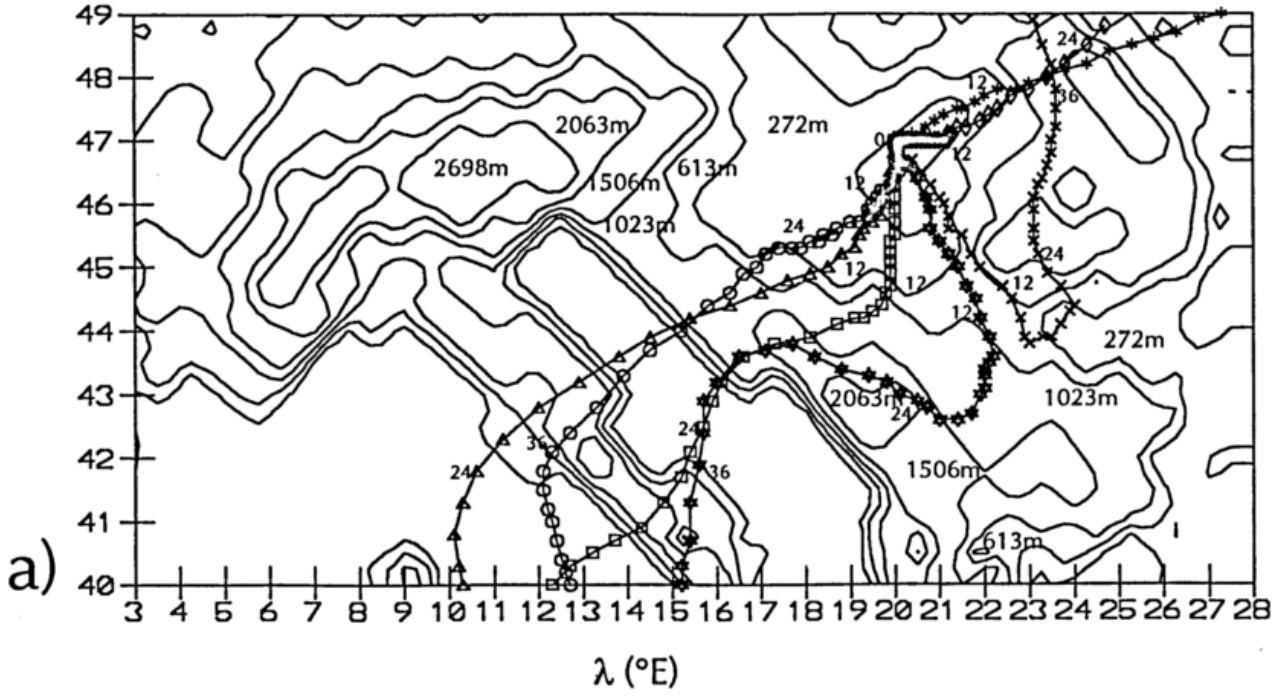

* LT=1 (z=3820m) ◊ LT=2 (z=3057m) O LT=3 (z=2380m) Δ LT=4 (z=1784m) □ LT=5 (z=1264m) ✡ LT=6 (z=818m) X LT=7 (z=442m)

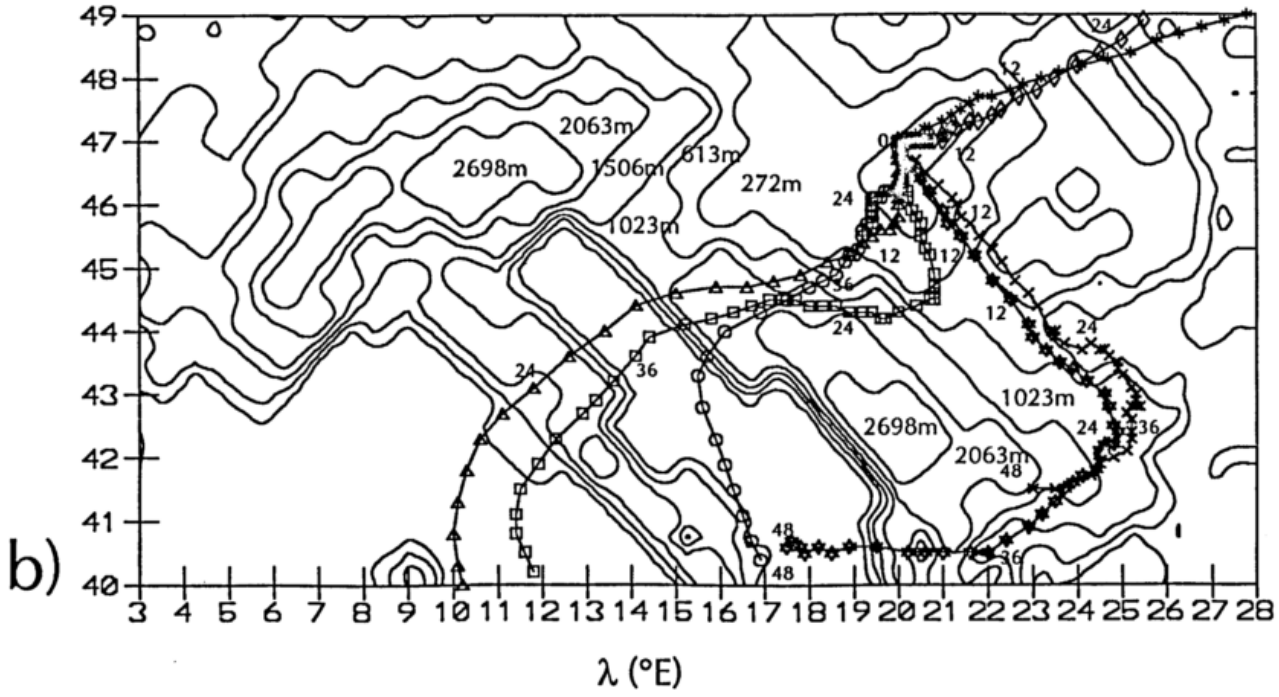

Fig.2 As in Fig.1, but for: a) with control mauntains, b) with 150% of control mountains over Adriatic coast.

A simple prognostic wind field model for complex areas: applications to local circulation prediction for an alpine region.

R. Salerno
° AMBIO s.r.l. corso Lodi 106 I-20139 Milan Italy

ABSTRACT

The evaluation of the local circulation in the alpine areas is difficult due to many interacting effects. The prevalence of the effects of the mountain-valley wind systems on the lower atmospheric levels, due to the protective role of the mountains, reveals the great importance of a correct computation of the local features effects and of the thermally driven systems. In this paper an attempt to compute the wind fields in a south alpine area is made using a simple elaboration of the ATM123 model, by which the conservation time-dependent equations are analitically solved under some limitations and assumptions for selected planes of the studied area, differing from the ATM123 model for which the solutions are all numericals, prescribing the correct thermal forcing and the boundary conditions. The solutions obtained on the planes, together with the boundary data are put in a mass-conservation three-dimensional model at selected times. The aim is to understand if such a simple mechanism is able to reproduce the evolution of the air flow pattern on the alpine area. Preliminary simulations have been performed, showing that the correct prescriptions of the thermal forcing and the boundary conditions might lead to interesting results in the absence of a relevant synoptic flow, giving the evolution of the wind in a very short time also on small computers.

SOME NUMERICAL SIMULATIONS OF DRY TEMPERATURE INVERSIONS AND ASSOCIATED WINDS IN ALPINE VALLEYS

Tomaž Vrhovec
University of Ljubljana, Department of Physics
Ljubljana, Slovenia

Abstract

A hydrostatic mesometeorological model APIKA (Vrhovec 1991) was improved by a new turbulence parametrisation using a complete prognostic equation for the turbulent kinetic energy with both horizontal and vertical advection of turbulent kinetic energy. An improved parametrisation of diabatic term in the air near the ground with the use of multi-level soil temperature model is used. Horizontal diffusion by turbulence is explicitly included and the model with the improvements was tested. With the model APIKA some simulations of the formation of inversion layers were performed. As the simulations were done for whole day also the morning dissipation of the inversion layers in valleys due to the diabatic heating are examined. Interesting vertical and horizontal temperature patterns are formed due to partial dissipation of inversion layer near the slopes exposed to the sun.

Introduction

In complex topography fair weather local winds are in absence of strong synoptic scale flow mostly forced by the differences in local diabatic heating or cooling. In daytime the differences in diabatic heating are due to the diverse inclination and aspects of the slopes, the intensity of local heating of the atmosphere is further modified by the differences in local surface reflexivity and in heat storage.During the night in absence of the clouds the forcing term in energy balance of the surface of the topography is IR terrestrial radiation. The absence of the clouds justifies the assumption that the incoming IR atmospheric radiation is horizontally homogenous (assuming also that water vapour content is homogeneous in the atmosphere) so IR atmospheric radiation, intercepted by the terrain surface is modified by the differences in topography and in emissivity only. Valley wind system were extensively studied in alpine regions (for review see Whiteman 1990).Four different flow regimes of valley winds were observed and explained by conceptual models (Whiteman 1990, Egger 1990): morning transition, daytime upvalley wind, evening transition and downvalley wind. In this extended abstract we will present some results of the simulations of valley and basin winds and of formation and dissipation of associated dry temperature inversion layers within valleys and basins performed with an improved version of mesometeorological model APIKA (Vrhovec 1991). The winds in the basins and in the valleys are more or less similar: the onset of the wind in a closed basin is forced by diabatic cooling or heating but due to diverse geometry of basin (a basin has no or only a small outflow) the basin winds are more confined into the basin and its surroundings. In the night the cold air formed along the slopes and at the bottom of the basin can not flow out of the basin as it does out of the valley creating downvalley wind. The basin cold air simply accumulates in the basin: the upper boundary of the cold air can be seen as rising elevated temperature inversion layer.

Recent changes in model APIKA

Parametrisation of diabatic term

In earlier versions of the model APIKA (Vrhovec 1991) the diabatic term was parametrised with the earth surface energy balance equation similar to that in Wallbaum (1982). In this version we parametrised surface energy equation similar to work of Virant (1993). In her work she made a

numerical model MEBIT for simulation of soil temperature profiles and of soil surface temperature. The model MEBIT uses astronomical, topographical, pedological and meteorological data: these derived from the mesometeorological model variables. The model MEBIT calculates conductive heath flux, mass flows of liquid water and vapour in the soil, transports of heath by water and air in the ground with the equations of soil physics and some empirical parameters concerning soil properties and so determines the soil temperature and humidity profiles.

Some additional parametrisation has to be done in very rugged topography: in case of very big differences in altitude on short horizontal distances great differences in the diabatic term and so also in the temperature can occur on short horizontal distances between the points near the mountain slopes and those already further horizontally away in the free air. Naturally these temperature differences are reason for slope winds but small scale turbulence mixes the air also horizontally. To obtain increased horizontal mixing (i.e. for the points in the model space that are horizontally near the topography surface but several model levels vertically away from the topography surface) also turbulence parametrisation scheme has to be modified.

Turbulence parametrisation with TKE

To determine turbulent diffusivities for the momentum and for the enthalpy in all three dimensions parametrisation using turbulent kinetic energy (TKE) was used. Turbulent diffusivity for momentum in vertical direction is determined by:

$$K_{mv} = l_m(aE)^{0.5} \tag{01}$$

where l_m is Monin Obukhov stability length and E is turbulent kinetic energy .

The turbulent kinetic energy is being transported, created by bouancy and shear, dissipated and turbulently mixed:

$$\frac{\partial E}{\partial t} = u\frac{\partial E}{\partial x} + v\frac{\partial E}{\partial y} + w\frac{\partial E}{\partial z} + K_{mv}\left(\left(\frac{\partial u}{\partial z}\right)^2 + \left(\frac{\partial v}{\partial z}\right)^2\right) \tag{02}$$

$$-K_{hv}g/\Theta\frac{\partial \Theta}{\partial z} - c_E/lE^{1.5} + \frac{\partial}{\partial x}K_{hh}\frac{\partial E}{\partial x} + \sigma_E\frac{\partial}{\partial z}K_{hv}\frac{\partial E}{\partial z} \tag{03}$$

The parameters a, c_E and σ_E are determined as in Bishoff-Gauss (1982), while turbulent diffusivities for entalphy K_{hh}, K_{hv} and for horizontal diffusion of momentum K_{mh} are determined according to Businger et al. (1971) The initial state of turbulent kinetic energy is determined as a fraction of total kinetic energy. There is a minimum requirement for turbulent kinetic energy and so also for turbulent diffusivity.

Meteorological and topographical input data

The new version of APIKA was tested on idealised topography that consisted of a single hill (elevation $500m$ above plain, base length $6km$). In this extended abstract we will only present some results obtained above the topography of an idealised symmetrical south - north oriented valley. Some other simulations will be presented in forthcoming paper. The valley mouth is towards the north. The bottom of the valley is at $50m$ and the slopes reach elevation of $400m$. The valley is surrounded by a plateau, the valley width is $4km$, length $10km$, while whole integration domain is $10x20km$. The valley bottom is flat and the slopes have maximum inclination of $20°, 35\%$. The model has horizontal resolution of $1km$ and 18 levels in vertical direction in the air and 10levels in the ground (down to the 1 m depth) . Vertical resolution at lower levels is between 25 and 50 meters while at higher levels the resolution is from 100 to 500 meters. It is assumed that there is

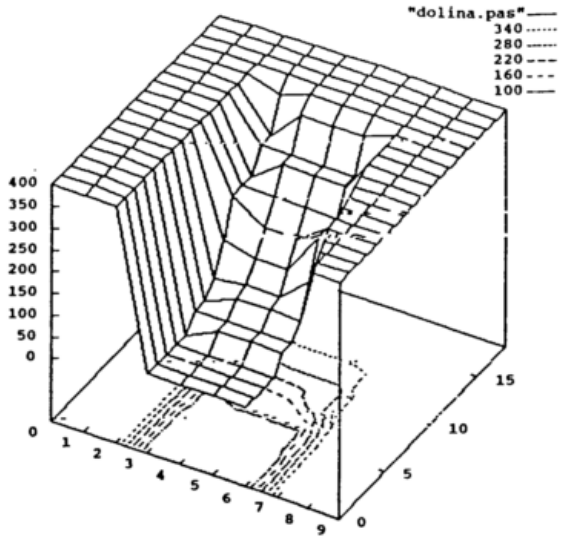

Figure 1: 3D representation of model topography: symmetrical valley, vertical dimensions are three times exaggerated

a geostrophic wind blowing at the upper model domain boundary at approximately $600hPa$ and the unperturbed part of the pressure field is adjusted to the geostrophic wind.The topography of the symmetric valley is presented at fig 1.

It is assumed that whole basin and plateau has same short wave albedo (0.5) and that all other thermal and frictional characteristics are same on all the places. The simulation was made for mid July day: the simulation started at 1^{00} local time and ended at midnight the same day. The initial temperature stratification was same everywhere in model space and stable with $\frac{\partial\theta}{\partial z} = 5.1K/km$ while humidity was set to be 50% at all the model levels.

Results

The results of the model simulation are presented for the time of morning and evening transition only. For each time three horizontal cross-sections of wind field within the valley at different altitudes, one vertical cross-section of the wind field along valley axis and a set of vertical potential temperature profiles along valley axis are presented. (See figs. 2 and 3).

For morning transition time it is interesting, that up-valley wind starts to blow first at upper part of the valley (fig. 2 d) while at lower part there is still down-valley wind. The boundary between the two winds coincides with change in vertical stratification: lower part is still under temperature inversion while upper part is above it.

For evening transition time the down-valey winds form first at lower part of the valley atmosphere (fig. 3 d) while in the upper part the up-valley wind is decreasing, just above the valej crest thete is still some updraft. The onset of down-valley wind is marked by "S" shape in vertical potential temperature profile. In three horizontal cross-sections various stages of onset of down-valley wind are presented.

Literature

Bishoff-Gauss I., 1982: Zur Verwerdung der Gleichung fuer Turbulenzenergie bei der Schliessung des Gleichungsystems fuer die atmosphaerische Grenzschicht, Diploma Thesis, Dept. Meteorol. Tech. Univ. Darmstadt.

Businger J.A. et al., 1971: Relationships in the atmospheric surface layer. J. Atm. Sci. 28, 181-189.

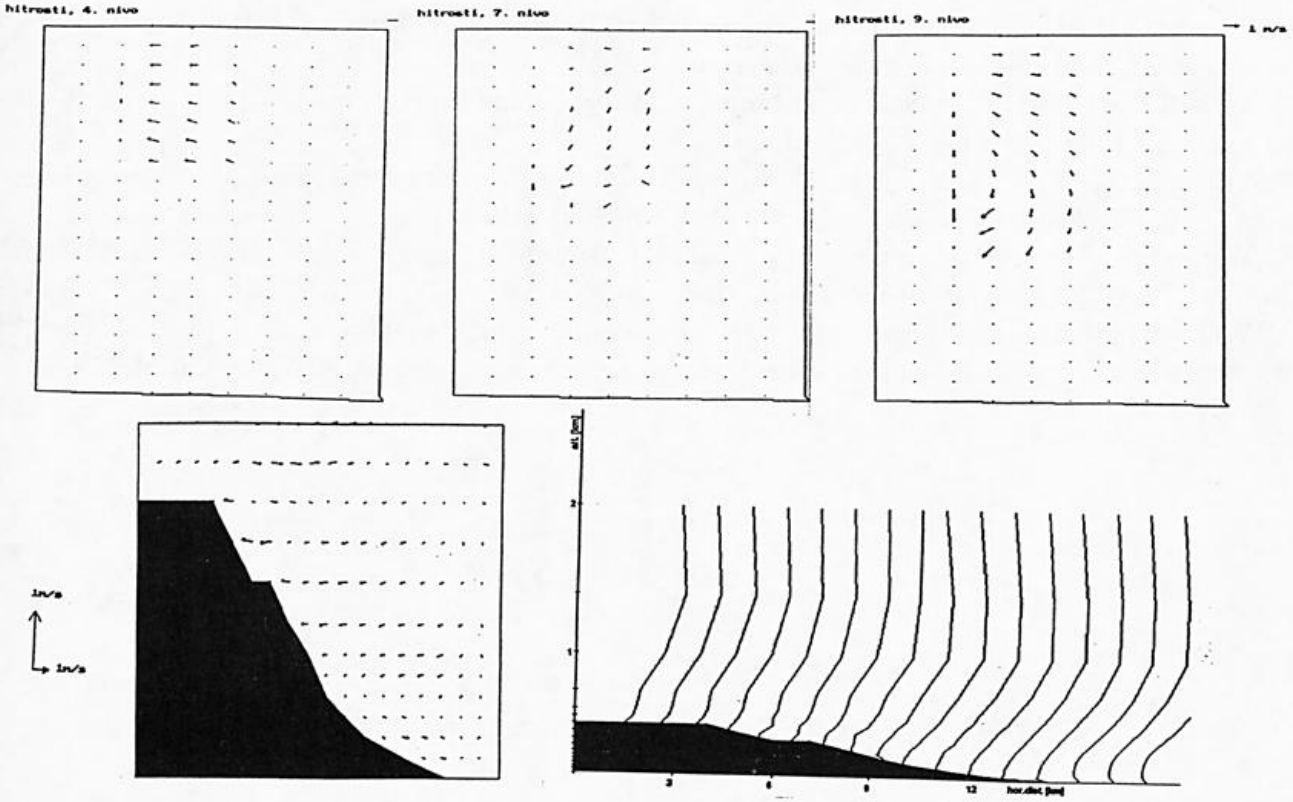

Figure 2: Winds and potential temperatures in a symmetrical valley at the time of **morning transition** (6.30 LT, 5. 30 h after beginirg of simulation, for a July day). Horizontal cross-sections of u and v components: **a** - at 120m, **b** - at 200 m, **c** - at 300 m above the valley bottom; **d** - vertical cross-section of v and w components alon valley axis; **e** - vertical pot. temperature profiles along vert. cross-section.

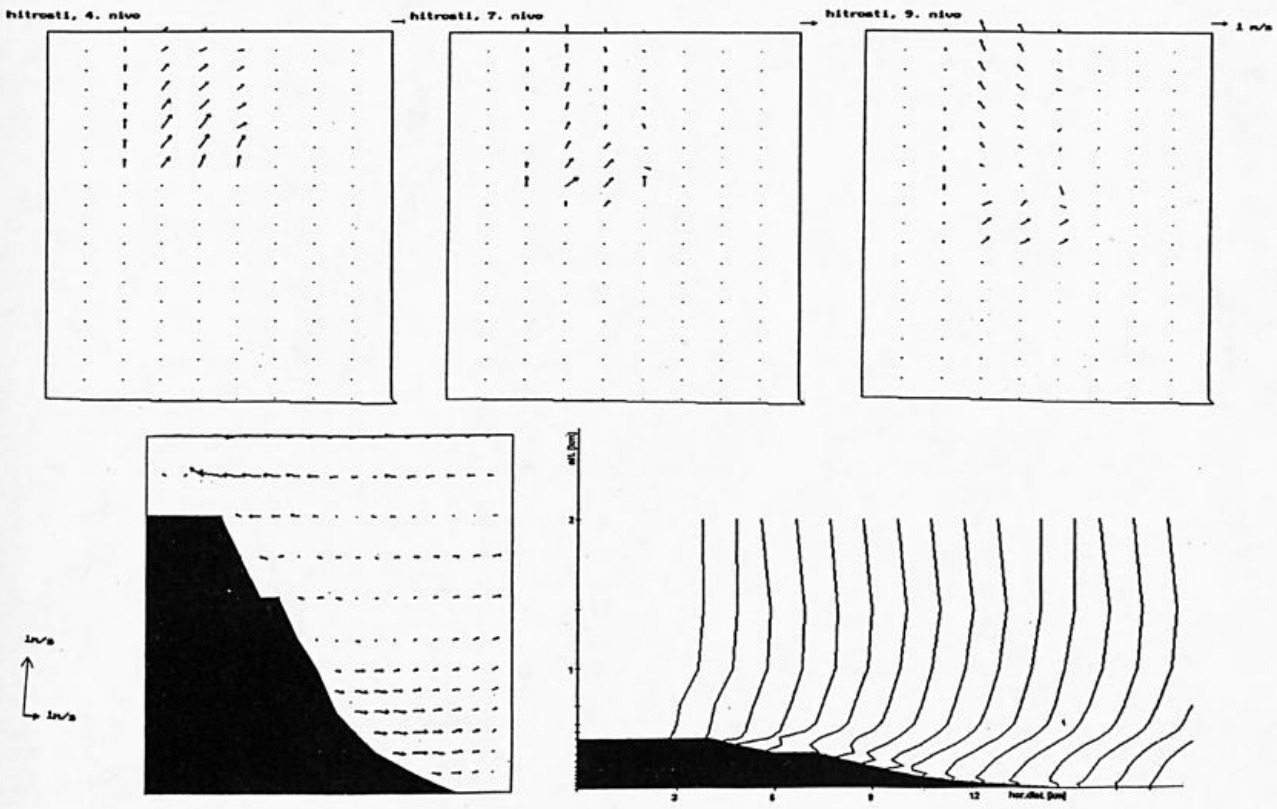

Figure 3: Winds and potential temperatures in a symmetrical valley at the time of **evening transition** (18.15 LT, 17.15 h after begining of simulation, for a July day). Horizontal cross-sections of u and v components: **a** - at 120m, **b** - at 200 m, **c** - at 300 m above the valley bottom; **d** - vertical cross-section of v and w components alon valley axis; **e** - vertical pot. temperature

Egger, J. 1990: Thermally forced flows: theory. Atmosperic processes over complex terrain, Am. metorol. Soc. Meteorological Monographs, 43-58

Virant, D. 1993: Dinamično modeliranje vpliva padavin na fizikalne lastnosti tal, M. Sc. Thesis, Univerza v Ljubljani, BTF, Agronomija, 96 pp.

Vrhovec, T. 1991: Mezometeorološki model vetrovnih in temperaturnih polj v razgibanem reliefu, Ph. D. Thesis, Univerza v Ljubljani, FNT- Fizika 101 pp.

Wallbaum, F. 1982: Numerische Simulation atmosphaerischer Stroemungen im Mesosacle Gamma, Ph. D. Thesis, Dept. Meteorol. Tech. Univ. Darmstadt, 183 pp.

Whiteman, C.D. 1990: Observations of thermally developed wind systems in mountainous terrain.Atmosperic processes over complex terrain, Am. metorol. Soc. Meteorological Monographs, 5 - 42.

INFLUENCE OF OROGRAPHY AND SURFACE THERMAL BUDGETS ON STORM DEVELOPMENT

Vlasta TUTIŠ and Branka IVANČAN-PICEK

Meteorological and Hydrological Service, Zagreb, Croatia

Abstract

Severe storms are mostly subsynoptic features. Since they are very difficult to be studied in the regions with scarce data (as the Adriatic area), it is desirable to broaden diagnostic analyses with the knowledge on their temporal and space environment which may show to be significant during the triggering phase.

It is wellknown that the wavelength of orography strongly influences the airflow. Therefore we analysed the characteristic wavelengths of mountains and mountain chains belonging to the eastern part of the Alps and the Dinaric Alps. We applied the standard Fourier analysis on data sets, each describing one cross-section of the mountaneous area (Fig.1). The results show that the dominant wavelengths of orography (Tab.1) have the strongest impact on atmospheric disturbances on the lower part of the meso-beta scale.

The strong influence of orography on severe weather can be divided into two major topics - the influence on storms within stably stratified flow (like leeward Bora windstorms along the eastern Adriatic coast) and the influence on convective storms. Our special attention is focused on the influence of orography on stably stratified flows. Calculations of the surface mountain drag show a significant correlation of the high drag periods with the Bora periods, so it seems that the surface mountain drag controlls the stably stratified stationary low-level flow /1/, to a large extent.

The convective storms are strongly influenced by thermal budgets of the surface (land or sea), as documented by the two recent examples on Adriatic severe weather /2/. On the days when there were a tornado touch-down at the northern Adriatic (on 10th August 1992) and a strong hailstorm at the middle Adriatic (on 10 October 1992), the sea temperatures were significantly higher than the average monthly sea temperatures in the 10 - year period, due to an extremly warm summer (Fig.2).

So, when discussing severe weather (in case-studies or in weather forecast) we have take into account that storms are mostly subsynoptic features, strongly influenced by local processes and orography and, therefore, very difficult to study by regular synoptic network. A knowledge on broader temporal "environment" of severe storms (like surface thermal budgets) should also be more exploited since it is often underestimated in standard case-study analyses.

Tab.1. Estimated dominant wavelengths of the Dinaric Alps along the cross-sections A, B and C:

dominat wavelengths of orography (km)		
traverse A	traverse B	traverse C
53	38	88
30	30	59
24	22	32
16	21	18

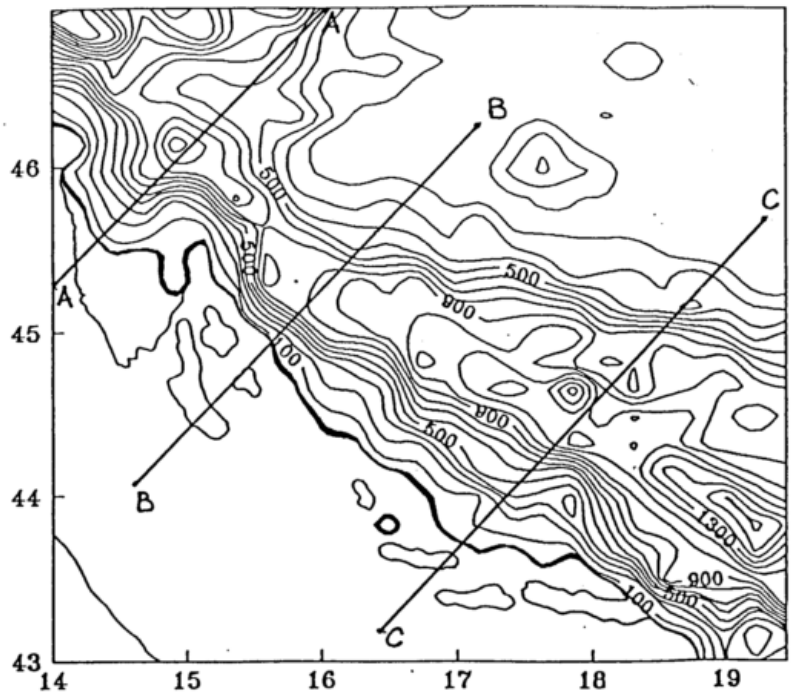

Fig.1. The surface domain including the corrugated topography (the south-east Alps and the most parts of the Dinaric Alps), the south Pannonian Valley and a greater part of the Adriatic sea. Isohypses every 100 m from the sea level; thick isoline is the 50 m height. The orography- reading every 5 km. The Fourier analysis is provided for crossections A, B and C.

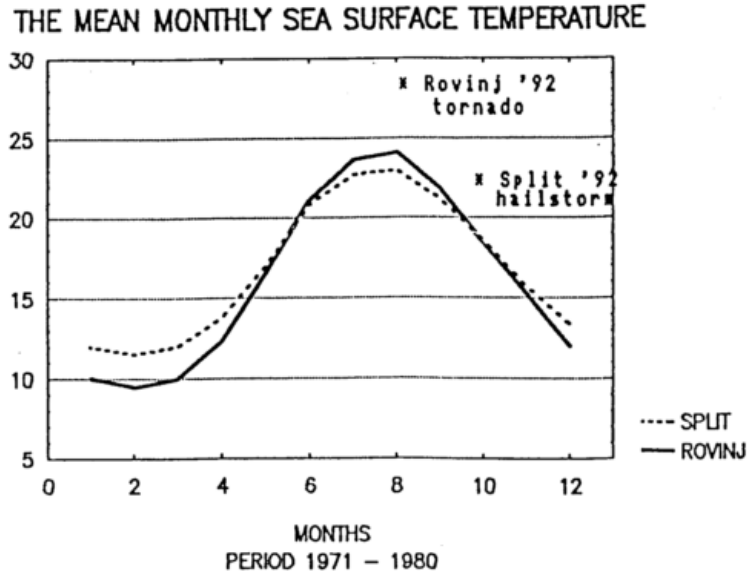

Fig.2. The mean monthly surface temperatures (1971-1980) near Rovinj (at the northern Adriatic) and Split (at the middle Adriatic). The measured values of the sea surface temperature on severe weather days are indicated by asterisks.

References:

/1/ Tutiš V. and B.Ivančan-Picek (1991): Pressure drag on the Dinaric Alps during the ALPEX SOP. Meteorol.Atmos.Phys.,47, 73-81.

/2/ Tutiš V.,D.Peti,S.Britvić, 1993: "Convective storms in 1992". (in Croatian), Extraordinary Meteorological and Hydrological Events in Croatia in 1992. Vol.16, 5-16

Climate change detection in Alpine valleys
The example of the Brera Observatory (Milan) rainfall series (1790 - 1990)

R. Sneyers*, A.M. Siani**, S. Palmieri**

*Institut royal météorologique de Belgique, **Department of Physics, University of Rome

Abstract

The series of annual and seasonal rainfall of Brera Obsvervatory (Milan) has been submitted to a statistical analysis of their internal structure by testing their randomness against serial correlation and trend. The results found in all cases is the succession of alternating abrupt changes. Statistical modeling of the annual series has been considered while, for this century, the existence of change-points has been related to the evolution of the general atmospheric circulation over the region. The statistical principles of the time series analysis have been first remembered and different examples given.

1. Introduction

The traditional characterization of climate has generally been limited to adjusting appropriate statistical distributions to climatological observations. However, an existent climate warming having been evidenced for certain regions already at the end of the 40s, it became obvious that this climate approach could no longer remain acceptable without testing the stability of the climatological time series (Sneyers, 1992). The interest of the Milan rainfall series is due to the fact that the instability found in the internal structure of the series could be related to changes in the general circulation over the region.

2. Internal structure analysis of climatological time series.

Simple randomness (signifying independence and identity of distribution of the elements of a series or, abbreviated: i.i.d.) being the underlying hypothesis necessary for validating statistical distribution adjustments, this validation reduces to testing both the independence and the stability of the distribution of the elements of this series. Moreover, in order to avoid biased conclusions, in the considered tests, the elements of the series are replaced by the corresponding ranks obtained when arranging the series in increasing order. For ties, the rank adopted is the average of the ranks occupied in the increasing series by the ties. Such tests are called non parametric ones. Due to the fact that under the hypothesis of randomness, these ranks are proportional to the unbiased estimation of the probability given to each element of the series by their distribution function, whatever this distribution function is, the conclusions of such tests are independent of the underlying distribution, while the loss of power relatively to the corresponding parametric tests is generally small.
For verifying the hypothesis of simple randomness, the tests are as follows:
(a) randomness against serial correlation (Wald-Wolfowitz, 1943). In this test, the test statistic is the serial correlation coefficient of first order.
(b) randomness against trend (Mann, 1945). In this test, the number of the preceding smaller elements is computed for each element of the time series, ties of the element being counted for .5, and the test statistic is the sum of the obtained numbers. Moreover, the analysis is completed by considering a point running from the beginning to the end of the series and in computing the trend test statistic for each of the subseries defined by its successive positions. It allows to detect eventual internal trends inside the series giving in this way a correct idea of the internal

structure of the series. Noting that actually, the trend test is especially sensitive to changes of the median, when applied to the absolute deviations of the elements to the general average, absence of trend in both cases ensures stability for distributions defined by two parameters.
A special well known case of heterogeneity in climatological time series is the one caused by changes in observational methods. When only one change occurs in a series, Pettitt (1979) has given a procedure for its determination, which is optimal when the change divides the total series into two i.i.d. subseries. Such a point is called a change-point. The interest of Pettitt's procedure is that the test statistic consists in computing progressively the deviations to their expectances of the cumulated sum (cusum) of the ranks of the elements of the series, the change-point being then given by the largest absolute deviation. Note, however, that the i.i.d. condition for the subseries makes its verification necessary before any final conclusion.
In the case of more than one change-point, Pettitt's procedure may be used as first indication, the sequential Mann trend test being then used for the final estimations.

3. Examples

3.1 The series of air temperature at Brussels-Uccle (Belgium) (1833-)
This method was applied to the seasonal averages of the air temperature (1833-1956), to verify the hypothesis of a correlation between consecutive seasons (Sneyers, 1958). Actually, existing change-points were found for each season, round 1910 for winter and spring and round 1930 for summer and autumn. Taking account of this feature, the suggested hypothesis of correlation could be rejected. The same conclusion was found for Paris. Extended up to 1988, the last analysis established increasing shifts of .9°C for winter, 1.1°C for spring, .7°C for summer and 1.0°C for autumn.

3.2 The Jones NH surface air temperature (1851-1987), (Demarée, 1990)
The global warming reduces in fact to an increasing shift of .3°C which occurred round 1920.

3.3 The homogenized regional Austrian air temperature series (1775-1989)
For this century, the same change-points at the seasonal scale were found as for Brussels and Paris. They are responsible for an increasing total shift of .7°C. However, the complete analysis revealed the existence of a change-point round 1830 responsible for an equivalent decreasing shift of .7°C (Sneyers, Böhm and Vannitsem, 1992).

3.4 The Genova annual averages of air temperature (1833-1990), (Sneyers, 1993)
Four change-points have been found respectively placed in 1860, 1877, 1919 and 1952. They produced alternatively increasing and decreasing shifts amounting from .6 to 1.0°C.

3.5 The regional U.S.A. annual air temperature averages (1895-1991)
Three change-points occurred respectively in 1921, 1959 and 1984. The successive alternatively increasing and decreasing shifts are: +.60°F, -.56°F anf +.94°F. Moreover, an abrupt increase of the variance occurred in 1972.

3.6 The annual air temperature averages at Oulou (Fld) (1847-1990)
Two change-points occurred respectively in 1938 and 1949. The shifts were successively +.74°C and -.57°C.

4. The Brera (Milan) rainfall record (1791-1990)

The assessment of the climate property of evolving in an abrupt way is a self sufficient information for practical applications at the condition that this evolution may be completely defined by a statistical model. On the other hand, for theoretical purposes, it is of major interest to be able to put this property in connection with special general circulation features. The interest of the Brera Observatory(Milan) rainfall record lies in the fact that this double question

could be answered (Sneyers, Siani and Palmieri, 1993).

Table 1. Rainfall amounts in Milano (Period 1790-1990) (mm)
Homogeneous subseries dividing the total series

	Period	m	s	s(m)	t	α	α'
Year	1790-1835	993.28	173.06	25.32			
	1836-1852	1175.00	158.74	38.50	2.73	.003	.01
	1853-1884	981.63	208.75	36.90	-2.64	.004	.02
	1885-1916	1064.43	171.36	30.29	1.46	.07	.20
	1917-1932	869.38	199.45	49.86	-2.55	.005	.02
	1933-1990	1014.62	230.28	30.24	1.77	.04	.10
Winter	1791-1852	204.82	95.54	12.13			
	1853-1884	164.25	97.73	17.28	-1.77	.04	.08
	1885-1990	200.08	89.89	8.73	1.63	.05	.07
Spring	1790-1834	228.71	84.53	12.60			
	1835-1918	289.77	107.78	11.76	2.85	.002	.003
	1919-1971	245.49	87.10	11.96	-1.89	.03	.04
	1972-1990	289.10	129.64	29.34	1.20	.12	.30
Summer	1790-1810	218.71	99.22	21.65			
	1811-1821	316.18	95.42	28.77	2.03	.02	.12
	1822-1832	204.46	59.82	18.04	-2.40	.008	.07
	1833-1852	283.25	92.91	20.78	2.28	.01	.06
	1853-1933	215.84	84.35	9.37	-2.45	.007	.01
	1934-1990	256.44	88.84	11.77	2.13	.02	.03
Autumn	1790-1907	331.49	127.00	11.69			
	1908-1990	282.49	125.49	13.77	-2.60	.005	
(9-3)	1791-1841	590.12	142.90	19.81			
	1842-1916	606.63	192.22	22.20	2.34td	.001	
	1917-1989	546.97	164.50	19.25	-1.77*	.04	

m, s = average and standard deviation of the subseries
s(m) = standard error on the estimation of the mean
t = standardized value of the Mann trend statistic characterizing the abrupt change with the preceding subseries (one sided test)
α = corresponding significance level
α' = corrected significance level for reduction to the total length of the series
td = standardized value of the Mann trend test for the absolute deviations to the average (abrupt change in the standard deviation)
* = standardized value of the Mann trend test statistic for the total series
(9-3): September to March period

4.1 Statistical modeling

Table 1 gives the result of the above described time series analysis made on the annual, seasonal and on the period September to March rainfall amounts. It evidences that spring and summer are the seasons with the more frequent changes in the mean. As a consequence, the year presents the same character. If we limit a further statistical analysis to the annual rainfall amounts, it may be shown that the six i.i.d. sequences have homogeneous variances and normal distributions. Moreover, if the three sequences with low amounts have homogeneous means, among the three other ones with high amounts, the two last sequences with high rainfall amounts have also homogeneous means, while the first one has a mean significantly higher than the two other ones. Note that it is not excluded that this heterogeneity is linked to an

instrumental one which occurred during the first high amount rainfall period. Finally, the fact that the distribution of the lengths of the sequences are well adjusted by a gamma distribution function completes entirely the statistical characterization of the long term evolution of the annual rainfall amounts.

4.2 The general circulation explanation

The search for this explanation has been limited to the period 1900-1991 by estimating the annual averages of two orthogonal components of the geostrophic wind over Central Mediterranean and Italy. For this purpose, four blocks surrounding this region respectively at the N, E, S and W have been considered and values proportional to the wind components have been deduced from the pressure differences S-N and W-E. From this computation it appears that the period with low rainfall yearly means (1917-1932) was characterized by a weak west-east yearly mean zonal flow, while the time intervals with larger mean precipitation amounts (1900-1916 and 1933-1990) were related to prevaling east-west surface flows. Though the complete analysis of threedimensional representation of the geostrophic flow reveals a less simple evolution than the one given by the statistical analysis of the annual rainfall, the final explanation may be found in the orography of the surroundings of Milan situated in the Po Valley open to the E and, thus, to the easterly winds coming from the Adriatic Basin. Low level convergence of the humidity carried by these winds, on one side, and a lowering effect on the humidity of the air masses crossing mountainous regions for the other winds, on the other side, give reasonable reasons for considering the climate instability as due to an orographic effect of general circulation heterogeneities.

5. Conclusion

The link found between the long range rainfall amounts evolution in Milan and the simultaneous changes in the general circulation over the region, suggests that the asynchronous evolutions found for the air temperature at the few different places considered are related to general circulation changes influencing but a limited region over the earth. It follows that global averages give but a poor picture of the actual global climate evolution and that, in particular, the 1920 shift observed at the global scale, may be but the witness of the effect observed at the middle latitudes damped by the integration of series of the other parts of the world poorly or not dependent of the middle latitude series. If still necessary, it demonstrates the complexity of the global climate change problem.

References

DEMAREE, G., 1990. Did an abrupt global climatic warming occur in the 1920s? in Contributions à l'étude des changements du climat, Ed. G. D. Schietecat, Inst. R. Météor. de Belgique, Pub. A, N°124, 32-37.

MANN, H. B., 1945. Non parametric test against trend, Econometrika, 13, 245-259.

SNEYERS, R., 1958. Connexions thermiques entre saisons consécutives à Bruxelles-Uccle. Inst. R. Météor. de Belgique, Pub. B, N°23, 24pp.

SNEYERS, R., 1992. On the use of statistical analysis for the objective determination of climate changes. Meteor. Zeitschrift, N. F., 247-256.

SNEYERS, R., 1993. Multimodal Stochastic Models. Application to Climate Modeling. Proc. 6th Intern. Symposium. Applied Stochastic Models and Data Analysis, Vol.II, Chania, Crete, Greece, May, 3-6, 1993, Ed. J. Janssen, Chr. H. Skiadas, World Scientific, 886-894.

SNEYERS,R., BÖHM, R. and VANNITSEM, S., 1992. Climatic changes in the Austrian Alps during the period 1775-1989. Geogr. Fis. Dinam. Quat., 15, 195-199.

SNEYERS, R., SIANI, A. M. and PALMIERI, S., 1993. Characterizing trends in climatological time series. An application to Brera observatory(Milan) rainfall series. Proc. Confer. on Applications of Time Series Analysis in Astronomy and Meteorology, Padova, 6-10 Sept. 1993, Chapman-Hall (London), in the press.

WALD, A. and WOLFOWITZ, J., 1943. An exact test for randomess in the non-parametric case based on serial correlation. Ann. Math. Statist., 14, 378-388.

U.S.A. and Oulou data kindly communicated respectively by the U.S.A. National climatic data center and by our collegue Raino Heino from the Finnish Meteorological Institute (unpublished analyses).

Temperature Trends in the Alpine Region in this Century

G. Stefanicki, P. Talkner and R.O. Weber
Paul Scherrer Institute, Villigen, Switzerland

Abstract

There exists quite general agreement that the global annual mean temperature raised by about 0.5°C during the last hundred years. Recently, it has become obvious that this trend is quite inhomogeneous in various respects. Besides the spatial and seasonal variability of the observed trend a diurnal asymmetry of increase in temperature has been observed. In large continental regions the daily minimum temperature has increased noticeably faster than the daily maximum. We found the same behaviour for low-lying stations in Central Europe. Moreover we demonstrated that the maxima are representative for the mean temperature during daytime on the respective day and the minima for the mean temperature during nighttime. Data from isolated mountain stations were also analyzed and show a consistent temporal behaviour. No diurnal asymmetry was observed for these stations. The good agreement of the times series led us to believe that the observed diurnal symmetry of the temperature change at mountain stations is not caused by observation errors.

Introduction

It is widely accepted that the annual global mean temperature of earth's surface has increased during the last hundred years by about half a degree Celsius [*IPCC*,1990; *IPCC*,1992]. The warming has been neither uniform throughout the year nor uniform over the globe. There are pronounced differences between both the seasons and various geographical regions [*IPCC*,1990; *IPCC*,1992; *Jones and Briffa*,1992; *Hunter et al.*,1993]. Whether the observed temperature changes are signs of natural fluctuations of the climate system or a sign of changing climate caused by man-made alterations of the greenhouse effect in the atmosphere is an open question.

Besides the observed seasonal differences in temperature change also a diurnal asymmetry in the trend became evident [*Karl et al.*,1984; *Karl et al.*,1991; *Karl et al.*,1993]. The daily minimum temperature has increased at a larger rate than the daily maximum. This asymmetry is termed day-night asymmetry [*Kukla and Karl*,1993], since the minimum temperature is assumed to be representative of the nighttime temperature and the maximum for the daytime. We tested this assumption using 10-minutes temperature data from Swiss stations.

Karl et al. [1993] and *Kukla and Karl* [1993] discussed several possible causes for the observed diurnal asymmetry. There are indications that an increase in cloud cover, including low clouds, is a possible and probable cause of the observed diurnal asymmetry [*Karl et al.*,1993].

It is not clear whether the observed diurnal asymmetric warming exists only in the near surface atmosphere or whether it takes also place higher up in the troposphere. The answer to this question may help to identify the mechanisms causing the diurnal asymmetry. As no daily minimum and maximum data from that part of the troposphere are available, we took data from some stations on isolated mountains in the Alps. For comparison, data from nearby midland stations at lower altitude were analyzed, too.

Data

Records from Swiss, German and Austrian stations were made available to us by the respective national weather services. Stations were selected which had a record extending back at least to the beginning of this century. Only three stations located on fairly high mountains had long enough records of daily extreme values. For comparison with stations at lower altitude some stations of the Swiss midland were chosen. A list of the selected stations and geographical information is given in Table 1.

For checking the temperature records the difference of the annual mean of daily minimum (maximum) for all pairs of stations was computed. Plots of these differences can reveal inhomogeneities of the records, especially sudden constant shifts. By comparing all difference plots for the seven stations listed in Table 1 and other Swiss and German stations, few inhomogeneities could be discovered. Those found were corrected by adjusting the means of the differences before and after the break to the same value [*Weber, Talkner and Stefanicki*,1994].

Station	Location	Height	Years
Sonnblick	47°03'N, 12°57'E	3105 m	1887-1990
Säntis	47°15'N, 09°21'E	2490 m	1901-1992
Zugspitze	47°25'N, 10°59'E	2960 m	1900-1992
Basel-Binningen	47°33'N, 07°35'E	316 m	1901-1992
Zürich SMA	47°23'N, 08°34'E	556 m	1901-1992
Bern-Liebefeld	46°56'N, 07°25'E	565 m	1901-1992
Neuchâtel	47°00'N, 06°57'E	485 m	1901-1992

Table 1. Location of the stations. In cases where a station was relocated the newest geographical location and height is given.

Säntis and Sonnblick had no inhomogeneities. They were chosen as representative for the mountain stations. Basel and Neuchâtel also had no corrections applied and were taken as representative for the midland stations. All four midland stations are situated close to towns and, hence, their data may have been influenced by changes in urbanization. Based on the growth of population during this century, we estimated from Table 7 of *Karl et al.* [1988] that the daily minimum has been enhanced due to urbanization by 0.1°C in the smallest town, Neuchâtel, and by 0.3°C in the largest town, Zürich. The respective estimate of the change in the daily maximum is about a factor of ten smaller and, hence, negligible. These urbanization effects are much smaller than the observed differences between daily minimum and maximum temperature as discussed below.

In order to test the representativity of the minimum for the mean nighttime temperature and the maximum for the mean daytime temperature we utilized the temperature values taken each 10 minutes on the Swiss stations by the SMA since 1978. For the nighttime mean temperature of a particular day the values starting at the sunset of the previous day and ending at the sunrise of the considered day were taken. For the daytime mean temperature we took the values from sunrise till sunset of that day. From these data nighttime and daytime mean temperatures were calculated for each year. A comparison with the respective minimum and maximum temperatures shows an almost constant difference and, hence, justifies the use of minimum and maximum for the calculation of trends, see Figure 1.

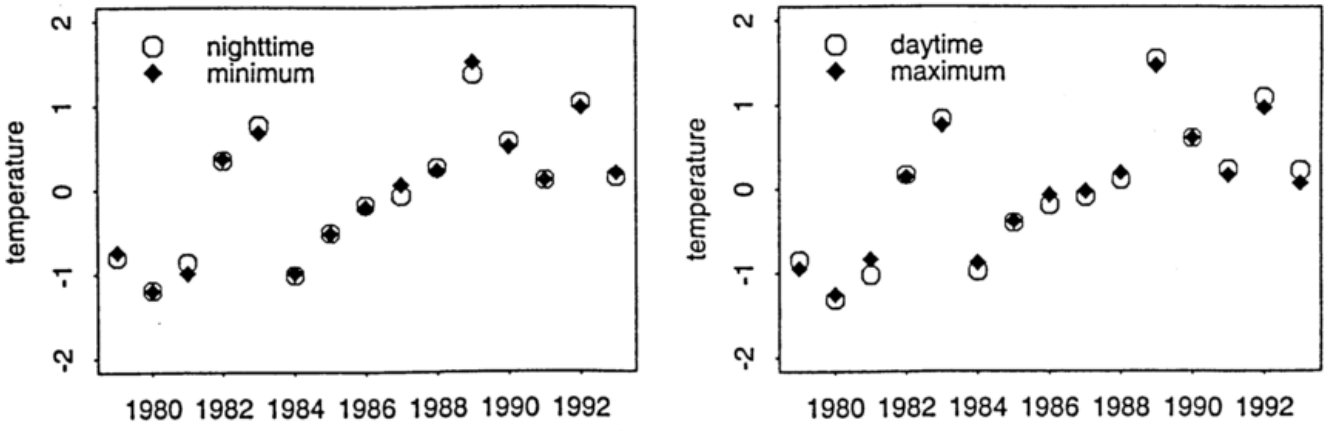

Figure 1. Anomalies of annual mean of daily minimum and maximum and daily nighttime and daytime temperature for the mountain station Säntis.

From daily minimum and maximum values monthly and seasonal means (winter (DJF), spring (MAM), summer (JJA) and fall (SON)) were computed for each year. Annual means were calculated as the arithmetic mean of all daily values of a year. At most 5 missing values were allowed for the monthly means and at most 10 missing values for the annual means. Under these constraints only the station on Zugspitze has four missing monthly means in 1945 .

Observed Changes of Mean Maximum and Minimum

The times series of annual mean minimum and mean maximum temperatures show a good coincidence within each group of mountain stations and midland stations, see *Weber, Talkner and Stefanicki* [1994]. This indicates that the data are not much influenced by local effects and are representative for the respective regions.

Both the minimum and the maximum of the mountain stations increased during the observed period. At the midland stations on the other hand only the minimum increased, whereas the maximum shows no obvious increase. In *Weber* [1993] this behaviour was already noticed for the Swiss stations over the period 1901-1970. In order to roughly determine the amount of warming, the linear trends were calculated over the common period 1901-1990. The results are shown in Table 2. The mountain stations and their average show a significant linear trend of the same size in minimum and maximum temperature. The midland stations have a significant linear trend in the minimum but no significant, or a very small, linear trend in the maximum temperature. As some of the mountain stations and midland stations are close together, the observed difference in the increase of minimum and maximum is hardly caused by the variability of the sites, but probably related to the different height of the two types of stations. This is in strong contrast to the results reported by Bücher and Dessens [1991] for the station on the Pic du midi in the French Pyrenees, where the same diurnal asymmetry in warming was observed as for the midland stations.

Station or region	MIN	MAX	Station or region	MIN	MAX
Mountain Stations			*Midland Stations*		
Säntis	1.12	1.36	Basel	1.77	*0.11*
Sonnblick	1.23	1.43	Neuchâtel	2.24	*0.59*
Zugspitze homogenized	0.99	0.74	Zürich homogenized	1.82	*0.52*
			Bern homogenized	1.96	1.12
Mountain average	0.93	1.18	Midland average	1.76	*0.26*

Table 2. Trends [°C/100 yr] of the annual means of daily minimum (MIN) and maximum (MAX) temperature. Linear trends which are not significant at the two-tailed 5% level are printed in italics. The representative average of a region is the arithmetic mean of the two representative stations as described in text.

In Table 3 the linear trends for three-months seasons are presented for the representative averages of the mountain and midland regions. At all representative stations the largest warming occurred during fall. A multiple testing, based on the binomial distribution of independent trials [Sneyers, 1990] shows that the largest seasonal increase is significant at the 5% level and can be localized within the year. A trend analysis of the monthly means confirms that most of the significant warming took place in fall, especially in September and October.

Season	Region	MIN	MAX	Mean	Region	MIN	MAX	Mean
	Mountain				*Midland*			
Winter	(representative	*0.95*	*1.06*	*1.01*	(representative	1.77	*0.46*	1.11
Spring	average)	*0.71*	*0.90*	*0.81*	average)	1.70	*-0.11*	0.79
Summer		1.04	1.23	1.13		2.16	*-0.24*	0.96
Fall		1.90	2.30	1.21		2.26	1.17	1.72
Annual		1.15	1.37	1.26		1.97	*0.32*	1.15

Table 3. Trends [°C/100 yr] of seasonal means of daily minimum (MIN) and maximum (MAX) temperature. Linear trends which are not significant at the two-tailed 5% level are printed in italics. The representative average of a region is the arithmetic mean of the two representative stations as described in text. The annual mean is defined as the arithmetic mean of the four seasons.

Conclusions

Long records of daily minimum and maximum temperature from three stations at high altitude in the Alps and four midland stations at lower altitude were taken, and monthly, seasonal and annual means of the daily extreme values were formed. The resulting time series show a good coincidence between the stations within each group. The midland stations have the same diurnal asymmetry in their temperature increase as is observed over large parts of the continents. Only a small part of this asymmetry can be attributed to growing urbanization. The mountain stations, on the other hand, show an almost equal increase of minimum and maximum temperature. We conclude from these findings that the cause of the diurnal asymmetry in temperature increase is confined to the lowest part of the troposphere. An increase in low level cloud cover or in aerosol content, for example, could be the reason for the observed behaviour of daily minimum and maximum temperature.

References

Bücher, A., and J. Dessens, Secular trend of surface temperature at an elevated observatory in the Pyrenees, *J. Climate, 4*, 859-868, 1991.

Hunter, D.E., S.E. Schwartz, R. Wagener, and C.M. Benkovitz, Seasonal, latitudinal, and secular variations in temperature trend: Evidence for influence of anthropogenic sulfate, *Geophys. Res. Lett., 20*, 2455-2458, 1993

Intergovernmental Panel on Climate Change (IPCC), *Climate Change: The IPCC Scientific Assessment*, edited by J.T. Houghton, G.J. Jenkins, and J.J. Ephraums, 365 pp., Cambridge University Press, 1990

Intergovernmental Panel on Climate Change (IPCC), *Climate Change 1992: The Supplementary Report to the IPCC Scientific Assessment*, edited by J.T. Houghton, B.A. Callander, and S.K. Varney, 200 pp., Cambridge University Press, 1992.

Jones, P.D., and K.R. Briffa, Global surface air temperature variations during the twentieth century: Part 1, spatial, temporal and seasonal details, *The Holocene, 2*, 165-179, 1992

Karl, T.R., G. Kukla, and J. Gavin, Decreasing diurnal temperature range in the United States and Canada from 1941 through 1980, *J. Climate Appl. Meteor., 23*, 1489-1504, 1984.

Karl, T.R., H.F. Diaz, and G. Kukla, Urbanization: Its detection and effect in the United States climate record, *J. Climate, 1*, 1099-1123, 1988.

Karl, T.R., G. Kukla, V. Razuvayev, M.J. Changery, R.G. Quayle, R.R. Heim, Jr., D.R. Easterling, and C.B. Fu, Global warming: Evidence for asymmetric diurnal temperature change, *Geophys. Res. Lett., 18*, 2253-2256, 1991.

Karl, T.R., P.D. Jones, R.W. Knight, G. Kukla, N. Plummer, V. Razuvayev, K.P. Gallo, J. Lindseay, R.J. Charlson, and T.C. Peterson, A new perspective on recent global warming: Asymmetric trends of daily maximum and minimum temperature, *Bull. Am. Meteorol. Soc., 74*, 1007-1023, 1993.

Kukla, G., and T.R. Karl, Nighttime warming and the greenhouse effect, *Environ. Sci. Technol., 27*, 1468-1474, 1993.

Sneyers, R., On the Statistical Analysis of Series of Observations, *Technical Note 143*, 192 pp., World Meteorological Organization, Geneva, 1990.

Weber, R.O., Influence of different daily mean formulas on monthly an annual averages of temperature, *Theor. Appl. Climatol., 47*, 205-213, 1993.

Weber, R.O., P. Talkner and G. Stefanicki, Asymmetric diurnal temperature change in the Alpine region, *Geophys. Res. Lett., 21*, 673-676, 1994.

POSSIBLE CHANGE OF THE CLIMATE CONDITIONS IN SLOVAKIA DUE TO THE EXPECTED GLOBAL WARMING BY 1 - 2 °C

(Extended Abstract)

M. Lapin

Slovak Hydrometeorological Institute Bratislava, Slovakia

ABSTRACT

Possible impacts of the supposed climate change in next 35 years are discussed. Calculation of the water balance elements change was carried out according to the Zubenok - Budyko method using monthly data of air temperature, air humidity and precipitation. An assessment of the climate warming impacts upon changes of precipitation, relative air humidity, snow cover characteristics and daily range of air temperature was provided by the correlation method and by warmer periods analysis.

Introduction

Predicted climate change connected with the increase in the atmospheric greenhouse effect will probably cause changes of atmospheric circulation and, from this, resulting changes of precipitation, cloudiness, air humidity and other climatic elements all over the world. These changes can seriously influence the natural environment and socio-economic activities. This paper represents a brief review of results obtained in completing some of the Czecho-Slovak and the Slovak National Climate Programme tasks from 1991 to 1994.

Methods and data

Two climatological stations (Hurbanovo, 115 m a.s.l., representing lowlands in southern Slovakia and Liptovský Hrádok, 640 m a.s.l., representing valleys in northern Slovakia near the High Tatras) were used as a basic source for all calculations, and seven other ones in Slovakia for the correlation method applications. The potential evaporation E_o was calculated according to the Zubenok nomograms using monthly air temperature and relative air humidity averages. For the actual evaporation E calculation, the complex Budyko method was adopted using E_o and monthly precipitation totals, as well as some parameters of the precipitation regime and optimal soil moisture.

For the period 1951 - 1991 we prepared means and totals of several climatological elements, both for warm (IV-IX) and cold (X-III) half-years in each year. Then a correlation analysis of relative air humidity and snow cover characteristics with air temperature and precipitation was done for nine stations in Slovakia. Selected results are shown in the Table 1. More detailed analysis was made for winter (XII-II) and summer (VI-VIII) values at the station Hurbanovo in the period 1903-1994 (Table 2 and Figure 2 present an example of results). All data have been tested for homogeneity by Craddock test and Double mass analysis.

Table 1. Correlation coefficients (r) and linear terms (l) of the linear regression equations for the relation of the variables: U - relative air humidity in %, T - air temperature in °C, P - precipitation in 100 mm, N - number of days with snowcover in 10 days, S - daily snowcover depth totals in 100 cm. In the columns 1 and 2 the values for warm half-years and in other ones for cold half-years of the period 1951-1991 are presented.

		C O R R E L A T I O N S							
Stations (altitude)	r l	1 (T,U)	2 (P,U)	3 (T,U)	4 (P,U)	5 (N,U)	6 (S,U)	7 (T,N)	8 (T,S)
Hurbanovo	r	-0,4	0,7	-0,3	0,4	0,4	0,4	-0,8	-0,7
(115)	l	-2,0	2,5	-0,6	1,2	0,4	0,3	-1,3	-1,8
Bratislava	r	-0,4	0,7	-0,2	0,5	0,2	0,2	-0,7	-0,6
Koliba (286)	l	-1,8	2,3	-	1,5	-	-	-1,6	-3,2
Piešťany	r	-0,3	0,6	-0,2	0,6	0,4	0,2	-0,7	-0,6
(165)	l	-1,2	2,0	-	2,1	0,6	-	-1,0	-1,3
Košice,	r	-0,5	0,7	0,0	0,6	0,1	0,0	-0,6	-0,5
letisko (230)	l	-2,3	2,5	-	1,7	-	-	-1,1	-1,9
Sliač,	r	-0,4	0,6	0,1	0,3	0,2	0,1	-0,7	-0,6
letisko (313)	l	-1,9	1,8	-	0,7	-	-	-1,5	-3,9
Liptovský	r	-0,4	0,6	0,0	0,4	0,4	0,1	-0,4	-0,5
Hrádok (640)	l	-1,2	1,4	-	0,9	0,3	-	-1,0	-4,3
Poprad,	r	-0,3	0,6	-0,3	0,4	0,4	0,2	-0,6	-0,6
letisko (695)	l	-1,1	1,6	-0,6	1,7	0,4	-	-1,1	-4,2
Telgárt	r	-0,4	0,5	0,1	0,4	0,2	0,1	-0,6	-0,6
(901)	l	-1,5	1,2	-	1,0	-	-	-1,4	-13,2
Štrbské	r	-0,5	0,4	-0,2	0,3	0,0	0,1	-0,1	-0,4
Pleso (1360)	l	-1,8	1,1	-	1,4	-	-	-	-13,9

Table 2. Correlation coefficients (r) and linear terms (l) of the linear regression equations for the relation of the variables: U - relative air humidity in %, PP - air pressure in Vienna in hPa, T - air temperature in °C, Ta - mean daily range of air temperature in °C, P - precipitation in 100 mm, N - number of days with snowcover in 10 days, S - daily snowcover depth totals in 100 cm. In the lines 1 and 2 the values for winters (XII-II) and in other ones for summers (VI-VIII) of the period 1903-1993/4 at the station Hurbanovo are presented.

	(T,N)	(T,S)							
r	-0.7717	-0.7383							
l	-0.66	-1.18							
	(U,Ta)	(P,Ta)	(PP.Ta)	(PP,P)	(T,P)	(T,U)	(T,Ta)	(P,U)	(PP,U)
r	-0.7579	-0.6064	0.4896	-0.3954	-0.3257	-0.5730	-0.5815	0.6285	-0.4963
l	-0.21	-1.1	0.53	-0.25	-0.24	-2.67	0.75	3.9	-1.9

Table 1. Correlation coefficients (r) and linear terms (l) of the linear regression equations for the relation of the variables: U - relative air humidity in %, T - air temperature in °C, P - precipitation in 100 mm, N - number of days with snowcover in 10 days, S - daily snowcover depth totals in 100 cm. In the columns 1 and 2 the values for warm half-years and in other ones for cold half-years of the period 1951-1991 are presented.

		C O R R E L A T I O N S							
Stations (altitude)	r l	1 (T,U)	2 (P,U)	3 (T,U)	4 (P,U)	5 (N,U)	6 (S,U)	7 (T,N)	8 (T,S)
Hurbanovo	r	-0,4	0,7	-0,3	0,4	0,4	0,4	-0,8	-0,7
(115)	l	-2,0	2,5	-0,6	1,2	0,4	0,3	-1,3	-1,8
Bratislava	r	-0,4	0,7	-0,2	0,5	0,2	0,2	-0,7	-0,6
Koliba (286)	l	-1,8	2,3	-	1,5	-	-	-1,6	-3,2
Piešťany	r	-0,3	0,6	-0,2	0,6	0,4	0,2	-0,7	-0,6
(165)	l	-1,2	2,0	-	2,1	0,6	-	-1,0	-1,3
Košice,	r	-0,5	0,7	0,0	0,6	0,1	0,0	-0,6	-0,5
letisko (230)	l	-2,3	2,5	-	1,7	-	-	-1,1	-1,9
Sliač,	r	-0,4	0,6	0,1	0,3	0,2	0,1	-0,7	-0,6
letisko (313)	l	-1,9	1,8	-	0,7	-	-	-1,5	-3,9
Liptovský	r	-0,4	0,6	0,0	0,4	0,4	0,1	-0,4	-0,5
Hrádok (640)	l	-1,2	1,4	-	0,9	0,3	-	-1,0	-4,3
Poprad,	r	-0,3	0,6	-0,3	0,4	0,4	0,2	-0,6	-0,6
letisko (695)	l	-1,1	1,6	-0,6	1,7	0,4	-	-1,1	-4,2
Telgárt	r	-0,4	0,5	0,1	0,4	0,2	0,1	-0,6	-0,6
(901)	l	-1,5	1,2	-	1,0	-	-	-1,4	-13,2
Štrbské	r	-0,5	0,4	-0,2	0,3	0,0	0,1	-0,1	-0,4
Pleso (1360)	l	-1,8	1,1	-	1,4	-	-	-	-13,9

Table 2. Correlation coefficients (r) and linear terms (l) of the linear regression equations for the relation of the variables: U - relative air humidity in %, PP - air pressure in Vienna in hPa, T - air temperature in °C, Ta - mean daily range of air temperature in °C, P - precipitation in 100 mm, N - number of days with snowcover in 10 days, S - daily snowcover depth totals in 100 cm. In the lines 1 and 2 the values for winters (XII-II) and in other ones for summers (VI-VIII) of the period 1903-1993/4 at the station Hurbanovo are presented.

	(T,N)	(T,S)							
r	-0.7717	-0.7383							
l	-0.66	-1.18							
	(U,Ta)	(P,Ta)	(PP.Ta)	(PP,P)	(T,P)	(T,U)	(T,Ta)	(P,U)	(PP,U)
r	-0.7579	-0.6064	0.4896	-0.3954	-0.3257	-0.5730	-0.5815	0.6285	-0.4963
l	-0.21	-1.1	0.53	-0.25	-0.24	-2.67	0.75	3.9	-1.9

Deviations of the period 1988-1993 water balance means from 1901-1980 normals at station Hurbanovo, south Slovakia

Fig. 1.

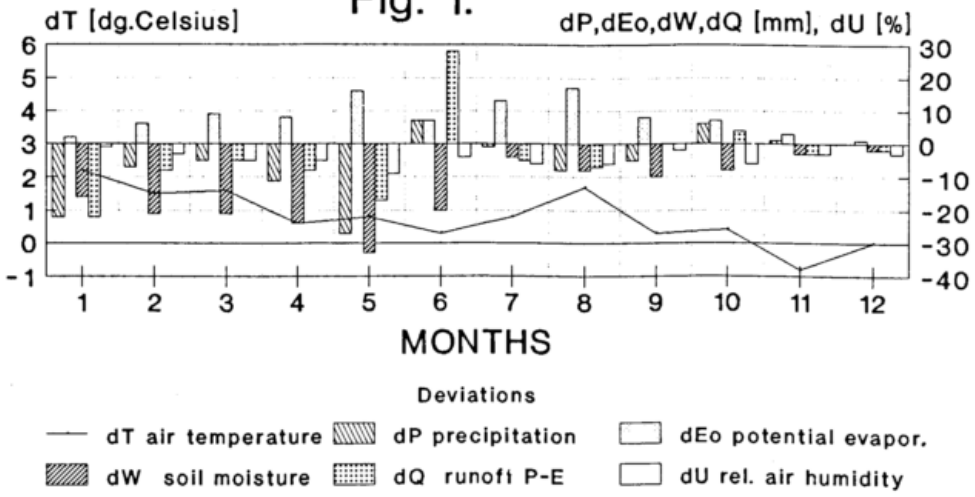

Values Eo, E and W are calculated according to Budyko-Zubenok method
Detail information is in text

Relation between mean air temperature T and number of days with snow cover N at Hurbanovo in winters 1920/21-1993/94

Fig. 2.

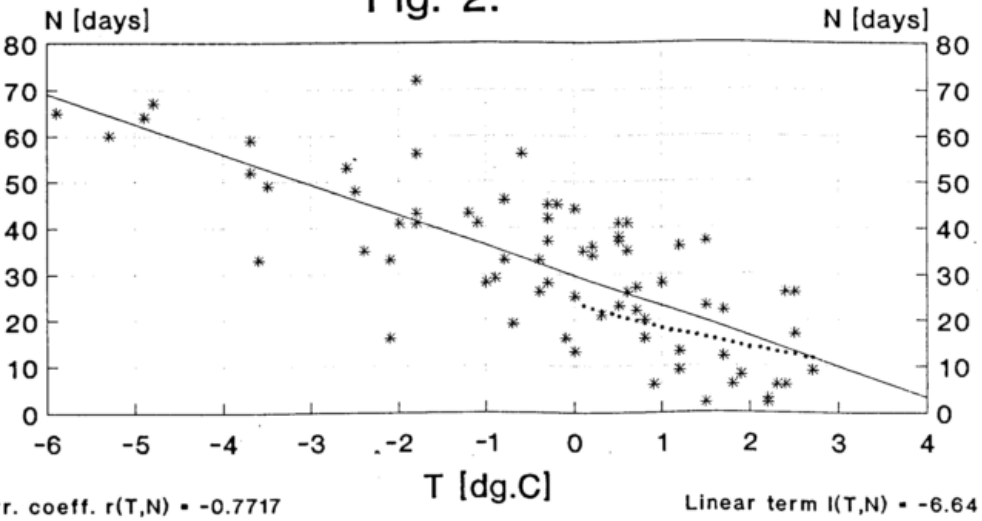

Winter 1950 are months XII.1949-II.1950

Results

Results of the water balance model calculations for stations Hurbanovo and Liptovský Hrádok showed a significant rise of potential evaporation calculated according to Zubenok method by about 15 % since 1901. Final results of the water balance calculations are the usable soil moisture W and the balance runoff Q values. A significant decreasing trend of W and Q by 10-20 % was found at both stations. Model calculation using scenarios of temperature T, precipitation P and relative air humidity U change confirmed continuous decreasing trends of W and Q in all territory of Slovakia in next four decades by further 10-20 % (decrease of Q in mountainous part of Slovakia is expected as a very unfavorable if T increase and no considerable P increase is supposed). Figure 1 shows (as an example of warmer periods analysis) deviations from normals 1901-1980 of some measured and calculated means at Hurbanovo for the period 1988-1993. This 6-year period was the warmest and driest one since 1871 in Slovakia. There can be seen significant deviations of all elements mainly in spring and summer months toward lowering of W values.

Some results of correlation analysis for selected nine stations are shown in the Table 1. Significantly close correlation was found between mean relative air humidity U and precipitation totals P in warm half-year on the whole territory of Slovakia. If P totals decrease by 100 mm in average, U will probably decrease by 2 % in lowlands and by 1 % in other regions. Acceptable correlation was found also between U and mean air temperature T in warm half-year. Snow characteristics are in a close correlation with mean air temperature of cold half-year. The average number of days with snow cover N will decrease probably by about 15 days if T increases by 1 °C. That is about 30 % in lowlands but only 10 % of the present average of N in mountains. The decrease of the daily depths of snow cover totals S is considered more important. The 1 °C rise of T in cold half-year will probably cause the decrease of S by 100 to 300 cm in lowlands (approx. by 50 %) and by 400 to 1400 cm in the middle altitudes (approx. by 35 to 15 %).

More detailed correlation analysis was made at the station Hurbanovo, where are to disposal reliable professionally observed data for all elements since 1903. Selected results for summer and winter periods of those analysis are presented in Table 2 and in Figure 2. We can see significant correlation between air temperature T rise and relative air humidity U decrease, between U decrease and daily range of air temperature Ta rise, between T rise in winter and snow characteristics decrease. Linear regression is only approximately significant at snow characteristics near zero, so we calculated exponential regression as well (Figure 2, dotted line).

Conclusion

In the next stage of this topic solving we plan to do some model calculations using regional climate change scenarios and more detailed methods. Further plan is based on analysis of the atmospheric circulation change impact upon climate characteristics (precipitation, air humidity, sun shine...) in Slovakia. This solving is included into the National Climate Programme tasks.

DECREASE OF THE ANNUAL AMOUNT OF THE HOURS WITH FOEHN AT ISPRA

by Claudio GANDINO

(Research Centre of European Communities)

I-21020- ISPRA (Italy) FAX i-0332-789413 -email: claudio.gandinoCjrc.it

ABSTRACT

Ispra is located on the eastern side of Lago Maggiore, ninety kms South of the Gotthard Pass. This position is ideally suited for a study of the characteristics of the North Foehn and every hour with this wind has been taken into account with related parameters from 1964 to 1993 (30 years).

Three different time scales have been considered on the horizontal axis of many drawings:

1) Starting with 1964 and going on to 1993, the annual amount of the hours with Foehn and the annual precipitations are decreasing, whereas, with some doubts about the instrument precision, the annual means of the atmospheric pressure, of the air temperature and of the water vapour pressure are increasing.
2) With every annual amount of the hours with Foehn on the horizontal axis in increasing order, the mean atmospheric pressure and the water vapour pressure are decreasing. This is consistent with point 1.
3) Only the events of strong Foehn which continued during a second day were chosen. On the horizontal axis the hours with Foehn during the first day are written, considering them as an index of Foehn intensity. With less evidence than in the two preceeding scales, the average relative humidity and the water vapour pressure are decreasing with a correlation coefficient equal to 0.6.

1. Introduction

The meteorological observatory of Ispra was established in 1959. Although 35 years involve a period of time which is shorter than the secular series of some famous observatories, during this last period the human race caused most damage to the Earth. Considering that our observatory is located in an agricultural area, where pasture-fields and woods have been maintained, its instruments can show the multiannual variation of the meteorological elements, as part of the climatic change (Gandino, 1993).

2. Variation of meteorological elements with time.

Figure 1 shows the decrease of the annual totals of the hours with Foehn, at a rate of thirteen hours per year. A regression line is drawn with a correlation coefficient =0.62. In part this is due to the growing of trees around the observatory, but the weather influence is the most important cause. In the upper part of Figure 1, the annual totals of precipitation are drawn. These decrease at a rate of about one millimeter per year with a correlation coefficient which is very small, but however could reach 0.22 if the precipitations from 1959 to 1963 are added.
This decrease is confirmed by the persistent dry weather in the Southern Europe during the last years (Maheras, 1994).

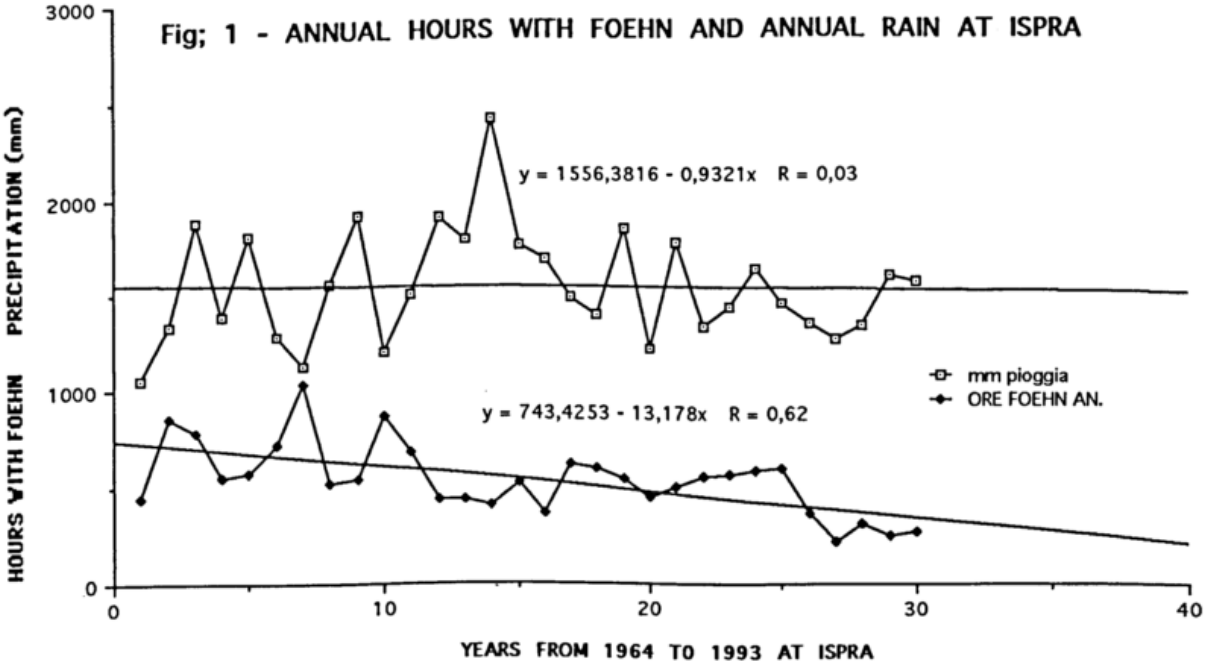

Drawing other diagrams which are similar to Figure 1, it could be possible to derive that during the last thirty years the air temperature increased about half centigrade degree and the water vapour pressure, which was computed with the air temperature and relative humidity, increased about one hPa with a correlation coefficient =0.74, but with some doubts about its accuracy.

The atmospheric pressure increased about three hPa, but we must remember that the precision of the three barographs was not always the same during thirty years. However, an agreement exists with the 100-years data series of measurements at Sonnblick, which recorded a similar increase of air temperature and atmospheric pressure (Auer, Bohhm and Mohnl). On the contrary, solar irradiation does not show any trend at Ispra.

3. Variation of meteorological elements with the annual Foehn hours.

In **Figure 2** the decrease of the annual average water vapour pressure and of the annual atmospheric pressure with the yearly totals of Foehn hours in increasing order are drawn. Both regression lines show a correlation coefficient about 0.6 , following a small decrease which means drier air with more hours with Foehn.

Fig. 2 - VAPOR PRESSURE AND ATMOSPHERIC PRESSURE vs ANNUAL FOEHN HOURS

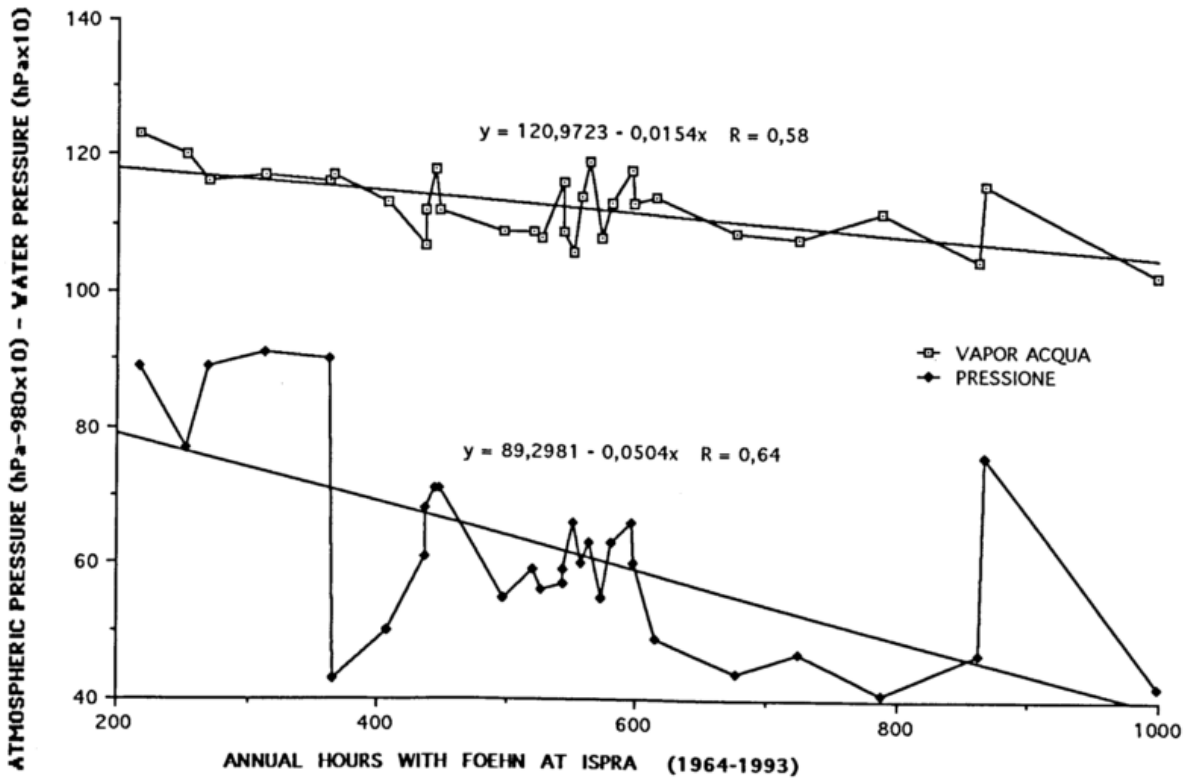

4. Variation of meteorological elements with the Foehn intensity.

The steep increase and the slow decrease of the wind speed during a typical Foehn event and the variation of atmospheric pressure, which is V-shaped, were shown during the 1966 and 1974 Meetings on Alpine Meteorology. In addition to that, this paper presents a correlation of the relative humidity and of water vapour pressure

with time while Fohn is blowing. Only the events of strong Foehn which continued during a second day were chosen. Because these conditions are rare, twenty events during 1988 and a second group of twenty events during 1991 and 1992 have been selected. On the horizontal axis the hours with Foehn during the first day are written, considering them as an index of Foehn intensity. With the group of 1991 and 1992 data the average relative humidity and the water vapour pressure are decreasing with a correlation coefficient about 0.6.

The maximum gust is not a representative parameter for the horizontal axis.

Moreover, considering 14 events of the 1988, a decrease of the water vapour pressure during the second day is correlated with the reascending of the atmospheric pressure after the typical minimum which characterize the starting of the Foehn, with a correlation coefficient =0.39.

5. Conclusions

Some multiannual trends of several meteorological parameters are evident, but they are so small that they do not completely exclude a possible effect of instrumental error.

The annual hours with Foehn halved, the air temperature increased about half centigrade degree and the atmospheric pressure increased by a few hPa. This is in partial agreement with Sonnblick measurements.

However, this thirty years period could have been a fortunate period to find the shown correlations and the trend for 1994 is already different .

6. References

1) AUER I., BOEHM R., MOHNL H., " Die troposphaerisce Erwaermungsphase des 20. Jahrhunderts ", *20° Congresso di Meteorologia Alpina, Vol.1, pp 145-159,* Sèstola,1988.

2) GANDINO C. "Atmospheric pressure and Foehn wind at Ispra", *Rivista Italiana di Geofisica, Vol.1, pp 44-46,* Saint Vincent, 1974.

3) GANDINO C. , DE BORTOLI M., "Andamenti della velocità del Foehn ad Ispra ", *pubblicazione N.4 della Centrale Meteorologica Svizzera* , 9. Tagung fuer Alpine Meteorologie, pp 255-260, Brig-Zermatt,1966.

4) GANDINO C. , MARANZANA E. ,"34° Annuario Meteorologico 1992 di Ispra", *rapporto EUR 14983* , Lussemburgo, 1993.

5) MAHERAS P.,"*Actes du Colloque de l'Association Internationale de Climatologie*" Thessaloniki, 1993.

Le precipitazioni nelle Valli di Lanzo durante il periodo 1915 - 1993

A. Biancotti, S. Paludi

Università di Torino - Dipartimento di Scienze della Terra
Comitato Glaciologico Italiano

ABSTRACT

Stura di Lanzo basin is located in Western Italian Alps, W of the city of Turin. In this area are installed about ten meteorological stations belonging to Italian Hydrographic Service network; some pluviometric series begin in 1913, other during the 30's. All stations show a pluviometric pattern characterized by main maximun during May, secondary maximum in October and winter main minimum. The mean yearly precipitation ranges between 1100 mm of highest stations and 1300 mm of lowest ones, showing an higher interannual variability. Most of daily rainfalls have an intensity of 1 to 5 mm, but are numerous events over 200 mm in 24 hours too. After the heavy rainfalls of the second half of 10's, the yearly amounts are close to the mean until the early 60's. The period 1960 - 1970 shows a pluviometric deficit, while the 70's represent the main positive anomaly, with yearly absolute maxima, reached in 1977, exceeding 2500 mm. From 1980 the precipitations become again lower than mean, coming back to normal values at the beginning of 90's. The Mann-Kendall test shows no trends.

RIASSUNTO

Il bacino della Stura di Lanzo è ubicato nelle Alpi occidentali italiane ad Ovest della città di Torino. In tale comprensorio sono ubicate circa dieci stazioni meteorologiche appartenenti alla rete del Servizio Idrografico Italiano, le cui serie pluviometriche iniziano in alcuni casi nel 1913, in altri durante gli anni '30. Tutte le stazioni mostrano un regime pluviometrico caratterizzato da massimo principale in maggio, massimo secondario in ottobre e minimo principale invernale. La piovosità media annua è compresa tra i 1100 mm delle stazioni più elevate ed i 1300 mm di quelle ubicate a fondo valle, ove la variabilità interannuale è maggiore. La maggior parte degli eventi piovosi giornalieri è di intensità compresa tra 1 e 5 mm, ma sono numerosi anche gli eventi superiori ai 200 mm in 24 ore. Dopo le abbondanti precipitazioni della seconda metà degli anni '10, i valori annui si mantengono intorno alla media fino all'inizio degli anni '60. Il decennio 1960 - 1970 mostra un deficit pluviometrico, mentre i successivi anni '70 rappresentano la principale anomalia positiva, con massimi annui assoluti, raggiunti nel 1977, superiori a 2500 mm. Dal 1980 le precipitazioni scendono nuovamente a valori inferiori alla media, ritornando a valori normali con l'inizio degli anni '90. Il test di Mann-Kendall non evidenzia tendenze.

1. Introduzione

Il bacino della Stura di Lanzo si trova nelle Alpi Graie ad W della città di Torino (Italia NW). All'interno dello sbocco nella pianura torinese (450 m s.l.m.), esso si dirama in tre valli parallele con asse W - E: la Val Grande a N, la Val d'Ala in centro e la Val di Viù a S; la superficie totale è di 627 Km^2, l'elevazione media di 1740 m e quella massima di 3676 m. In Val di Viù sono presenti tre laghi artificiali, utilizzati per la produzione idroelettrica, contenenti circa 11 milioni di m^3 d'acqua; è inoltre in progetto un quarto sbarramento, capace di contenere $50*10^6$ di m^3 d'acqua destinata ad incrementare le risorse idropotabili della città di Torino. Nel bacino esistono attualmente 11 stazioni meteorologiche appartenenti alla rete Servizio Idrografico e Mareografico Nazionale - Sezione di Torino, quasi tutte installate presso impianti idroelettrici dell'ENEL; alcune di esse (Viù, Usseglio, Ceres e Balme) hanno iniziato la loro attività nel 1913, mentre la stazione meteorologica del Lago della Rossa (2725 m s.l.m.) attiva fin dal 1938, assume un ruolo fondamentale nello studio della climatologia di alta montagna, trattandosi di uno dei pochi punti di osservazione meteorologica ubicati a circa 3000 m. I dati pluviometrici giornalieri sono stati digitalizzati per mezzo di Ashton-Tate DB3, sottoposti a validazione ed elaborati cercando di interpolare le informazioni provenienti dai singoli punti di misura. Si ringrazia il Dott. Furio Dutto (Servizio Idrografico e Mareografico Nazionale - Sezione di Torino) per aver consentito agli autori di consultare dati di archivio inediti.

2. Regime pluviometrico

La definizione del regime pluviometrico rappresenta il primo passo per conoscere la distribuzione annua delle precipitazioni. Premettiamo fin d'ora che abbiamo considerato l'anno idrologico (ottobre - settembre) ed utilizzato la classificazione dei regimi pluviometrici in Italia proposta da PINNA & VITTORINI (1985). Tutte le stazioni considerate presentano due massimi e due minimi: il massimo assoluto cade in primavera (maggio), quello secondario in autunno (ottobre); i minimi principale e secondario sono invece caratteristici rispettivamente dell'inverno (gennaio) e dell'estate

(luglio). Sulla base di questa distribuzione si può concludere che il bacino della Stura di Lanzo ha un regime pluviometrico di tipo padano - prealpino, caratteristico di quasi tutto il Piemonte, della bassa pianura lombarda e della pianura veneta. Nel corso del mese più piovoso, maggio, si concentrano percentuali degli apporti medi annui comprese tra il 13.3 ed il 15.8%; anche ottobre ed aprile sono mesi piuttosto umidi, durante i quali la frazione pluviometrica mensile supera il 10%. Passando ai periodi meno piovosi, i mesi invernali ed estivi, specialmente luglio ed agosto, presentano percentuali di precipitazione dell'ordine del 5% e, comunque, mai superiori al 10%. Introducendo la variabile indipendente elevazione, oltre i 2000 m la frazione pluviometrica mensile assume, in novembre e nel corso della primavera (marzo - maggio), valori minori rispetto a quelli calcolati per le stazioni ubicate più in basso; tale situazione si inverte dall'estate inoltrata all'inizio dell'autunno. Confrontando le frazioni pluviometriche dei due sottobacini della Stura di Viù e della Stura d'Ala - Stura di Lanzo non si notano differenze di particolare rilievo, salvo che il massimo principale di maggio si presenta più accentuato in Val d'Ala, dove varia dal 13,9 al 15,8%, mentre in Val di Viù le percentuali si mantengono inferiori al 15%; un comportamento analogo caratterizza anche il massimo secondario. Relativamente al minimo di luglio si può invece rilevare come, al disotto dei 1000 m, la Val d'Ala riceva apporti lievemente superiori a quelli della Val di Viù, situazione che si capovolge al disopra di tale limite. Una miglior sintesi territoriale è resa possibile considerando la percentuale delle precipitazioni medie stagionali. Gli apporti maggiori appartengono, in tutto il bacino alla primavera, seguiti da quelli autunnali, estivi ed invernali. In Val di Viù gli apporti sono maggiori al disotto dei 2000 m in primavera ed al disopra di tale elevazione nel corso dell'estate. A livello di differenze tra i due sottobacini, in Val d'Ala sono leggermente più cospicui gli afflussi primaverili ed autunnali, mentre nelle due stagioni meno piovose le precipitazioni favoriscono la Val di Viù. La quantità di pioggia e neve fusa che cade, in media, durante ogni anno idrologico nel comprensorio considerato, si mantiene superiore ai 1000 mm, decrescendo dai 1396,7 mm di Ceres fino ai 1098.7 mm del Lago della Rossa. L'andamento medio mensile delle precipitazioni si apre con il massimo secondario di ottobre, i cui apporti sono compresi tra i 124.0 mm del Lago della Rossa ed i 177.2 mm di Funghera. A partire da novembre, quando si registrano ancora quantità di pioggia e neve fusa superiori ai 100 mm, eccetto che in Val di Viù oltre i 1000 m s.l.m., inizia il decremento delle precipitazioni che persiste fino al minimo principale di gennaio, oscillante tra i 44.9 mm di Funghera ed i 60.6 di Balme. Da febbraio i totali mensili crescono fino a raggiungere il massimo principale di maggio, mese durante il quale, in Val di Viù, gli apporti oscillano tra 148.4 mm (Lago della Rossa) e 196.9 mm (Viù), mentre in Val d'Ala l'intervallo si restringe e si sposta verso l'alto, risultando compreso tra i 180.0 mm di Balme ed i 221.3 mm di Ceres. Una brusca caduta degli afflussi conduce al minimo secondario di luglio, dopodichè si verifica una ripresa che si protrae durante i mesi di agosto e settembre. A livello mensile la minor variabilità interannuale spetta ai mesi che vanno dalla metà della primavera alla metà dell'autunno; più precisamente l'estate mostra i minimi scostamenti dalla media, in particolar modo oltre i 2000 m, dove il coefficiente di variazione di agosto scende al disotto del 50% (49.5% al Lago dietro la Torre e 48.3% al Lago della Rossa). Dall'autunno inoltrato all'inizio della primavera le oscillazioni interannuali degli apporti sono decisamente più marcate, soprattutto in novembre, gennaio e febbraio. A livello annuo in Val di Viù sono le stazioni ubicate più in basso ad avere coefficienti di variazione maggiori, eccezion fatta per il Lago della Rossa ove tale parametro raggiunge il 26.2%, valore confrontabile con quelli di Usseglio e Malciaussia, stazioni site al disotto dei 2000 m. In Val d'Ala, ove la variabilità interannuale è più marcata che in Val di Viù, spicca il dato di Ceres, il cui coefficiente di variazione ammonta appena al 21.9% (minimo del bacino), mentre i valori delle altre stazioni della valle si aggirano intorno al 27 - 29% circa.

3. Andamento delle precipitazioni con l'elevazione

Contrariamente a quanto riportato in bibliografia, nel bacino della Stura di Lanzo la quantità media annua di pioggia e neve fusa caduta diminuisce dal fondo valle verso l'alta montagna. Tale comportamento, segnalato da MENNELLA (1967) per altre valli delle Alpi occidentali, è confermato dall'analisi di regressione, in base alla quale il decremento medio degli apporti può essere quantificato in circa 10 mm ogni 100 m. La spiegazione di questo comportamento delle precipitazioni può essere rappresentata dal sollevamento della masse d'aria umida ad opera delle prealpi, fenomeno che riduce drasticamente il loro contenuto di umidità, limitando l'entità degli apporti a mano a mano che ci si addentra nella catena alpina. Localmente sono riscontrabili inversioni di tendenza minime, la cui ragion d'essere risiede, piuttosto che in cause dinamiche, nella disposizione degli strumenti in siti che, per la presenza di ostacoli perlopiù artificiali, favoriscono la raccolta delle idrometeore all'interno dei collettori dei pluviografi.

4. Distribuzione di frequenza delle precipitazioni giornaliere

In tutte le stazioni del bacino le precipitazioni più frequenti sono quelle di debole intensità, cioè comprese tra 0.1 e 5 mm nel corso delle 24 ore: tali eventi rappresentano circa il 50% di tutti quelli finora registrati. Ben rappresentati, sebbene di gran lunga subordinati, anche i casi pluviometrici apportanti da 6 a 10 mm e da 11 a 20 mm: le loro frequenze oscillano intorno al 20 ed al 17% rispettivamente. Con la classe di intensità 21 - 30 mm la frequenza scende al disotto del 10%, mentre quella successiva 31 - 50 mm rappresenta appena il 4 - 5% delle manifestazioni meteoriche. Gli eventi con intensità compresa tra 51 e 70 mm sono gli ultimi ad avere una frequenza superiore all'unità percentuale. Si noti, infine, come oltre i 1800 m gli

apporti giornalieri superiori a 150 mm, sebbene possibili, perdano ogni significato per la climatologia media, diventando però interessanti nell'analisi degli eventi estremi.

5. Giorni piovosi e sequenze di giorni asciutti e piovosi

Il numero medio annuo di giorni piovosi, compreso tra 84 (Funghera) e 112 (Lago della Rossa e Lago dietro la Torre), aumenta con l'elevazione, risultando inferiore a 100 fin verso i 1500 m ed oltrepassando tale soglia alle quote superiori. La distribuzione mensile ricalca abbastanza fedelmente il regime pluviometrico, raggiungendo il massimo assoluto (11 - 13 giorni) in maggio ed il minimo, compreso tra 4 e 7 giorni, in gennaio; in luglio, mese in cui si situa il minimo secondario del regime pluviometrico, i giorni piovosi oscillano tra 7 e 9, mostrando un divario non particolarmente ampio rispetto ai mesi più piovosi, quando il parametro in esame si mantiene superiore ai 10 giorni. Se nei mesi con precipitazioni più frequenti il numero medio di giorni piovosi non presenta particolari tendenze all'aumentare dell'elevazione, quello dei mesi con apporti più rari, almeno in Val di Viù, mostra un lieve incremento, passando dai 4 di Viù agli 8 del Lago della Rossa. I giorni piovosi, come quelli asciutti, tendono ad associarsi in gruppi. La lunghezza media delle sequenze di giorni piovosi è di circa due giorni; non esistono significative tendenze all'aumentare dell'elevazione. Venendo ai periodi asciutti, il loro protrarsi persiste, in media, dai 5 ai 6 giorni, con un massimo a Funghera di circa 6 giorni ed un minimo al Lago della Rossa di appena 4 giorni. Il più lungo periodo piovoso verificatosi nel bacino è stato, a Viù, di 27 giorni (3 - 29 maggio 1984), mentre l'assenza di precipitazioni è durata, a Funghera, ben 78 giorni (4 dicembre 1988 - 19 febbraio 1989); solo al Lago della Rossa non si sono mai contati più di 50 giorni asciutti consecutivi, infatti il massimo è stato di 38 giorni, dal 18 dicembre 1975 al 24 gennaio 1976.

6. Massimi pluviometrici giornalieri e mensili

I massimi pluviometrici giornalieri raggiungono e superano i 400 mm in diverse stazioni (Viù, Lemie, Ala di Stura e Balme), altrove oscillano tra 200 e 300 mm (Usseglio, Malciaussia, Lago dietro la Torre, Funghera e Ceres), mentre solo al Lago della Rossa non sono mai stati superati i 158.2 mm in 24 ore. Nella maggior parte dei casi, il massimo è stato raggiunto durante l'evento del 26 settembre 1947 che apportò ben 472 mm a Viù, 430 mm a Lemie e 410 mm a Balme; anche laddove il primato spetta ad un altro giorno, le precipitazioni di quel 26 settembre rappresentano il massimo apporto giornaliero assoluto per il mese di settembre, come a Malciaussia (115.0 mm), al Lago della Rossa (102.0 mm) e ad Ala di Stura (210.0 mm). Altri eventi pluviometrici giornalieri significativi furono quelli dell'8 novembre 1962 e del 1° aprile 1981: in entrambi i casi molte stazioni ricevettero più di 200 mm nel corso delle 24 ore ed alcune oltre 300 mm. Il massimo totale mensile di precipitazione fu registrato a Viù nel maggio 1949 ed ammonta a 735.4 mm, pari al 373% della media mensile; sempre a Viù, nell'aprile 1918 caddero 730.7 mm di pioggia, con uno scostamento dalla media del 417%. Altri dati interessanti sono rappresentati dai 715.0 mm e dai 677 mm del maggio 1949 misurati a Funghera e Balme rispettivamente, dai 639 mm rilevati ad Ala di Stura durante il maggio 1937 e dai 635.4 mm caduti, nel corso del novembre 1962, ancora a Balme. Tra i massimi pluviometrici mensili subordinati, segnaliamo quelli del giugno 1957, dell'aprile 1986 e del giugno 1992. Nel primo caso le abbondanti precipitazioni (da 400 a 550 m), associate all'incremento delle portate prodotte dalla fusione nivale, provocarono l'esondazione delle Sture in diversi punti del bacino, con danni alla rete viaria e, più ridotti, ai fabbricati. Nell'aprile 1986 e nel giugno 1992 non furono segnalati dissesti di particolare entità, tuttavia gli apporti, dell'ordine dei 350 - 600 mm rappresentano il massimo assoluto per i mesi di aprile e giugno in molte stazioni o, comunque, uno dei principali massimi degli ultimi vent'anni.

7. Evoluzione cronologica delle precipitazioni ed individuazione di tendenze

La sufficiente omogeneità delle serie pluviometriche esaminate ha permesso di sintetizzare i totali annui a livello bacinale per mezzo dello Standardized Anomaly Index. Per il periodo anteriore al 1939 l'analisi è stata compiuta considerando i dati di tre sole stazioni (Viù, Usseglio e Ceres); dal 1939 in avanti sono invece state utilizzate le informazioni fornite da 9 stazioni sulle 11 disponibili. L'applicazione ai valori del S.A.I. del test di Mann-Kendall non ha evidenziato tendenze. Durante la seconda metà degli anni '10 i totali annui di precipitazione mostrano un picco positivo; tuttavia, dalla fine di questo decennio ai primi anni '20, esse decrescono fino a raggiungere valori prossimi alla media che mantengono per circa 10 anni. Nella seconda metà degli anni '30 si colloca un nuovo periodo piuttosto piovoso che persiste fino ai primi anni '40; anche la seconda metà di questo decennio presenta totali pluviometrici superiori alla norma, mentre tra il 1950 ed il 1965 circa le precipitazioni tornano a mantenersi più o meno conformi alla media, salvo alcuni lievi scostamenti. La seconda metà degli anni '60 evidenzia invece un importante minimo pluviometrico, seguito, però, da una rapida ripresa che persiste per tutta la prima metà del decennio 1970/'79 e lascia spazio ad una fase di abbondanti precipitazioni, protrattasi per buona parte degli ultimi anni '70. Dal 1979 i totali annui di pioggia e neve fusa diminuiscono nuovamente, scendendo ai valori fortemente deficitari del 1989/'90; dal 1991 si profila, invece, una nuova ripresa. L'anno più piovoso è stato il 1977, quando,

in quasi tutto il bacino, caddero oltre 2000 mm di pioggia e neve fusa: fanno eccezione il Lago dietro la Torre ed il Lago della Rossa, stazioni che ricevettero comunque apporti superiori ai 1900 mm. Anche 1972, 1946 e 1920 furono anni con precipitazioni piuttosto copiose, specialmente nella medio - bassa Val di Viù e nella media Val d'Ala. Meno univoco è, invece, l'anno idrologico che registrò gli apporti più scarsi; nella maggior parte delle stazioni risulta essere il 1990 con circa 600 mm, tuttavia a Viù fu il 1970 (650.4 mm) e ad Usseglio il 1979 (619.4 mm).

8. Bibliografia

BIANCOTTI A. (1982) - *Ricerche di geografia fisica nel bacino del Fiume Varaita (Alpi Cozie, Piemonte).* Torino

BIANCOTTI A., BRANCUCCI G., MASSAGLIA L. & MERCALLI L. (1991) - *La serie termopluviometrica di Cuneo 1877-1990.* Stud. Ric. Geogr., 14(2), 214-223, 7 ff., 2 tabb.

BIANCOTTI A. & MERCALLI L. (1991a) - *Variazioni climatiche nell'Italia Nord-Occidentale.* Mem. Soc. Geog. It., 46, 385-408, 9 ff., 12 tabb.

BIANCOTTI A. & MERCALLI L. (1991b) - *Variazioni climatiche a breve termine (1927 - 89) a Gressoney (Valle d'Aosta, Italia), 1850 m s.l.m..* Rev. Valdôtaine Hist. Nat., 45, 5-19, 10 ff., 5 tabb.

BRIZIO D. & MERCALLI L. (1992) - *Pioggia e neve a Bra. 130 anni di osservazioni (1862 - 1991).* Meteo Bra Quad. Oss. Meteor. Mus. Civ. Craveri St. Nat., 64 pp., 37 ff., 18 tabb.

GIUFFRIDA A. & CONTE M. (1989) - *Variations climatiques en Italie: tendances des températures et des précipitations.* Publ. de l'Ass. Int. Clim., 2, 209-216, 4 ff., 3 tabb.

MENNELLA C. (1967) - *Il clima d'Italia.* Editrice E.D.A.R.T., Napoli

ORGANISATION METEOROLOGIQUE MONDIALE (1990) - *Guide des pratiques climatologiques. OMM - N° 100.* Genève

PINNA M. & VITTORINI S. (1985) - *Contributo alla determinazione dei regimi pluviometrici in Italia.* Mem. Soc. Geog. It., 39, 147-167, 6 ff.

Spatial Differences of Precipitation in the Eastern Swiss Alps

Felix P. Blumer & Herbert Lang
Swiss Federal Institute of Technology, Department of Geography, Hydrology Section,
Winterthurerstr. 190, 8057 Zurich

On the northern slope of Gamserrugg (eastern Swiss Alps) precipitation was measured at 5 observation sites at different elevations over a three-year period. No increase in precipitation with increasing altitude could be found. In order to prevent wind-influenced measurement losses, a double fence intercomparison reference (DFIR) was installed to protect the measurement site at the top of Gamserrugg (2074 m a.s.l.). Measured solid precipitation increased then by about 45% at this site, but there was no evidence of altitudinal increase in the annual precipitation amount. Local orographic influences seem to determine the precipitation conditions in this region. For this reason, a dense precipitation network with more than 50 observation sites over an area of about 500 km^2 was installed in summer 1991. The maximum value (1108 mm) for the period from June 1st to September 30th was nearly 3 times higher than the minimum value (380 mm) in a horizontal distance of only 8 km. Based on the results of this dense network and the network of the Swiss Meteorological Institute, it can be concluded that the distance between the observation sites and Säntis mountain, which at 2500 m a.s.l. ist the highest peak in the region, is a more important factor than altitude alone.

EXTREME SEASONAL PRECIPITATION IN MOUNTAIN REGIONS OF BULGARIA

L. Kristev, Ek. Koleva

National Institute if Meteorology and Hydrology
blvd. Tzarigradsko shousse 66, Sofia 1784, Bulgaria

Besides the "normal" or the most probable events, extreme meteorological events are also fundamental elements of the climate. Knowledge of extreme event statistics, including event probabilities, return periods and design values, for various climatological elements is of great practical importance.

In the paper data of seasonal precipitation amounts were used for identification and fitting the desired extremal probability distributions. Data for seven mountain stations were used. The basic period was 1935-1992. The homogeneity of the time series was tested. The data were fitted by normal, gamma and lognormal distributions. The Jenkinson's method was applied to estimate the expected precipitation maxima for various return periods.

Semidiurnal Solar Tides in the Mountain Atmosphere

C. David Whiteman and X. Bian

Pacific Northwest Laboratory
P.O. Box 999
Richland, Washington 99352

1. Introduction:

In this paper, harmonic analysis is applied to hour-average wind profiles obtained from pulsed Doppler radars at three sites on the west side of the Rocky Mountains. The analysis identifies a coherent semidiurnal wind system that is present at all three sites. The wind system characteristics suggest that it is a semidiurnal solar tide.

2. Data Analysis

Clear air, pulsed Doppler, radar wind profilers (Neff, 1990) were developed for meteorological applications in the 1980s. Data sets from these instruments are now becoming available for mountainous areas, and the analyses to be reported in this paper come from 915 MHz wind profilers at the sites shown in Figure 1 and listed in Table 1.

Available horizontal wind data during the period of record at each of the sites were averaged vectorially for each hour of the day at each range gate (i.e., altitude) to produce a time-height cross section of hourly vector winds for a mean day, as illustrated for Page, Arizona, in Figure 2 and for Temple Bar, Arizona, in Figure 3. An intriguing feature of the wind fields at all three sites is the apparent semidiurnal wind oscillation at heights above the wintertime atmospheric boundary layer.

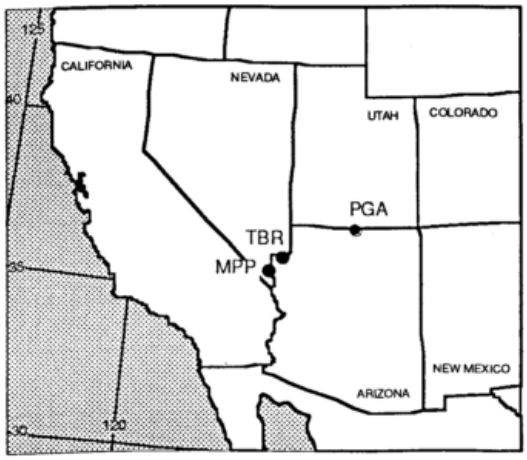

Figure 1. Radar profiler locations.

To investigate the semidiurnal wind oscillations further, the wind data were broken into u (eastward directed) and v (northward directed) components and harmonic analyses were performed for each range gate. The results for the semidiurnal components (subscript 2) are shown in Figures 4 and 5. Figure 4 shows that the amplitudes of the semidiurnal components generally increase with height. Except in the near-surface boundary layer, the diurnal (not shown) and semidiurnal components are of roughly equal amplitudes, attaining speeds near 1 m/s at 4 km. Figure 5 provides phase information on the semidiurnal harmonic components, expressed in terms of the times at which the u_2 and v_2 components reach a maximum. Each of the semidiurnal components reach a maximum twice per day at times separated by 12 hours. The phases of the semidiurnal components above the boundary layer are generally consistent between the sites, with the u_2 component maxima occurring between 1 and 4:30 am (and 1-4:30 pm) and the v_2 maxima occurring at around noon (and at midnight).

Table 1. Site Information.

Site	ID	latitude (°N)	longitude (°W)	elevation (m MSL)	period of record
Page, Arizona	PGA	36.90	111.50	1332	01/08/90-04/03/90
Temple Bar, Arizona	TBR	36.02	114.33	460	01/03/92-04/19/92
Mohave Power Plant, Nevada	MPP	35.15	114.60	226	01/05/92-03/31/92

3. Results and Discussion

The most interesting result from the harmonic analysis is the significant semidiurnal oscillation seen at all three sites. This oscillation has about the same amplitude as the diurnal oscillation and has a phase that is consistent among the sites and with elevation. Hodograms of the sum of the mean and semidiurnal components at Page and Temple Bar are presented in Figure 6 to illustrate the twice-daily clockwise turning of the semidiurnal winds at selected heights. The semidiurnal winds have an amplitude of 1.5 m/s at altitudes where the mean winds have amplitudes of about 6 m/s. They are thus seen to be a significant feature of the

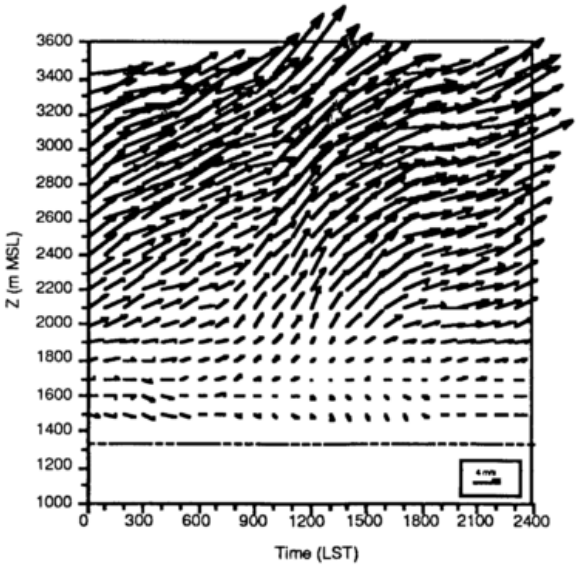

Figure 2. Time-height cross section of mean hourly horizontal winds at Page, Arizona. A vector pointing up represents a wind blowing from south to north, a vector pointing to the right blows from west to east, etc. The dashed line indicates the surface.

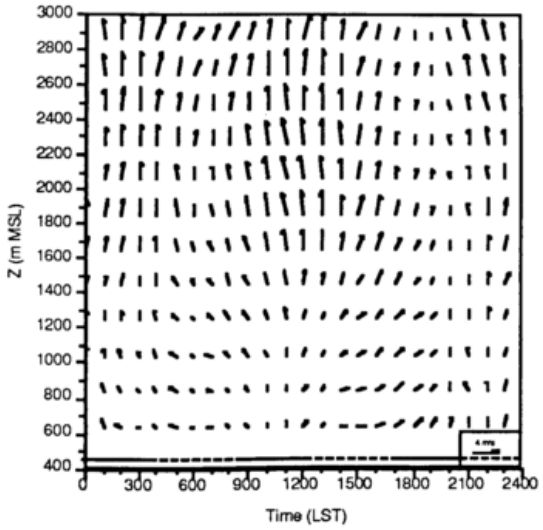

Figure 3. Same as Figure 2 for Temple Bar.

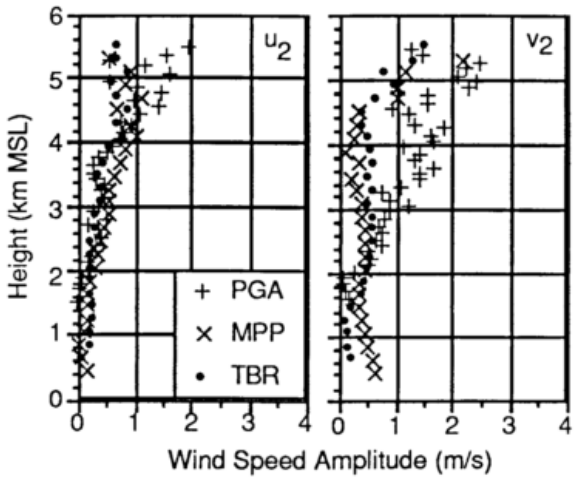

Figure 4. Amplitudes as a function of height.

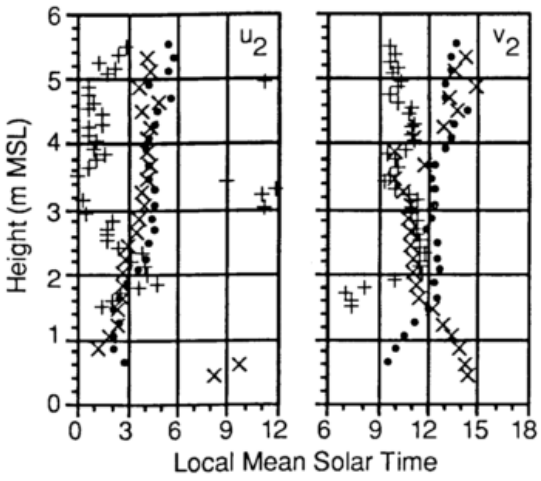

Figure 5. Times of the wind maxima for the u and v semidiurnal harmonic components.

overall mean daily wind system above the Rocky Mountains. The physical origin of this wind system is of interest, as its characteristics differ so significantly from the diurnal wind systems that are a feature of most complex terrain areas. We have considered and rejected several hypotheses regarding the origin of these semidiurnal winds, settling on the hypothesis that the winds are semidiurnal solar tides. The semidiurnal solar tide (Chapman and Lindzen, 1970) is produced by solar heating in the stratosphere and mesosphere by ozone absorption (Butler and Small, 1963). Heating by water vapor absorption also plays a lesser, though significant, role (Siebert, 1961). The heating occurs above the terminators where the solar radiation path lengths are longest. Since the terminators sweep around the earth twice per day this produces two cycles of heating (and winds) per day. Large semidiurnal tidal wind oscillations are produced by the upward propagation of this heating into the mesosphere and lower thermosphere (Greenhow and Neufeld, 1961). The semidiurnal solar tides are also responsible for semidiurnal surface pressure oscillations, whose general variation with latitude θ and longitude ϕ have been described by Haurwitz (1956), using the formula

$$S_2(p) = 1.16 \cos^3\theta \sin(2t'+2\phi+158°) \quad \text{mb} \qquad (2)$$

where $S_2(p)$ represents the semidiurnal surface pressure component and t' is Universal Time measured in degrees from lower transit (midnight), with one hour corresponding to 15°. The form of this equation illustrates the essential wave nature of the oscillation with two complete waves around the earth and with highest

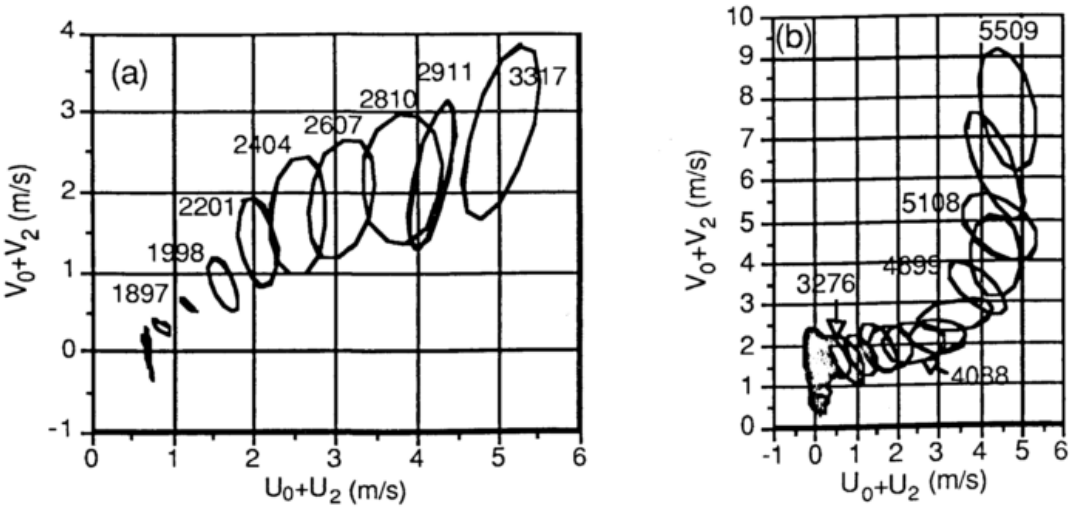

Figure 6. Hodograms of the sum of the mean daily wind (u_0,v_0) and the mean hourly semidiurnal components (u_2, v_2) at different indicated heights (m MSL) above (a) Page, Arizona, and at ~200-m height intervals beginning at 637 m at (b) Temple Bar, Arizona. The 24 points making up each hodogram represent the hours of the day and each point defines the tip of a wind vector which originates at the coordinate origin (0,0). This vector rotates clockwise twice per day around each of the hodograms.

amplitudes at the equator. Since the tide follows the apparent path of the sun, the times of maximum pressure are 0944 and 2144 local mean solar time (LMST) at all longitudes.

Long time series observations of surface pressure (U.S. Weather Bureau, 1943) are available for the U.S., and Spar (1952) has used these data to produce more detailed maps of semidiurnal surface pressure oscillations that show significant perturbations in the Rocky Mountains.

4. Equations of Motion

The hypothesis that the observed semidiurnal winds are semidiurnal solar tides can be evaluated by comparing the wind system characteristics with those of the semidiurnal solar tide, where the tidal characteristics are determined by substituting Haurwitz's formula (2) for the semidiurnal pressure oscillation into the perturbation equations of motion for the atmosphere on a rotating earth, ignoring friction

$$\frac{\partial u}{\partial t} - 2\Omega v \sin\theta = -\frac{1}{\rho R_E \cos\theta}\frac{\partial p}{\partial \phi}$$
$$\frac{\partial v}{\partial t} + 2\Omega u \sin\theta = -\frac{1}{\rho R_E}\frac{\partial p}{\partial \theta} \qquad (3)$$

In this formula, u and v are velocities, t is time, Ω is the angular velocity of the earth, ρ is air density, R_E is the earth's radius, and p is the semidiurnal pressure oscillation, assumed independent of height.

The solutions (Chapman and Lindzen, 1970) at Page's latitude are $u = u_2 = 0.31 \sin(2t + 338°)$ and $v = v_2 = 0.30 \sin(2t + 68°)$ m/s, and are considered valid just above the planetary boundary layer, where the effect of friction becomes negligible. The pressure and wind patterns follow the apparent path of the sun with the maximum u_2 (v_2) component occurring at 0344 and 1544 (0044 and 1244) LMST at all longitudes (Figure 7). The tidal wind components are 90° out of phase and the vector wind rotates clockwise with time. The amplitudes, times, and sense of rotation are in general agreement with the radar profiler data.

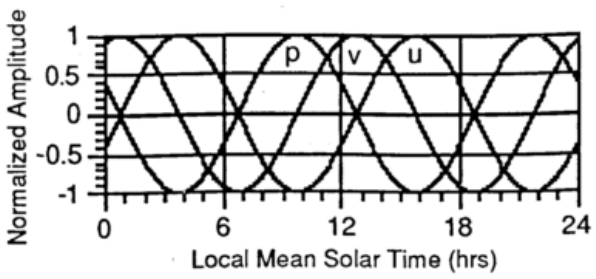

Figure 7. Phase relationships between pressure and the u and v wind components.

5. Conclusions

Harmonic analysis of Doppler radar wind profiler data west of the Rocky Mountains has identified a coherent semidiurnal wind system above the wintertime boundary layer at multiple sites in the region. The unusual characteristics of this mountain wind system (its semidiurnal frequency, amplitude, phase, and direction of rotation) suggest that it is a semidiurnal solar tide. Such tides have not been well documented in the mountain atmosphere or in the troposphere generally but, because semidiurnal signatures are well known in surface barometric traces, and large amplitude semidiurnal tides are known in the upper atmosphere, they are not unexpected.

Our interpretation of these winds as tidal wind systems is supported by a solution of the momentum equations for frictionless flow on a rotating earth in which a simplified fit to global semidiurnal surface pressure observations is used to drive the equations. The resulting solution generally matches the observed winds in frequency, amplitude, phase, and direction of rotation. The phase of the observed winds varies somewhat from site to site and in the vertical at individual sites, producing some discrepancies between the observations and model. This is probably due to statistical uncertainty in the observations resulting from the short period of record, and the falloff in the number of observations with height. The model also lacks detail on phase and amplitude variations of the semidiurnal surface pressure fields in the Rocky Mountain cordillera.

Our future research on this semidiurnal cordilleran wind system will focus on obtaining sufficient data to resolve further the vertical structure, seasonal variation, and spatial variations of the wind system. Of particular interest is the role of the Rocky Mountains and other cordilleras in modifying the global tides. It remains to be seen whether semidiurnal cordilleran circulations will be of sufficient magnitude to be observed across major arcuate-shaped east-west-oriented mountain massifs such as the Alps. There, from the work of Frei and Davies (1993), we may expect wind systems to develop in response to pressure gradients that form across the Alps due to differences in the amplitudes and phases of semidiurnal and diurnal pressure oscillations on the north and south sides of the mountain barrier. Such pressure gradients appear to be of the same order of magnitude as the pressure gradients producing the semidiurnal tides.

Acknowledgments

Radar data were collected by NOAA's Environmental Technology Laboratory (ETL) as part of the Salt River Project's 1990 Winter Visibility Study and the 1992 MOHAVE Project. Mr. Dan Wolfe is thanked for useful discussions on radar profiler operation. Dr. John Gaynor of ETL and Mr. Norm Robinson of Desert Research Institute supplied the MOHAVE radar profiler data.

Research was supported by the U.S. Department of Energy under Contract DE-AC06-76RLO 1830 at Pacific Northwest Laboratory as part of DOE's Atmospheric Studies in Complex Terrain program. Pacific Northwest Laboratory is operated for the DOE by Battelle Memorial Institute.

References

Butler, S. T., and K. A. Small, 1963: The excitation of atmospheric oscillations. *Proc. Roy. Soc.*, **A274**, 91-121.

Chapman, S., and R. S. Lindzen, 1970: *Atmospheric Tides.* D. Reidel Publishing Co., Dordrecht, 200 pp.

Frei, C., and H. C. Davies, 1993: Anomaly in the Alpine diurnal pressure signal: Observations and theory. *Quart. J. Roy. Meteor. Soc.*, **119**, 1269-1289.

Greenhow, J. S., and E. L. Neufeld, 1961: Winds in the upper atmosphere. *Quart. J. Roy. Meteor. Soc.*, **87**, 472-489.

Haurwitz, B., 1956: The geographical distribution of the solar semidiurnal pressure oscillation. *Meteor. Pap.*, **2**(5), New York University.

Neff, W. D., 1990: Remote sensing of atmospheric processes over complex terrain. Chapter 8 in Atmospheric Processes Over Complex Terrain (W. Blumen, Ed.), *Meteor. Monogr.*, **23** (45), 173-228. Amer. Meteor. Soc., Boston, Massachusetts.

Siebert, M., 1961: Atmospheric Tides. *Advances in Geophysics*, **7**, 105-182.

Spar, J., 1952: Characteristics of the semidiurnal pressure waves in the United States. *Bull. Amer. Meteor. Soc.*, **33**, 438-441.

U.S. Weather Bureau, 1943: 10-year normals of pressure tendencies and hourly station pressures for the United States. *U. S. Weather Bureau Tech. Pap. No. 1*, U. S. Government Printing Office, Washington, D.C.

Changes in temperature extremes at the Pic du Midi (Pyrenees, 2862 m), period 1882-1984.

A. Bücher, J. Dessens and B. Pech
Observatoires du Pic du Midi et de Toulouse
B.P. 136, 65201 Bagnères-de-Bigorre Cedex, France

The subject of Global Change and more particularly of global warming has received much attention from the scientific community in the past decade (IPCC 1990, IPCC 1992). The investigation of such warming requires the observation of changes in temperatures over long periods of time. Historical data sets can be very valuable in forming assessments of any recent change caused by greenhouse gases. The coverage quality of the data has been discussed in detail, the most crucial problem being probably the effect of urban warming in most of the land stations. On this point, the long series of data taken by professional meteorologists at elevated observatories (Bücher and Dessens 1991, Weber et al. 1994) are of particular interest because no urban warming occurs in these locations. Moreover, mountain stations can give the only available indication of a temperature trend in the middle atmosphere.

This paper summarizes the data obtained at the Pic du Midi, a mountain observatory at 2862 m a.s.l. in the French Pyrenees, after these data have been corrected for a systematic deviation due to a relocation of the station in 1971. The temperature data now cover the 1882-1984 period. A detailed discussion on the quality of the temperature data at the Pic du Midi has already been presented by Bücher and Dessens (1991).

Mean seasonal and annual temperatures

From the beginning to the end of the 1882-1984 period, it has been observed that the mean night-time temperature has increased by 2.49°C while the mean daytime temperature has decreased by 0.49°C. In consequence, the mean temperature has increased by 1.00°C and the mean annual temperature range has dropped by 2.98°C. All seasons are affected by this evolution (Table 1).

	DJF	MAM	JJA	SON
Mean T min, °C	- 10°08	- 7°21	2°34	- 3°06
1882-1984 trend, °C	+ 2°38*	+ 2°58*	+2°07*	+ 2°92*
Mean T max, °C	- 3°93	- 0°16	9°35	2°99
1882-1984 trend, °C	-0°18	- 1°76*	- 0°91*	0°90

Table 1. Mean seasonal and annual values of minimum and maximum temperatures at the Pic du Midi. Changes significant at the 1% level are marked by an asterisk.

Mean monthly temperature extremes

Table 2 gives the monthly mean values of the minimum and maximum temperature extremes and the 1882-1984 trends for these mean values. The trends of the mean temperatures and of the mean extremes are similar, with a dramatic increase of the minimum extremes in January, February and March. Such a large winter temperature increase certainly has some impact on the ecology and economy of the Pyrenees.

J	F	M	A	M	J	J	A	S	O	N	D
-20°39	-18°76	-17°85	-15°65	-11°99	- 7°18	- 4°19	- 4°40	- 7°19	-11°89	-15°45	-18°76
6°03	4°12	5°46	1°95	2°06	0°52	1°51	2°49	2°76	3°10	1°63	2°88
-34°8	-32°9	-29°0	-23°0	-18°6	-11°8	- 9°1	- 9°0	-13°8	-20°3	-24°0	-27°1
1981	*1956*	*1883*	*1910*	*1902*	*1914*	*1910*	*1945*	*1936*	*1936*	*1890*	*1917*
4°17	3°71	4°98	6°75	9°69	13°98	16°45	16°44	13°81	10°06	6°63	4°49
0°14	- 2°17	- 1°65	- 2°61	- 2°17	- 1°07	0°20	- 1°26	- 0°15	2°31	0°19	- 0°16
11°0	11°2	11°0	11°6	15°3	18°7	20°2	22°0	18°1	15°5	13°1	9°4
1951	*1903*	*1893*	*1891*	*1969*	*1968*	*1981*	*1923*	*1966*	*1946*	*1979*	*1891*

Table 2. - Mean monthly minimum and maximum temperature extremes at the Pic du Midi, with 1882-1984 trends.
- Minimum and maximum mean monthly extremes, with indication of the year.

Comparison with Säntis and Grand-Saint-Bernard

The Pic du Midi mean temperatures can be compared with those available for two other mountain stations in western Europe: Säntis, Switzerland (47°15'N, 9°20'E, 2500 m a.s.l.), and Grand-Saint-Bernard, Switzerland (45°52'N, 7°10'E, 2479 m a.s.l.). The trends are similar at the three stations (Fig. 1), with a marked increase of the mean temperature in the fall (Table 3).

	D J F	M A M	J J A	S O N	Year
Pic du Midi	- 7°00	- 3°69	5°84	- 0°05	- 1°23
Trend	1°10	0°41	0°58	1°91	+ 0°97
Säntis	- 8°36	- 3°95	4°40	-0°74	- 2°16
Trend	0°42	0°94	1°11	1°48	+ 0°99
Gd St Bernard	- 7°95	- 3°30	6°03	- 0°12	- 1°34
Trend	0°83	0°77	1°68	1°96	+ 1°31

Table 3. Mean seasonal and annual trends of mean temperatures at three mountain stations in western Europe.

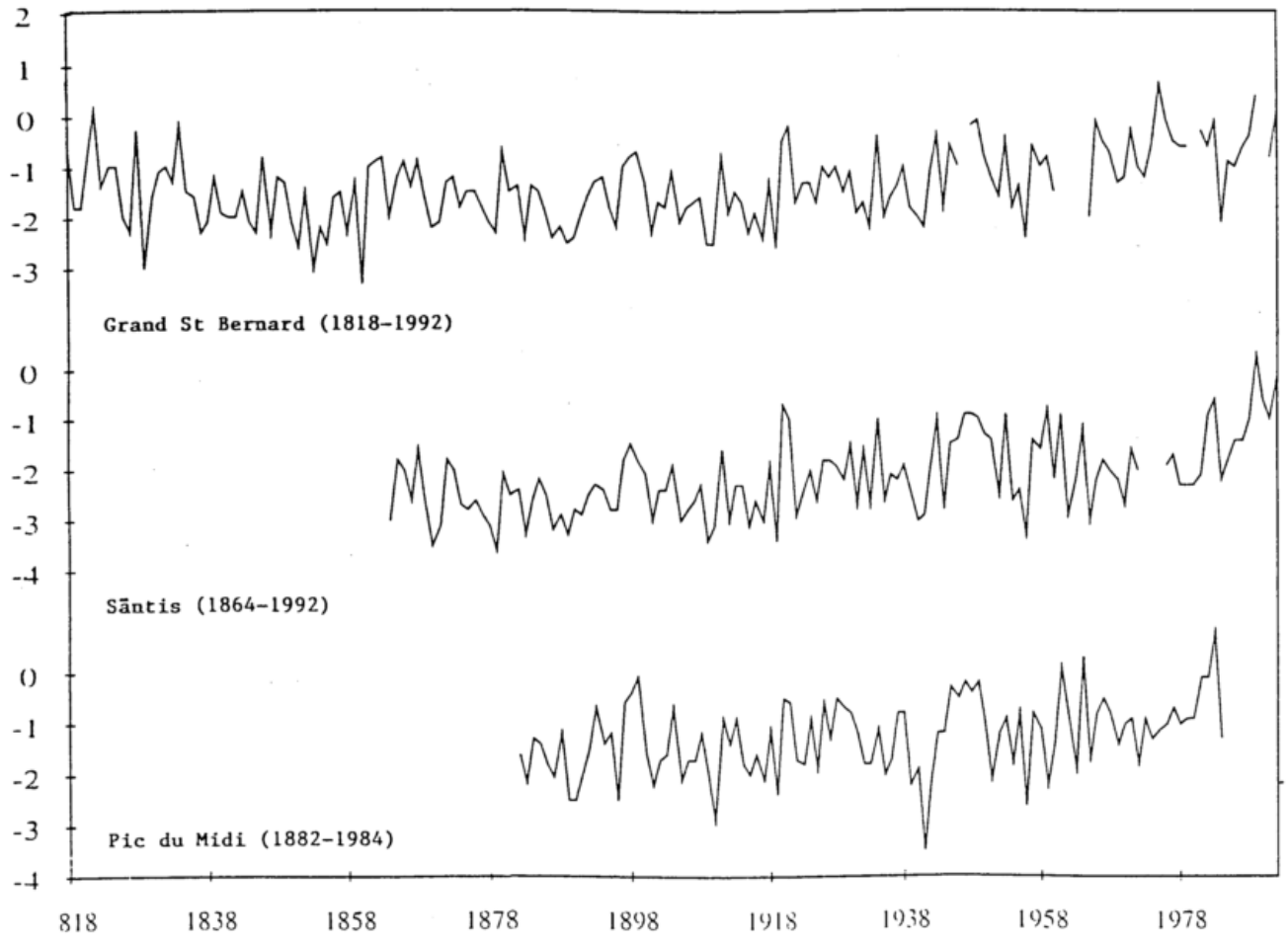

Fig. 1 : Original series of annual mean temperatures at three mountain stations in western Europe.

Conclusion

We have examined historical series of minimum and maximum temperature data at an elevated observatory in the Pyrenees, and we have found a large increase of the mean night-time temperature in all seasons. In the meanwhile, the mean daytime temperature has slowly decreased in all seasons except the fall. In consequence, most of the warming observed at the Pic du Midi during the 1882-1984 period took place in the fall.

Weber et al. (1994) have examined historical series of minimum and maximum temperature data at Säntis and at Sonnblick (47°03'N, 12°57'E, 3105 m), and while they also found a maximum warming in the fall, they did not observe any difference in the increase of the minimum and maximum temperatures. In another paper (Dessens and Bücher 1994), we have suggested that, in addition to the widely discussed greenhouse effect, there may be compensating effects caused by the cloud cover, and we have examined humidity and cloud cover data at the Pic du Midi for the same 1882-1984 period. We have concluded that the decrease in the maximum temperature at the Pic du Midi is related to a concomitant increase of 15-16 % in both the relative humidity and the cloud cover.

References

- Bücher, A., and J. Dessens, 1991: Secular trend of surface temperature at an elevated observatory in the Pyrenees. *J. Climate*, 4, 859-868.
- Dessens, J., and A. Bücher, 1994: Changes in minimum and maximum temperatures at the Pic du Midi in relation with humidity and cloudiness, 1882-1984. In "*Asymetric Change of Daily Temperature Range*", United States Department of Energy, CONF-9309350, 1994, 253-272.
- Intergovernmental Panel on Climate Change (IPCC), 1990: *Climate Change: the IPCC Scientific Assessment*, edited by J.T. Houghton, G.J. Jenkins, and J.J. Ephraums, Cambridge University Press, 365 pp.
- Intergovernmental Panel on Climate Change (IPCC), 1992: *Climate Change 1992: The Supplementary report to the IPCC Scientific Assessment*, edited by J.T. Houghton, B.A. Callender and S.K. Varney, Cambridge University Press, 200 pp.
- Weber, R.O., P. Talkner and G. Stefanicki, 1994: Asymmetric diurnal temperature change in the Alpine region. *Geophys. Res. Letters*, 21, 673-676.

The influence of the Carpathian mountains to the variability of the Romanian precipitation in wintertime

Aristiţa BUSUIOC
National Institute of Meteorology and Hydrology
Bucharest, ROMANIA

ABSTRACT

The patterns of the Romanian precipitation variability in the winter season have been obtained by using EOF analysis. This analysis has been applied to the observed precipitation data as well as to the simulated data by three extended-range GCM experiments run at the Max-Planck-Institute für Meteorologie. The first three EOFs for the observed data as well as for the simulated data by GCM at four grid points covering the Romanian area present same spatial features. If the first EOF presents same sign of the variability for the entire country, the folowing two EOFs present two extended regions with opposite signs of variability which divide the country in intra-Carpathian - extra-Carpathian and West - East, respectively, that shows the influence of the Carpathians to the variability of the Romanian winter precipitation.

1. Introduction

About the rôle of the Romanian Carpathians to the evolution of the Romanian weather many papers have been written out of which we mention only some (Bâzâc, 1983; Drăghici, 1988; Ion-Bordei, 1988). These papers have pointed out the influence of the Carpathians especially through case studies or statistical analyses on some profiles. The present paper studies the main space and time features of the winter precipitation variability through an objective method by using EOF analysis. The influence of the Carpathians is well pointed out. 14 locations which cover almost evenly Romania's territory over 1901-1987 interval have been considered. EOF analysis of the monthly precipitation amount for a grater number of locations but for a shorter period has been achieved by Mareş (1988). This paper has not emphasized the rôle of the Carpathians, the EOF analysis results being not so conclusive for the monthly precipitation amount. The present paper compare the results of the observed data with those obtained from the analysis of the GCM simulated data (Cubasch et all, 1992).

2. Data and analysis method.

Romanian seasonal precipitation amount in the wintertime and the grid point winter precipitation simulated by GCM experiments performed at Max-Planck Institute (Cubasch et all, 1992) have been used in this paper. 14 locations over the interval 1901-1987 have been considered (fig. 3). The GCM outputs over 100 years have been considered for the "control" experiment, the "$2CO_2$" experiment and the "IPCC Scenario A" experiment. For all data sets the anomalies relative to the long-term mean have been calculated, GCM simulated precipitation anomalies being computed relative to the long-term mean in the control experiment. The main time and space features of the precipitation variability have been established by using EOF analysis (Barnett and Preisendorfer, 1978). The space features are given by the the first significant eigenvectors emphasizing the regions with the same variability. The time features of the variabilty are given by the coefficient time series associated to every EOFs. The coefficient time series corresponding to the first EOF contains the climate signal in the data sets.

3. Results

a. The main variability modes achieved from the observed data

The analysis of the first three EOFs for the Romanian winter precipitation has pointed out the main areas with the same sign of variability. Fig. 1 shows the patterns of the first tree EOFs, the explained variances by every EOF being represented. The first EOF explains 46% of the total precipitation variance and presents the same sign of variability for the entire country with higher absolute values in the South-West. The second EOF explains 20% of the total variance and presents two regions with opposite signs (intra-Carpathian and extra-Carpathian).

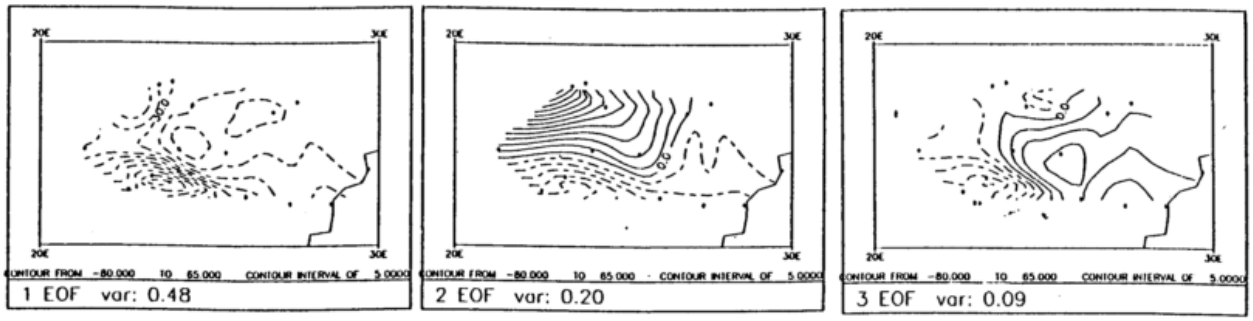

Figure 1. The patterns of the first 3 EOFs for the Romanian winter precipitation over 1901-1987 interval.

The demarcation line between the two regions follows almost exactly the Carpathian curvature emphasizing the rôle of the Carpathian mountains in the variability of the Romanian winter precipitation. The value close to zero are emphasized in the North-Eastern region, consequently the country could be divided into aproximatively two regions disposed in the North-South direction. This shows the significant influence of the Southern Carpathians (which are the highest) on the flow circulation, being an obstacle for the Northern-Northwestern and South-Southwestern circulation. The third EOF explains only 9% of the total variance and presents two regions with opposite signs disposed in the West-East direction. This pattern emphasizes the orographic perturbation efect of the Eastern Carpathians to the western and eastern circulation.
The coeficient time series (principal component) of the first EOF (fig. 2) has been analysed to point

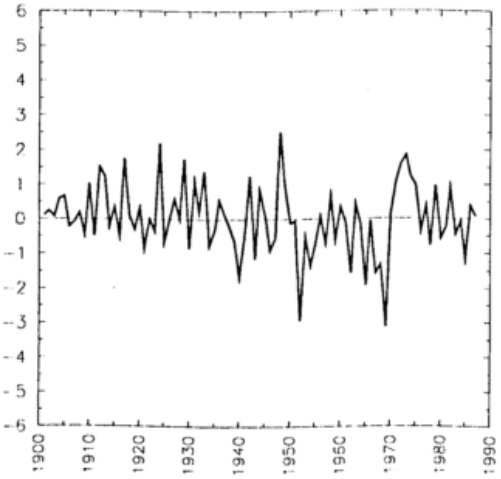

Figure 2. The principal component corresponding to the first EOF for the Romanian winter precipitation.

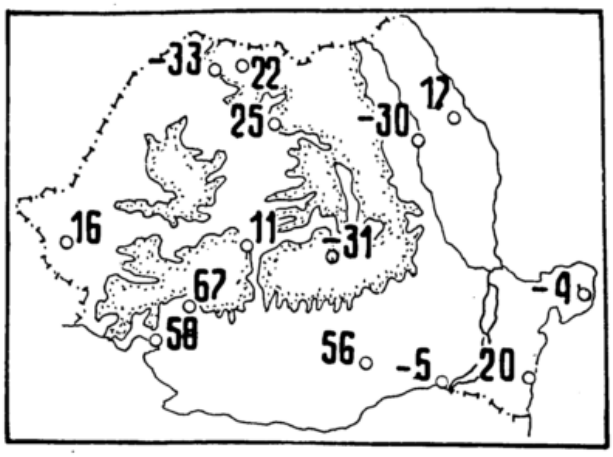

Figure 3. Climate change of the Romanian winter precipitation (mm/season/100 years).

out the climate signal over the considered period. A significant decrease trend is emphasized and taking into consideration the pattern of the first EOF, this explains a decrease trend for the negative anomalies or an increase trend for the positive anomalies. The spatial averaged climate signal shows an increase trend of about 12 mm / season in 100 years while in detail at the station scale (fig. 3) some differences are pointed out. The highest values are in the South-Western area that explain the pattern of the first EOF.

b. Variability modes resulted from the GCM simulated data

The first three EOFs of the winter precipitation anomalies for four grid points corresponding to the Romanian area were calculated by using the monthly precipitation amount simulated by GCM.

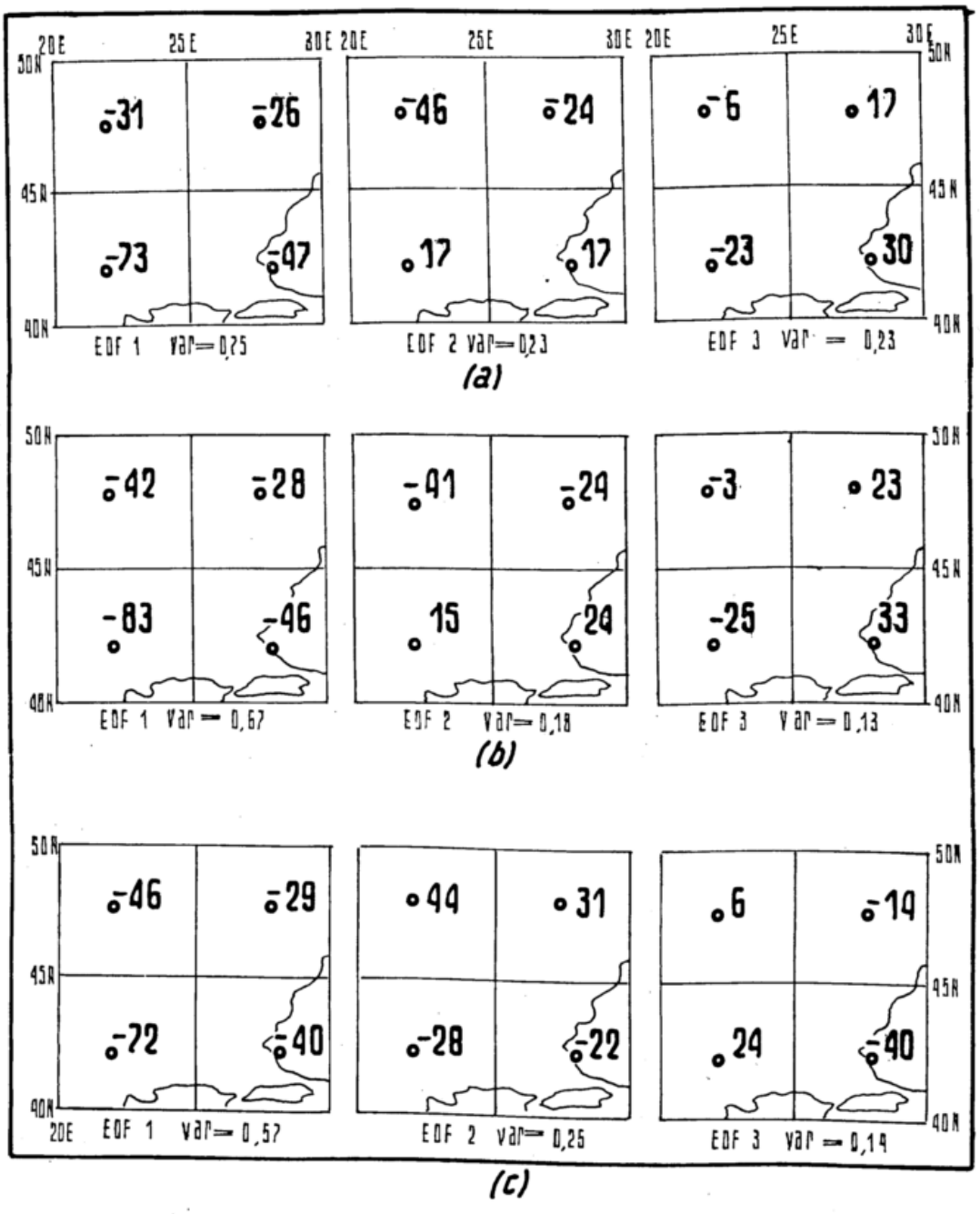

Figure 4. The patterns of the first 3 EOFs for the four grid point Romanian winter precipitation derived from: GCM control experiment (**a**); $2CO_2$ experiment (**b**); and from scenario A experiment (**c**).

Fig. 4(a, b, c) presents the patterns of these EOFs for the "control" experiment, "$2CO_2$" experiment and the Scenario A experiment, respectively. The main space features of the observed data variability are well represented by these patterns. The first EOF presents the same sign in all grid points with higher absolute values in the South-Western area. The second EOF presents two regions with opposite signs disposed in the North - South direction with higher absolute values in North-West for the Northern area and in the South - West for the Southern area. The third EOF presents two regions with opposite signs disposed in the West - East direction with higher absolute values in the South - West.

4. Conclusion

EOF analysis for the Romanian winter precipitation field emphasizes objectively three main variability modes: same sign variability for the entire country and twoo regions with opposite variability (intra-Carpathian - extra-Carpathian and West-East). These variability modes are well pointed out by GCM experiments too, in spite of the complexity of the topography in the region. The influence of the Carpathian Chain upon the regional atmospheric flow are emphasized by the second and third variability modes. The Southern Carpathians are an orographic obstacle for the Northly - Northwesterly circulation and the Eastern Carpathians for the westerly and easterly circulation.

Ackowledgments . *These results were supported by the European Community (Contract no. ERB- CIPA- CT- 92-2045) under Dr. H. von Storch scientific assistance at Max- Planck- Institut für Meteorologie (MPI). We thank Prof. Dr. K. Hasselmann (MPI) for having accepted the proposal, E. Zorita (MPI) for graphic subroutines and U. Cubasch (MPI) for the GCM outputs .*

REFERENCES

BARNETT, T., PREISENDORFER, R., 1978.
Multifield analog prediction of short - term climate fluctuation using a climate state vector. *J. Atmos. Sci.* ,35, 1771-1787.

BÂZÂC, Gh., 1983.
The influence of Relief upon the Main Features of Romanian Climate, *Ed. Acad. R. S. R.*, 179p (in Romanian).

CUBASCH, U., HASSELMANN, K., HÖCK, H., MAIER-REIMER, E., MIKOLAJEWICZ, U.,SANTER, B.D., SAUSEN,R., 1992.
Time-dependent greenhouse warming computations with a coupled ocean-atmosphere model. *Clim. Dyn.* 8, 55-69.

DRĂGHICI, I., 1988.
Dynamics of the Atmosphere, *Ed. Acad.R.S.R.*, 475p (in Romanian).

ION-BORDEI, N., 1988.
Meteoclimatic Phenomena induced by the Carpathian configuration in the Romanian Plain, Ed. *Acad. R.S.R.*, 174p (in Romanian).

MAREŞ, I., 1988.
Factor analysis of monthly temperature and precipitation and determination of their homogenities over Romania's territory. *Metorology and Hydrology.* Vol. 18, 2 / 1988.

Variations of Extreme Air Temperatures Across the Dinaric Alps

B. Čapka, M. Gajić-Čapka

Meteorological and Hydrological Service, Zagreb, Croatia

ABSTRACT

The results in this paper are part of the study on the climatic characteristics of extreme air temperatures over the entire Croatia. They refer to the transact of about 230 km in length stretching from the island of Rab in the northern Adriatic, across the northern Dinaric Alps and to the very southern edge of the Panonian lowland. Seven selected stations were located in different climatic zones. Measured temperature extremes and expected extremes for various return periods estimated after the Jenkinson method, were compared. The frequency distribution of maximum and minimum temperatures during the year was analysed in relation to the synoptic situations.

1. Introduction

Over the areas with different orographical characteristics and under the maritime and continental influence, very different temperatures could be expected. Therefore, a knowledge about extreme high or low air temperatures which may be attained is important for a number of engineering design applications so that the designer may make his decisions regarding cost and safety on as sound a basis as possible.

Up to now, there are some works dealing with extreme value analysis over Croatia. Pleško (1976) investigated the appropriate record length necessary for estimation of maximum temperature conditions in a "normal" climate. The estimates of maximum temperatures were deduced for entire Croatia by means of Jenkinson model for the periods ending with 1969. Gajić-Čapka (1985) applied Jenkinson model for estimation of extreme temperatures necessary as input data for design of nuclear power plant at one location in Croatia. Bajić (1986) compared the results of maximum temperature estimates along the Adriatic coast after Jenkinson and Gumbel method for the data records from the period 1950-1979.

2. Data and method

Input data for this analysis are annual extreme temperatures for the period 1951-1990 at 7 stations.

Estimates of the maximum and minimum values are determined by means of Jenkinson model (Jenkinson, 1955, 1969; Makjanić, 1977; Faragó and Katz, 1990): $t = t_0 + \alpha W(k,y)$ where $W(k,y) = (1 - e^{-ky}) / k$. The extreme values t are related to return period T by means of the reduced variate y, where $y=-lnlnT/(T-1)$, t_o is extreme value expected once in a year, where $y = 0$, α is the slope of the t,y curve at $y = 0$, and k is a curvature parameter, giving three distribution types for negative, zero, and positive values of k.

Fifty- and hundred-year return period values of maximum and minimum temperatures were calculated. Clearly for longer return periods, any estimates of extreme temperatures might be unreliable because of long-term climatic fluctuations. The users can estimate maximum and minimum temperatures t(°C) for specified return periods T (years), by use of the theoretical

curves of extremes taking into consideration the relation between reduced variate y and return period of T years and calculated values of the parameters.

The relation between temperature extremes and synoptic situations was analysed using the weather type classification after Poje (1965) with 10 main groups:

C.....cyclone
t.....pressure trough
A.....anticyclone
r, b.....pressure ridge, high pressure bridge
B.....gradientless field (small gradients of pressure) with anticyclonic curvature of isobars
B.....gradientless field (small gradients of pressure) with cyclonic curvature of isobars
N,NE,E.....northerly, north-easterly, easterly transitory type
SE.....south-easterly transitory type
S, SW.....southerly, south-westerly transitory type
W, NW....westerly, north-westerly transitory type

3. Results

The absolute temperature maxima recorded along the studied transact are similar at the Adriatic coast and in inland, and their values were in the interval from 37.0°C to 39.8°C, while on summit of mount Velebit (northern Dinaric Alps) it was 27.6°C. On the contrary, the differences in absolute temperature minima are the greatest between the Adriatic coast (-8,2°C at Rab - island and -16.6°C at Senj - coast), and the highland and inland (from -25.2°C to -28.6°C).

Tab. 1. Measured absolute temperature maxima (M) and minima (m), mean and standard deviation values, and estimated once-in-50-years values (T_{50}) and once-in-100-years values (T_{100}) according to the Jenkinson model. Period: 1951-1990.

a) maximum temperatures

Station	H(m)	M	mean	std	k	T_{50}	T_{100}
Rab	24	37.0	33.9	1.47	0.31	36.7	37
Senj	26	39.0	34.6	1.45	0.00	37.9	38.4
Zavižan	1594	27.6	23.5	1.59	0.01	27.6	28.4
Ogulin	328	38.0	32.9	1.57	0.01	37.0	37.9
Karlovac	112	38.2	34.2	1.59	0.09	38.0	38.6
Zagreb-Maksimir	128	39.8	33.5	1.86	0.02	38.2	39.1
Varaždin	167	37.4	32.7	1.90	-0.05	37.8	39.0

b) minimum temperatures

Station	H(m)	M	mean	std	k	T_{50}	T_{100}
Rab	24	-8.2	-2.6	2.39	0.19	-7.8	-8.5
Senj	26	-16.6	-5.8	3.35	0.07	-13.7	-14.9
Zavižan	1594	-28.6	-18.5	3.51	0.00	-26.6	-27.8
Ogulin	328	-28.5	-18.2	4.75	0.34	-27.2	-28.0
Karlovac	112	-25.2	-15.3	4.62	0.30	-24.4	-25.3
Zagreb-Maksimir	128	-27.3	-15.7	4.72	0.25	-25.4	-26.5
Varaždin	167	-28.0	-19.0	5.17	0.50	-27.2	-27.7

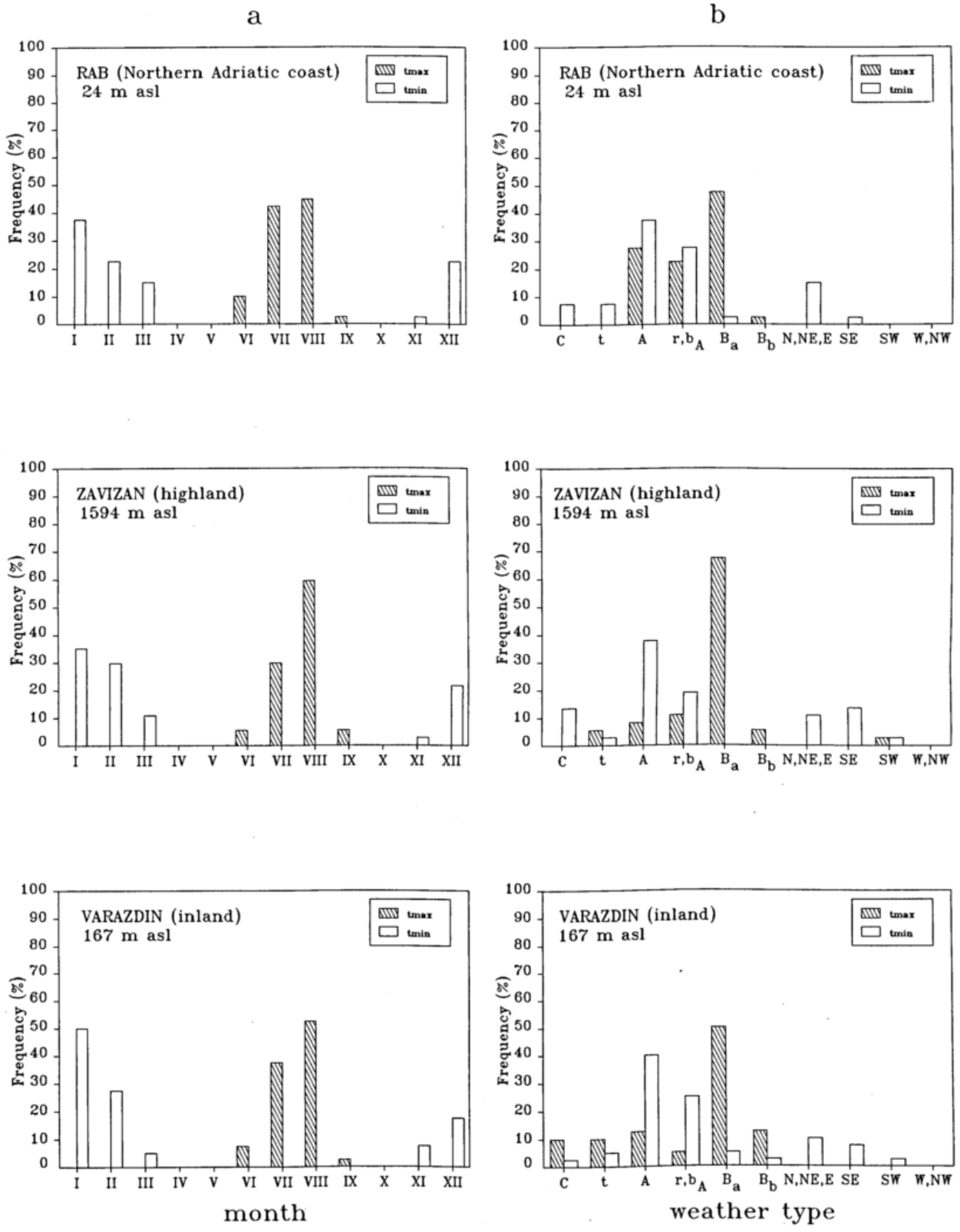

Figure 1. Frequency of absolute minimum and maximum temperatures during the year (a), and frequency of weather types for occurrence of temperature extremes (b). Period: 1951-1990.

According to the standard deviation values, the variability of annual temperature maxima and minima increase from the coast toward inland, and it is higher with temperature minima than maxima for all stations.

The Jenkinson solution for temperature maxima gave small positive values of k at six stations, and even negative value of k in lowland (Varaždin) (Tab. 1). With minima positive values of k were obtained in the interval from 0.50 (Varaždin) to 0.00 (Zavižan).

The highest once-in-100-years temperatures can be expected in the continental lowland (about 39°C), a little bit lower at the sea (37-38°C), while the mountainous areas at higher altitudes are supposed to experience temperature maxima about 10 C lower (Tab. 1).

The lowest once-in-100-years temperatures are expected on summits or high slopes (-27.8°C at Zavižan) and in valleys, where the effect of strong temperature inversions is present (-28.8°C at Ogulin), as well as in the continental lowland. However, the expected minima are much milder at the coastal sites (from -8.5°C to -14.9°C), where the sea has a large warming effect in winter months.

Absolute maximum temperatures appear during a year mainly in August and July, and they are connected with the synoptic situation characterised by small gradients of pressure with anticyclonic curvature of isobars.

Absolute minimum temperatures appear in winter (mainly in January) during the anticyclonic situations (Fig. 1).

4. Conclusion

The obtained results show that the highland would experience maximum temperatures about 10°C lower than continental lowland or seaside, while its minimum temperatures can be expected similar to lowland minima, and 10-20°C lower than minima at the coast.

Acknowledgement:
The authors are grateful to M.Sc. Edita Lončar for completing of weather type data set.

References

Bajić, A., 1986: Contribution to the study of air temperature maxima on the Adriatic, (in Croatian, Summary in English), Pomorski zbornik, 24, 407-427.

Faragó, T. and R. W. Katz, 1990: Extremes and Design Values in Climatology, World Meteorological Organisation, WMO/TD- NO. 386, WCAP - 14, pp 46.

Gajić-Čapka, M., 1985: Extreme meteorological conditions at the power plant site, (in Croatian, summary in English). Energija, 34, (1), Časopis elektroprivrednih organizacija Hrvatske, Zagreb, 13-20.

Jenkinson, A. F., 1955: The frequency distribution of the annual maximum (or minimum) values of meteorological elements. Quart. J. R. Met. Soc. 87, 158-171.

Jenkinson, A. F., 1969: Statistics of Extremes, Estimation of Maximum Floods. World Meteorological Organisation, Geneve, WMO Technical Note No. 98, Chapter 5.

Makjanić, B., 1977: Application of extreme value theory in geophysics, (in Croatian), Hydrometeorological Institute of Croatia, Zagreb, pp 84.

Pleško, N., 1976: Distribution of maximum annual air temperatures in Croatia, (in Croatian), M. Sc. Theses, Faculty of Sciences, Zagreb, pp 107.

STATISTICAL STUDY ON THE SNOW STORM PHENOMENON IN THE MOUNTAIN AREA OF ROMANIA

Liana Cazacioc
National Institute of Meteorology and Hydrology
Bucharest, Romania

ABSTRACT

The first part presents certain climatologic considerations on the snow storm phenomenon occurred in the mountain area of Romania as compared to the one occurring in the hill or plain areas, by watching the wind frequency and intensity on various directions, the mean precipitation amounts fallen during the snow storms, their duration over consecutive days.
The second part of the paper contains a spectral analyses of the hemispheric geopotential field at 500 hPa in November 1993, when the wether was extremely severe in Romania due to the snowstorms occurred and the cooling that followed. The 60°N latitude was chosen in order to decompose the geopotential field in the domain of latitudinal wave diagram. By means of Hovmöller diagram the space-time wave distribution was expressed with various wave numbers, looking for correlations between the variations of the temperature field in Romania and those of the geopotential field at the hemispheric level.

1. INTRODUCTION

The snow storm is a complex meteorological phenomenon frequently occurring in Romania during the cold season. The snow storm is defined by its two elements, the wind that has to exceed a certain intensity threshold and the snow that is transported by the wind. For the present paper, snow storm was considered when during the snowfall, the wind exceeded 8 m/s, drifting the snow.
In order to establish certain climatic characteristics of the phenomenon, six mountain stations were studied: Iezeru (1785 m), Rarău (1541 m), Ceahlău-Toaca (1898 m), Lăcăuţi(1776 m), Vf.Omu (2508 m) and Ţarcu (2180 m). The studied period was 1961-1975, except for the station of Ceahlău-Toaca for whith the interval 1964-1975 was used.
A day with snow storm is considered the day when at least at one observation time (1,7,13,19 - local time) the snow storm conditions were accomplished.

1 a. Annual distribution of the number of days with snow storm

In the mountain area in Romania the annual mean number of days with snow storm is much higher than the one corresponding to the field and hill areas where it can reach 7 days /1/.
From Table 1, a conclusion can be reached that the highest values of the annual mean number of days with snow storm is recorded at the Omu, Ţarcu and Ceahlău-Toaca peaks, which suggests the existence of a relationship between the station height and the frequency of the phenomenon.

Table 1. The annual mean number of recorded snowstorms

Station	Frequency (no of days)
Iezeru	49
Rarău	40
Ceahlău-Toaca	73
Lăcăuţi	66
Vf.Omu	94
Ţarcu	79

Table 2. Monthly frequency (%) of the mean number of days with snow storm

Station \ Month	I	II	III	IV	V	VI	VII	VIII	IX	X	XI	XII
Iezeru	17.5	18.3	16.6	8.3	2.8	1.2	-	0.7	1.3	4.5	12.6	16.1
Rarău	14.4	16.3	18.1	10.6	4.0	1.1	-	-	1.7	5.8	11.4	16.3
Ceahlău-Toaca	15.8	18.3	17.1	10.9	3.8	0.5	0.2	-	2.4	6.6	10.6	13.7
Lăcăuţi	16.3	17.7	15.7	11.3	3.6	1.2	0.1	0.1	1.7	5.4	10.5	16.3
Vf.Omu	13.4	13.8	13.4	12.9	7.2	3.0	1.3	0.6	2.6	5.8	11.2	14.6
Ţarcu	13.6	15.0	16.0	11.6	5.4	1.2	0.7	0.2	1.2	4.7	12.8	17.5

In the northern part of the Eastern Carpathians, that is the region of the Rarău Mountains and of the Iezeru peak, the presence of the phenomenon is more moderate.

1 b. The monthly distribution of the number of days with snow storm

In the mountain areas, the snow storm can occur during the entire year, differently from the field areas where the phenomenon occurs during the interval October-April, being more significant in January and February /2/.

Concerning the occurrence probability of this phenomenon every month, the following aspects can be emphasized at the mountain stations (Table 2):

a. In the months of February and December the highest frequency of this phenomenon is recorded.

b. In the months of March the snow storms occur almost as often as in the winter months.

c. In the mountains, snow storms can occur even in the summer (e.g. Omu peak, Ţarcu ,Lăcăuţi).

d. At high altitudes, the snow storm phenomenon being frequent, it occurs in a very high number of days in a month. Therefore, 20 days were recorded at Omu Peak in January, February, March and December and at Ţarcu, 23 days were recorded in March 1962.

The record was reached at Ceahlău Montain with 25 days in February 1970.

1 c. Wind direction and speed during the snowstorms

There are significant indicators for the assessment of the phenomenon intensity and consequences. Differently from the plain /1/, where the predominant wind directions are Northerly and north-easterly (in the South of the country), in the mountain area, the southern and south-western components are comparable with the northern one occurence even with strong, violent snow storms. This is a very significant conclusion as it shows the possibility of the phenomenon only in the mountains, when in the other areas there are no conditions favouring its occurrence.

The wind speed during the snow storms in the mountains is clearly higher than in the plain. This value depends on height and season, higher in the winter (over 40 m/s at Ţarcu, Omu Peak and Lăcăuţi), but for the stations of Omu Peak and Tarcu the speed is high also in the summer.

Table 3 shows the mean values of the wind speed during the snow storms occurred in the mountains, values distributed on 8 selected directions ranging from 8 m/s (at Rarău) to 20.3 m/s (at Ţarcu).

The record of the highest mean values, irrespective of the wind direction belongs to the Omu Peak and Ţarcu. The speed interval for the first station ranges from 13.5 to 17.6 m/s, and for the second station from 11.1 to 20.3 m/s.

In order to watch the snow storm frequency in various countries, the percentage was calculated for the occurrence of three wind speed classes, that is: moderate (8-12 m/s), strong (13-19 m/s) and violent (≥ 20 m/s). The result was that the frequency of the weaker snow storms exceeds that of the strong and violent snow storms as it was to be expected. However, at Omu Peak and Ţarcu , the percentage of violent snow storms is higher, as at Ceahlău-Toaca too.

Table 3: The wind mean speed (m/s) during the snow storms

Direction / Station	N	NE	E	SE	S	SV	V	NV
Iezeru	10.7	11.4	10.8	11.5	12.0	12.6	11.7	10.7
Rarău	9.0	9.0	8.0	9.0	11.0	10.0	11.0	9.0
Ceahlău-Toaca	11.6	11.3	14.7	15.0	14.5	13.1	16.5	13.8
Lăcăuţi	11.9	13.9	14.7	12.9	11.0	11.6	15.1	14.0
Vf.Omu	16.4	15.3	16.9	17.6	17.5	16.0	13.5	16.5
Ţarcu	20.3	18.4	12.4	13.8	12.9	11.4	11.1	16.0

Table 4. The maximum precipitation amounts (l/m²) fallen during the snow storms on the wind directions

Direction / Station	N	NE	E	SE	S	SV	V	NV
Iezeru	24.4	25.3	27.2	41.8	14.1	27.9	9.0	23.0
Rarău	30.2	19.5	16.2	15.1	18.4	10.6	16.0	15.2
Ceahlău-Toaca	8.9	16.8	9.4	6.1	6.6	9.7	17.1	14.7
Lacăuţi	9.6	18.1	23.4	13.4	9.5	12.4	21.9	18.0
Vf.Omu	23.1	55.8	28.0	48.2	22.6	29.7	36.0	39.3
Ţarcu	126.0	21.4	21.7	23.4	15.1	22.2	18.3	40.5

Table 5. Mean (monthly and annual) amounts of precipitation fallen during the snow storms (l/m²)

Month / Station	I	II	III	IV	V	VI	VII	VIII	IX	X	XI	XII	Annual
Iezeru	46.0	66.5	51.4	26.5	13.1	5.5	-	4.2	2.9	19.2	48.2	43.5	327.0
Rarău	9.0	23.6	25.3	23.5	19.1	1.4	-	-	8.9	12.0	16.4	15.1	154.3
Ceahlău-Toaca	30.6	40.3	33.8	20.9	12.1	0.4	0.4	-	8.4	14.9	27.9	23.9	213.6
Lăcăuţi	33.7	35.7	27.4	27.0	17.2	6.8	-	0.7	12.5	15.9	25.7	34.1	236.7
Vf.Omu	59.9	74.8	70.1	72.4	75.0	26.4	19.8	4.1	19.4	35.3	51.8	74.6	583.6
Ţarcu	58.2	49.2	46.0	40.6	26.8	6.1	3.7	1.4	3.0	16.2	38.5	64.2	353.9

1 d. The amounts of precipitation fallen during the snow storms

The maximum precipitation amounts were considered from the six mountain stations, irrespective of year and month when they were recorded.

A distribution was thus achieved of these values on the eight selected wind directions (Table 4).

The largest amount of precipitation during a snow storm in 1961-1975 period was recorded at Tarcu on the northern direction and was 126 l/m².

Significant information connected to the regions where the largest amount of snow falls during the snow storms, can be obtained also from the mean monthly and annual values of precipitation fallen during the selected period (table 5).

In most of the cases the month of February is the one corresponding to the largest amounts of precipitation fallen during the snow storms.

By comparing the monthly mean values of precipitation recorded at the mountain stations, the result is 74,8 l/m² for the Omu Peak, 64,2 l/m² for Ţarcu, as well as 66,5 l/m² for Iezeru.
In the mountain area, significant amounts of precipitation fall annually as snow, especially at high altitudes. Therefore, at the Omu Peak, 583 l/m² and 353 l/m² at Ţarcu were recorded as the highest values.
1.e. Snow storm duration in the mountain area
For this analysis the 1-day, 2-day, 3-day etc. storm frequency was calculated, in terms of the total number of snow storm cases (table 6).

Table 6. Frequency (%) of the 1-day, 2-day, etc. snow storms/consecutive days.

Station \ Consecutive days	1	2	3	4	5	No. of days
Iezeru	67.9	25.0	4.7	1.6	0.8	504
Rarău	80.0	16.5	3.0	0.2	0.2	491
Ceahlău-Toaca	74.3	19.5	5.0	0.9	0.3	650
Lăcăuţi	75.0	20.8	3.8	0.4	-	762
Vf.Omu	65.0	26.0	5.0	3.0	0.2	987
Ţarcu	71.4	23.0	4.3	1.2	-	875

It is to be noticed that most snow storms last for one or two days, reaching 5 consecutive days in exceptional cases.
By comparing the various stations, it can be noticed that at Rarău, where, during the analyzed period, the lowest number of snow storms was recorded (491 as against 987 at the Omu peak) the percentage of day snow storms is the highest (80%) and at the Omu Peak, the lowest (65%).

2. SPECTRAL ANALYSIS OF THE GEOPOTENTIAL FIELD AT 500 hPa LEVEL IN NOVEMBER 1993

In November 1993, four snow storms occurred in Romania on the 10th and 11th, 16th and 17th, 20th and 21st an on the 30th. These phenomena, which are not specific to the month of November in Romania, affected maily the southern areas, where the plain is predominant. Here, the maximum values of the air temperature recorded large negative deviations as against the normal, during the period 11-30 November.
In the mountains, however, the temperature was very low during the interval 10-22 November (Fig. 1).

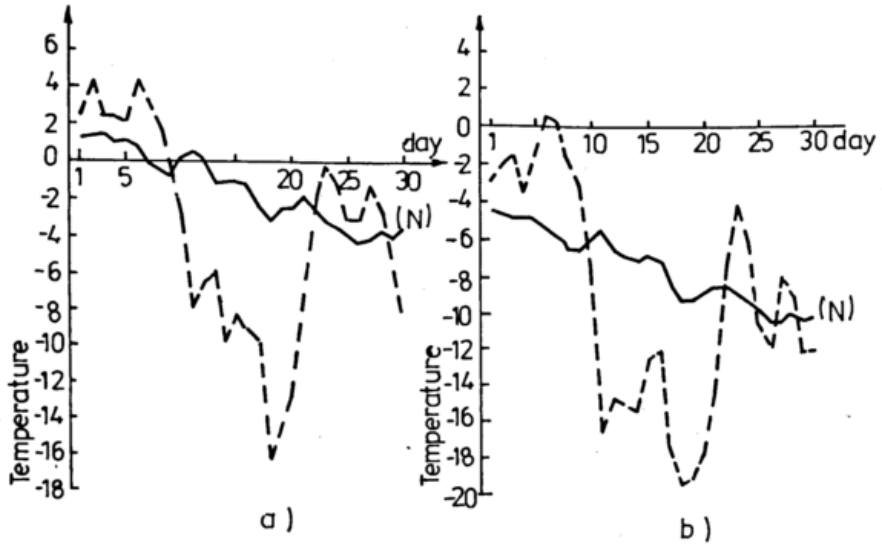

Figure 1. Maximum temperature (**a**) and minimum temperature (**b**) in November 1993 at the station of Omu Peak (N indicates the multiannual daily mean evolution).

In order to find a relationship between the severe aspect of the weather in Romania in the month of November 1993 and the general atmospheric circulation, the 60°N latitude was considered for which decompositions were made of the 500 hPa geopotental field in the domain of latitudinal wave numbers.
By a development in the Fourier series of the daily geopotential values during the interval 1-30 November 1993 the amplitude of the waves 1-18 was calculated.
Figure 2 shows the range of the 1-3 amplitudes, representative at the global scale for the general atmospheric circulation. It must be noticed that for the first part of the month, wave 1 has lower amplitudes than the other two. Then, the amplitudes of the first two waves become significant. During the period 10-22 November, the significant decrease of the air temperature (Fig.1) is very well correlated with the evolution of waves 2 and 3 (Fig.3).
The space-time evolution of wave 2 by a Howmöller diagram /3/, as it is represented on Figure 3, emphasizes an almost stationary movement along the entire month. The vertical arrow indicates the meridian of our country being under the persistent influence of the East-European anti-cyclone ridge, responsable for the severe weather phenomena in our country.

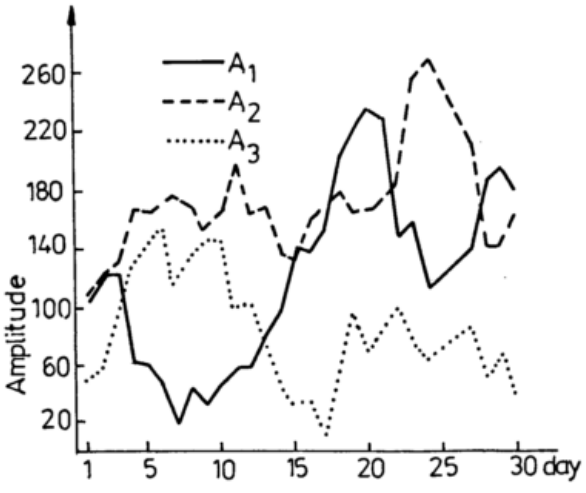

Figure 2. Amplitudes of waves 1, 2 and 3 of the 500 hPa geopotential values for 60°N latitude in November 1993.

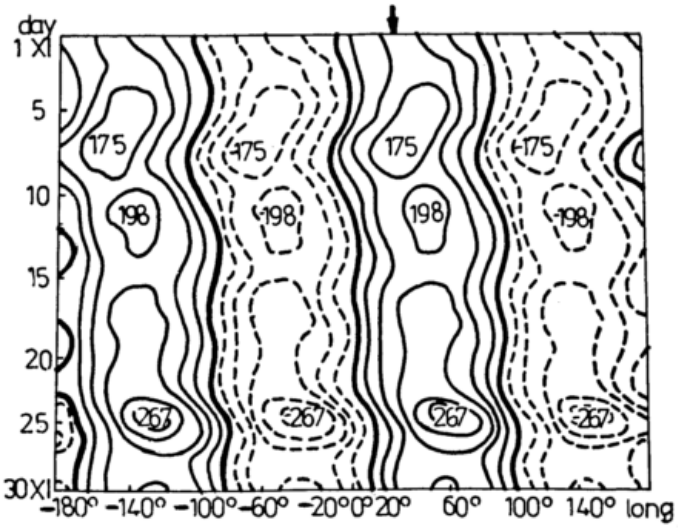

Figure 3. Hovmöller spectral diagram at 500 hPa and 60°N for wave 2 in November 1993. The dotted lines are the negative values. The isolines are drawn from 50 to 50 units.

CONCLUSIONS

* In the mountain area of Romania the frequency of the snow storm is high, these phenomena occurring also in the summer.
* The strongest snow storms are recorded at stations located above 2000 m hight (Omu Peak and Ţarcu) but also at Ceahlau-Toaca, where the local conditions are extremely favourable.
* The snow storms occur in the mountains and in the south and south-western directions, when in the other areas there are no conditions favouring their occurrence.
* In November 1993, waves 2 and 3 of the 500 hPa geopotential field were in "resonance" with the temperature evolution in the mountain area in Romania.

REFERENCES

1. Balescu, O. I., Besleaga, N., (1959)
Teritorial distribution of snow storms in Romania, Meteorology, Hydrology and Water Administration, no.1.
2. Balescu, O. I., Besleaga, N., (1962)
Snow storms in Romania, CSA Publishing House, Bucharest.
3. Hovmöller, E., (1949)
The Trough-and-Ridge diagram, Tellus, Vol. I, no.2, 62-66.

A new look at tree rings

Peter Kahlig

Applied Analytical Meteorology, Institute of Meteorology and Geophysics
University of Vienna, Hohe Warte 38, A-1190 Vienna

ABSTRACT

Annual tree ring widths may be interpreted as stroboscopical views of a dynamical system - the living tree. Growth is controlled by environmental parameters, e.g. precipitation. A nonlinear model for tree ring growth exhibits realistic qualitative features. Within the limits of the model, nature appears to utilize bifurcations, but to avoid chaos.

Dendrochronology has often been used in the past to reconstruct paleoclimates from tree rings of wooden pieces by statistical correlation of ring widths with meteorological elements. Dynamical systems theory can be a useful supplement to correlational statistics: the growth of tree rings is treated stroboscopically, and meteorological elements are viewed as control parameters.

The method appears to offer some insight into the adaptation of tree species to climate. For example, the growth of tree rings of a certain Poplar follows an operating curve with a transcritical bifurcation, thereby achieving an optimum efficiency in the use of precipitation, but normally never touches chaotic regions.

The Föhn Phenomenon in the Romanian Carpathians

G. Bâzâc, R. Cotariu, Carmen Simen

National Institute of Meteorology and Hydrology
Bucharest, Romania

ABSTRACT

The paper aims at analyzing the Föhn phenomenon on the basis of meteorological data resulted from measurements carried-out at meteorological stations situated in characteristic orographic profiles within Romanian Carpathians.
To this aim, differentiated data processing methods are used, depending on the case, to reveal the occurrence mechanism, its maintenance and to disambiguate its weight in reaching the thermal hygric and nephic regime of regions subjected to Föhnal precesses.

The display of the Carpathian-Balkan mountainous chain as a reversed "S" is an important physical barrier in front of the air masses with different physical characteristics depending on their origin.
These air masses' crossing the mountainous massifs generates in some cases catabatic phenomena with Föhn effects in the downwind slopes. These slopes, depending on frequency and duration may create local climatic conditions either beneficial, or, on the contrary with negative effects.
The Föhn phenomenon occurs with different intensities in many slope-surfaces over areas more or less wide, under circumstances of transversal wind.
To analyze the Föhn phenomenon over the Romanian territory, two specific areas were chosen equipped with meteorological stations that allow revealing the mentioned phenomenon. Due to the siting of these meteorological stations in the area of interest, revealing the main characteristics of the Föhn phenomenon was made through various methods, adapted from case to case, on the basis of data in the 1961-1993 interval.
Thus, in the southern slope of the Meridional Carpathians, where there exist meteorological stations sited in a north-to-south profile, the following stations were taken into account: Omu Peak (2507m), Sinaia (1500m), Predeal (1090m), Câmpina (461m) and Ploieşti (177m.
Data concerning air temperature and relative humidity from these stations were selected for situations where the wind readings at the climatological terms (01,07,13,19 hrs.) simultaneously pointed at a northern prevailing circulation. The some parameters were simultaneously selected for the observation terms when calm wind was reported. In these situations it is considered that air temperature directly depends on the transformational potential of the active surface in the area. On this basis the variation graphs were drawn of air temperature and relative humidity, depending on height (figure 1). From analyzing these graphs it results that, under Föhn conditions, when northern winds blow from the high mountainous areas to the low southern areas, air temperature gradually rise. Thus, the descending air, though it experiences a warning process, keeps cooler than in calm wind circumstances up to altitudes of about 1600m. In the lower areas of the southern slope, the calm air, whose temperature depends on the thermal contribution of the active surface, marks constant values between 1100 and 1500m and rises in the lower areas where it reaches values higher than 9.5°C.

Under Föhn circumstances, the descending air is subject to warning processes, so that at altitudes lower than 200m temperatures of 16°C are recorded.
The relative humidity under Föhn circumstances naturally experiences a reversed variation as compared to that of temperature but at a different scale and with different ratios (figure 1).
It must be pointed out that in the southern slope of the Meridional Carpathians, the Föhn phenomenon has a relatively rare occurrence, anytime throughout the year, depending on the circulation type.
The profile in figure 2 renders the variation of the difference between temperatures recorded at the Omu Peak station (2507m) and those reported simultaneously at the slope stations, depending on the windspeed under specific Föhn circumstances.
The graph in figure 2 renders the difference variation between temperatures recorded at Omu Peak station (2507m) and those simultaneously observed at slope stations depending on Föhnal specific circumstances. From these data it results that in descending situations, air temperature may rise from -6°C at Omu Peak to 0°C at altitudes of 1400m when windspeed ranks between 21 and 24ms^{-1}. At speeds of 6-10ms^{-1}, air temperature in descending situations in the downwind slopes rises by 10°C downwards the profile.
The lack of a higher number of meteorological stations in altitudinal profile has led to using an adequate method to stress the Föhn phenomenon on the basis of data from a single station correspondingly sited in the territory. Thus, the method of the isoplethary roses was used, achieved for the main climatic parameters characteristic to Föhn, depending on wind direction.
Being placed in the western border of Semenic Mountains, which display within the mountainous Carpathian-Balkan fit, the meteorological station Oravitza (308m) holds a typical position to Föhn phenomenon exposure. This phenomenon is generated by strong, warm and dry winds known in Romania and Serbia as "Cashava".
To analyze the mentioned phenomenon, a selection on computer was made of temperature and humidity values over 16 wind directions and the necessary parameters were computed in grid points, made up of monthly rings and wind directions respectively.
In this case, the meteorological station is situated in the central point of the wind roses. For each month–from the centre to the periphery–, mean monthly values were inscribed of air temperature and relative humidity.
To close the isopleths, the circle formed in the periphery repeats the month of January that holds first position in the centre of the rose.
To reveal Föhn contribution to air warning in the area, the difference was computed between mean temperature in calm conditions and mean air temperature when the wind blew at the station over 16 directions.
On the basis of the resulted differences, the rose was achieved of the corresponding differences of the mean temperature over wind directions (figure 3). The analysis of this rose points at the fact that from early autumn till late spring, descending streams in the western slopes of Semenic and Anina Mountains record temperatures higher by 6-9°C as compared to autochthonous air warmed by the active surface in calm conditions.
As can be noted from this distribution rose, northwesterly winds preserve or diminish temperature differences at values lower than 0°C as compared to local air calm conditions.
The rose of differences between relative humidity values over the wind directions as against air temperatures in calm conditions points at its diminishing by more than 30% when the wind blows from the southeast.
North-westerlies keep relative humidity values close to those of local air or cause their increment but only in slightly significant amounts (figure 4).
This time-distribution normally correlates with air temperature space-distri-

bution. The lowest values show a space-lay towards the east-north-eastern sector. Both roses ascertain the Föhn phenomenon occurred due to the accumulation of an important pressure potential within the Balkan-Carpathian sink in the cold season of the year when in the extra-Carpathian area the Siberian high evolves. Its coupling with Mediterranean cyclones induces necessary circumstances to an east-to-west air-mass discharge over the Carpathian-Balkan fit. This generates gale-force winds over its western slope.

The meteorological station Oravitza, placed at the foot of the mentioned slope, meets this phenomenon in its full complexity.

The Föhn-type "coshava" phenomenon that frequently occurs on the background of gale-force winds causes severe damage in the area. Thus during the spell February 16-18, 1979, the gusts exceeded speeds of 50ms-1 inducing massif wood wreckings, afflicting buildings over a large area in the downwind slopes of the Semenic-Anina mountains.

Violent winds, accompanied by the entire complex of phenomena specific to Föhn, often occur in the September-April interval, afflicting both the southwestern part of the Carash-Severin district and the Serbian adjacent area.

Conclusions

1. The display of the Carpathian mountains arch favors the occurrence of the Föhn phenomenon in many parts of the Romanian territory, but with various frequencies and intensities.
2. In most situations, due to the lack of adequately sited meteorological stations, Föhn is hard to approach, although it is locally ascertained through its constant effects.
3. At most of the sites over the territory the frequency and intensity of the Föhn phenomenon do not have enough weigh to be evident in the mean monthly and annual air temperature and humidity values in the respective areas.
4. The yearly duration of the interval when the Föhn phenomenon occurs, its frequency and intensity over the western border of the Carpathian-Balkan fit do have an important weigh. In the cold interval of the year, the Föhn phenomenon occurring on the background of highspeed worm and dry winds is the main factor that induces an individualization of the regional climatic regime within the wider context of the southwestern part of Romania.

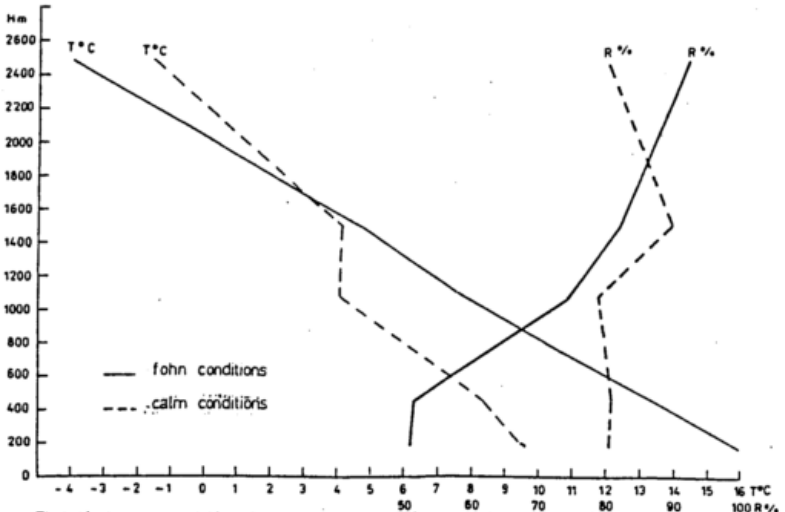

Fig.1. Air temperature (°C) and relative humidity (%) mean value variation in föhn circumstances and calm conditions in the southern slope of the Meridional Carpathians accross the profile : Omu Peak, Sinaia (1500), Predeal, Câmpina, Ploiesti.

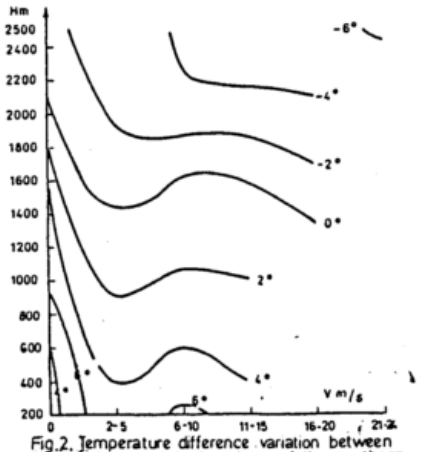

Fig.2. Temperature difference variation between Omu Peak and the low parts of the southern slope of the Meridional Carpathians depending on windspeed (ms^{-1})

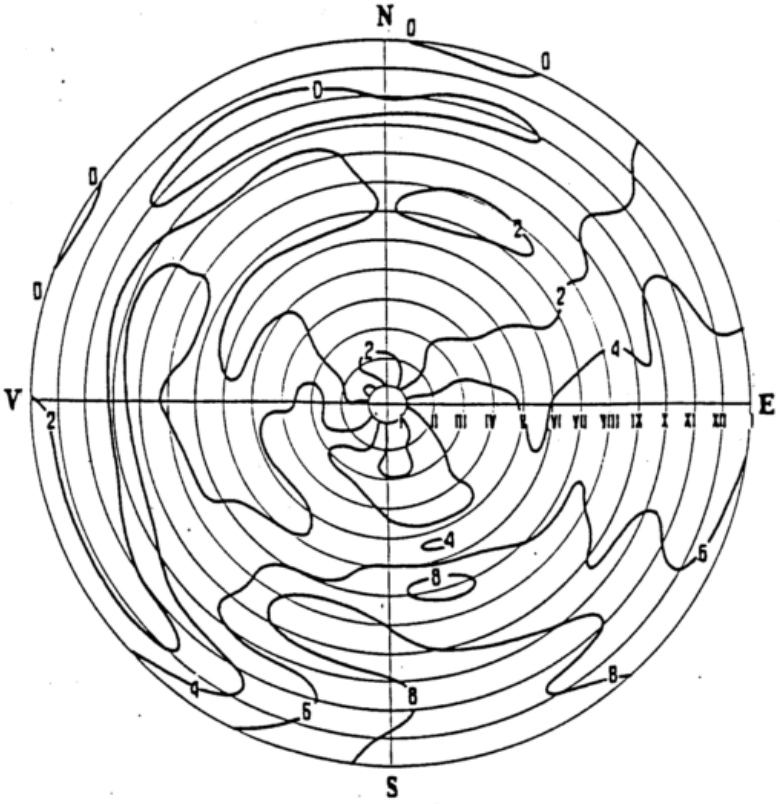

Figure 3 ANNUAL VARIATION OF DIFEERENCES BETWEEN THE MEAN MONTHLY AIR TEMPERATURE OVER THE WIND DIRECTIONS AND MEAN MONTHLY TEMPERATURE IN CALM CONDITION (°C) METEOROLOGICAL STATION ORAVIZA

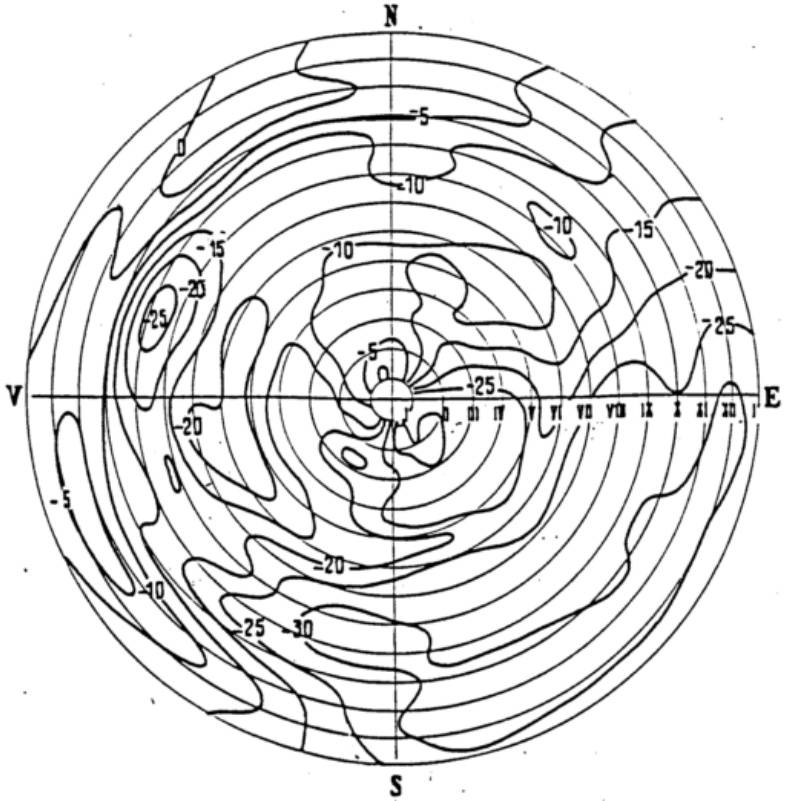

Figure 4 ANNUAL VARIATION OF DIFFEREUCES BETWEEN MEAN MONTHLY RELATIVE HUMIDITY OVER THE WIND DIRECTIONS AND MEAN MONTHLY RELATIVE HUMIDITY IN CALM CONDITION (%) METEOROLOGICAL STATION ORAVIZA

Climatological Basis for Prediction of Road Slipperiness: Minimum Air and Soil Temperatures

K. Zaninović, M. Gajić-Čapka

Meteorological and Hydrological Service Centre for Meteorological Research
HR 41000 Zagreb, Grič 3, Croatia

ABSTRACT

This paper is part of an investigation dealing with the temperature basis for increased traffic safety and road maintenance which aims to predict hazard weather situations favourable for road slipperiness at the foot of the mountain Medvednica in the Sava river valley.

In the lack of the data on air and road surface temperatures, the climatological data from the site of the meteorological station have been used to determine temperature relations needed for predicting of road slipperiness. The present analysis involves the relations in minimum air temperatures at 2m height and soil temperatures at depth of 5cm at 7am during various weather situations defined by means of average cloudiness and wind conditions as well as situations with fog and frozen ground during the night preceding the occurrence of minimum temperatures.

Relations between minimum air temperatures and soil temperatures do not differ significantly for different weather types. However, they are pronounced between months. According to these conclusions, soil temperatures should be predicted particularly by means of regression equations deduced for each month.

KEY WORDS: road slipperiness, minimum air temperature, soil temperature, weather situations

1. Introduction

The climatological data from the regular meteorological network present the valuable material for applied road weather climatological studies. The results can serve as the first information about the temperature climatological conditions that can cause the road slipperiness in different parts of the country, as well as a base for instalation of road weather information system. The following analysis refer to the minimum temperature relations at two levels under different weather conditions at the foot of the mountain Medvednica in the Sava river valley.

2. Data and method

The analysis is deduced for station Zagreb-Maksimir at the foot of the mountain Medvednica in the Sava river valley in the 10-year period (1981/82-1990/91) for the cold period of the year (September to May) when the minimum temperatures less than 0°C could be expected. The correlations between minimum air temperatures at 2m and soil temperatures at depth of 5cm at 7am are determined for eight different weather situations. Six of them were classified by means of mean cloudiness (C) and mean wind velocity (v), and two of them were the situations with fog and frozen ground during the night (from 21pm till 7am). Namely, it was supposed that minimum temperatures appear mostly early in the morning, influencing air and surface cooling. The following weather situations were defined:

a) clear ($C < 2/10$) - calm ($v \leq 3.3$ m/s)

b) clear ($C < 2/10$) - windy ($v \geq 3.4$ m/s)

c) partly cloudy ($2/10 \leq C \leq 8/10$) - calm ($v \leq 3.3$ m/s)

d) partly cloudy ($2/10 \leq C \leq 8/10$) - windy ($v \geq 3.4$ m/s)

e) cloudy ($C > 8/10$) - calm ($v \leq 3.3$ m/s)

f) cloudy ($C > 8/10$) - windy ($v \geq 3.4$ m/s)

g) fog (visibility $\leq$ 1000m)

h) frozen ground

3. Results

The relations between minimum air temperatures at 2m height and soil temperatures at the depth of 5cm are linear: $y = a + bx$, where y is expected soil temperature (t_{soil}), x is minimum air temperature at 2m height (t_{min}), *a* denotes y value for $x = 0°C$, and *b* is the slope of y.

It turned out that relations between minimum air temperatures at 2m (t_{min}) and soil temperatures at the depth of 5cm (t_{soil}) do not differ significantly for different weather types, but they are pronounced between months. The relations between t_{min} and t_{soil} are determined for all months in the cold part of the year when the soil temperatures less than 0°C can be expected (from November till March) (Fig. 1). The following relations are obtained:

November:	$t_{soil} = 3.3 + 0.63\ t_{min}$	r= 0.86	n= 300
December:	$t_{soil} = 1.9 + 0.52\ t_{min}$	r= 0.84	n= 309
January:	$t_{soil} = 1.3 + 0.34\ t_{min}$	r= 0.72	n= 289
February:	$t_{soil} = 1.2 + 0.27\ t_{min}$	r= 0.69	n= 282
March:	$t_{soil} = 2.2 + 0.69\ t_{min}$	r= 0.89	n= 310

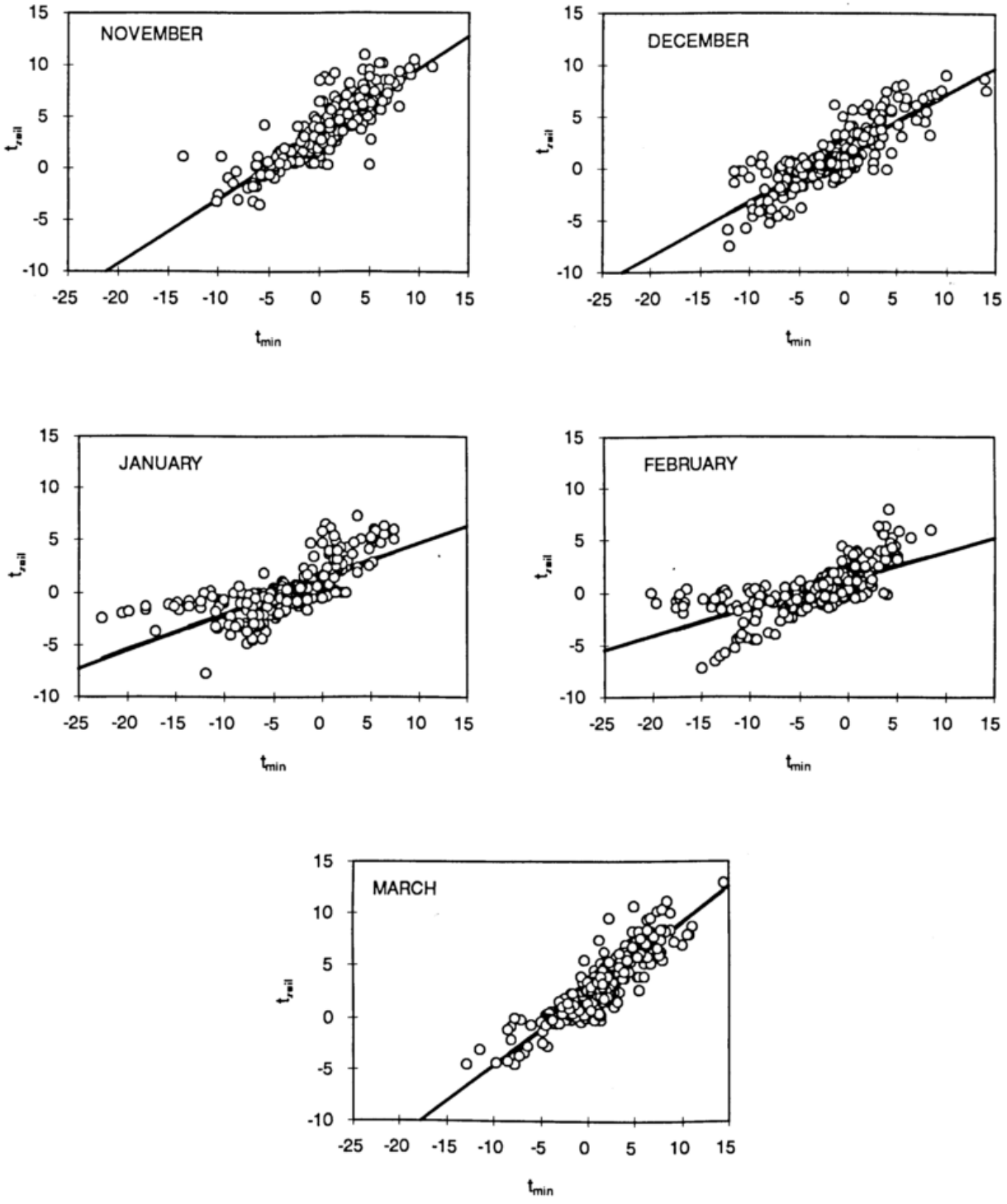

Figure 1. Regresion lines of minimum air temperatures at 2m height (t_{min}) and soil temperatures at 5 cm depth at 7 am (t_{soil}) from November to March. Zagreb-Maksimir, period: 1981/82-1990-91.

Highly significant correlation coefficients (r) indicate that knowing minimum air temperatures one can estimate soil temperatures very well by means of these equations. However, for very low minimum air tempoeratures (<-10°C) the differences between real and estimated soil temperatures can be greater.

The slope b<1 indicates that the soil temperature changes slower than the minimum air temperature. The changes of t_{soil} are the slowest in the coldest months - if t_{min} changes 1°C, the change of soil temeperature will be about 0.3°C in January and February, while in November and March the change will amount 0.6-0.7°C.

At lower temperatures the soil temperatures are higher than the minimum air temperatures at 2m height, and oposite at higher temperatures. The limits at which t_{soil} become lower than t_{min} differ from month to month (Tab. 1). In November soil temperatures will rarely be lower than minimum air temperatures because the limit values of t_{min} at which it happens are almost the same as maximum values they can reach. On the other side, during January and February this condition will be fulfilled already for t_{min} greater than 1.6 or 2°C.

Tab. 1. The values of t_{min} above which t_{soil} become lower and the values of t_{min} below which t_{soil} become negative. Zagreb-Maksimir, period: 1981/82- 1990/91.

	XI	XII	I	II	III
$t_{soil}=t_{min}$	8.9	4.0	2.0	1.6	7.1
$t_{soil}<0°C$	-5.2	-3.7	-3.8	-4.4	-3.2

For the trafic safety it is much more interesting to determine the minimum air temperatures at which the soil temperatures will be negative. Namely, in these situations slipperiness can appear. In November this condition will be very rare because the minimum temperature has to be lower than -5.2°C. what is not very often. During the winter the slipperiness could appear if minimum air temperature is lower than about 4°C (-4.4°C in February and -3.7°C in December) (Tab. 1).

4. Conclusions

The presented analysis is an example how the climatological data are usefully used for the applied studies which help the society to ensure the safer road traffic. In this case the analysis deals with soil temperauture conditions which can cause road slipperiness. The deduced results can help in forecasting of such situations in the Sava river valley at the foot of mount Medvednica.

References

Meteorological and hydrological service, Centre for meteorological research, 1993: Relations between minimum air temperatures and surface temperatures for road traffic safety (unpublished), pp 40.

Pressure Singularity Detected by a Mountain Station

E. Lončar[1], N. Šinik[2], K. Zaninović[1]

1 Meteorological and Hydrological Service, Zagreb, Croatia
2 Department of Geophysics, Faculty of Science, University of Zagreb, Croatia

ABSTRACT

An analysis of the air pressure annual course at various parts of Croatia has revealed a new peculiarity typical for shorter i.e. ten-day time intervals. It was a pressure decrease in the second decade of February, mostly pronounced at Zavižan (h = 1594 m). Zavižan is the mountain meteorological station situated on one of the tops of Velebit mountain (Dinaric Alps). An increased cloudiness followed by a decay of insolation and the greatest number of rainy days during the mentioned ten-day period (determined for the years 1961-1990) are also typical for Zavižan.
A further expansion of this investigation clearly indicates that a pressure decrease, accompanied by cloudy, rainy, (snowy), weather, recured each year in the second decade of February, so it became obvious that an overall climatic characteristic of the whole of Croatia had come out. This peculiarity is related to a steadiness of cyclonic weather types during the second decade of February. Such features are presumably related to some characteristic pattern of the general circulation of the atmosphere and the authors consider the weather characteristics of this short period in February as the relevant ones for the climate of Croatia just like the appearance of "etesia" or "European monsoon".

1. Introduction

An analysis of the air pressure indicates the month April to have the minimum air pressure monthly mean value all over Croatia. The exception was the mountain meteorological station Zavižan with the air pressure minimum in February. This intriguing deviation stimulated a more detailed investigation which made use of ten day mean values.
The analysis of the air pressure annual course based on the ten-day means corresponds well with the annual course of the monthly means, but it has revealed some new peculiarities typical for shorter i.e. ten-day time intervals (Fig.1.). The most prominent feature appeared now to be a pressure decrease in the second decade of February, which was pronounced all over Croatia.That value at Zavižan represents even annual pressure minimum (Fig.1.). The investigations, performed by other authors (Gajić-Čapka and Zaninović, 1993), revealed an increased cloudiness followed by a decay of insolation and the greatest number of rainy days during the mentioned ten-day period all over Croatia (illustrated here only by two locations on the figure 2.).
These findings were compared with annual courses of monthly and ten day frequencies of the main weather types in Croatia and also with other authors statements on weather dependence upon the

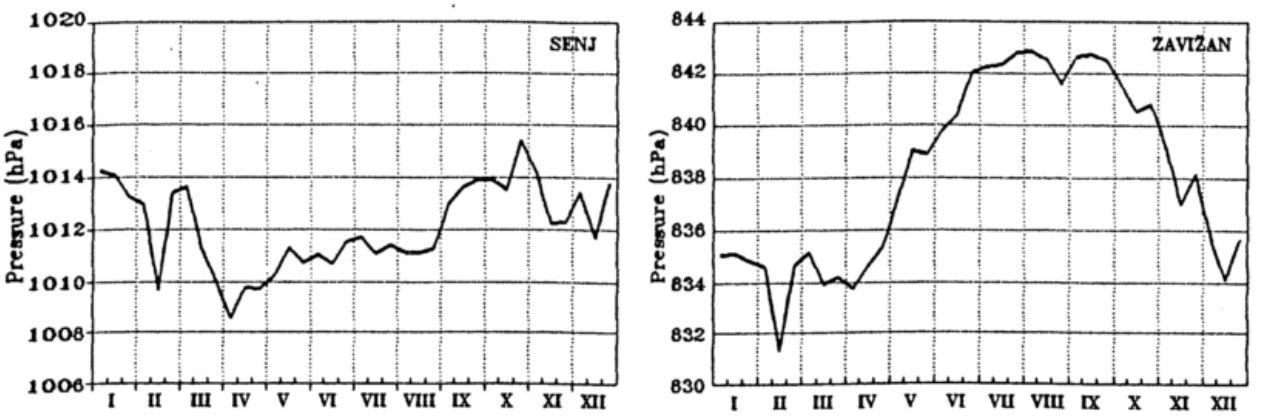

Fig.1. Annual course of ten-day pressure means. Period:1961-1990.

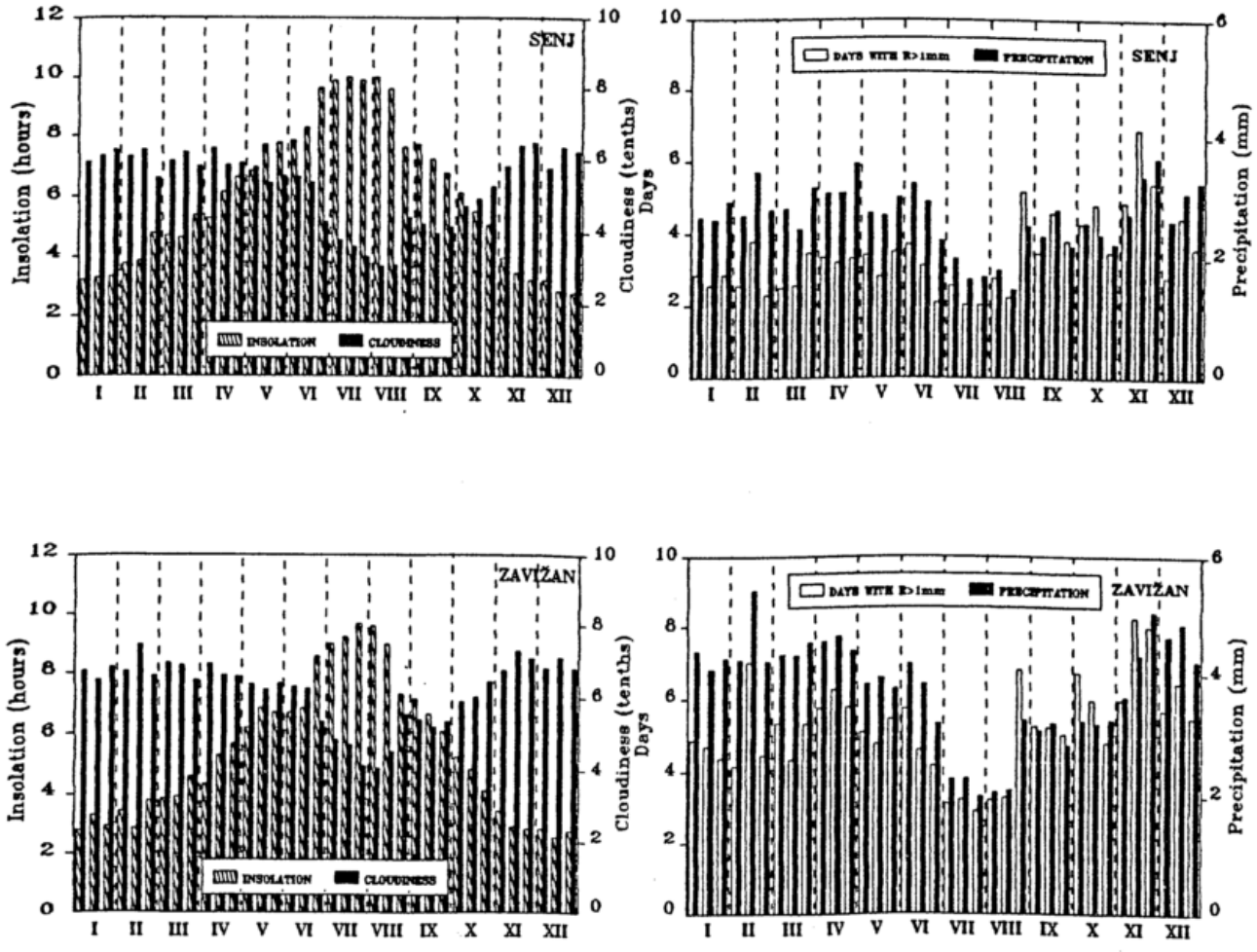

Fig. 2. Mean daily insolation and cloudiness (left), rainy days and mean daily precipitation rates (right) for ten-day period during the year. Period: 1961-1990.

frequency of cyclones and anticyclones (Čatlak and Penzar B. 1975, Lončar and Šinik, 1993, Penzar B., 1968,1977, Šinik 1970). The results have made it possible to postulate that a decrease in pressure during the second decade of February is a climatic characteristic of the whole of Croatia connected with the fairly regular appearance and prevailing influence of cyclones upon the weather during that short period.

2. Annual course of the air pressure ten-day means

Air pressure annual variation differences between the mountain meteorological station Zavižan and the other parts of Croatia, represented here by Senj and Zavižan, are illustrated on the figure 1. Here we want to underline, that no matter the differences amongst the air pressure annual variations, the peak of a lowered pressure in the second decade of February appears to be almost equally intensive all over Croatia.

3. Annual variation of the weather types ten-day frequencies

Ten-day pressure means annual peculiarities can be enlighten by means of the accompanied weather types. The minimum of pressure in the second decade of February accompanied by cloudy, rainy, (snowy), weather (Fig.2.) has resulted from the great frequency of the low pressure weather types over southeastern Europe and Mediterranean (e.g. "Grosswetterlagen" WZ, WS, BM, TM, HB, HFA, HFZ, HNFZ, SEA, SEZ, SZ, TRW, in accordance with "Katalog der Grosswetterlagen Europas nach Paul Hess und Helmuth Brezowski 1881-1992"). The weather types significant for mentioned short period over our small region have been determined by the more detailed classification, developed by Poje (1965) and they are depicted on the figure 3.

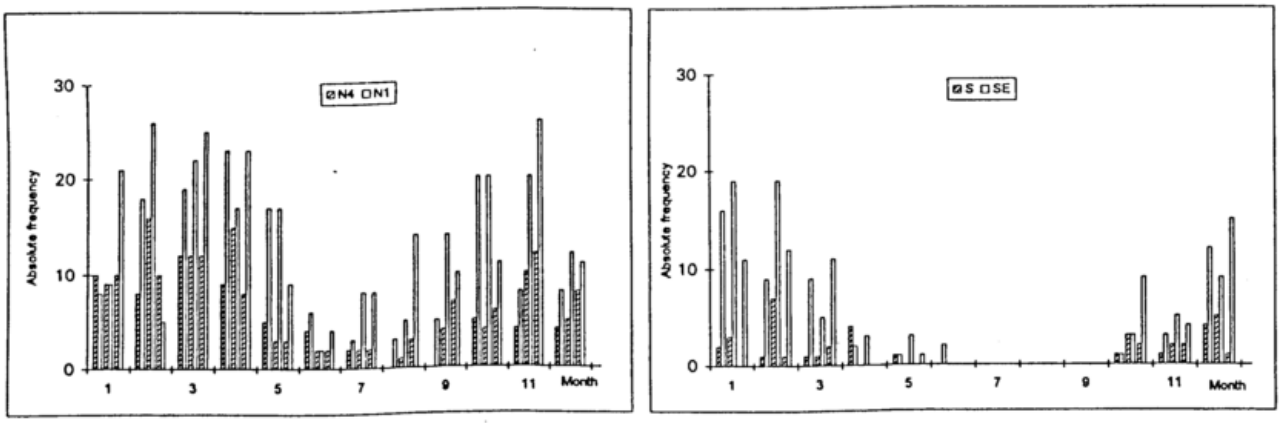

Fig.3. Annual course of weather types ten-day frequencies. Period: (1971-1990). N1 - eastern sector of a cyclone, N4 - northern sector of a cyclone, SE - south-easterly transitory type, S - southern transitory type

4. Conclusion

The pressure decrease in the second decade of February, detected all over Croatia, being related to the simultaneous maximum frequency of the cyclonic weather types is an overall climatic characteristic of the whole of Croatia. This peculiarity is presumably related to characteristic patterns of the general circulation of the atmosphere. The weather characteristics of this short period in February might be relevant for the climate of Croatia just like the appearance of "etesia" or e.g. the "European monsoon". Still, such an assumption should be proved by the further research.

References

Čatlak M.,Penzar B.,(1975): Contribution to the knowledge of the cyclones over the Adriatic sea. in Croatian, Hidrografski godišnjak, pp 67-87.

Gajić-Čapka M., Lončar E., Zaninović K.,(1993): Climatic, bioclimatic and dispersion characteristics over the Senj area, in Croatian, unpublished, pp. 66.

Gerstengarbe F.W., and all (1993):Katalog der Grosswetterlagen Europas nach Paul Hess und Helmuth Brezowski 1881-1992. Berichte des Deutschen Wetterdienstes 113, pp 249.

Lončar E.,Šinik N.,(1993): Some peculiarities of the annual air pressure variation in Croatia. in Croatian, Croatian meteorological journal, 28. pp.81-88.

Penzar B.,(1968): Some characteristics of weather types over the Adriatic sea. in Croatian, Hidrografski godišnjak, pp 99-124.

Penzar B.,(1977): Air pressure, wind. in Croatian, Sav. hidromet. zavod pp.117.

Poje D. (1965): Weather types in Yugoslavia and their dependence on the general circulation of the atmosphere. in Croatian, Dissertation,.pp.215.

Šinik N.,(1970): Spectral analyses of the prevailing weather types frequences on the middle part of the eastern coast of the Adriatic sea. in Croatian, Hidrografski godišnjak, pp 89-104.

The Influence of the Major Relief on the Climate Variability of the Temperature and Precipitation Fields from Romania

Ileana Mares, C. Mares, Ionela Musat, Simona Valcu

National Institute of Meteorology and Hydrology, Bucharest

ABSTRACT

The temperature and precipitation fields from two stations from Romania were analyzed. The two stations are Vf.Omu (Man Peak) and Bucharest - Filaret, with altitudes of 2509 m and 82 m respectively, and with observations from 1928 to 1992 (which is the common period for the two stations). In order to emphasize the tendencies and climatic jumps, Pettitt and Mann - Kendall nonparametric tests have been applied. At the same time the existence of some quasiperiodicities was tested by applying MEM's power spectrum.
The experiments were made for seasonal and annual values. For the mountain station the results concerning the change points, are more significant, especially in the precipitation field.
The link between the two categories of stations was quantified by considering the common signal for both stations.

1.Introduction

In order to study the climate variability in the mountain zone of Romania, Vf. Omu station was considered which is situated at 2509m altitude, representing the highest Romanian station.
The temperature and precipitation fields from this station was analyzed in parallel and compared with the ones from Bucharest - Filaret, a plain station, for the common observational period 1928-1992. The results obtained for Bucharest for the whole observation data series (1896 - 1992, 136 years for temperature and 128 years for precipitation) appear in Mares (1994).
In order to find out the change points, Pettitt (1979) nonparametric test was applied. Then each one of these points was tested, according to the method described by Sneyers(1992,1993), by applying Mann-Kendall nonparametric test.
The estimation of signal - to - noise ratio for these points was realized using the procedure described by Yamamoto (1986).
Because the series of observations for the mountain zone are not very long, for estimating the quasiperiodicities a MEM (maximum entropy method) power spectrum suitable for short data series, was applied. This power spectrum was estimated using a 30 order AR model, for which the parameters were calculated using Burg's (1968) algorithm.
In order to see if a significant signal exists between the temperature and precipitation fields of the two stations, a common signal was estimated for the two data series, using "common elements" method described by Trenberth (1992).

2. Results of the comparative statistical analysis of the temperature and precipitation series from Vf. Omu and Bucharest

Following there are presented the results obtained from the statistical analysis of the internal structure of the temperature and precipitation series from Vf. Omu and Bucharest stations. The best way for showing evident climate change is to consider annual and seasonal averages (Sneyers et al. 1993).

Table 1. Signal to noise ratio in temperature and precipitation fields from Vf.Omu and Bucharest stations (1928-1992).

	Change-point	α	α'	M_1	M_2	LAG	$R_{S/N}$
Temperature Vf.Omu							
Year	1949	0.18	0.19	-2.89	-2.25	10	0.42
Winter	1968/69	6.10^{-3}	6.10^{-3}	-10.08	-8.71	15	0.56
Spring	1945	0.01	0.01	-5.20	-3.40	15	0.51
Summer	1964	5.10^{-3}	6.10^{-3}	5.16	4.23	20	0.61
Autumn	1969	5.10^{-2}	5.10^{-2}	-0.51	-1.67	10	0.68
Temperature Bucharest							
Year	1969	0.06	0.08	11.49	10.95	10	0.53
Winter	1946/47	0.02	0.02	-1.75	-0.20	18	0.41
Spring	1965	0.11	0.17	10.70	11.78	10	0.51
Summer	1966	1.10^{-3}	1.10^{-3}	22.51	21.29	20	0.76
Autumn	1969	1.10^{-3}	1.10^{-3}	12.20	11.20	20	0.55
Precipitation Vf.Omu							
Year	1940	2.10^{-5}	1.10^{-3}	733.74	1359.39	10	**1.00**
Year	1979	1.10^{-3}	1.10^{-3}	1361.41	667.24	10	**2.26**
Winter	1938/39	4.10^{-3}	5.10^{-3}	145.02	342.08	10	0.97
Winter	1978/79	1.10^{-3}	1.10^{-3}	260.83	120.71	10	0.95
Spring	1940	8.10^{-3}	1.10^{-2}	214.15	356.10	10	0.51
Spring	1979	1.10^{-4}	1.10^{-4}	350.97	146.30	10	**1.03**
Summer	1946	1.10^{-4}	5.10^{-4}	291.79	438.70	15	0.51
Summer	1979	1.10^{-3}	4.10^{-3}	500.33	299.18	10	**1.08**
Autumn	1939	1.10^{-3}	4.10^{-3}	110.10	217.62	10	0.85
Autumn	1978	3.10^{-4}	1.10^{-3}	253.23	105.19	10	**1.03**
Precipitation Bucharest							
Year	1953	0.07	0.08	517.86	619.25	10	0.51
Year	1981	0.05	0.08	647.07	553.41	10	0.42
Winter	1951/52	0.06	0.09	103.12	140.37	10	0.41
Winter	1969/70	0.05	0.09	163.47	103.75	10	0.45
Spring	1940	2.10^{-2}	0.05	164.47	124.94	10	0.44
Spring	1953	0.19	0.27	124.94	183.65	10	0.74
Summer	1941	0.02	0.03	241.86	170.81	10	0.40
Summer	1968	0.09	0.13	160.44	227.91	10	0.65
Autumn	1981	0.08	0.09	148.44	92.96	10	0.53

In Tab. 1 there are presented change points (according to Pettitt), significant level α , which is deduced from the standardized statistics, corrected significance level for reduction to the total length of the series α' , averages of the periods with length of a lag before the change point M_1 and after this point, M_2. The last column of Tab. 1, contains the values of signal to noise ratio, corresponding to these change points, estimated using first and second orders statistical moments. Values greater than 1 for the signal to noise ratio, were obtained for the precipitation series from Vf. Omu, for annual values as well as for the seasonal ones, except winter season for which this ratio is a little bit smaller than 1. A change point with a significance greater enough appears between a wet period and one with less precipitation in the years 1978-1979.
Although significant, but with a lower level, appears a change point in 1939 - 1940 when a transition from a dry period to a wet one exists. The change point divides two periods for which the averages differ by a 2 factor for the mountain zone. For the plain zone, the results are not so evident because the significance level are relative lower and the same change point cannot be found in all seasons and also in the annual series.
In the temperature series from Vf. Omu change points with significance level so great as in case of precipitation, didn't appear. Considering value 0.5 as having practical importance for signal to noise ratio, significant results were obtained only for the seasonal values. In these cases, for autumn and winter, the same change point for year 1969 was obtained, with the specification that for the autumn period the transition is from warm to cold and for winter, from cold to warm. At the same time, an interesting result was obtained for summer, where year 1964, marks a transition point from a warmer 20 years period to a colder one. In case of summer and autumn the transition faze, as well as change points are characteristic also for Bucharest.
In order to see if the anomalies of the temperature and precipitation series go hand in hand in case of the two stations, the common signal in the two series is considered (Trenberth, 1992).

Table 2. The common signal in the two observations series from Vf.Omu and Bucharest stations (1928-1992).

	Temperature		Precipitation	
	Correlation coefficient	Signal/noise	Correlation coefficient	Signal/noise
Year	**0.69**	**2.26**	0.16	0.19
Winter	**0.69**	**2.26**	**0.24**	0.32
Spring	**0.65**	**1.83**	0.15	0.18
Summer	**0.84**	**5.33**	**0.27**	0.37
Autumn	**0.65**	**1.84**	**0.53**	**1.12**

The signal to noise ratio for the standardized series shown in Tab. 2, suggests that only for the temperature field can be induced a signal from a series to another and for the

precipitation the single season that has this feature ($s/n \geq 1.0$) is autumn. The bold numbers have a significance at least of 5%. The greatest ratio (s/n=5.33) in the temperature series of the two stations was found for summer, fact also shown by the change points with a good significance from the two stations. Although in Tab. 1 only year 1964 for Vf. Omu and 1966 for Bucharest have been noted, significant signals appear in the period 1964-1966. Using a 30-th order AR model (this order was considered in order to find possible periodicity caused by the 22 year double cycle of the sun spots), power spectrum has been estimated by MEM, for which the results were noted in Tab 3.

Table 3. Quasiperiodicities in temperature and precipitation fields for Bucharest-Filaret and Vf.Omu stations.

	Temperature		Precipitation	
	Bucharest	Vf.Omu	Bucharest	Vf.Omu
Year	**25; 30**	**2.2; 4; 26**	**2.4; 3.7**	**15.0; 32**
Winter	65	2.0; 26	**5.2**	18.0; **32**
Spring	**21; 30**	2.1; **12**	2.2; **8.0**	**1.5**; 33
Summer	**25; 30**	**4.0; 8; 27**	**4.2; 7.0**	2.4; **10**
Autumn	**30**	**3.6; 8; 15**	**4.7**; 33.0	16.0; **32**

The bold numbers have a significance better then the other ones. The period of about 2 years can be noticed at the annual, winter and spring temperatures from Vf. Omu, as well as at the summer precipitation from this mountain station. This can be associated with QBO (Quasi-Biennial Oscillation) phenomena. For the plain station this period appears only in the annual and spring precipitation series. At the same time for the precipitation at Vf. Omu, a 15 or 16 year period appears in all cases, except summer when the period is only of 10 years.

3. Conclusion

The tests by the mentioned methods revealed periods with distinct features in temperature and precipitation regim in the mountain area, in comparison with the plain zones.
So, for the period of instrumental measurements, 1928-1992, climatic jumps with good significance have been determined especially for precipitation series. It was found out that 1979 year is a change point in the precipitation field in the mountain area making the transition towards a dry period which continues in the present. Remarkable is also the change in the temperature component of the climate structure that reveals the transition from a colder period (1954 - 1968) to a warmer one (1970 - 1984) in the winter season and from a warmer one (1944 - 1963) to a colder one (1965 - 1984) in the summer season and even in the autumn season.

A good significance level of the changes occurred in the mountain area, in comparison with the changes in the plain area, suggests that high zones are more sensitive at the factors that modify the climate.
Unfortunately, the short data series of the mountain area from Romanies don't allow us to make comparison with the results obtained by other authors that have made similar analysis with long data series, for example with that made for Austrian Alps by Sneyers (1992).

References

Burg,J.,P., 1968 : A new analysis technique for time series data. Paper presented at Advanced Study Institute on Signal Processing,NATO,Enschede,Netherlands.

Mares, Ileana and C. Mares, 1994 : Statistical Methods for estimating the Signal to Noise Ratio.
The paper has been prepared for the "Contemporary Climatology",August 15-20,Brno,Czech Republic.

Pettitt,A.N., 1979 : A non-parametric Approach to the Change-Point Problem.Appl.Statist.28,No 2,126-135.

Sneyers,R., 1992 : On the use of Statistical Analysis for the Objective Determination of Climate Change.
Meteorol. Zeitschrift, N.F.1,247-256.

Sneyers,R., R. Bohm and S. Vannitsem, 1992: Climatic Changes in the Austrian Alps during the Period 1775-1989.Proc. 6th Italian Glaciological Meeting, Gressoney, Italy.

Sneyers,R., A.M.Siani and S.Palmieri ,1993 : Characterizing Trends in Climatological Time Series.An Application to Brera Observatory (Milan) Rainfall Series (in press).

Trenberth,K.E. 1992 : Signal and Noise in the Surface Temperature Record.Proc.Amer.Meteorol.Soc. 12th Conference on Probability and Statistics in the Atmospheric Sciences and 5th International Meeting on Statistical Climatology.J7

Yamamoto,R.T.et al.,(1986): An analysis of Climate Jump.
J.Met.Soc.Japan, 64, 273 - 281.

LONG-TERM AIR TEMPERATURE FLUCTUATIONS IN THE RUMANIAN CARPATHIANS

Ion-Florin MIHAILESCU * Adrian RABAEA * Ion BUCSA **

Abstract

Time series of air temperature fluctuations, as indicative of the main climatic variations in the Rumanian Carpathians, are analyzed by means of mixed parametrical model of autoregression and the sliding average .

The analysis is based on the recordings of the mountain meteorological station of Sinaia, established 1886 the station with the longest series of observations in the Rumanian Carpathians. Until 1960 the station functioned at an altitude of 879 m ; ever since it has been functioning at an altitude of 1510 m .

a) **b)**

The 1886-1960 period (879 m)

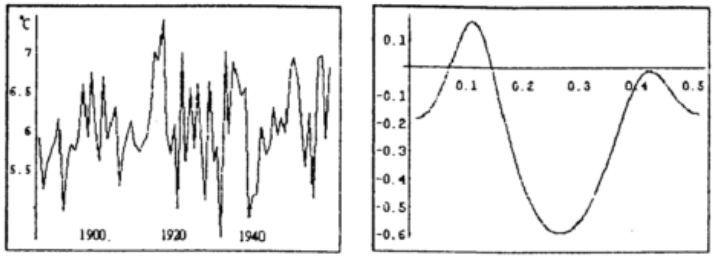

The 1961-1986 period (1510 m)

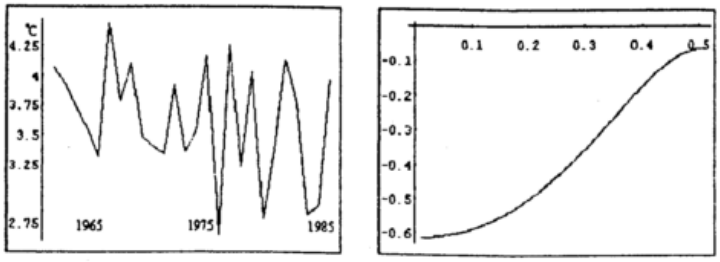

The variation ofthe average annual air temperature **(a)** and the logarithm of the spectral density **(b)** at Sinaia .

The time series of air temperature from Sinaia have ben compared with the century-old observations of lower altitude meteorological stations, as wel as with thoose of the stations on the highest peaks in the Rumanian Carpathians, such as Omul, 2509 m , the latter , with observations since 1928 .

* The "OVIDIUS" University of Constanta , Romania
** Departament of Meteorology , Constanta , Romania

Precipitation rate as a possible signal of recent climatic variations

V. Pasquale, G. Russo, A. Sacchini, M. Verdoya

Università di Genova, Dipartimento di Scienze della Terra, Settore di Geofisica,
I-16132 Genova, Italia

ABSTRACT

The precipitation rate of the last 160 years (1833-1992) at Genoa shows a clear tendency to increase versus time, but no particular trend has been observed in the annual rainfall. The rise in number of the dry days, on average 0.23 day/year, is apparent in every season and it plays a decisive role in the occurrence of such processes. The progressive growth in stability of the dry weather depends on a corresponding increase in the southerly circulation in the Mediterranean basin. The rather stable rate of the annual rainfall indicates that drought periods alternate periods with more intense and concentrated precipitation.

Within the framework of surveys devoted to investigate the recent climate fluctuation in Europe, we have already found an evident tendency to a temperature increase of about 0.006 K/year during the last hundred years, on the base of the analysis of several temperature time series (Pasquale et al., 1990). In particular, temperature has had an increase of about 0.4 °C from 1850 to 1865; then underwent a strong drop until 1885. Since then, a main rise of about 0.8 °C begun again and lasted until 1945. This period was followed by a slight cooling of 0.2 °C, for about 25 year. Afterwards, a warming period took place which still seems to keep on, bringing back temperature to the levels of 1865 and 1945. The temperature increase cannot be ascribed only to urbanization as it is observed also outside urban areas. The temperature trend compared to the wind direction indicates that changes in the general circulation of the atmosphere are the primary cause of such climatic variations.

In this paper we report some additional results which have been obtained by analyzing the precipitation data recorded at Genoa since 1833. Observations on the daily precipitation amount as well as the count of dry days with precipitation lower than 0.3 mm allow to obtain the related monthly and annual average, and the precipitation rate, defined as the ratio between the amount of

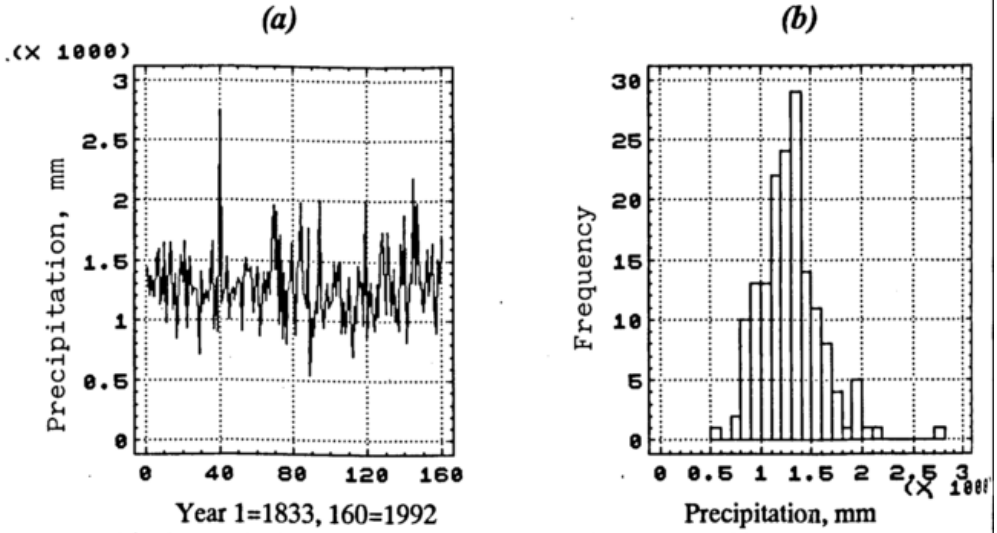

Fig. 1 - Amount (a) and frequency histogram (b) of annual rainfall at Genoa during the period 1893-1992.

precipitation on the number of rainy days. By means of the available observations, it is here defined the weather trend which can be also inferred from the average duration of the drought periods.

During the time span studied in this paper, the annual precipitation amount is rather stable, i.e. it varies around a mean value of 1292±308 mm (mean deviation 17.6%), without showing any significant trend (Fig. 1a). The frequency distribution (Fig. 1b) is close to normal and its fitting, verified by the chi-squared test, is pretty good at 5% significance level. It is 95% confident that the mean precipitation in the population falls between 1244 and 1440 mm per year. Annual precipitation greater than 1800 mm has probability of occurrence by about 5% and those lower than 900 mm by 10%. The years in which these limits have been overcome are:

#	Year	Below 900 mm	#	Year	Above 1800 mm
1	1849	849	1	1872	2752*
2	1861	720	2	1901	1965
3	1871	899	3	1903	1906
4	1894	872	4	1916	1978
5	1906	844	5	1926	2007
6	1908	803	6	1951	1991
7	1913	877	7	1972	1879
8	1921	543**	8	1977	2186
9	1923	872	9	1979	1977
10	1940	899			
11	1944	705			
12	1952	864			
13	1973	830			
14	1989	900			

* Absolute maximum value
** Absolute minimum value

The highest precipitation amount (2752 mm) pertains to 1872; such a value is more than twice the average value of the series. That year was characterized in October-December by rainfalls yielding floods which produced about 1850 mm. This unusual event has very long return period and regional character as it affected the whole northwestern Italy and surrounding countries. The lowest value (543 mm) occurred in 1921, which was preceded by a year with a precipitation amount exceeding the mean of the time series by about 500 mm.

The annual precipitation rate shows short-period fluctuations which, however, indicate a clear increase with time, with a maximum of 22.3 mm/day in 1970 and a minimum of 8.0 mm/day in 1884 (Fig. 2a). The time series averages 12.6 mm/day with standard deviation of 2.6 mm/day. A tendency to increase by 0.23 day/year can be observed for dry days. They are on average 261.9±17.9 and range from 307 to 205 (Fig. 2b); these extreme conditions occurred in the years of absolute minimum and maximum precipitation amounts, respectively. Even though the number of rainy days tends to rise in the years with the largest precipitations, a close relation between annual precipitation amount and rainy days cannot be recognized. Any season seems to contribute to the increase of dry days (Figs. 3 and 4). Spring shows a noticeable decrease during the second half of last century, whereas winter shows it from 1960 to 1980.

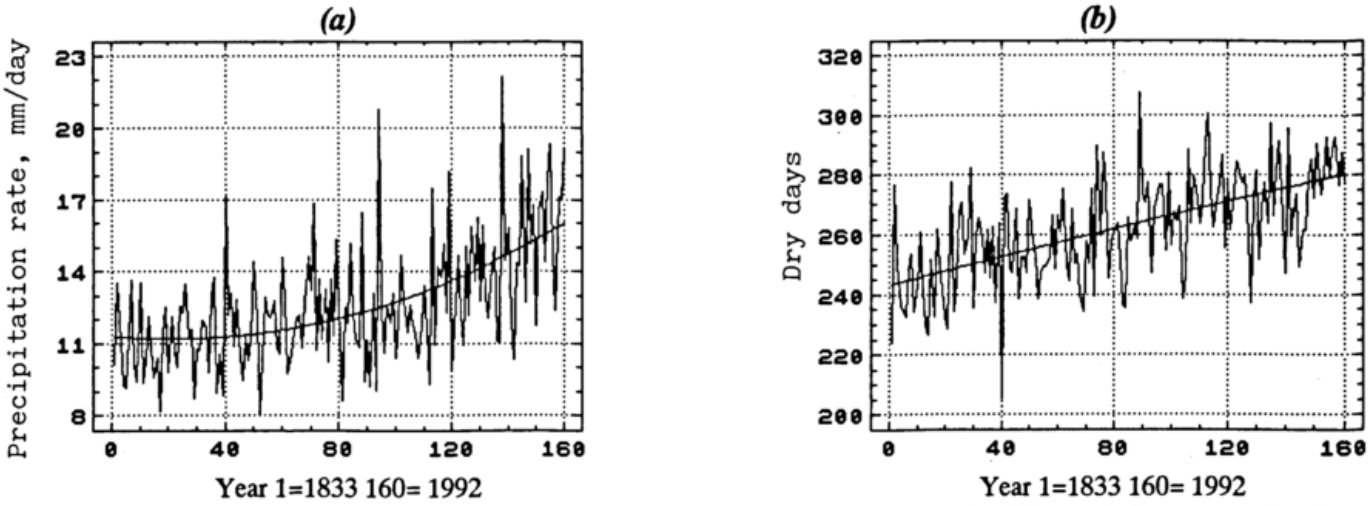

Fig. 2 – Rate of precipitation (a) and dry days (b) at Genoa together with the related interpolation curves showing quadratic and linear trend, respectively.

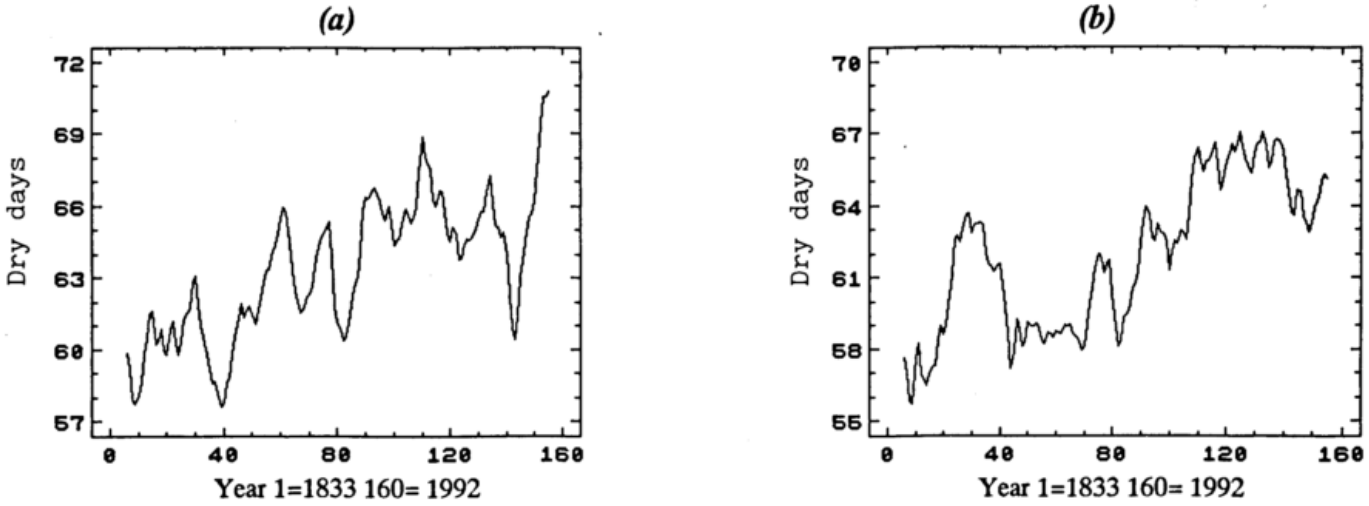

Fig. 3 – Smoothed series of the number of dry days per year at Genoa in winter (a) and spring (b) obtained by means of a 10–term moving average.

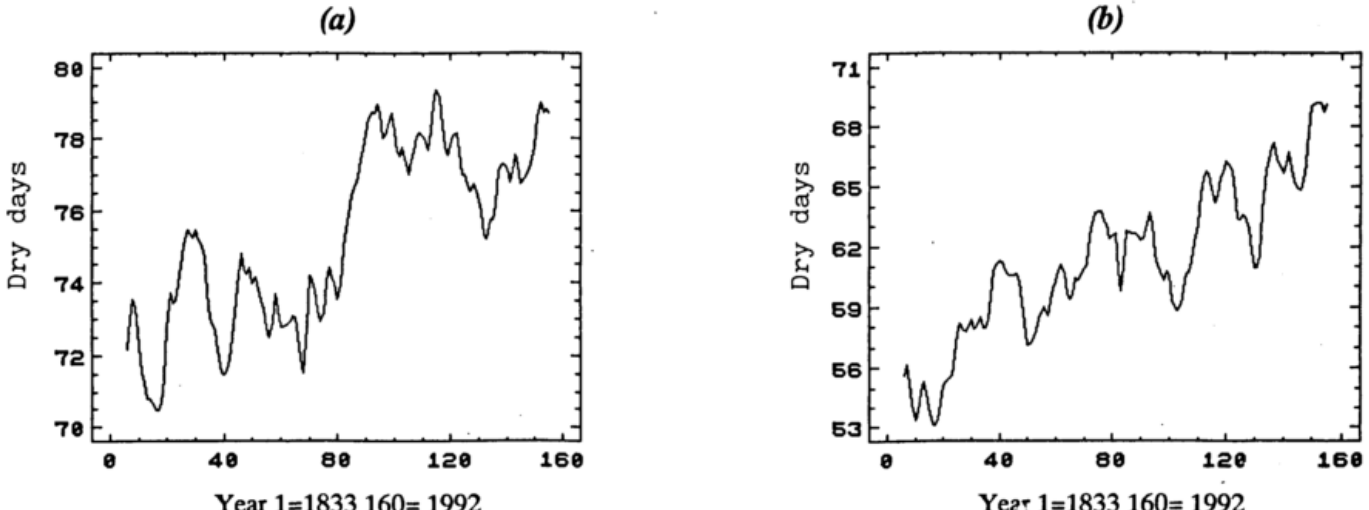

Fig. 4 – As in Fig. 3 for summer (a) and autumn (b).

The increase of periods with abnormal dry weather confirms the fact that the precipitation rate is characterized by a global rise. If we take account of the average length of the periods of consecutive dry days, it is possible to state they have progressively grown, with a remarkable difference between the period 1841–1930 and the subsequent period of 60 years (Table 1). This is confirmed by the global number of rainy periods and by their progressive decrease, which indicate that the average length of the steady weather is increased, particularly since last century to the present one (Bossolasco, 1950).

Table 1. Seasonal average duration of the dry periods

Station	Time span	Winter	Spring	Summer	Autumn	Year
Genoa	1841–1870	11.4	9.8	11.1	8.9	10.30
«	1871–1900	11.8	8.9	12.1	10.2	10.75
«	1901–1930	11.5	9.2	11.9	10.2	10.70
«	1931–1960	11.7	11.4	14.0	10.9	12.00
«	1961–1990	11.9	10.5	13.8	11.8	12.00
Chiavari	1901–1930	10.7	9.6	12.8	9.9	10.75
«	1901–1945	10.7	9.7	12.9	9.7	10.75
Milan	1901–1930	11.8	8.8	10.0	9.6	10.05

An analogous behaviour is observed at Chiavari which is located along the coast, 35 km east of Genoa. Even though the time span investigated is shorter, Chiavari data show differences only in the seasonal trend of the mean duration of the dry days. Compared to that of Genoa, this parameter is lower both in autumn and winter. A progressive fall in the weather variability has occurred also in this site, in terms of a slight increase in duration of the periods with dry steady weather. If we compare these results with those obtained for Milan, which represents the typical continental climate of the Po Valley, it can be inferred that dry periods are longer, on average, near the Ligurian Sea coast (Table 1). However, variability is slightly larger at Milan because the mean duration of the stable weather periods is here smaller.

The increase of drought periods and dry weather stability observed in the present century, justifies the rise of the air mean temperature which occurred in Europe during the same period and which is still going on. This phenomenon is nothing else but the effect of the increase in the southerly circulation which is clearly illustrated by the change in the mean annual wind at the ground observed in Genoa (Pasquale et al., 1990, Fig. 4). Generally, a warm period corresponds to a growth of the southern components of the ground wind direction; the increase in the southerly circulation in the Mediterranean yields increased stability of the dry weather.

References

Bossolasco, M., 1950. La persistenza del tempo in Liguria ed in talune località continentali. Geof. Pura ed Appl., 16, 163–180.

Pasquale, V., Flocchini, G., Russo, G., 1990. Surface temperature field along an European traverse. Atti del XXII Intern. Conf. on Alpine Meteor., pp. 345–349.

Sulle variazioni climatiche del numero di giorni con nevicate in alcune localita' delle Alpi italiane

Cosimo Todaro*, Franco D'Abramo**, Ernesto Migliardi.
* Soc. Ital. Meteor. Appl. (SIMA) Roma
** Servizio Meteor. Aer. Ital. Roma

Zusammenfassung:

Es werden monatliche Zeitreihen an sieben Ortschaften untersucht mit Hilfe angemessener test und ein Signifikanzniveau von 1%. Autokorrelationen liegen vor: in Bric della Croce in Jannuar, in Tarvisio im Dezember, in Paganella im November und Dezember. Die Reihen von Toblach, Passo Resia und Passo Rolle sind aleatorisch. Am Pian Rosa' liegt eine Autokorrelation in den Monaten Juli, November und Dezember vor; diese Monate, zusammen mit Mai und Juni tragen zur Persistenz von Jahr zu Jahr bei; eine negative Tendenz ist in allen Monaten vorhanden außer im April. Ordnet man die 12 Monate indem man mit April anfängt hat die "Jahres" Zeitreihe einen negativen Trend und läßt sich in drei Teile trennen, ohne Autokorrelation und ohne trend.

Testo:

Lo studio destinato a questo Congresso concerne l'analisi di serie cronologiche del numero di giorni al mese con nevicate sulle localita' delle Alpi elencate nella Fig. 1 e nella tab. I. Soltanto per Pian Rosa' si prende in esame la frequenza indicata in un particolare aggregato di 12 mesi. Poiche' la finalita' da perseguire e' la ricerca di variazioni climatiche, e' opportuno chiarire che si ritiene accertata l'esistenza di un mutamento climatico allorche' la serie cronologica denuncia uno scostamento significativo dalla casualita' perche' i suoi termini non sono indipendenti o perche' la sua media non e' costante oppure perche' tali proprieta' sono coesistenti. Pertanto, in un primo tempo occorre indagare sull'esistenza di un'eventuale autocorrelazione e di una eventuale tendenza. Quando la serie non risulta casuale pura nel senso detto, l'indagine deve proseguire per cercare di dividere la serie stessa in due o piu' parti, ciascuna priva di autocorrelazione e di tendenza; in tal caso la separazione tra due serie parziali puo' essere assimilita a una discontinuita' climatica. Ogni conclusione alla quale si perverra' e' basata su un'ipotesi di zero al livello di significativita' rigoroso dell'uno per cento(α_0=0,01). I test di cui si fara' uso sono: per le serie mensili quello di **Wald-Wolfowitz** (2) per la autocorrelazione e quello di **Kendall-Mann** (2) per la tendenza, in forma normalizzata rispettivamente u(r) e u(t); per l'aggregato dei 12 mesi il "chi quadrato" di **Fisher**(3), combinato con il test derivante dalla legge binominiale (2); per la separazione in serie parziali il test della mediana, applicato sequenzialmente,FT(4).

Le analisi effettuate suggeriscono di ripartire le localita' almeno in due gruppi, l'uno formato dalle prime 6 stazioni meteorologiche, l'altro soltanto da Pian Rosa'.

I risultati ottenuti nel primo gruppo sono sintetizzati nella tab. II, i mesi esclusi dall'analisi sono quelli in cui il numero di casi e' nullo in piu' di 20 anni. Si vede che la persistenza e' presente solo in un mese nelle due localita' piu' basse e in due mesi in quella piu' alta e che una tendenza negativa si ha a Tarvisio soltanto in gennaio. Con questi risultati si ritiene che non vi sia interesse ad approfondire ulteriormente l'indagine. Per quanto concerne Pian Rosa', un primo studio fu gia' presentato al VI Congresso Glaciologico italiano, tenutosi a Gressoney nel settembre 1991 (4). In esso una pseudo-stagione delle nevicate invernali venne definita in maniera a priori, escludendo i mesi da marzo a luglio. Qui invece l'indagine e' piu' approfondita perche' il numero dei giorni còn nevicata e' preso in esame in base ai risultati di analisi eseguite su tutte le serie cronologiche mensili. Infatti si vedra' che, anche ai fini della variabilita' climatica, la frequenza delle

precipitazioni nevose nella primavera e nell'estate, spesso associate a rovesci e temporali, non sono da trascurare.

La tab.III relativa a Pian Rosa', per ciascun mese, contiene tutti gli elementi per l'analisi dell'autocorrelazione. Si vede che una significativita' individuale dell'autocorrelazione positiva e quindi della persistenza non e' prevalente e si ha solo nei mesi di luglio, novembre e dicembre. Il test multiplo di Fisher: $\chi^2=92,635$ applicato all'aggregato dei 12 mesi indica che anche da un anno all'altro esiste un autocorrelazione significativa. In particolare , sequendo la tab. IV, se a cominciare dal valore 92,635 si selezionano i contributi di ciascun mese alla significativita' di tutto l'aggregato, si vede che a luglio, novembre e dicembre bisogna associare anche giugno e maggio. Infatti aggiungendo alle selezioni precedenti il contributo di maggio il valore di χ^2 diviene piu' piccolo del valore soglia corrispondente e quindi si deve concludere che tale mese, nell'ordine k indicato, e' l'ultimo che fornisce un apporto significativo. Questa affermazione acquista maggior valore per il fatto che in giugno e maggio le probabilita' $\alpha(r)$ di tab. II sono ben piu' piccole dei loro limiti superiori α_1 (2). Con identica metodologia si possono analizzare i test mensili di Kendall-Mann sulle tendenze.

Dalla tab. V si vede che in tutti i mesi si ha una tendenza negativa, e che e' molto prevalente la significativita', infatti solo in aprile la probabilita' di superamento del test e' appena superiore a 10^{-2}. I mesi indicati con un asterisco sono quelli nei quali si e' riscontrata un'autocorrelazione significativa, percio' e' possibile che il test di tendenza in essi risulti sovrastimato. Il test multiplo di Fisher, applicato all'aggregato dei 12 mesi, indica che anche da un anno all'altro esiste una tendenza negativa. In particolare, seguendo la tab. VI, se si selezionano i contributi di ciascun mese alla significativita' di tutto l'aggregato, si vede che, nell'ordine k indicato, l'ultimo contributo e' quello di ottobre e che l'unico mese da escludere e' aprile. In questo caso tutte le probabilita' $\alpha(t)$ sono molto piu' piccole dei loro limiti superiori α_1.

Aggregando i 12 mesi da gennaio a dicembre, da febbraio a gennaio, da luglio a giugno e da aprile a marzo si previene ai risultati indicati nella tab.VII, tutti significativi perche', compatibilmente con il livello $\alpha_0=0,01$ per ciascun mese, i valori soglia per ogni aggregazione sono:

$$u'_0(r)=3,143 \;;\; \alpha'_0(r)=0,837\cdot10^{-3} \;;\; u'_0(t)=\pm3,345 \;;\; \alpha'_0(t)=0,835\cdot10^{-3}.$$

E' interessante costatare che la serie cronologica che presenta il piu' grande scostamento dalla casualita' e' quella in cui l'aggregazione comincia dal mese di aprile che da' il minimo contributo al trend.

Per questo motivo si e' data la preferenza a tale serie per studiare la possibilita' di suddividerla in serie parziali aleatorie mediante l'applicazione del test FT. Il suo andamento per le n-1 possibili divisioni della serie totale in due parti e' mostrato nella fig.2. In corrispondenza del massimo principale che localizza una prima divisione tra il 1970-71 e il 1971-72 (tra i primi 19 e gli ultimi 21 termini) si ha : $FT_{max1}=28,97$ che proviene dalla sequente ripartizione nelle due parti delle frequenze assolute dei ranghi, in termini di valori minori o uguali(-) e di valori maggiori(+) del rango mediano (20,5):

	1ªparte	2ªparte	totale
-	1	19	20
+	18	2	20
	19	21	40

Poiche' FT_{max1} e' un estremo tra n-1=39 valori, il livello di significativita' α'_0, in una specificazione bilaterale con α_0=0,01, e' dato da α'_0=2,57·10^{-4}. La probabilita' di superamento di FT_{max1} e' α'=5,82·10^{-8} . Pertanto $\alpha' < \alpha'_0$ indica la significativita' dell'estremo. Nella prima serie parziale si ha: n'=19

$$u(r)=1,19 \ ; \ \alpha(r)=0,117 \ ; \ u(t)=0,24 \ ; \ \alpha(t)=0,810 .$$

Sebbene si tratti di una serie parziale, poiche' i valori delle α sono gia' grandi, non e' necessario incrementarli con le dovute "correzioni" per decidere che bisogna accettare l'ipotesi di zero, quindi la casualita' per assenza di autocorrelazione e di tendenza. Nella seconda si ha: n'=21

$$u(r)=3,42 \ ; \ \alpha(r)=3,16\cdot10^{-4} \ ; \ \alpha_c(r)=6,02\cdot10^{-4} \quad u(t)=-3,96 \ ; \ \alpha(t)=7,65\cdot10^{-5} \ ; \ \alpha_c(t)=1,46\cdot10^{-4}.$$

nelle quali le α_c sono le probabilita' "corrette".

Contrariamente al caso precedente, essendo tali probabilita' inferiori al livello di significativita', la seconda serie parziale non risulta casuale perche' presenta ancora autocorrelazione e tendenza. Percio' tale serie puo' ulteriormente essere suddivisa in due parti.

Con un procedimento analogo, con una nuova determinazione dei ranghi, si trova l'andamento di FT riprodotto nella fig. 3, nella quale si vede che il massimo si localizza tra il 1979-80 e il 1980-81 (tra i primi 9 e gli ultimi 12). Si trae FT_{max2}= 17,33; il livello di significativita' e': α''_0=5,01·10^{-4}; la probabilita' "corretta" e':α''_c=1,30.10^{-4} . Pertanto, essendo $\alpha''_c < \alpha''_0$, l'ulteriore divisione della seconda serie parziale in due parti e' anch'essa significativa. Per la prima parte, compresa tra il 1971-72 e il 1979-80, si ha n'=19

$$u(r)=-0,12 \ ; \ \alpha(r)=0,548 \ ; \ u(t)=1,50 \ ; \ \alpha(t)=0,134 .$$

Anche in tal caso, considerate i valori delle α già grandi, non e' necessario effettuare le "correzioni" dovute al fatto che si tratta di una serie parziale per concludere che ha caratteristiche aleatorie.

Per la seconda parte, compresa tra il 1980-81 e il 1991-92, si ha: n'=12

$$u(r)=2,64 \ ; \ \alpha(r)=4,15\cdot10^{-3} \ ; \ u(t)=-2,33 \ ; \ \alpha(t)=0,0198 .$$

Correggendo le due α rispettivamente risulta: $\alpha_c(r)=0,0138$ $\alpha_c(t)=0,0645$.

Percio' anche in questo caso, allo stato attuale, si puo' accettare l'aleatorieta' della serie, ma, poiche' il valore relativo al test sull'autocorrelazione supera di poco il livello α_0=0,01, si potrebbe fare una riserva in attesa di un congruo prolungamento della serie totale con i dati del futuro. Tuttavia quest'ultima considerazione va pure temperata dalla seguente circostanza: le ultime due serie parziali appena trattate sono con pochi termini (9 e 12) e l'uso di test piu' appropriati, al posto di quelli che sono valevoli asintoticamente, avrebbe certamente fornito valori delle probabilita' "corrette" ancora piu' grandi.

In definitiva la serie totale risulta divisibile in tre serie parziali, caratterizzate dalle medie e varianze riportate nella tab.VIII. Le medie sono rappresentate nella fig. 4. Si puo' agevolmente dimostrare che tra le varianze, considerate a due a due, non vi e' differenza significativa, percio' una stima della varianza puo' trarsi da una media ponderale; risulta: s^2=279,060. Al contrario, tra la prima e la seconda media e tra la seconda e la terza le differenze sono alquanto significative. Cio' da' ulteriore credito alle due discontinuita' climatiche individuate e all'interpretazione del trend negativo della serie totale in termini di decremento cronologico della media in tre serie parziali successive, tutte aleatorie.

Fig. 1 - Ubicazione delle stazioni: 1 Bric della Croce, 2 Tarvisio, 3 Dobbiaco, 4 Passo Resia, 5 Passo Rolle, 6 Paganella, 7 Pian Rosà.

Stazione	altitudine (m)	periodo di riferimento
Bric della Croce	710	1953 - 1992
Tarvisio	778	1952 - 1992
Dobbiaco	1226	1954 - 1992
Passo Resia	1524	1952 - 1992
Passo Rolle	2006	1959 - 1992
Paganella	2129	1952 - 1992
Pian Rosà	3488	1952 - 1992

Tab. I - Dati relativi alle stazioni meteorologiche

	numero anni (n)	altitudine (m)	mesi esclusi dall'analisi da	a	valori significativi u(r)>2,326	|u(t)|>2,576
Bric della Croce	40	710	aprile	ottobre	gennaio	-
Tarvisio	41	778	maggio	ottobre	dicembre	gennaio (-)
Dobbiaco	39	1226	maggio	settembre	-	-
Passo Resia	41	1524	giugno	settembre	-	-
Passo Rolle	34	2006	luglio	agosto	-	-
Paganella	41	2129	luglio	agosto	novembre dicembre	-

Tab. II - Mesi con valori significativi di autocorrelazione positiva e tendenza.

mese	k	r	u(r)	α(r)	α_t
lug	1	0,673	4,19	$1,40.10^{-5}$	0,000837
nov	2	0,481	3,20	$3,87.10^{-4}$	0,0128
dic	3	0,443	2,96	$1,54.10^{-3}$	0,0396
giu	4	0,320	2,18	$1,46.10^{-2}$	0,0759
mag	5	0,277	1,91	$2,81.10^{-2}$	0,1214
ago	6	0,260	1,80	$3,59.10^{-2}$	0,1746
apr	7	0,198	1,41	$7,93.10^{-2}$	0,2349
gen	8	0,177	1,28	0,1003	0,3024
set	9	0,126	0,96	0,1685	0,3775
mar	10	0,084	0,69	0,2451	0,4627
feb	11	0,080	0,66	0,2546	0,5606
ott	12	0,006	0,20	0,4207	0,6813

Tab III - Pian Rosà - Coefficiente di autocorrelazione di *lag* 1 r tra i ranghi del numero di giorni al mese con nevicata; u(r): test di Wald-Walfowitz; α(r) sua probabilità di superamento; α_t limite superiore di α(r) secondo il test multiplo basato sulla legge binomiale. I mesi sono disposti secondo la graduatoria k per α(r) crescente (cioè per contributo decrescente al test multiplo χ^2 di Fisher). Autocorrelazione significativa per α(r) < 10^{-2} [u(r) > 2,326].

mese	k	χ^2	$k_{selez.}$	ν	α_χ	χ^2_α
		92,635		24	0,01	42,98
lug	1	70,280	1	22	0,0092	40,6
nov	2	55,713	1,2	20	0,0083	38,25
dic	3	42,761	1,2,3	18	0,0075	35,8
giu	4	34,307	1,2,3,4	16	0,0067	33,25
mag	5	27,716	1,2,3,4,5	14	0,0058	30,85

Tab. IV - Pian Rosà - Selezione graduale dei contributi mensili di Wald-Walfowitz, da k=1 a k=5, al test multiplo di Fisher (χ^2 = 92,635) sull'intero aggregato dei mesi. ν gradi di libertà; α livello di significatività; χ^2 valore soglia del test.

aggregazione da	a	n	u(r)	α(r)	u(t)	α(t)	NOTE
gen	dic	41	4,76	$9,96.10^{-7}$	-6,01	$1,88.10^{-9}$	anno calendariale
feb	gen	40	4,98	$3,25.10^{-7}$	-5,83	$5,74.10^{-9}$	inizio dal mese più freddo
lug	giu	40	4,81	$7,62.10^{-7}$	-5,69	$1,29.10^{-8}$	inizio dal mese più caldo
apr	mar	40	5,44	$2,76.10^{-8}$	-6,02	$1,79.10^{-9}$	inizio dal mese di min. trend

Tab. VII - Pian Rosà - Valori dei test relativi alle indicate aggregazioni di 12 mesi.

mesi	k	t	u(t)	α(t)	α_t
giu*	1	203	-4,65	$3,41.10^{-6}$	0,000837
lug*	2	222,5	-4,21	$2,565.10^{-5}$	0,0128
nov*	3	244	-3,73	$1,946.10^{-4}$	0,0396
dic*	4	247,5	-3,65	$2,67.10^{-4}$	0,0759
ago	5	257,5	-3,43	$6,116.10^{-4}$	0,1214
mag*	6	258,5	-3,40	$6,74.10^{-4}$	0,1746
feb	7	260,5	-3,36	$7,908.10^{-4}$	0,2349
set	8	260,5	-3,36	$7,908.10^{-4}$	0,3024
gen	9	263,5	-3,29	$1,007.10^{-3}$	0,3775
mar	10	268	-3,19	$1,43.10^{-3}$	0,4627
ott	11	291	-2,67	$7,58.10^{-3}$	0,5606
apr	12	299,5	-2,48	$1,314.10^{-2}$	0,6813

Tab. V - Pian Rosà - Statistica t del test di Kendall-Mann tra i ranghi del numero di giorni al mese con nevicata; u(t) test di Kendall-Mann; α(t) probabilità di superamento del suo valore assoluto; α_t limite superiore di α(t) secondo il test multiplo basato sulla legge binomiale. I mesi sono disposti secondo la graduatoria k per α(t) crescente, cioè per contributo decrescente al test multiplo χ^2 di Fisher. Tendenza significativa per α(t) < 10^{-2} [|u(t)| > 2,576]. Gli asterischi indicano i mesi nei quali è anche presente una correlazione interna.

mese	k	χ^2	$k_{selez.}$	ν	α_χ	χ^2_α
		183,169		24	0,01	42,98
giu	1	157,991	1	22	0,0092	40,6
lug	2	136,849	1,2	20	0,0083	38,25
nov	3	119,760	1,2,3	18	0,0075	35,8
dic	4	103,304	1,2,3,4	16	0,0067	33,25
ago	5	88,505	1,2,3,4,5	14	0,0058	30,85
mag	6	73,900	1,.....,6	12	0,0050	28,3
feb	7	59,615	1,.....,7	10	0,0042	25,7
set	8	45,330	1,.....,8	8	0,0033	23,0
gen	9	31,529	1,.....,9	6	0,0025	20,2
mar	10	18,429	1,.....,10	4	0,0017	17,3
ott	11	8,664	1,.....,11	2	0,0008	14,15

Tab. VI - Pian Rosà - Selezione graduale dei contributi dei test mensili di Kendall-Mann, da k = 1 a k = 11, al test multiplo di Fisher (χ^2 = 183,169) sull'intero aggregato dei mesi. ν gradi di libertà; α_t livello di significatività; χ^2 valore soglia del test.

Serie parziale	n'	media	varianza
1952-53/1970-71	19	220,7	262,538
1971-72/1979-80	9	178,1	209,861
1980-81/1991-92	12	139,7	365,424

Tab. VIII - Pian Rosà - Parametri relativi alle tre serie parziali.

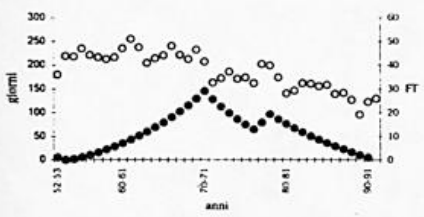

Fig. 2 - Pian Rosà - In alto: numero di giorni con nevicata nell'aggregato di 12 mesi da aprile a marzo nel periodo 1952-53/1991-92. In basso: andamento del test FT per ogni possibile divisione della serie in due parti.

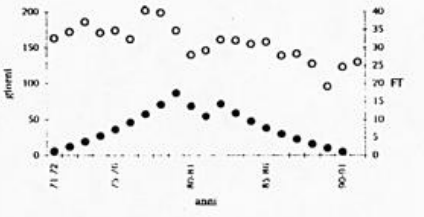

Fig. 3 - Pian Rosà - In alto: numero di giorni con nevicata nell'aggregato di 12 mesi da aprile a marzo nel periodo 1971-72/1991-92. In basso: andamento del test FT per ogni possibile divisione della serie in due parti.

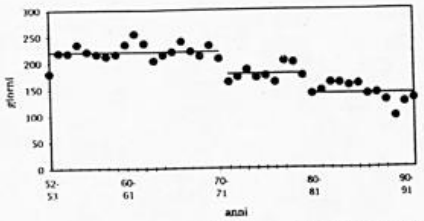

Fig. 4 - Pian Rosà - Numero di giorni con nevicata nell'aggregato di 12 mesi da aprile a marzo nel periodo 1952-53/1991-92. I segmenti rappresentano le medie nelle tre serie parziali.

Bibliografia

2. Sneyers R. - *Sur l'analyse statistique des séries d'observations.* - OMM, Note Tech. n. 143, 1975, Genève.

3. Fisher R. A. - *Metodi statistici ad uso dei ricercatori.* - UTET, 1948, Torino.

4. Todaro C. - *Sulle fluttuazioni climatiche del numero di giorni con nevicata a Plateau Rosa (Alpi Pennine).* - Geogr. Fis. e Dinam. Quater., vol. 15 (1 e 2), 1992.

AIR TEMPERATURE CHANGES IN THE BULGARIAN MOUNTAINS

Ek.Koleva

National Institute of Meteorology and Hydrology
blvd.Tzarigradsko shousse 66. Sofia 1784. Bulgaria

Long-term air temperature fluctuations in Bulgarian mountains are examined. This fluctuations are studied by the seasonal and annual mean, maximum and minimum air temperature. In the analysis the emphasis are on the existence of trends and periodicities in the time series.

To verify the stability of seasonal and annual air temperature a test of randomness against trend is applied and more especially Mann-Kendall trend test in a progressive forward and backward manner. In a case of an abrupt climate change the Pettitt non-parametric change-point test has been used for estimating the change point and for finding confirmation of its significant character.

Generally, decreasing trend in annual maximum temperature and decreasing trend in annual minimum temperature is present during the period 1935-1992.

Long-term variability of the potential foehns due to circulation conditions in the Western Carpathians

Tadeusz Niedźwiedź, Zbigniew Ustrnul
Institute of Meteorology and Water Management - Cracow, Poland

Abstract

The present study concerns an attempt of characterizing the long-term variability of situations with foehn winds in the Western Carpathians. The analysis was based upon determination of the daily synoptic situations over the investigated area.

1. Introduction

Among many problems concerning climate change in the mountains, frequency of the foehn winds variability seems to be quite interesting for research. Foehns are the typical phenomena in mountains all over the word and as many different investigations show they exert large influence on many aspects, not only meteorological. The basic difficulty during foehns' variability studies is the lack of long and homogeneous data series from at least from two stations situated close but located at the top of mountains and in the valley bottom. Additionally, the data should contain some particular information concerning the speed and wind direction, cloudiness and air humidity. It is unusually difficult to find such data for the long-term series where only some elements (mainly temperature and precipitation) have homogeneous data.

2. Method and data

According to the lack of data for the Western Carpathians, mentioned above, the authors took for consideration synoptic situations' variability. We have used the mesoscale synoptic calendar by T. Niedźwiedź (1993). As some earlier research has proved there is very strict dependency between occurrence of the particular situation type and the foehn winds in the Western Carpathians (Ustrnul 1992). It refers to the typical strong foehn phenomena which appear in 100 percent cases during the distinct air advection from the Southern sector. Taking into account the good correlation one can identify occurrence of the synoptic types with the distinct advection from the Southern directions with the occurrence of the potential foehns.

The variability of circulation situations during the seasons and the year was presented by applying index of southerly circulation (S). It is one index from several simple indices devised by R. Murray and R.P.W. Lewis (1966) with further modification to Polish classification of circulation types

(Niedźwiedź 1993). Index of southerly circulation - S was counted by summation of scores (points) for days with different air flow as follows: +2 for type S, +1 for types SW and SE, -1 for NW and NE, and -2 for type N. Hence, the high positive values of index point to an intensive advection of air masses from the South, while negative ones point to the advection from the North. That method above was used in order to obtain more synthetic results. In the specified way types of atmospheric circulation were determined for each day during the period of 1873-1994 for the Western Carpathians.

Variability of circulation index was presented throughout the seasons and the year as a whole by curves smoothed using 9-term low-pass Gauss filter (Schönwiese 1992).

3. Results

Occurrence of the potential foehn periods has relatively rather straight course with only some fluctuations in the whole investigated period (1873-1994). Changes most frequently observed have the character of short time oscillations of several-years period. Slight maximum of potential foehn situation around 1890 and then in the 1920-s and the 30-s has been observed (fig. 1). The final period with rather high number of foehn situation lasts from the beginning of the 50-s until beginning of the 70-s. The general changes of the potential foehn variability is even better expressed by the frequency of the airflow from directions SE+S+SW, which have been calculated independently (fig. 2).

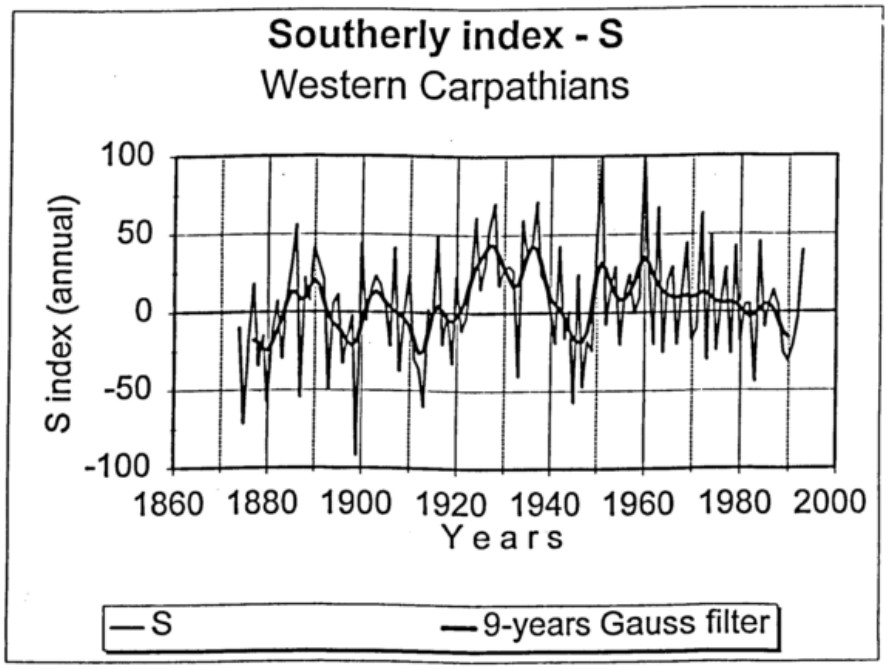

Fig. 1.

Both courses concern annual values. Besides, taking into account the frequency distribution of the foehn situations in particular seasons, the analysis of S index was given for spring and autumn when the highest number of foehns was observed (fig. 3-4). The highest frequency of air advections causing foehns in spring was observed in the middle of the 30-s although during the whole investigated period many fluctuations can be observed. In autumn the most foehns occurred in the early of the 60-s and then very rapid decrease of them was noticed.

It should be stressed that described variability of the potential foehns in the Western Carpathians is very well related with the observed foehn changes detected for Altdorf in Reuss valley in Switzerland (Bader, Gutermann, Imhof, 1992). For example the lowest annual frequency of the foehn situation in both regions is being noticed around 1900, 1920 and especially in 1950.

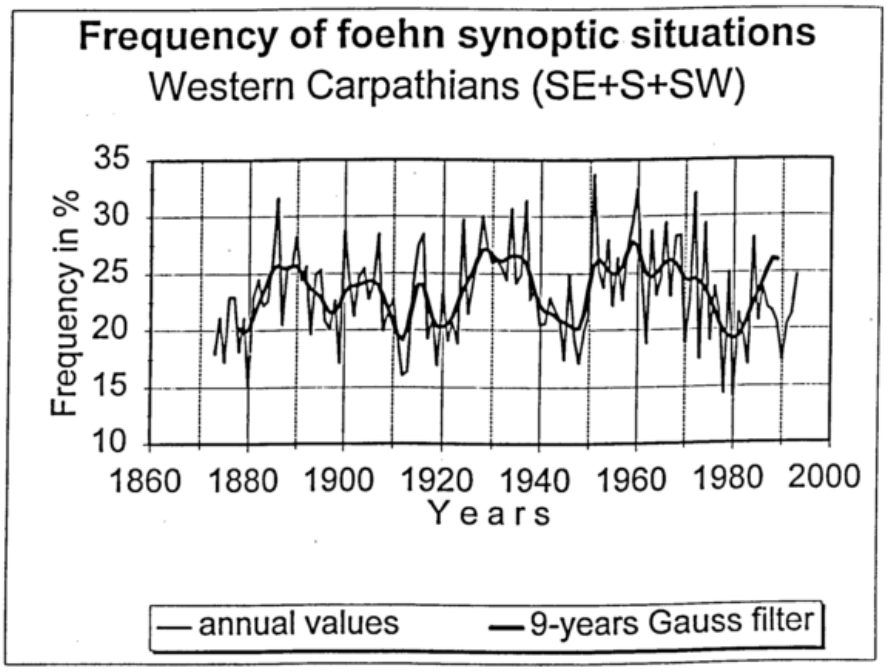

Fig. 2.

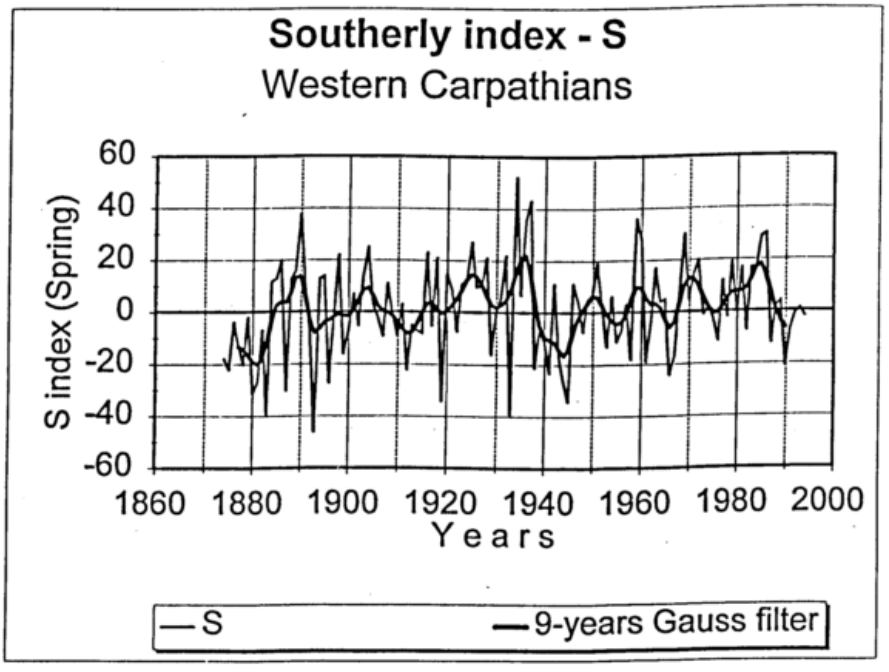

Fig. 3.

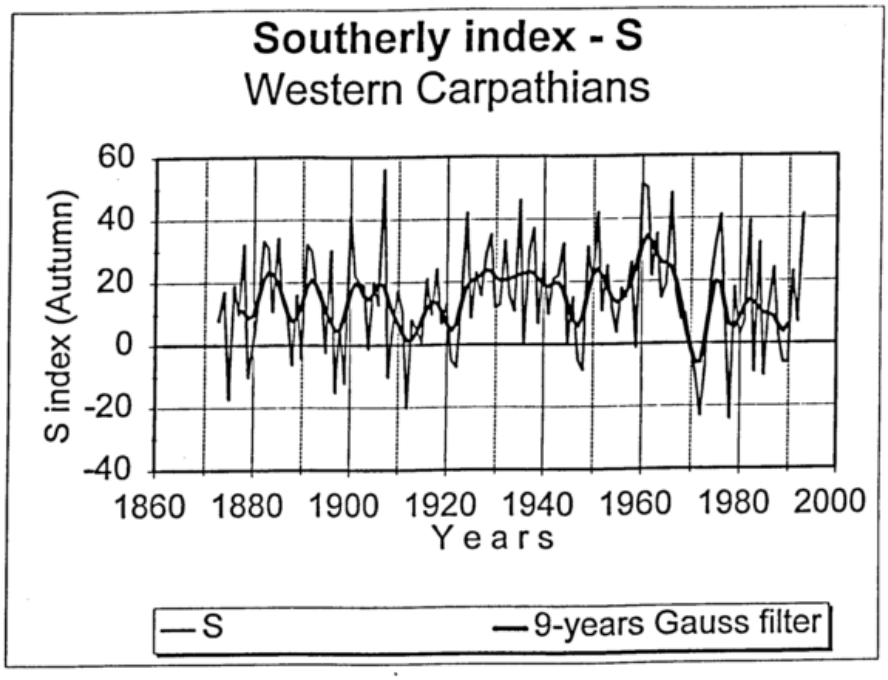

Fig. 4.

On the other hand, the highest frequency of these situations can be observed in the 30-s and on the turn of the 50-s and 60-s. It seems that convergence is not occasional and it confirms the dominant meaning of the circulation factor for the foehns' creation. Simultaneously, on the basis of the mentioned materials (though the data originated from Altodorf station has not been homogenized yet) one can see the close relationship of the circulation conditions (i.e. strong southern advection) between both regions (i.e. in the Western Carpathians and in the Alps) in spite of their quite far location.

Acknowledgments

This study was partially supported by State Committee for Scientific Research, grant No. 6 P202 057 05.

References

Bader S., Gutermann T., Imhof M., 1992, Foehn frequencies in Altorf (Reusstal, CH) from 1864 to 1991 (128 years) - a climatological approach, Alpex-Regional Bulletin, No. 19, pp. 22-23.

Murray R., Lewis R.P.W., 1966, Some aspects of the synoptic climatology of the British Isles as measured by simple indices, Meteorological Magazine, Vol. 95, No. 1128, pp. 193-203.

Niedźwiedź T., 1993, Changes of atmospheric circulation (using the P, S, C, M indices) in the winter season and their influence on air temperature in Cracow, Zeszyty Nauk. UJ, Prace Geogr., z. 95 "Early Meteorological Instrumental Records in Europe", pp. 107-113.

Schönwiese Ch. D., 1992, Praktische Statistik fur Meteorologen und Geowissenschaftler, Gebruder Borntraeger, Berlin-Stuttgart, p. 232.

Ustrnul Z., 1992, Potential conditions of foehn effects in the Polish Carpathians (in Polish, English summary), Zeszyty Nauk. UJ, Prace Geogr., z. 90, pp. 97-112.

Automatisches Meßnetz des Lawinenwarndienstes Tirol

R. Mair

Amt der Tiroler Landesregierung, Lawinenwarndienst

Abstract

According to a law detailing the technical equipment needed by avalanche warning commissions and specifying community responsibility, a building plan of automatic weather stations has been worked out by the avalanche warning service of the Tyrol. The intention of this plan is to extensively build such stations in meteorologically interesting places. The avalanche warning service is responsible for the technical planning of station equipment. Thus, the installation and adjustment of measuring instruments to the high mountain surroundings and permanent data access for all authorized users is of utmost importance. Currently, another topic of interest is the development of a user-friendly software package for graphical analysis and the statistical processing of data.

Zusammenfassung

Aufbauend auf ein Gesetz, das den Gemeinden die technische Ausstattung der Lawinenkommissionen vorschreibt, entwarf der Lawinenwarndienst Tirol einen Ausbauplan automatischer Wetterstationen. Ziel dieses Ausbauplanes ist die flächendeckende Errichtung solcher Stationen an jenen Standorten, die meteorologisch und nivologisch besonders geeignet erscheinen. Das technische Konzept für die Ausstattung dieser Meßstationen liefert der Lawinenwarndienst, wobei besonders auf die Hochgebirgstauglichkeit der Meßgeräte sowie auf permanenten Datenzugriff aller berechtigten Nutzer Wert gelegt wird. Einen weiteren Schwerpunkt bildet die Erstellung und laufende Weiterentwicklung einer benutzerfreundlichen Software zur graphischen Auswertung und statistischen Weiterbearbeitung der Daten.

1) Einleitung

Tirol als Hochgebirgsland ist im Winter naturgemäß mehr oder weniger permanent von Lawinen bedroht. Einen wesentlichen Beitrag zum Schutz von Bevölkerung und Siedlungsraum vor Lawinengefahren bieten neben Schutzverbauungen die örtlichen Lawinenkommissionen. In 160 von 279 Tiroler Gemeinden ist die Einrichtung und Ausstattung dieses Expertengremiums daher gesetzlich vorgeschrieben. Die Beurteilung der momentanen Lawinensituation und nachfolgend zu treffende Schutzmaßnahmen ist ein äußerst komplexer Vorgang, der wesentlich auf der langjährigen Erfahrung eines Kommissionsmitgliedes aufbaut. Zur Unterstützung der Entscheidungsfindung liefern aber die Daten einer automatischen Wetterstation einen wertvollen und zunehmend unentbehrlichen Beitrag dieser verantwortungsvollen Tätigkeit.

2) Ausbauplan

Um eine unkontrollierte Errichtung automatischer Stationen zu verhindern, erarbeitete der Landeslawinenwarndienst einen Ausbauplan. In diesem Plan sind großräumig Standorte eingetragen, die meteorologisch und nivologisch besonders geeignet erscheinen. Der genaue Standort einer Station wird dann in der Vor-Ort-Besichtigung von Vertretern des Lawinenwarndienstes und der örtlichen Lawinenkommission festgelegt. Anschließend erfolgt die genaue technische Planung sowie die Ausschreibung der Bauarbeiten. Die Finanzierung obliegt der betreffenden Gemeinde mit Beiträgen eventuell betroffener Liftgesellschaften oder Nachbargemeinden. Eventuell schon vorhandene Stationen anderer Betreiber (z.B. die TAWES-Stationen der Zentralanstalt für Meteorologie und Geodynamik) können problemlos in das System integriert werden. Diese Stationen werden dann mit einer Schneehöhenmeßeinrichtung ergänzt.
Der Landeslawinenwarndienst unterstützt die Gemeinden nicht nur bei der Planung, sondern übernimmt auch einen Großteil der anfallenden Wartungskosten. Von insgesamt 30 geplanten Stationen sind derzeit 8 in Betrieb und 3 in Planung bzw. Bau.

3) Aufbau einer Station

Die Grundausstattung einer automatischen Wetterstation zusammen mit der Meßmethodik, Aufbereitung und Speicherung der Werte ist aus folgender Tabelle zu entnehmen:

Meßgröße	**Meßmethode/ Art des Gebers**	**Geber-abfrage**	**Aufbereitung der Werte**	**Speicherung der Werte für Zeitintervall 10min**
Lufttemperatur	Pt100, belüftet	10s	1-Minuten-Mittel	Mittelwert der letzten Minute des Intervalls; Extremwerte des Intervalls
Luftfeuchte	kapazitiv	10s	1-Minuten-Mittel	Mittelwert der letzten Minute
Windrichtung	Ultraschall	2s	vektorielles Mittel über 1 Minute	vektorielles Mittel über Zeitintervall
Windgeschwindigkeit	Ultraschall	2s	vektorielles Mittel über 1 Minute	vektorielles Mittel über Zeitintervall
Böe	Ultraschall	2s	-	maximaler 2s-Wert der Geschwindigkeit im Intervall und zugehörige Richtung
Globalstrahlung	Sternpyranometer	2s	1-Minuten-Mittel	Mittel über Zeitintervall
Schneehöhe	Ultraschall	10s	-	arithmetisches Mittel über Intervall
Schneetemperatur	NTC	3 Stunden	-	3-Stunden-Wert

Ist eine Stromversorgung vorhanden, sind die Meßgeräte kontinuierlich in Betrieb und werden ab Erreichen von Minustemperaturen geheizt. Ist keine feste Stromversorgung vorhanden, kann die Meßstation auch mit einer Solaranlage versorgt werden. In diesem Fall schaltet sich zwischen den Messungen die komplette Meßanlage ab und wacht nur zu den eingestellten Intervallen zum Messen

und Speichern auf. Um die Solaranlage wirtschaftlich zu halten, sind bei Solarversorgung keine Meßgeräte mit Heizung möglich.
Da die Windwerte üblicherweise an einem exponierten Standpunkt (Grat, Gipfel, o.ä.) besonders interessant sind, die Schneehöhe hingegen an einem möglichst windunabhängigen Meßfeld, werden diese zwei Sensoren meist räumlich getrennt (oft mehrere hundert Meter).

Die Erfassung der Daten erfolgt in einem 16-Kanal-Datenlogger. Die analogen Meßeingänge werden nacheinander (multiplex) mit einem integrierenden AD-Wandler gemessen, digitalisiert und auf Plausibilität getestet. Die gültigen Meßwerte werden mit einer eingegebenen Formel auf physikalische Werte umgerechnet und mit Echtzeit in komprimierter Form gespeichert. Der Datenspeicher ist normal als Ringspeicher konfiguriert und hat eine Kapazität von etwa 40.000 Meßwerten. Bei Belegung aller Kanäle und einem Speicherintervall von 10 min. entspricht das einem Speicherzeitraum von etwa 3 Wochen. Im Falle einer Störung wird ein Reset und Neustart ausgelöst, wobei alle Daten und Meßwerte erhalten bleiben. Die Echtzeituhr, Arbeits- und Datenspeicher sind außerdem über eine Batterie gegen Versorgungsausfall gesichert.

4) Datenübertragung

Der Abruf der Daten aus dem Datenlogger erfolgt über eine serielle Schnittstelle. Die weitere Übertragung erfolgt je nach örtlicher Situation über Direktleitung, Modem-Telefon, Modem-Mobiltelefon oder Funkmodem-Funkgerät. Eine Übertragung über Funkstrecken kommt z.B. insbesondere dann in Betracht, falls ein Teil der Station (wie die Schneehöhenmessung) von der übrigen Anlage räumlich getrennt ist. Am Ende der Übertragungskette steht aber immer ein Telefonmodem und das öffentliche Telefonnetz, über das die Daten für berechtigte Nutzer jederzeit fernabfragbar sind. Die Modems verwenden zur Erhöhung der Datensicherheit und des Datendurchsatzes Korrektur- und Kompressionsalgorithmen. Bei der üblichen Übertragungsrate von 2400 bd (1200 bd im Mobilnetz und über Funkstrecken) und 4-facher Datenkompression kann daher ein Datendurchsatz von maximal 9600 bd erreicht werden. Da sich Hochgebirgsmeßstationen üblicherweise am Ende der Leitungen befinden und die Verbindungen daher oft sehr schlecht sind, schalten sich die Modems selbständig auf geringere Übertragungsraten zurück.
Der Vorteil dieses Systems liegt darin, daß eine Gemeinde von mehreren Orten aus, z.B.: dem Gemeindeamt und dem Büro des Schiliftunternehmers, auf die Daten zugreifen kann. Zum Vergleich können aber auch die Daten von Nachbarstationen fernabgefragt werden. Sämtliche Stationen stehen natürlich auch dem Landeslawinenwarndienst zur täglichen Abfrage als Grundlage des "Lawinenlageberichtes" zur Verfügung.

5) Auswertesoftware

Zu Beginn der Arbeiten mit automatischen Wetterstationen zeigte sich, daß vor allem die Praktiker vor Ort (= Mitglieder der Lawinenkommissionen) mit der vorhandenen Standardauswertesoftware

Probleme hatten. Einerseits war die Programmbedienung sehr kompliziert, andererseits die graphische Darstellung zu wenig anschaulich. Der Lawinenwarndienst Tirol entwickelte daher eine Software, die dem Praktiker einfache (Ein-Tasten-) Handhabung, dem zusätzlich interessierten Fachmann aber eine Fülle von weiteren Möglichkeiten bietet. Die Software ist auf jedem IBM-AT-kompatiblen PC unter DOS lauffähig. Für den täglichen Routinebetrieb werden üblicherweise am Morgen die letzten 24 Stunden eingelesen, graphisch ausgewertet und anschließend ausgedruckt. Weitere Interessenten ohne eigene Auswertestation können direkt einen Faxausdruck erhalten.

Darüber hinaus besteht eine Schnittstelle zu einem sogenannten "Next-day-Modell". Dafür benötigte Daten, die nur händisch zu messen sind (z.B.: Einsinktiefe der Rammsonde) oder beobachtet werden (z.B.: Lawinenabgänge), können über Tastatur in den Datensammler eingegeben und damit ebenfalls direkt in das Statistikprogramm übernommen werden.
Mit diesem Programm werden sämtliche Daten des aktuellen Tages samt der drei vorhergehenden Tage (mit unterschiedlicher Wichtung) mit den Daten aller vorhandenen Tage verglichen. Mittels der Methode des nichtlinearen Vektorabstandes zweier Tage werden nun die zehn Tage ausgesucht, die mit dem aktuellen Tag die größte Ähnlichkeit aufweisen. In einem Ausdruck erhält man die gereihte Liste dieser Vergleichstage samt der Lawinentätigkeit an jedem einzelnen. Um die unterschiedliche Charakteristik verschiedener Beobachtungsorte einzubeziehen ist es möglich, jeden Meßwert für jede Station unterschiedlich zu wichten. Neben dieser Vergleichsmethode kann mit diesem Programm aber auch eine graphische Übersicht der meteorologischen und nivologischen Verhältnisse an einer Meßstation samt der Lawinentätigkeit erstellt werden. Damit läßt sich sehr anschaulich die Entwicklung über einen Monat oder den gesamten Winter verfolgen (siehe nachfolgende Abbildung).

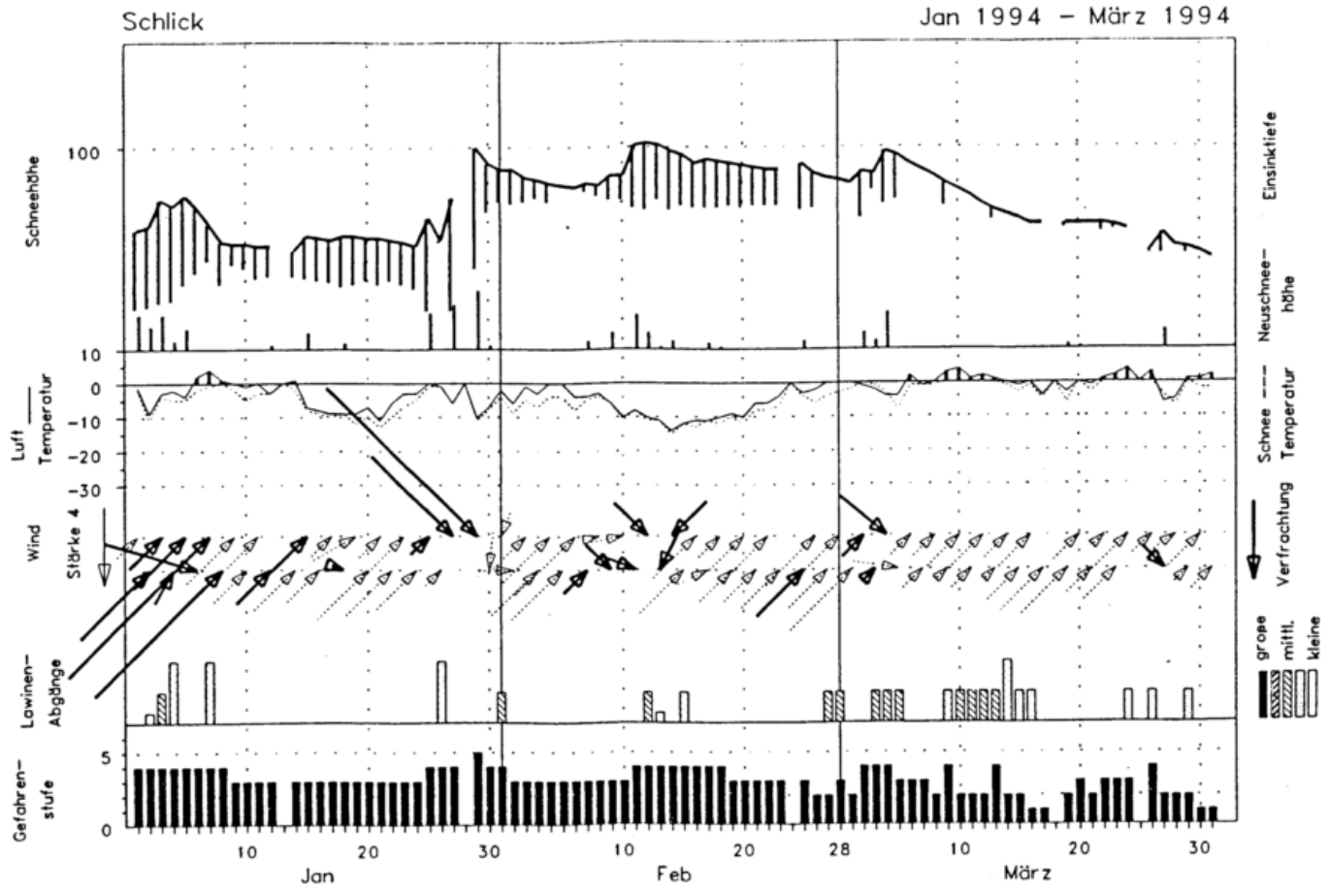

A MODEL FOR THE SUDDEN EXTINCTION OF CIRQUE AND VALLEY GLACIERS BASED ON A CASE IN THE WESTERN ALPS

Luigi MOTTA & Michele MOTTA
Comitato Glaciologico Italiano

ABSTRACT

Marked reduction of the extent and volume of the glaciers in the Conca del Dragone (Valtournanche, Aosta Valley, Italy), to the point of total extinction in all but one case, has been documented through glaciological surveys over the past sixty years. The climatic and morphological factors responsible for this recession are discussed, and a model that may be applicable to other small glaciers in the
Western Alps is proposed .

1 - Introduction

An evaluation is made of the process that led to the disappearance by 1993 of 87% of the glaciated area of the Conca del Dragone, including the total extinction of the Colle di Valcournera, Fontanella and Dragone glaciers and the Glacionevato del Colle di Bella Tsà, and the very marked reduction of the only remaining glacier (Chateau des Dames SW).

2 - Recent changes

In the 19th century, the Ghiacciaio del Colle di Valcournera covered the entire valley of the same name, and shared a common tongue with the Ghiacciaio di Fontanella. By 1934, this tongue had disappeared,
and the two glaciers, though still united, had separate fronts. A period of severe regression between 1952 and 1957 resulted in their total separation. The Valcournera was already well covered with morainic débris when two landslides completely buried it in rock waste between 1957 and 1971. Between 1989 and 1992, its original catchment basin, where the bedrock cropped out, became thinner and the glacier itself was again covered by a rockfall. The upper part became a thin layer of ice and débris, with the result that the lower part was no longer fed from above. The front made some slight progress until 1991 and then regressed. In the autumn of 1992, the glacier disappeared, leaving only a mass of decaying ice in a sheltered cirque on the hydrographic left-hand side of the valley.
In 1957, the Ghiacciaio di Fontanella had already retreated behind its innermost frontal moraine. It was covered with morainic débris by a series of small rockfalls between 1971 and 1975. Later, much of the front became exposed and in 1989 formed an amphitheatre with two drumlins and a tarn on flat ground at its feet. Two large rockfalls struck the glacier between 1989 and 1991 and radically altered its dynamics. The hydrographical right-hand side was eroded by these falls and became extinct in 1991. In the centre, the débris protected and compressed the ice at first, causing its rapid advance over the whole of the flat ground in front of it. Most of its accumulation zone, however, had been removed by the rockfalls, and this sector disappeared altogether in 1992-93. The hydrographic left was untouched by the rockfalls and held out a little longer. By 1992, however, it ,too, was confined to an ice fan nourished from a gully and a few masses of decaying ice. Subsequent heavy snowfalls covered the remains of the glacier throughout the summer of 1993, but were not enough to bring about its reconstitution.
The geometry of the moraine patterns shows that in the 19th century the Ghiacciaio del Dragone was joined to the Colle di Bella Tsà and Chateau des Dames SW formations. In 1934, it still occupied the whole of its cirque and had only just parted company with the Glacionevato del Colle di Bella Tsà. By 1957, the S-facing eastern part had broken up into simple snowfields, whereas the SE and E-facing western part was substantially intact. Small rockfall deposits accumulated on this part in 1970-72. In 1975, the original long and continuous snout had spilt into two distinct tongues, whereas the rest of the front had moved well back. During 1985-1986, the snowline rose (shown by the disappearance of several snowfields) and another small tongue was formed. The appearance of crevasses in several areas showed that the glacier was still active, and the Glacionevato del Colle di Bella Tsà also expanded and developed small transverse crevasses. Between 1985 and 1987, the central tongue retreated 21.5 m. A smaller regression (1.5 m) in 1988 was none the less accompanied by marked thinning. Nearly all the snow-filled corries on the flat ground below also disappeared during the same period. In 1988-89, the right-hand tongue was almost completely buried by a landslide. This shifted it forward about ten metres and thinned the uncovered part by some 2-3 metres. The main tongue retreated 25 metres. The right-hand tongue disappeared in 1992, while the glacier itself dwindled to a narrow band alongside Monte Dragone. The Glacionevato del Colle di Bella Tsà also shrank to a simple snowfield. By the autumn of 1992, all that remained were a few masses of decaying ice separated by piles of débris, pools of water and roches moutonnées. The central mass alone could still be regarded as a glacionevato. The other masses, each no more than a few tens of
metres long, occupied corries in which the redrock cropped out, so that the presence of ice masked by débris could be excluded. In the summer of 1973, the residual snow covered the area as far as the tarns below. The glacier, however, was extinct.
In 1934, the Ghiacciaio dello Chateau des Dames SW extended as far as its furthermost lateral moraine. Between 1940 and 1972, considerable thinning of the entire glacial body took place and a talus cone was formed. A large prismatic block of limestone also broke off from the Chateau des Dames and fell almost unbroken onto the glacier, dividing it into two

ESPOSIZIONE DEI GHIACCIAI DELLA CONCA DEL DRAGONE

GHIACCIAIO DEL COLLE DI VALCOURNERA

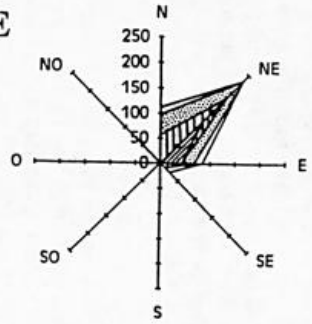

GHIACCIAIO DI FONTANELLA

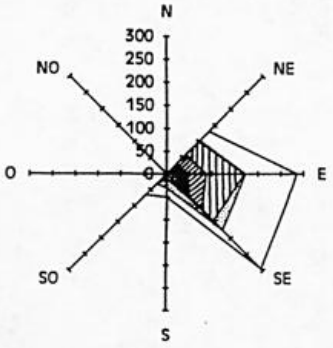

GHIACCIAIO DEL DRAGONE

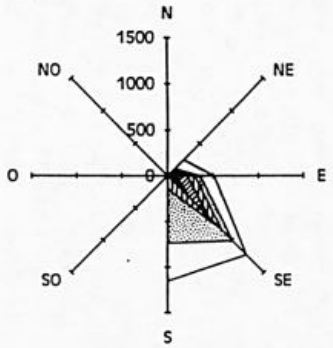

GLACIONEVATO DEL COLLE DI BELLA TSA'

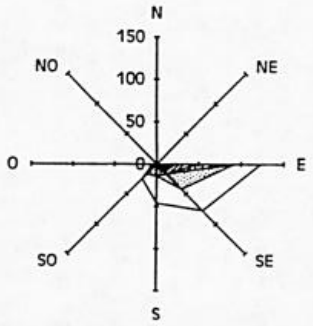

GHIACCIAIO SUDOCCIDENTALE DELLO CHATEAU DES DAMES

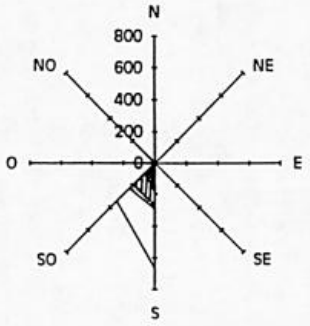

DISTRIBUZIONE ALTIMETRICA AREALE DEI GHIACCIAI DELLA CONCA DEL DRAGONE

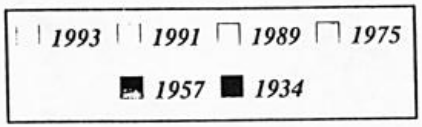

Ghiacciaio del Colle di Valcournera

Ghiacciaio di Fontanella

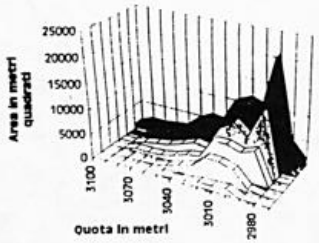

Ghiacciaio del Dragone

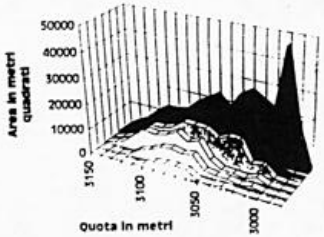

Glacionevato del Colle di Bella Tsà

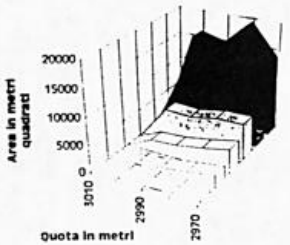

Ghiacciaio Sudoccidentale dello Chateau des Dames

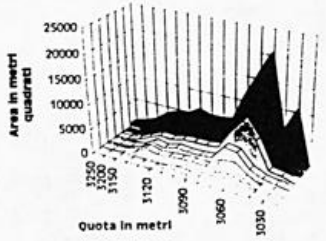

small sectors and thus accelerating its regression. By 1984-87, the western sector had already shrunk to the level of a glacionevato, whereas the eastern sector, joined to it by a thin band of snow, still possessed a small tongue of clean ice with longtitudinal crevasses. In 1988-89, the upper part of the western sector shrank considerably and its front became very thin. A tarn formed at 3045 m and the morainic cover became abundant. The better-preserved eastern sector displayed a scanty morainic cover and a slab of residual snow. The western sector disappeared in 1992, while in the following year massive landslides cut the glacier off from its neighbours. The eastern sector escaped extinction and appeared to be stationary or advancing.

3. Extinction dynamics

The altitude of the firn line can be reconstructed from the Comitato Glaciologico Italiano's summer snowfall records. This is very useful as the strictly local deglaciation process displays a microclimate greatly different from that of even nearby weather stations. The years just before the extinction (1986-91) were marked by exceptionally scanty summer snowfalls. Between 1934 and 1952, the area of the Conca del Dragone glaciers shrank by 54.4% (the highest reduction in the whole of the Valtournanche), 44.0% and 51.7%, compared with the mean 27.6% for the Aosta Valley (DE GEMINI F. et al., 1953, "I ghiacciai della Valle d'Aosta", Boll. CGI, s.2, 4). Examination of the exposures (fig.1) shows that the 1934-57 regression primarily affected areas facing south, whereas in Valtournanche and the whole of the Aosta Valley, SE and E-facing areas were spared, despite their "more favourable position with respect to insolation and ablation" (DE GEMINI et al., op. cit.), and areas facing east suffered most. Regression in the Conca del Dragone, therefore, was clearly anomalous.
The effects of the slow retreat that took place between 1934 and 1975 varied according to the exposure. During the 1975-1993 regression, on the other hand, exposure was of secondary importance compared with the change in albedo brought about by extension of the morainic cover, and by rockfalls from the cirque backwalls. The feet of the Fontanella, Dragone and Chateau des Dames SW cirques correspond to the extent of their glaciers in 1934, when they were occupied by true cirque glaciers. The first regression phase involved these small, but dynamically "normal" glaciers, whereas the second phase involved those spread in horseshoe fashion around the backwalls. These, in fact, were so small that in very poor years they were left completely below the snowline. Rapid destruction of their thin snowcover was followed by leopard-skin shrinkage and sudden regression.
A higher-order corrie in the Dragone cirque roughly corresponds to the extent of its glacier in 1975. The area and elevation distribution of this glacier has been determined by this morphology. In 1934, it was plurimodal with maxima at 3060 m (as shown by the upper corrie), 3030 m (corresponding to the central cirque), and 3000 m (the tongue). The lower tongue disappeared in 1957 and the distribution remained bimodal until 1975, when it became unimodal.
The same pattern was followed by the Fontanella and Chateau des Dames SW glaciers. Here, too, disappearance of the tongue and survival of the glacier at the foot of its cirque only correspond to the passage from bimodal to unimodal distribution.
The Colle di Valcournera, on the other hand, was a valley-glacier not a cirque-glacier. Its curve was constantly unimodal, and moved gradually downwards, shifting its maximum to higher altitudes in keeping with the regression of the ice-mass along the valley floor. The Glacionevato del Colle di Bella Tsà, lies almost entirely at the same elevation, and its situation is again different. Its evolution simply consisted of the lowering of a poorly defined, but substantially plurimodal curve, which none the less displayed, like the others, a tendency to become increasingly rectilinear, and hence unimodal.
Extinction by sectors has made it necessary to consider the fluctuations of their fronts. All sectors have advanced since 1989 in step with pronounced thinning of the ice-mass and a very great reduction in the area of their high-altitude parts. This advance has been faster for fronts at lower elevations, while it has equally been slower in the centre of a front as opposed to the sides, and delayed by 1-2 years in the Colle di Valcournera and Chateau des Dames SW glaciers. Elsewhere in the Valtournanche, the SW-facing Valtournanche and Forca glaciers were in slight regression in 1989, whereas the others, which are exposed ot the SE, began to advance. In 1993, on the other hand, the Ghiacciaio della Forca was advancing, whereas the Ghiacciaio della Valtournanche was receding much faster than before. The advance of the mainly SE-facing Conca del Dragone glaciers cannot be regarded as evidence of renewed glaciation, since it has been accompanied by great shrinkage of both their overall volume and the area of their upper sections. It is thus of very different origin to that of the other Valtournanche glaciers, which are free from any substantial signs of regression in their catchment basins or marked thinning of their fronts. The most likely explanation is that ablation due to contact with the bedrock resulted in the formation of a cushion of meltwater. This, coupled with the extra weight added to the ice-mass by rockfalls, would have led to an advance of the front, due solely to faster rotational slipping, just before complete extinction.

4. Conclusions

The 1993 extinctions were brought about by negative mass balances in 1989-91, when the snowline rose above the glacier-heads and the summer snow supply was confined to the small quantities brought down by avalanches. The similarities between them suggest that a common model can be proposed. The first step was reduction by these negative mass balances of the already very thin accumulation zones. This trigered three extinction mechanisms:
- modification of the albedo and the thermal insulation afforded by the snow mantle, resulting in more intense ablation;

- disappearance of the ice cementing fissures in the rock, resulting in great instability of the cirque backwalls and their coverage of the glacier surface with low-albedo scree;
- outcropping (surfacing) of the englacial moraine in the former feeder areas, resulting in further reduction of the albedo and even greater ablation, since the surface moraine was too thin to protect the ice below it.

These processes eventually speeded up the reduction of the ablation areas, too, thanks to:
- fragmentation of the glaciers into smaller units less likely to survive;
- thermokarst on the part of down-flowing water;
- partial or total reduction of the uphill ice supply, due to shrinkage or disappearance of the original catchment basins;
- greater surface abrasion owing to the increase in débris-laden ice.

The final step was dismemberment into patches of decaying ice. The continued survival of the small remnant of the Chateau des Dames SW glacier is probably due to its having been nourished by large-scale avalanches.□

Oscillazioni frontali del Ghiacciaio del Colle di Valcournera e del Ghiacciaio di Fontanella

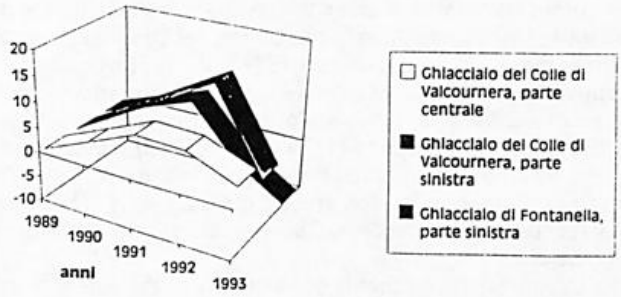

Oscillazioni della lingua destra idrografica del Ghiacciaio del Dragone

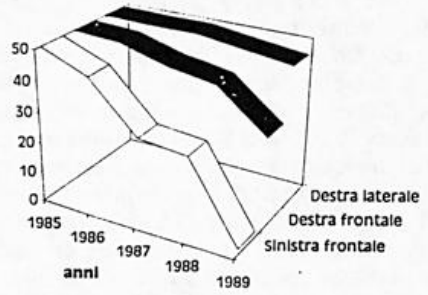

Oscillazioni frontali del settore destro idrografico del Ghiacciaio Sudoccidentale dello Chateau des Dames

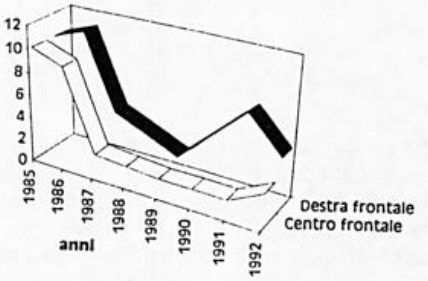

Estimation of the heat budget over a glacier snowfield, Franz Josef, New Zealand

Sturman, A.P.[1], Owens, I.F.[1], Kelliher, F.M.[2], Clark, M.P.[1], Byers, J.N.[2], Hunt, J.E.[2] and McSeveny, T.M[2].

[1] Department of Geography, University of Canterbury, Christchurch, New Zealand.
[2] Landcare Crown Research Institute, Christchurch, New Zealand.

Abstract

An evaluation is made of the heat budget components over a snow surface in the neve region of the Franz Josef Glacier during a summer melt period. Approaches to the estimation of these components are evaluated using a comprehensive data set, including snowpack and atmospheric profile information, as well as some eddy correlation measurements. An aerodynamic approach to estimation of sensible and latent heat fluxes is applied based on Monin-Obukhov similarity theory, and good agreement is achieved with eddy correlation measurements. Changing weather conditions experienced during the field period provided some interesting variability in the heat budget components. Sensible heat flux peaked at over 150 Wm^{-2} towards the surface during morning periods of strongest temperature gradient, but remained less than 40 Wm^{-2} for much of the rest of the time. Latent heat flux reached a maximum approaching 150 Wm^{-2} away from the surface, with values tending to lag behind sensible heat flux. For two twelve hour periods the latent heat fluxes varied around 10 Wm^{-2} towards the surface, the first period occurring during light drizzle associated with a cold front and the second during the formation of a surface hoar frost over night. In addition to the close relationship with local weather changes, estimated fluxes obtained from the energy balance model showed reasonable correspondence with field measurements of snow ablation.

1. Background and methods

Glaciers are known to advance and retreat in response to climatic fluctuations (Oerlemans, 1992), while the production of water from alpine glaciers may be of considerable regional significance, for example, in hydro-electric power generation. It may also provide irrigation water for downstream agricultural activities, as well as being a local flood hazard under strong melt conditions.

The atmosphere plays an important role in both the contribution of snow and ice to glacier mass balance, as well as to the loss of water from the surface through melting, evaporation and sublimation. This loss of glacier mass, or ablation, is the result of the exchange of heat above and within the frozen surfaces. There are distinct problems associated with the study of heat budget components over mid-latitude, alpine glaciers in maritime regions. In addition to logistical and safety problems, there are also significant problems in applying contemporary theoretical and measurement approaches to estimation of heat budget components. Ideally, the eddy correlation approach should provide useful measurements of turbulent heat fluxes, but technical problems are often encountered in operating the sensitive equipment in harsh alpine environments. It is also operating near its threshold limits in this strongly stable environment. Estimating heat fluxes by the aerodynamic approach tends to be cheap, relatively simple to set up, more robust and better suited for unattended operation, but there are a number of analytical problems associated with this method.

The present paper examines some of the problems involved in deriving estimates of surface heat balance components and their contribution to snowmelt over an alpine glacier snow field, comparing a number of different approaches to the solution of these problems. The study of short term variations in the heat budget components allows an assessment of the sensitivity of these components to local and mesoscale weather changes. This research should therefore have downstream benefits in terms of improved short and long term predictions of water yield in alpine catchments, as well as a clearer understanding of the atmospheric processes that are responsible for changes in glacier form.

The heat budget of a neve surface can be expressed as:

$$Q_m - (Q^* + Q_h + Q_e + Q_p + Q_g) = 0 \qquad (1)$$

where Q_m is the heat flux used for melting ice, Q^* the net radiation, Q_h the sensible heat flux, Q_e the latent heat flux, Q_p the precipitation heat flux and Q_g the conductive heat flux into the snowpack. Of these components, Q^* was measured directly, while Q_p *and* Q_g were derived from field measurements as described in Ishikawa et al (1992) and McComb et al (1992) respectively. The turbulent fluxes were estimated for the field period using an aerodynamic method based on Monin-Obukhov similarity theory, supported by comparison with shorter periods of eddy correlation data.

The location of the field study site on the Franz Josef neve is indicated in Figure 1. This basin-shaped neve field was covered in a smooth layer of fresh snow in the days preceding the field study and the instrumentation was located at least 1 km from any significant terrain features. Surface ablation and micrometeorological measurements were made during the field period of 1 to 5 March 1992.

2. Results and conclusion

The weather of the study period was generally fine, but included the passage of a weak front (2 March 1992) and other subtle local variations as evident from the daily pattern of net radiation shown in Figure 2. However, although the radiation components showed a clear diurnal variation, this was less clear in other micrometeorological parameters. Application of Monin-Obukhov similarity theory to heat flux estimation produced some useful results, which corresponded well to the localised variability of atmospheric conditions (Figure 2). The brief periods of eddy correlation data also support the usefulness of the aerodynamic heat flux estimates, with the correlation between latent heat flux estimates being rather stronger than for sensible heat (Figure 3). The results so far obtained provide optimism that the simple and more robust instrumentation required for use with the aerodynamic model can provide useful information about the energy budget over glacier snowfields, from which estimates of snowmelt can be derived.

References

Ishikawa, N., Owens, I.F., Sturman, A.P., 1992: Heat balance characteristics during fine periods on the lower parts of the Franz Josef Glacier, South Westland, New Zealand. *International Journal of Climatology*, 12: 397-410.

McComb, T.J.L., Rimmer, A.B., Rodgers, M.L.B., Turver, K.E. and Vickers, A.F. 1992: A mathematical model for the prediction of temperature in a dry snow layer. *Cold Regions Science and Technology*, 20, 247-259.

Oerlemans, J., 1992: Climate sensitivity of glaciers in southern Norway: Application of an energy-balance model to Nigardsbreen, Hellstugubreen, and Alfotbreen. *Journal of Glaciology*, 38: 255-265.

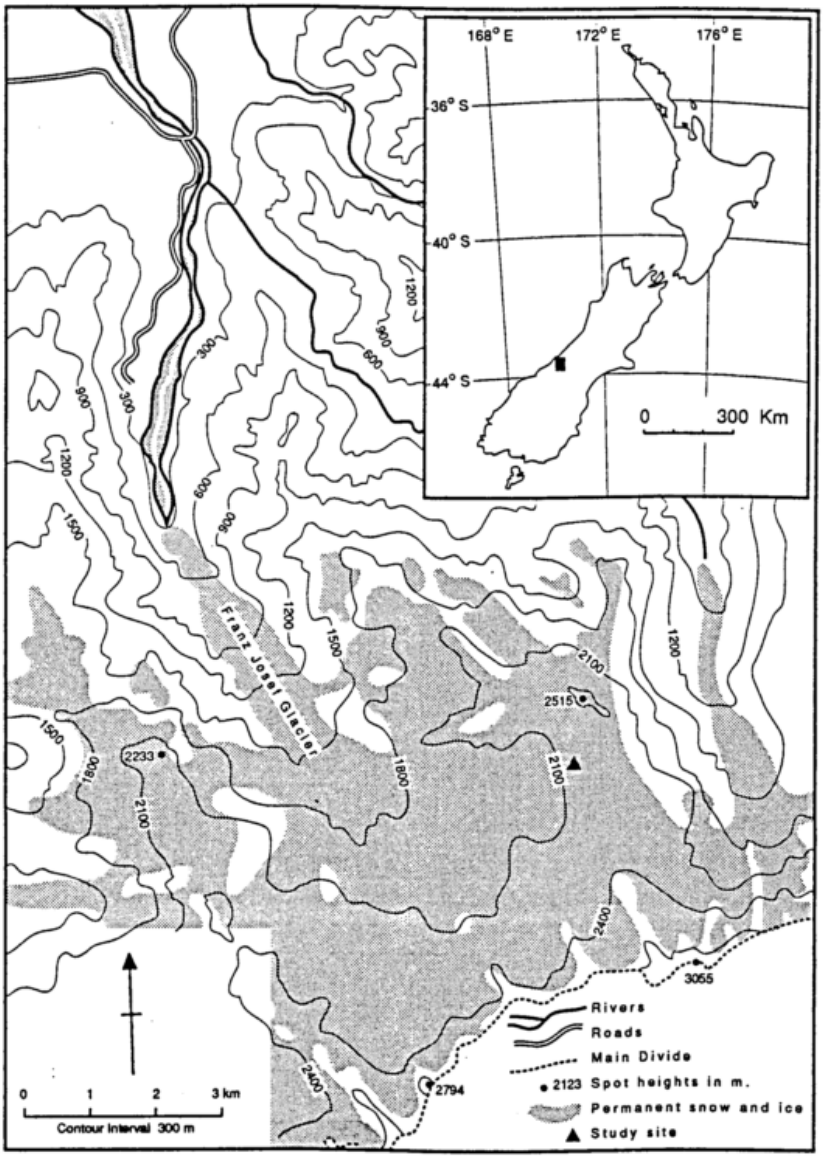

Figure 1 Location map of the Franz Josef Glacier, showing the location of the field site on the neve field.

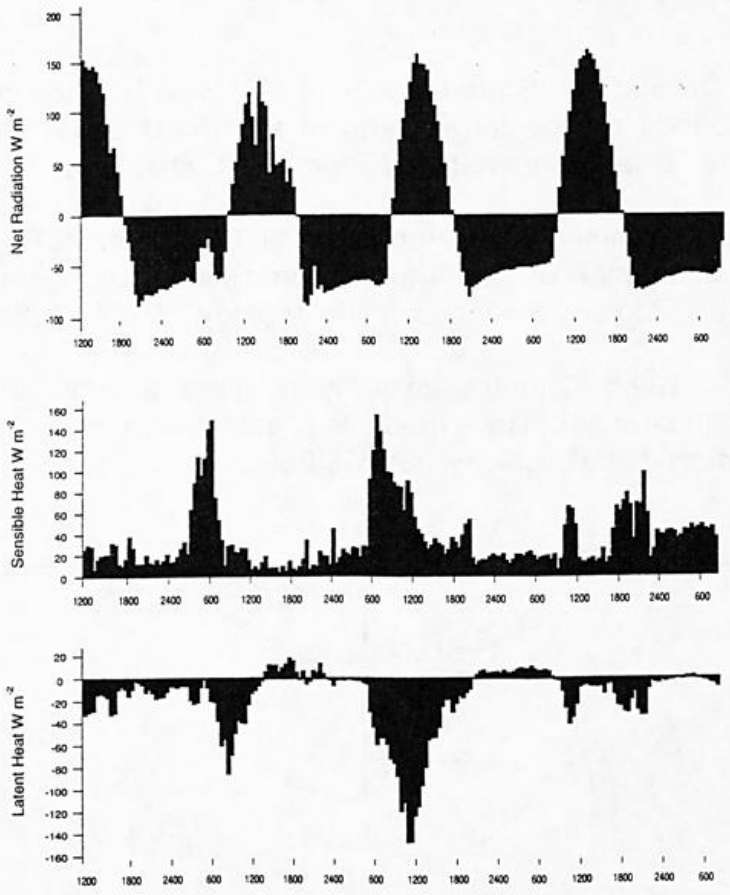

Figure 2 Half-hourly time series of net radiation and turbulent heat fluxes derived using Monin-Obukhov similarity theory during the field period (1-5 March 1992).

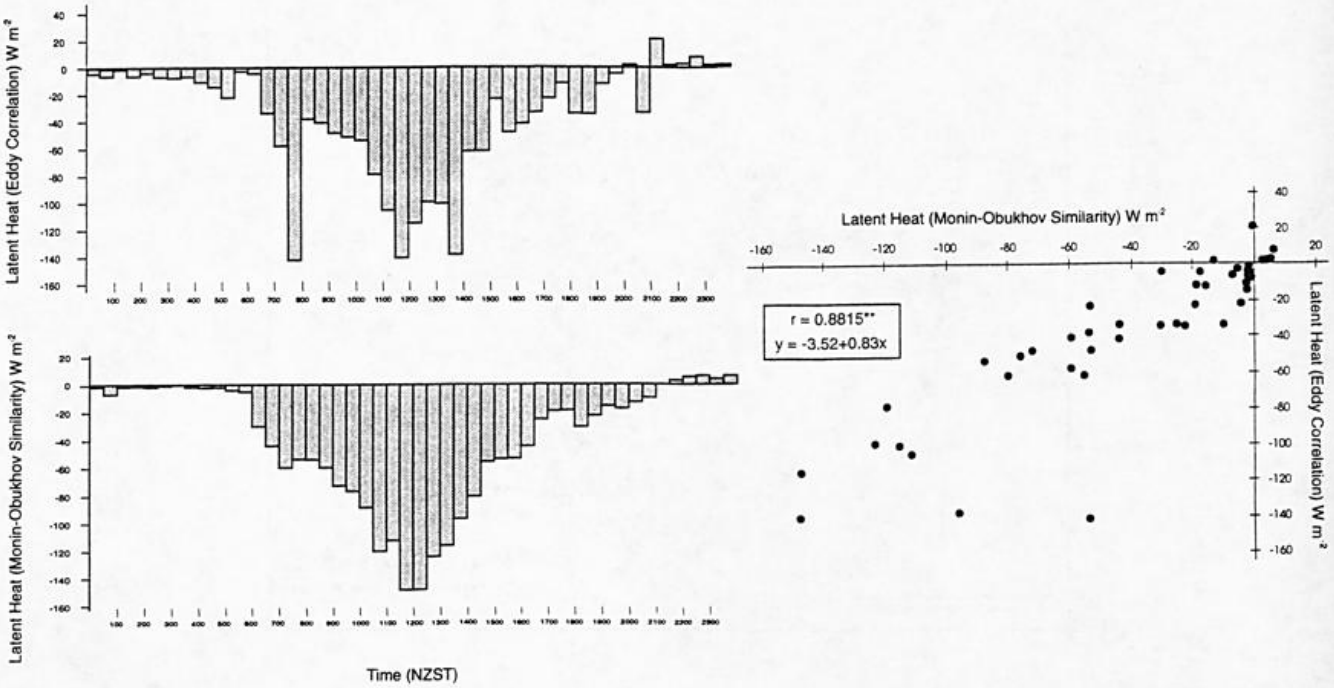

Figure 3 Latent heat flux estimates obtained over the Franz Josef neve field using the eddy correlation technique (upper left) and the Monin-Obukhov model (lower left), 3 March 1992. The correlation between the two sets of estimates is shown in the right hand diagram.

SNOWFALL ANALYSIS IN THE EASTERN PYRENEES

C. García Sellés (*), F. Salvador Franch (**)

(*) Servei Geològic de Catalunya. Generalitat de Catalunya.
(**) Servei de Gestió i Evolució del Paisatge. Universitat de Barcelona.

ABSTRACT

Studies on snow regime in the southern side of the Eastern Pyrenees are very scarce. Nevertheless, that kind of studies are interesting both from scientific point of view due to the Pyrenees range position between the Atlantic and Mediterranean climatic zones, and from environmental planning point of view because of the avalanches impact in man and constructions.

Analysed data have been recorded at La Molina (1702 m a.s.l.). This study site is the unique meteorological observatory with climatic snow data series in Eastern Pyrinees, which belongs to the "Instituto Nacional de Meteorología" network. The studied data are from the 1961-1993 period summing only 30 years because of some lacks. The snow regime has been analysed in relationship with synoptic situations especially over the period 1984-1993, being particularly interesting the estimation of maximum daily snowfall amounts by means of the Gumbel distribution.

1. INTRODUCTION

La Molina (1702 m a.s.l.) observatory is located at 42° 20' N, 1° 56' E in the northfacing slope of the La Cerdanya valley. This area is sited in the southern side of the Eastern Pyrenees. The Eastern Pyrenees are distinguished by a high mountain climate with mediterranean influence. The effects of the high mountain climate are both high anual precipitation more than a 1000 mm and fresh temperatures over all the year (annual average lower than a 5°C). The mediterranean influence results both in a high interannual irregularity of the precipitations and in the ocurrence of high intensity daily precipitation events, specially in autumn season.

2. CHARACTERISTICS OF THE SNOWFALL PRECIPITATION

2.1. Amounts of precipitation

The annual average precipitation is 1157 mm. From that amount, 362 mm are registered in snowfall days. So, the snowfall coefficient reaches the 31%. It is interesting to remark the elevated interannual irregularity (figure 1) showing a Pearson variation coefficient of 22% for the annual precipitation and a variation coefficient of 33% for the snowfall amounts. In the atlantic climate area of the Iberian Peninsula the Pearson variation coefficient fluctuates about 10% and even less.

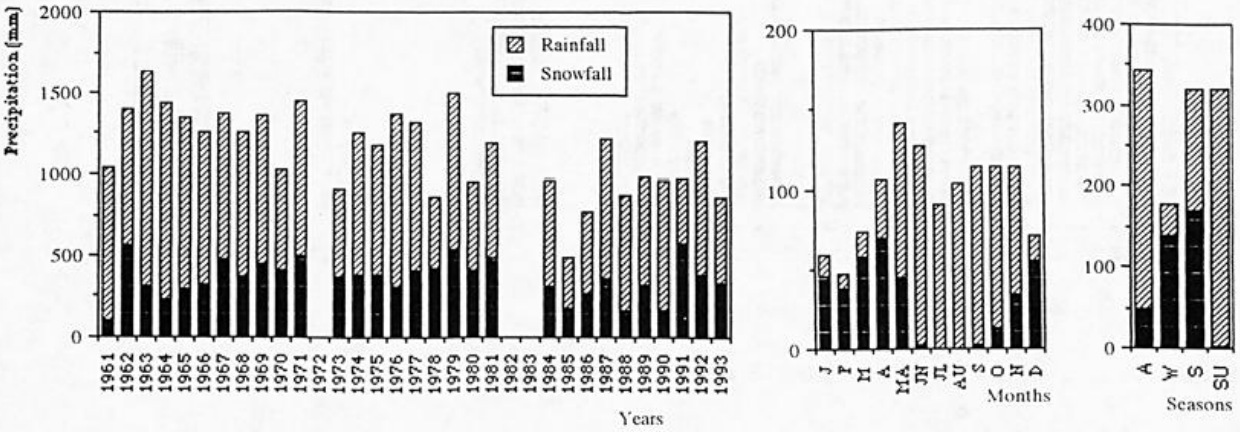

Figure 1.- *Annual, monthly and seasonal amounts of precipitation and snowfall amounts.*

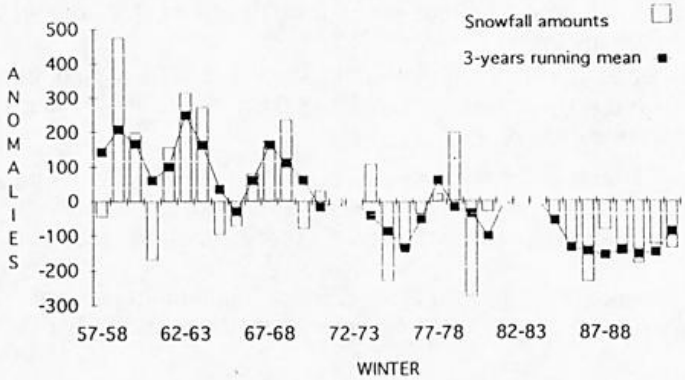

Figure 2.- *Deviation of the snowfall amounts in winter from the average and 3-years running mean.*

The winter precipitation (November to May) from 1957/58 to 1992/93 seems to reveal a decreasing tendency by means of applying 3-years running mean (figure 2). Winters from 1957/58 to 1973/74 were more snowing than winters from the last two decades.

2.2. Days of precipitation

The annual average of precipitation days is 124. From them, the 40% belongs to snowfall days. The maximum number of snowfall days are registered on the spring months, March and April (figure 3) (XERCAVINS, 1983).

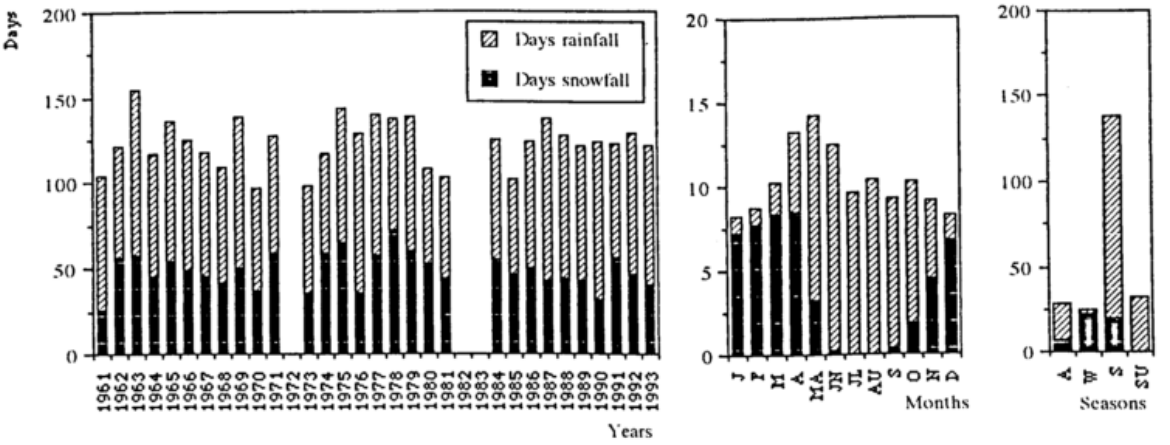

Figure 3.- *Annual, monthly and seasonal number of days of precipitation and days of snowfall.*

2.3. Days with snowcover

The average of days with snowcover is 120. In spite of the fact that both the maximum number of snowfall days and the snowfall amounts occur on March and April, the maximum number of days with snowcover is recorded on January and February due to radiation balance reasons (figure 4) (SALVADOR, 1986).

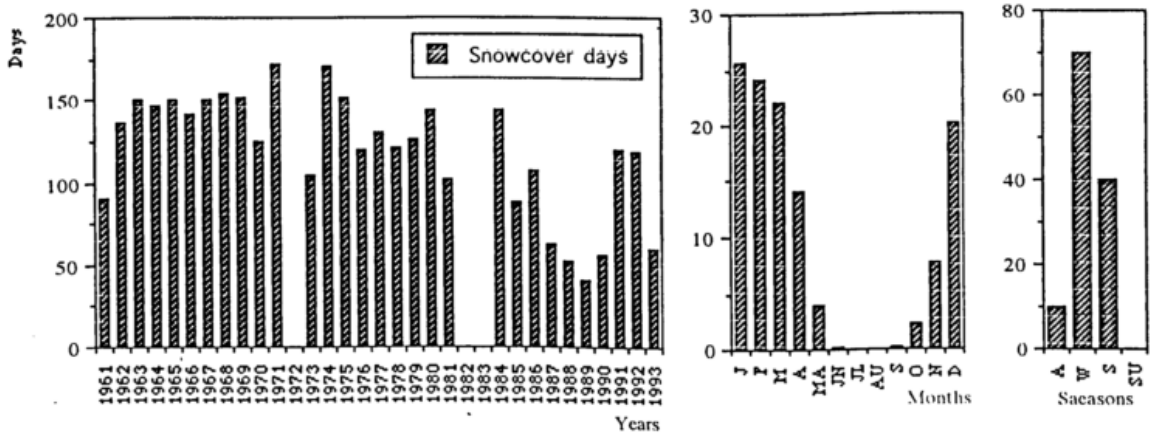

Figure 4.- *Annual, monthly and seasonal number of days with snowcover.*

3. SNOWFALLS AND SYNOPTIC SITUATIONS

3.1. Days of precipitation

The relationship between precipitation in winter season and synoptic situations causing has been studied over period of 10 winters (1983-84 - 1992-93) from November to May.

The maximum number of days of precipitation is observed in trough synoptic situations with a cold fro associated (17,2% from the whole of the precipitation days), in east situations (15,6%), in cyclone situatior (11,6%), in north-west situations (10,9%) and in west situations (10,9%).

Because of the height of the meteorological station (1702 m a.s.l.), a significative part of the precipitation da in winter is registered as rainfall days; so, the ratio of snowfall days only reaches a 36% from the whole of tl days of precipitation in winter season. Thereby, rainfall days are frequent not only on November and May but the coldest months like January and February.

The ocurrence of rainfall days depends more on the aerological characteristics of the incoming airmass than the monthly average temperature. The south-west synoptic situation is the rainiest one, since the 65% of t

precipitation days in south-west situation are registered as rainfall days. The east and west weatner types are rainy synoptic situations in winter time too.
With regard to snowfall days situations, the north, north-est, north-west and cyclonic synoptic situations show the highest rates with values of snowfall days among 97% and 88% from the whole of theirs precipitation days.

3.2. Daily snowfall amounts

The daily snowfall amounts (DSA), given in cm of fresh snow, have been analysed over the winter period 1983-84 to 1992-93 from November to May. It has been impossible to dispose of more data since the observation of DSA in La Molina was started on 1983. Table I gives the absolute frequencies of DSA for each class gathered by the causing synoptic situations.
It is significant the share corresponding to the haviest snowfalls in the obtaining of the total sum of DSA. So, considering the amount of 30 cm as treshold to select heavy snowfalls, it is observed that days with snowfall amounts higher than 30 cm are only a 2% from the snowfall days, but they give a 15% from the sum of DSA. That lack of equidistribution has been confirmed for daily precipitation amounts in other sites located in the mediterranian basin of Iberian Peninsula (GUILLÓ and PUIGCERVER, 1970).
Amounts of snowfall classified in the corresponding weather type show that the highest amounts are fell in cyclone, easterly and trough synoptic situations. The highest means of DSA are brought by cyclone and east weather situations with 10,4 cm and 9,8 cm per day respectively. The means pointed out are meaningful greater than the average calculated for the whole of the DSA which is 6,1 cm per day.
Results from relationship between DSA and weather situations are:
- The slight importance of west and north-west synoptic situations in the bringing of DSA, which are uppermost cause of snowfalls in Western Pyrenees. Contrarywise, Eastern Pyrenees are affected by westerly zonal circulation in upper air with less frequency and in a minimized way.
- The great importance of cyclone and east synoptic situations in the frequency, intensity and quantity of snowfall amounts. That fact is due to the mediterranean maritime influence, which is not very considerable in Western Pyrenees.
East weather situation is caused by the presence of a blocking anticyclone in zonal position over the north of Europe and the presence of a cyclone over the north of Africa (CLAVERO and RASO, 1979). Both cells lead a polar airmass modified because of its staying on Mediterranean sea. Precipitacions intensify when in upper level (500 hPa) a cold airmass loose from zonal circulation is detected (MARTIN, 1987). Figure 5 shows east weather situation on 22 January 1992 bringing heavy snowfalls in Eastern Pyrenees.
Cyclone synoptic situation causes intense precipitations when the surface vortex is located at south of the Eastern Pyrenees. So, the cyclone leads easterly and south-easterly winds over the southern side of the range increasing the precipitation by means of orographic lifting of maritime airmass. Figure 6 shows cyclone synoptic situation on 31 January 1986.

CLASSES	SYNOPTIC SITUATION									SUM	SUM
(cm)	C	E	SW	TRG	NW	NE	W	N	OTH.	Event	(cm)
0.1-4.9	13	15	8	38	29	14	24	12	16	169	286
5.0-9.9	14	6	2	15	11	1	6	6	2	63	414
10.0-14.9	9	5	2	6	5	2	1	2	1	33	378
15.0-19.9	4	3		2	2					11	173
20.0-24.9	2	2		1						5	110
25.0-29.9	3	2		1						6	157
30.0-34.9				1						1	30
35.0-39.9	1		1							2	73
40.0-44.9											
45.0-49.9											
50.0-54.9				1						1	50
55.0-59.9	1	1								2	116
Events	47	34	13	65	47	17	31	20	19	293	
SUM (cm)	490	303	87	402	209	54	87	79	46		1787
MEAN	10,4	9,8	6,7	6,2	4,4	3,2	2,8	2,5	2,4		6,1

Table I.- *Absolute frequencies of daily snowfall amounts given in cm of fresh snow, gathered in synoptic situations (C, cyclone; E, east; SW, south-west; TRG, trough; NW, north-west; NE, north-east; W, west; N, north; OTH, others synoptic situations).*

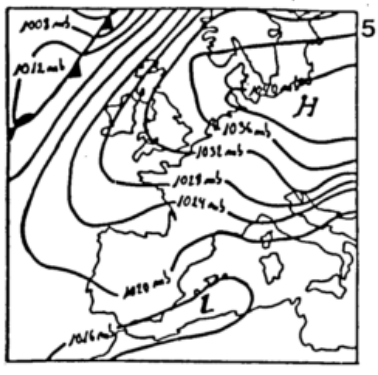

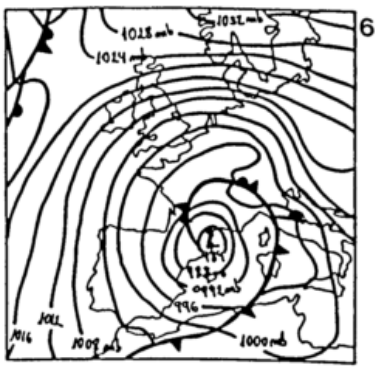

Figure 5.- *Surface synoptic situation. East weather type. 22-I-92.*

Figure 6.- *Surface synoptic situation. Cyclone weather type. 31-I-86.*

3.3. Estimation of maximum daily snowfall amounts

Heavy snowfalls are considered as a natural hazard because of the possibility of triggering avalanches, which frequently do damage to man and his constructions. It is necessary to know the magnitude of maximum daily snowfall amounts in order to improve the high mountain planning, specially relating ski resorts management. Table II shows the estimated maximum daily snowfall amounts for the return periods of 3, 5, 10, 15, 20, 25, 30, 50, 75 and 100 years according to the Gumbel distribution given by:

$$P(x) = \alpha\, e^{-[\alpha (x-\mu) + e^{-\alpha (x-\mu)}]} \qquad \text{where } \alpha = 0{,}041 \text{ and } \mu = 36.358$$

The data used are daily maximum snowfall amounts given in water equivalent (mm) from the period 1961-1993. In some cases part of the snowfall amounts corresponds to rain. From table II it is observed that a day with a snowfall amount higher than 119.3 mm is expected once per 30 years. In fact the pointed out maximum was exceeded once in the period 1961-1993, exactly on November 1962 when 149.0 mm were registered.
The greater part of the daily maximum snowfall amounts fell both from March to May and from November to December (ALBENTOSA, 1983). It may be remarked that winter period is the driest season of the year in the Eastern Pyrenees, especifically on February and January. Over the last ten years the cyclonic situations have been the main synoptic cause of maximum snowfall amounts with surface vortex centered at the south of the Eastern Pyrenees leading surface easterly winds from Mediterranean sea.

	RETURN PERIODS (YEARS)									
	3	5	10	15	20	25	30	50	75	100
LA MOLINA (1700 m)	58,5	73,1	91,5	101,9	109,2	114,8	119,3	132,0	142,0	149,1

Table II.- *Maximum daily snowfall amounts estimated (given in mm) according to the Gumbel distribution for different return periods.*

4. CONCLUSIONS

The Eastern Pyrenees present the minimum seasonal amount of precipitation in winter. It implies low amounts of snowfall respect to the Western Pyrenees. The maximum amount of fresh snow is registered on March and April, but the maximum number of days with snowpack on the ground occurs on January and February.
In spite of the low monthly amounts of snowfall, high daily snowfall amounts are frequent, which implies a natural hazard by means of the avalanche activity. The main synoptic situations leading to intense snowfalls are cyclonic and east situations, wich are linked to the mediterranean influence.
The insignificance of the west and north-west weather types in the generation of snowfalls is another typical feature of the snow regime of the Eastern Pyrenees.

REFERENCES

Albentosa, L. 1983: "Los contrastes espaciales de las precipitaciones en el Pirineo Catalán". *VII Coloquio de Geografía. A.G.E.*, pp. 61-64. Salamanca.

Clavero, P., and Raso, J. M. 1979: "Catálogo de tipos sinópticos para un estudio climático del Este de la Península Ibérica y Baleares". *Aportacions en homenatge al geògraf Salvador Llobet*, pp. 63-68. Barcelona.

Guilló, A. M. and Puigcerver, M. 1970: "Sobre las contribuciones relativas de las precipitaciones local y generalizada a la precipitación total en Catalunya". *Revista de Geofísica, XXIX, 3*, pp. 205-216. Madrid.

Martín, J. 1987: "Característiques climatològiques de la precipitació en la franja costera mediterrània de la Península Ibèrica". Institut Cartogràfic de Catalunya. Barcelona.

Salvador, F. 1986: "Application of some topoclimatic methods for the assessment of snow covering, distribution and permanence in La Molina (Eastern Pyrenees)". *Abstracts Study Group of Topoclimatical Investigation and Mapping*, p. 14. Barcelona.

Xercavins, A. 1983: "El regimen anual de nieves en el Pirineo Oriental". *VII Coloquio de Geografía. A.G.E.*, pp. 69-74. Salamanca.

Untersuchungen zum Niederschlag- und Abflußverhalten eines stark vergletscherten Einzugsgebietes in den Ötztaler Alpen

H.Escher-Vetter, O.Reinwarth

Kommission für Glaziologie der Bayerischen Akademie der Wissenschaften

Abstract

Using the twenty-years records of runoff and precipitation of a highly glacierized drainage basin (Vernagt-Basin/Oetztal Alps), the influence of mass balance on the relationship between the maximum rainfall of each year and peak runoff values is investigated. It can be shown, that in spite of peak rainfall events mainly below 30 mm without a rising tendency, the share of rainfall in the total runoff is constantly growing. The reason lies in the growth of the bare ice area, caused by very high negative mass balances especially since 1982.

Zusammenfassung

Anhand der 20-jährigen Meßreihen von Abfluß und Niederschlag in einem stark vergletscherten Einzugsgebiet (Vernagt-Gebiet/Ötztaler Alpen) wird der Einfluß der Massenbilanz des Gletschers auf die Koppelung von höchsten Regenniederschlagsbeträgen und maximalen Abflußbeträgen untersucht. Es zeigt sich, daß immer größere Anteile des Abflusses an den Tagen mit den höchsten Regenfällen des Jahres vom Regen geliefert werden, obwohl die Niederschlagshöhen überwiegend unter 30 mm liegen und keine steigende Tendenz aufweisen. Die Ursache hierfür ist in der Vergrößerung der aperen Gletscherfläche durch hohe negative Massenbilanzen vor allem seit 1982 zu sehen.

1. Einleitung

Im Herbst des Jahres 1973 wurde die Pegelstation Vernagtbach (2640 m NN) am Gletscherbach des Vernagtferners (2747 m NN - 3633 m NN) in den Ötztaler Alpen errichtet. Für das 11,44 km² große, zu 80 % vergletscherte Einzugsgebiet der Station liegen nunmehr zwanzigjährige Meßreihen des Abflusses (Escher-Vetter et al.,1994), des Niederschlags und verschiedener meteorologischer Parameter (Lufttemperatur, Luftfeuchte, Luftdruck, Globalstrahlung, Windgeschwindigkeit und -richtung) für die Monate Mai bis Oktober in nahezu lückenloser Form auf der Basis von Stundenmitteln (Niederschlag i.d.R. als Tagessummen) vor; während der Wintermonate treten - vor allem in den ersten Jahren - gelegentlich längere Unterbrechungen auf. Darüber hinaus wird am Vernagtferner seit 1965 die Massenbilanz glaziologisch bestimmt.

Im folgenden Beitrag wird der sich aus den Veränderungen der glaziologisch/hydrologischen Randbedingungen seit 1974 ergebende Zusammenhang von Spitzenwerten des Abflusses und maximalen Tagessummen des Regens näher untersucht.

2. Jährliche Höchstwerte von Regen und Abfluß

Bei der hier vorgestellten Untersuchung lag das Hauptaugenmerk auf der etwaigen Erhöhung des Schmelzwasserabflusses durch den am gleichen Tag gefallenen Niederschlag. Dazu mußte als erstes die Art des Niederschlags - Regen oder Schnee - bestimmt werden, da auf die Gletscheroberfläche fallender fester Niederschlag zunächst zwischengespeichert wird, den Abfluß also nicht direkt bezuschußt. Deshalb wurde anhand der Temperaturregistrierung an der Pegelstation Vernagtbach ermittelt, bis in welche Höhe des Einzugsgebietes der Niederschlag in Form von Regen fällt, wobei eine Isotherme von +2°C als Grenzlinie gewählt wurde. Zusätzlich diente die tägliche Photographie des Gletschergebietes zur Kontrolle der Niederschlagsart; seit 1978 wird etwa von Anfang Mai bis Ende Oktober einmal pro Tag ein großer Bereich der Gletscheroberfläche mit einer Kamera automatisch photographiert, primär, um den Ausaperungsstand und damit die Albedoverteilung im Verlauf des Sommers zu dokumentieren.

In Tabelle 1 sind die maximalen Regen- bzw. Abflußbeträge für die Jahre 1974 bis 1993 an der Pegelstation Vernagtbach zusammengestellt. Zusätzlich sind - im linken Teil der Tabelle - für das Datum der höchsten Regentagessummen die jeweiligen Tagesmittel des Abflusses angegeben, im rechten Teil entsprechend die Niederschlagsbeträge (Schnee *kursiv* gesetzt) am Tag des maximalen Abflusses.

Im Jahr	Max.Regen am	Regen [mm]	Abfluß [m*m*m/s]	Max.Abfluß am	Abfluß [m*m*m/s]	Regen [mm]
1974	8.August	25	2.38	5.August	2.90	6
1975	28.Juli	14	1.52	18.Juli	3.91	?
1976	2.Juli	28	2.83	18.Juli	4.76	5
1977	18.August	30	2.33	30.August	2.99	18
1978	**7.August**	**29**	**2.82**	**8.August**	**3.09**	***6***
1979	31.Juli	16	3.02	2.August	3.63	1
1980	**8.August**	**11**	**4.46**	**8.August**	**4.46**	**11**
1981	3.Juli	21	2.24	17.August	4.04	4
1982	28.August	26	2.26	17.Juli	4.79	10
1983	2.August	18	4.54	1.August	5.61	4
1984	5.August	23	2.76	14.Juli	**3.52**	**0**
1985	5.Juli	26	1.05	30.Juli	4.56	*27*
1986	18.Juli	23	1.58	5.August	5.59	2
1987	24.August	39	5.55	19.Juli	6.12	31
1988	29.August	21	1.80	3.August	5.42	15
1989	7.Juli	31	2.34	17.August	4.72	16
1990	1.Juli	24	2.83	5.August	**4.63**	**0**
1991	14.Juli	22	3.69	12.Juli	4.53	1
1992	29.Juli	11	4.08	22.August	5.03	4
1993	10.Juli	33	2.15	23.August	6.00	25

Tab.1: Datum und Menge von Regen und Abfluß am Tag mit höchster Regenmenge des Jahres (linker Teil) und mit höchstem Abflußbetrag des Jahres (rechter Teil) an der Pegelstation Vernagtbach

Betrachtet man Tabelle 1, so fällt als erstes auf, daß die höchsten Regentagessummen (Spalte 3) in 12 der vorliegenden 20 Jahre zwischen 20 mm und 30 mm liegen, nur in drei Jahren werden mehr als 30 mm erreicht, in fünf Jahren liegen sie sogar unter 20 mm. Dies bestätigt die Charakterisierung des hinteren Ötztals als eines inneralpinen Trockentals mit geringen Niederschlagsmengen vor allem im Sommer (Kuhn et al.,1982). Vergleicht man das Auftreten des maximalen Abflusses (Spalte 5) mit dem der maximalen Regenmenge (Spalte 2), so sieht man, daß nur in zwei von zwanzig Jahren (1978 und 1980) beide Spitzenwerte am gleichen bzw. an aufeinander folgenden Tagen registriert wurden. 1984 und 1990 fällt kein Regen am Tag mit Höchstabflußbeträgen, in den übrigen Jahren variieren die Regenmengen für diesen Tag zwischen 1 mm und 31 mm. Die lineare Interpolation der Abflußmaximalwerte ergibt eine jährliche Zunahme von 0.11 m^3/s, bezogen auf die Tagesmittel.

3. Bestimmung des relativen Anteils des Regen- und des Eisschmelzabflusses am Gesamtabfluß

Trotz der von vielen Autoren (z.B. Schädler, 1985; Bernath,1992) beschriebenen Schwierigkeiten bei der Bestimmung des Gebietsniederschlags, insbesondere in teilweise vergletscherten Gebieten im Gebirge, wird hier der Versuch unternommen, über das

Tab.1: Ergebnis der Energiebilanzrechnungen mit dem Programm MEMI, freundlicherweise von P. Höppe bereitgestellt.

Personendaten (JW): 30 Jahre, 62 kg, 1,72 m, männlich																					
		Ta	Tmrt	V	f	Vpa	p	Icl	Arb	Tsk	Tcl	H	Rsum	Csum	Ed	Esw	Ere	Wsum	wetsk	K-Wert	K-Wert
12.06.1991	11:40	3,7	58	4,0	36	2,7	571,0	1,5	310	35,0	21,0	348	378	-511	-23,0	-145	-47,0	305	0,17	899	sehr kühl
Sonne	12:07	3,7	69	5,1	34	2,7	571,0	1,5	310	35,0	22,0	348	508	-631	-23,0	-154	-47,0	318	0,18	949	kalt
Sonne	12:18	4,0	72	4,9	34	2,8	571,0	1,5	310	35,0	23,0	348	538	-648	-23,0	-166	-48,0	336	0,19	931	kalt
Sonne	12:50	4,1	73	5,6	37	3,0	571,0	1,5	310	35,0	22,0	348	557	-675	-23,0	-160	-47,0	326	0,18	956	kalt
Sonne	13:02	4,0	72	5,6	37	3,0	571,0	1,5	310	35,0	22,0	348	546	-666	-23,0	-157	-47,0	322	0,18	959	kalt
Sonne	14:00	4,6	83	5,4	33	2,8	571,0	1,5	310	35,0	26,0	348	672	-759	-22,0	-189	-48,0	371	0,21	932	kalt
3/8 Wolken	15:40	4,8	60	3,2	34	3,2	571,0	1,5	310	35,0	23,0	348	381	-489	-22,0	-169	-48,0	340	0,21	822	sehr kühl
Sonne	15:50	5,1	59	2,8	33	2,9	571,0	1,5	310	35,0	24,0	348	362	-463	-22,0	-176	-48,0	351	0,22	789	sehr kühl
Sonne weg	18:45	3,6	-1	3,1	34	2,8	571,0	1,5	310	32,0	8,6	348	-74	-147	-22,0	-57	-47,0	173	0,08	851	sehr kühl
13.06.1991	10:40	6,6	76	1,3	30	2,9	571,8	1	310	36,0	36,0	348	450	-445	-21,0	-282	-50,0	510	0,3	629	kühl
Sonne	11:10	6,5	87	1,5	32	3,1	571,7	1	310	36,0	39,0	348	576	-528	-20,0	-326	-49,0	573	0,33	652	kühl
Sonne	12:10	7,1	61	1,0	30	3,0	571,6	1	310	35,0	32,0	348	294	-338	-21,0	-233	-50,0	438	0,27	584	kühl
Sonne	13:55	7,5	84	2,2	29	3,0	571,4	1	310	36,0	36,0	348	563	-561	-22,0	-277	-51,0	506	0,26	683	kühl
Sonne	15:20	7,9	83	2,4	28	3,0	571,3	1	310	36,0	35,0	348	556	-564	-22,0	-266	-51,0	490	0,25	685	kühl
Sonne	17:25	8,8	41	0,7	26	2,9	570,9	1	310	35,0	27,0	348	118	-219	-22,0	-173	-52,0	353	0,23	509	kühl
S.Untergang	17:59	3,2	37	1,1	45	3,5	571,0	1	310	34,0	22,0	348	118	-283	-23,0	-113	-46,0	255	0,14	686	kühl
	18:06	2,0	18	1,8	52	3,7	571,0	1	310	32,0	15,0	348	12	-255	-22,0	-39	-45,0	140	0,05	793	sehr kühl
	18:20	1,5	0	1,9	56	3,8	571,1	1	310	30,0	10,0	348	-85	-198	-21,0	0	-44,0	80	0	816	sehr kühl
	18:45	0,6	0	1,0	62	3,9	571,2	1	310	31,0	12,0	348	-95	-172	-21,0	-16	-43,0	103	0,03	731	sehr kühl
19.06.1991	08:47	-1,0	43	2,0	89	5,0	564,7	2	372	35,0	17,0	403	254	-388	-18,0	-205	-47,0	381	0,34	891	sehr kühl
Schneefall	09:43	-1,4	39	3,8	95	5,1	564,9	2	372	34,0	12,0	403	250	-422	-20,0	-164	-47,0	322	0,26	1043	kalt
8/8 Wolken	13:39	-1,4	48	2,1	85	5,2	565,6	2	372	35,0	18,0	403	303	-429	-18,0	-213	-46,0	390	0,35	911	sehr kühl
Schneefall	15:00	-0,1	19	1,7	95	5,8	565,6	2	372	34,0	11,0	403	61	-232	-18,0	-167	-47,0	325	0,29	837	sehr kühl
20.06.1994	08:17	-2,2	20	1,4	86	4,8	568,7	2	310	34,0	11,0	348	72	-242	-21,0	-117	-40,0	245	0,21	853	sehr kühl
8/8 Wolken	10:13	0,1	59	2,5	80	4,3	568,9	2	310	35,0	21,0	348	410	-513	-20,0	-182	-42,0	346	0,29	907	sehr kühl
8/8 Wolken	10:55	0,2	33	2,6	61	3,8	569,0	2	310	34,0	13,0	348	177	-335	-21,0	-124	-43,0	264	0,2	912	sehr kühl
6/8 Wolken	13:26	1,5	47	4,4	63	4,3	569,0	2	310	34,0	15,0	348	314	-465	-21,0	-132	-43,0	275	0,2	987	kalt

Arb: Arbeit, d.h. Aktivitätsumsatz des Körpers (W), **Csum**: Wärmefluß durch Konvektion (W), **Ed**: Energiefluß durch Wasserdampfdiffusion (W), **Ere**: Energiefluß in die Atemluft (W), **Esw**: Leistung der aktuellen Schweißverdunstung (W), **f**: Luftfeuchtigkeit (%), **H**: innere thermische Leistung (W), **Icl**: Wärmedurchgangswiderstand der Kleidung (clo), **K-Wert**: Abkühlung (W/m²), **p**: Luftdruck (hPa), **Rsum**: Strahlungsbilanz des Körpers (W), **Ta**: Lufttemperatur (°C), **Tcl**: mittlere Temperatur der Kleidungsoberfläche (°C), **Tmrt**: mittlere Strahlungstemperatur (°C), **Tsk**: Hauttemperatur (°C), **V**: Windgeschwindigkeit (m/s), **Vpa**: Wasserdampfdruck (hPa), **wetsk**: Hautbenetzung (%), **Wsum**: gesamter Wasserverlust (g/h)

Tab.2: Vergleich der Mittelwerte aus den Energiebilanzrechnungen für Sonnentage (12., 13.6.91) und Wolkentage (19., 20.6.91).

	weiblich					männlich					Mittelwert (männlich-weiblich)					
	Mittel	Mittel	Mittel	S-W	S-W	Mittel	Mittel	Mittel	S-W	S-W	Sonne	Sonne	Wolke	Wolke	alle Werte	
	Sonne	Wolken			(in %)	Sonne	Wolken			(in %)	absolut	(in %)	absolut	(in %)	absolut	(in %)
Ta	5,9	-0,6	2,7	6,5												
Tmrt	70	33	52	38												
V	3,1	2,9	3,0	0,2												
f	32	72	52	-40												
Vpa	3,0	3,0	3,0	0,0												
p	571,3	567,1	569,2	4,1												
Icl	1,3	2,0	1,7	-0,7												
Arb	300	330	315	-30	-0,10	375	415	395	-40	-0,11	-75	-0,20	-85	-0,20	80	0,20
Tsk	35,7	34,9	35,3	0,8	0,02	35,1	34,4	34,8	0,7	0,02	0,6	0,02	0,5	0,01	-0,5	-0,01
Tcl	28,5	12,4	20,5	16,1	0,56	28,5	12,1	20,3	16,4	0,57	0,0	0,00	0,3	0,02	-0,2	-0,01
H	332	359	346	-27	-0,08	416	453	435	-36	-0,09	-84	-0,20	-94	-0,21	89	0,20
Rsum	425	171	298	254	0,60	512	200	356	311	0,61	-86	-0,17	-29	-0,15	58	0,16
Csum	-494	-332	-413	-163	0,33	-589	-391	-490	-197	0,34	95	-0,16	60	-0,15	-77	0,16
Ed	-22,0	-20,0	-21,0	-2,0	0,09	-24,6	-22,1	-23,4	-2,5	0,10	2,6	-0,11	2,1	-0,10	-2,4	0,10
Esw	-194	-136	-165	-58	0,30	-256	-186	-221	-70	0,27	61	-0,24	50	-0,27	-56	0,25
Ere	-47,0	-42,5	-44,8	-5	0,10	-58,7	-53,2	-56,0	-6	0,09	12	-0,20	11	-0,21	-11,2	0,20
Wsum	378	277	328	100	0,27	486	365	426	121	0,25	-109	-0,22	-88	-0,24	98	0,23
wetsk	0,22	0,23	0,23	-0,01	-0,05	0,24	0,26	0,25	-0,02	-0,08	-0,02	-0,08	-0,03	-0,12	0,02	0,08

Da der Vernagtferner in den siebziger Jahren auf Grund seiner großen Altschnee- und Firnflächen beim Auftreten der höchsten Regenfälle über ein beträchtliches Speichervolumen verfügte, lieferten Regen und Eisschmelzwasser nur einen geringen Anteil des Gesamtabflusses. Dagegen überlagerten sich am 23. August 1993 beträchtliche Eisschmelzwassermengen und sehr hohe Regenabflüsse, sie bildeten zusammen etwa die Hälfte des Gesamtabflusses. Besonders interessant ist das Regenereignis vom 19.Juli 1987. Hier war zwar die ausgeaperte Gletscherfläche noch klein, trotzdem wurde an diesem Tag der absolut höchste Tagesmittelwert des Abflusses in der 20-jährigen Reihe registriert. Durch günstige Schmelzbedingungen an den vorangegangenen Tagen und einen Regenfall von 22 mm am Vortag war so viel Flüssigwasser im Firn vorhanden, daß sich der Gesamtabfluß zum größten Teil aus diesem Reservoir speiste.

4. Ausblick

Die hier dargestellten Zusammenhänge zwischen den Spitzenwerten des Regens und den Abflüssen, wie sie an der Pegelstation Vernagtbach seit nunmehr 20 Jahren registriert werden, legen den Schluß nahe, daß bei unverändert negativen Massenhaushalten, die im Jahr 1991 erstmals zu einer Gleichgewichtslinienhöhe oberhalb des Gletschers geführt haben, ein weiteres Anwachsen der maximalen Abflußbeträge zu erwarten ist. Sollte sich auf Grund ungünstiger zeitlicher Überlagerung ein Starkregen auf ein großes Eisgebiet mit hoher Schmelzwasserproduktion ergießen, so würde das nicht nur eine Gefährdung der Meßstelle, sondern auch ein erhebliches Hochwasserrisiko für ein weitaus größeres Gebiet zur Folge haben.

5. Danksagung

Nahezu lückenlose Zeitreihen hydrologischer und meteorologischer Parameter im Hochgebirge können nur durch großen Arbeitseinsatz aller am Projekt beteiligten Mitarbeiter gewonnen werden; stellvertretend für die zahllosen Mitarbeiter und Helfer soll hier Dipl.Ing.(F.H.) Erich Heucke genannt werden. Die Untersuchungen wurden von der DFG im Rahmen des SFB81, TP A1 und vom Bayerischen Klimaforschungsprogramm (BayFORKLIM) gefördert.

6. Literatur

Bernath,A.(1992): Precipitation measurements in the alpine basin Gletsch during the ALPEX/RHONEX-Project: Distribution and elevation dependency. XXIIème Conf. Intern.d.Météorolgie Alpine, Toulouse, 7-11 Septembre 1992 (Hrsg.: Météo-France et la Société Météorologique de France). S. 156-160, Toulouse.

Escher-Vetter,H.(1980):Der Strahlungshaushalt des Vernagtferners als Basis der Energiehaushaltsberechnungen zur Bestimmung der Schmelzwasserproduktion eines Alpengletschers. Wiss.Mitt.Met.Inst.München, Nr. 39, München.

Escher-Vetter,H.,Reinwarth,O.(1994): Zwanzig Jahre Abflussmessung an der Pegelstation Vernagtbach (Ötztaler Alpen) 1974-1993. Monographie, herausgegeben von der Kommission f. Glaziologie der Bayer. Akademie d. Wissenschaften, München.

Kuhn,M.,Nickus,U.,Pellet,F.(1982): Die Niederschlagsverhältnisse im inneren Ötztal. 17. Tagung f. Alp. Meteorol., Berchtesgaden,21.-25.9.1982 (Hrsg.: Deutscher Wetterdienst), S.235-237, Offenbach.

Lang,H.(1985): Höhenabhängigkeit der Niederschläge. In: Der Niederschlag in der Schweiz. Beiträge zur Geologie der Schweiz - Hydrologie, Bd. 31, S. 149-157, Zürich.

Moser,H.,Escher-Vetter,H.,Oerter,H.,Reinwarth,O.,Zunke,D.(1986): Abfluss in und von Gletschern. Abschlußbericht TP A1, SFB 81, TU München. GSF-Bericht 41/86, T.I, S.208-226 bzw. S.76-107, München.

Schädler,B.(1985): Gebietsniederschläge. In: Der Niederschlag in der Schweiz. Beiträge zur Geologie der Schweiz - Hydrologie, Bd. 31, S. 171-186, Zürich.

Meteorological Influences on Air and Snow Pollution in the High Alps - Results of the Project ALPTRAC

Petra Seibert[1], Helga Kromp-Kolb[1], Anne Kasper[2], Hans Puxbaum[2],
Urs Baltensperger[3], Dieter T. Jost[3], Margit Schwikowski[3]

[1]Institut für Meteorologie der Universität Wien, Austria
[2]Institut für Analytische Chemie der Technischen Universität Wien, Austria
[3]Paul Scherrer Institut, Labor für Radio- und Umweltchemie, Villigen, Switzerland

ABSTRACT

ALPTRAC is a EUROTRAC subproject devoted to the study of air and snow pollution at high-alpine sites. Meteorological influences on the concentrations of chemical species relevant for acidification were investigated on the basis of long-term measurements at Sonnblick, Jungfraujoch and Monte Rosa. During winter, the concentrations are extremely low and represent the free troposphere for most of the time. In the warm season, a diurnal cycle probably caused by regional slope winds is often observed. Sometimes, air from the Po Valley's boundary layer gets advected to the high-alpine peaks; this requires the reduction of atmospheric stability through the release of latent heat. A statistical trajectory analysis was applied to investigate potential source regions relevant to long-range transport of secondary aerosol. This analysis shows that relevant source areas are not only to the east, but also to the south, while air coming from the northwest - though passing over regions of considerable emissions - is relatively clean on the average, probably due to precipitation scavenging during transport.

1. ALPTRAC - an overview

ALPTRAC is an international (F, I, CH, D, A) and interdisciplinary subproject of EUROTRAC (a co-ordinated research programme on the transport and transformation of environmentally relevant trace constituents in the troposphere over Europe) devoted to the investigation of air and snow pollution at high-alpine sites. ALPTRAC consists of four studies with different foci: In the alpine-wide snow sampling programme SNOSP is devoted to the determination of deposition of the major ions in the winter and spring snow cover at about 15 sites in the Alps at elevations between 3000 and 4500 m. The aim of the CORE programme is to reconstruct the history of air pollution through the analysis of firn and ice cores drilled in cold alpine glaciers. In the ALASS programme, the phase distributions of pollutants in the air and the scavenging mechanisms in and below clouds are investigated at the mountain observatories Jungfraujoch (Swiss Alps, 3450 m) and Sonnblick (Austrian Alps, 3106 m), and on the Rigi in the Swiss Alps (sites at 1030 m and 1620 m). Automatic stations for measurements of aerosol and/or meteorological parameters are operated also at Colle Gnifetti in 4450 m and at Colle Vincent in 4086 m in the Monte Rosa region. Finally, the aim of the meteorological support study SNOWMET is the meteorological interpretation of the chemical and physical measurements as well as the investigation of the transport mechanisms and of the likely source regions of pollutants. Information on ALPTRAC and the groups involved can be found in [1]; a directory of the field data collected until spring 1993 and some related information including a bibliography of ALPTRAC has been published in [2].

2. Data sets and their characteristics

Long-term measurements of airborne pollutants are the primary basis of the meteorological investigations. Paul Scherrer Institute has been operating so-called epiphaniometers at Jungfraujoch, Colle Gnifetti, and Sonnblick since several years, and did so for a limited period near La Grave in the French Alps [3]. The epiphaniometer measures the aerosol surface concentration in relative units with a time resolution of 30 min at very high sensitivity, and can be operated on solar-powered batteries [4,5]. A modified epiphaniometer at Jungfraujoch measures the concentration of radon decay products with a time resolution of 1 h [4,6].

At Sonnblick, the Institute of Analytical Chemistry in Vienna operated a filter pack from November 1991 until November 1993, which yielded concentration data for all major water-soluble particulate and gaseous species relevant for acidity with a time resolution of 12 or 24 h [7].

Figure 1 shows the time series of the daily mean values of the concentration of particulate sulphate at Sonnblick from November 1991 until November 1992. Two features are prominent: the strong annual cycle with a minimum in winter, and considerable variation in the synoptic time scale.

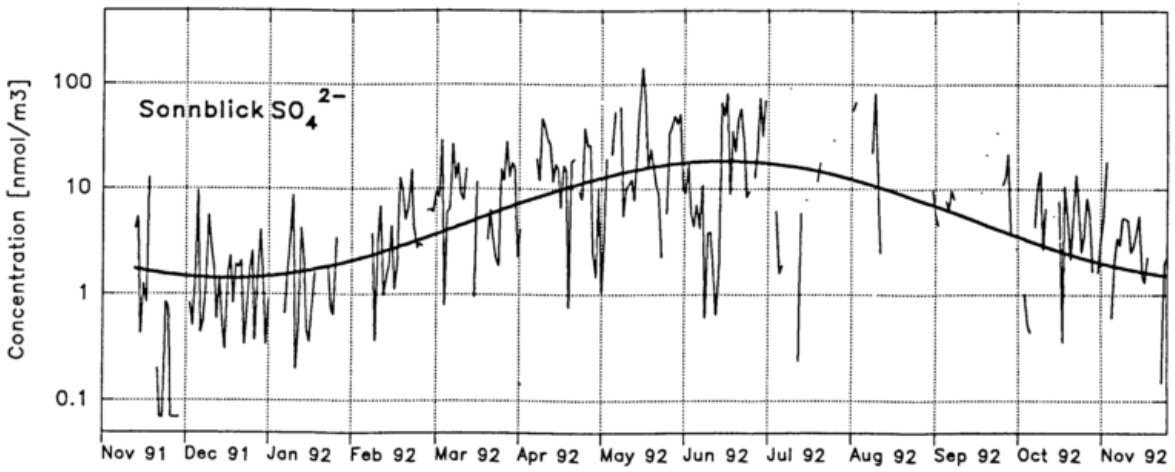

Fig. 1: Daily means of the particulate sulfate concentration at Sonnblick, Nov 1991 - Nov 1992. The heavy line indicates the annual cycle estimated by harmonic regression (yearly period only).

The annual cycle is observed in all species but SO_2 and at all sites. The ratios between the mean summer (JJA) and winter (NDJ) concentrations in air at Sonnblick were 1 for SO_2, 5 for HNO_3 and NH_3, 8 for NO_3^-, 11 for SO_4^{2-}, and 17 for NH_4^+ [7]. It is obvious that it is related to the stability of the atmosphere and not to the intensity of photochemical reactions as it is shown also by chemically inert tracers such as radon decay products [4,6]. Undisturbed winter situations represent free tropospheric background conditions with concentration levels comparable to those found in Greenland.

Variations with a time scale of one or several days are likely to be caused by long- or medium range transport. Their analysis has been a major focus of SNOWMET (see sections 4 and 5). In addition, a diurnal cycle was found on many summer days which is discussed in section 3.

An important tool for meteorological analysis were back trajectories, computed for 00 and 12 UTC of each day for 8 sites on the basis of ECMWF wind fields. As only wind data on main pressure levels were available, trajectories were computed on isobaric surfaces only (levels 850, 700 and 500 hPa).

3. Regional-scale transports and the diurnal cycle of pollution

On a number of days, mainly during the warm season, a distinct diurnal cycle of the aerosol concentration can be observed at Jungfraujoch and (to a lesser extent) at Sonnblick (Fig. 2), with maxima in the late afternoon or evening. Parallel observations of radon decay products show that this is a transport phenomenon. The diurnal cycle of the aerosol concentration has also been found at Colle Gnifetti in 4450 m [5]. At a first glance, convective mixing in the boundary layer seems to be a possible explanation. However, the differences of potential temperatures between Jungfraujoch and a valley station on the windward side turned out to be an insufficient predictor of the occurrence of the typical diurnal cycle. Replacement of the potential by the equivalent-potential temperatures for cases where the mountain station was in clouds also failed. There are many cases with a distinct vertical transport of pollutants (and also humidity, see Fig. 2) under stable stratification. Windshear may produce turbulence which might provide the necessary fluxes. However, inclusion of wind speed at Jungfraujoch still does not allow a statistical discrimination of days with and without the cycle. This implies

that another diabatic transport mechanism is responsible. Slope winds are diabatic and thus, in principle, a potential explanation. However, to the south of Jungfraujoch we find the vast snow areas of Aletschgletscher, the largest glacier in the Alps, while on the north side a steep and largely ice-covered wall drops. The expectation that typical slope winds will rarely develop at this site was confirmed by the investigation of hourly wind data from Jungfraujoch.

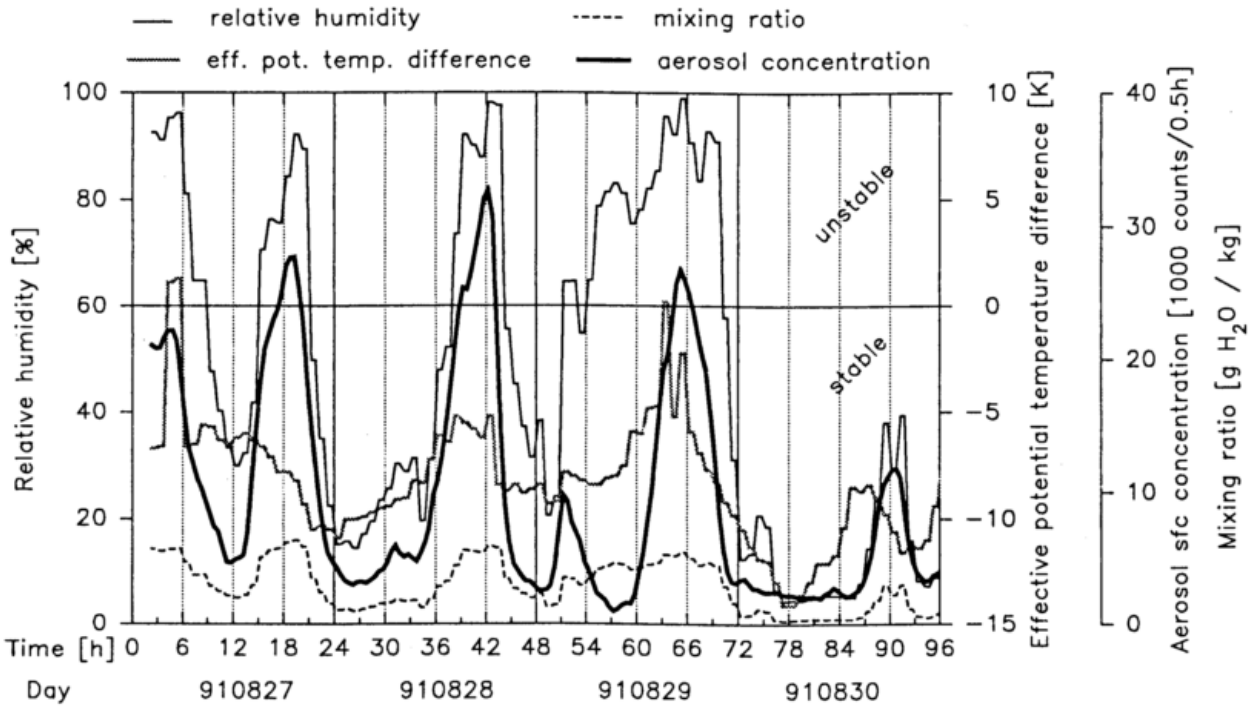

Fig. 2: Hourly means of the effective potential temperature difference between Jungfraujoch and Montana/Napf (stable <0, unstable >0), relative humdity and mixing ratio at Jungfraujoch, and half-hourly means of the epiphaniometer signal at Jungfraujoch.

A hypothetical explanation matching the observations would be that slope winds all over a certain catchment area carry pollutants from the plains and valley floors up to the ridge height of surrounding mountains (which have typical heights of 2500 m north of Jungfraujoch), and the synoptic wind at these levels then advects them to the highest peaks. Different transport mechanisms are possible for the vertical displacement in this uppermost layer: dynamic lifting (as indicated by a maximum fraction of days with pollutant cycle at medium wind speeds), sometimes facilitated by the release of latent heat in capping clouds, transport in cumulus clouds, or in small thermals developing over rock outcrops. This theory is supported by simulations with the ALPTHERM model [8], a 1D convection model including orographic effects and developed for soaring flight forecasts [9].

4. Transports from the Po Valley

Transports from the Po Valley are of special interest as it is the most important source area for pollutants adjacent to the Alps. However, the boundary layer air there is often trapped by strong stability, especially during southerly flows.

The height of origin of air coming from the Po Valley and arriving at Sonnblick and Jungfraujoch was determined under the assumption of conservation of the potential (or equivalent-potential, in the case of condensation) temperature, while the horizontal path was given by the isobaric trajectories. Results are shown in Figure 3. Origins below 1500 m are found in 19% of the cases at Sonnblick and 28% at Jungfraujoch. They are always associated with condensation at Jungfraujoch and in 97% at Sonnblick. These cases are connected, on the average, with cooling in the previous 24 hours, indicating that these are not foehn cases, but rather associated with cold front passages.

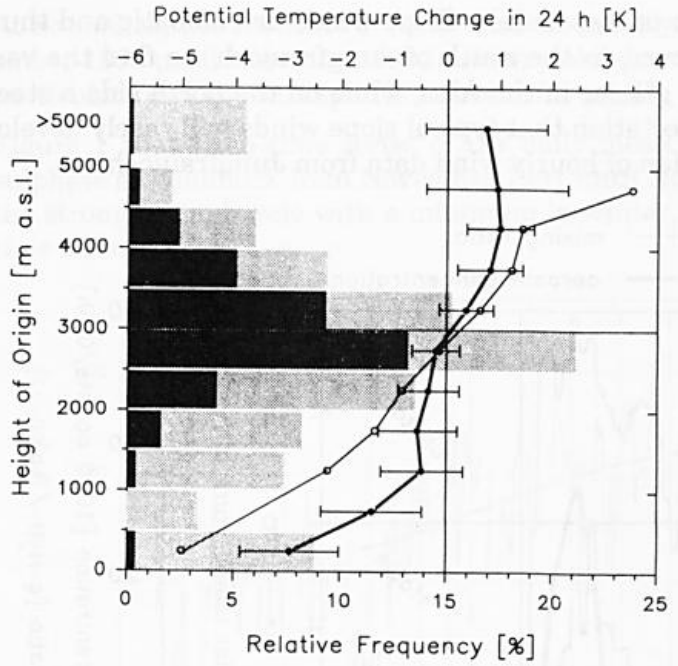

Fig. 3: Relative frequencies of the height of origin of air passing from the Po Valley to Sonnblick (bars) and associated temperature change in the previous 24 h at Sonnblick (lines). All height intervalls of dry plus wet cases add up to 100%.

5. Statistical trajectory analysis of potential source areas

In order to find potential source regions, pollution time series have been statistically evaluated together with the back trajectories. A grid was laid over Europe and the Northern Atlantic, and for each grid cell (side length about 150 km) the average concentration observed on arrival at Jungfraujoch or Sonnblick of each trajectory passing through this cell was computed. Concentration data were logarithmized to make them normally distributed and the annual cycle was eliminated using a spectral fit. Resulting fields were smoothed. A more detailed description can be found in [10]. Fig. 4 shows one example of the results, which is based on epiphaniometer measurements at Jungfraujoch in the period November 1991 until November 1992. Three major potential source areas, namely northeastern central Europe, the Iberian and the Italian Peninsulas were found. Low concentrations are observed with origins from most ocean areas, and interestingly, the British Isles, though considerable emissions of pollutants there. This pattern is probably to be explained by the probability of precipitation during different flow situations and in different areas; precipiation is by far the most important removal mechanism for atmospheric aerosol. The high contribution from southern Europe is most pronounced in winter.

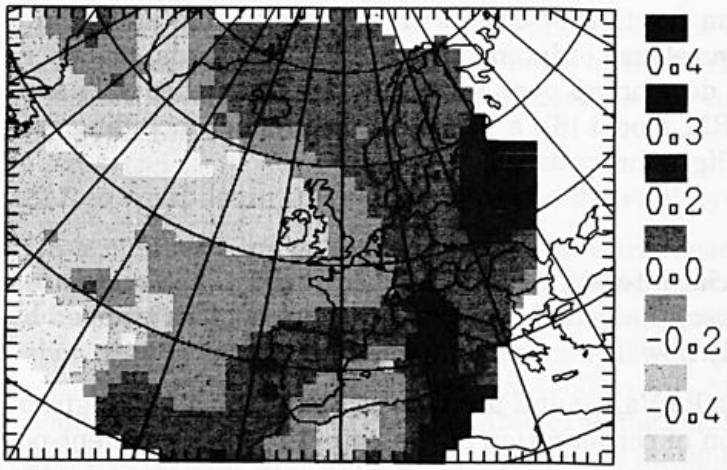

Fig. 4: Spatial distribution of the potential source areas for aerosol observed at Jungfraujoch (period Nov. 1991 - Nov. 1992). The scale is logarithmic, thus -0.4 corresponds to 40% of the mean, -0.2 to 63%, 0 to 100%, 0.2 to 158%, 0.3 to 200%, and 0.4 to 251%).

Saharan dust transport was investigated in a case study [11]; due to the limitations of the regularly available trajectories (no vertical motion, only 72 h back) statistical analyses were less suitable here. Saharan dust transports are quite sporadic [12] but of decisive influence on the acidity of the alpine snowpack; in extreme cases, a single event may balance the acidity input of a whole year [13].

6. Outlook and Conclusions

High mountain stations in the Alps offer the possibility to continuously monitor the concentration of atmospheric trace constituents. During most of the cold season, they experience tropospheric background conditions. However, synoptic systems cause intermittent transports of more polluted air, and during favourable conditions thermal wind systems and convection carry potentially polluted low-level air up to the highest peaks of the Alps. Concentrations can thus vary by 3 orders of magnitude. The use of these sites as background stations in the Global Atmospheric Watch (GAW), as planned for Jungfraujoch, Sonnblick and Zugspitze, therefore requires a good knowledge of the local meteorological conditions and their consideration in any evaluations of measurement data.

EUROTRAC and its subprojects will be continued until 1995. The working plan of SNOWMET for this period contains the completion of the statistical analysis of all available data sets, including chemical composition of wet deposition. The Po Valley transports shall be related to observed pollution events. A topic which will certainly remain important beyond ALPTRAC is the Alpine boundary layer, and especially the quantification of vertical exchange in this layer.

The ability of state-of-the art numerical models to simulate mesoscale pollutant dispersion in the Alpine region is presently under investigation in co-operation with the EUROTRAC subproject EUMAC. Their EURAD model system consists of a nested meteorological model (MM-5 model used in hydrostatic version with grid sizes 60 and 20 km) and a Eulerian transport and chemistry model (same grid size) based on the RADM model. If results are good enough, the simulation of the two periods selected is expected to give more insight into the role of different mechanisms which determine pollutant concentrations in the high Alps.

Acknowledgements

This work was funded by the Austrian Fonds zur Förderung der wissenschaftlichen Forschung (P7809-GEO, P7806-GEO), the Swiss National Science Foundation, and the Swiss Bundesamt für Bildung und Wissenschaft. In addition, we want to thank the staffs of the observatories at Jungfraujoch and Sonnblick for their support. B. Neininger made valuable contributions in a discussion about the role of slope winds in the transport of boundary layer air to Jungfraujoch.

References

[1] EUROTRAC Annual Report 1992, Part 2: ALPTRAC, TRACT. EUROTRAC ISS, D-82467 Garmisch-Partenkirchen (1993 report to become available soon)

[2] Kromp-Kolb H., W. Schöner, P. Seibert, 1993, *ALPTRAC Data Catalogue.* EUROTRAC ISS Garmisch-Partenkirchen, May 1993, 137 pp.

[3] Schwikowski M., U. Baltensperger, H.W. Gäggeler, D.T. Jost, 1992, Measurements of concentration, chemical composition and size distribution of background aerosol at high alpine stations. *J. Aerosol Sci.*, **21**, Suppl. 1, S321-S324.

[4] Baltensperger U., H.W. Gäggeler, D.T. Jost, M. Schwikowski, 1993, Aerosol, radon, thoron and ^{210}Pb measurements with the epiphaniometer at the Jungfraujoch. P.M. Borell et al. (eds.), Proc. EUROTRAC Symposium '92, SPB Acad. Publ. bv The Gaure, pp. 550-554.

[5] Baltensperger U., H.W. Gäggeler, D.T. Jost, M. Emmenegger, W. Nägeli, 1991, Continuous background aerosol monitoring with the epiphaniometer. *Atmos. Environ.*, **25A**, 629-634.

[6] Gäggeler H.W., D.T. Jost, U. Baltensperger, M. Schwikowski, P. Seibert: Radon and thoron decay product and ^{210}Pb measurements at Jungfraujoch, Switzerland. Subm. to *Atmos. Environ.*

[7] Kasper A., H. Puxbaum, 1994, Determination of SO_2, HNO_3, NH_3 and aerosol components at a high-alpine background site with a filterpack method. *Analytica Chimica Acta*, **291**, 297-304.

[8] Baltensperger U. et al., in preparation.

[9] Liechti O., B. Neininger, 1993, ALPTHERM - a PC-based model for atmospheric convection over complex topography. Proc. OSTIV Congress 1993.

[10] Seibert P., H. Kromp-Kolb, U. Baltensperger, D.T. Jost, M. Schwikowski, A. Kasper, H. Puxbaum: Trajectory Analysis of Aerosol Measurements at High Alpine Sites. Proc. EUROTRAC Sympos. '94.

[11] Schwikowski M., P. Seibert, U. Baltensperger, H.W. Gäggeler: A study of Saharan dust at the high-alpine site Jungfraujoch. Submitted to *Atmos. Environ.*

[12] Prodi F., G. Fea, 1978, Transport and deposition of Saharan dust over the Alps. Proc. 15. ITAM, Grindelwald. Publ. SMA, **40**, 179-182.

[13] Maupetit F., 1992, Chimie de la neige de très haute altitude dans les Alpes Francaises. Thèse, CNRS-LGGE Grenoble / Univ. Paris VII, 246 pp.

INCREASE OF ERYTHEMAL EFFECTIVE IRRADIANCE WITH ALTITUDE BETWEEN INNSBRUCK (577 m a.s.l.) AND THE HAFELEKAR (2269 m a.s.l.)

Roland Silbernagl, Michael Salzgeber, Martin Huber, Mario Blumthaler, Walter Ambach

Institut für Medizinische Physik, Müllerstraße 44, 6020 Innsbruck

Abstract

The increase of solar irradiance with altitude between Innsbruck (Austria, 577 m a.s.l.) and the Hafelekar (Austria, 2269 m a.s.l.) was measured from October until December 1993 with Robertson-Berger Sunburn Meters, Eppley filterspectrometers and pyranometers. For the Robertson-Berger Sunburn Meter data, the increase with altitude amounts to 20±3 % per 1000 m on snow-free terrain in Innsbruck and snow-covered terrain at the Hafelekar, and to 15±2 % per 1000 m on snow-covered terrain at both stations showing the influence of albedo. On the contrary, the altitude effect of total irradiance determined with pyranometers amounts to 10±3 % per 1000 m, independent of the snow situation in Innsbruck. The altitude effect decreases with increasing wavelengths. Within the UV range this was determined to -0.5 % per 1000 m and per nm with the Eppley filterspectrometer. No systematic influence of turbidity and troposheric ozone was found.

1. Introduction

Solar UV irradiance is increasing with altitude above sea level, which is a consequence of smaller optical air masses at higher altitudes. On clear days, this increase (called altitude effect) depends on the wavelength and on the albedo at the stations. Turbidity and tropospheric ozone show minor influence. Therefore, the altitude effect varies in time and location, and no generally valid figure can be presented. An increase of UV irradiance results in a number of deleterious effects on the human organism, especially on the human skin (Ambach and Blumthaler, 1993). The Robertson-Berger Sunburn Meter (Berger, 1976) is generally accepted as an instrument to record erythemal effective irradiance, as its spectral sensitivity is well adapted to the erythemal action spectrum (Fig. 1). Because of the similarity between the action spectra for erythema and non-melanoma skin cancer (Madronich and de Gruul, 1994), the Robertson-Berger Sunburn Meter data are also relevant for non-melanoma skin cancer formation.

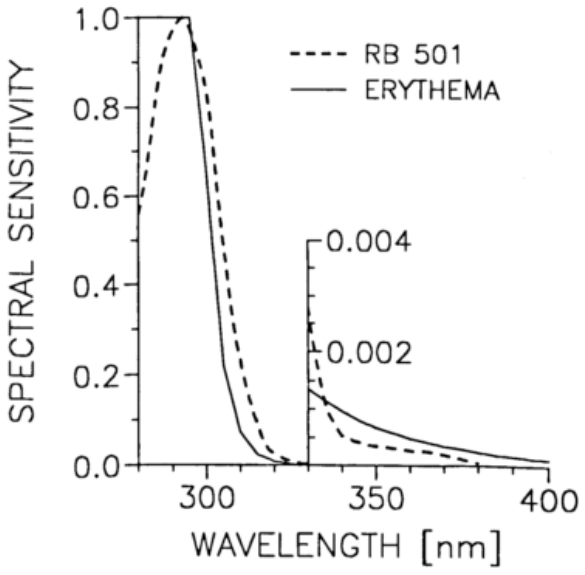

Fig. 1: Spectral sensitivity of the Robertson-Berger Sunburn Meter (RB 501) and the erythemal action spectrum according to McKinlay and Diffey (1987).

2. Materials and Methods

Between October 10, 1993, and December 31, 1993, measurements in Innsbruck (Austria, 577 m a.s.l.) and at the Hafelekar (Austria, 2269 m a.s.l.) were performed simultaneously. These two locations are appropriate for determination of the altitude effect because a relatively high difference in altitude (1692 m) is paired with a small horizontal distance (5.8 km). During the measurement period the surrounding of the mountain station was always snow-covered, whereas the situation at the valley

station changed from snow-free to completely snow-covered terrain. Identical atmospheric conditions can be assumed on clear days. Two Robertson-Berger-Sunburn Meters (Model 501) were used to measure the erythemal effective irradiance, and two Eppley filterspectrometers were used to determine the wavelength dependency of the altitude effect. Additionally, total irradiance (300 nm - 3000 nm) at both stations was determined with pyranometers. All instruments measured irradiances from the upper hemisphere (global irradiance). At the Hafelekar and in Innsbruck average values were taken over a time span of 10 minutes. Intercomparisons of the Robertson-Berger Sunburn Meters took place in Innsbruck from October 1 until October 9, 1993 and from January 9 until January 19, 1994 showing a mean deviation of less than 1 %. An intercomparison of the pyranometers in May 1994 showed a systematic deviation of less than 2 %. These systematic deviations are taken into account for the calculation of the altitude effect. The Eppley filterspectrometers were calibrated relatively to each other in April 1993 showing a statistical variation of ±2 %.

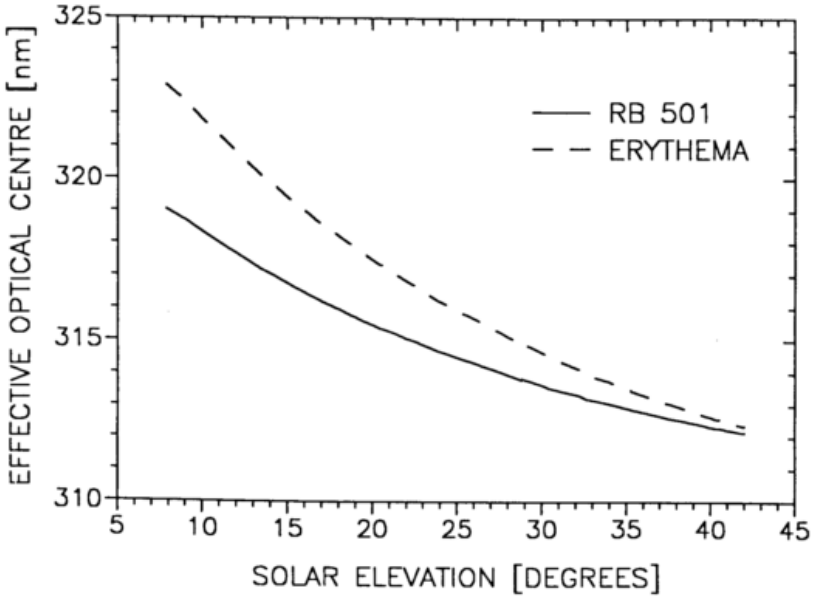

Fig. 2: Effective optical centres of the Robertson-Berger Sunburn Meter (RB 501) and the erythemal action spectrum as a function of solar elevation. The effective optical centres were calculated from high resolution spectral measurements of global solar irradiance with a double monochromator in Innsbruck on September 25, 1991. On this day, the total atmospheric ozone content amounted to 265±3 DU.

The Robertson-Berger Sunburn Meter is a broadband detector with its maximum sensitivity in the UVB region (Fig. 1). Its effective optical centre λ_{oc} is defined by

$$\lambda_{oc} = \frac{\int \lambda\, s(\lambda)\, I(\lambda)\, d\lambda}{\int s(\lambda)\, I(\lambda)\, d\lambda}$$

with $I(\lambda)$ specifying the spectral solar irradiance and $s(\lambda)$ specifying the instrument's spectral sensitivity. Fig. 2 shows the effective optical centre of the Robertson-Berger Sunburn Meter as a function of solar elevation, calculated from high resolution spectral measurements of global irradiance in Innsbruck on September 25, 1991. At high solar elevations the higher share of the short wavelengths in the solar spectrum causes a shift of the effective optical centre to lower wavelengths (Piazena, 1991).

The Eppley filterspectrometer (Goldberg and Klein, 1974) consists of a rotating filterwheel with eight interference filters centred every five nanometers between 290 nm and 325 nm with a halfbandwidth of about ±3 nm. The absolute spectral sensitivity in the channels was determined at the Physical-Technical Federal Institute in Braunschweig (Germany). Due to the small halfbandwidth the effective optical centres of the channels remain constant within ±0.3 nm for all solar elevations. In this study three channels with the effective optical centres at 313 nm, 317 nm and 324 nm were used (Blumthaler and Ambach, 1991).

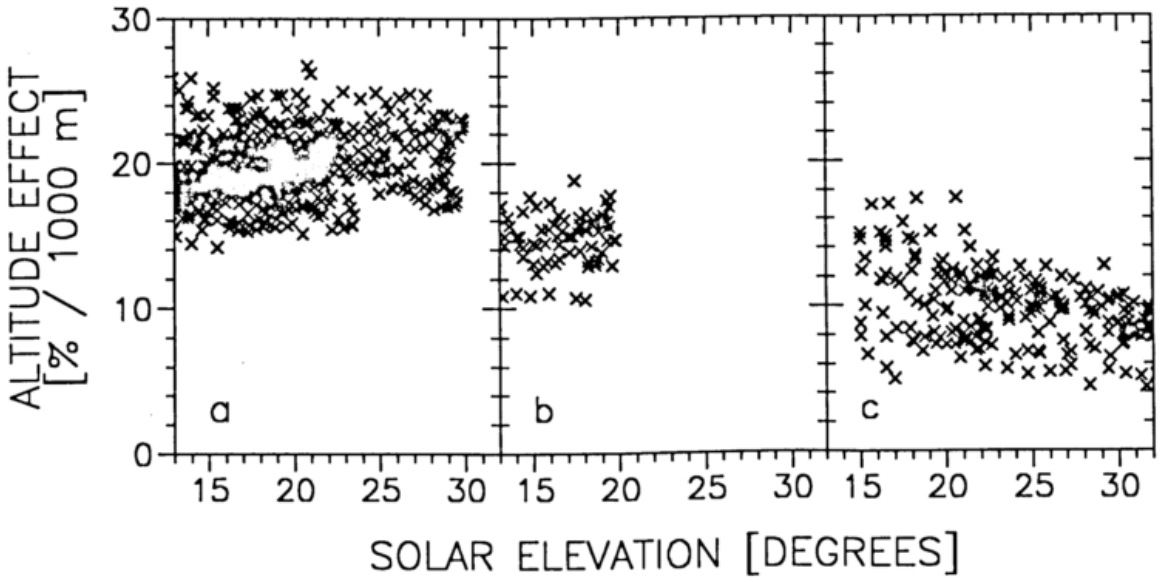

Fig. 3: Altitude effect between Innsbruck (577 m a.s.l.) and the Hafelekar (2269 m a.s.l.)
a: Robertson-Berger Sunburn Meter data, snow covered terrain at the Hafelekar, snow free terrain in Innsbruck
b: Robertson-Berger Sunburn Meter data, snow covered terrain at the Hafelekar and in Innsbruck
c: total irradiance (pyranometer data) for all conditions

3. Results

Fig. 3a shows the altitude effect of Robertson-Berger Sunburn Meter data on clear days with high albedo at the Hafelekar (snow-covered terrain) and with low albedo in Innsbruck (snow-free terrain). It amounts to 20±3 % per 1000 m (relative to the valley station) and is independent from solar elevation. Comparing this with the altitude effect obtained on snow-covered terrain at both stations leads to the conclusion that the altitude effect of the Robertson-Berger Sunburn Meter data decreases by 5 % per 1000 m on snow covered terrain at both stations (Fig. 3b). Due to the minor influence of turbidity and tropospheric ozone, no significant dependency of the altitude effect on these parameters could have been determined during this measurement period.

The altitude effect between Innsbruck and the Hafelekar is in accordance with the altitude effect for daily totals of the Robertson-Berger Sunburn Meter between Innsbruck and the Jungfraujoch (Switzerland, 3576 m a.s.l., horizontal distance Innsbruck - Jungfraujoch: 270 km), which amounts to 18±2 % per 1000 m in summer and to 23±6 % per 1000 m in winter (Blumthaler et al., 1993). Reiter et al. (1982) determined the altitude effect of daily totals within the spectral range from 310 nm to 340 nm between 14 % per 1000 m and 27 % per 1000 m, depending on the actual weather situation, including also clouds.

For comparison, Fig. 3c shows the altitude effect of total irradiance between Innsbruck and the Hafelekar on clear days determined with two pyranometers, which amounts to 10±3 % per 1000 m with a slight dependency on solar elevation. Again, this is in accordance with the altitude effect of total irradiance between Innsbruck and the Jungfraujoch amounting to 9 % per 1000 m for daily totals (Blumthaler et al., 1992). The stronger altitude effect of the Robertson-Berger Sunburn Meter data compared to that of total irradiance is due to the more effective backscattering of short wavelengths, which is a result of Rayleigh-scattering in the airmass between the two stations. Furthermore, the influence of albedo on global irradiance is caused by multiple scattering between the earth's surface and the atmosphere, which is also more effective for short wavelengths. Consequently, the influence of

albedo on the altitude effect can only be seen in the Robertson-Berger Sunburn Meter data and not in total irradiance.

The wavelength dependency of the altitude effect can be determined with the Eppley filterspectrometers. In September 1993, at 30° solar elevation the altitude effect for the channels with the effective optical centres at 313 nm, 317 nm and 324 nm amount to 21.0 %, 19.3 % and 15.6 % per 1000 m (relative to the valley station). From these values, the decrease of the altitude effect with increasing wavelength can be deduced to -0.5 % per 1000 m / nm. This also accounts for solar elevations others than 30°.

Due to small differences in the spectral sensitivity of the Robertson-Berger Sunburn Meter and the erythemal action spectrum, the effective optical centre for the erythemal action spectrum is slightly shifted to longer wavelengths compared to that of the Robertson-Berger Sunburn Meter, e.g. by 2 nm at 20° solar elevation and by less at higher solar elevations (Fig. 2). As a consequence, the Robertson-Berger Sunburn Meter overestimates the erythemal altitude effect, for example by 1 % per 1000 m at 20° solar elevation and by less at higher solar elevations, which is within the range of uncertainty and therefore practically negligible.

Acknowledgement

Gratitude is expressed to the "Daniel-Swarovski - Leopold-Franzens-Universität Innsbruck - Förderungsfond" and to the Austrian Academy of Sciences for financial support.

References

Ambach, W., Blumthaler, M. (1993) Biological effectiveness of solar UV radiation in humans. Experientia 49, 747-753

Berger, D. (1976) The sunburn ultraviolet meter: design and performance. Photochem. Photobiol. 24, 587-593

Blumthaler, M. , Ambach, W. (1991) Spectral measurements of global and diffuse solar ultraviolet-B radiant exposure and ozone variations. Photochem. Photobiol. 54, 429-432

Blumthaler, M., Ambach, W., Rehwald, W. (1992) Solar UV-A and UV-B radiation fluxes at two alpine stations at different altitudes. Theor. Appl. Climatol. 46, 39-44

Blumthaler, M., Ambach, W., Huber, M. (1993) Altitude effect of solar UV radiation dependent on albedo, turbidity, and solar elevation. Meteorol. Zeitschrift 2, 116-120

Goldberg, G., Klein, W. (1974) Radiometer to monitor low levels of ultraviolet irradiance. Applied Optics 13, 493-496

Madronich, S., de Gruul, F. (1994) Stratospheric ozone depletion between 1979 and 1992: Implications for biologically active ultraviolet-B radiation and non-melanoma skin cancer incidence. Photochem. Photobiol. 59, 541-546

McKinlay, A., Diffey, B. (1987) A reference spectrum for ultraviolet induced erythema in human skin. Commision Internationale de l'Eclairage (CIE)-Journal 6, 17-22

Piazena, H. (1991) Zum Einfluß atmosphärischer Ozonkonzentrationsänderungen auf die Erythemwirksamkeit der ultravioletten Sonneneinstrahlung an der Erdoberfläche. Z. Meteorol. 41, 273-282

Reiter, R., Munzert, K., Sladkovic, R. (1981) Results of 5-year concurrent recordings of global, diffuse and UV-radiation at three levels (700, 1800 and 3000 m a.s.l.) in the Northern Alps. Arch. Met. Geoph. Biokl., Ser. B 30, 1-28

O_3 and ^7Be Measurements in Atmosphere for the Study of Vertical Exchanges and Transport

R. Vecchi, G. Valli

Istituto di Fisica Generale Applicata - Universita' di Milano
Via Celoria, 16 - 20133 Milano (Italy)

In this paper we show the results of an ozone measurements campaign carried out during the years (1992-1994).
The monitoring station, managed by our Institute, is placed in Brunate (800 m sl) near Como, on Italian pre-Alps. This site is placed next to the lake Como, on the first mountains which separate the Po Plain from the Alps.
O_3 measurements carried out continuously are then analyzed as regards seasonally, daily and hourly trends.
Particular interest is addressed to the study of probable exchanges stratosphere-troposphere using the radionuclide ^7Be as natural tracer; correlations between high ^7Be activities and O_3 peaks contribute to the comprehension of these exchanges□

Ergebnisse der biometeorologischen Untersuchungen im Basislager des Broad Peak, Juni 1991

Cornelia Lüdecke
Valleystr. 40, D-81371 München

Abstract

During the German Medical Research Expedition Karakoram 1991, meteorological parameters, among others, were measured at basecamp of Broad Peak (4850 m) to describe environmental influences to human body due to height. Calculations with an energy budget model for different weather situations throw light on human energy budget in high mountain areas. Besides, there are indications for a higher pressure on the mountain peak in 8048 m than predicted by US-Standard Atmosphere.

Zusammenfassung

Während der Deutschen Medizinischen Forschungsexpedition Karakorum 1991 wurden im Basislager des Broad Peak (4850 m) u.a. auch meteorologische Parameter gemessen, um die höhenbedingten Umwelteinflüsse auf den Menschen beurteilen zu können. Rechnungen mit einem Energiebilanzmodel für verschiedenen Wetterlagen ergeben Anhaltspunkte über den menschlichen Energiehaushalt im Hochgebirge. Außerdem gibt es Hinweise auf einen höheren Druck am Gipfel in 8048 m als er als er von der US-Standardatmosphäre vorhergesagt wird.

1. Einleitung

Die Deutsche Medizinische Forschungsexpedition Karakorum 1991 (GEMEX K91) hatte sich zum Ziel gesetzt, während der Besteigung des Broad Peak (35°50'N und 76°38'0, 8047 m) die Auswirkung höhenbedingter Umwelteinflüsse auf den menschlichen Organismus zu untersuchen. So wurden neben den bergsteigerischen Tätigkeiten zeitweise im Basislager auch meteorologische Parameter zur Beschreibung der Umweltbedingungen im Hochgebirge gemessen.

2. Meteorologische und bergsteigerische Bedingungen

Am 6.6.91 wurde das Basislager auf der Mittelmoräne des Godwin-Austen-Gletschers in 4850 m am Fuße des Broad Peak aufgebaut. Die Einrichtung der Höhenlager in 5750 m, 6400 m und 7100 m mußte mehrfach wegen Schlechtwetterperioden (11.-12.6., 17.-23.6., 25.6., vgl. Abb.1) unterbrochen werden. Anschließend wehte bei meist klarem Himmel ein stetiger Höhenwind, der den ersten Gipfelversuch am 30.6.91 in ca. 7200 m beendete. Die Handanalyse des Indischen Wetterdienstes für 250 hPa 0000UTC zeigt die Wetterverhältnisse während des zweiten Gipfelversuches am 2.7.1991. Dieser Tag war durch ein ausgeprägtes Hoch mit Zentrum über Tibet gekennzeichnet, an dessen nordwestlichem Rand das Karakorum im Einflußbereich westlicher Winde lag (Abb.2). Nach den Modellrechnungen aus Radiosondendaten (West-Ost Höhenschnitt des Amtes für Wehrgeophysik) war in Gipfelhöhe des Broad Peak zur selben Zeit mit einer Windgeschwindigkeit von etwa 23 m/s (83 km/h) zu rechnen (Abb.3). Dieser Gipfelversuch scheiterte schließlich in ca. 7600 m vor allem wegen der dicken Neuschneedecke.
Im Mittel ergaben die meteorologischen Messungen im Basislager (8.6.-28.6.91) tagsüber zwischen 8 Uhr und 19 Uhr folgende Werte (Abweichungen): 3 (±5) °C Lufttemperatur, 60 (±30) % Luftfeuchtigkeit, 3 (±3) m/s Windgeschwindigkeit und 570 (±4) hPa Luftdruck (Abb.1).

3. Druckverhältnisse am Gipfel des Broad Peak

Da für die Besteigung von Achttausendern ohne Sauerstoff der Luftdruck in Gipfelhöhe von ausschlaggebender Bedeutung ist, wurde aus den Messungen im Basislager mit der barometri-

schen Höhenformel der Druck am Gipfel des Broad Peak (8047 m) abgeschätzt. Im Mittel lag er im dort Juni 1991 bei 381 hPa und damit um 11 hPa höher als der US-Standardwert für Juni bei 36°N (370 hPa). Dies würde einer Erniedrigung der Gipfelhöhe um rund 210 m auf 7837 m entsprechen. Die große Differenz beruht zum gewissen Teil auf der Wetterlage und der unterschiedlichen Temperaturabnahme im Hochgebirge im Vergleich mit der freien Atmosphäre. Leider gibt es keine Messungen in Gipfelhöhe, um die Abschätzung verifizieren zu können. Am Gipfel des Mt. Everest (8848 m) wurde beispielsweise eine Druckerniedrigung von 5,7 hPa gegenüber dem langjährigen Mittel aus Radiosondendaten in Dehli festgestellt (West 1983).

4. Biometeorologische Untersuchungen

4.1 Abkühlung

Zur Beschreibung der menschlichen Behaglichkeit im Basislager wurde die Abkühlung (K in W/m²) an je zwei Strahlungstagen und bedeckten Tagen mit folgender Formel bestimmt:

$$K = (33 - T)\,(12{,}12 + 11{,}6\sqrt{v} - 1{,}16\,v) \qquad T \text{ in } °C,\ v \text{ in m/s.}$$

Im Juni 1991 wurde das Wetter am Broad Peak bei Sonnenschein, geringer Luftfeuchte und hoher (niedriger) Windgeschindigkeit als „kalt" („kühl") empfunden und unter einer geschlossenen Wolkendecke bei hoher Luftfeuchte als „sehr kühl" (vgl. Tab.1). Hier zeigt sich vor allem der Einfluß der Windgeschwindigkeit.

4.2 Energiebilanz

Die menschliche Energiebilanz wurde in Abhängigkeit von den meteorologischen Bedingungen für alle Expeditionsteilnehmer (2 weibliche, 11 männliche) mit dem Programm MEMI (Höppe 1984) berechnet, wobei als Aktivität Wandern auf holprigen Untergrund angenommen wurde.

Personendaten				**Allgemeine Daten**	
	Alter	Gewicht	Größe		Aktivität
weiblich (N=2)	26 Jahre	60 kg	1,63 m	Tage ohne Schneefall	5 W/kg
männlich (N=11)	31 Jahre	76 kg	1,82 m	Tage mit Schneefall	6 W/kg

Für den Expeditionsteilnehmer (JW), der am 2.7.91 bis auf 7600 m vordrang, sind die vollständigen Ergebnisse der Energiebilanzrechnung zuzüglich der meteorologischen Daten beispielhaft in Tab. 1 zusammengefaßt. Tab. 2 gibt den Vergleich zwischen den weiblichen und männlichen Teilnehmern bzw. der unterschiedlichen Wetterbedingungen wieder. Die einzelnen Parameter unterscheiden sich an beiden Wetterlagen geschlechtsspezifisch. Durch die höhere Schweißrate und den entsprechend um 8 % höheren Benetzungsgrad der Bergsteiger ergibt sich im Vergleich mit den Bergsteigerinnen eine um 0,5 °C niedrigere Hauttemperatur, während der Gesamtwasserverlust bei bedecktem Himmel im Vergleich zum Sonnentag bei den Bergsteigern im Mittel um 25 % niedriger ausfällt und bei den Bergsteigerinnen um 27 %.

5. Schlußbemerkung

Die hier aufgeführten Ergebnisse können nur grobe Anhaltspunkte für die menschliche Energiebilanz im Hochgebirge geben, da nur bruchstückhafte Tagesgangmessungen vorliegen und die Meteorologie hinter den bergsteigerischen Tätigkeiten zurücktreten mußte. Die Ergebnisse sollen jedoch Anregungen für weitere Studien geben.

6. Literatur

Höppe, P., 1984, Die Energiebilanz des Menschen, Wiss. Mitt. Meteor. Inst. Univ. München, Nr. 49, 171 S.

West, J. et al., 1983, Barometric pressures at extreme altitudes on Mt. Everest: physiological significance, American Physiological Society, 1188-1194

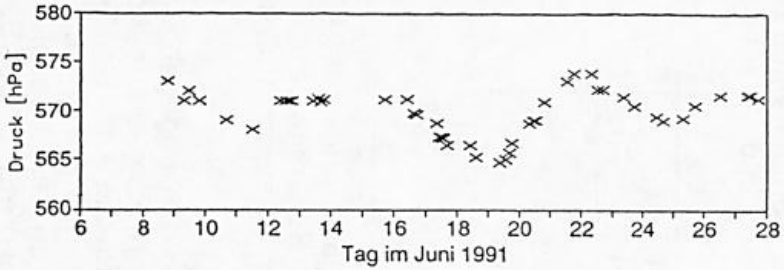

Abb.1: Luftdruck im Basislager des Broad Peak in 4850 m Höhe (8.6.-28.6.1991).

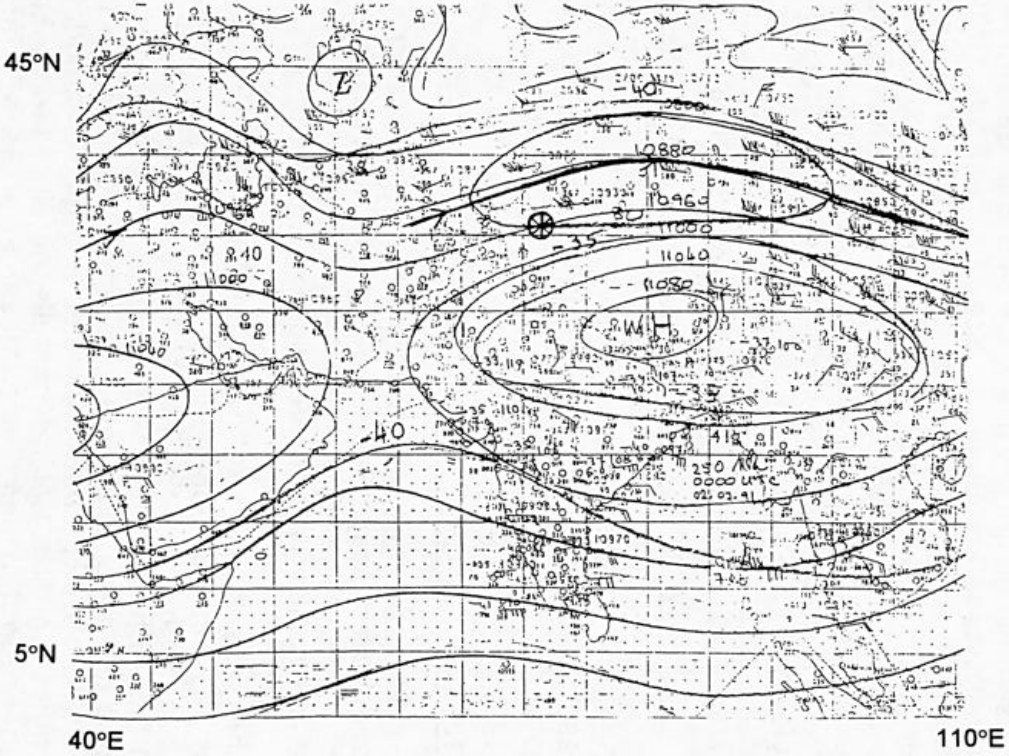

Abb.2: Handanalyse der Höhenwetterkarte für 250 hPa (2.7.1991, 0000UTC), freundlicherweise vom Indischen Wetterdienst, Dehli, bereitgestellt. + Gipfel des Broad Peak.

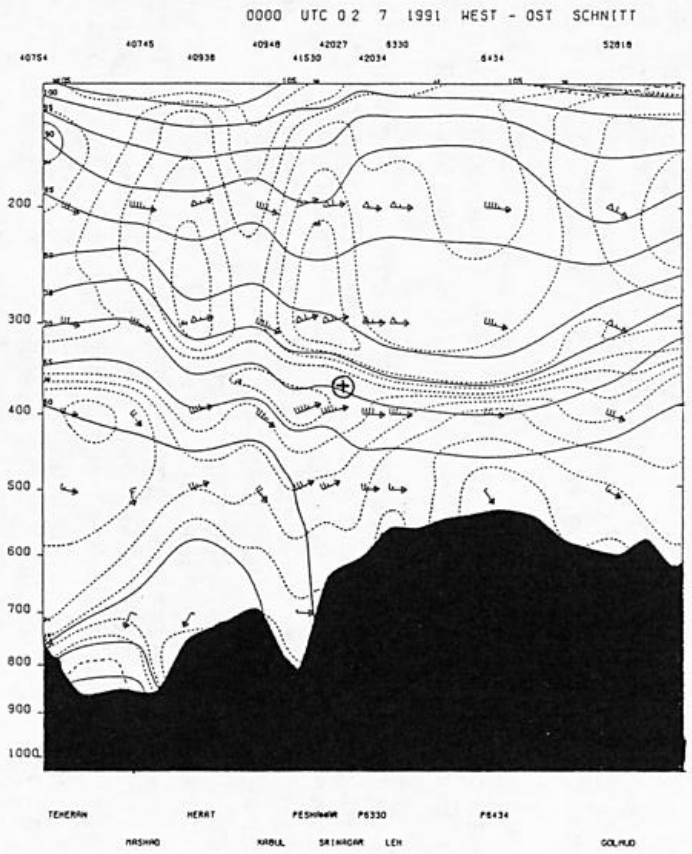

Abb.3: Aus Radiosondendaten berechneter W-O-Höhenquerschnitt (2.7.1991, 0000UTC), freundlicherweise von Amt für Wehrgeophysik, Traben-Trarbach, bereitgestellt. + Gipfel des Broad Peak.

Gebietsintegral des Regenniederschlags den Regenanteil am Abfluß abzuschätzen. Dabei werden folgende Annahmen gemacht:

- Der Höhengradient der Regenmenge wird vernachlässigt. Obwohl das Gesamteinzugsgebiet ein Höhenintervall von rund 1000 m umfaßt, ist dies zumindest für Einzelregenereignisse, um die es hier geht, gerechtfertigt, bei denen auf Grund des Niederschlagsbildungsprozesses nahezu keine Höhenabhängigkeit besteht (Lang, 1985).
- Die Fläche des aktuellen Regen-Einzugsgebietes umfaßt das konstante Gletschervorfeld und die apere Eisfläche des Gletschers, die mit guter Genauigkeit den bereits erwähnten täglichen Photographien des Gletschers entnommen werden kann.

Der Regenanteil am Abfluß ergibt sich damit aus der registrierten Niederschlagsmenge an der Pegelstation Vernagtbach, multipliziert mit der Fläche des Niederschlags-Einzugsgebietes, d.h. er wird wesentlich gesteuert von der Größe des aperen Eisgebietes. Dieser Parameter hat sich jedoch durch die vor allem seit 1982 aufgetretenen starken Massenverluste des Vernagtferners erheblich verändert, in dem Sinne, daß die apere Eisfläche, d.h. der Flächenanteil des Gletschers mit fehlender Zwischenspeicherung des Abflusses sukzessiv größer wurde. Hingegen nahm der Firnbereich, in dem Regen und Schmelzwasser gespeichert werden, fortschreitend an Ausdehnung ab. Für die Tagesmittelwerte des Gebietsniederschlags bedeutet das, daß eine vergleichsweise geringe Regenmenge im Jahr 1993 den gleichen Abflußbetrag liefert wie hohe Regenniederschläge in den ersten Jahren der Abflußregistrierungen. Umgekehrt ergeben z.B. 29 mm Regen, die am 7. August 1978 auf einen nur gering ausgeaperten Gletscher fallen, einen Abflußbeitrag von 0.67 m^3/s im Tagesmittel, während 25 mm Regen am 23. August 1993 bei weit ausgeapertem Gletscher 1.59 m^3/s lieferten.

In Tabelle 2, Spalte 3 sind diese Werte für fünf ausgewählte Tage aus dem Gesamtzeitraum zusammengestellt. Zusätzlich sind der Gesamtabfluß (Spalte 2), die Beträge der Eisschmelzwasserkomponente (Spalte 4) und die Größe des aktuellen Regen-Einzugsgebietes ("Regen-Fläche",Spalte 5) angegeben. Die letzte Spalte zeigt das Verhältnis aus der Summe von Regen- und Eisabfluß zum Gesamtabfluß, es gibt also an, wieviel Prozent des Gesamtabflusses an diesem Tag aus Regen und Eisschmelzung resultieren. Dies ist deshalb von großem Interesse, da diese beiden Abflußkomponenten die Tagesspitzen im Abfluß verursachen, während Schmelzung von Firn- und Altschnee nicht am gleichen Tag zum Abfluß beiträgt.

Datum	Gesamtabfluß [m*m*m/s]	Regenabfluß [m*m*m/s]	Eisabfluß [m*m*m/s]	Regen-Fläche km*km	%
7.Juli 1978	2.82	0.67	0.14	1.99	28
8.August 1980	4.46	0.24	0.08	1.98	7
19.Juli 1987	6.12	0.77	0.12	2.15	14
24.August 1987	5.55	1.34	0.43	3.00	32
23.August 1993	6.00	1.59	1.35	5.50	49

Tab.2: Tagesmittel des Gesamtabflusses (gemessen), des Regen- und des Eisschmelzabflusses (berechnet) in m^3/s, Einzugsgebiet des Regenabflusses in km^2 und prozentualer Anteil von Regen- und Eisabfluß am Gesamtabfluß für ausgewählte Tage im Vernagt-Einzugsgebiet

In den Jahren 1978 und 1980 umfaßte das Regen-Einzugsgebiet an den angegebenen Tagen nur das Vorfeld, dagegen war am 24. August 1987 das apere Eisgebiet schon mehr als 2 km^2 groß, am 23. August 1993 betrug die Fläche mehr als 3.5 km^2. Der Eisschmelzabfluß, d.h. der Teil des Abflusses, der aus dem Eisgebiet stammt, wurde unter Verwendung der meteorologischen Registrierungen an der Pegelstation Vernagtbach für die Jahre 1978 bis 1985 mit Hilfe eines Energiebilanzmodells (Escher-Vetter, 1980) auf der Basis eines digitalen Geländemodells mit einer räumlichen Auflösung von 100 m, einer zeitlichen von 1 h berechnet (Moser et al.,1986); für die späteren Jahre wurden Tagesmittelwerte mit vereinfachten Energiebilanzansätzen bestimmt.

THE STUDY OF INDUSTRIAL POLLUTION OF LINZ USING A DIFFUSION MODEL BY INCORPORATING THE MASS CONSISTENCY CONCEPT.

Thara V. Prabha , Erich Mursch -Radelgruber
Institut fur Meteorologie und Physik, Turkenchanzstrasse-18, Wien

ABSTRACT

Application of a K-type diffusion model is discussed for the city of Linz. The model runs are done for 24 hours by incorporating wind field for each hour from the mass consistent wind model. This study is intended to investigate the effect of the ambient flow on the locally generated wind and to look into the changes in the pollutant distribution with the routinely measured wind and the air pollution related data. The situation for 21st December 1991 is simulated with a changing (north westerly to south easterly) ambient wind .

INTRODUCTION

Linz is one of the big industrial city of Austria, which is situated in the basin of the Danube in the north of the 'Alpenvorland' and the southern edge of the 'Bohmische Masse '. To the north of the city, there are mountain ranges with a mean height of 800m. and to the south, a basin nearly 300m. above sea level. Under different ambient wind conditions, the local effects do have a significant role in the transport of pollutants. The aim of this study is to look into this aspect and to study the interaction between the ambient flow and the locally generated flow making use of the normally available observations.

An eulerian model based on the continuity equation for a pollutant is used. The available observations are incorporated in a mass consistency approach to get a better representation of the flow field . This is used as the wind input to the diffusion model to predict the pollutant levels.

DATA

The topography of Linz along with the locations of the stations are given in the figure(1). There were 9 surface stations including the observations at a 150 meters high tower. The wind observation taken at Giselawarte (situated 927m above sea level) is representative of the ambient wind. The temperature observations at the tower of Frienberg is the only one giving the information about the stability of the domain. All the available emission rates of SO_2 from the main sources are considered.

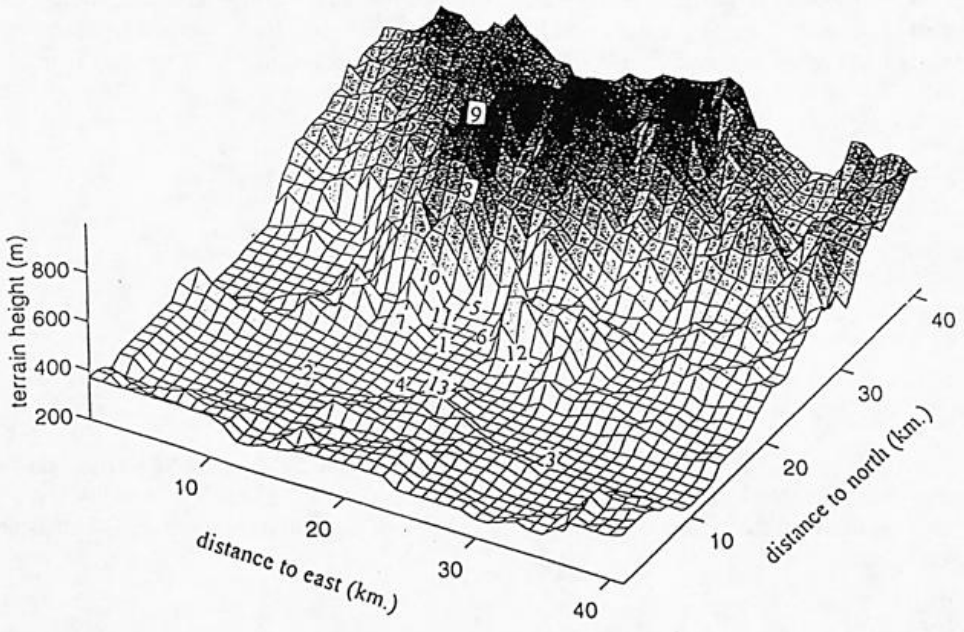

Fig. (1) : The topography of linz with the stations.

(1) - Hauserhof	(2) - Traun	(3) - Asten
(4) - Kleinmünichen	(5) - 24er-Turm	(6) - ORF-Zentrum
(7) - Freinberg (150m. tower)	(8) - Lichtenberg	(9) - Giselawarte
(10) - BH-Urfahr	(11) - Ursulinenhof	(12) - Steyregg
(13) - Berufschulzentrum		

K-MODEL

The advection diffusion equation for a passive scalar 'C' is given by,

$$\frac{\partial C}{\partial t} + \nabla . (UC) = D \nabla^2 C + R + Q \qquad (1.1)$$

(1) (2) (3) (4) (5)

where, the terms are (1) local rate of change , (2) the advection , (3) molecular diffusion , (4) chemical reaction rate and (5) the source for a pollutant with concentration ' C=<C>+C' ' and with the ambient wind 'U=(u,v,w)'. The molecular diffusivity is negligible compared to other terms. The velocity components and the concentration are expressed in terms of mean and turbulent parts and the Reynolds averaging gives,

$$\frac{\partial v<C>}{\partial y}+\frac{\partial u<C>}{\partial x}+\frac{\partial v<C>}{\partial y}+\frac{\partial w<C>}{\partial z}+\frac{\partial <u'C'>}{\partial x}+\frac{\partial <v'C'>}{\partial y}+\frac{\partial <w'C'>}{\partial z}=<R>+<Q>$$

The turbulent terms are parametrized in terms of K- theory, i.e., by expressing the turbulent fluxes in terms of the mean gradients of the concentration.,

$$<u'C'> = -K_{xx} \frac{\partial <C>}{\partial x}, \qquad <v'C'> = -K_{yy} \frac{\partial <C>}{\partial y}, \qquad <w'C'> = -K_{zz} \frac{\partial <C>}{\partial z}$$

where, '$K=(K_{xx}, K_{yy}, K_{zz})$'is the turbulent diffusivity tensor which is diagonal. This method can be applied only when the scales of changes in <C> is much greater than the scale of turbulent transport. The chemical reactions of the pollutant and the deposition at the surface are not incorporated in the present version of the model. The vertical advection is also assumed to be negligible. A terrain following co-ordinate system with $x \Rightarrow x$, $y \Rightarrow y$, $z \Rightarrow \sigma = H [(z-h(x,y)) / (H(x,y)-h(x,y))]$ is used . The sources are initialized with the available emission data. The boundary conditions are set to no turbulent transport across the boundaries. The horizontal components of the eddy diffusivities were kept constant and the vertical component was formulated based on the horizontal velocity (Reynolds,1973) . This does not include the effect of wind shear and vertical temperature structure. A (41 x 41 x 12) grid is used with a horizontal resolution of one kilometer and in the vertical, variable grid spacing is used. Method of fractional steps is used to solve the advection-diffusion equation. Each term is solved separately as a time dependent part and added up, to get the resultant concentration . Carlsons method (Richtmayer 1967) was used to solve the advection and Crank - Nicholson's (Crank-Nicholson,1947) method is used for the diffusion part.

$$\text{Source :} \quad \frac{\partial C}{\partial t} = Q_r \, \delta(x-x_r). \, \delta(y-y_r). \, \delta(z-z_r).$$

$$\text{Advection :} \quad \frac{\partial C}{\partial t} = -u \frac{\partial C}{\partial x}, \qquad \frac{\partial C}{\partial t} = -v \frac{\partial C}{\partial y}$$

$$\text{Diffusion :} \quad \frac{\partial C}{\partial t} = K_h \frac{\partial^2 C}{\partial x^2}, \qquad \frac{\partial C}{\partial t} = K_h \frac{\partial^2 C}{\partial y^2}, \qquad \frac{\partial C}{\partial t} = K_v \frac{\partial^2 C}{\partial \sigma^2}$$

The advection-diffusion equation is integrated with the inputs of wind fields and eddy-diffusivities and the emission rates. The time step used is 360 sec. The integration is done for 24 hrs.The wind field used must be divergence free to avoid the artificial generation or the loss of the pollutant. So a mass-consistent wind model is used .

WIND MODEL

Mainly two steps are involved in this procedure. First to objectively analyze the available observations to the regular grid points and then to reduce the divergence in the field using a divergence minimization criteria (Endlich ,1984). Thus the pattern of the observed phenomena is well inherent in the final flow field. The inputs of the model are the terrain heights at all grids and the available surface, upper level observations of temperature and wind and the average boundary layer height. The geostrophic wind is

calculated using the surface wind , temperature and the pressure observations and is used for the upper level wind interpolations.

RESULTS AND DISCUSSION

The wind model is able to represent the flow structure much accurately. The considered day of simulation is characterized by north-westerly ambient wind during the first half of simulation and later a south-easterly ambient wind. There was considerable mixing going on after 1000 hrs. Results at 1200 hrs. and 2100 hrs. are shown in figure (2) and (3) respectively.

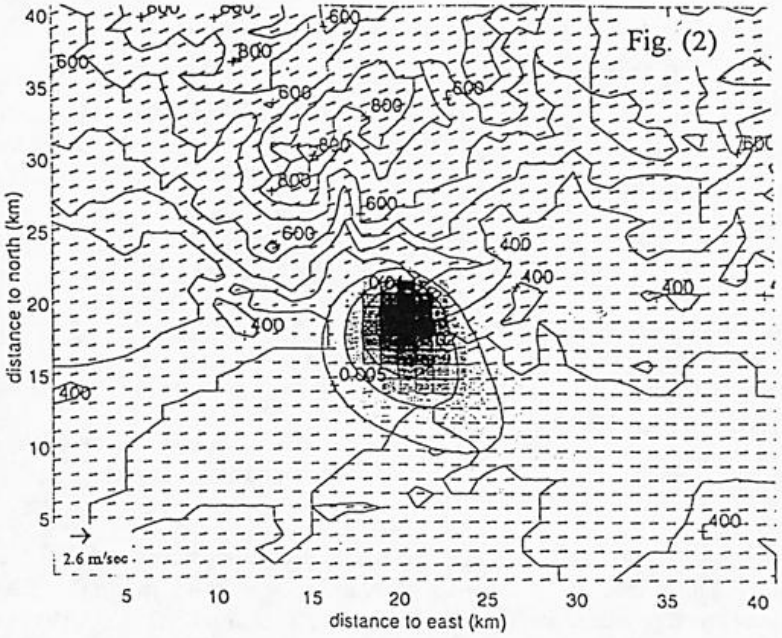

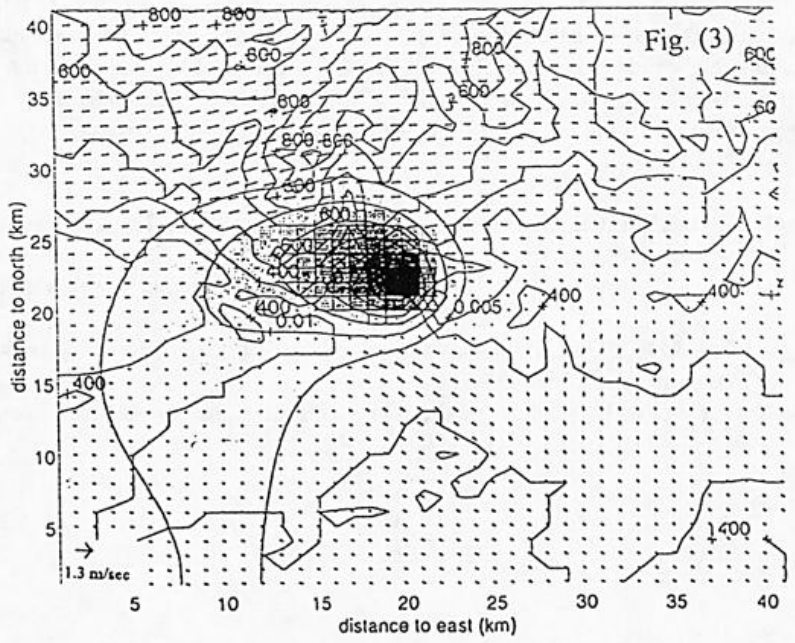

Fig. (2) & (3) : The distribution of SO_2 (in mg/m^3) at 1200 hrs. and 2100 hrs. respectively along with the elevation of the topography.

The model is able to simulate the meandering of the plume during the course of the day. The advection part is working well compared to the diffusion part. It is noted that the predicted concentrations are in better agreement with the observations in the first 1200 hrs.of integration at most of the stations especially at Steyregg, Berufschulzentrum, 24-er Turm, ORF-Zentrum (fig.(4)), Ursulinenhof, BH-Urfahr and Kleinmünichen. The deviations from the observation are less than a factor of three or less.

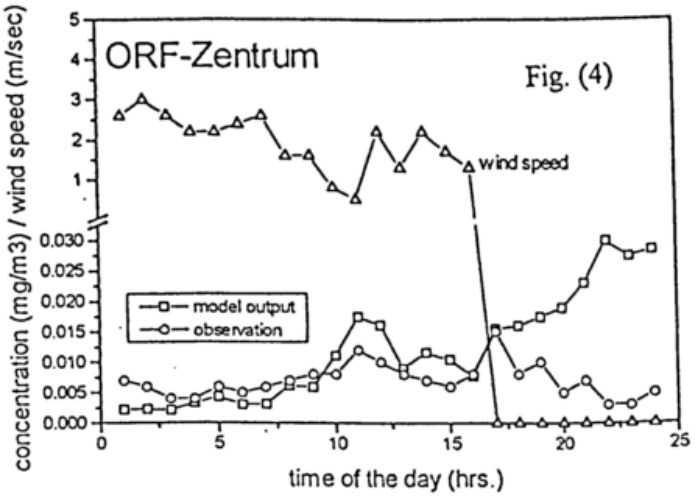

Fig. (4) : Diurnal variation of the concentration of SO_2 (observation and the model output) and the wind speed

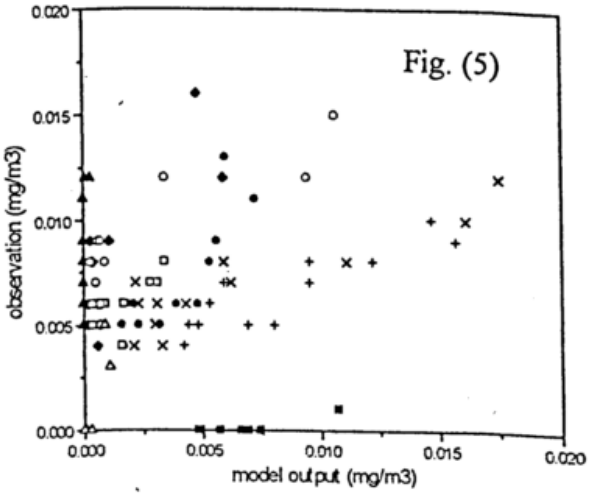

Fig. (5) : A comparison of the model outputs with the observations.

At Hauserhof there is an over prediction and at Traun, an under prediction through out the 24 hrs. compared to the observations. The predicted SO_2 verses obervations are shown in fig.(5). The daily changes in the SO_2 variations are reproduced well in the model output up to 1700 hrs. The observed changes in the ambient wind speeds are reflected well in the pollutant distributions through out the 24 hour simulation. There is an overestimate after 1600 hrs. attributed to the calm wind conditions. This feature is seen in the case of almost all stations. In the case of the station, ORF-Zentrum, this is shown in fig.(4). The diffusion parametrization, depending only on the kinetic energy of the ambient atmosphere, is failing to diffuse the pollutants even though the atmosphere is turbulent. The accumulation of the pollutant results in over predicting during low ambient winds (<1.5 m/sec). This proposes the need for including the effects due to atmospheric stability, which has not been considered in the present parametrization of the diffusivity. Further improvements to both the wind and the diffusion models are in progress.

REFERENCES

Crank,J.,Nicholson,P., (1947), A practical method for numerical solution of partial differential equations of heat conduction type. Proc. Cambridge Philos. Soc., 43, pp. 50-67

Endlich,R.M.., (1984), Wind energy estimates by use of a diagnostic model., Bound.-Layer Meteor., 30, pp.375-386

Reynolds,S.D., Roth,P.M.,Seinfeld, J.H.,(1973), Mathematical modelling of photochemical air pollution I. Formulation of the model . Atmos. Environ. 7, pp.1033-1061

Richtmayer,R.D., Morton,K.W.,(1967), Difference methods for initial value problems. Intrscience, NewYork.

Air Pollution on the hills around the Thermal Power Plant Šoštanj

T.Planinšek, I. Čuhalev
Hydrometeorological Institute of Slovenia
Milan Vidmar Electroinstitute

ABSTRACT

The Thermal Power Plant Šoštanj lies in the valley, surrounded by forests overgrown slopes. Its SO2 emission varies from 80000 to 90000 tons per year. Monitoring system for air quality around Šoštanj power plant consist of six fixed and one mobile station. Results of measurements show that 2 to 5 % of time concentrations exceed 500 µg/m3. There are different weather conditions causing high SO2 concentrations. About half high concentrations appear at anticyclone weather connected with subsidential temperature inversion. Another half of cases are caused by moderate to strong winds from different directions, bringing plume gases directly from the stacks to surroundings.

1. INTRODUCTION

The Thermal Power Plant Šoštanj is the greatest SO2 emission source in Slovenia. It has 750 MW electrical power and burns the lignite from the nearby Velenje coal-mine. This lignite has high content of sulphur which causes high SO2 emission Complex terrain around Šoštanj at disadvantageous weather conditions causes high SO2 concentrations and damage on vegetation on the slopes of the hills around Šaleška dolina valley, where the Thermal Power Plant Šoštanj is located. SO2 emission The Thermal Power Plant Šoštanj influences on air quality not only on near surroundings but also on greater distances, in southern Austria too /4/.

2. SITE AND SO2 EMISSION

Šoštanj is situated in the valley which is about 10 km long and 4 km wide. It lies on 360 m altitude. The peaks of the hills in Northeast, Northwest and directions at the distance about 20 km from the power plant exceed the altitude of 1500 m. About 5 km to the North from the power plant rises a ridge with 700 m to 900 m altitude, on the south there are smaller hills with altitudes between 500 m and 700 m.
The Thermal Power Plant Šoštanj consists of 5 blocks with electrical powers: block I-III 150 MW, block IV 275 MW and block V 325 MW. It has 3 stacks, 100 m for blocks I-III, 150 m for block IV and 230 m for block V. When projects for blocks IV and V have been made, desulphurisation was provided for later time. The stack heights for blocks IV and V were determined to protect settlements in Šaleška dolina valley. Because of the low ground inversion the height of those two stacks are sufficient for that purpose.
The lignite from the nearby Velenje coal-mine has low heating value, about 10 MJ/kg and contains about 1.5 % of sulphur. This is the reason of great SO2 emission which varies from 80000 to 90000 tons per year. This emission is greater than total SO2 emission in whole Austria. The greater part of SO2 is released from the height two stacks. SO2 emission is measured on blocks IV and V. Desuphurisation device on block IV is in construction and is planned to begin to operate in autumn 1994. Desulphurisation for block V is also planned, but the financial problems has to be solved.

3. THE INFLUENCE OF THE SO2 EMISSION IN THE SURROUNDINGS.

Šaleška dolina valley is seldom influenced by SO2 emission from the power plant. It occurs only at strong southerly wind, which causes a vortex on the lee side of 100 m high hill 200 m south from the power plant and pushes flue gases from the stack down towards the ground. On the hills around the high SO2 concentrations appears in two weather situations /1,2/:
- subsidential temperature inversion due to anticyclone at approximately 1000 m altitude
- moderate to strong Southwest wind connected with approaching weather front

On slopes Northwest from the power plant, where the most severe damage on forest was observed, very high SO2 concentrations occur at night and early morning in case of temperature inversion and very weak wind. During daytime, the highest SO2 concentrations occur if the wind blows in direction from the power plant, moving upwards the mountain slopes. On the ridge Northwest from the power plant high concentrations prevail at Southwest wind. On the top of the hill south from the power plant high concentrations are frequent at Northwest wind.

4. MEASURING NETWORK

A network of six monitoring stations was built around the Thermal power plant Šoštanj to monitor the influence of SO2 emission from the power plant. Three of them are located in the Šaleška dolina valley in two towns Šoštanj and Velenje and in spa Topolšica. Other three were put on the slopes of the valley where the most severe damage on forests were observed: Veliki vrh, 550 m altitude, 2.6 km south from the power plant, Zavodnje, 770 m altitude, 7.6 km Northwest

from the power plant and Graška gora, 774 m altitude, 7.2 km Northeast from the power plant. System includes also a mobile unit, which is monitoring air pollution at several locations for a period of few months. Continuous SO2 concentrations, air temperature, relative humidity and wind speed and direction measurements are recorded as half-hour measurements on monitoring stations and are transferred to central unit in power plant. At Zavodnje NOx and ozone concentration monitoring also take place. On the basis of that data the regional authority for environment are taking emergency measurements for episode control. By taking emergency measurements appears the problem that duration of high concentrations is mostly limited on short period, mostly from one to few hours. In some situations, about 30-40 % of high concentrations, the air pollution pattern from stack to monitor lasts some hours and immediate reduction of emission from the power plat after measured high concentration at one monitoring site has no effect. Because of that reason prediction of high SO2 concentrations probability is necessary as long as desulphurisation on blocks IV and V do no operate and this work is a small contribution to the basis for such predictions.

5. WORKING METHOD

In this work monitoring the results for years 1992 and 1993 from three upper stations of monitoring system are considered. At first high SO2 concentrations above 500 µg/m3 were chosen from all data. For this cases the frequency distribution by half-hour intervals during the day was made. We also considered the wind condition and stability of the atmosphere in two layers at such situation. The temperature differences from station Veliki vrh and Zavodnje for layer between 550 and 770 m altitude and temperature differences from station Zavodnje and Kum (a station from the monitoring system of Thermal Power Plant Trbovlje, 31 km south from Šoštanj) for layer between 770 m and 1210 m altitude were computed. Temperature differences were classified into four stability classes.
Table 1 shows SO2 concentrations frequency distribution at Veliki vrh, Zavodnje and Graška gora. About 1,5 to 2 % of half-hour SO2 concentrations measurements exceed value 500 µg/m3. Higher SO2 concentrations are more frequent at Veliki vrh than at Zavodnje and Graška gora.

Table 1: Distribution of SO2 concentrations into intervals for measurements in years 1992 and 1993 (number of cases):

SO2 concentration	Veliki vrh	Zavodnje	Zavodnje
0 - 250	30612	28909	30261
250 - 500	1598	1057	1036
500 - 750	534	278	280
750 - 1000	134	83	82
1000 - 1250	49	39	30
1250 - 1500	18	19	16
1500 - 1750	13	6	7
1750 - 2000	2	3	2
2000 - 3000	2	4	4
3000 - 4000	0	3	1
> 4000	0	0	1
missing	1795	2401	2326

Picture 1 shows half-hour SO2 concentrations frequency during the day. Higher SO2 concentrations at Veliki vrh are the frequent in early morning and morning but they are rare in afternoon. In the afternoon the atmosphere is less stable, plume rise is higher and SO2 emission from power plant less affect Veliki vrh area. There are two peaks of high SO2 concentration frequency at Zavodnje: after midnight and in morning and forenoon. The first peak is connected with downslope night breeze which brings polluted air from the polluted air layer on altitude between 800 and 1000 m /3/. The most often this polluted layer is created due to weak wind under subsidential temperature inversion at anticyclone weather situation. In forenoon, often after night high concentrations, wind turns due to warming valley slopes by sunshine, to Southeast direction bringing the plume from the power plant directly to Zavodnje area. In the afternoon the atmosphere is less stable, plume is diluted into greater volume and concentration fall. At Graška gora high SO2 concentration is more frequent during the night because of more stable atmosphere.

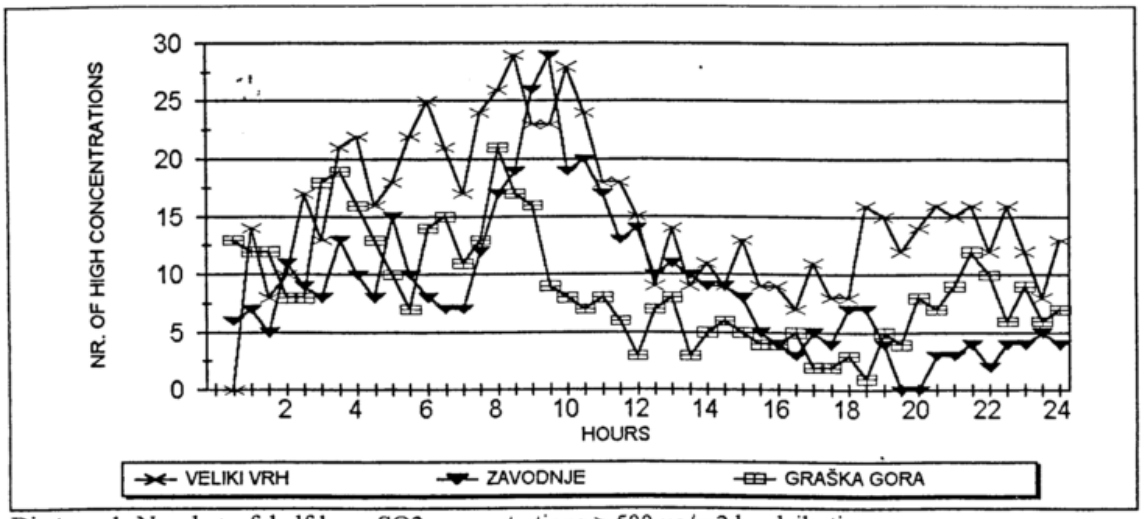

Picture 1: Number of half-hour SO2 concentrations > 500 µg/m3 by daily time.

Table 2: Wind data for situations with SO2 concentration > 500 µg/m3 for three stations (number of cases divided into wind speed classes and wind direction).

		wind direction							
	wind speed	N	NE	E	SE	S	SW	W	NW
VELIKI VRH	< 1 m/s	49	134	42	11	4	4	8	7
	1 - 3 m/s	99	319	9	6	0	0	5	4
	3 - 5 m/s	0	0	0	0	0	0	0	0
	> 5 m/s	7	38	0	0	0	0	0	0
ZAVODNJE	< 1 m/s	47	52	39	62	19	15	24	25
	1 - 3 m/s	9	5	0	114	18	5	1	0
	3 - 5 m/s	0	0	0	0	0	0	0	0
	> 5 m/s	0	0	0	0	0	0	0	0
GRAŠKA GORA	< 1 m/s	2	3	18	14	28	33	14	4
	1 - 3 m/s	10	9	11	5	10	238	15	1
	3 - 5 m/s	0	0	0	0	0	0	0	0
	> 5 m/s	0	0	0	0	0	6	0	0

The wind data is shown in table 2. Data are distributed into intervals according wind direction and wind speed. The first establishment is, that high SO2 concentration appears at weak wind. Significant wind direction for locations Veliki vrh and Graška gora at high SO2 concentration is from the power plant, that means north wind at Veliki vrh and Southwest wind at Graška gora. Average half-hour wind speed have been most frequent in the range from 1 to 3 m/s. In some cases wind speed was considerably great. Wind situation at high SO2 concentration at Zavodnje is different. In the most cases the wind was blowing upslope - Southeast wind, but there are also a lot of cases at downslope breeze with prevailing northeast direction. Considering picture 1 the cases with SE wind belong to morning hours...

Table 3: Atmosphere stability classes frequency for two layers for situations with SO concentration > 500 µg/m3 (number of cases).

		atmosphere stability				
	layer	-	U	N	s	S
VILE HRH	550 - 770 m	23	9	350	264	106
	770 - 1210 m	216	53	355	97	31
ZAVODNJE	550 - 770 m	1	3	230	174	27
	770 - 1210 m	75	39	221	83	17
GRAŠKA GORA	550 - 770 m	15	90	268	48	1
	770 - 1210 m	41	54	206	20	1

For the cases with high SO2 concentration the analysis of the temperature differences between tree stations: Veliki vrh (550 m), Zavodnje (770 m) and Kum (1210 m) was made. They were divided into four classes: U (unstable) if temperature gradient was < -1°C/100 m, N (neutral) if temperature gradient was >= -1°C/100 m and < 0 °C/100 m, s (slightly stable) if temperature gradient was >= 0°C/100 m and < 1°C/100 m and S (very stable) if temperature gradient was >=1°C/100 m. Sign - denotes missing measurements. Number of high SO2 concentrations at Veliki vrh and Zavodnje is about the same at stable and at neutral atmosphere and are seldom at unstable condition. The situation at Graška gora is different while most of observed high SO2 concentration cases appear at neutral and unstable atmosphere.

Table 4: Comparison of atmosphere stability classes for two layers for situations with SO concentration > 500 µg/m3 (number of cases).

	STABILITY OF 550 - 750 m LAYER	STABILITY OF 770 - 1210 m LAYER			
		N	3	S	-
VELIKI VRH	U	3	18	0	1
	N	201	58	11	77
	s	118	18	13	69
	S	31	0	7	50
	-	2	0	0	19
ZAVODNJE	U	2	20	0	1
	N	142	49	2	31
	s	76	14	7	39
	S	1	0	8	4
	-	0	0	0	0
GRAŠKA GORA	U	84	17	0	3
	N	185	2	1	27
	s	29	0	0	8
	S	0	1	0	0
	-	8		0	3

There is no sense to make correlation between SO2 concentrations from three monitoring stations for all the data because of small portion of high concentrations. Therefore the comparison was made only for concentration > 500 µg/m3 at each station. Table 5 shows SO2 concentration frequency distribution at other two stations when at first station SO2 concentration exceeded 500 µg/m3. It can be seen from the table 5 that there are some situations with high concentration both at Veliki vrh and Zavodnje and very seldom high concentration at the same time at Graška gora and at one of other two stations.

Table 5: SO2 concentration frequency distribution at other two stations when at first station SO2 concentration exceeded 500 µg/m3 (number of cases).

station with > 500 µg/m3	Veliki vrh		Zavodnje		Graška gora	
SO2 concentration	Zavodnje	Graška gora	Veliki vrh	Graška gora	Zavodnje	Veliki vrh
0.0 - 250.0	571	673	341	397	386	374
250.0 -500.0	67	15	52	14	10	22
500.0 -750.0	18	2	19	5	1	6
750.0 -1000.0	4	0	3	3	1	4
1000.0 -2000.0	2	0	3	2	0	0
2000.0 -3000.0	1	0	0	0	0	0
>3000.0	0	0	0	0	0	0
missing data	0	39	17	14	22	14

6. CONCLUSION

High SO2 concentration over 500 µg/m3 on the slopes around the thermal power plant Šoštanj appears at about 1.5 to 2 % of time. They are most frequent in morning and forenoon. At location Zavodnje, Northwest from Šoštanj, high concentration are most common at presence of anticyclone and subsidential temperature inversion. Weak downslope wind at night brings polluted air from the polluted cloud, formed at night above the valley and morning upslope wind brings pollution directly from the power plant. The transport from stack to monitor station lasts at night some hours, in the morning about one hour. Some night SO2 high concentrations at Veliki vrh and Graška gora are caused mostly by similar mechanism as at Zavodnje. But most of that situations are the consequence of moderate to strong wind in direction from the power plant. The situations with simultaneous high concentration on more than at one monitoring station is not very frequent. High SO2 concentration around the Thermal Power Plant Šoštanj can be avoided only to put in operation desulphurisation units on blocks IV and V and to stop operating blocks I - III.

7. LITERATURE

1. Hydrometeorological Institute of Slovenia: Air Pollution in Slovenia, April 1990 - March 1991
2. Hydrometeorological Institute of Slovenia: Air Pollution in Slovenia, April 1991 - March 1992
3. Jožef Stefan Institute: Pollution Analyses of the Šoštanj Basin, Work report N°.:6680, Ljubljana, february 1993
4. K. Radunsky: Abshätzung der Immissionbelastung für die Umgebung des Dampfkraftwerkes Šoštanj/ Slowenien, Umweltbundesamt Wien, Dezember 1993

BACK-GROUND AIR POLLUTION ON MOUNTAIN MEDVEDNICA

[1]N. Šinik, [2]E. Lončar, [1]A. Marki

[1] Department of Physics, Faculty of Science, University of Zagreb, Croatia.
[2] Meteorological and Hydrological Service, Zagreb, Croatia.

ABSTRACT

A theory of the background pollution has been derived which enables to determine a local background pollutant concentration, C_b, by means of simultaneous series of wind velocities and pollutant concentrations data. The value of C_b can be obtained as a limit of a pollutant concentration, C, when wind velocity approaches its maximum. That way the background value of SO_2 concentrations at Puntijarka (988 m high, Medvednica mountain) was determined for the general case and particularly for winds from the city of Zagreb (southeastern foot of Medvednica). An intercomparison of these C_b values proves the top of Medvednica reliable for the detection of pollutants brought to the northeastern Croatia by air streams from distant emission sources.

1. INTRODUCTION

An exact definition of the background pollution, C_b, is not generally adopted and it is often described as a concentration of pollutants brought to a given locality by the long-range transport (Szepesi & Fekete, 1987). Having no such data, as might be the case elsewhere, we have evaluated a specific approach, which enables a determination of the local background pollution by means of local series of wind velocities and measured concentrations of a given pollutant.

For that purpose we define the local background pollution as a possible minimum concentration that cannot be cleaned away any longer by local winds and turbulent diffusion - and derive a theoretical basis for such an approach (Lončar & Šinik, 1993). We have solved analytically a simplified form of the equation of diffusion for a stationary case of the background pollution. Making use of the surface layer similarity one finally gets to the following form of the solution:

$$C = C_o \exp\left[\frac{u_* s}{V S} + \left[\frac{z}{k S}\right]^{1/2} \Phi_m\right] \qquad (1)$$

Here, C is the concentration of the given pollutant, C_o its minimum value at the ground, u_* is friction velocity, V wind velocity, Φ_m universal similarity function, S length of the area under consideration, s and z horizontal and vertical coordinates and k - von Karman's constant. For constant values of s, z and S the concentration C changes only with u_*/V and Φ_m (which implies the influence of turbulent diffusion). A background pollution is now defined as:

$$C_b = \lim_{\substack{V \to \infty \\ \Phi_m \to 0 \text{ (unstable PBL)}}} C \qquad (2)$$

Based on (1) and (2) a practical graphical method has been evaluated to determine the local value of background pollution by means of simultaneous

series of C and V with Φ_m implicit in the procedure. One enters the diagram with axes lnC and u_*/V. According to (1) lnC should decrease with decreasing values of u_*/V. Intersection of straight lines through points on such a diagram with the axes $u_*/V=0$ present various $\ln C_o$ values, corresponding to the limit case of $V\to\infty$. The uppermost and lowest enveloping straight lines (see figures) determine the interval of possible $\ln C_o + (z/kS)^{1/2}\Phi_m$ values. The lower boundary value corresponds to $\ln C_b = \lim_{\Phi_m\to 0} [\ \ln C_o + (z/kS)^{1/2}\Phi_m\ ]$, i.e. it gives the final C_b value.

2. BACKGROUND POLLUTION ON PUNTIJARKA

Puntijarka is the meteorological station at 988 m height near the top (1033 m) of the mountain Medvednica. If its background pollution is negligible it can be included into the network of regional stations for monitoring long-range pollutants transport.

We applied our method to series of daily SO_2 concentrations and wind velocities, V, during the winter months of the period 1987-1990 (completed with data from 1981-1984). Simultaneous $C(SO_2)$ and V data are presented on the figure 1a with the values of $lnC(SO_2)$ against u_*/V (u_* taken to be 1.0 m/s) on the figure 1b.

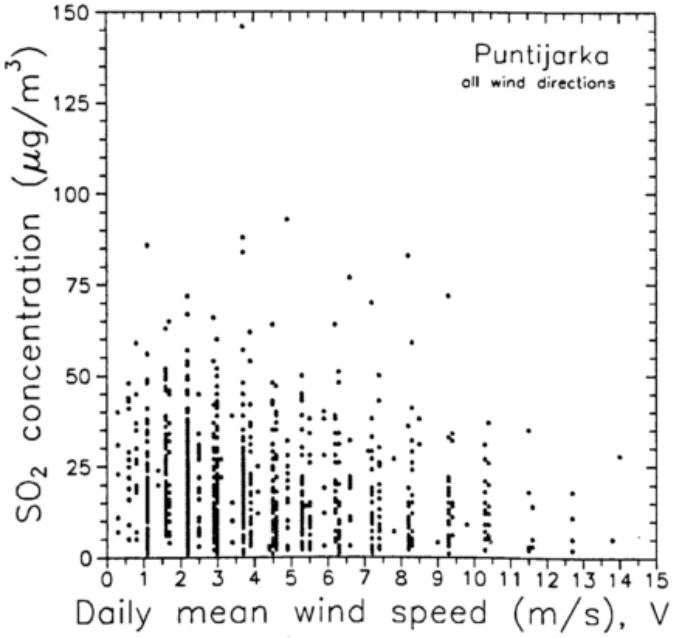

Figure 1a

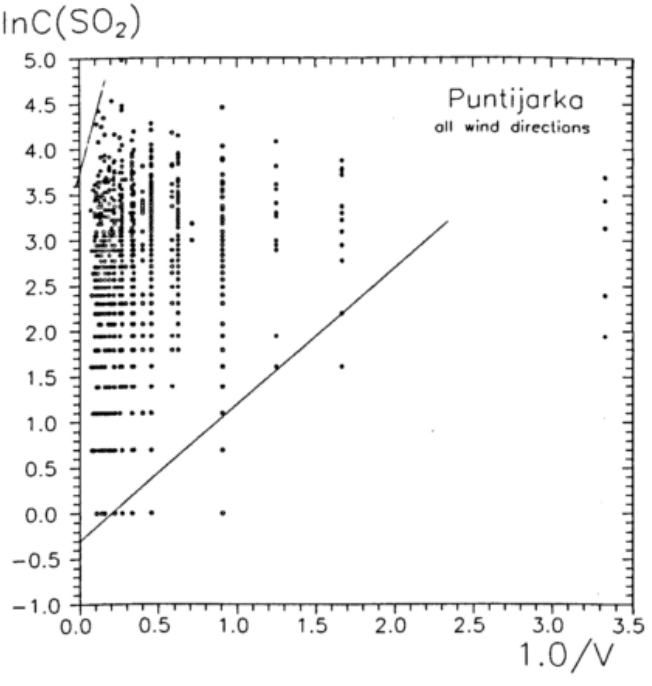

Figure 1b

Figure 1a. $C(SO_2)$ dependence upon wind velocity, V, Puntijarka, 988 m, December, January and February (1987-1990).

Figure 1b. Graphical determination of C_b.

SO_2 concentrations illustrate first an increase with the wind velocity up to about V = 2.0 m/s and further on they decrease very slowly (Fig. 1a). Two enveloping straight lines (for V > 2.0 m/s) define on the (1.0/V) = 0 axes the interval $-0.3 \le \ln C_o \le 3.7$, whose lower boundary gives $C_o = 0.74\ \mu g/m^3$. Obviously, the background pollution on Medvednica top is almost negligible.

3. C_b DEPENDENCE UPON THE WIND DIRECTION

The increase of $C(SO_2)$ with wind velocity up to V = 2.0 m/s indicates rather strong emission sources in the surrounding of a radius around 170 km (2.0 m/s * * 3600 s * 24 hours). Since Zagreb, the capitol of Croatia, is situated inside this area on the southeastern part of Medvednica, we have repeated the analysis only for wind directions from Zagreb to Puntijarka. The results (Figs. 2a and 2b) suggest that, in spite of having a maximum of SO_2 concentrations in winter, Zagreb is "not guilty" for maximum concentrations at Puntijarka, since now the upper values of $C(SO_2)$ are less (Figs. 2a and 2b).

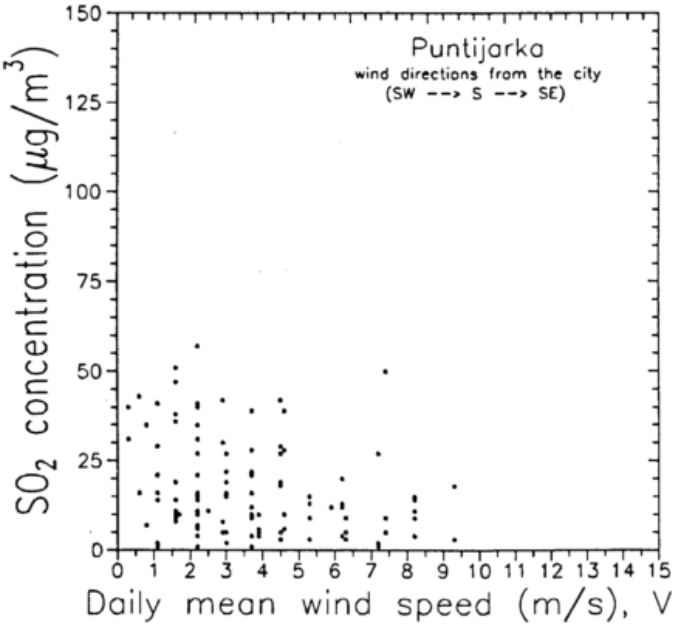

Figure 2a

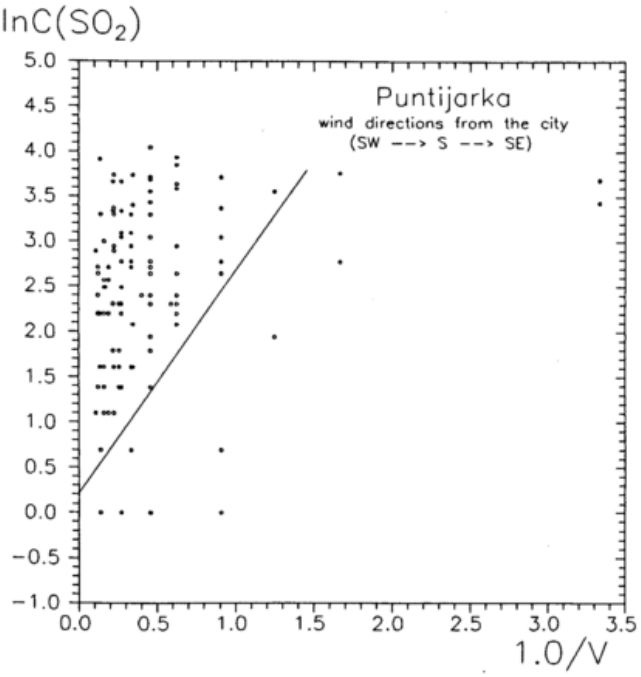

Figure 2b

Figure 2a. $C(SO_2)$ dependence upon wind velocity, V, Puntijarka, 988m, December, January and February (1987-1990).

Figure 2b. Graphical determination of C_b.

Still, if we exclude some separated points on the diagram, the background pollution at Puntijarka appears to be a little bit greater (C_b = 1.22 $\mu g/m^3$, i.e. $\ln C_b$ = 0.2). This is again very small value and allows Puntijarka to remain representative for the long-range pollutant transport assessment.

A possible relationship between background pollutions in Zagreb and at Puntijarka intrigues additional investigations.

4. REFERENCES

Lončar, E. & N. Šinik (1993): Local background air pollution in response to coastal circulation. 20th International Technical Meeting on Air-Pollution Modelling and its Application, Valencia, Spain, November 29 - December 3 1993, 469-471.

Szepesi, D.J. & Fekete, K.E. (1987): Background levels of air and precipitation quality for Europe, Atm. Environ. 21, 1623-1630.

METEOROLOGICAL CONDITIONS DURING ELEVATED OZONE CONCENTRATIONS IN SLOVENIA

T. Cegnar, M. Lešnjak

Hydrometeorological Institute of Slovenia, Vojkova 1/b, 61000 Ljubljana, Slovenia

1. Introduction

For the period 1991-1993 the occurrences of short-term elevated ozone concentrations were examined. The hourly value of 150 $\mu g/m^3$ was used in comparisons for the following two reasons: firstly, this value has been proposed as the UN ECE critical level for ecosystems (ECE, 1988) and secondly, it is the lower limit of the WHO guideline value aimed for the protection of human health (WHO, 1987).

For meteorological analysis of the elevated ozone concentrations, synoptic situations, local meteorological conditions (solar radiation, wind speed, air temperature) and trajectories at the 850 and 700 hPa pressure level were checked.

Ozone measurements are performed by continuous UV absorption instruments (Monitor Labs, Model 8810) being calibrated automatically once a day. The two sites were examined: Krvavec (1740 m a.s.l.), a mountain site, and Ljubljana-Bežigrad (299 m a.s.l.), an urban site. Mt. Krvavec is situated on the ridge of the south-eastern Alps, 25 km north of Ljubljana. The measurement site is situated on the south-western slope at the height of 1740 m a.s.l., while the nearby mountain peak is 1853 m high above the sea level. The top of the mountain and its surroundings are covered with grassland, conifers and rocks while slopes at the lower altitudes are mostly wooded. The site is opened towards the most frequent wind directions over Slovenia. Mt. Krvavec is a ski-resort with no permanent inhabitants and no substantial local emission sources. Ozone is sampled on the broadcasting station, 12 m above the ground. Ozone measurements started in March 1991. From 1992 it is also an EMEP and EUROTRAC TOR measurement site.

The station Ljubljana-Bežigrad is situated 1 km from the city centre; the monitoring site is not directly influenced by the vehicular emissions. Ljubljana has about 300.000 inhabitants and lies in the Ljubljana basin, which is the central and the largest basin in Slovenia. The local climate is typical for the basin location with the prevailing weak winds. The ground-level temperature inversions occur frequently in calm weather.

2. Results and discussion

The highest monthly concentrations occurred during spring and summer. In Ljubljana, the low level of ozone in winter is associated with the comparatively high NO_x concentrations and frequent nocturnal inversions, when ozone is consumed in the reaction with NO. For Krvavec, the seasonal variation curve has a broad maximum with high monthly mean concentrations extending into September. The curve is however of the similar shape than those reported for the elevated Alpine sites.

In Ljubljana the distinct diurnal minima appear in the morning (6-7 a.m.) and evening (20-22 p.m.), while during the afternoon (12-16 p.m.) a pronounced ozone maximum is observed. The ozone cycle displays a typical trend for the urban site where the ozone diurnal variation is influenced mainly by the chemical reactions in polluted air. The difference between the spring/summer and autumn/winter peak values ranges 80 $\mu g/m^3$.

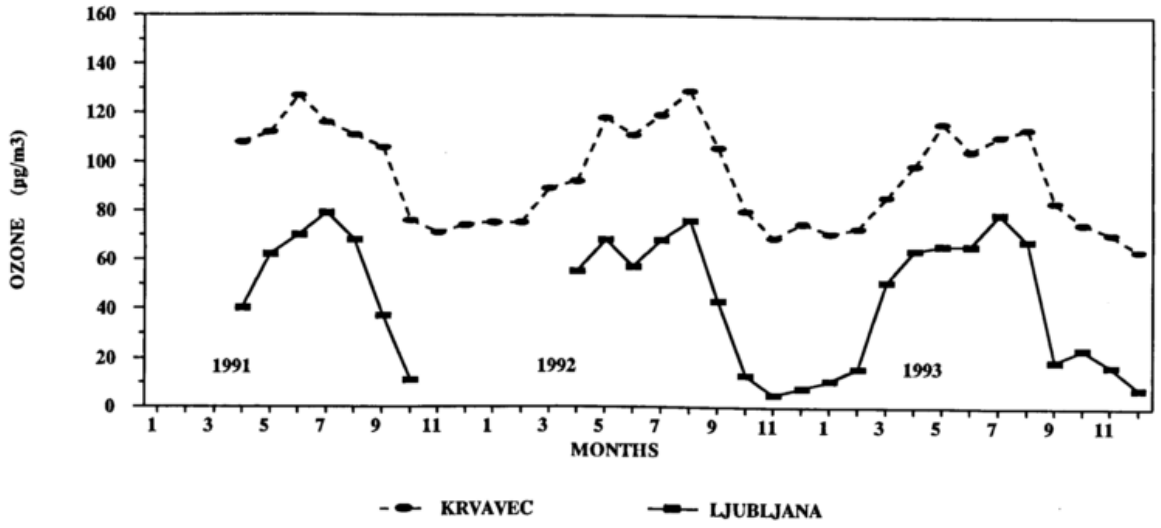

Fig. 1. Mean monthly concentrations of ozone in 1991, 1992 and 1993.

Smoother curve is observed however on Mt. Krvavec where the cycle is almost totally suppressed even in the summer period. The average daily level of ozone is about 110 $\mu g/m^3$ in spring/summer and 80 $\mu g/m^3$ in autumn/winter season. These concentrations are comparable to the ozone levels in a lower troposphere (Logan, 1985).

The results of ozone measurements in Slovenia indicate that in summer months the so called "ozone-episodes" occur pretty frequently in urban area, rural area as well as on the mountains in the Alps.

In 1991 the severest ozone episode occurred in June. In 24-26 June, sunny and hot weather with weak winds prevailed over northern Mediterranean and central Europe. The cold front approaching the Alps on 26 June forced the winds to turn to southwest. Sunny and hot weather prevailed over the northern Italy over which the air moved to Slovenia. The meteorological conditions on a local scale as well as long the path of air were highly favourable for the photochemical reactions. On 27 June the cold front caused the winds strengthened, it was cloudy, air temperatures dropped substantially, precipitation and thunderstorm occurred. Consequently, the ozone concentrations dropped noticeably. The episode on 26 June in Slovenia was not of a local character (Lešnjak et al., 1992). Increased concentrations covered also a part of southern Austria.

The exceedences of 150 $\mu g/m^3$ were the most frequent in August 1992, what contributed also to the high mean monthly concentrations. August 1992 has been the hottest month since the data for Slovenia have been existing. In Ljubljana, the mean monthly temperature was 23.7°C what is for 4.5°C higher than the 30-year average. The daily maximum temperature in Ljubljana was 29 days above 25°C, and 22 days more than 30°C. This month was also characterised by the high sunshine duration, more than 10 hours per day, and the outstanding drought. The meteorological conditions were therefore highly favourable for photochemical reactions and ozone accumulation.

The number of hours with average concentration over 150 $\mu g/m^3$ in Ljubljana is rising from year to year, but the average concentrations show no significant trend.

May 1993 was unusually warm and sunny; the mean daily maximum temperature is for 3.2°C higher than the 30-year average. The meteorological conditions in July 1993 were close to 30-year average values, except for a number of sunny days and sunshine duration, which was in Ljubljana more than 9.9 hours per day. The severest ozone episode that occurred during the considered three-year period was on 30 July, when the maximum 1/2-hour concentration in

Ljubljana was 236 $\mu g/m^3$. Again it was evident that the synoptic (air mass characteristics, wind strength and direction in the lower part of the free troposphere) and local meteorological conditions (intensive solar radiation, high air temperature, absence of strong winds and precipitation) play the dominant role in determine the ozone concentrations.

Table 1. Mean monthly concentrations (c_{ave}) and maximum hourly concentrations (c_{max}), and number of hours with ozone concentrations exceeding 150 $\mu g/m^3$ (N_{150}) over the period April-September 1991, 1992 and 1993.

	KRVAVEC			LJUBLJANA		
Period	c_{ave}	c_{max}	N_{150}	c_{ave}	c_{max}	N_{150}
April 91	108	151	1	40	164	1
May 91	112	179	3	62	206	8
June 91	127	228	102	70	212	34
July 91	116	187	41	79	212	55
August 91	111	163	12	68	186	36
September 91	106	119	27	37	178	8
April-September 91	**114**	**228**	**186**	**60**	**212**	**142**
April 92	92	142	0	55	189	19
May 92	118	173	37	68	197	34
June 92	111	156	2	57	149	0
July 92	119	193	82	68	193	29
August 92	129	189	127	76	225	116
September 92	106	172	14	43	181	10
April-September 92	**113**	**193**	**262**	**61**	**225**	**208**
April 93	99	156	4	64	178	31
May 93	116	210	60	66	210	34
June 93	105	159	5	66	184	21
July 93	111	191	49	79	236	109
August 93	114	186	90	68	222	81
September 93	84	126	0	19	96	0
April-September 93	**105**	**210**	**208**	**60**	**236**	**276**

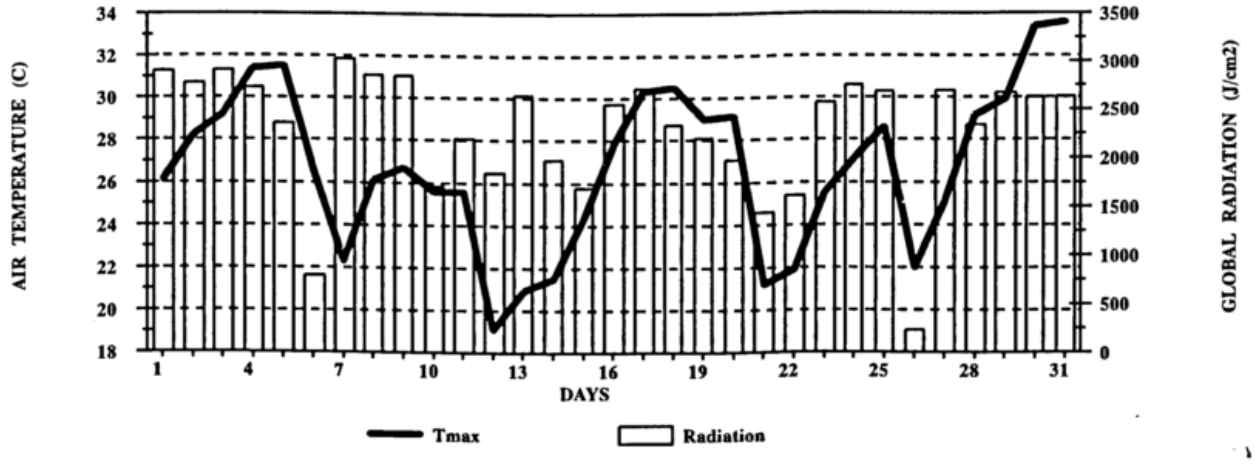

Fig. 2. Sunshine radiation and maximum daily temperatures in Ljubljana in July 1993.

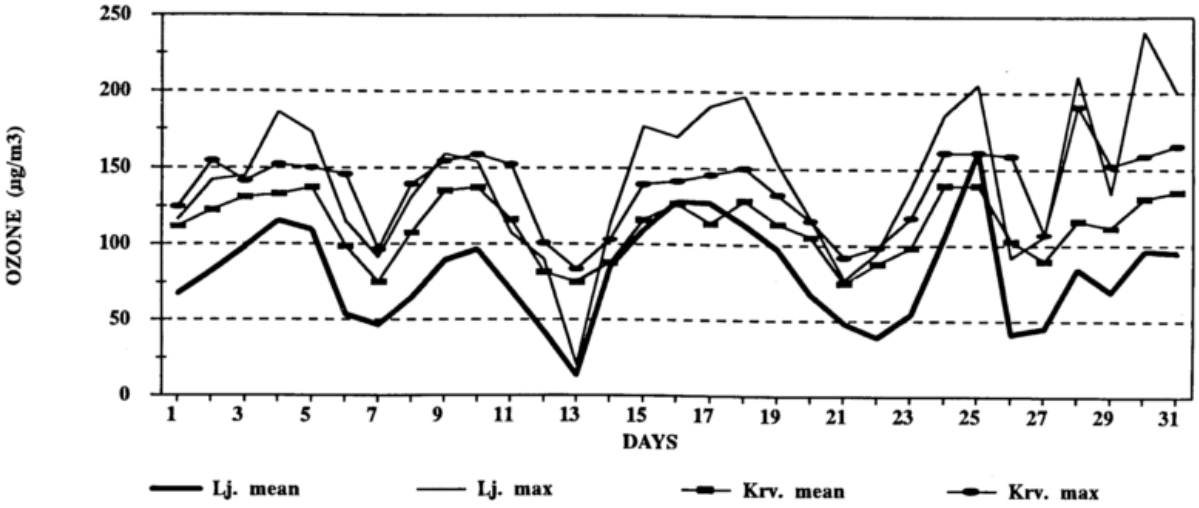

Fig. 3. Daily mean and maximum 1/2-hour ozone concentrations in Ljubljana and on Mt. Krvavec in July 1993.

September was unusually cold with a lot of days with precipitation; the mean monthly temperature in Ljubljana was 3.3°C bellow the average value for this month. Consequently also the ozone concentrations were relatively low.

At the 850 hPa level (standard pressure level close to the altitude of the measurement site Krvavec) the influence of the Alps on the air flow is still very pronounced, for this reason we considered also the trajectories at 700 hPa level.

3. Conclusions

Taking into account the data on spatial distribution of the ozone precursor emissions in Europe, NO_X and VOCs, as well as the known phenomena of ozone few-days accumulation and transport in the lower troposphere, our data on ozone measurements suggest that the main origin of the elevated surface ozone concentrations in Slovenia is a transport of polluted air from the highly industrialised and densely populated northern Italy. The weaker ozone episodes may be however attributed mainly to the in situ ozone production rather than transport as the density of NO_X and VOCs emissions within few hundred kilometres eastern of Slovenia is not high.

Some common characteristics were found for such periods lasting typically from one to several days: (i) high air temperatures, (ii) intensive solar radiation, (iii) weak-gradient pressure field implying slow movement or retention of air masses and (iv) the western or south-western winds prevailing in the free lower troposphere.

The ozone sank however either: (i) at the change of a trajectory direction, (ii) at strengthening of the wind speed, or (iii) at the passage of the cold front.

4. References

ECE, 1988: ECE Critical Level Workshop, Bad Harzburg, Federal Republic of Germany, 14-18 March 1988

Lešnjak M., Planinšek A: 1992: Ozone Episode in Slovenia. Ujma, 101-105

Logan, J. A., 1985: Tropospheric ozone: seasonal behaviour, trends, and anthropogenic influence. J. Geophys. Res., 90(6), 10463-10482

WHO, 1987: Air Quality Guidelines for Europe. WHO Regional Publications, European series No. 23, Copenhagen.

Ozone Concentration Characteristics In and Over a High-Altitude Forest

Gene L. Wooldridge
Karl F. Zeller
Robert C. Musselman

USDA Rocky Mountain Forest and Range Experiment Station
240 West Prospect Road, Fort Collins CO 80526 U.S.A.

ABSTRACT

Four years of atmospheric ozone data from a subalpine forest site at an elevation of 3180 m above mean sea level (msl) about 55 km west of Laramie, Wyoming, U.S.A., and at a 2680 msl forest-steppe ecotone site 15 km to the southeast, have been analyzed. These sites appear to be free of any urban or industrial pollutants. Data for January through June show that the amplitude of the diurnal cycle of hourly mean values is small in winter, then increases through June. The highest monthly mean concentrations occur in April or May, and decrease in June. Episodal high O_3 values were measured during spring months in connection with cutoff low pressure centers aloft and probable stratospheric intrusions. Spectral analyses yield a peak at the diurnal period and broad peaks at longer periodicities, particularly during the spring season.

1. INTRODUCTION

The Glacier Lakes Ecosystem Experiments Site, or GLEES, project provides data on landscape habitats, floristics, geology, soils, aquatics, meteorology, hydrology, snow, and air quality. It contains three small alpine lakes with their corresponding watersheds. An extension of the GLEES to the southeast includes a subapline fir-Engelmann spruce forest in which a 30-m tower is used to measure meteorological variables and O_3 above the forest floor (R.C. Musselman, 1994).

Ambient O_3 concentrations depend on a large number of chemical reactions and a variety of atmospheric circulations and dispersion phenomena. One of the atmospheric mechanisms is known as "tropopause folding", which produces stratospheric intrusions of high concentrations of O_3. This has been described by Danielsen (1980), and usually occurs concurrent with a low pressure trough and a cutoff low pressure center in the upper troposphere. These intrusions occur in mid-latitudes during spring and early summer months, and somewhat later in the year at more northerly latitudes. During the intrusion, a thin layer of dry, ozone-rich air flows on a long downward trajectory toward the surface; turbulent erosion of the layer elevates concentrations in the atmospheric boundary layer. On rare occasions, the undiluted layer can be measured at the surface (Arlette, 1958) or detected by odor. Austin and Follows (1992) calculated that the intrusions were the source of 25% of the O_3 mixing ratio at 300 hPa at midlatitudes during winter and spring months, occurring once or twice a month. Surface ambient O_3 characteristics have been catagorized as: (1) Urban, where anthropogenic precursors strongly affect O_3 concentrations; (2) Rural, where low-level circulation systems may carry urban plumes over distances of up to hundreds of km; and (3) Remote.

Large coherent eddies over the rough canopy of a forest dominate the penetration of gaseous constituents downward. These are called "sweeps", which reach deep into and below the canopy space. Finding concentrations of ozone very low at the ground during nighttime, Fontan et al. (1992) concluded that the chemical

destruction of O_3 at night was weak in comparison with its deposition at the surface. O_3 can cause injury to plant tissue and reductions in forest growth if the exposure is sufficient (LeFohn, 1992). The magnitude of the impact depends on the concentration of ozone and the length of the exposure.

2. OBSERVATIONS AND ANALYSES

A 30-m tower stands in a small clearing at 3180 m msl, near the edge of the 17-m tall subalpine fir-Engelmann spruce forest of the southeastern extension of the GLEES, and will be referred to here as the Brooklyn tower. A 10-m tower has provided O_3 data 140 m southwest of the taller tower, 70 m downwind of the forest edge. This is called the Brooklyn NDDN (National Dry Deposition Network) site. This 10-m tower, earlier located at 2680 m msl and about 15 km southeast of the GLEES, will be referred to as the Centennial NDDN site. The winds at the GLEES blow predominantly from the west to west-northwest over the forest. Precipitation falls mostly as snow during the winter months, with snowmelt nearly complete by late June. The O_3 measurements at all levels and sites were made using Thermo Electron COrporation (TECO) Series 49 UV photometric ambient analyzers. Analyses are limited here to the first six months of 1990-1993.

Figure 1 compares 1990-91 data from the Centennial NDDN site with 1992-93 data from the Brooklyn NDDN site for the months of January, March, and May. The January mean hourly O_3 values show a small diurnal amplitude, and little difference between the data sets. By March, the amplitude of the diurnal cycles of the Centennial data is greater than that for the Brooklyn data; by May, the Centennial data has an amplitude much greater than at the higher Brooklyn site. These differences appear largely due the depth and length of snow cover. Smowmelt at the Brooklyn site occurs between late May and late June, while it occurs during March and April at the Centennial site. The mean monthly O_3 concentrations at the two elevations differ only slightly.

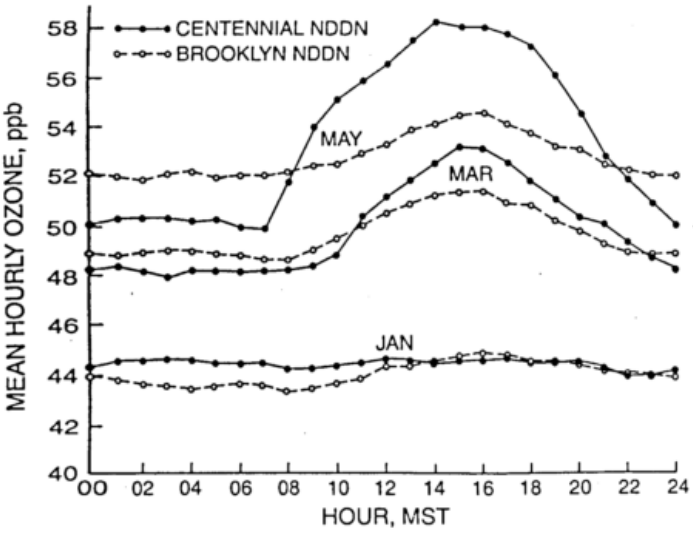

Fig.1. Averages of Centennial NDDN O_3 for 1990-91 (dashed lines) and Brooklyn NDDN for 1992-93 (solid lines).

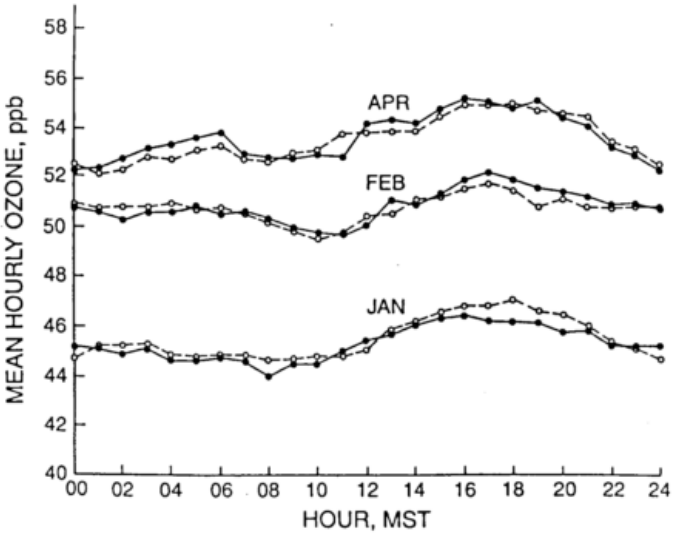

Fig.2. O_3 values for Brooklyn tower over the forest canopy (dashed lines) and Brooklyn NDDN (solid lines), 1993.

The O_3 concentrations over the GLEES forest (Fig. 2), normalized on the Brooklyn NDDN data, show an increase in mean values through the period of January to April, 1993. The highest monthly mean occurred in April, with a slightly lower value in May; the June mean decreased further (not shown here). The diurnal amplitude for January was 2.4 ppb; for June, it increased to 3.8 ppb. Ozone data taken at a height of 3 m at the Brooklyn tower in 1990 are represented

in Fig. 3. The diurnal amplitudes of the mean hourly O_3 values differ significantly from those over the top of the canopy. Unfortunately, data for 1990 over the forest canopy are not available; interannual variations may be responsible for the higher May values. The diurnal amplitudes during and after May 1990 are much greater under the canopy level than above. By June the amplitude reached 9.3 ppb, mostly due to much lower nighttime concentrations under the canopy; snowmelt in 1990 occurred on June 9.

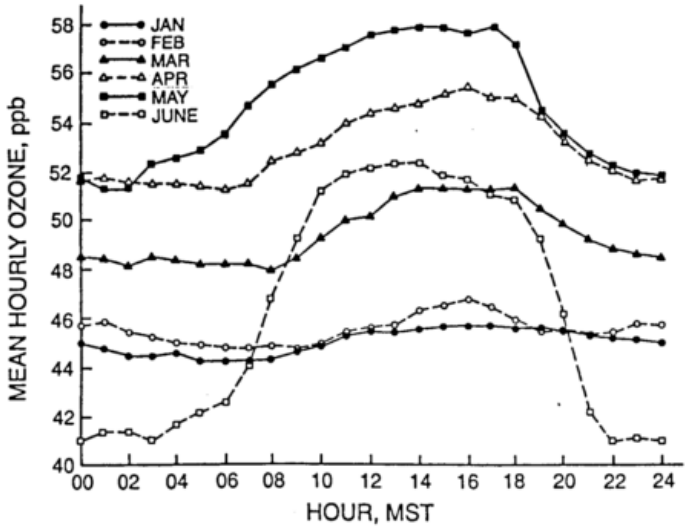

Fig.3. Mean hourly O_3 values in ppb at 3 m above the surface in the small clearing at Brooklyn tower, 1990-91.

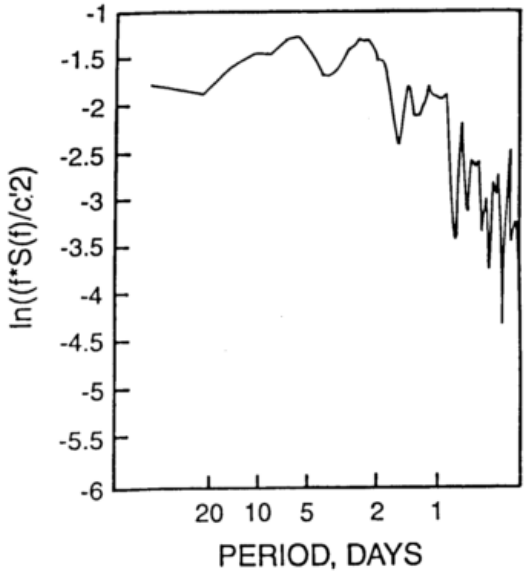

Fig.4. Spectral representation of April-June 1992 Brooklyn NDDN mean hourly O_3 data.

Fig. 4 shows the distribution of the variance of the O_3 concentrations at the Brooklyn NDDN 10-m site from April through June, 1992. The spectrum shows a peak near the diurnal period and a broad peak at longer periodicities. The longer period of the double peaks approximates the frequency of stratospheric intrusions identified in Table I below, and indicates the significance of the intrusions to O_3 concentrations during the spring months. The January-March spectrum (not shown here) indicates a much sharper peak for the 1-day period, and a single broad peak near an 11-day period.

Table I. Stratospheric Intrusions Identified (Id.) and Verified (Ver.), 1990-93.

Year	1990			1991			1992			1993		
Month	Id.	Ver.	Mean (ppb)	Id.	Ver.	Mean (ppb)	Id.	Ver.	Mean (ppb)	Id.	Ver.	Mean (ppb)
Jan.	0	0	44.0	0	0	45.7	0	0	43.0	0	0	45.3
Feb.	0	0	45.3	0	0	45.8	0	0	44.9	0	0	50.8
Mar.	1	1	50.6	0	0	48.4	0	0	49.4	0	0	49.9
Apr.	2	1	53.3	4	3	55.2	3	2	52.8	3	2	52.7
May	3	2	53.3	4	4	56.3	1	1	52.7	4	3	52.6
June	2	1	47.8	2	1	46.1	3	3	51.7	2	2	51.1

In order to further examine the contributions to O_3 concentrations by stratospheric intrusions, two criteria were applied to the data. Intrusions were presumed identified when the O_3 concentrations exceeded 60 ppb for ten hours or more and the relative humidities were 25% or lower. When the intrusions prevailed over the tree canopy, they were also found at 3 m below the canopy. Table I lists the number of episodes identified in the O_3 data, and those verified by the passage of a closed low pressure center at 500 hPa between Central Colorado and Central Wyoming. The monthly mean O_3 concentrations were calculated using the 3-m Brooklyn tower height in 1990 and 1991, and using the

10-m Brooklyn NDDN site for 1992 and 1993. The number of episodes identified averaged 3 per month in April and May and 2 in June. The application of the criterion of a closed low pressure at 500 hPa appears too restrictive for verification of all episodes.

3. SUMMARY

3.1. There appears to be no significant difference in monthly average O_3 concentrations with elevation between the Brooklyn and Centennial observational sites, a vertical distance of 500 m.

3.2. There is a difference between sites in the amplitudes of the diurnal traces of monthly mean hourly O_3 values during late spring-early summer months. This appears to be due to the presence or absence of snow on the ground. During these months, increased surface deposition after snowmelt sharply decreased nighttime ambient concentrations near the ground. There is also a greater diurnal amplitude under the forest canopy than over the top of the canopy.

3.3. Episodes with O_3 values over 60 ppb for ten hours or more appear to elevate mean values less than 6% during the months of April and May. These episodes occur with nearly equal frequency at any hour of the day, rather than during daytime hours as reported by Lisac et al, 1993.

4. ACKNOWLEDGEMENTS

The authors appreciate the support of Project RWU 4452 of the USDA Rocky Mountain Experiment Station and Project Director Linda Joyce. Richard Sommerfeld supplied snowmelt information; Bernadette Connell and Ted Hehn provided meteorological and O_3 data. Discussions of meteorological processes with William Massman proved very helpful. The USEPA Atmospheric Resources and Exposure Assessment Laboratory edited and provided the NDDN data.

5. LITERATURE

Arlette, V., 1958: Concentration de l'air en ozone a la station scientifique du Jungfraujoch: influence des fronts froids. Seance du 22 decembre 1958. Comptes Rendue, de l'Academie des Sciences, Paris, t256. 2404-2411.

Austin, J.F., and M.J. Follows, 1991: The ozone record at Payerne: an assessment of the cross-tropopause flux. Atmos. Environ. 25A, 9. 1873-1880.

Danielsen, E.F., 1980: Stratospheric source for unexpectedly large values of ozone measured over the Pacific Ocean during Gametag, August 1977. J. Geophys. Res., 85. 410-412.

Fontan, J., A. Minga, A. Lopez, and A. Druilhet, 1992: Vertical ozone profiles in a pine forest. Atmos. Environ., 26A. 863-869.

LeFohn, A.S., 1992: Surface Level Ozone Exposures and Their Effects on Vegetation. Lewis Publishers, Chelsea MI. pp 7-282.

Lisac, I., A. Marki, D. Tiljak, L. Klisinc, and T. Cvitas, 1993: Stratospheric ozone intrusion over Zagreb, Croatia. Meteor. Zeits. 2. 2224-231.

Musselman, R.C., 1994: The Glacier Lakes Ecosystem Experiments Site. USDA Forest Service, RMS General Technical Report (in press). Fort Collins, Co.

Human-biometeorologische Bewertung des thermischen Milieus in den höheren Gebirgsregionen von Griechenland

A. Matzarakis (*); H. Mayer (*); C. Balafoutis (**)

(*) Meteorologisches Institut der Universität Freiburg, Werderring 10, D-79085 Freiburg

(**) Department of Meteorology and Climatology, Aristotelian University of Thessaloniki, GR-54006 Thessaloniki

ABSTRACT

The effect of the thermal component of climate on humans can be assessed by use of human energy balance models and derived thermal indices. For the construction of monthly bioclimate maps for Greece the "KLIMA-MICHEL-MODELL" with the calculation of the PMV-index has been applied. The bioclimate maps contain spatial information on the thermal sensation of humans in different zones of Greece. In the summer month July humans feel thermal comfort in montainous regions between 1200 and 1500 m asl, whereas differently strong heat stress is characteristic for the interior, coasts and islands of Greece.

ZUSAMMENFASSUNG

Die Wirkung der thermischen Komponente des Klimas auf Menschen läßt sich über die Anwendung von menschlichen Energiebilanzmodellen bzw. daraus abgeleiteten Indizes beurteilen. Für die Erstellung von monatlichen Bioklimakarten von Griechenland wird der auf dem "KLIMA-MICHEL-MODELL" basierende Bewertungsindex PMV verwendet. Die Bioklimakarten enthalten flächendeckende Aussagen über das thermische Empfinden von Menschen in den verschiedenen Zonen Griechenlands. Im Sommermonat Juli fühlen sich die Menschen in den Gebirgsregionen zwischen 1200 und 1500 m NN thermisch behaglich, während sie im Landesinneren, an den Küsten und auf den Inseln unterschiedlich starke Wärmebelastungen empfinden.

1. Einleitung

Die geographische Situation von Griechenland läßt sich nicht nur durch seine Lage am Mittelmeer, sondern auch durch sein ausgeprägtes Relief kennzeichnen. Die Gipfel der Gebirgsregionen reichen dabei bis ca. 2900 m NN. Dadurch weist Griechenland eine verhältnismäßig große Variabilität bei der thermischen Komponente des Klimas auf (BALAFOUTIS und MAHERAS, 1986). Ihre Wirkung auf Menschen läßt sich über die Anwendung von menschlichen Energiebilanzmodellen bzw. daraus abgeleiteten Indizes beurteilen. Derartige Untersuchungen sind für Griechenland aus zahlreichen Gründen - u.a. für den Fremdenverkehr oder medizinische Belange - von großem Interesse.

2. Methodik

Die Erstellung von flächendeckenden, monatlichen Bioklimakarten für Griechenland, die eine human-biometeorologische Bewertung des thermischen Milieus in den höheren Gebirgsregionen von Griechenland ermöglichen, beruhte auf dem "Klima-Michel-Modell" bzw. dem damit in Zusammenhang stehenden Bewertungsindex PMV (JENDRITZKY et al., 1979). Zur Umsetzung von punktuellen PMV-Resultaten in den Raum wurde ein Verfahren angewendet, das auf Untersuchungen von JENDRITZKY (1990) basiert.

Aufbauend auf meteorologischen Daten aus dem Zeitraum von 1980 bis 1989 wurde PMV zum 12 UTC-Termin für eine Auswahl von Stationen des Griechischen Wetterdienstes berechnet. Dabei war die Art der Bekleidung bzw. der im "Klima-Michel-Modell" zu berücksichtigende Wärmedurchgangswiderstand I_{cl} der Bekleidung an die jeweiligen Lufttemperaturverhältnisse angepaßt, um möglichst realitätsnahe Bedingungen simulieren zu können.

Über multiple Regressionsanalysen zwischen diesen PMV-Werten einerseits und den Parametern "geographische Breite", "Höhe über NN", "Kontinentalität", "Exposition", "Hangneigung" und "Meereseinfluß" andererseits wurden Bioklimakarten für einzelne Monate erstellt. Dabei wurde für Griechenland ein Geländemodell mit einem Gitternetz in 1 min Auflösung eingesetzt.

3. Ergebnisse

3.1 Ausgewählte Stationen

Im Untersuchungszeitraum nahm die Anzahl von Tagen mit sehr starker Wärmebelastung (PMV > 3) in der Reihenfolge der ausgewählten Stationen Larisa (im Landesinneren in Zentralgriechenland, 73 m NN; 89.5 d/a), Corfou (Insel im Ionischen Meer, 4 m NN; 68.1 d/a), Florina (in Nordwestgriechenland, 650 m NN; 67.1 d/a), Samos (Insel in der Ägäis, 2 m NN; 58.0 d/a), Helliniko (Flughafen von Athen, 28 m NN; 47.9 d/a), Andravida (auf dem Westpellopones, 17 m NN; 44.4 d/a), Tripolis (in der Mitte des Pellopones, 644 m NN; 38.3 d/a), Alexandroupolis (in Nordostgriechenland, 7 m NN; 38.2 d/a), Mikra (Flughafen von Thessaloniki, 4 m NN; 35.0 d/a), Rhodos (Insel in der Ägäis, 4 m NN; 23.8 d/a), Heraklion (auf Kreta, 37 m NN; 21.3 d/a) und Limnos (Insel in der Nordägäis, 17 m NN; 16.5 d/a) ab.

Die Analyse von zusammenhängenden Tagen (mehr als drei Tage) mit extrem starker Wärmebelastung (PMV > 4.0) an den untersuchten Stationen in Griechenland (Höhen nicht über 650 m NN) ergab für die 80-er Jahre witterungsabhängig 9 Perioden mit extrem hoher Wärmebelastung. Sie traten im August 1980, Ende Juni / Anfang Juli 1981, Ende Juli 1981, im Juni 1982, Mitte Juli 1984, Ende Juli / Anfang August 1985, Ende Juli 1987 (große Hitzewelle von 1987, siehe u.a. MATZARAKIS und MAYER, 1991), Mitte Juli 1988 und am Anfang August 1988 auf. Für die Jahre 1984 und 1989 wurden keine zusammenhängende Tage (mehr als drei) mit extrem starker Wärmebelastung ermittelt.

3.2 Bioklimakarte von Griechenland für den Juli

Von den für jeden Monat erstellten Bioklimakarten von Griechenland ist in der Abb. 1 exemplarisch diejenige für den Sommermonat Juli enthalten. Im Gegensatz zu den Originalkarten, in denen die flächendeckende Verteilung der über die PMV-Werte bestimmten thermischen Belastungsstufen in Analogie zu JENDRITZKY (1979) in 10 Klassen farbkodiert ist, wurde die Abb. 1 zur besseren Übersichtlichkeit bei der Schwarz-Weiß-Darstellung nur in drei verschiedene Graustufen unterteilt. In der Abnahme der Schwärzung repräsentieren sie die Bereiche PMV $\leq$ 0.5, 0.5 < PMV $\leq$ 2.0 sowie PMV > 2.0.

Der Juli ist in Griechenland der Monat mit der höchsten Wärmebelastung für Menschen. Die Geländehöhe und die Nähe zum Meer, die generell als Steuerfaktoren für die human-biometeorologisch relevanten Parameter "Lufttemperatur", "Dampfdruck", "Windgeschwindigkeit" und "mittlere Strahlungstemperatur" wirken, bestimmen hier besonders deutlich die räumliche Variabilität der Wärmebelastung. Sie ist in den Gebirgsregionen am geringsten, wobei in Höhen zwischen 1200 und 1500 m NN die Zone des thermischen Behaglichkeitsbereiches (|PMV| $\leq$ 0.5) liegt. Für die noch höher gelegenen Gebirgsregionen wurde sogar leichter Kältereiz (PMV < -0.5) ermittelt. Demgegenüber ergab sich extrem starke Wärmebelastung (PMV > 4) in den niedrig gelegenen Regionen (unterhalb von 150 m NN) im Landesinneren. Die Küstenregionen des Festlandes zeigen überwiegend eine etwas geringere Wärmebelastung (3 < PMV $\leq$ 4) als im Landesinneren. Sie ist aber höher als auf den meisten Inseln. Dort hängt PMV primär von der Geländehöhe ab und schwankt zwischen 2 und 3 im Küstenbereich sowie zwischen 0.6 und 2 in den höheren Regionen. Eine Sonderstellung nehmen die großen Inseln, vor allem Kreta, mit ihren hohen Gebirgen ein. Dort tritt im Juli in größeren Höhen sogar leichter Kältereiz auf.

Die human-biometeorologisch relevanten, thermischen Empfindungen im Monat August stimmen mit denen im Juli weitgehend überein. Der einzige Unterschied liegt darin, daß das Niveau der PMV-Werte in den niedrigen Regionen im Landesinneren geringfügig kleiner ist. Der Juni bildet in Griechenland der Sommermonat mit der generell niedrigsten Wärmebelastung - gleichgültig ob im Landesinneren, an der Festlandsküste oder im Landesinneren.

LITERATUR

BALAFOUTIS, C.; MAHERAS, P., 1986: Geographical distribution and grouping of bioclimate types in Greece related to air enthalpy. Z. Meteorol. **36**, 259-264.

JENDRITZKY, G.; SÖNNING, W.; SWANTES, H.-J., 1979: Ein objektives Bewertungsverfahren zur Beschreibung des thermischen Milieus in der Stadt- und Landschaftsplanung ("Klima-Michel-Modell"). ARL-Beiträge Nr. 28.

JENDRITZKY, G., 1990: Bioklimatische Bewertungsgrundlage der Räume am Beispiel von mesoskaligen Bioklimakarten. In: Jendritzky, G.; Menz, G.; Schmidt-Kessen, W.; Schirmer, H.: Methodik zur räumlichen Bewertung der thermischen Komponente im Bioklima des Menschen. ARL-Beiträge Nr. 114, 7-69.

MATZARAKIS, A.; MAYER, H., 1991: The extreme heat wave in Athens in July 1987 from the point of view of human-biometeorology. Atmospheric Environment **25B**, 203-211.

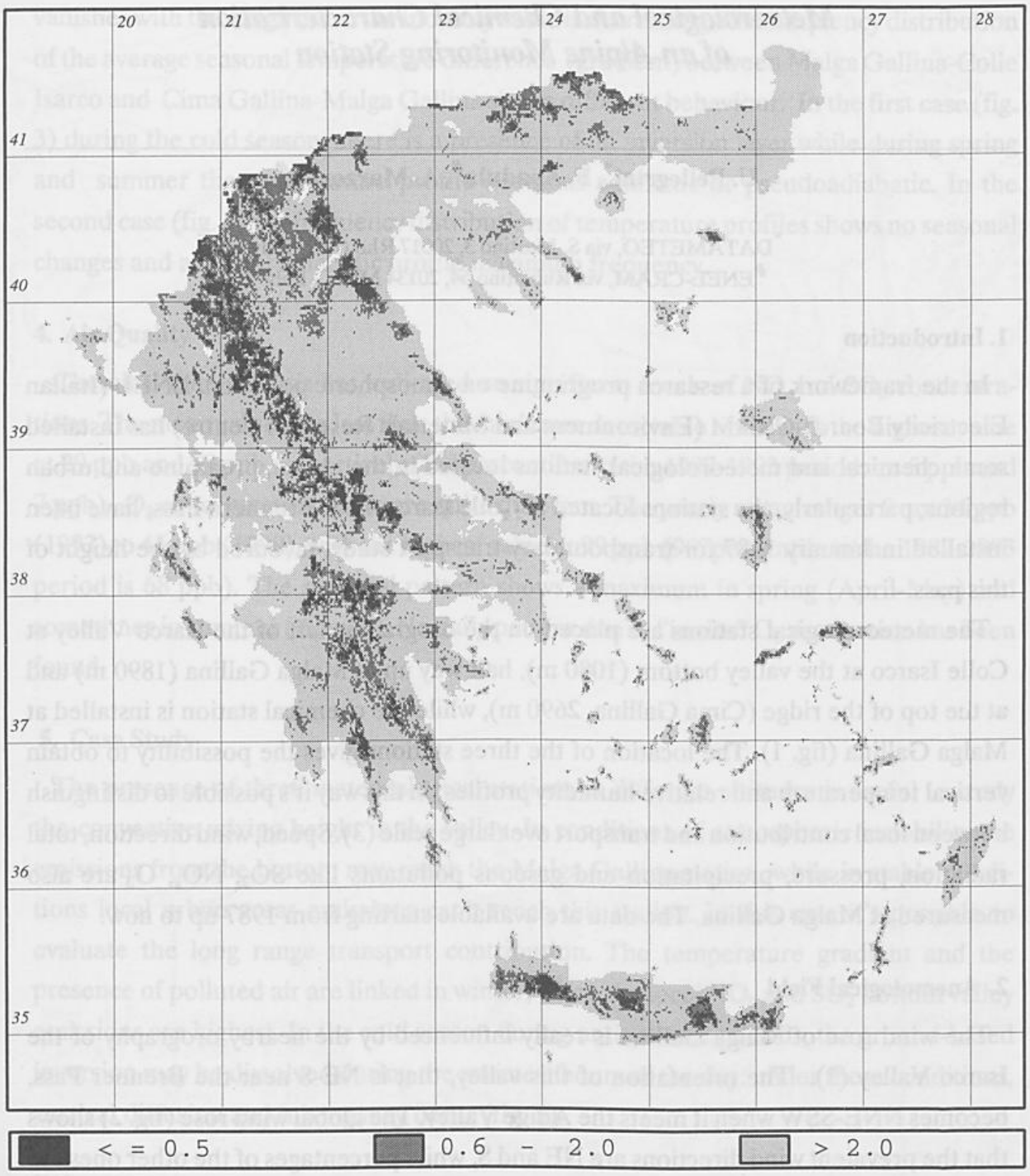

Abb. 1: Bioklimakarte von Griechenland für den Juli: mit unterschiedlichem Schwärzungsgrad sind die Gebiete mit PMV ≤ 0.5, 0.5 < PMV ≤ 2.0 und PMV > 2.0 angegeben

Meteorological and Chemical Characterization of an Alpine Monitoring Station

U. Pellegrini*, F. Apadula#, A. Marzorati#

*DATAMETEO, via S. Martino 3, 20017 Rho (Mi)- Italy
#ENEL-CRAM, via Rubattino 54, 20134 Milan - Italy

1. Introduction

In the framework of a research programme on atmospheric pollution, ENEL (Italian Electricity Board)-CRAM (Environment and Materials Research Centre) has installed some chemical and meteorological stations located in the alpine, prealpine and urban regions; particularly, the stations located at Colle Isarco, near Brennero Pass, have been installed in January 1987 for transboundary transport study, favoured by the height of this pass.

The meteorological stations are placed on the orographic left of the Isarco Valley at Colle Isarco at the valley bottom (1080 m), half way up at Malga Gallina (1890 m) and at the top of the ridge (Cima Gallina, 2690 m), while the chemical station is installed at Malga Gallina (fig. 1). The location of the three stations gives the possibility to obtain vertical temperature and relative humidity profiles; in this way it's possible to distinguish between local contribution and transport over large scale (3). Speed, wind direction, total radiation, pressure, precipitation and gaseous pollutants like SO_2, NO_x, O_3 are also measured at Malga Gallina. The data are available starting from 1987 up to now.

2. Anemological Field

The wind rose of Malga Gallina is really influenced by the nearby orography of the Isarco Valley (1). The orientation of this valley, that is NE-S near the Brenner Pass, becomes NNE-SSW when it meets the Adige Valley. The global wind rose (fig. 2) shows that the prevalent wind directions are NE and S, while percentages of the other ones are lower than 10%. The wind speed shows a maximum in the frequency distribution at about 4 m/s. The daily and nightly wind roses allow to explain the important role of the breeze circulation, due to the different warming between the bottom and the top of the valley, especially during spring and summer (2); there is a clear wind rotation to W during the day and to E during the night.

3. Temperature Field

The temperature distribution has permitted to evaluate the different behaviour in the three stations. The daily temperature variation is very evident at Colle Isarco and

vanishes with the height; also the monthly value is decreasing. The frequency distribution of the average seasonal temperature difference (gradient) between Malga Gallina-Colle Isarco and Cima Gallina-Malga Gallina shows different behaviour. In the first case (fig. 3) during the cold seasons there is a presence of an inversion layer while during spring and summer the temperature profile becomes adiabatic or pseudoadiabatic. In the second case (fig. 4) the frequency distribution of temperature profiles shows no seasonal changes and a typical adiabatic profile maximum frequency.

4. Air Quality

Chemical data analysis has indicated no significant levels of NO and SO_2 concentrations. The mean values are less than the minimum detectable limit, with the highest value at 29 ppb and 58 ppb respectively (98° percentiles in the 1987-1993 period are 5 ppb and 7 ppb). O_3 concentration levels are quite different. The yearly mean ranges from 34 ppb (1993) to 45 ppb (1990), with the highest value at 99 ppb (98° percentile in the 1987-1993 period is 68 ppb). The seasonal pattern shows a maximum in spring (April-May) and sometimes in summer (August). No daily pattern due to "in situ" O_3 production has been found.

5. Case Study

The presence of three meteorological stations at different altitudes is useful to study the convective mixing height in the valley. In conditions of atmospheric instability the emissions from the bottom may reach the Malga Gallina station, while in stable conditions local urban areas emissions can't reach this station. In this case it's possible to evaluate the long range transport contribution. The temperature gradient and the presence of polluted air are linked in winter, when the local NO_x and SO_2 bottom valley emissions are highest. In the cold season during anticyclonic periods, the ground-based inversion may be dissolved during the warmest hours of the day: under these conditions, vertical diffusion and mixing may occur (fig. 5).

References

- (1) APADULA, F., BANDA, L., CARBONI, G., MANZI, G., MINA, L., NOVO, A., VANNINI, C., VENTURA, A. (1990): Caratterizzazione Chimico Meteorologica della Stazione Dedicata allo Studio del Trasporto Transfrontaliero degli Inquinanti Atmosferici nella Zona del Brennero; E5/90/15/MI, documento ENEL, 23
- (2) ATKINSON, B. (1981): Meso-scale Atmospheric Circulation; Academic Press, London
- (3) CAMUFFO, D., BERNARDI, A., BACCI, P. (1991): Transboundary Transport of Atmospheric Pollutants through the Eastern Alps; Atmos. Environ.; 25A, 12
- (4) REITER, R. (1991): On the Mean Daily and Seasonal Variations of the Vertical O_3 Profiles in the Lower Troposphere; Atmos. Environ.; 25A, 9
- (5) ROSINI, E. (1988): Introduzione all'Agroclimatologia; ERSA, Bologna

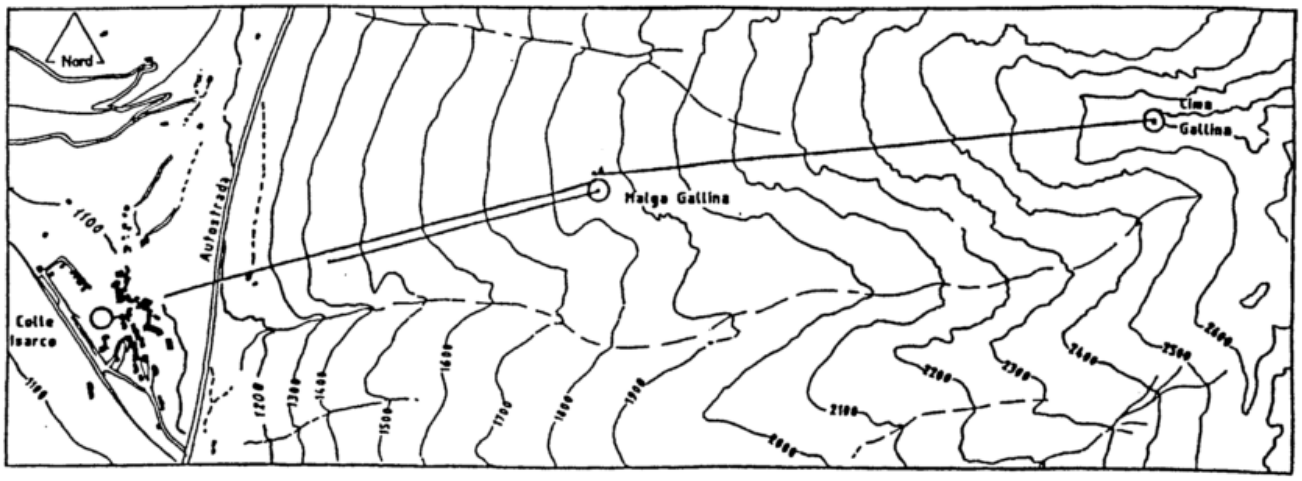

Fig. 1. Location of the three stations at Brennero Pass.

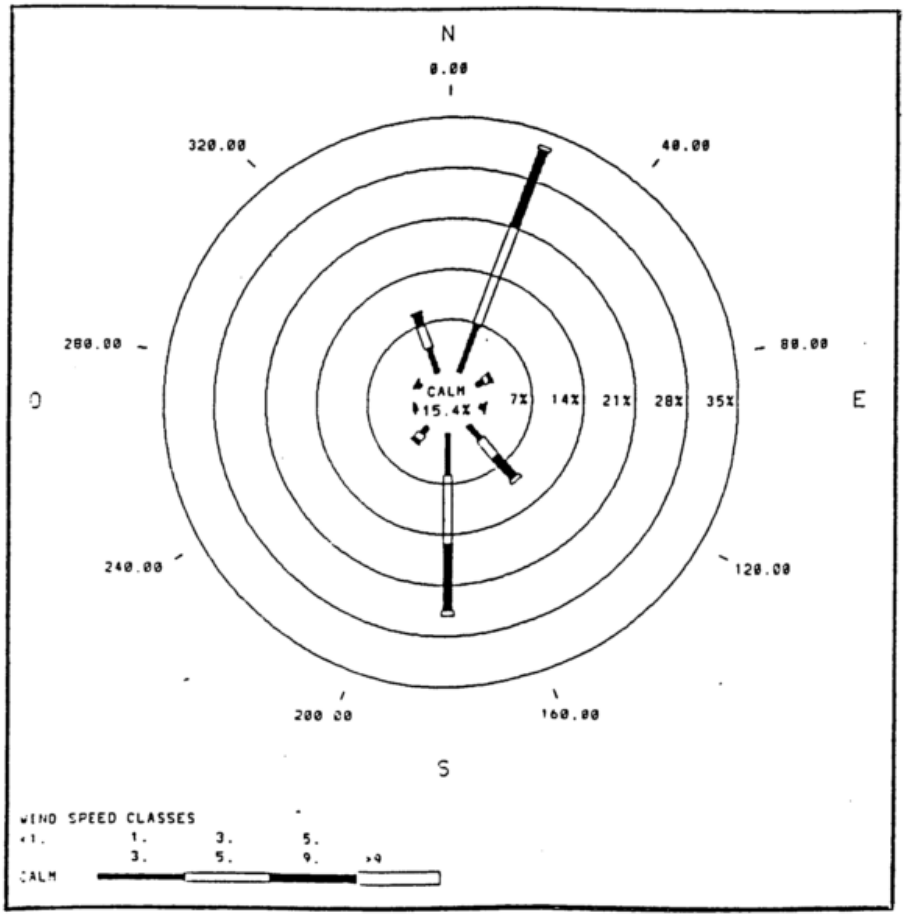

Fig. 2. Wind roses at Malga Gallina in the 1987-1992 period. Wind speed in m/sec.

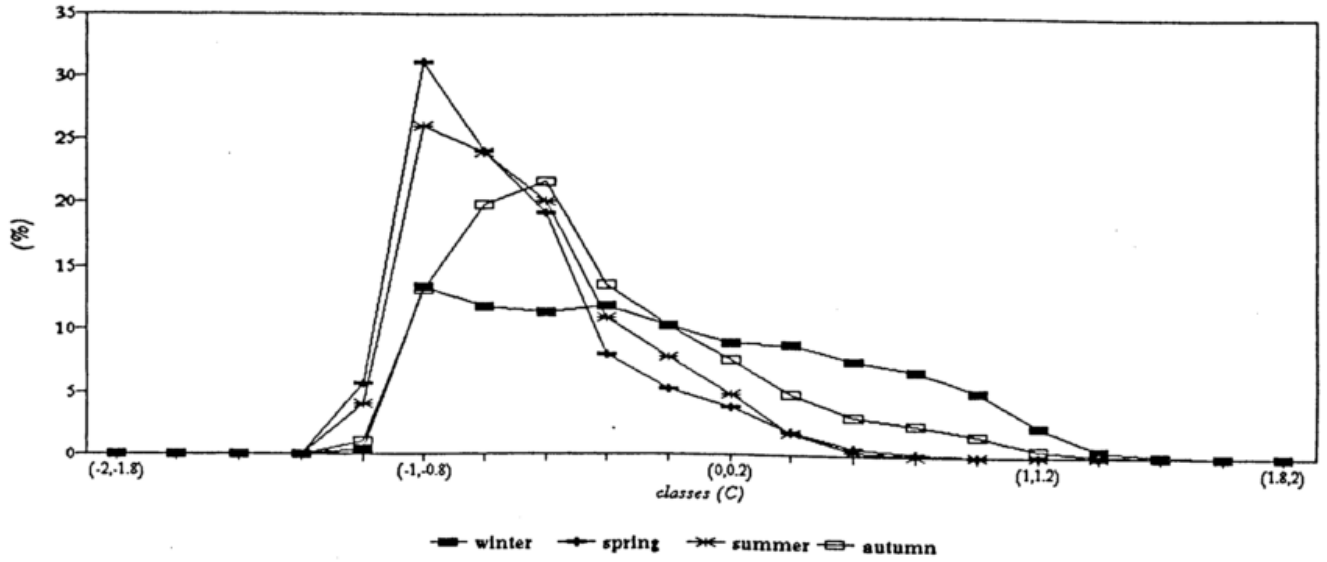

Fig. 3. Frequency distribution of the mean seasonal temperature gradient between Malga Gallina and Colle Isarco.

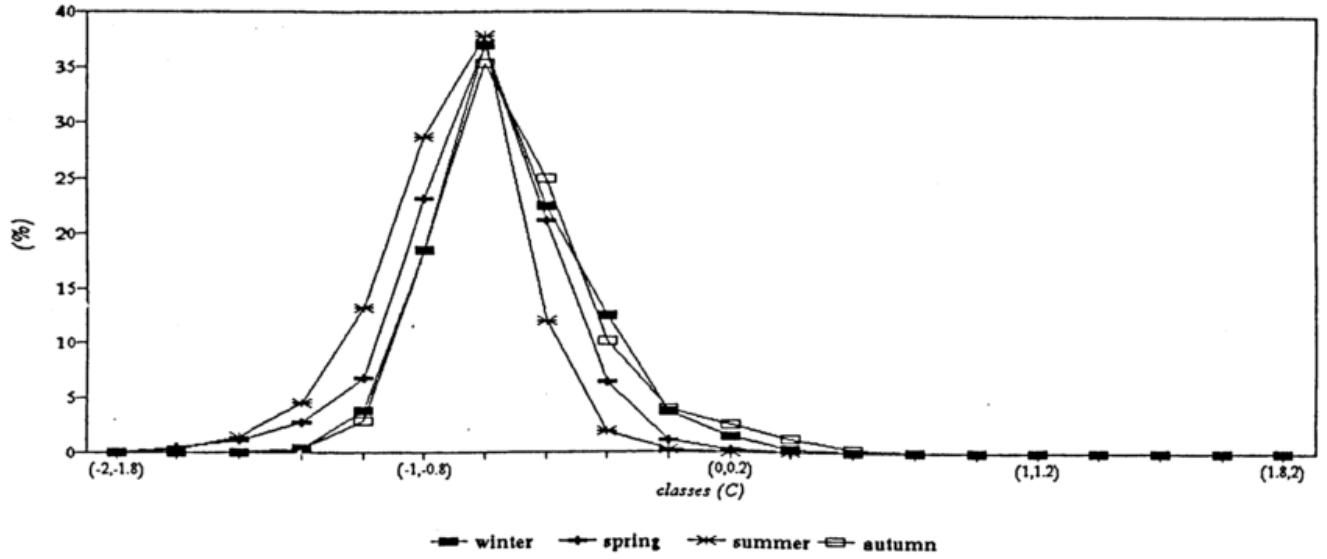

Fig. 4. Frequency distribution of the mean seasonal temperature gradient between Cima Gallina and Malga Gallina.

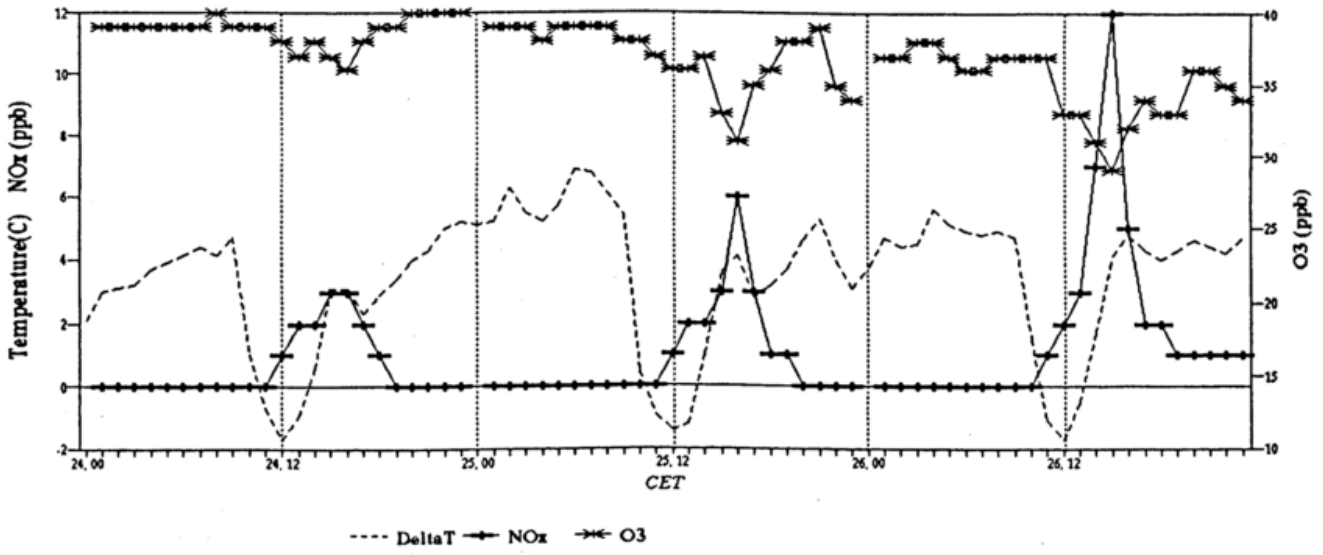

Fig. 5. Case study (24-26/01/1989): NO_x and O_3 hourly average at Malga Gallina and temperature gradient hourly average between Malga Gallina and Colle Isarco.

DEPENDENCE OF CHILDREN'S SINO-BRONCHIAL SYNDROME ON WEATHER IN CONTINENTAL PART OF CROATIA

Nada Pleško[1], Milica Krstić-Burić [2], Sanja Pleško[3]

[1] *Meteorological and Hydrological Service of Croatia, Zagreb*
[2] *Children's Hospital for Respiratory Diseases, Srebrnjak, Zagreb*
[3] *Sanitary Service, Trešnjevka, Zagreb*

SUMMARY

Our goal was to research the weather influence on incidence of children's sino-bronchial syndrome in Zagreb, the capitol of Croatia, and to find the characteristics of this weather. Zagreb is a town of about 900.000 inhabitants, developed industry and the strong road traffic. Therefore the influence of air pollution on disease frequency was analyzed as well. The weather has been classified according to man's thermal sensation, namely, according to daily bioclimatic index, separately for the cold and warm part of a year. Especially consideration was given to duration of some weather conditions and simultaneous disease frequency.
Results indicate that chronic patients are more sensitive to weather conditions than acute. In the warm part of the year they most frequently react to becoming cold and opposite in the cold part. The acute patients before all react to weather situations with high air humidity and longer duration (a few days) of warm periods in a cold part of the year and cold in the warm one.

1. Introduction

The respiratory tract diseases are frequently related to weather conditions and air pollution according to guess of many patients and their relatives, and even by many researchers (Tromp, 1963, 1980 et al.; Ayres, 1986; Katzschner, 1990; Krstić-Burić et al, 1991). Some authors emphasize a highly significant statistical relationship between the asthma attacks and atmospheric cooling, as a result of simultaneous effect of the air temperature and wind speed (Tromp 1980). Meanwhile, an extensive increase of heat, especially in combination with high air humidity, can cause the strong attacks of asthma as well. The cold fronts are significant for an increase of asthmatic attacks too.

The goal of this study was to find if inflammatory processes of upper and lower respiratory tracts (sino-bronchial syndrome) at children and adolescent in Zagreb could be connected with some weather conditions and air pollution in this town.

2. Data

For this study were used three kinds of daily data: medical, meteorological and chemical, collected or measured at Children's Hospital for Respiratory Diseases, Srebrnjak, Zagreb and at Meteorological and Hydrological Service of Croatia, Zagreb. They contain:

a)-number of patients for each day with:

- chronic sino-bronchial syndrome and
- acute disease of upper and lower respiratory tracts for period 1988-90, for children and adolescents (age 0-19) admitted to hospital at Srebrnjak.

b)-mean daily values of bioclimatic index i/H (enthalpy/cooling power) calculated on the basis of meteorological measurements (air temperature, relative humidity, wind speed and air pressure) at Observatory Zagreb-Maksimir.

c)-24-hour concentrations of SO_2 and smoke measured at Observatory Zagreb-Grič.

3. Method

All analyses have been performed separately for the cold (October- March) and warm (April-September) part of a year (period 1988-90).

A correlation analysis have been made for:

- daily number of chronic and acute patients in the period and
- daily values of bioclimatic index i/H (Pleško, 1976), including thus the joined influence of temperature, humidity and wind speed at cooling of man s body, respectively defining the man's thermal sensation. This index (i/H) is combined by two known bioclimatic indices: air enthalpy **i** (Böer, 1964) and cooling power **H** (Landsberg 1972, Conrad and Pollak, 1950).

It can be calculated from the equtions:

$$i = 1004(t_w + \frac{1555}{p} E_t)$$

where is: i - air enthalpy (J/kg); t_w - wet bulb temperature (°C), p - barometric pressure (hPa) at air temperature t; E_t- saturated vapour pressure at temperature t; v - wind speed (m/s); H - cooling power (kJ/m^2 s) and

$$H = 0.042(0.20 + 0.40v^{0.5})(36.5 - t) \quad \text{for v} < 1 \text{ m/s}$$
$$H = 0.042(0.13 + 0.47v^{0.5})(36.5 - t) \quad \text{for } v \geq 1 \text{ m/s},$$

with belonging bioclimatic classification (Pleško 1983):

THERMAL SENSATION	i/H
EXTREMELY COLD	<5
COLD	5 - 15
COOL	15 - 35
COMFORTABLE	35 - 85
WARM	85 - 155
UNPLEASANTLY WARM	155 - 255
SULTRY	205 - 310
DANGEROUSLY WARM	>310

The correlation analysis have been repeated for:

- three-, five- and seven-day moving averages of chronic and acute patients number and simultaneous moving averages of bioclimatic index i/H.

4. Results and discussion

The study is based at group of 207 chronic patients (134 boys, 73 girls) living in the town territory with many industrial objects and intensive road traffic; and at group of 100 patients cured for acute disease of upper and lower respiratory tracts. A correlation with meteorological parameters was studied on the basis of hospital admission date.

One can see (Tab.1) the significant increase of chronic sino-bronchial syndrome ($P < 0.01$) in the warm part of the year if the cooling lasts at least a day. A similar correlation was observed for the year as a whole (although with smaller significance); but if the year is divided in the warm and cold parts, the signs of correlation are opposite.

The acute upper and lower respiratory tracts disease is not related to meteorological conditions lasting only a day at all, concluding at the basis of thermal sensation. A sensitivity of chronic patients to thermal sensation during the whole year is remarked for the three-day moving averages very clearly in the warm as in the cold part of a year, indicating that in the warm part are significant three-day cold periods ($P < 0.0001$) and in the cold parts of a year the warm one ($P< 0.001$). Still more significant relationship with same characteristics between weather and chronic sino-bronchial syndrome is obtained for five- and seven-day moving averages (Tab.1). Meanwhile, a significant increase of acute disease frequency is obtained not before the seven day of warming in the cold part of a year ($P < 0.05$). The shorter warming periods in the cold part of a year, seems, do not cause yet the acute disease manifestation in the predisposed children or they do not come still in a hospital for the help. Thermal sensation in the warm part of a year is not significant for acute patients even for the seven-day moving periods.

Table 1. Linear correlation coefficients between 1-,3-,5- and 7-day moving averages of chronic sino-bronchial syndrome as well acute disease of upper and lower respiratory tracts and bioclimatic index i/H for the warm and cold part of a year; in Zagreb, period 1988-90.

COLD PART OF THE YEAR

		$(i/H)_1$	$(i/H)_3$	$(i/H)_5$	$(i/H)_7$
CHRONIC	r	0.0803	0.1410	0.1804	0.2174
	n	(546)	(546)	(548)	(548)
	P	0.0608	0.0009	0.0000	0.0000
ACUTE	r	0.0553	0.0688	0.0812	0.0863
	n	(546)	(548)	(548)	(548)
	P	0.1968	0.1074	0.0576	0.0435

WARM PART OF THE YEAR

		$(i/H)_1$	$(i/H)_3$	$(i/H)_5$	$(i/H)_7$
CHRONIC	r	-0.1163	-0.2226	-0.2897	-0.3382
	n	(549)	(549)	(549)	(549)
	P	0.0064	0.0000	0.0000	0.0000
ACUTE	r	0.0153	0.0364	0.0575	0.0596
	n	(549)	(549)	(549)	(549)
	P	0.7210	0.3947	0.1782	0.1629

r - correlation coefficient, P - signifcance level, n - number of cases

A measuring of SO_2 and smoke concentrations were performed by West-Gaeke spectrofotometric method. The station is situated in the green oasis of hill Grič at 150 m a.s.l. in the central part of town and far from industrial zone. At the same time it is about 30 m above the main town roads with dense traffic and above the territory where the observed children live. The extremely 24-hour concentrations for SO_2 was 148 µg/m and for smoke 260 µg/m in the period 1988-90. There were many days when 0 µg/m was registered for SO_2 and smoke according to mentioned method. For such data we did not get any significant correlation of the air pollution with chronic and acute diseases.

5. Conclusion

The results of our study correspond to results for asthma of Tromp and others, but it moreover brightened the differences between the warm and cold part of a year and between the chronic and acute disease incidence. Besides it indicate that chronic patients have the lower sensitivity threshold and react earlier to weather stress than acute ones. Air pollution with SO_2 and smoke was not significant in studied three years nor for chronic or acute disease incidence. The concentrations were within the law permitted boundaries.

REFERENCES:

Ayres J. G., 1986: Seasonal pattern of acute bronchitis in general practice in the United Kingdom 1976-83, Thorax 41, 106-110.

Böer W., 1964: Tehnische Meteorologie, Teubner Verlags gesellschaft, Leipzig, 290

Conrad V., L. W. Pollak, 1950: Methods in Climatology, Cambridge

Katzschner L., 1990: Atemwegserkrankungen in Abhängigkeit von Klima, Luftblastung und Stadtstrukturen, Ost Gesundh.-Wes. 52, 14-21.

Krstić-Burić M., N. Pleško, B. Momčilović, M. Bašić-Grbac, M. Medar-Lasić, Đ. Milković, M. Šumić, 1991: Sino-Bronchial Syndrome in a Children Population of an Industrialized Urban Area, Lung and Environment, 8 Congress of Pneumology, Trieste - Italy, November 8-9, 1991, Alpe - Adria - Pannonia, 57-58.

Landsberg H.E., 1972: The Assessment of Human Bioclimate, WMO, Tech. Note No.123, 36.

Pleško N., 1983: Biometeorološki indeksi u ocjeni termičkog komfora Zagreba za vrijeme različitih sinoptičkih situacija, Rasprave RHMZ SRH, 18, 3-16.

Tromp S. W., 1980: Biometeorology, Heyden, London, 346

Tromp S. W., 1963: Medical Biometeorology, Elsevier, Amsterdam, 991

Vukelić B. und N.Pleško, 1990: Der Einfluß von Maritimen Umweltfaktoren auf den Verlauf des Bronchialasthmas in Kindesalter - Ergebnisse nach einjähriger Beobachtung, Zeitschrift für Klinische Medizin, Band 45, Heft 20,

Degree Days in the Mountain Area of Croatia

M. Vučetić and V. Vučetić
Meteorological and Hydrological Service
Zagreb, Croatia

ABSTRACT

The growth of plants is more or less closely correlated with the accumulated air temperature below or above some temperature thresholds T. When computed from mean temperatures, these temperature differences are called degree days or temperature sums. Different types of degree days in the mountain area for the period 1961-1990 have been analysed. The mean annual of growing degree days (T = 5 °C) reached 2000-2300 °C at an altitude of 400-600 m. The range of the mean annual cooling degree days when CDD < °0 C was -250 to -200 °C at the same altitude. For the Zavižan meteorological station, situated in the northern part of the Velebit mountain at 1594 m, these degree days were 950 °C and -550 °C respectively.

1. Introduction

Air temperature is one of the significant meteorological elements by which the entire life on earth is governed. Since it is a known fact that the effect of air temperature on the flora is extraordinary, it seems of invaluable importance to include the best possible correlation. The simplest presentation of the influence of temperature on plants is the sums of the necessary physiological inactive and active air temperature. Thus, air temperature has an effect on the physiological process in a plant, not only during the period of vegetation, but equally in the period of winter rest. Mutual correlation of the inactive and active temperature effect is most marked in fruit trees and forest trees which are the most numerous in the mountain area of Croatia. Therefore the aim of this paper was to determine for this area the degree days or temperature sums for certain thresholds and estimate their linear trend. The meteorological data of the stations Skrad (675 m), Plaški (385 m), Ogulin (382 m), Gospić (564 m) and Zavižan (1594 m) were used for this purpose. Simultaneously the monthly precipitation amount and insolation duration have been presented.

2. Degree day analysis for different temperature thresholds

An analysis of heating degree days, HDD, was undertaken for temperature thresholds of 0 °C, 5 °C and 10 °C by means of application of relation (V. Vučetić and M. Vučetić, 1994):

$$HDD = \sum_{i=1}^{n} (S_i - T) \qquad S_i > T \qquad (1)$$

$$S = \frac{t_{max} + t_{min}}{2} \qquad (2)$$

where T - temperature threshold, t_{max} - maximum daily temperature, t_{min}- minimum daily temperature and n - number of days in a certain period. If $S \leq T$,$t_{max} > T$ °C and $t_{min} \geq 5$ °C, a correction was made in the estimate (1) and the heating degree days are calculated according to the relation $HDD = (t_{max} - T)/2$. Under the same conditions, except in the case of $t < 5$ °C it is taken that the temperature sum is zero. This correction is significant in spring, when already a small amount of warmth contributes to the beginning of vegetation but from the relation (1) follows that there is no temperature contribution. It is known that plants which do not accumulate a certain quantity of negative (inactive) temperatures during the winter, in the vegetation period may have a lower fertilization and thus also a poorer crop is obtained (Krpina, 1993). For this reason the cooling degree days were also analysed:

$$CDD = \sum_{i=1}^{n} S_i \qquad S_i < 0 \qquad (3)$$

where S is computed according to relation (2).

The commencement of vegetation depends on the duration and intensity of the winter. This is particularly importance in the mountain area, where the vegetation period is considerably shorter than in the other parts of Croatia. Therefore knowing the mean monthly temperature sums it is possible to give an estimate of the temperature conditions in a region in a certain period of the year and thus plan the growing of plant species.

Under normal conditions during the winter about -150 to -250 °C of CDD accumulate in the area considered, with the exception of Zavižan station where CDD are between -350 and-450 °C. If the

Table 1 Monthly degree days for different temperature thresholds, precipitation amount and insolation duration in the mountain area of Croatia for the period 1961-1990 except for Plaški station (1961-1986).

	MONTH	CDD [°C]	HEATING DEGREE DAYS T = 0 °C	T = 5 °C	T = 10 °C	PRECIPITATION [mm]	INSOLATION [hours]
	1	-85.9	44.9	5.6	0.1	110.6	
	2	-52.9	57.2	8.9	0.4	117.0	
	3	-21.6	128.5	37.7	5.0	127.3	
S	4	-0.4	232.4	98.3	21.4	157.4	
K	5	0.0	382.4	228.7	90.7	139.7	
R	6	0.0	466.1	316.1	169.0	140.0	
A	7	0.0	545.8	390.8	236.4	126.8	
D	8	0.0	532.0	377.0	222.6	149.0	
	9	0.0	425.9	276.1	133.6	152.2	
	10	-0.2	295.8	149.9	46.8	158.0	
	11	-13.4	140.3	47.0	7.9	197.2	
	12	-60.5	62.3	12.3	0.8	146.0	
	1	-86.9	57.7	12.1	0.9	101.6	
	2	-46.6	69.0	16.2	1.8	104.7	
	3	-13.5	157.0	54.1	7.8	124.2	
P	4	0.0	273.1	131.2	36.4	142.9	
L	5	0.0	422.1	267.7	122.2	116.5	
A	6	0.0	502.6	352.6	203.9	128.6	
Š	7	0.0	569.7	414.7	259.8	111.0	
K	8	0.0	558.1	403.1	248.4	130.9	
I	9	0.0	453.7	303.7	158.0	126.9	
	10	-0.1	321.8	171.3	59.0	141.6	
	11	-9.3	165.6	66.7	16.7	168.2	
	12	-58.5	72.7	19.8	2.4	135.1	
	1	-75.1	64.1	14.41	1.5	105.8	68.6
	2	-37.5	83.3	20.8	2.6	109.8	85.4
	3	-11.8	176.1	65.7	11.9	122.3	139.9
O	4	-0.1	293.7	148.6	44.6	137.6	157.1
G	5	0.0	438.6	283.9	136.0	124.7	210.0
U	6	0.0	519.4	369.4	219.9	129.3	224.4
L	7	0.0	593.5	438.5	283.6	118.8	272.2
I	8	0.0	578.8	423.9	268.9	135.5	242.3
N	9	0.0	467.0	317.0	169.6	138.6	185.1
	10	0.0	335.8	184.2	66.0	139.0	123.7
	11	-7.9	176.3	69.9	17.9	174.5	76.4
	12	-48.8	83.1	24.0	4.0	141.3	67.8
	1	-95.9	42.3	5.7	0.4	107.0	64.3
	2	-50.8	59.7	9.7	0.7	107.8	84.2
	3	-17.6	135.4	37.7	3.8	104.4	130.3
G	4	-0.1	242.1	102.6	19.5	107.6	163.7
O	5	0.0	387.2	232.8	90.5	107.4	217.6
S	6	0.0	469.6	319.6	171.0	91.6	237.5
P	7	0.0	547.0	392.0	237.1	66.3	295.8
I	8	0.0	538.0	383.0	228.1	101.1	263.0
Ć	9	0.0	424.8	274.8	130.4	118.1	190.6
	10	-0.2	297.8	148.4	42.4	136.4	134.4
	11	-14.7	145.9	49.3	9.4	179.1	70.2
	12	-72.7	59.4	13.3	1.7	142.1	49.1
	1	-138.5	10.0	0.3	0.0	143.1	93.0
	2	-125.4	11.4	0.5	0.0	149.8	95.1
Z	3	-90.6	32.7	4.1	0.4	154.7	128.2
A	4	-26.3	77.9	14.2	1.5	177..5	153.0
V	5	-1.7	208.7	76.7	15.3	157.4	204.0
I	6	-0.1	301.4	155.7	48.8	144.2	220.5
Ž	7	0.0	393.2	238.6	100.0	95.5	287.2
A	8	0.0	391.0	236.3	98.3	139.9	265.5
N	9	-0.3	289.0	146.2	43.6	153.9	198.6
	10	-8.7	179.0	63.0	12.1	179.8	1145.3
	11	-47.3	66.0	10.2	0.9	221.8	91.9
	12	-111.2	24.3	1.3	0.0	181.1	85.1

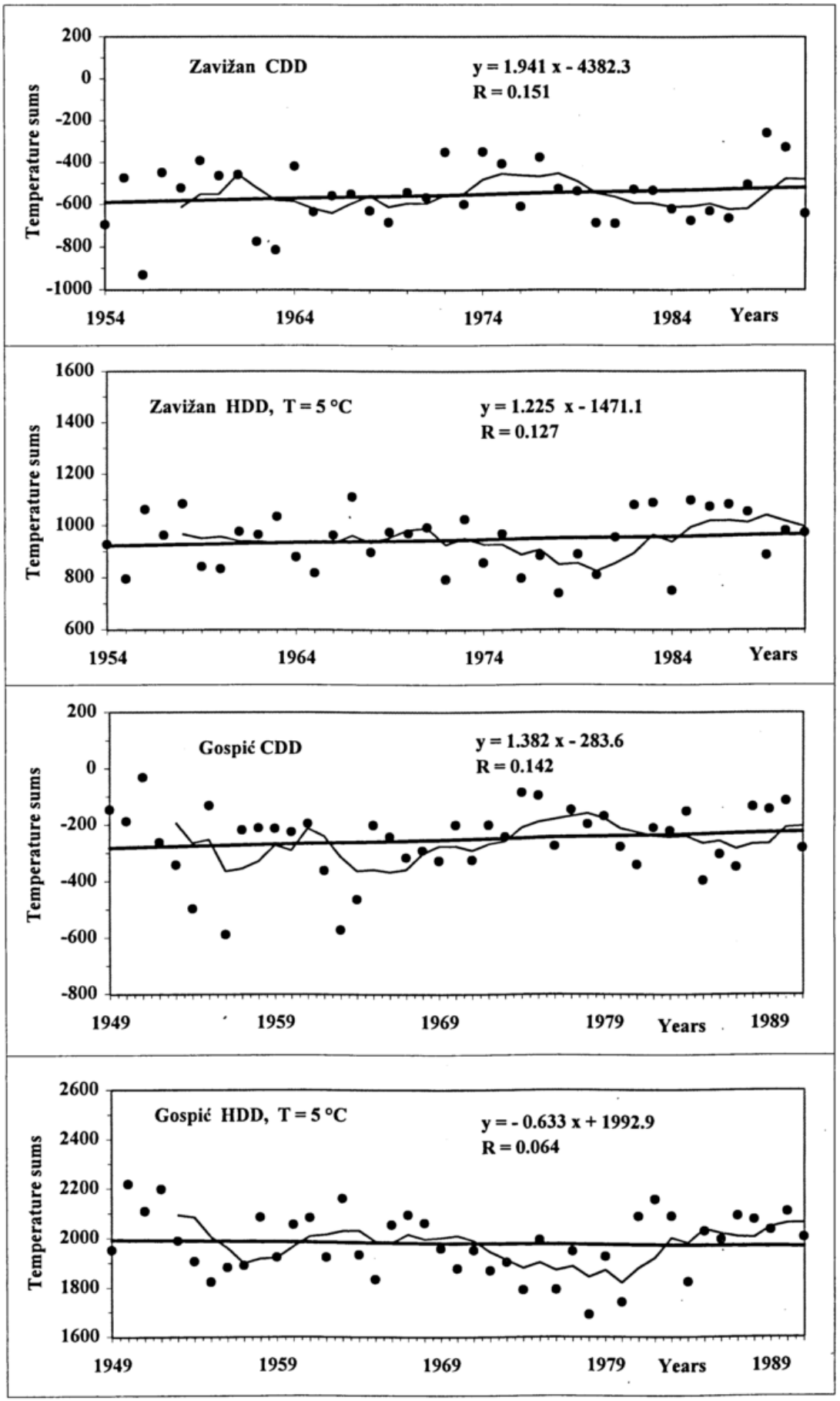

Figure 1 Time series of mean annual degree days (dots), the 5-year moving average (thin line) and the linear trend (bold line) for Zavižan (1954-1991) and Gospić (1949-1991).

temperature sum at an altitude of 400-600 m is less than -300 °C, this may be considered a severe winter. In the higher mountain regions the CDD is lower than -500 °C. Contrary to this, the winter will be mild if CDD is greater than -100 °C and on Zavižan greater than -250 °C. Short periods of milder weather during the winter are associated with special weather situations in which the foehn effect becomes marked. In these cases the heating degree days over the threshold of 10 °C were observed in meteorological stations located on a lower altitude above sea level (Table 1).
Vegetation begins for most plant species when sufficient warmth over the threshold of 5 °C has accumulated. On Zavižan the commencement of vegetation may be expected in May and in lower mountain regions in the transition period from March to April (Table 1). The highest mean values of HDD are noted in July (Table 1). At that time occurr the longest mean duration of insolation (250-300 hours) and the minimum of monthly precipitation amount (about 100 mm). In the summer months the deviation of HDD is approximately 150 °C between the lower mountain region and Zavižan. A sudden drop of HDD occurs in autumn. In November the annual maximum of the monthly precipitation amount appears.

3. Linear trend of mean annual degree days for different temperature thresholds

One of the methods which enables us to estimate statistically significant changes of the level around which are distributed the terms of the time series i. e. linear trend estimate of existence is the non-parametric Mann-Kendal rank test. This test is based on the value of the individual term in the series and the position of this term in the series. Namely, if a linear trend exists, then the values ought to be chronologically more or less increased or decreased. A detailed description of this method may be found in Mitchell et al. (1966). The results of this test application on the degree days above certain temperature thresholds, are presented in Table 2 where τ is the Kendall coefficient and α is the level of significance. The closer the τ-values are to zero, the higher is the level of significance i. e. the analysed values do not increase or decrease chronologically.
The greatest probability, that no linear trend exists, is in the series for Gospić and the least in the series for Ogulin and Plaški. According to the α coefficient the CDD for Skrad stands out and has the greatest probability for the linear trend (in the sense of increase of CDD with $\alpha = 0.06$, Table 2).

Table 2 The Kendall coefficient (τ) and corresponding level of significance (α) for the time series of mean annual degree days in the mountain area of Croatia.

	Skrad 1961-1991		Plaški 1961-1991		Ogulin 1949-1991		Gospić 1949-1991		Zavižan 1954-1991	
HDD	τ	α	τ	α	τ	α	τ	α	τ	α
0 °C	0.145	0.24	0.231	0.09	0.121	0.25	0.063	0.55	0.110	0.33
5 °C	0.113	0.36	0.174	0.20	0.161	0.13	0.011	0.92	0.090	0.43
10°C	0.149	0.23	0.105	0.44	0.152	0.14	0.014	0.89	0.070	0.54
CDD	0.232	0.06	0.123	0.37	0.055	0.60	0.060	0.57	0.037	0.74

However, it may be assumed that the testing of a longer data series would show results similar to those seen in the other stations. Thus, the statistical significance estimate in the change of level around which are distributed the terms of the time series, has not established the existence of a significant linear trend not even for one degree day of the stations considered. Fig. 1 represents only selected trends of annual degree days and the corresponding moving average for the Zavižan and Gospić stations.
According to the curves of a 5-year series of moving average, which eliminate very short-term fluctuations, a somewhat colder period was noticed in all stations during the period of transition from the seventies to the eighties.
Thus, the results of linear trend analysis may give the first significant information concerning the general characteristics of a time series.

References:

Krpina I. 1993: Zimsko smrzavanje voćaka , Hrvatski voćarski glasnik 2(3), Voćarski centar, Zagreb, 9.
Mitchell, J.M.Jr. et al; 1966: Climatic Change, WMO Tech. Note 79, Geneva, 58-75.
Vučetić M, V. Vučetić, 1992: Analysis of phenological characteristics in the Zavižan region, 22 ITAM, Toulouse 7-11 September 1992,
Vučetić V., M. Vučetić, 1994: Influence of weather conditions on agriculture during the period October 1992-September 1993, Izvanr. meteorol. hidrol. prilike Hrvat., Vol.17, DHMZ RH, Zagreb, 113-121.

M E T L I S

Das LITERATURINFORMATIONSSYSTEM METEOROLOGIE des DWD

Michael K. Goesch

Deutscher Wetterdienst, Zentralamt, Bibliothek/Fachinformation

ABSTRACT

METLIS, the Literature Information System METeorology, is a bibliographic database to aid literature searches, which was set up by the library at the Deutscher Wetterdienst. The database contains all catalogue entries that have been drawn up in the library since 1967. At the moment there are over 134,000 bibliographic records, mainly on meteorology, but also on other related fields.

ZUSAMMENFASSUNG

METLIS, das Literaturinformationssystem Meteorologie, ist eine bibliographische Datenbank, mit deren Hilfe Literaturrecherchen durchgeführt werden können. Sie wurde von der Bibliothek des Deutschen Wetterdienstes aufgebaut. Die Datenbasis umfaßt alle Titelaufnahmen, die in der Bibliothek seit 1967 erstellt worden sind. Zur Zeit sind das über 134 000 Literaturnachweise, in erster Linie aus dem Fach Meteorologie, teilweise aber auch aus verwandten Fachgebieten.

1 Einleitung

Jeder kennt die Situation: Man sucht Fachliteratur und ist mit dem, was man findet, nicht zufrieden, weiß nicht, wo man suchen soll, oder hat Schwierigkeiten, aus der Fülle das Wesentliche herauszusuchen.

Vielleicht fällt einem dabei eine der online recherchierbaren, öffentlich zugänglichen Literaturdatenbanken ein. Hierfür benötigt man jedoch meist eine Einweisung (Lehrgang), eine Nutzerkennung und man muß obendrein (hohe) Gebühren für die Anschlußzeit am Hostrechner sowie auch für die gefundenen Literaturzitate bezahlen.
Eine vollständige, rein meteorologische Literaturdatenbank findet sich bei diesen Hosts nicht. Die Meteorologie ist dort jeweils nur Rand- , nicht Kerngebiet, bzw. der "scope" der auswertenden Institution ist ein anderer.

Aus diesem Dilemma hilft Ihnen **METLIS**

Seit 1989 unterhält die Bibliothek des Deutschen Wetterdienstes das **LITERATUR - INFORMATIONSSYSTEM METEOROLOGIE**, kurz **METLIS** genannt. Es steht seit 1990 allen DWD-Mitarbeitern, die über ein Terminal auf die MFA (CY 860) des Meteorologischen Rechenzentrums (MRZ) des DWD zugreifen können, zur Verfügung und wird rege benutzt, Tendenz steigend.

METLIS ist eine bibliographische Datenbank und stellt das Kernstück eines künftig anzustrebenden Fachinformationssystems Meteorologie (FIS) dar. Mit Hilfe von METLIS werden Literaturrecherchen zu meteorologischen Themen für Mitarbeiter des DWD sowie für Interessenten von außerhalb durchgeführt.
Das Literaturinformationssystem Meteorologie wurde im Sachgebiet Dokumentation der Bibliothek mit Unterstützung durch das MRZ des DWD entwickelt. Durch die Bibliothek wird es unterhalten (Programmpflege) und laufend um die Neuzugänge ergänzt (update).

2 Was ist in **METLIS** enthalten ?

METLIS enthält zur Zeit über 134 000 Dokumentationseinheiten (DE). Das sind die Titelaufnahmen des gesamten meteorologischen Schrifttums, das bei der Bibliothek des DWD seit 1967 gesammelt und ausgewertet wurde, so daß **METLIS** Ende 1993 die Literaturnachweise von 27 kompletten Jahrgängen umfaßte, also auf eine große Datenbasis zugreift.

Die Literatur wird nicht nur formal bibliographisch beschrieben, sondern auch inhaltlich erschlossen. Die inhaltliche Erschließung, d.h. eine sorgfältige Klassifizierung nach fachlichen Gesichtspunkten, erfolgt mittels DK-Zahlen (Universelle Dezimalklassifikation).

Die ausgewertete Literatur umfaßt neben Monographien und Aufsätzen aus Zeitschriften Diplom- und Doktorarbeiten, Projekt- und Konferenzberichte, Reports u.s.w., also auch die sogenannte Graue Literatur. Die gesamte in **METLIS** zitierte Literatur ist in der Bibliothek des DWD vorhanden und unter bestimmten Bedingungen ausleibar. Literatur, die nicht in der Bibliothek des DWD vorhanden ist, wird nicht nachgewiesen. Da aber die Bibliothek das gesamte meteorologische Schrifttum weltweit sammelt, ist der Vollständigkeitsgrad hoch.

3 Wie kommt man an **METLIS** heran ?

Da die Benutzeroberfläche von **METLIS** nur für EDV- und Bibliotheksinsider im DWD geeignet ist, und auch noch gewisse organisatorische sowie verwaltungstechnische Hindernisse bestehen, können bisher nur Mitarbeiter des DWD online recherchieren. Die Bibliothek des DWD nimmt jedoch Aufträge zur Durchführung von Literaturrecherchen an. Die Recherchen sind unter bestimmten Bedingungen kostenlos: Wenn die Ergebnisse für rein wissenschftliche Zwecke, für Schule, Studium, Forschung oder Lehre verwendet werden. Andernfalls fallen gem. Gebührenordnung des DWD Gebühren an. Bei der Bibliothek des DWD sind Formulare für Rechercheaufträge, ein Merkblatt zu **METLIS** sowie eine ausführliche Gebrauchsanweisung für **METLIS** - Einsteiger erhältlich. Die Recherchen, die schriftlich angefordert werden müssen, werden kurzfristig erledigt, sofern es keine Probleme mit der EDV gibt.

4 Technische Informationen über **METLIS**

Der DWD unterhält eine Vielzahl verschiedener Datenbanken. Bei den meisten handelt es sich um sogenannte numerische oder Faktendatenbanken (mit meteorologischen Meß- oder Beobachtungsergebnissen u.s.w.). Um diese Datenbanken geht es hier nicht!

METLIS ist vom Inhalt und Zweck her a u s s c h l i e ß l i c h eine b i b l i o g r a p h i s c h e D a t e n b a n k , die Literaturnachweise (keinen Volltext !) enthält. Da METLIS mit einem nicht für Bibliothekszwecke konzipierten Datenbanksystem entwickelt wurde, bietet es nicht den Komfort, den Bibliotheksbenutzer bei einem Online-Katalog (OPAC, siehe Ausblick!) erwarten können.

Informationstechnisch hat die Datenbank folgende Eigenschaften:
METLIS ist eine IM/BASISplus-Datenbank. IM/BASISplus, ein Datenbanksystem der Battelle-Tochter IDI Inc. für Großrechner, nutzt als Host die CYBER 860 des MRZ des DWD. IM/BASISplus kann von 512 Usern gleichzeitig benutzt werden.

Wenngleich die Benutzeroberfläche von **METLIS** aufgrund der vorgenannten Unzulänglichkeiten noch nicht optimal ist, so ist **METLIS**, was die Performance betrifft, sehr leistungsfähig: Die Zugriffszeiten sind aufgrund der Anwendung moderner Datenbanktechnik (be-tree-Technik) bei IM/BASISplus (sofern der Hostrechner nicht anderweitig sehr strapaziert wird) sehr kurz und quasi unabhängig von der (großen) Anzahl der Datensätze in der Datenbasis. Und gerade das ist wichtig, denn **METLIS** wird weiter an Umfang zunehmen, nämlich ca. 5 0 0 0 DE pro Jahr.

5 Was leistet **METLIS** ?

Man kann sich aus **METLIS** alle zu einem gegebenen meteorologischen Thema in der Datenbasis enthaltenen Literaturzitate ausgeben lassen. Für die thematische Suche, wie z.B. die nach "anthropogenen Einflüssen auf das Klima", "Treibhauseffekt", "Ozonloch", aber auch weniger "modischen" Themen wie "Vorticityadvektion", "Klima-" oder "Ausbreitungsmodellen" und "Num. Vorhersagemodellen" werden in erster Linie die DK-Zahlen benutzt. Die Suche nach frei gewählten Begriffen aus dem Titel der Veröffentlichung (Stichwörter) oder auch z.B. nach Verfassernamen bzw. nach Kombinationen verschiedener Suchbegriffe in einem oder mehreren Feldern ist möglich. Das Ergebnis wird übersichtlich formatiert ausgegeben, je nach Wunsch sortiert, z.B. in chronologischer Reihenfolge.

6 Die Vorgeschichte von **METLIS**

Zur Arbeit der Bibliothek des DWD gehört seit jeher neben den klassischen Aufgaben einer Bibliothek (Erwerbung, Katalogisierung, Ausleihe und einfache Literaturauskünfte) die Literaturdokumentation, deren wesentliche Aufgabe die Auswertung und Nutzbarmachung der Fachliteratur für ihre Benutzer ist. Ziel ist die rasche Erteilung von Literaturauskünften mittels EDV-gestützten Literaturrecherchen. Das nennt man heute Fachinformationsvermittlung, und diese ist ohne den Einsatz moderner EDV-Verfahren nicht mehr denkbar.

Die ersten Dokumentationsarbeiten, Klassifizierung der meteorologischen Fachliteratur nach der Universellen Dezimalklassifikaktion (DK), begannen schon bei der Bibliothek des Reichswetterdienstes im Jahre 1935. Sie hatte sich bereits seit 1929, vertreten durch ihren damaligen Leiter Karl Knoch, an der Ausarbeitung des Bereichs Meteorologie, Klimatologie der DK beteiligt. Schon in den 60er Jahren ging man dazu über, die Titelaufnahmen auf elektronisch lesbaren Datenträgern (zunächst Lochstreifen, danach Magnetbänder) zu speichern (ab 1967 routinemäßig). Diese Titelaufnahmen enthielten bereits als Merkmale der Inhaltserschließung DK-Zahlen sowie zu einem kleinen Teil auch Schlagwörter und Referate. Diese Entwicklung mündete 1987 in den Aufbau der bibliographischen Datenbank METLIS.

7 Aktive Information

Mit Hilfe von **METLIS** werden die monatlich erscheinenden "Zugänge der Bibliothek des Deutschen Wetterdienstes" erstellt.

Darüberhinaus werden sogenannte PROFILDIENSTE angeboten: Wissenschaftler, denen die "Zugänge" zuviel "Ballast" enthalten, die aber ständig über die neueste Literatur unterrichtet sein wollen, können eine Literaturrecherche speziell für ihr Interessengebiet "abonnieren", wenn sie, wie bei einer Einzelrecherche, ihr "scope" genau definieren. Sie bekommen dann in bestimmten Abständen Literaturhinweise zu ihrem "Spezialthema" ausgegeben.

8 Ausblick

Die Bibliothek des DWD plant die Beschaffung eines integrierten Bibliotheksverwaltungssystems, das auch einen Online - Benutzerkatalog (OPAC = online public access catalogue) enthält. Ein OPAC ist ein elektronischer Bibliothekskatalog, der von jedem Laien ohne besondere Vorkenntnisse über einen Bildschirm (mit und ohne Bedienerführung) leicht und effektiv benutzt werden kann.

Voraussichtlich dann werden Online - Recherchen in **METLIS** auch von außerhalb des DWD möglich sein. Bis dahin sind allerdings noch einige grundsätzliche technische und verwaltungsmäßige Fragen (Datensicherheit, Zugriffssberechtigung, Gebühren für Anschlußzeit und Ergebnisse) zu regeln.

Ein weiteres Problem, das zu lösen wäre, ist die Ablösung der DK als Mittel der inhaltlichen Erschließung durch ein anderes System, da die DK nur von Insidern beherrscht wird und auch gewisse Schwächen aufweist.

Dies sind die Voraussetzungen für eine Verbesserung der Vermittlung von Fachinformation durch die Bibliothek des DWD. Aber auch in der jetzigen Form ist das METLIS ein "mächtiges Werkzeug" für die Durchführung von Literaturrecherchen.

LITERATUR

Aniol, R.: Literaturdokumentation im Deutschen Wetterdienst. Meteorol. Rdsch. 21 (1968) Nr. 3, S. 81-84.

Goesch, M. K.: METLIS: das meteorologische Literaturinformationssystem des DWD. Annalen der Meteorologie. 27 (1992), S. 360-361.

Keil, K.: Dezimaklassifikation des meteorologischen Schrifttums.
Meteorol. Zeitschr. 53 (1936) Nr. 7, S. 260-263.

Schlegel, M.: Die Bibliothek des DWD im Wandel der Zeiten <1847-1983>.
PROMET, Offenbach a.M., 13 (1983) Nr. 3/4, S. 61-64.

Abramo, F.d' 282
Abreu, Sa L. 176
Aebischer, U. 125
Apadula, F. 348
Aprano, L.d' 109
Attie, J.L. 176

Bajic, A. 113
Balafoutis, C. 344
Balut, G. 32
Bazac, G. 260
Benech, B. 152, 163
Bian, X. 239
Biancotti, A. 233
Binder, P. 89, 129
Blumer, F.P. 43, 237
Bougeault, P. 151
Bucsa, I. 277
Bücher, A. 243
Busuioc, A. 247

Caccia, J.-L. 163
Cagnati, A. 6
Campins, J. 159
Capka, B. 251
Cazazioc, L. 255
Cegnar, T. 336
Chen, B. 130, 143
Chmelik, M. 196
Cotariu, R. 260
Cuhalev, I. 329

Damrath, U. 85
Dessens, J. 243
Dima, V. 32
Druilhet, A. 152, 176

Egger, J. 71
Elkhalfi, A. 180
Elomaa, E. 61
Emde, K.v.d. 171
Emeis, S. 188
Escher-Vetter, H. 307

Fuentes, U. 21

Gajic-Capka, M. 251, 264
Gandino, C. 229
Garcia Selles, C. 303
Genoves, A. 159
Georgelin, M. 156, 180
Goesch, M. 360

Haase-Straub, S. 28
Hagen, M. 28
Haiden, T. 93
Heimann, D. 21, 28
Held, E. 52
Hereil, Ph. 171
Herzog, H.-J. 89
Huang, F. 134
Huber, M. 316
Huntrieser, H. 13

Ivancan-Picek, B. 200, 215

Jansa, A. 159
Joss, J. 52
Jude, O. 32

Kahlig, P. 259
Kasper, A. 311
Kelliher, F.M. 299
Kerkmann, J. 6
Klaus, V. 163, 167
Klose, B. 184
Koffi, E. 152,
Koleva, E. 238, 286
Krames, K. 67
Kristev, L. 238
Kromp-Kolb, H. 311
Krstic-Buric, M. 352
Kuettner, J. 121
Kurz, M. 1

Lang, H. 237
Lapin, M. 225
Lazic, L. 204
Lesnjak, M. 336
Li, Ch. 139
Li, L. 56
Liu, X. 147
Loncar, E. 268, 333
Lüdecke, C. 321

Mair, R. 291
Majewski, D. 85
Mares, C. 272
Mares, I. 272
Marki, A. 333
Marzorati, A. 348
Matsuo, T. 96
Matzarakis, A. 344
Maurer, Chr. 43
Mayer, H. 344
Mayr, G.J. 10
McKee, Th. B. 10
Migliardi, E. 282
Mihailescu, I. 277
Moiseyev, N. 104
Motta, L. 295
Motta, M. 295
Murakami, M. 96
Mursch-Radelgruber, E. 60, 325
Musat, I. 272
Musselman, R.C. 340

Nejedlik, P. 196
Nespor, V. 47
Niedzwiedz, T. 287

Owens, I.F. 299

Palmieri, S. 109, 217
Paludi, S. 233
Pasquale,V. 278
Paul, G. 80
Pech, B. 243
Pellegrini, U. 348
Peristeri, M.K. 25
Pichler, H. 78
Planinsek, T. 329
Plesko, N. 352
Plesko, S. 352
Pöttschacher, W. 39
Prabha, T.V. 325
Pristov, N. 105, 192

Qian, Zh. 130, 143

Rabaea, A. 277
Rakovec, J. 105, 192
Reinwarth, O. 307
Richard, E. 156, 180
Russo, G. 278

Sacchini, A. 278
Saito, K. 96
Salerno, R. 209
Salvador Franch, F. 299
Salzgeber, M. 316
Saulacic, I. 204
Schär, Chr. 125
Schiesser, H.H. 17
Schmid, W. 13, 56
Seibert, P. 311
Seloyan, I. 167
Sept, V. 21
Sevruk, B. 48, 61
Siani, A.M. 109, 217
Silbernagl, R. 316
Simen, C. 260
Sinik, N. 268, 333
Sneyers, R. 217
Stastny, P. 196
Stefanicki, G. 221
Stein, J. 152, 171
Steinacker, R. 39, 122
Steinegger, U. 43
Steppeler, J. 85
Sturman, A.P. 299
Sun, G. 139, 147

Tafferner, A. 73
Takano, I. 100
Talkner, P. 221
Tannhauser, D. 163
Tannhauser, D.S. 104
Todaro, C. 282
Tutis, V. 200, 215

Ustrnul, Z. 287

Valli, G. 320
Vecchi, R. 320
Verdoya, M. 278
Vogt, H. 65
Volkert, H. 117
Vrhovec, T. 210
Vucetic, M. 356
Vucetic, V. 113, 356

Weber, R.O. 221
Werner, R. 35
Whiteman, C.D. 239
Willemse, S. 17
Wooldridge, G.L. 340

Yang, D. 61

Zahlavova, L. 48
Zaninovic, K. 264, 268
Zeller, K.F. 340
Zhang, L. 139
Zhou, Y. 139, 147

17. 1982: Berchtesgaden, 21.–25. September
17. Internationale Tagung für Alpine Meteorologie. Annalen der Meteorologie, N.F. Nr. 19 (1982), 293 S.

18. 1984: Opatija, 25.–29. September
18th International Conference for Alpine Meteorology. Zb. Meteorol. i Hidrol. Radova 10 (1984), 374 S.

19. 1986: Rauris, 1.–6. September
Tagungsbericht, hersg. v. d. Österr. Ges. f. Meteorol. Wien 1987, 457 S.

20. 1988: Sestola, 18.–25. September
20. Congresso Internazionale de Meteorologia Alpina. Organiz. dal Servizio Meteorologico Italiano ..., Roma 1988.

21. 1990: Engelberg, 17.–21. September
Verhandlungen der 21. Internationalen Tagung für Alpine Meteorologie, Zürich: Schweizer. Meteorol. Anstalt 1990 u. 1991, 437 und 135 S. Veröffentlichungen d. Schweizerischen Meteorologischen Anstalt Nr. 48 und 49.

22. 1992: Toulouse, 7.–11. September
22ème Conference Internationale de Météorologie Alpine. Toulouse: Société Météorologique de France 1992, 452 S. und in La Météorologie 7. Ser., 1992, 45, S. 1–64.